REFERENCE
ONLY

The Study of the Process Dynamics and Control of a Continuous Stirred Tank Reactor using a Partial Simulation Technique

A Thesis submitted to the University of Aston in Birmingham for the Degree of Doctor of Philosophy

Thesis

16.JUN.71 138369
660·200623 BUX

Brian Buxton, B.Sc.

Department of Chemical Engineering

March 1971

SUMMARY

The problem was to analyse the stability and controllability of a continuous stirred tank reactor which was effecting an exothermic reaction. The approach chosen was a partial simulation technique by which it was hoped to retain some of the real plant characteristics whilst eliminating some of the more undesirable aspects. In this way it was anticipated that the gap between the completely theoretical approach and real plant analysis would be narrowed.

The equipment employed was a typical well stirred vessel which received a flow of water representing feed to the reactor. The vessel was cooled by water flowing through a coil which was situated in the vessel. Heat equal to that released from the exothermic reaction was generated by means of immersion heaters. The kinetics were simulated on an analogue computer which monitored the feed flowrate into the tank and also the temperature of the water within the tank. The computer was programmed with the idealised model of the process's material balance and by continually integrating this in real time it calculated the heat generation for the current value of temperature and concentration in the tank. This value was then transformed into real heat release in the vessel by means of immersion heaters through a servomechanism.

The stability and controllability of the partially simulated stirred tank reactor was then investigated, the

results being obtained in phase-plane portrait form. The control of the reaction temperature was effected by employing a standard feedback control loop in real plant hardware.

The research showed that the partial simulation technique offered more versatility than real plant analysis whilst the outlay necessary to conduct the work was much reduced. When compared with complete simulation it was evident that the demand on computer space was much reduced yet more of the real system character was retained.

NOMENCLATURE

The nomenclature in use throughout the thesis is given in the following list. Special symbols which appear from place to place are defined where they occur.

English letter symbols

A	Area
A	Constant in Arrhenius equation
A	Non-singular matrix
a_{ij}	Constants in matrices where i and j are the numbers of rows and columns respectively
B	A constant matrix
c	Concentration (gmole/litre)
c_o	Concentration of reactant in feed to the reactor (gmole/litre)
c_1	Concentration of reactant in the reactor (gmole/litre)
c_p	Specific heat (cal/g ^{o}C)
COP	Controller output pressure (lbf/in^{2}gauge)
C	Constant matrix
D	Diagonal matrix
E	Activation energy (cal/gmole)
e_s	Error from set-point (deg C)

G Transfer function

G_L Load transfer function

G_c Controller transfer function

G_v Valve transfer function

G_p Plant transfer function

G_m Measurement transfer function

g Acceleration due to gravity (cm/s^2)

ΔH Heat of reaction (cal/gmole deg C)

I Identity matrix

J Jordan canonical matrix

j $\sqrt{-1}$

K Overall gain

K_v Control valve gain $\left(\frac{\text{litre/min.}}{\text{lbf/in}^2}\right)$

K_c Controller gain $\left(\frac{\text{lbf/in}^2}{\text{deg C}}\right)$

K_p Plant gain $\left(\frac{\text{K cal/h deg C}}{\text{litre/min.}}\right)$

k Velocity constant (s^{-1})

L Time constant (s)

LMTD Log mean temperature difference (deg C)

M Mass holdup in the reactor (kg or g)

m_c Mass flowrate of coolant (g/s or kg/min.)

m_f Mass flowrate of feed (g/s or kg/min.)

N Describing function

P	Diagonalisation matrix
Q	Heat output from immersion heaters (Kcal/h)
Q_G	Rate of heat generation (Kcal/h)
Q_R	Rate of heat removal (cal/s)
R	Universal gas constant (cal/gmole ^oK)
R	Resistance (ohms)
r	Rate of reaction (gmole/litre s)
s	Laplace transform complex variable
T	Temperature (^oC or ^oK)
T_o	Temperature of feed inlet to reactor (^oC or ^oK)
T_1	Temperature in the reactor (^oC or ^oK)
T_{set}	Set-point temperature (^oC or ^oK)
T_{c1}	Inlet temperature of coolant (^oC or ^oK)
T_{c2}	Outlet temperature of coolant (^oC or ^oK)
T_{cav}	Average coolant temperature (^oC or ^oK)
T_R	Integral reset time (s)
t	Time (s)
UA	Heat transfer coefficient x Area [(cal/deg C s) or (Kcal/deg C h)]
u	Volumetric feed flowrate [(litre/min.) or (cm^3/s)]
u	A vector
u_c	Volumetric coolant flowrate (litre/min.)
V	Volumetric holdup in reactor (litres)
V	Voltage
V(x)	Liapunov function

x	Variable
x	A state vector
y	Variable
y	A state vector

Greek letter symbols

ω	Frequency
μ	Viscosity (P)
ρ	Density (gm/cm^3)
λ	Eigenvalue
τ	Time
θ_o	Outlet variable
θ_i	Inlet variable
θ_L	Load variable
Φ	State transition matrix

Simulation terminology used in the Thesis

Complete simulation

This term is used when the entire process is modelled and then implemented on a computer to obtain a solution.

Partial simulation

This term is used when some of the process exists in real plant whilst a particular part of it is chosen to be modelled and simulated on a computer. The computer operates on-line to the real equipment and the two operate together, thus representing the whole of the process for the purposes of the investigation.

INDEX

Page No.

Page No.

- o O o -

INDEX TO FIGURES

INDEX TO TABLES

ACKNOWLEDGEMENTS

The author wishes to thank Mr. A. R. Cooper of the Department of Chemical Engineering for his guidance and encouragement throughout the research, and Mr. J. Hamilton of the Department of Electrical Engineering for advice given with regard to servomechanism design.

I also wish to express my gratitude to my wife, Tricia, for typing the thesis.

CHAPTER 1
INTRODUCTION

The problem is to analyse the stability and controllability of a continuous stirred tank reactor. The system is usually not very difficult to model but the models obtained are often cumbersome and highly nonlinear. Consequently complete solutions are usually complicated and hence difficult to obtain. Computers have been utilized in the more extensive analyses but even so the research conducted has been on idealised mathematical models which have suffered modification in order to simplify the computations. Little work, if any, has been carried out on actual chemical plant. The present research intends to simplify calculations by retaining some of the nonlinear entities in real plant and thus reduce the demands on modelling by incorporating these effects directly in the solutions obtained. Thus a partial simulation technique was developed. It could be used to analyse any CSTR system effecting an exothermic reaction, which lends itself to be partially modelled. Further, the technique offers versatility in that it could be applied to other processes in which it is convenient to simulate a particular part or parts of a process while retaining the rest of the plant in its real form.

CHAPTER 2. LITERATURE SURVEY

2.1. Relating the particular problem for research to the field of Control Engineering

Control engineering is a subject which at the moment encompasses sections of many fields of well established engineering faculties. The most relevant ones to this project are Chemical, Electrical and Mechanical Engineering. All the fields are linked by a common mathematical basis viz. the study of a set of linear or nonlinear equations which describe the relevant system in the form of a mathematical model. This particular project does, in fact, have its roots in chemical engineering but the simulation requires a limited study of both electrical and mechanical engineering control fields. This is fortunate in that it allows consideration of control as a subject in its own right rather than as a subsection of chemical engineering.

2.2. Classification of the problem

When invited to consider the stability and controllability of a continuous stirred tank reactor, the problem posed in reality is the consideration of a set of nonlinear equations which represent this chemical process by means of well established mathematical descriptions. Once committed to an exothermic reaction, with temperature sensitive kinetics, then a nonlinearity is immediately imposed on the set of equations by the rate of reaction term which is a function of both temperature and concentration (except for zero order kinetics). The velocity constant is usually defined by the Arrhenius equation:

$$k = Ae^{-E/RT} \qquad \text{(Eq.2.1.)}$$

The rate for a first order irreversible reaction is then:

$$r = cAe^{-E/RT} \qquad \text{(Eq.2.2.)}$$

Consider a reaction with this form of kinetics being carried out in a CSTR which is cooled by water flowing through a coil. Taking as constants:

$$u, \rho, c_p, Q_r, T_o, V, \Delta H$$

then the transient material balance is given by:

$$uc_o = uc_1 + \underline{\underline{rV}} + V\frac{dc_1}{dt} \qquad \text{(Eq.2.3.)}$$

and the transient energy balance by:

$$\rho uc_pT_o + \underline{\underline{rV(-\Delta H)}} = u\rho c_pT_1 + \rho Vc_p\frac{dT_1}{dt} + Q_r \qquad \text{(Eq.2.4.)}$$

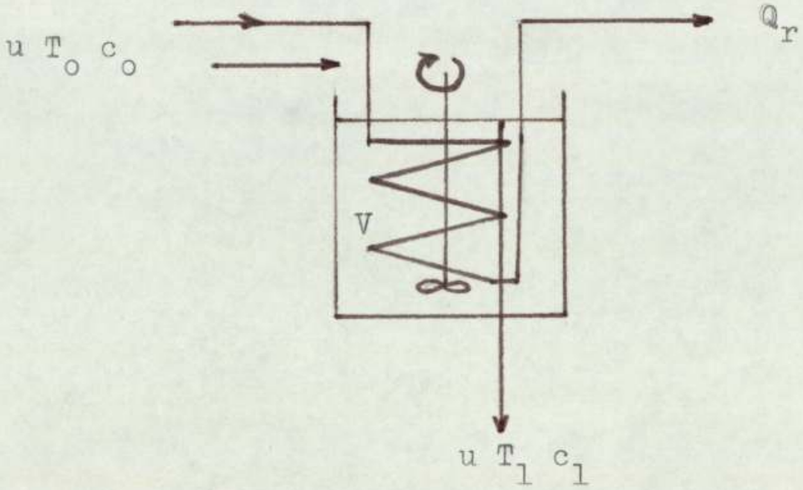

(Fig.2.1.)

In these equations the nonlinear terms are underlined. It is easy to conceive more complex cases by simply removing the constraints of constancy on the above list and also by increasing the complexity of the kinetics. Hence in general the system can be described by:

$$y_1 = f(y_1, y_2, y_3, y_4 \ldots\ldots\ldots\ldots\ldots\ldots y_n, t)$$

$$y_2 = f(y_1, y_2, y_3 \ldots\ldots\ldots\ldots\ldots\ldots\ldots y_n, t)$$

$$\vdots$$

$$y_n = f(y_1, y_2 \ldots\ldots\ldots\ldots\ldots\ldots\ldots\ldots y_n, t) \qquad \text{(Eq. 2.5.)}$$

wherein some y's may be zero.

The functions all contain at least one nonlinearity, and the general question now posed is how to analyse and solve such a set of equations.

2.3. Methods currently available for investigating this class of problem

A great deal of literature is available on the analysis of linear systems and the field of study is at a very advanced stage. Although much work has also been conducted in the study of nonlinear systems, it is meagre in comparison and the results less flexible than in the former case. Consequently one is hesitant to discard linear control theory on the grounds that the equations contain nonlinearities. Instead it is usual to salvage the equations by remodelling them in linear form i.e. by making a linear approximation to the nonlinear system. Perhaps the most popular technique is that utilising a truncated Taylor series to represent the nonlinear term. However having linearised the system equations it is then necessary to accept the limitations imposed on the conclusions which can be now obtained by analysing the simplified model. By the perturbation method the point of concern is moved to the origin and thus the initial conditions become zero by definition.

Hence transfer functions can be defined and block diagrams constructed for controllability analysis. Obviously for small deviations from the origin this approximation is a good one and it can be concluded that the linear set of equations describes the real system acceptably. However as the deviations from the origin increase then so do the errors introduced by the linearisation.

In regulator control problems when only small deviations are encountered the approximation will be quite good enough. For servo control with large deviations the approximation may suffer large errors and be entirely useless. When analysing system stability using the linearised equations many methods are available. The conclusions obtained are however restricted to being local i.e. if the system is found to be stable by a particular criterion it can only be concluded that the operating point is a stable point and no indication of the size of the region of stability involved can be obtained.

Therefore in summarising the usefulness of reducing the system model to linear form it can be said that if the engineer is prepared to accept restricted conclusions then he has at his disposal the entire linear control theory which is a powerful mathematical technique.

2.4. Analysis of Linear Systems

In the domain of linear systems there exists classical control and modern control techniques. Classical methods usually employ the Laplace Transformation type of analysis of the systems which have a limited number of variables. For multivariate systems modern control theory is used which employs state space representation and analysis of control systems, and requires a good knowledge of matrix theory. Modern control theory is being used in ever increasing situations but is at the moment largely confined to mechanical, electrical and aerospace engineering literature, while there is a noticeable lack in chemical engineering. This is most probably due to the greater difficulty encountered when trying to construct dynamic multidimensional models of chemical processes.

2.5. Nonlinear Systems Analysis

This deals with the mathematical expressions in their original nonlinear form. There are no general methods for the analysis of nonlinear systems. It is generally believed that such a general method is impossible because the response of the system depends in some way upon the input for its character. It is however possible to develop analyses which are applicable to a particular class of nonlinearities. Popular methods include phase plane analysis, Liapunov's direct method and the Describing Function technique. The phase plane method in its most complete form requires the actual integration of the nonlinear differential equations by either analogue or digital computers and subsequent cross plotting of the state variables with time being eliminated. This technique can be carried over into the multivariable domain but the essential advantage of the complete system representation by a single portrait is lost above second order systems. It would clearly be possible to construct three-dimensional models for the third order systems but the merit would be questionable considering the work involved.

The Liapunov method for the analysis of nonlinear systems in their nonlinear form is called the Direct or Second method of Liapunov. The first method is strictly a justification of the linearisation technique for nonlinear systems stability study i.e. it states that at the steady state the stability of the nonlinear equations will be the same as the linearised ones. The second or direct method of Liapunov can be used for either linear or nonlinear systems. In this approach it is not necessary to actually solve the differential equations describing the system.

Instead the problem is changed to that of constructing a Liapunov function for the system and having achieved this one can then claim stability (or instability) in the sense of Liapunov by observing various stability criteria for the function. The major disadvantage of this technique is that there are no standard procedures for constructing these functions for nonlinear systems in general.

The third powerful technique is the "describing function method" which belongs to the frequency response class of stability analyses. Nyquist plots can be obtained for the nonlinear systems which have been split into linear and nonlinear parts and stability criteria for the systems so arranged have been determined. A general background to the method is given in ref.(1). Application to a reactor (nuclear) control system in ref.(2).

Other methods such as the "Tracking Function technique" and the "Averaging Technique" (see refs.(3) and (4)) have also been developed which appear to be helpful in this type of system analysis and whilst the most famous methods have been mentioned the reader should not assume that the survey has attempted to include all of the approaches available. In general the approach taken is likely to depend on which class the nonlinearity or nonlinearities come into.

Having briefly summarised the possible ways of tackling the problem as presented by the current literature it is now intended to cover in more detail particular aspects of interest.

2.6. Classical Control Theory for Linear Systems

After linearisation the set of nonlinear equations can be represented in linear form in vector matrix notation:

$$\dot{x}(t) = Ax(t) \qquad \text{(Eq.2.6.)}$$

where: x is an n vector

A is an nxn non-singular matrix

and the equation is a homogeneous (i.e. unforced) linear time invariant differential equation. Considering a two-dimensional system for classical purposes the system may be described in the form:

$$\begin{bmatrix} \dot{x}_1 \\ \dot{x}_2 \end{bmatrix} = \begin{bmatrix} a_{11} & a_{12} \\ a_{21} & a_{22} \end{bmatrix} \begin{bmatrix} x_1 \\ x_2 \end{bmatrix} \qquad \text{(Eq.2.7.)}$$

or:

$$\dot{x}_1 = a_{11}x_1 + a_{12}x_2$$

$$\dot{x}_2 = a_{21}x_1 + a_{22}x_2$$

or in terms of temperature and concentration:

$$\begin{aligned} \dot{c}_1 &= a_{11}c_1 + a_{12}T_1 \\ \dot{T}_1 &= a_{21}c_1 + a_{22}T_1 \end{aligned} \qquad \text{(Eq.2.8.)}$$

where c_1 and T_1 are perturbation variables and are the only system variables, and where the constants a_{11}, a_{12} etc. are defined by the fixed parameters of the system.

In classical theory the Laplace transformation technique is used to obtain the transfer functions for the system. Hence from Eq.2.8. :

$$\frac{\bar{c}_1}{\bar{T}_1} = G_1 = \frac{K_1}{L_1 s + 1}$$

and:

$$\frac{\bar{\bar{T}}_1}{\bar{c}_1} = G_2 = \frac{K_2}{L_2 s + 1} \qquad \text{(Eq.2.9.)}$$

$$\therefore \quad \bar{T}_1 = \frac{K_2}{L_2 s + 1} \quad \frac{K_1}{L_1 s + 1} \quad \bar{T}_1$$

$$\bar{T}_1 \left[(L_1 s + 1)(L_2 s + 1) - K_1 K_2 \right] = 0$$

or:

$$\bar{T}_1 \left[a s^2 + b s + c \right] = 0 \qquad \text{(Eq.2.10.)}$$

This is the characteristic equation of the system from which a stability analysis can be made.

Reference (5) and more basically reference (6) describe much of the pioneer work conducted on the stability and control of a CSTR. From the linearised equations they put forward conditions which had to be satisfied for reactor stability. These were identical to the Routh - Hurwitz criteria which is dealt with in Section.2.7.14.

From Eq.2.10. the roots can be obtained using:

$$s_1, s_2 = \frac{-b \pm \sqrt{b^2 - 4ac}}{2a} \qquad \text{(Eq.2.11.)}$$

where a, b and c are constants (not necessarily positive) and L_1 and L_2 are time constants for the system.

If either of these roots is positive the system is unstable. If both are negative the system is stable. Further if the roots are complex an oscillatory response is obtained. If the real parts are zero then the oscillation is sustained whilst if the real parts are positive or negative the response oscillates in an unstable or stable manner respectively. As the number of variables increases and the orders of the polynomials increase so this method of solution becomes more difficult to manage.

In close connection with this method is the root locus technique which is described in many texts. Here the roots of the characteristic equation (or denominator of the transfer function set equal to zero) are obtained as a function of some varying parameter and plotted on an imaginary/real axis graph. All roots in the imaginary part of the graph give rise to stable solutions; if even one root lies in the positive half then an unstable solution is obtained. There are a number of available short cuts (Refs. (7) and (8)) which make it possible to construct the root locus without having to repeatedly solve the characteristic equation. It is in these short cuts that the true advantage of root locus analysis emerges.

Further information can be found in ref.(9) which illustrates the application of the root locus method in the design of a control system for a theoretical CSTR and ref.(10) which compares the root locus technique applied to the CSTR to the analogue simulation method.

Nonhomogeneous Time Invariant Systems

Similar analyses can be applied to forced systems (i.e. nonhomogeneous) which are time invariant.

In this case the system model would take the form:

$$\bar{\theta}_o = G_p \bar{\theta}_i + G_L \bar{\theta}_L \qquad \text{(Eq.2.12.)}$$

or in vector/matrix notation:

$$\dot{x} = Ax + Bu \qquad \text{(Eq.2.13.)}$$

where A and x are as defined previously,

and: u is an r vector

B is an nxr constant matrix.

In this category is the possibility of control systems already alluded to. In classical theory the block diagram technique is used and an overall transfer function for the complete negative feedback control loop of the system obtained.

Fig.2.2. shows a typical block diagram for the process under consideration. The overall expression is given by:

$$\bar{\theta}_o = \frac{G_L}{(1 + G_m G_v G_c G_p)} \bar{\theta}_L + \frac{G_v G_c G_p}{(1 + G_m G_v G_c G_p)} \bar{\theta}_S \qquad \text{(Eq.2.14.)}$$

For load changes only this reduces to:

$$\bar{\theta}_o = \frac{G_L}{(1 + G_m G_v G_c G_p)} \bar{\theta}_L \qquad \text{(Eq.2.15.)}$$

which can be expressed in the form:

$$\bar{\theta}_o = \frac{(s^n + a_1 s^{n-1} + a_2 s^{n-2} \ldots\ldots)\ \bar{\theta}_L}{(s^m + a_3 s^{m-1} + \ldots\ldots\ldots\ldots)}$$

where $m > n$ and a_1 to a_3 are constants.

This equation can be solved by inversion into the time domain.

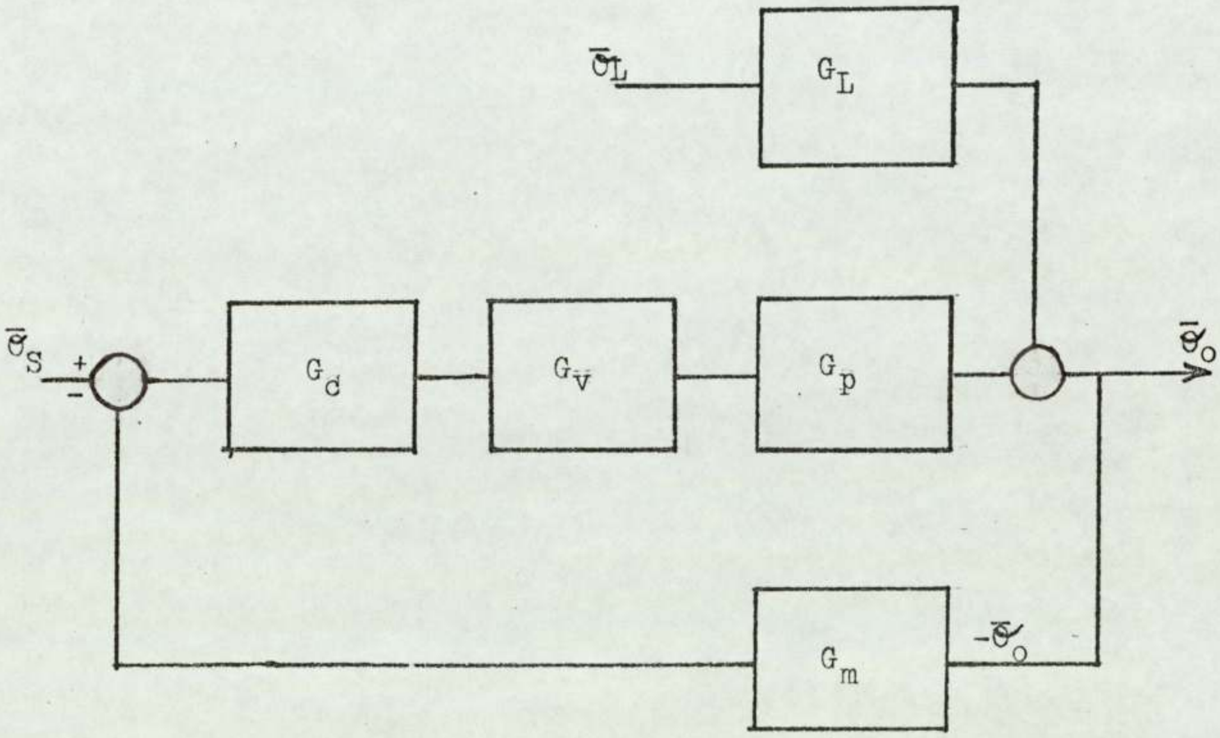

Fig.2.2. Block diagram illustrating a typical feedback control loop on a system undergoing load and/or setpoint changes.

Stability Criteria utilising the requirement that attenuation should not exceed unity

Frequency response analysis of classical systems also yields some stability criteria. From the modified sine wave obtained Bode and Nyquist plots can be made and open and closed loop system stability can be analysed from these graphs. Briefly the Nyquist criterion uses observations on open loop behaviour for the deductions of closed loop stability. A closed loop control system is stable if (and only if) the open loop Nyquist curve does not enclose the critical point at -1. The Nyquist graph is a polar plot of the vector $G(jw)$ where $G(s)$ is the open loop transfer function for the system.

The Bode plots consist of two graphs of logarithm of the magnitude, and angle of $G(jw)$ with a common abscissa logarithm of w. Here the stability criterion is based on the fact that there is a critical frequency at which the angle curve crosses the -180° level. The open loop magnitude of attenuation at this frequency will establish stability or otherwise according to its value relative to unity. Ref.(11) shows the application of frequency response techniques to the study of CSTR controllability.

Classical control theory is particularly suitable for the design of single (or limited) input output linear time invariant systems. The design is based on frequency response analysis. Using this technique of transmitting a sine wave through a process and observing the modification of this sine wave by the process the system dynamics can be estimated and a mathematical model proposed. From these models a block diagram can be constructed and the system controllability analysed.

It is clear that the eq.2.15. is subject to the same stability criteria as previously put forward for the unforced system.

More complicated block diagrams which arise from examples which include more variables still reduce to the same form of equation as above (multivariable systems) but the more complicated they become the more difficult is the utilisation of the classical techniques and the greater the justification for state space analysis techniques.

2.7. Modern Control Theory of Linear Systems

2.7.1. Unforced Systems - Co-ordinate Transformation

Consider the free dynamic multidimensional system:

$$\dot{x} = Ax \qquad \text{(Eq.2.16.)}$$

in which x is a state vector (n)
and A is an nxn matrix (non-singular).

The state vector may be defined in several ways. A set of state variables is the smallest set of numbers which must be stated in order to predict the dynamic behaviour of the system in question. The dimension is therefore fixed and the different methods of definition can be considered as co-ordinate transformations of the system.

Information on the system dynamics can be obtained by such a transformation. By putting the coefficient matrix of the state vector into a canonical form the eigen values can be displayed on the matrix diagonal. For unrepeated eigen values the simplest form is given, i.e.

$$\begin{bmatrix} \lambda_1 & & & & O \\ & \lambda_2 & & & \\ & & \lambda_3 & & \\ & & & \ddots & \\ O & & & & \lambda_n \end{bmatrix}$$

For multiple eigen values there are several possible forms depending on the linear independence of the eigen vectors. If all are linearly independent then the original form still stands. e.g. for three repeated eigen values in a five-dimensional system:

$$\begin{bmatrix} \lambda_1 & 0 & & & O \\ 0 & \lambda_1 & 0 & & \\ & & \lambda_1 & & \\ & & & \lambda_4 & 0 \\ O & & & 0 & \lambda_5 \end{bmatrix}$$

If only two are linearly independent then the form is modified to:

$$\begin{bmatrix} \lambda_1 & 1 & & & O \\ 0 & \lambda_1 & 0 & & \\ & & \lambda_1 & & \\ & & & \lambda_4 & 0 \\ O & & & 0 & \lambda_5 \end{bmatrix}$$

and if none are independent:

$$\begin{bmatrix} \lambda_1 & 1 & 0 & & O \\ 0 & \lambda_1 & 1 & & \\ & & \lambda_1 & 0 & \\ & & & \lambda_4 & 0 \\ O & & & 0 & \lambda_5 \end{bmatrix}$$

Obtaining the Jordan Canonical Matrix

Considering again the linear dynamic unforced system:

$$\dot{x} = Ax$$

Any other state vector say y is related to x by:

$$x = Py$$

where: P is an nxn non-singular matrix

This is sometimes called the diagonalisation matrix.

A useful state vector for the engineer analysing stability is defined by:

$$\dot{y} = P^{-1}APy = Jy \qquad \text{(Eq.2.18.)}$$

where: J is the Jordan Canonical matrix.

Determination of the Matrix P

For distinct eigen values P can be computed by utilising the system eigen values. Details of the procedure can be obtained from several standard texts on the subject (e.g. Ref.(12)). Briefly:

$$P = \begin{bmatrix} A_{111} & A_{211} & \cdots\cdots\cdots & A_{n11} \\ A_{112} & A_{212} & \cdots\cdots\cdots & \\ \vdots & & & \\ A_{11n} & \cdots\cdots & \cdots\cdots\cdots & A_{n1n} \end{bmatrix} \qquad \text{(Eq.2.19.)}$$

where the first subscript figure relates to a particular eigen value used for calculation and A stands for the cofactor of the element a_{11} of the original matrix.

Similar transformation matrices are calculable for systems with multiple eigen values and/or complex conjugate pairs. The simplest possible representation of the system has now been obtained in the Jordan Canonical form. Frequently occurring in control problems are n^{th} order scalar differential equations. (e.g. when using transfer functions to obtain a complicated block diagram the final representation will be produced in this form). It should be noted at this point therefore that it can be easily reduced to the form:

$$\dot{x} = Ax$$

i.e. a set of first order differential equations and in this case the computation of P is simplified.

2.7.2. Solutions of Linear Time-Invariant Vector Matrix Differential Equations

Most physical systems are more or less time-varying. However, as many of them change very slowly compared with their input forcing functions these may be approximated by linear time-invariant models. This allows a simplification in finding the solutions of these equations, the advantage being that as the system response does not depend on the input time of the forcing function the initial time can be conveniently taken as zero. As the system for research was taken as time-invariant this approach is presented here. However, the extension to time-varying parameter systems is straight-forward.

The Unforced Dynamic System (Homogeneous)

The linear time-invariant equation is:

$$\dot{x}(t) = Ax(t) \qquad x(o) = x_o$$

where $x(t)$ is an n vector defining the state of the system at time t

and A is an $n \times n$ constant matrix.

Taking: $x = Py$

then: $\dot{y} = Jy$

where J is the Jordan Canonical matrix.

For distinct eigen values $J = D$, the diagonal matrix, and the solution is:

$$y(t) = \begin{bmatrix} e^{\lambda_1 t} & & & 0 \\ & e^{\lambda_2 t} & & \\ & & \ddots & \\ 0 & & & e^{\lambda_n t} \end{bmatrix} y(0) = e^{Dt}\, y(0) \qquad \text{(Eq.2.20.)}$$

$$= Q(t)y(0)$$

where $Q(t) = e^{Dt}$.

Then reverting to the original variable of interest:

$$x(t) = PQ(t)P^{-1}x(o) \qquad \text{(Eq.2.21.)}$$

where $PQ(t)P^{-1}$ is the state transition matrix (Φ).

For multiple eigen vectors which are linearly dependent the state transition matrix is obtained in the form:

$$\Phi = P \begin{bmatrix} e^{\lambda_1 t} & te^{\lambda_1 t} & \frac{1}{2}t^2 e^{\lambda_1 t} \dots \\ 0 & e^{\lambda_1 t} & te^{\lambda_1 t} \dots \\ 0 & 0 & e^{\lambda_1 t} \dots \end{bmatrix} P^{-1}$$

(Eq.2.22.)

or $PS(t)Q(t)P^{-1}$

where $$S(t) = \begin{bmatrix} 1 & t & t^2/2 & \cdots\cdots\cdots \\ 0 & 1 & t & \cdots\cdots\cdots \\ 0 & 0 & 1 & \cdots\cdots\cdots \end{bmatrix}$$

It is interesting to note that the solution is a linear combination of motions. The amount of each motion can be considered separately and the single contributions noted. The contribution of each factor is dependent on the initial condition and for some particular starting points there may be a zero contribution by a particular factor throughout the transience. Hence the transition matrix is sometimes referred to as the weighting factor, i.e. it gives weights to various modes of motion, there often being some negligible ones compared with other dominant ones. This information can be put to good use by increasing the contribution of desired modes and reducing the effect of the undesirable modes. Hence parameter manipulation can play an important role in stability, controllability and optimisation.

Another method of solving the homogeneous vector matrix differential equation is by analogue computer simulation. The simulation utilises 'n' integrators, e.g. considering again:

$$\dot{x} = Ax$$

where:
$$x = \begin{bmatrix} x_1 \\ x_2 \\ x_3 \end{bmatrix} \qquad A = \begin{bmatrix} a_{11} & a_{12} & a_{13} \\ a_{21} & a_{22} & a_{23} \\ a_{31} & a_{32} & a_{33} \end{bmatrix}$$

The figure 2.3. illustrates the circuit for solving the third order system.

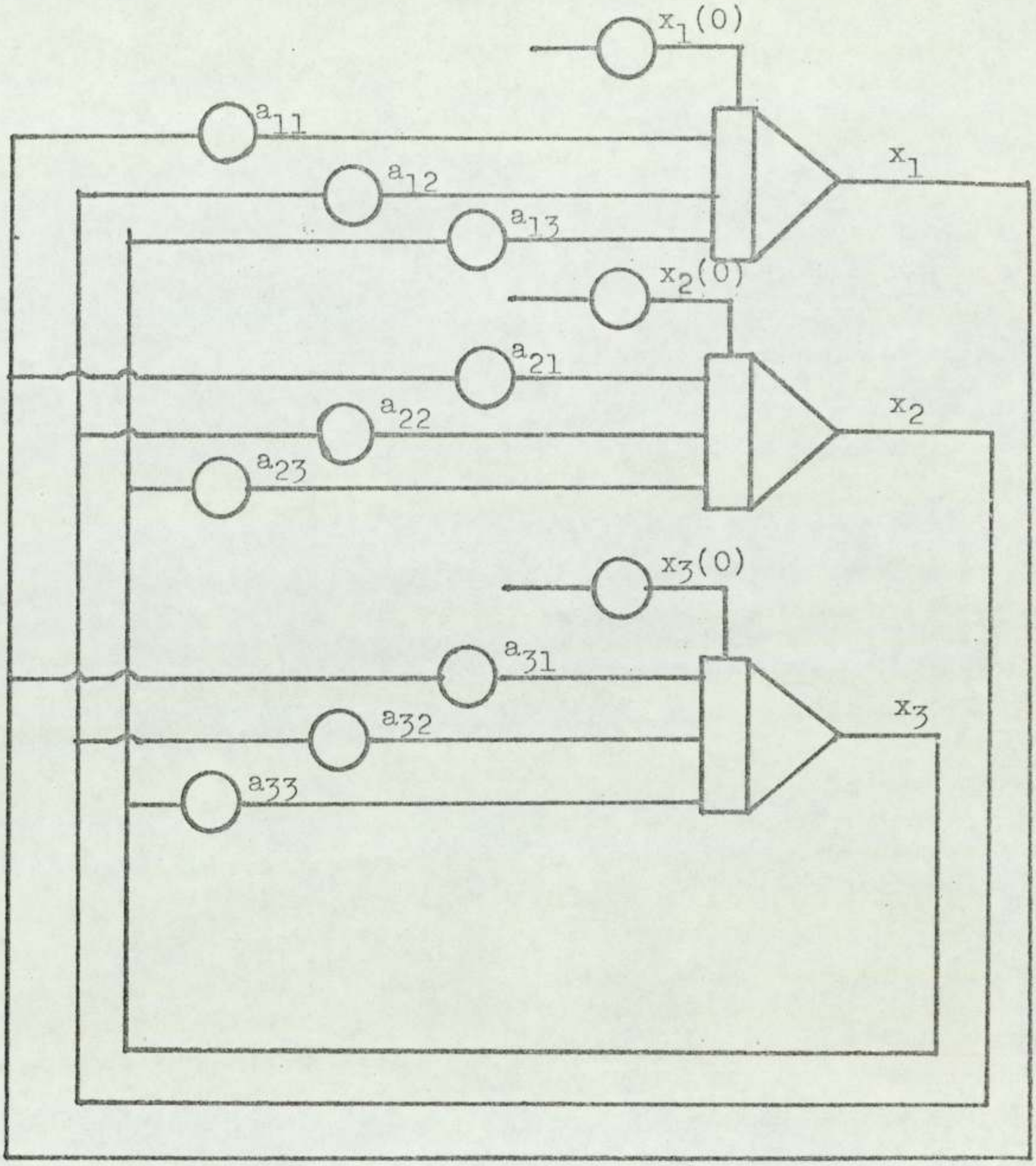

Fig.2.3. The Unforced Dynamic System (homogeneous).
Analogue Circuit for Solution.

To simplify the circuit convenient assumptions have been made:

$$a_{ij} \quad \text{negative}$$

$$|a_{ij}| \leq 1$$

These constraints are easily lifted and it is a simple matter to programme any real system under investigation which fits into this class.

Forced Dynamic System (Linear Time-Invariant)

Considering the vector matrix differential equation:

$$\dot{x}(t) = Ax(t) + Bu(t) \qquad x(0) = x_o \tag{Eq.2.23.}$$

where: x is an n vector

u is an r vector

A is an nxn constant matrix

B is an nxr constant matrix.

The solution of this expression is of the form:

$$x(t) = e^{At}x_o + \int_o^t e^{-A(\tau - t)} Bu(\tau)d\tau \tag{Eq.2.24.}$$

where: $\Phi(t) = e^{At}$ is the unique fundamental matrix.

It should be noted that x(t) is obtained from the addition of the motions due to initial condition and those due to the forcing function. The latter depend on the matrix B. If B is chosen in the correct form it is possible to ensure that a particular motion can only be excited by say the initial condition and not by the system forcing functions.

The equation can also be solved by analogue computational means in a similar way to that used for the unforced system.

2.7.3. Evaluation of e^{At}

The next stage in solving the equations is the computation of e^{At}. It is necessary to express e^{At} as a square matrix in order to obtain numerical solutions of x(t). For systems of dimensions greater than three, hand computation becomes tedious and it is usual at this stage to use a digital computer for performing the necessary arithmetic. Most computer manufacturers would probably offer such a subroutine as a standard piece of computer software.

Methods of computation include expansions into a power series, i.e.

$$e^{At} = e^{W} = I + W + \frac{W}{2}\left(\frac{W}{1!}\right) + \frac{W}{3}\left(\frac{W^2}{2!}\right) + \ldots\ldots\ldots \qquad \text{(Eq.2.25.)}$$

This method has the advantage of programming simplicity but the form of the mathematics is uneconomical in computer time and also suffers the loss of insight into the dynamic behaviour of the system by failure to separate the responses of different modes.

The Jordan Canonical form has therefore several advantages in this field, i.e. computation for distinct λ's

$$e^{At} = P\,e^{Dt}\,P^{-1} = P \begin{bmatrix} e^{\lambda_1 t} & & 0 \\ & \ddots & \\ 0 & & e^{\lambda_n t} \end{bmatrix} P^{-1}$$

For multiple eigen vectors a similar slightly more complicated form is obtained. Nevertheless computational effort is still greatly reduced over the series technique.

A standard subroutine could be constructed for this solution without much extra difficulty in programming, and also other methods of computing e^{At} exist.

2.7.4. Transfer Matrices

It should also be mentioned that the equation can be analysed by the use of the classical Laplace transform by constructing transfer matrices for zero initial conditions. The transform of Eq.2.23. is:

$$sX(s) = AX(s) + BU(s) \qquad \text{(Eq.2.26.)}$$

or:

$$X(s) = (sI - A)^{-1} BU(s)$$

The problem then presented is that of computing $(sI - A)^{-1}$ in which both analogue and digital computers are readily useful. Application to the CSTR has been made in ref.(13).

2.7.5.

Summarising, the representation and solution of multivariable systems in terms of state space has been considered. Ways have been indicated of obtaining an actual solution to the model in question. It has been noted that much can be learnt about the system without actually obtaining an explicit solution. Simply by manipulating the equation's co-ordinates information can be obtained about the system's behaviour. The next section employs this new system representation to obtain information about controllability, observability and stability without actual solution of the equations themselves.

2.7.6. Controllability and Observability

These two terms have special definitions in modern control theory. If a system of the form shown in Fig.2.4. is considered:

Fig.2.4.

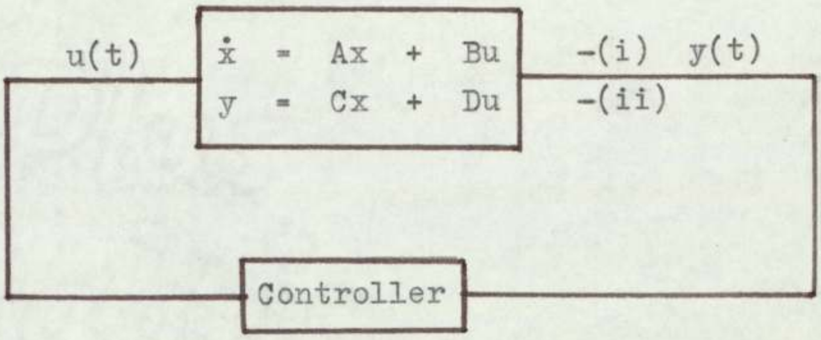

the state is described by equation (i) and the output by equation (ii) where A, B, C and D are constant matrices. A and B have already been mentioned. C specifies the constraint on the output with respect to x and D represents the direct transmission of u into y. Kalman introduced these concepts (ref.(14)) and the definitions are as follows:

2.7.7. Controllability

A system is completely state controllable if for any initial time it is possible to construct an unconstrained control vector which will transfer any initial system state to any final state in a finite time interval.

It should be noted that complete state controllability is neither necessary nor sufficient for complete output controllability which must therefore be defined separately.

Complete output controllability is obtained if it is possible to construct an unconstrained control vector which will transfer any initial output to a desired one in finite time.

Further, if the control process is confined to fixed intervals total controllability is necessary. This requires the system to be completely controllable on every time interval.

2.7.8. Observability

A system is completely observable on a time interval if for any initial time and some other time every state can be determined from a knowledge of the output vector, i.e. a system is completely observable if every transition of the system's state eventually affects the system output. Similar to total controllability, total observability can be defined as complete observability for every initial time and every subsequent time.

A determination of the controllability and observability of a system may give sufficient information to render the actual solution of the system's equations unnecessary.

2.7.9. Determination of Complete Controllability

The controllability of a continuous time and linear time-invariant system can be determined by the following analysis.

The equation of the system is:

$$\dot{x} = Ax + Bu$$

where: x = n vector (state vector)

u = r vector (control vector)

A = nxn matrix

B = nxr matrix.

The system is said to be completely state controllable if and only if the composite matrix nxnr P where:

$$P = [B \vdots AB \vdots \ldots\ldots\ldots\ldots A^{n-1}B] \qquad \text{(Eq.2.27.)}$$

is of rank n. (The matrix P has nr columns).
The proof of this theorem and the observability theorem can be found in ref.(15).

There is a similar theorem for the Laplace transformation representation. If the linear time-invariant system:

$$\dot{x} = Ax + Bu \qquad x(0) = 0 \qquad \text{(Eq.2.28.)}$$

where: x = n state vector

u = scalar (control signal)

A = nxn matrix

B = nx1 matrix

is considered then the solution in the Laplace domain is of the form:

$$X(s) = (sI - A)^{-1} BU(s)$$

where: $(sI - A)^{-1}B$ is an n vector

I = nxn identity matrix

s = complex variable such that $(sI - A)^{-1}$ exists.

A necessary and sufficient condition that the system defined above is completely state controllable is that $(sI - A)^{-1}B$ has no cancellation. If there is cancellation then the rank of the matrix:

$$P = [B \vdots AB \vdots \ldots\ldots\ldots\ldots \vdots A^{n-1}B]$$

is less than n. In this case then the system cannot be controlled in the direction of the cancelled mode.

2.7.10. Output Controllability

For the system:

$$\dot{x} = Ax + Bu$$
$$y = Cx \qquad \text{Eq.2.29.)}$$

in which:

$m \leqslant n$

x = n vector $\qquad$ A = nxn matrix

u = r vector $\qquad$ B = nxr matrix

y = m vector $\qquad$ C = mxn matrix

complete output controllability is obtainable if and only if the composite mxnr matrix P when:

$$P = [CB \vdots CAB \vdots CA^2B \vdots \dots\dots\dots\dots CA^{n-1}B] \qquad \text{(Eq.2.30.)}$$

is of rank m. (i.e. It is made up of m linearly independent equations.)

A similar theorem exists for the continuous time system described by:

$$\dot{x} = Ax + Bu$$
$$y = Cx + Du \qquad \text{(Eq.2.31.)}$$

(i.e. with the additional direct transmission of u to y.

Observability of Linear Time-Invariant Systems

Consider the system defined by the equations:

$$\dot{x} = Ax$$
$$y = Cx \qquad \text{(Eq.2.32.)}$$

where: A = nxn $\qquad$ x is an n vector (state vector)

C = mxn $\qquad$ y is an m vector (output vector)

$m \leqslant n$

(N.B. It can be shown that for determining observability it suffices to consider the system wihtout any input $u(t)$.)

The system can be proved to be completely observable if and only if the composite nxmn matrix P where:

$$P = [C^* : A^* C^* : \ldots\ldots\ (A^*)^{n-1} C^*] \qquad \text{(Eq.2.33.)}$$

is of rank n. The asterisk stands for the conjugate transpose of the matrix.

A similar theorem exists for the transfer matrices approach and also time varying systems.

2.7.11. Connection between Controllability and Observability

It should be noted that there is a relationship between the controllability and observability of dynamic systems. The analogies were expressed in the principle of duality which was presented by Kalman. Since observability is the dual of controllability, a knowledge of one implies a knowledge of the other.

These concepts give a complete solution to the optimal regulator control problem. Furthermore, they clarify the linear dynamic system and the transfer function relationship.

2.7.12. Stability Analysis of Multidimensional Linear Systems

A steady state x_{ss}, of a system:

$$\dot{x} = f(x,t) \qquad \text{(Eq.2.34.)}$$

is said to be stable if for each real number $\alpha > 0$ there exists a real number β which is a function of α and the initial time (t_o) in such a way that:

$$\|x_o - x_{ss}\| \leqslant \beta \qquad \text{(Eq.2.35.)}$$

implies:

$$\|\varphi(t;\, x_o\,, t_o) - x_{ss}\| \leqslant \alpha \qquad \text{(Eq.2.36.)}$$

for any $t \geqslant t_o$.

N.B. $\|x\|$ is the Euclidean length or norm of the vector x. i.e.

$$\|x\| = \sqrt{(x_1^{\;2} + x_2^{\;2} + \dots\dots\dots)}$$

If β is only dependent on α then the state can be called uniformly stable.

Considering a two dimensional system as an illustration then from Figure 2.5.:

Fig. 2.5

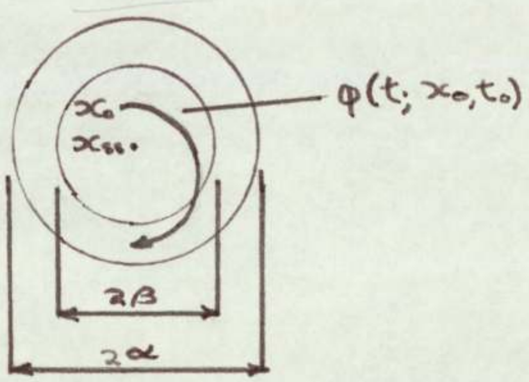

any initial value of $x\,(x_o)$ which lies within the circle radius β the motion does not leave the circle of radius α. The definition can be extended to three dimensionality by considering spheres and n-dimensionality by considering bounded surfaces.

The solutions of $\dot{x} = f(x\,,\,t)$ are said to be bounded if for a given $\beta > 0$ a constant α, which is a function of β and initial time, exists and that

$$\|x_o - x_{ss}\| \leqslant \beta \qquad \text{(Eq.2.37.)}$$

implying:

$$\left\|\varphi(t ; x_o, t_o) - x_{ss}\right\| \leq \alpha(\beta, t_o) \qquad \text{(Eq.2.38.)}$$

for all time $t \geq t_o$.

For α only dependent on β, uniformly bounded solutions can be concluded.

It should be noted that these may not be satisfactory stability criteria from the chemical engineer's point of view in that the new steady state will not necessarily be an acceptable operating point. A more useful concept of stability is asymptotic stability which is discussed in the next section.

Asymptotic Stability

A steady state is said to be asymptotically stable if it is stable and if every solution converges to this state as time increases indefinitely when starting from an initial condition sufficiently near to the steady state. Mathematically this can be stated as follows:

Consider two real numbers $\beta > 0$ and $\gamma > 0$ then there are real numbers $\alpha > 0$ and $\eta(\gamma, \beta, t_o)$ in such a way that:

$$\left\|x_o - x_{ss}\right\| \leq \beta \qquad \text{(Eq.2.39.)}$$

which implies:

$$\left\|\varphi(t ; x_o, t_o) - x_{ss}\right\| \leq \alpha \qquad \text{(Eq.2.40.)}$$

for all time $t \geq t_o$.

and:

$$\left\|\varphi(t ; x_o, t_o) - x_{ss}\right\| \leq \gamma \qquad \text{(Eq.2.41.)}$$

for all time $t \geq t_o + \eta(\gamma, \beta, t_o)$.

Figure 2.6. illustrates the motion for the second order system:

Fig.2.6.

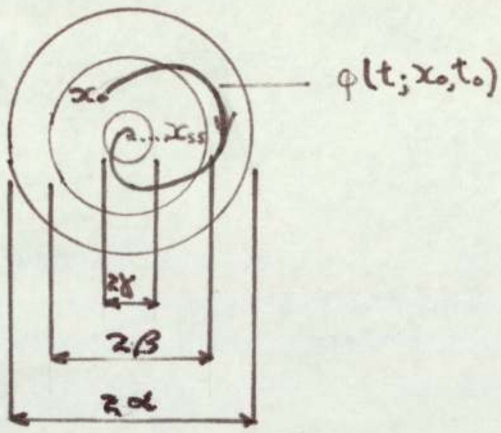

The circle, radius γ , represents the region that the φ will have entered after the time elapse $t_o + \mathfrak{h}$. The motion starts from the point x_o in the circle of radius β . Every motion converges to the origin without leaving the circle radius α .

These conditions establish local rather than global stability, i.e. there is a region of asymptotic stability within which starting from any initial condition the steady state will be approached. This region is called the "domain of attraction". Some knowledge of the size of the largest region of asymptotic stability is usually required and consequently many stability analyses deal with computing the boundaries of such a region.

Asymptotic Stability in the large

If the above criteria hold for all initial conditions in the state space, the system is said to be globally stable or asymptotically stable in the large. Obviously if this condition exists there can be only one steady state. The foregoing criteria are those desired by the control engineer.

Failing this he must compromise and calculate a large enough region of stability which will not be transcended.

2.7.13. Instability

A steady state is said to be unstable if it is neither stable nor asymptotically stable. In this case for some real number $\alpha > 0$ and any real number $\beta > 0$ no matter how small, there is always in the circular region a state x_0 such that the motion starting from this state reaches the boundary circle.

2.7.14. Routh and Hurwitz Stability Criteria

The criteria are applicable to linear time-invariant systems and can be applied to both classical and modern control problems. In the classical case the polynomial which is the denominator of a feedback control loop transfer function, or simply the system's characteristic equation if free response stability information is needed, is required for the test. In modern control theory from the free dynamic system:

$$\dot{x} = Ax$$

the nature of the solution is determined from the eigen values of A or the roots of the characteristic equation.

$$|A - \lambda I| = 0 \qquad \text{(Eq.2.42.)}$$

Hence the polynomial can be generated.

For forced systems the application of Cramer's rule produces the corresponding polynomial for this case.

The polynomial finally obtained after equating to zero will be of the form:

$$a_o \lambda^n + a_1 \lambda^{n-1} + a_2 \lambda^{n-2} + \dots\dots a_{n-1} \lambda + a_n = 0$$

(Eq.2.43.)

where the coefficients a are real quantities.
If any of the coefficients are zero or negative the system is known to be unstable and further analysis is unnecessary.

The Routh and Hurwitz criteria can be shown to be equivalent to each other. Taking the Routh method as an example of the technique then all the coefficients are arranged in rows and columns according to:

$$\begin{array}{llllll}
\lambda^n & a_o & a_2 & a_4 & a_6 \dots\dots & \text{first row} \\
\lambda^{n-1} & a_1 & a_3 & a_5 & a_7 \dots\dots & \\
\lambda^{n-2} & b_1 & b_2 & b_3 & b_4 \dots\dots & \\
\lambda^{n-3} & c_1 & c_2 & c_3 & c_4 \dots\dots & \\
\vdots & \vdots & \vdots & \vdots & \vdots & \\
\lambda^2 & d_1 & d_2 & 0 & & \\
\lambda & e_1 & 0 & & & \\
\lambda^o & f_1 & & & & \\
 & \begin{array}{c}\text{first}\\ \text{column}\end{array} & & & &
\end{array}$$

The first two rows are obtained directly from the polynomial and subsequent rows are calculated from:

$$b_1 = \frac{a_1 a_2 - a_o a_3}{a_1} \qquad b_2 = \frac{a_1 a_4 - a_o a_5}{a_1}$$

$$c_1 = \frac{b_1 a_3 - a_1 a_2}{b_1} \qquad \text{etc.}$$

(Eqs.2.44.)

This technique is continued until a zero appears in the first column.

If there are no sign changes the system is stable. If there is at least one sign change the system is unstable. The instability is due to the existence of at least one complex conjugate pair of roots which have a positive real part. If stability is proved it should be remembered that this proves only local stability for the nonlinear system.

2.7.15. The Liapunov Methods of Stability Analysis

The First Method of Liapunov

Consider the nonlinear system:

$$\dot{x} = f(x) \qquad \text{(Eq.2.45.)}$$

where:

x = state vector (n)

$f(x)$ = n vector, and is continuously differentiable in $x_1, x_2 \ldots\ldots x_n$

In the first method each steady state, if more than one exists, is investigated separately. As in the classical case the nonlinear vector function can be expanded in a Taylor series about the steady state and the system expressed as:

$$y = Ay + F(y)y \qquad \text{(Eq.2.46.)}$$

where:

$y = x - x_{ss}$

If the Taylor series is truncated at the first derivative, the Jacobian matrix is then formed, given by:

$$A = \begin{bmatrix} \frac{\partial f_1}{\partial x_1} & \frac{\partial f_1}{\partial x_2} & \cdots\cdots\cdots & \frac{\partial f_1}{\partial x_n} \\ \frac{\partial f_2}{\partial x_1} & \frac{\partial f_2}{\partial x_2} & \cdots\cdots\cdots & \vdots \\ \vdots & \vdots & & \vdots \\ \frac{\partial f_n}{\partial x_1} & \vdots & \cdots\cdots\cdots & \frac{\partial f_n}{\partial x_n} \end{bmatrix}$$

(Eq.2.47.)

Thus near the origin and neglecting the higher order terms $F(y)$ the linearised equation obtained is:

$$\dot{y} = Ay$$

Liapunov proved that if the eigen values of this matrix A have nonzero real parts then the stability of the steady state linear equations is the same as that of the nonlinear equation, i.e. if all eigen values have negative real parts then both steady states for linear and nonlinear cases are asymptotically stable. If the real parts of one or more of the eigen values are zero then the stability depends on higher order derivatives in the Taylor series.

It is important to remember that these stability conclusions apply only to the close proximity of the steady state. No indication as to the size of region is given. Liapunov's second method deals with the dimensions of such a region.

The Second (or Direct) Method of Liapunov

This technique is applicable to both linear and nonlinear systems. It determines the system stability without having to resort to solving the system's equations. When analysing linear problems it has the advantage of a standard technique for constructing a Liapunov function (ref.16)). No such general method exists for nonlinear systems. As nonlinear system investigation is of greatest concern here the theorem is dealt with in detail in the nonlinear stability analysis section (2.8.3.). An important point to note, however, is that if a linear free dynamic system is found to be locally asymptotically stable by this method then it is also asymptotically stable in the large.

2.7.16. Phase Plane Analysis

This technique can be applied to linear systems (both single and multivariable) and nonlinear systems. Basically a phase-plane portrait is the tracing of the motion of the free response of a continuous, or discrete, system as it moves through space. The state variables are the co-ordinates of the plot and from a knowledge of their values at various points in the space a complete picture of the system stability can be constructed.

Consider a two-dimensional linear system as would be obtained from the linearised material and energy balances.

$$\begin{bmatrix} \dot{T}_1 \\ \dot{c}_1 \end{bmatrix} = \begin{bmatrix} a_{11} & a_{12} \\ a_{12} & a_{22} \end{bmatrix} \begin{bmatrix} T_1 \\ c_1 \end{bmatrix} \qquad \text{(Eq.2.49.)}$$

To obtain a phase-plane portrait from this equation it is first necessary to select state variables. Although c_1, $\dot{c}_1$, T_1 and $\dot{T}_1$ could be used it is convenient to use the pair T_1 and c_1 as these will be the most meaningful to the system analyst. It is generally more simple to use whatever dependent variables appear when the system is written in a set of first order differential equations. The important step to remember is to manipulate the equations in such a way that the independent variable is eliminated whilst the state variables are retained. This can be done by simply dividing time out, i.e.

$$\frac{\dot{T}_1}{\dot{c}_1} = \frac{a_{11}T_1 + a_{21}c_1}{a_{12}T_1 + a_{22}c_1} \qquad \text{(Eq.2.50.)}$$

After plotting trajectories from various initial conditions a picture is soon built up. Time could strictly be plotted along the length of each trajectory.

Methods of solving the equations or alternative routes of obtaining sufficient information to plot the portrait are given in the section on nonlinear systems (2.8.1.). Clearly for linear systems, solution is comparatively simple by direct integration, though for higher order systems the mathematics would become tedious without the assistance of a computer.

Accepting then that the information for constructing portraits for linear systems is readily obtained the two-dimensional system is now considered further as an example of a linear system.

For this two-dimensional case the portrait can be plotted directly on two co-ordinates and the stability of the system is completely defined.

For a stable system with unequal negative eigen values a node is obtained (Fig.2.7.(a)). If the eigen values had been equal the curved lines would have been straight. For an

Fig.2.7.

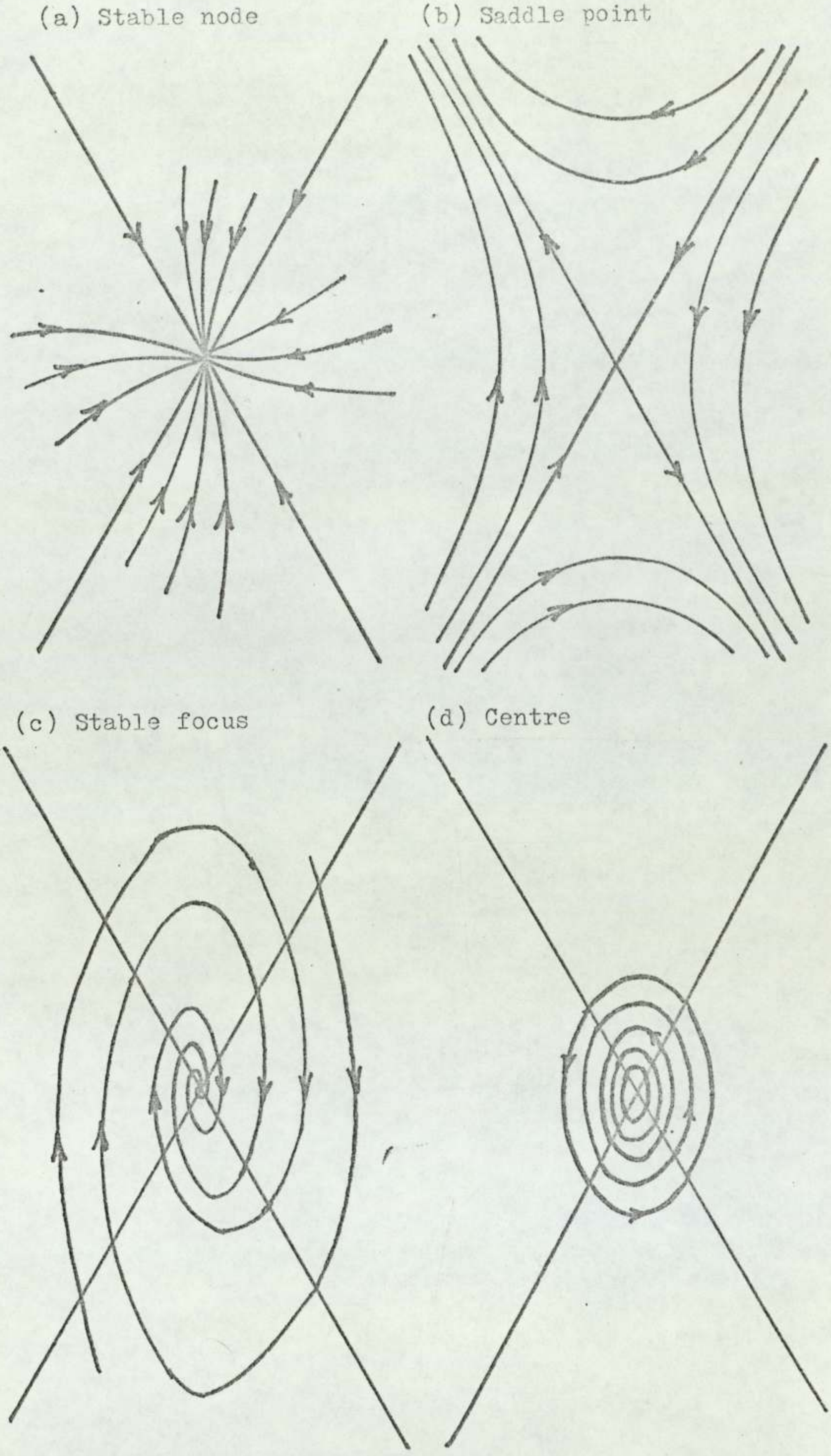

unstable node the arrows are merely reversed (i.e. both eigen value signs are reversed). If one eigen value is positive and the other negative a saddle point is obtained (Fig.2.7.(b)). Complex eigen values produce foci, their stability depending on whether their real parts are negative or positive. An example of a stable focus is given in Fig.2.7.(c) (i.e. negative real part). For a positive real part the direction of the arrows is reversed. For zero real parts a "centre" is obtained (Fig.2.7.(d)).

Considering multivariable systems (i.e. three or more variables) it is obvious that the two-dimensional phase plane portrait is lost. Recalling that in the section on solution of multidimensional unforced systems it was possible to present the solution in its separate modes for both distinct and repeated eigen values then this form of presentation can be utilised in the phase plane technique. In spite of the fact that the two-dimensional portrait is lost an extension can be offered if it is noted that the motion of the individual modes can be visualised as separate phase plots. The total motion can then be obtained by the superposition of the individual plots. A similar type of analysis can be done for forced systems by utilisation of the Jordan Canonical type of presentation of the solutions.

2.7.17. Functional Analysis

Before concluding this section on modern control theory it should be mentioned that functional analysis is playing an ever increasing part in the analysis of systems (refs. 17 and 18)). This approach takes a more abstract view than has been presented hitherto and classifies the systems in a more basic structure.

As an introduction to this subject a mathematically based approach is taken. Extensive mathematical theory of functions exists and this can be applied to control problems. There are many similarities between functional analysis and vector analysis. Many problems can be constructed with either technique and hence the other may be avoided. The application of functional analysis is readily appreciated in such problems which require steepest-descent and mean square minimisation solutions.

The initial consideration in this study is a concept of sets, the elements of which may be points, numbers or functions. A set which is the universe or set of elements used to compose all the sets under consideration is called a space. Then from various assumptions and definitions and theorems certain types of spaces can be defined, such as metric and linear spaces. The metric space provides a measure of distance whilst the linear space defines linear operations on the set. Hence through the understanding of linear independence of the equations the dimension of a space and its basis are defined.

After obtaining a "feel" for this type of system representation the norm axioms are clearly outlined. It can then be seen that any normed linear space is a metric space and convergence criteria which apply to the latter therefore are applicable to the former. A complete normed linear space is called a Banach space. A particular normed linear space which has many important properties is the Hilbert space, which is a finite or infinite dimensional set with the following properties:

(i) It is a linear space

(ii) An inner product is defined for each pair of elements which belong to the space, with the quantity:

$$\|f\| = \sqrt{\langle f, f \rangle} \qquad \text{(Eq.2.51.)}$$

being taken as the norm.

(iii) The space is a complete metric.

The Hilbert space is effectively an extension of Euclidian space into infinite dimensional space and is the natural one in which to study functions.

A Banach space is defined as:

A normed linear space which is also a complete metric space with respect to the metric:

$$\varepsilon\ (x, y) = \|x - y\| \qquad \text{(Eq.2.52.)}$$

induced by the norm.

Hilbert space is defined as:

A linear space is called a Hilbert space if it is an inner product space that is complete with respect to the norm induced by the inner product. i.e. A Hilbert space is a special case of a Banach space whose norm is induced by an inner product.

Applications of this theory can be made to sensitivity and optimal control problems for Banach spaces which represent a continuous system. A similar more restricted application can be made by utilising the Hilbert space concept.

Functions and Transformations

A function can be considered as a transformation or mapping of one subset into another.

Linear transformations then follow if linear mapping from one linear space to the next is considered, the transforms being defined by the linear dynamic systems. The first order homogeneous system may be dealt with as a transformation, the mathematical matrix manipulation of which has already been covered in the section on modern control theory. Similarly nonhomogeneous systems can be considered in terms of transformations.

From the foregoing a forced response of a continuous linear dynamic system can be defined as being representable as a linear transformation, bounded for a finite time interval, from one Banach space into another.

Linear functionals are the next important concept. Many can be defined depending on the type of space. They are necessary for the solution of many optimal control problems.

By means of a projection operator and a linear subspace of a Hilbert space the latter can be reduced to two components, one in the linear subspace and the other the orthogonal of every element of that subspace.

This can then be applied to the theory of mean square minimisation, the projection theory yielding the defining equations for optimum filters in the mean square sense. Also the solution of these mean square error problems by steepest-descent techniques can be formulated using theorems of functional analysis.

An alternative solution depends on a knowledge of the eigen values and eigenfunctions of the operator and uses the minimum norm concept. The Hilbert space has a relatively simple solution but when the minimum norm concept is applied to Banach spaces the analysis becomes much more complex delving into the question of uniqueness and existence of a minimum norm.

It should be noted that the complexity of the original equations may be unimportant as long as they define a linear space, as the analyst may often turn to critical norms which provide the constraints whose limits it is required to work within. If small deviations only are to be tolerated from the desired equilibrium point the nonlinear equations when linearised may provide the required linear transformation defined on the Banach space.

Another application of this functional approach is that of stability criteria. A Banach space criterion has been developed which is applicable to both linear and nonlinear systems.

In summary, the stage has now been reached where the current methods available for linear system analysis and control have been covered to a reasonable extent. It is now necessary to progress to nonlinear system study.

2.8. More detailed Analysis of Nonlinear Systems

The first approach is naturally that which has already received much attention. That is the linearisation of the nonlinear system and subsequent analysis.

Probably the most readily usable truly nonlinear study is the phase plane technique.

2.8.1. Phase Plane Analysis for Nonlinear Systems

This method was considered for linear systems for both the two- and multidimensional cases (Section 2.7.16.). The actual methods of obtaining sufficient information to construct either exact or approximate portraits were postponed until this section.

The solution of the linearised system was considered as far as equation 2.50. The original nonlinear system equation would be of the form:

$$\frac{\dot{T}_1}{\dot{c}_1} = \frac{a_1 T_1 \quad + \quad f(T_1,\ c_1)}{a_2 c_1 \quad + \quad f(T_1,\ c_1)} = \frac{dT_1}{dc_1} \tag{Eq.2.53.}$$

where the nonlinear term is the rate of reaction. The trajectories could be graphically estimated for both linear or nonlinear cases by the following numerical procedure. For a chosen point in the plane $(T_1,\ c_1)$ the function f and hence the derivative $\frac{dT_1}{dc_1}$ can be evaluated. This derivative is the trajectory gradient at the point chosen. If this calculation is repeated at an adequate number of points a diagram can be constructed of the tangents to the trajectories. The route of each trajectory from various initial conditions to the steady state can then be sketched by interpolating between the points of known gradient.

The Isocline Method

This method provides an alternative calculation of the gradients which reduces the computation necessary. Instead of calculating the slope of selected points a locus can be determined algebraically on which all trajectories possess the same slope. This locus is called an isocline. From these isoclines tangents can be drawn and the trajectory paths plotted as before. All the isoclines and trajectories pass through the steady state. At this value of c_1 and T_1 $\frac{dc_1}{dt} = \frac{dT_1}{dt} = 0$ and $\frac{dc_1}{dT_1}$ is indeterminate. (i.e. any value of the gradient will satisfy this point.) This point is called the critical or singular point.

Phase plane representation has value over and above its applicability to numerical estimation: it is an ideal way of presenting results no matter which numerical method of obtaining them is employed. If the nonlinear equations provide a portrait which is stable from any initial condition in the plane of interest then the stability is global or the system can be called stable in the large. Alternatively it might be stable in some bounded region or, of course, unstable.

It is interesting to compare the portraits obtained by analysing the nonlinear and linearised equations. The two portraits are found to agree very closely in the region of the steady state. Thus phase-plane analysis provides an important confirmation of Liapunov's first method.

Having mentioned the limitations of linearisation in comparison with the phase-plane portrait produced by the nonlinear equation it is also important to point out the limitations of the phase-plane method. As constant forcing functions are assumed in the construction of the trajectory only simple system inputs are examinable. Step inputs can be dealt with by assuming that the initial condition of a trajectory represents the old steady state that existed before zero time. A similar approach allows the analysis of impulse disturbances by taking the initial condition to be an instantaneous jump from the steady state at zero time. It is possible to extend possible inputs to that of the ramp type but this is the most complicated input which can be dealt with. In general, simple transients only can be analysed.

Integration of the Nonlinear Equations

The nonlinear equations can be integrated by using either analogue or digital computers. Aris and Amundson (ref.(5)) conducted a most detailed study of a two-dimensional CSTR system by means of phase plane analysis. They obtained plots of the trajectories of the state variables, temperature and concentration by integrating the nonlinear equations numerically using the Runge-Kutta technique (ref.(19)) and a digital computer. This involved extensive computations but the result was an excellent set of phase-plane portraits obtained to a high degree of accuracy. The portraits described the stability of a triple state system with two stable states and one unstable state.

Disadvantages of the approach include the time consuming way in which the digital computer integrates and also the fact that the solution is discrete giving for each computation only one point on one trajectory. It is for reasons such as these that the analogue computer was used rather than the digital computer in this research. This is considered later in section 3.4. In spite of the high accuracy of the digital computer the paper presented by Lapidus (ref.(4)), published recently, pointed out that by his own method called an "averaging technique", which operated to an even higher degree of accuracy, trajectories which appear to be limit cycles in Aris's analysis were in fact extremely slowly inward-winding foci. The percentage of decrease in size of the cycle was extremely small and whilst this is an academic point the effect on a real chemical process would be of little interest if the reactor was desired to operate at the steady state. If on the other hand the reactor was a chemical oscillator and was to be designed to operate for long periods of time in such a manner the inward-winding tendency could well become a more important factor. The averaging technique involves measuring the distance between the steady state and the trajectory, redetermining the distance after one limit cycle and averaging the result.

A machine which more readily lends itself to the integration of linear and nonlinear differential equations is the analogue computer. With relative simplicity and great speed in comparison to digital computer programming a complete simulation of the nonlinear process can be implemented (ref.(10)). Furthermore, a phase-plane plot between the two chosen state variables can be obtained directly from the machine. This can be done by setting the initial conditions of reactor temperature and concentration at various values in order to give a coverage of all relevant regions and then allow the computer to integrate until the final steady state is reached. In this way the complete trajectory is plotted in one computer operation.

The simulation is based on the nonlinear equations and these models often require simplification before implementation on the analogue computer in order that the complexity of the circuit required does not become excessive. As in the case of multidimensional linear systems the technique can be extended by superposition of the plots obtained from the computer from the various combinations of the state variables. For problems of dimensionality greater than five it is thought that even large analogue computers would have limited space and therefore a digital computer would necessarily have to be used to conduct this analysis using modern control theory techniques. While the accuracy obtainable on the analogue computer is less than that on the digital machine the results are usually accurate enough for chemical engineering purposes.

2.8.2. Tracking Function Technique

This method is mentioned here as it is closely related to the phase plane technique. It was devised by Perlmutter and Paradis (ref.(3)). The functions are used to determine practical regions of stability and ultimate boundedness. This is done by enclosing the steady state by an unbroken trajectory path which then gives a region of asymptotic stability for all initial conditions within this region. However, there is no guarantee that this region does not enclose a limit cycle but only that a trajectory once inside this region is bound to stay within its limits. This method although similar to Lapidus's "averaging technique" is in fact basically different. Sabo (ref.(20)) has shown a way of defining a general region of ultimate boundedness and a set of natural tracking functions for the system.

2.8.3. The Second (or Direct) Method of Liapunov

As indicated in section 2.7.15. this method is an important approach for analysing nonlinear system stability. Here again it is necessary to refer to the work of Aris et al. (ref.(21)) as one of the most informative articles on the application of this method to the analysis of CSTR stability. However, Perlmutter and Berger (refs.(22) and (23)) and Lueke and McGuire (refs.(24) and (25)) have also considered this subject in much detail.

Considering first the theorem which is an extension of Lagrange's work on the stability of conservative mechanical systems.

As mentioned in section 2.7.15. instead of solving the nonlinear equations the method relies on the discovery of a "Liapunov function" which can be used to ascertain the stability of the system in question. For two-dimensional systems the function can be plotted on ordinary cartesian co-ordinates as with phase plane analysis. However also as with phase plane analysis the extension to n - dimensional systems is possible mathematically but above three-dimensional a diagram cannot be constructed. The purpose of the function is that it shall establish a form of boundary, i.e. a region within whose limits any initial condition will remain at least near the origin.

The three stability criteria considered in section 2.7.12. can be established by the Liapunov function. The choice of which criterion to use depends on the information required by the analyst.

The criteria relating to the bounded region of a Liapunov function for the system can be stated in a concise form as follows:

(i) Stability

Stability has been achieved if for any initial condition near the origin the trajectory remains within the bounded region.

(ii) Asymptotic Stability

Asymptotic stability has been achieved if the initial condition trajectory finally goes to the origin.

(iii) Instability

The system is unstable if the trajectory leaves the origin and finally crosses the function boundary.

If the systems analyst can find a function which contains a region for which all system trajectories obey (i) and/or (ii) of the above criteria then a Liapunov function for the system has been obtained. It should be understood that several Liapunov functions may exist for a particular system and when one has been found it is not necessarily the best one, i.e. it may be possible to find another function which defines a larger region of stability.

Theorems for Stability

Consider the system:

$$\frac{dX(t)}{dt} = f(X, t) \qquad \text{(Eq.2.54.)}$$

where: X is a vector.

The control engineer usually requires to know whether the system is asymptotically stable. The question therefore posed is: "Does the forced system solution as a function of time approach the steady state solution?". If the distance between these solutions at a given time is defined as the error then the question can be redefined as: "Does the error defined by:

$$\frac{dx(t)}{dt} = f(x,t) \qquad x(0) = 0 \qquad \text{(Eq.2.55.)}$$

depart from or approach the origin as time increases?". Simplifying the analysis by assuming that the equations are autonomous (i.e. time does not appear explicitly) then the following approach can be taken:

Consider $V(x)$ as a measure of the error then conditions can be laid down which guarantee that the error will be small and will decrease monotonically. Mathematically the conditions are:

$V(x)$ must be (i) real

(ii) positive definite

(at least locally)

This implies that in the region of close proximity to the equilibrium state $V(x)$ is continuous, has continuous first partial derivatives, and of great importance:

$$V(x) > 0 \qquad x \neq 0$$

$$V(0) = 0$$

Hence defining for the autonomous system a type of projection of V along a solution (trajectory) of the differential equation above, then:

$$\dot{V}(x) = \frac{dV(x)}{dt} = (\text{gradient } V) \times \left(\frac{dx}{dt}\right) \qquad \text{(Eq.2.56.)}$$

$$= \frac{\partial V}{\partial x_1}\frac{dx_1}{dt} + \frac{\partial V}{\partial x_2}\frac{dx_2}{dt} + \dots\dots\dots$$

Hence $\dot{V}$ can be calculated directly (direct method) from the system equation if a valid V is known without solving the system's equations.

For a particular solution $x(t)$ if the error is to be maintained small then:

$$\dot{V}(x) \leqslant 0$$

in the region close to the origin. If the error is to decrease in size then:

$$\dot{V}(x) < 0 \qquad\qquad x \neq 0$$

If the steady state in considered to be the condition of the system after the elapse of a long period of time then the following stability theorems can be proposed:

(i) <u>Local Stability Theorem</u>

If (a) $V(x)$ is definite in the region of the steady state

(b) $V(0) = 0$

(c) $\dot{V}(x)$ is semidefinite with opposite sign to $V(x)$, or vanishes identically

N.B. definite $f > 0$ $\quad f < 0$

semidefinite $f \geqslant 0$ $\quad f \leqslant 0$

then the steady state is stable.

(ii) <u>Local Asymptotic Stability Theorem</u>

If (a) $V(x)$ is definite in neighbourhood of equilibrium state

(b) $V(0) = 0$

(c) $\dot{V}(x)$ is definite and of opposite sign to $V(x)$

then the steady state is asymptotically stable.

(iii) Theorem for Asymptotic Stability in the large (global)

If the system is asymptotically stable by theorem (i) above and also for all $x \neq 0$

$V(x)$ goes to infinity

as $||x||$ goes to infinity

then the steady state is asymptotically stable in the large.

If attempts to produce conditions for stability fail it does not necessarily follow that the system is unstable. Furthermore, as inferred earlier the multiplicity of functions, when considering the conclusions for stability, are often very conservative in that the conditions are sufficient but perhaps not necessary. In other words the Liapunov function may have a region which is too limiting in which case a greater region would also be stable.

(iv) Instability Theorem

If (a) $V(x)$ is definite in the region of the origin

(b) $V(0) = 0$

(c) $\dot{V}(x)$ is definite and not always of the opposite sign to that of $V(x)$

then the steady state is an unstable equilibrium point.

Having stated the conditions which are required in order to ensure the type of stability desired it is then necessary to consider the important point of how to construct a Liapunov function. There are no standard techniques of generating Liapunov functions for general nonlinear systems. There are however certain procedures which are applicable to particular classes of nonlinear systems. Some are therefore of direct interest to this particular project whilst others are of no interest as they deal with a different class of equation.

Warden and Aris (ref.(21)) pieced together a complicated route for the construction of a Liapunov function for a two-dimensional system which was linear in our variable and nonlinear in another. Comparisons were made to Lienard's equation and the system which had been transformed into a y, z plane. A conclusion was made that the Liapunov function in both cases was obtained from the sum of the positive definite function of y and a square term of $f(x+y)$. In this way they constructed their own Liapunov function and added on higher order terms to increase the size of the enclosed region of the function. The computations were however found to be very time consuming and they concluded that the results obtained were not commensurate with the computational effort required to obtain them. They decided that their method of solution of the differential equations by numerical integration and the plotting of the phase plane portraits was the most rewarding current technique then available. They did state, however, that if a standard more simple way of constructing Liapunov functions for nonlinear systems became available the method could then be reconsidered in this light.

The standard method which is applicable to linear systems and hence linearised systems yields too small an area of stability to be of practical use to the chemical engineer.

The only other method of constructing Liapunov functions which will be covered here is that due to Krasovskii. This deserves individual consideration because so much work has been done in this field using the CSTR as the subject for mathematical application. This method treats the important class of nonlinear systems represented by:

$$\dot{x} = f(x) \qquad f(0) = 0 \qquad \text{(Eq.2.57.)}$$

If they are representable in this form then they are subject to the theorem of Krasovskii. The theorem states that if f has a continuous first partial derivative and its Jacobian matrix:

$$F(x) = [\partial f_{ij} / \partial x_{ij}] \qquad \text{(Eq.2.58.)}$$

satisfies the condition that:

$$\hat{F}(x) = F(x) + F^T(x) \qquad \text{(Eq.2.59.)}$$

is negative definite, then the steady state:

$$x_{ss} = 0$$

of the system is asymptotically stable in the large and:

$$V(x) = \|f(x)\|^2 \qquad \text{(Eq.2.60.)}$$

is a Liapunov function for the system. In the proof it is shown that the sign of $\dot{V}(x)$ depends on the sign definiteness of the matrix $\hat{F}(x)$. If $\hat{F}(x)$ is negative definite, then the scalar $\dot{V}(x)$ will be negative. If negative definiteness cannot be proved for the entire region then a compromise can be accepted for a bounded region of asymptotic stability. The system is stable in the large if:

$$f(x)^* f(x) \longrightarrow \infty \qquad \text{as} \qquad \|x\| \longrightarrow \infty$$

The Krasovskii approach assumes V to be a Hermitiam form or a quadratic form in $f(x)$. Such an assumption is unnecessarily restricting because such a form of Liapunov function may not exist for a given function.

Other methods based on the second method of Liapunov include:

(i) Schultz Gibson's variable gradient method for constructing Liapunov functions

(ii) Lur'e's method applicable to stability of certain nonlinear control systems

(iii) Zubov's method of constructing domain attraction.

(Ref.(26))

For a CSTR defined by Aris's equations asymptotic stability in a bounded region can be determined by Krasovskii's method with or without control applied to the system. Lueke and McGuire showed how to optimise the technique in order to define a maximum region of stability. This method seems to be largely successful.

Recently Gurel and Lapidus have summarised the application of Liapunov's second method to various engineering applications. Chemical engineering is included amongst these and for the interested reader a wealth of references are obtainable in this article (ref.(27)).

2.8.4. The Describing Function Technique

This method is applicable to any nonlinearity for which a periodic function is obtained from a sinusoidal input. It is assumed that the system equations are separable into linear and nonlinear parts. Then the dominant first harmonic is taken as the most important piece of nonlinear information while the other harmonics are neglected. The method was originally developed in this country for relay or on/off devices but it has subsequently been extended to a much wider class of system. As the technique becomes more refined its applications are more general and thus the method is becoming a powerful one.

In Fig.2.8. y, an original output, is shown and also the first two terms of the Fourier series expansion of the function. The sum of all the terms would yield the original function. However the fundamental component $B_1 \sin wt$ is seen to yield the most significant contribution. Good results are obtained in the analysis of such nonlinear control elements by approximating the output by the fundamental component:

$$y \simeq B_1 \sin wt \qquad \text{(Eq.2.61.)}$$

The two major reasons why the fundamental component yields good results when used to approximate the characteristics of the nonlinear element are:

(i) The fact that it yields the most significant contribution to the output.

(ii) The higher frequency terms are progressively attenuated (i.e. $B_3 \sin 3wt$, $B_5 \sin 5wt$) more by the other linear components in the system. Consequently they have less effect on the operating characteristics of the system.

For an input:

$$x = x_o \sin wt$$

the describing function is defined by:

$$N = \frac{y}{x} = \frac{B_1 \sin wt}{x_o \sin wt} = \frac{B_1}{x_o} \qquad \text{(Eq.2.62.)}$$

as it describes the relationship between the output and input.

The nonlinearities have additive describing functions.

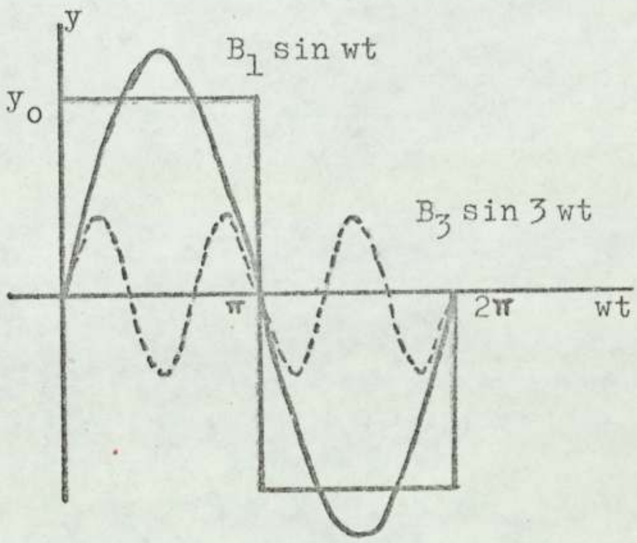

Fig.2.8. Graphical representation of a series expansion for a sine wave.

Criteria for Stability

Consider a control system with nonlinear component N where N is a dead band (Fig.2.9.). The value N may be considered as a variable gain which depends upon the amplitude of the input signal e_o. The frequency response of linear elements depends on frequency only. If the linear element's transfer function is of the form:

$$G(s) = \frac{K}{s(1 + a_1 s)(1 + b_1 s)} \tag{Eq.2.63}$$

then a polar plot can be constructed which, for example, could be of the form illustrated in Fig.2.10. The actual position of the line depends on values chosen for the constants a_1, b_1 and the gain, K. In the example the plot intersects the real axis at $-\frac{1}{2}$ and therefore if the gain were doubled the system would be marginally stable. Hence in this case if $N < 2$ the system is stable.

If $G(jw)$ and $-\frac{1}{N}$ are plotted as shown in Fig.2.11. then an unstable system is indicated if the curve $G(jw)$ and the line $-\frac{1}{N}$ intersect (Fig.2.11(a)). An example of a stable system is illustrated in Fig.2.11(b).

A similar analysis can be made on Bode diagrams or on Root Locus plots.

Phase Shift

The discussion so far has been limited to zero phase shift. If there is such a shift then a different describing function must be defined, i.e.

$$N = \frac{y}{x} = \frac{B_1 \sin(wt + \sigma)}{x_o \sin wt} = |N| \angle \sigma \tag{Eq.2.64.}$$

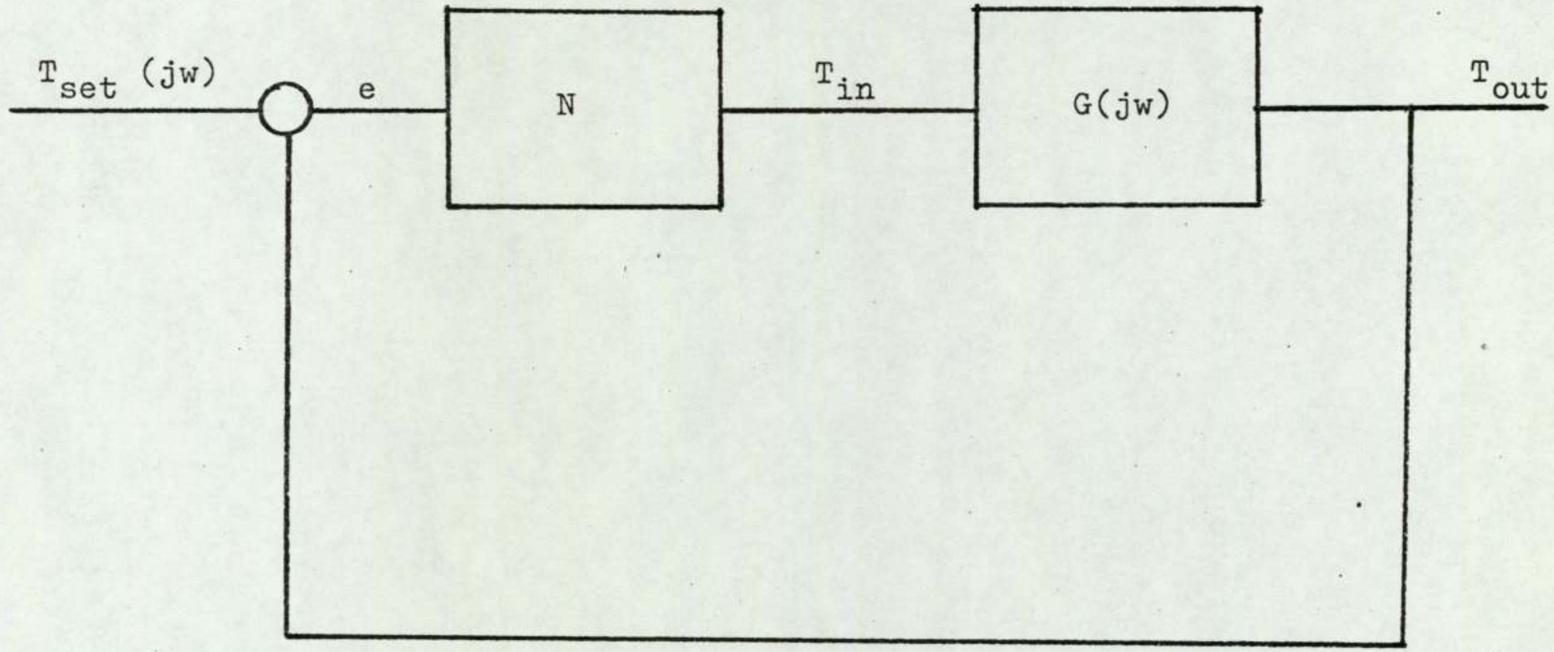

Fig.2.9.

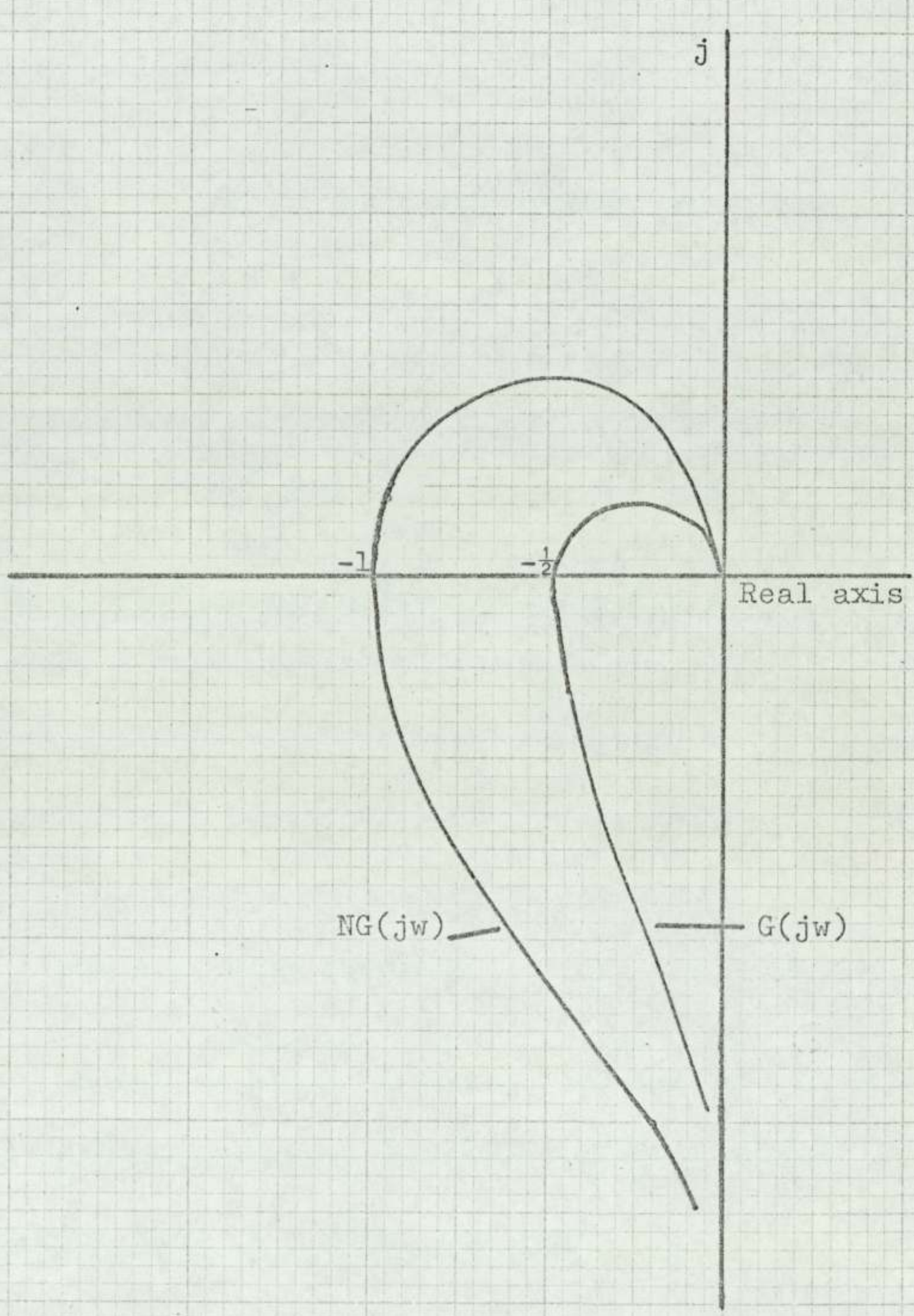

Fig.2.10.

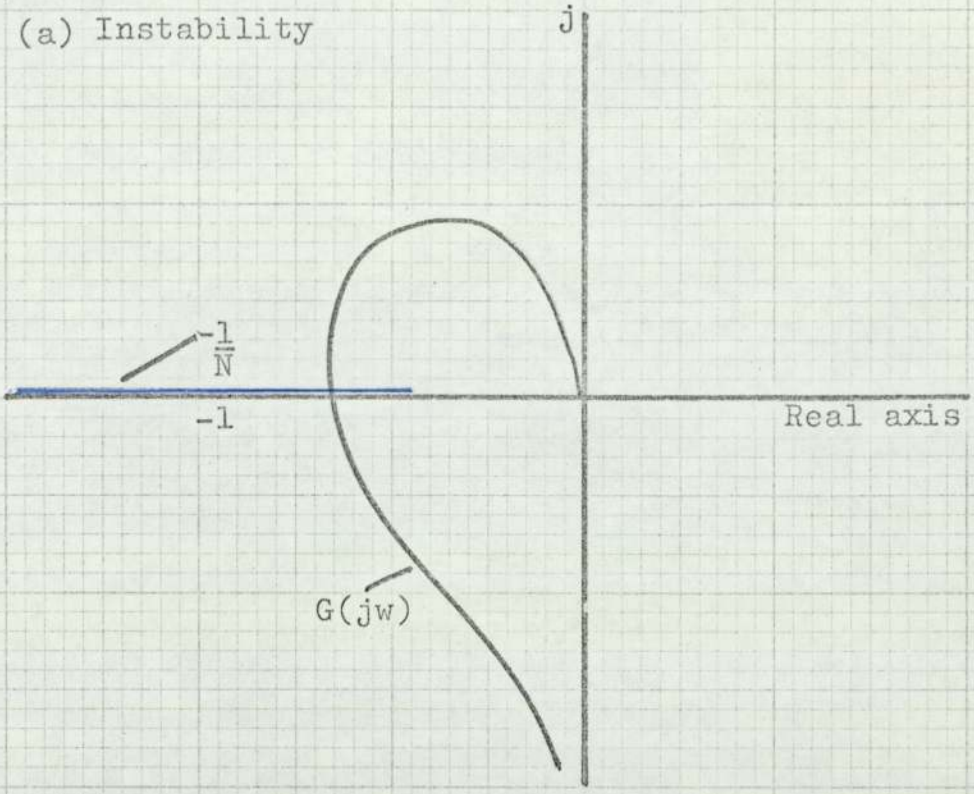
(a) Instability
j
$-\frac{1}{N}$
-1
Real axis
G(jw)

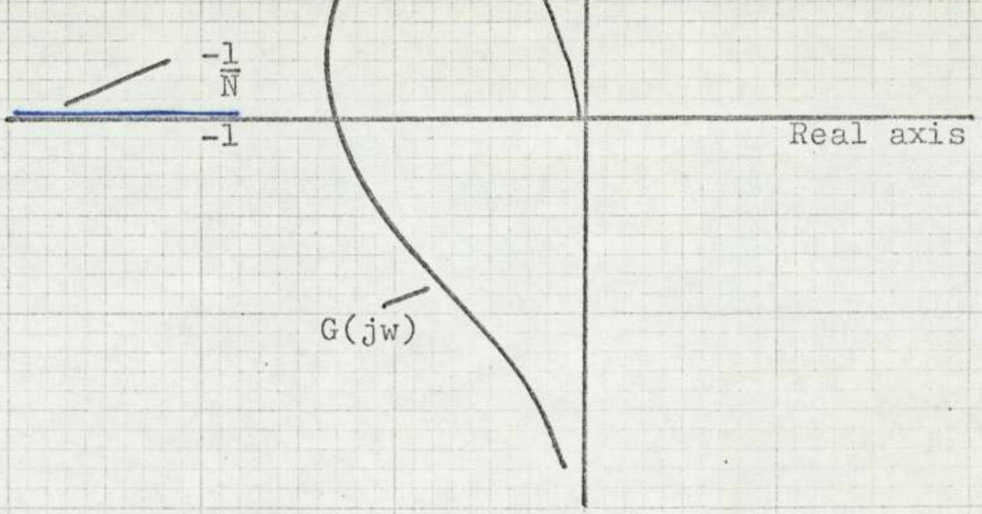
(b) Stability
j
$-\frac{1}{N}$
-1
Real axis
G(jw)

Fig.2.11.

The describing function has a phase shift when for a given input there is more than one output depending on the history of the input. In this case the root locus technique is not applicable.

Frequency sensitive describing functions and optimum switched systems are further realms of describing function methods. The former is applicable to nonlinear differential equations and the latter is an application of the theory for determining the switching schedule of an on/off controller so as to obtain optimum performance.

As the first of these has relevance to the research an indication of the technique will be given.

The system is redefined as:

$$y = y_0 \sin wt$$
$$\text{and } x = x_0 \sin (wt - \sigma) \qquad \text{(Eq.2.65)}$$

instead of the previous notation:

$$\text{input } x = x_0 \sin wt$$

and fundamental component of the output of the form:

$$y = y_0 \sin (wt + \sigma)$$

Hence a new describing function is obtained and a similar polar analysis follows.

The new definition of x and y is, in general, more convenient for nonlinear differential equation analysis and of course the equations which describe the system for the research come into this class.

This now concludes the section on current methods of analysing nonlinear systems.

2.9. Summary

In conclusion a review of current methods for analysing linear and nonlinear systems has been presented with particular emphasis on the study of controllability and stability. It has been intended in this first part of Chapter 2 to classify the problem and put into a setting and perspective the intended method of solution.

The next section deals with the approach to be taken by the research in the light of the literature survey.

2.10. The approach chosen for the research and the reasons for this choice

The literature survey showed a strong tendency for researchers to analyse the system by considering the idealised mathematical models only. Little work appeared to have been done on real plant and therefore it seemed that research conducted with at least some real chemical engineering apparatus was desirable.

In the theory on nonlinear analysis it was shown that only a limited insight into system behaviour is obtainable from the linearised models and it is very desirable to retain and solve the nonlinear equations whenever possible. As the Department had available two analogue computers and these machines lend themselves particularly well to solving nonlinear differential equations it was a reasonable step to try to include them in the research.

In order to reduce the gap between the completely theoretical approach and the entirely practical method it was decided to adopt a partial simulation technique. The kinetics and material balance were chosen for simulation on an analogue computer whilst the energy balance was to be carried out as in the real system. This reduced the demands on the complexity of mathematical modelling and therefore analogue simulation and yet retained several facets of the real system.

It was necessary for the computer to monitor the temperature of the liquid in the tank and from this value it could compute the appropriate heat generation which could then be released by immersion heaters in the stirred tank. A servomechanism was chosen to convert the computed heat generation into actual heat release. Full details of the equipment are given in Sections 5 and 6. The justification of the approach, assumptions necessary and limitations imposed are given in Section 3.

The method chosen for analysing system stability was phase plane analysis. This was chosen as the state variables, temperature and concentration, were directly available for plotting the system portrait.

CHAPTER 3

3.1. Justification for the approach of the research and consideration of the implications of this approach

The reasons for the type of research to be conducted were presented at the end of Chapter 2. It was hoped that by adopting this partial simulation technique and hence retaining some of the real chemical plant more representative results for the system would be obtained. As the results show later this was achieved.

The first part of Chapter 3 deals with the assumptions and implications of this technique and the latter part with the technique's theoretical advantages.

3.2. Assumptions

3.2.1. Mixing consideration

It was assumed that the classical well stirred mathematical model for the stirred tank reactor would hold in this case. Preliminary tests therefore had to be carried out in order to ascertain whether the liquid in the tank was well mixed.

3.2.2. Immersion heater time lag

Another important factor which should be considered here is the thermal capacity of the immersion heaters. This will cause a time lag which is imposed on the partial simulation which, of course, could not arise in the real plant. Whilst a time delay will certainly be present it can be shown to be negligible in comparison with the system time constant. In Chapter 5 calculations are given which justify the assumption that the immersion heaters cause a negligible time lag.

3.2.3. Time delays in the servomechanism and variable monitoring

It is important to ensure that all components in the partial simulation such as the monitoring variables and servomechanism operation introduce no significant time delays or other features which would be inconsistent with the real plant operation. These factors were checked and thus the assumption that their operation distorted the results to no appreciable extent was justified. The checks are considered when the component in question is discussed.

3.3. Implications and limitations

3.3.1. Heat transfer coefficients

Water was chosen to represent the flow of feed and products and the liquor in the tank. Consequently the heat transfer from the liquor to the coolant was much simplified in the partial simulation case. In the real plant, viscosity, degree of mixing and scaling up of the cooling coil must be taken into consideration. However in any initial design internal and external heat transfer coefficients would have to be estimated in the light of physical data available. Therefore for a chosen process reaction to be analysed, heat transfer data would still have to be estimated in the normal way. When the true heat transfer conditions have been determined the cooling system in the partial simulation could be loaded accordingly so as not to give the too optimistic picture for controllability which would otherwise be given by a water to water heat transfer relationship. Alternatively some other fluid instead of water could be employed in the reactor which has similar viscosity, specific heat, etc. properties to the actual liquor to be used in the real plant. The most innocuous fluid with these properties could then be used as an analogue to the real liquor.

If the mixing of the real liquor cannot be done to the required degree (i.e. well mixed) then the heat transfer calculations on the equipment and the mathematical model on the computer would have to be altered to fit the new situation. As long as the final model is of acceptable form for analogue computational solution, no difficulty should arise in either case.

3.3.2. Ranges under investigation

Limitations of the equipment will be imposed by various constraints. The choice of water as the fluid for feed etc. limits the range of temperature for consideration to between 0 and 100 deg.C. The range was further restricted by the power available from the immersion heaters since if a continuous feed of say 3 litre/min. is to be heated from 10 to 90 deg.C. the heat consumed is very large. Furthermore instantaneous demands of heat input are also restricted as the servomechanism would be wound off scale if the power in excess of the upper limit was required.

3.3.3. Time delays in real plant operation

As real plant is incorporated in the equipment the inherent time delays in dynamic operations must be determined in order that the results can be correctly analysed. However the incorporation of these delays is advantageous in that the real system is more closely represented. The calculation of time delays is dealt with in Chapter 5.

3.3.4. Accuracy consideration and checks necessary for analogue computation

In analogue computers, due to the inaccuracy of various components when complicated circuits are constructed, accumulated error may occur which could seriously affect the accuracy of the results. If the circuit incorporates a major programming fault then an incorrect result may be easy to detect but with slightly inaccurate results care must be taken to see that these discrepancies do not go unnoticed. Apart from components giving rise to inherent error small mistakes in actual programming (e.g. attenuator settings) can also be made. Furthermore when applying a gain of ten to a value, small errors become magnified and such gains are usually unavoidable in most circuits. It is considered therefore advisable to obtain a check on the final results obtained. Charts were therefore constructed for the feedrates chosen for investigation of temperature versus concentration at the steady state. These gave a ready check on the analogue computed steady state values. The construction and use of the charts are discussed in Section 6.11.

3.3.5. Real time computations

As the analogue computer operates on-line to the real equipment it must operate in real time in order that the material and energy balances are in phase with each other. Therefore the solutions cannot be speeded up and phase-plane portraits will take much longer to plot than the time scaled solutions obtained from complete simulations.

3.4. Theoretical advantages of the approach

In theory by retaining as much of the system in real hardware as possible some of the plant's nonideal characteristics are still present without requiring simulation or mathematical modelling. Also, heat transfer between liquor and coolant can be calibrated empirically and again no mathematical representation is necessary.

Other obvious immediate advantages are the avoidance of corrosive and dangerous reactants and also of effluent disposal and product recovery problems at the other end. Further, equipment can be built which needs to stand up only to the fluid chosen to represent the liquor, which will be the least corrosive and cheapest obtainable for the physical properties required of it. Thus the initial outlay on materials of construction and design is much smaller.

Apart from these immediate advantages the partial simulation equipment offers versatility in that fairly complex kinetics can be programmed on the computer for many different reactions. Although some changes would probably be necessary in the hardware or choice of fluid to change the ranges of certain parameters the outlay for change of the equipment to investigate different reactions would be low.

Advantages over total simulation are the retention of some of the real system character without excessive complexity of mathematical modelling and subsequent simulation. If the total simulation were to be conducted on a parallel logic machine such as the Hybrid 48 adequate space would not be available to include all the facets of the system and complexity of the kinetics would be severely restricted. Therefore, the simulation would have to suffer approximations which would reduce the accuracy of the results. By retaining some of the real system at least some of the dead time lags are incorporated in the analysis which are often ignored in the mathematical models and hence the complete simulations. Indeed, even if included, the analogue computer presents a large problem when attempting to programme these lags. There are various approximations such as the Padé one but these are known to be difficult to set up or to be erroneous.

Complete digital simulation would effectively impose no restriction on the size of problem to be simulated even with all the nonlinear characteristics represented. However with digital simulation the "hands on" experience of direct intervention in the solution is lost and also the solution is discrete rather than time continuous requiring a great many computations and therefore much computer time in order to obtain enough points to plot a phase-plane portrait of the system for one chosen set of conditions. Although work is being conducted at the moment on greater accessability to the digital simulation packages, at this stage it appears that whilst improvements are being made there is still much ground to be covered. Eventually however, if greater conversational facility between computer and operator does become obtainable this method will become very competitive indeed. At that stage also, digital computers will be in a position to better the analogue computer in nearly every field and the latter may become obsolete. However, partial simulation still offers the advantage of retaining system characteristics without having to define or model them. In complete simulation all these characteristics must be known and incorporated in the programme.

Having considered on a theoretical basis the approach of the research and highlighting difficulties and limitations, attention is now turned to designing and building the apparatus necessary to effect the partial simulation.

CHAPTER 4

4.1. Development of the apparatus

As water was the fluid chosen to represent the reactants and products in the tank a wide choice of materials was available for construction. The viscosity of water is such that ideal mixing should be closely approachable but the high specific heat of water could well prove to be very demanding on heat consumption.

4.2. Preliminary apparatus (Fig.4.1.)

It was decided in the first instance to make use of existing apparatus and from this obtain the necessary information for building the final plant. The existing equipment consisted of a tank with sides of Q.V.F. glass and the base made of perspex. Feed entered the base of the tank and left through a constant head device. Piping was constructed in Prestex and flexible plastic hose. The tank was fitted with a single 3 kW immersion heater and a stirrer. A Cressall Torovolt was used to control the power to the immersion heater and a rheostat to control the stirred speed.

The tank and accessories were incorporated into a large 'handy angle' frame and a cooling coil constructed of coiled copper pipe was made to fit inside the tank. Two 0.5 to 5 litre/min. rotameters were used to monitor coolant and feed flowrates.

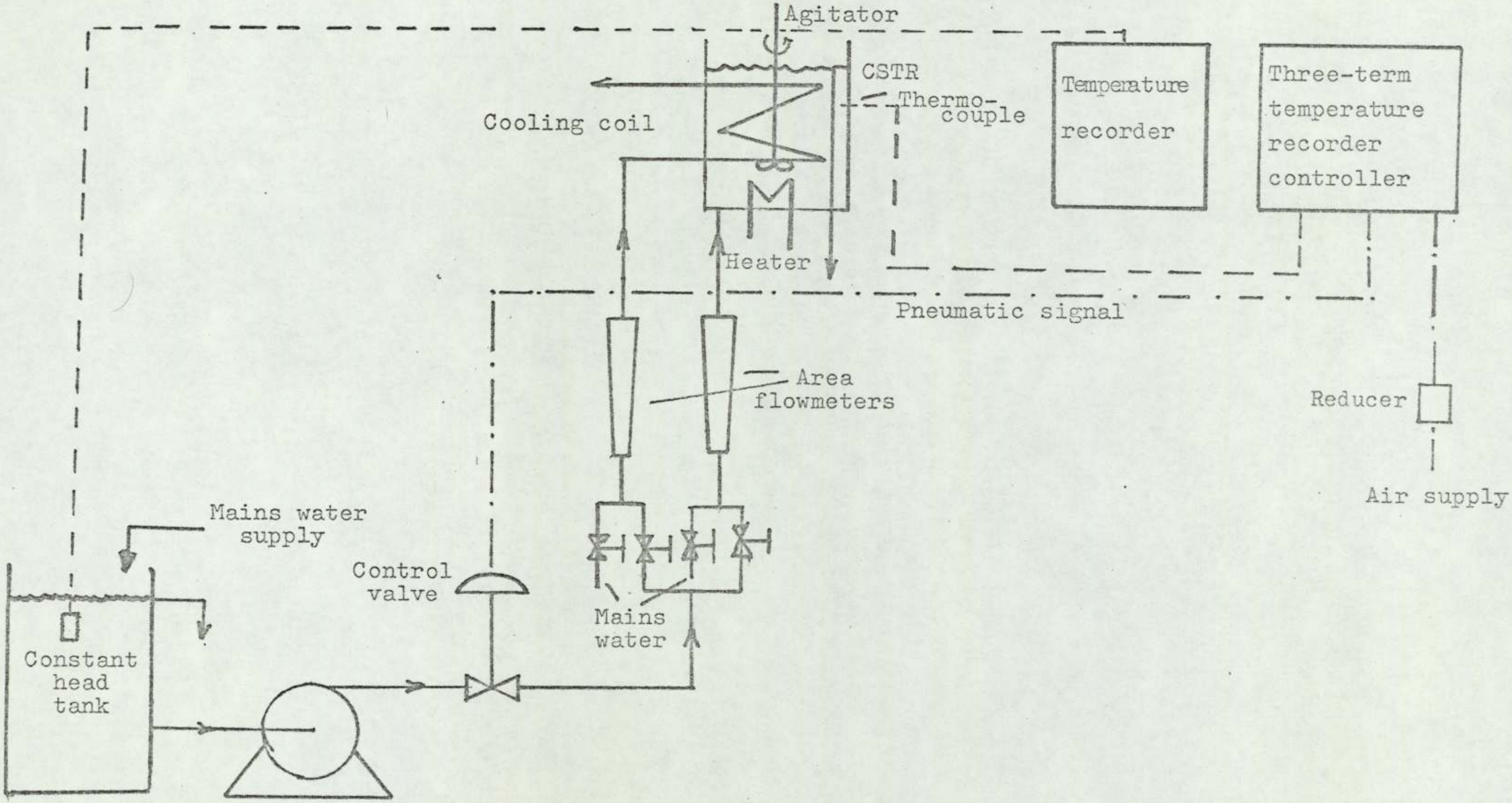

Fig.4.1. Preliminary apparatus

4.2.1. Feedback control loop

A Bristol three-term temperature recorder controller 0 to 200 deg.C. range and a Fisher automatic control valve were in stock and these were used in a simple feedback control loop. The controller monitored the temperature in the tank by means of a chromel / alumel thermocouple, determined the deviation from a chosen set-point and hence transmitted the corresponding pneumatic signal to a control valve which manipulated the flowrate of coolant through the cooling coil. As the range of temperature covered by the controller was excessive, a new controller of range 0 to 100 deg.C. was ordered for greater accuracy. It was intended to install this after arrival, when convenient.

Water was supplied to the pump feeding the control valve from a constant head tank which provided a constant pressure of water supply and reduced fluctuations which a direct mains supply suffers. The piping was so arranged that the feed or coolant could be the controlled flowrate. This was done to allow versatility of control variable and hence increase the flexibility of the equipment. Pipe diameters varied between half an inch and one inch but were not found to be critical.

4.2.2. Demonstration of equipment

The equipment was at this stage required for demonstration in an exhibition at the University. No time to this date had been available for developing the computer simulation and thus a simplified situation had to be presented for demonstration purposes. Heat was simply input at a fixed rate by manual setting of the power to the single immersion heater. When the set-point temperature or feed flowrate was changed the heat input by the immersion heater was stepped to the new value it would attain at the new final steady state condition. Calibration curves between temperature of liquor versus power setting and feedrate versus power setting were computed for this purpose. When temperature was varied by changing the set-point the feedrate was held constant and vice versa. The transience between initial and final steady states for the heat generation was ignored. In the true case it will vary according to the current value of rate of reaction which is itself dependent on the temperature and concentration in the reactor.

To carry out the demonstration it was necessary to calibrate the heat output from the immersion heater and consider the effectiveness of the cooling coil. The heat transfer coefficient was found to depend dominantly on coolant flowrate for a fixed stirrer speed. Heat lost to surroundings at temperatures less than $40^{\circ}C$ was found to be negligible.

The tests showed the system to be dynamically very slow moving. The heat input was found to be inadequate if any real stability problems were to be encountered and the cooling coil was rather too narrow in internal diameter which restricted the coolant flow through it severely and was also too long in that by the time the coolant had passed through half the length of coil the temperature of water in the coil had closely approached the temperature in the tank. Thus the heat removal capacity of the coil was much lower than necessary and also very inefficient for the length of coil.

4.3. Modifications for the final apparatus

Since inadequate heat was available from the single immersion heater it was decided to insert two more into the tank, bringing the total power available up to 9 kW.

The old cooling coil was discarded in favour of one with a larger internal diameter and fewer number of turns. This would allow greater coolant throughput with no wasted heat transfer area. Later, a larger rotameter was fitted which could monitor flowrates up to 10 litre/min.

It was decided to retain the same vessel size as it was a useful intermediate between real plant and the pilot plant. Furthermore, a tank of smaller size would not be able to accommodate the three immersion heaters, a stirrer and a cooling coil. Thus the size of the vessel was largely dependent on heat input and output devices rather than other constraints. The hold-up in the vessel was kept at 16 litres and with feedrate variable between 0.5 and 4 litre/min., a reasonable time constant was obtained (i.e. between four and thirty-two minutes).

Mixing was found to be good with a single propeller but a second one half-way up the stirrer shaft was added to encourage even better mixing. A support was also inserted at the base of the tank for the stirrer shaft to prevent 'whipping'. A small baffle was placed in the tank and this, in conjunction with immersion heaters and coil, was found to be sufficient to prevent vortexing.

A brass base was used instead of the perspex one in order to simplify construction work.

A Bristol 3-point temperature recorder was also installed into the plant. It was used to monitor the temperatures of the water flowing in and out of the coil and the feed to the tank.

CHAPTER 5

5.1. Calibrations and verification of assumptions

Now that the equipment design, hold-up and flowrates have been chosen it is possible to verify some of the assumptions made in Chapter 3 by test or calculation.

5.2. Mixing tests

One of the basic assumptions was that the liquid in the tank was well mixed. Two simple tests were done to see if this was the case.

5.2.1. Probing with a thermocouple

Stirring speed set at 40 on the Torovolt

All areas in the tank were probed with the thermocouple from the temperature recorder controller. No fluctuations in measured temperature were observed except near the feed inlet where some noise was monitored. This, of course, would be expected.

5.2.2. Ink tracer

With the same setting of stirrer speed, ink was dropped into the tank. This was seen to disperse rapidly to an even concentration in two seconds.

Therefore, the assumption that the vessel is well mixed is acceptable.

5.3. Time delay in immersion heater response

The thermal capacity of the immersion heaters must be compared to that of the hold-up of water in the tank plus the amount of feed entering in a chosen time (neglecting heat losses to vessel and surroundings).

Volume of the coils

For a diameter of 1 cm. and total length of approximately 300 cm. for the three heaters then the total volume is in the region of 240 cm^3. For a specific heat of 0.11 cals/g deg C and specific gravity of 7.1 the water equivalent can be calculated at about 190 cals/deg.C.

The heat absorbed by water in one minute equals:

(hold-up + feedrate/min.) x specific heat

For a 3 litre/min. feedrate then the heat absorbed is 19000 cals/deg.C.
Therefore, the percentage of the total heat absorbed by the immersion heater coils is about 1%. Thus it is a reasonable assumption to state that the time delay caused by this factor will be negligible.

5.4. Time delay in the cooling coil

The distance velocity lag can be obtained as follows:

5.4.1. Coolant flowrate 1 litre/min.

$$\text{Time lag} = \frac{\text{Holdup}}{\text{Coolant rate}} \qquad \text{(Eq.5.1.)}$$

The internal diameter of the coil is 1 cm. and the length immersed in the tank is 280 cm. Therefore the holdup is 220 cm^3.

$$\therefore \text{ the time lag} = \frac{220}{1000} \; [\,cm^3 (\frac{min}{cm^3})\,]$$

$$= 0.22 \text{ min}$$

$$\text{or: } \simeq 13 \text{ s}$$

For a 10 litre/min. flowrate the time delay is of course 1.3 seconds.

It can therefore be concluded that the distance velocity lag in the coil will not cause very large time delays in the feedback control loop action.

5.4.2. Calculation of Reynolds number in the coil

$$\text{Reynolds number} = \frac{D\,u_c\rho}{\mu\,A} \qquad \text{(Eq.5.2.)}$$

where: D is the internal diameter of the coil

A is the internal cross-sectional area of the coil.

For a flowrate of 1 litre/min. and a viscosity of 0.01 P at 20°C then:

$$Re = \frac{1 \times 1000 \times 1}{0.01 \times \frac{\pi}{4}} \; [\,(\frac{cm^3}{min})(\frac{g}{cm^3})\;\frac{cm}{P\,cm^2}\,]\,[P(\frac{cm.s}{g})(\frac{min}{60s})\,]$$

$$Re = 2130$$

Therefore even at this low flowrate the flow is turbulent and for flowrates in the region of 9 litre/min. when the temperature drop along the coil is small the well mixed concept can be used to determine the coil's time constant.

5.5. Time constant for the cooling coil

Considering the energy balance on the cooling coil and assuming the water in the coil to be well mixed then:

Steady state balance:

$$m_c c_p T_{c1} + UA\,(T_1 - T_{c2}) = m_c c_p T_{c2} \qquad \text{(Eq.5.3.)}$$

Transient balance:

$$m_c^1 c_p T_{c1} + U^1 A (T_1 - T_{c2}^1) = m_c^1 c_p T_{c2}^1 + M c_p \frac{dT_{c2}^1}{dt} \qquad \text{(Eq.5.4.)}$$

taking T_1 and T_{c1} as constants.

Then by subtracting equation 5.3. from equation 5.4. and linearising, the energy balance can be expressed in perturbation variables as:

$$m_c (c_p T_{c1}) + U(T_1 A) - U(A T_{c2}^o) - T_{c2}(U^o A)$$

$$= m_c (T_{c2}^o c_p) + T_{c2}(m_c^o c_p) + M c_p \frac{dT_{c2}}{dt} \qquad \text{(Eq.5.5.)}$$

$$\therefore \left[\frac{Mc_p}{m_c^o c_p + U^o A} \right] \frac{dT_{c2}}{dt} + T_{c2} = m_c \frac{(c_p T_{c1} - T_{c2}^o c_p)}{(m_c^o c_p + U^o A)} + \frac{UA(T_1 - T_{c2})}{(m_c^o c_p + U^o A)}$$

or: $$L \dot{T}_{c2} + T_{c2} = K_1 m_c + K_2 U \qquad \text{(Eq.5.6.)}$$

where the system time constant is:

$$L = \frac{M c_p}{m_c^o cp + U^o A}$$

and K_1 and K_2 are the gains for the system.

Therefore for a step change of coolant flowrate of 1 litre/min. taking UA from the calibration chart, for 4 to 5 litre/min. (Fig.A.6.)

$$L = \frac{220 \text{ g} \frac{\text{cal}}{\text{g deg C}}}{1000 \frac{\text{g}}{\text{min}} \frac{\text{cal}}{\text{g deg C}} \left[\frac{\text{min}}{60\text{ s}}\right] + \frac{5.5\text{ cal}}{\text{s deg C}}}$$

$$= \frac{220}{22.3}$$

$$= 9.9 \text{ s}$$

For a 10 litre/min. flowrate change then:

$$L = \frac{220}{\frac{1000}{60} + 87.4} = 0.87 \text{ s}$$

It can be concluded that the coil time constant is small for flowrate changes greater than 1 litre/min. and negligible in comparison with the time constant for the tank. For small flowrate changes some allowance should be made for delay in the coil response if rapid control action is required.

5.6. Time delays in controller, control valve and measurement devices

Tests on monitoring equipment showed all but one of the time delays to be small. The large one was in flow monitoring equipment for the computer and this is dealt with in the appropriate section.

The delay in controller action was only of the order of one or two seconds. In the control valve a delay of nine seconds was calculated when changing from fully shut to fully open. With the valve positioner in action the delay was five seconds. For closing, the time delays were five and three seconds respectively.

5.7. Calibration of the heat transfer coefficient / coolant flowrate relationship

An experiment was conducted in which the variacs were set at a fixed heat input. No feed flow entered the tank and thus heat was only removed by the coolant. Various coolant rates were set and the steady state values of tank temperature and coolant inlet and outlet temperature recorded.

A programme was written in Algol which utilised the relationship:

$$m_c c_p (T_{c2} - T_{c1}) = UA(LMTD) \qquad \text{(Eq.5.7.)}$$

and from this UA was evaluated.

The results, programme and chart obtained are presented in the Appendix in Table A.2., Programme 2 and Fig.A.6. respectively.

5.8. Calibration of heat output from the three immersion heaters

The variacs were connected electrically to give the maximum power output which was in the region of 11 kW for full scale. However, due to scale limits on the variacs just over 9 kW was actually available. The variacs were then set at intervals of ten on the scale and when steady state was reached, between heat from immersions and heat absorbed by feed, the inlet and outlet feed temperatures were recorded. The heat generated was calculated from:

$$Q = m_f c_p (T_1 - T_0) \qquad \text{(Eq.5.8.)}$$

The value when compared with the corresponding power output calculated in a different experiment confirmed negligible heat losses for temperatures up to 42.5°C.

A table of results is given in the Appendix and the calibration graph obtained in Fig.A.3. (Table A.1.).

CHAPTER 6

6.1. Apparatus for partial simulation

A line diagram of the equipment to be employed to implement the partial simulation is shown in Fig.6.1.

The hardware used was considered in Chapter 4. Therefore it is only necessary to consider here the extension for partial simulation.

The kinetics were simulated on an analogue computer (TR 10. EAL PACE). In order that the computer could determine the current value of rate of reaction and hence heat generation, it had to monitor the current values of temperature in the tank and feed flowrate into the tank. It was therefore necessary to design such monitoring devices.

Initially feed flowrate was held constant until the monitoring equipment became available. This meant a careful watch on the feed rotameter to ensure no drifting. Further, step changes in feed had to be imposed simultaneously on the computer and the rotameter. Clearly, also feed flowrate control was out of the question at this stage.

6.2. Initial temperature monitoring equipment

Temperature in the tank was measured by means of a chromel / alumel thermocouple. This was chosen as water would certainly not attack it and it gave a reasonably linear output of millivoltage with temperature (Fig.A.1.).

The problem then was the amplification of a millivoltage to a value in the range 0 to 10 V which was acceptable by the

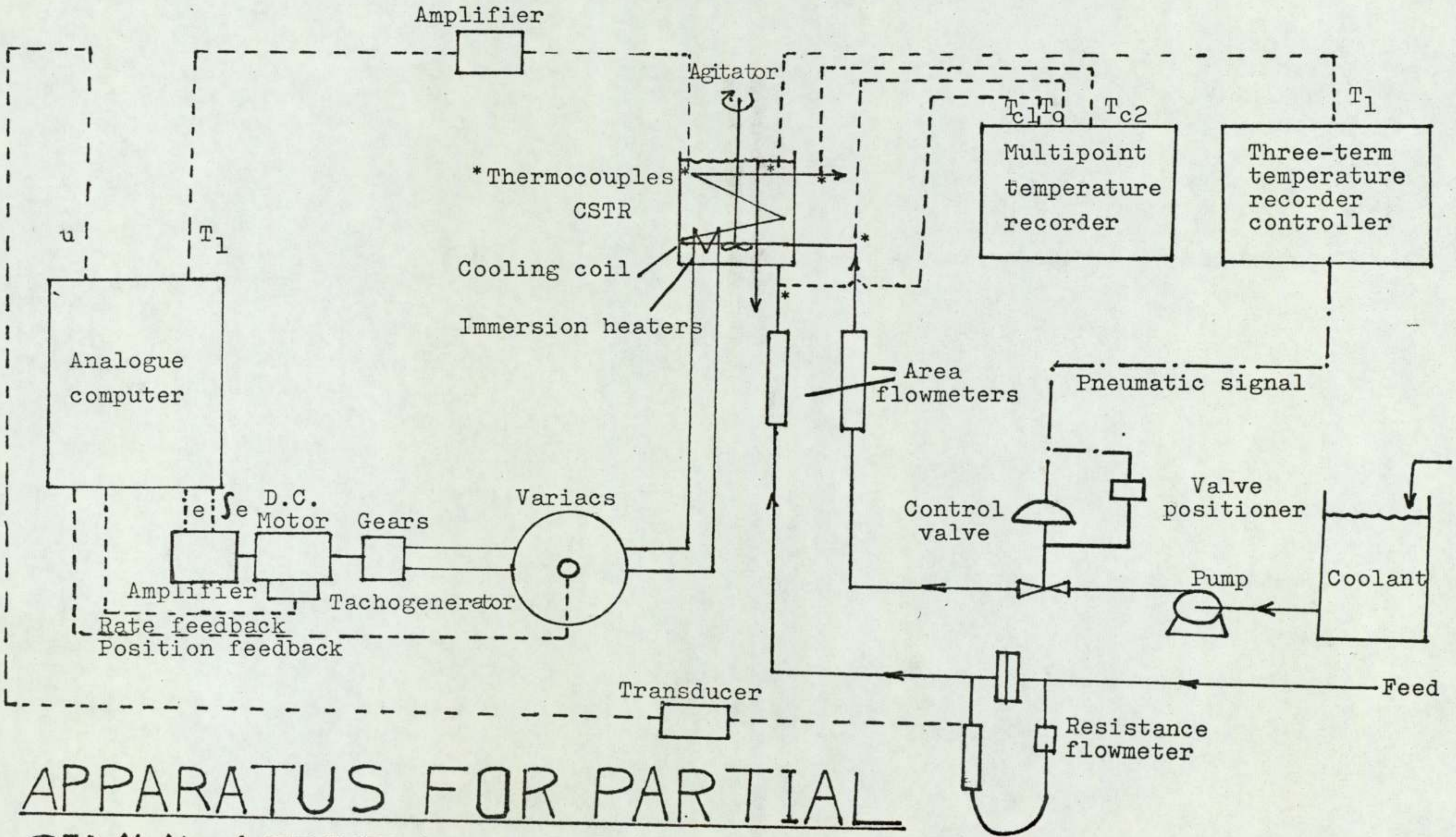

APPARATUS FOR PARTIAL SIMULATION

Fig.6.1.

Partial Simulation Equipment

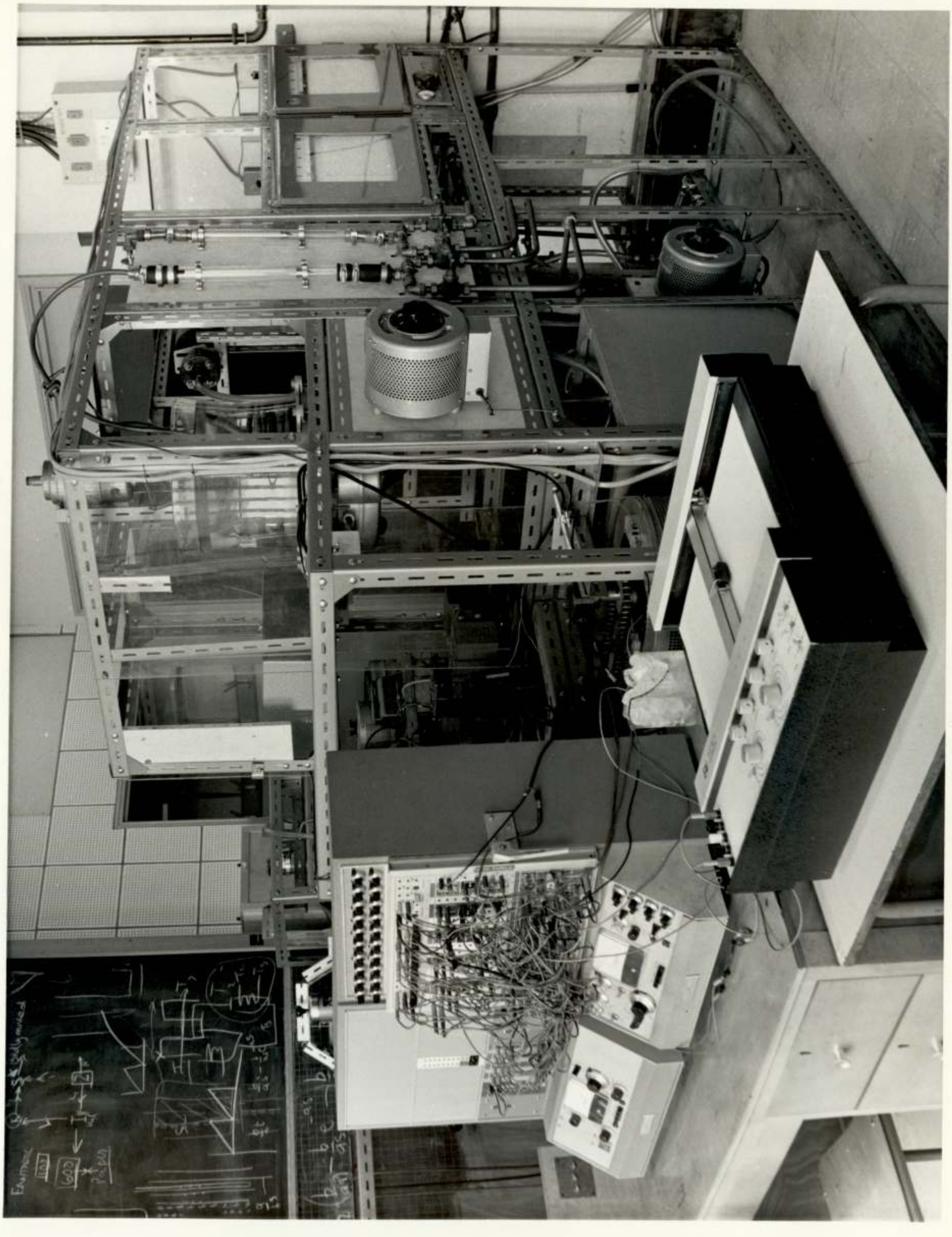

computer. First attempts were made to do this on the analogue computer with reasonable success; later, however, problems arose due to certain inaccuracies. However, early experiments were conducted with this device and the results obtained are considered in Chapter 7.

The circuit employed to monitor and amplify the thermocouple voltage is shown in Fig.6.2. The cold junction was left at room temperature and the final reading adjusted to compensate for this. Later, as drift was encountered, a cold junction was included in the circuit. The circuit operated on the Wheatstone bridge principle, noise being filtered out by a feedback / integrator circuit.

6.3. Final temperature monitoring equipment

As the first mechanism was felt to be one of the greatest contributors to the error encountered in the results obtained due to drift, it was finally decided to replace this device with an Elliott Automation TDC 2 (Fig.6.3.) amplifier which was specially designed to convert thermocouple millivoltages into 0 to 10 V which was the range required by the computer. This was found to be more reliable than the other device as far as drift was concerned; however, other difficulties were encountered most of which were overcome in the latter stages of the research.

6.4. Flowrate monitoring device

The equipment chosen for monitoring flowrate was proposed by Elliott Process Automation Limited. A diagramatic sketch is given in Fig.6.4. and a simplified electric circuit in Fig.6.5.

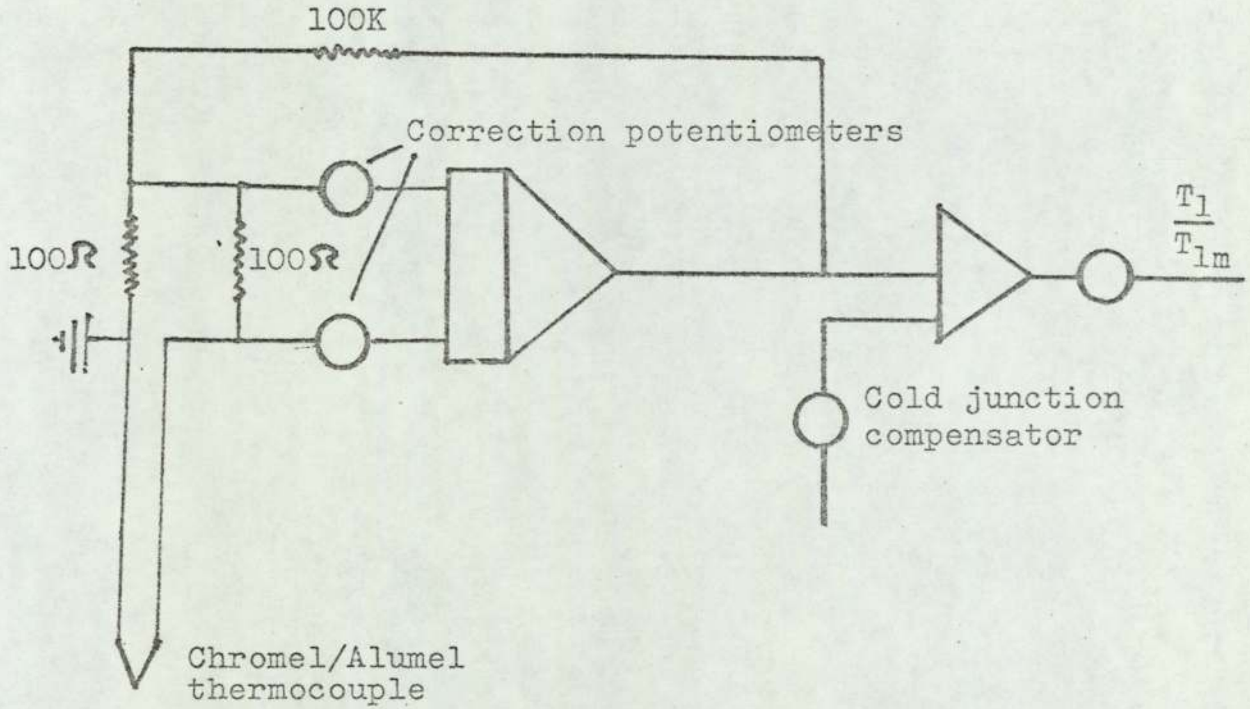

Fig.6.2. Temperature monitoring and amplification of the thermocouple output by analogue computer.

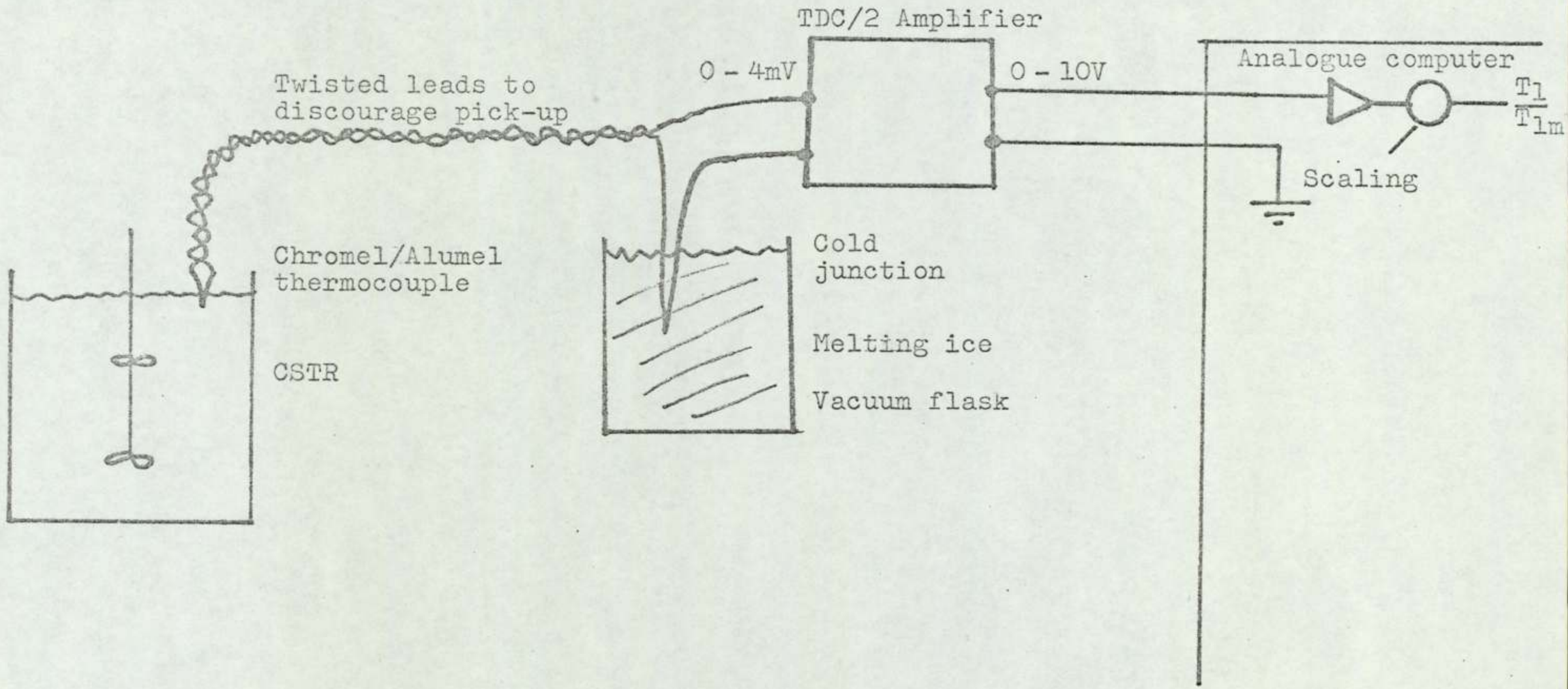

Fig.6.3. Final temperature monitoring circuit.

Fig. 6.4. Flow monitoring equipment

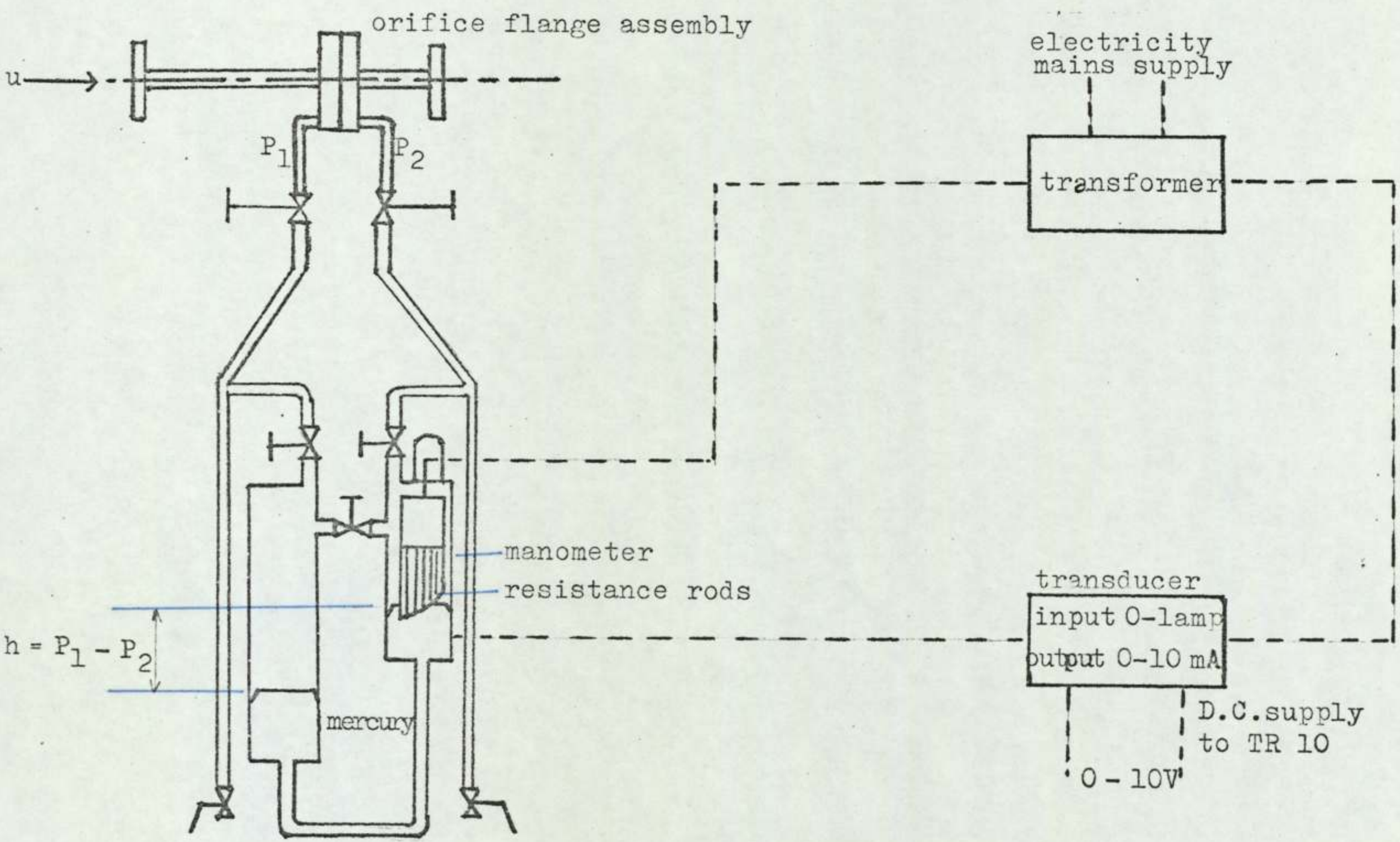

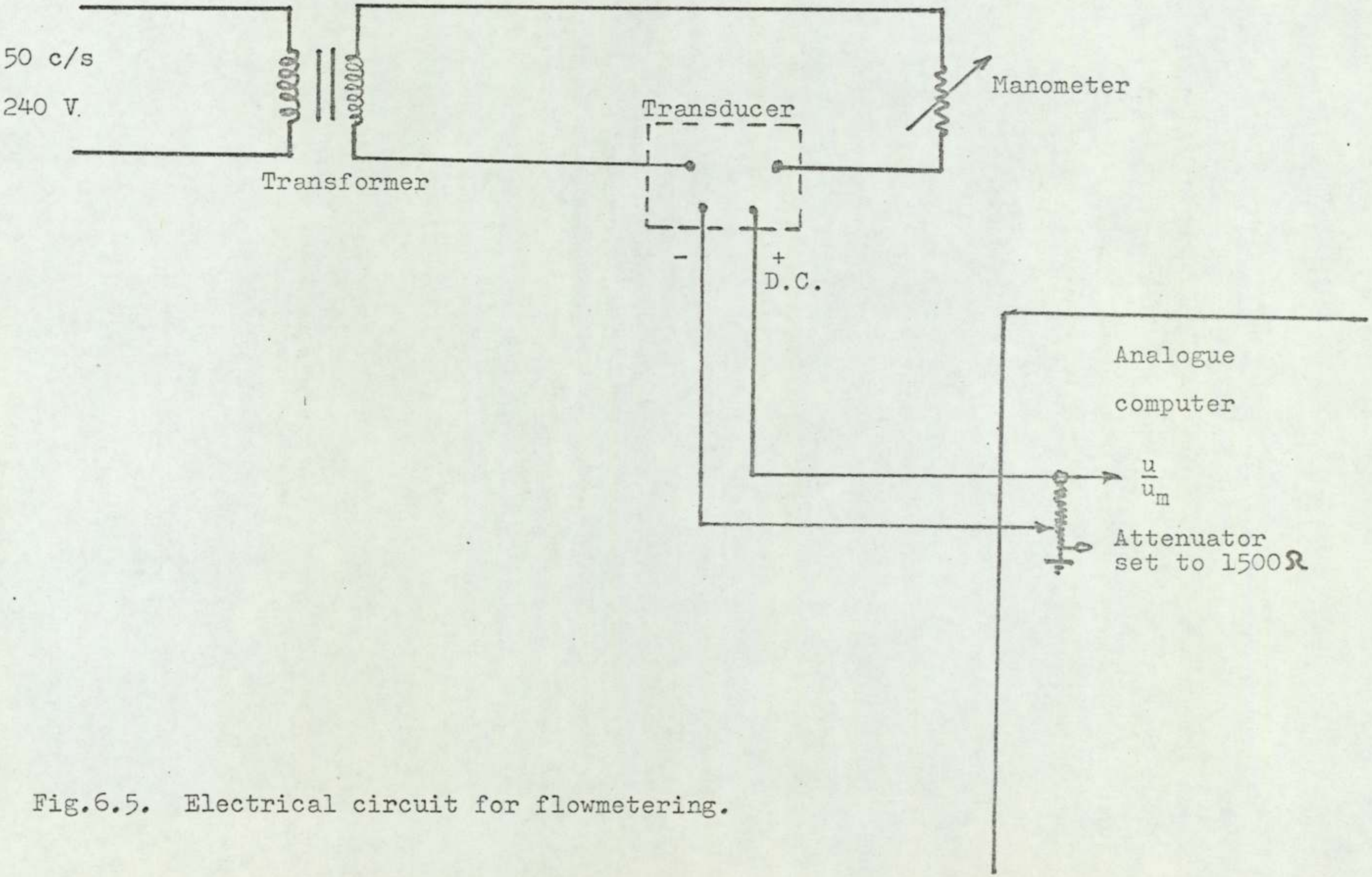

Fig.6.5. Electrical circuit for flowmetering.

The equipment consists of a pressure difference device orifice flange assembly (model 812,750) which connects to an E.P.A. double tube manometer. The pressure drop across the orifice plate is applied to the high and low pressure limbs of the manometer. The mercury 'U' tube then enables the rate of flow to be measured from the differential pressure. It is proportional to the square root of the pressure difference, the mathematical relationship being:

$$u \propto \sqrt{2gh}$$

The mercury in the manometer, rising under pressure, contacts and shorts out successively the conductor rods, and their associated coils, of the resistance element in the instrument circuit. Since the ends of the rods describe a parabolic profile to the mercury, the current which flows is then directly proportional to the square root of the differential pressure. In this way the power law is extracted from the relationship leaving flowrate directly proportional to the reciprocal of the resistance, i.e:

$$u \propto \sqrt{h} \propto \frac{1}{R}$$

A linear relationship between flowrate and voltage is then obtained for transmission to the computer. The current is input into an English Electric current transducer which converts the supply of 0 to 1 A A.C. to 0 to 10 mA D.C. across a load of 0 to 1500 ohms. This gives an output of 15 V on maximum. The circuit is powered from the mains via a transformer (type E.P.A. model 731).

For further details of all of this equipment the manufacturers' manual can be referred to.

The analogue circuit for material balance necessary to accommodate the feed flowrate as a variable is given in Fig.6.6. (Details of the general circuit construction for constant feed flowrate are given in Section 6.5.). The most significant extra requirement was a multiplier which was necessary to multiply the variables temperature and flowrate together. The potentiometer settings required are indicated in symbols in Table 6.1.

6.5. Analogue computer operations

The mathematical model chosen for implementation on the computer was based on the well stirred vessel concept. As the computer is required to simulate the chemical reaction side of the process it is necessary for it to carry out the following operations:

(1) Receive and scale information of the variables upon which its calculations depend

(2) From this information, calculate the velocity constant for chosen kinetics

(3) Integrate continuously in real time the mathematical model of the material balance for the system taking into account current values of kinetics and other variables as it does so. This yields the vessel operating concentration.

(4) From the calculation in (2) and (3) compute the current rate of reaction and hence the corresponding heat generation.

(5) Institute any further operations which may be required to help convert the computed value

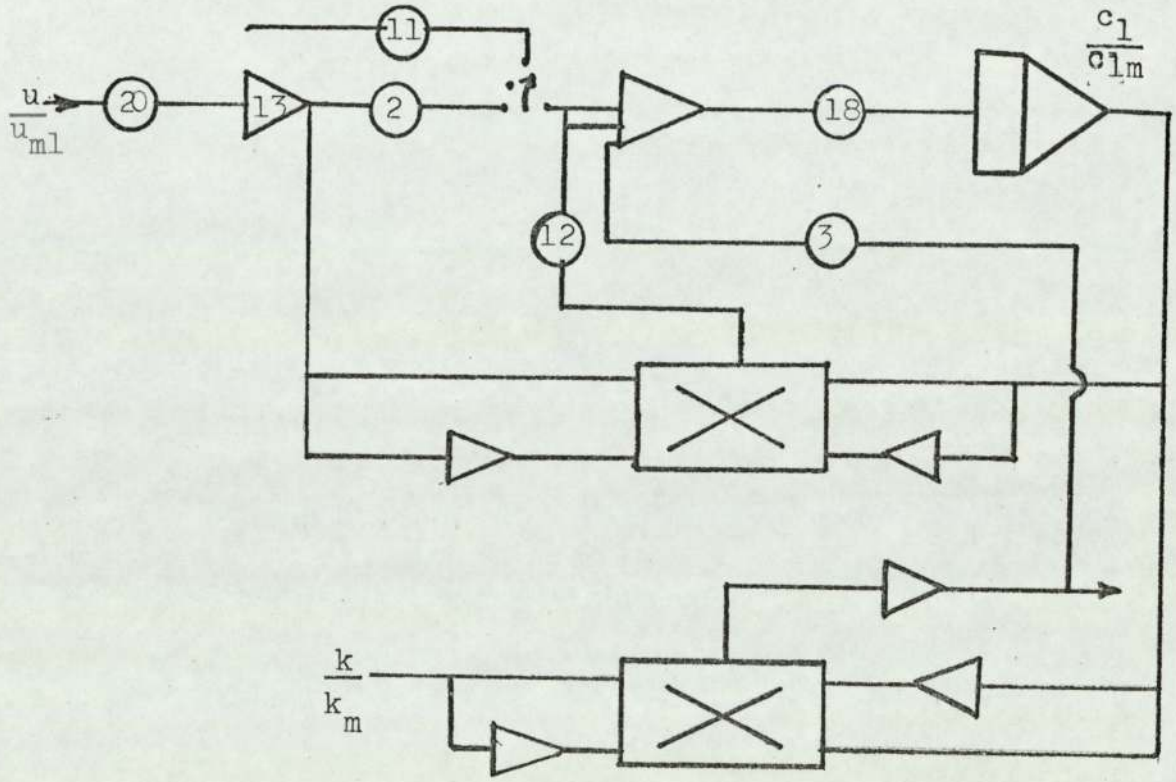

Fig.6.6. Modification of on-line analogue circuit to accommodate an input of feed flowrate as a variable

<u>Table 6.1.</u> Potentiometer settings definitions for circuit diagram shown in Fig. 6.6.

Potentiometer number	Parameters involved
2	$\left[\frac{u_m c_o}{V \dot{c}_{1m}} \right]$ where c_o = 1 gmole/litre
3	$\left[\frac{c_{1m} k_m}{\dot{c}_{1m}} \right]$
11	$\left[\frac{u_m c_o}{V \dot{c}_{1m}} \right]$ where $c_o > 1$ gmole/litre
12	$\left[\frac{c_{1m} u_m}{V \dot{c}_{1m}} \right]$
18	$\left[\frac{\dot{c}_{1m}}{c_{1m}} \right]$
20	$\left[\frac{u_{m1}}{u_m} \right]$

of heat into actual heat release in the stirred vessel.

The computer therefore has three major operations to conduct:

(1) Interpretation of the monitored input variables

(2) Simulation of the chemical reaction and hence computation of the heat release rate

(3) Generate an output signal to initiate the actual production of heat release in the stirred tank.

6.5.1. Calculation of velocity constant for chosen first order kinetics

Simple kinetics were chosen for convenience and to avoid demands on computer space beyond the available capacity. More complex kinetics can be implemented if bigger analogue computers are available.

Reaction kinetics

A first order irreversible exothermic reaction $A \xrightarrow{k} B$ was chosen for investigation, where the velocity constant was defined by the Arrhenius equation:

$$k = Ae^{-E/RT} \qquad \text{(Eq.6.1.)}$$

where T is the only variable and hence:

$$k = f(T)$$

The rate of reaction is then given by:

$$r = kc_1$$

The most convenient way to implement the Arrhenius equation on the analogue computer is to use a variable diode function generator (VDFG). Information on this module and other analogue computational techniques is available in the E.A.L. handbooks and many texts and therefore no elaboration is presented here. Scaling of all variables is necessary and this will be covered in detail elsewhere. The VDFG effectively constructs a reference calibration curve. For a particular value of temperature input to the module the appropriate velocity constant will be output. Initially the VDFG has to be set up to approximate the desired calibration curve. The generator approximates the curve by several straight lines the gradients of which are set by the operator. [See Fig.6.7.(a) and (b).]. In actual fact since the curve is exponential in shape, the change of gradient from one point to the next becomes too great and exceeds the setting range available on the VDFG. It is therefore better to effect the simulation in a different way. [See Fig.6.7.(c) and (d).]. The curve is approximated over a chosen range by a straight line and the error from the actual curve is subtracted from this value. The error curve then becomes the one actually implemented on the VDFG. This curve undergoes much less gradient change and can therefore be accommodated within the setting range of the function generator.

The complete analogue circuit which includes the kinetics simulation, material balance and servomechanism control is given in Fig.6.9. The latter two are dealt with in the next subsections.

Fig.6.7. Kinetics simulation

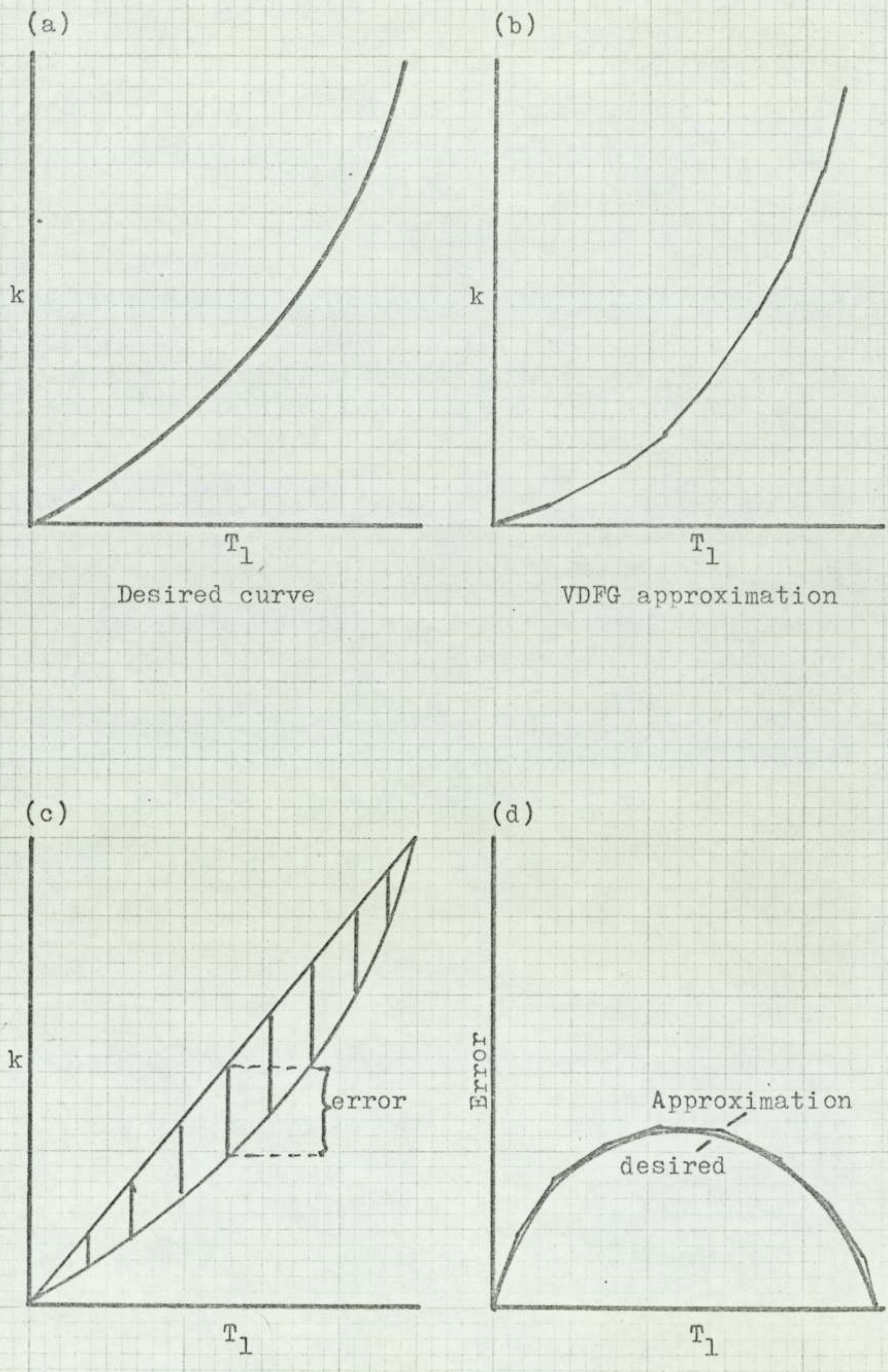

6.5.2. <u>Simulation of the material balance for the system and subsequent heat generation evaluation</u>

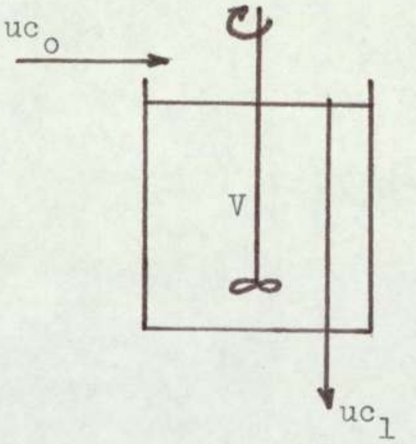

Fig.6.8.

Material balance on component A taking temperature and concentration in the tank as the only variables:

$$uc_o = uc_1 + rV + V\frac{dc_1}{dt} \qquad \text{(Eq.6.2.)}$$

which for a first order forward reaction becomes:

$$uc_o = uc_1 + k\,c_1 V + V\frac{dc_1}{dt}$$

or:

$$\dot{c}_1 = \frac{uc_o}{V} - \frac{uc_1}{V} - kc_1$$

Amplitude scaling in terms of the maximum variables gives:

$$\frac{\dot{c}_1}{\dot{c}_{1m}} = \frac{u}{V}\frac{c_o}{\dot{c}_{1m}} - \frac{u}{V}\frac{c_{1m}}{\dot{c}_{1m}}\left(\frac{c_1}{c_{1m}}\right) - \left(\frac{k}{k_m}\right)\left(\frac{c_1}{c_{1m}}\right)\left(\frac{k_m c_{1m}}{\dot{c}_{1m}}\right)$$

(Eq.6.3.)

This was the form of the mathematical model patched on the analogue computer.

Having obtained a value for rate of reaction from this equation the heat generation can then be computed from:

$$Q = rV(-\Delta H) \qquad \text{(Eq.6.4.)}$$

where ΔH is the heat of reaction and is assumed constant.

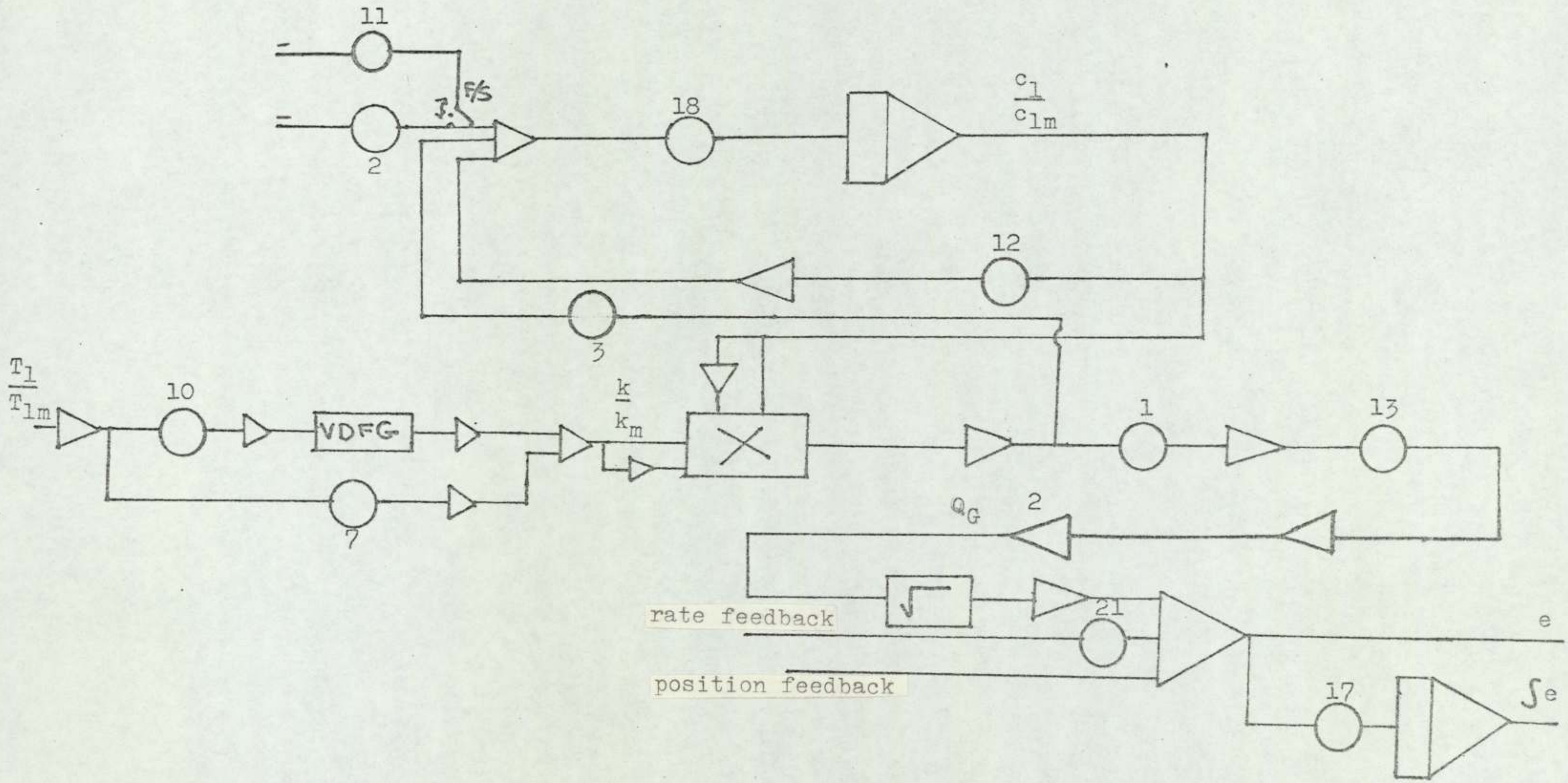

Fig.6.9. Analogue circuit for Arrhenius equation and material balance simulation and servomechanism control. (Feed flowrate constant)

Table 6.2. Potentiometer settings definitions for circuit diagram shown in Fig.6.9.

Potentiometer number	Parameters involved
1	$V\Delta H$
2	$[\frac{u\,c_o}{V\,\dot{c}_{1m}}]$ where $c_o = 1$ gmole/litre
3	$[\frac{k_m\,c_{1m}}{\dot{c}_{1m}}]$
7	Gradient of linear approximation to Arrhenius curve
10	VDFG factor
11	$[\frac{u\,c_o}{V\dot{c}_{1m}}]$ where $c_o > 1$ gmole/litre
12	$[\frac{u\,c_{1m}}{V\,\dot{c}_{1m}}]$
13	Gain for servomechanism
17	$\frac{1}{T_R}$ where T_R is the constant for integral control of servomechanism (0.286)
18	$[\frac{\dot{c}_{1m}}{c_{1m}}]$
21	Gain for rate feedback from tachogenerator (0.039)

Another feature included in the analogue circuit (Fig.6.9.) was the means of altering the inlet concentration in the manner of a step change using a function switch. This allowed the system to be disturbed rapidly to any desired initial condition of reactor concentration within the equipment's range. Once the initial condition was achieved the inlet concentration was switched back to the original value used for the steady state.

6.5.3. Analogue servomechanism control

Having obtained the heat generation required for the chosen kinetics and heat generation in computed form, it was now necessary to convert this value in volts and milliamps to actual heat release in the stirred tank.

As direct electrical conversion would be very difficult due to the large transformers required, it was decided to carry out the operation mechanically by using a servomechanism. The computer was then required to act as the controller of the servomechanism.

In actual fact a value of heat generation represented in volts was being converted into heat release which can be considered in power as $\frac{V^2}{R}$. Therefore in order to retain a linear relationship between voltage and power the computed value of heat generation had to have the square root extracted. Having done this, the value was compared with a position feedback from a potentiometer connected to the variac shaft and also a rate feedback generated by a tachogenerator fitted to the D.C. reversible motor which drove the variac shaft. The details of the servomechanism are dealt with in Section 6.6. The subtraction was done on a summer and the result produced the error which was required to drive the servomechanism. The feedbacks ensured the stability of the servomechanism.

Initially only the error was transmitted to the servomechanism which meant that it was under proportional control only. As deadband errors were found to persist after experimentation and modification, it was later found more satisfactory to include integral action as well. The two-term control proved satisfactory.

The setting for the potentiometer on the feedback of the tachogenerator was found by trial and error and only a small rate feedback was actually necessary.

The time constant of the integral control of the servomechanism was also determined by trial and error so as to give a suitably rapid response.

6.6. Servomechanism design

It was decided to adopt this route for conversion of computed to actual heat release as it was expected to be the most economical and simple way. Furthermore it offered a brief exploration, for a chemical engineer, of servomechanism theory which is in a related field to process control. Both of these subjects fall under the general heading of control engineering. Thus a greater insight into the general field by making comparisons between the two was anticipated. To delve too deeply into the subject would be too time-consuming and would detract from the main purpose of the research. However it was essential to ensure that such a mechanism would not distort the simulated reaction kinetics due to:

(1) Lengthy response time in comparison to the rest of the equipment. (Ideally it should be instantaneous.)

(2) Instability introduced by the servomechanism rather than by the actual system dynamics.

(3) Introduction of nonlinearities.

6.6.1. Hardware used for constructing the servomechanism

The layout of equipment used in the servomechanism is given in Fig.6.10. When integral control action was not used then points 2 and 3 on the amplifier were linked to make them common.

6.6.2. Supply to motor

The mains supplied the transformer which converted the current to 3 amps and peak voltage to 300 volts. This then passed through a diode rectifier bridge which produced a D.C. output of 3 amps / 250 volts. This power was supplied to the D.C. reversible motor.

6.6.3. Amplifier

The supply to the amplifier had to be stabilised before being input. This was done by a D.C. voltage stabiliser. The amplifier received the error and integral error inputs from the analogue computer and amplified these to the required value for the field input of the D.C. motor.

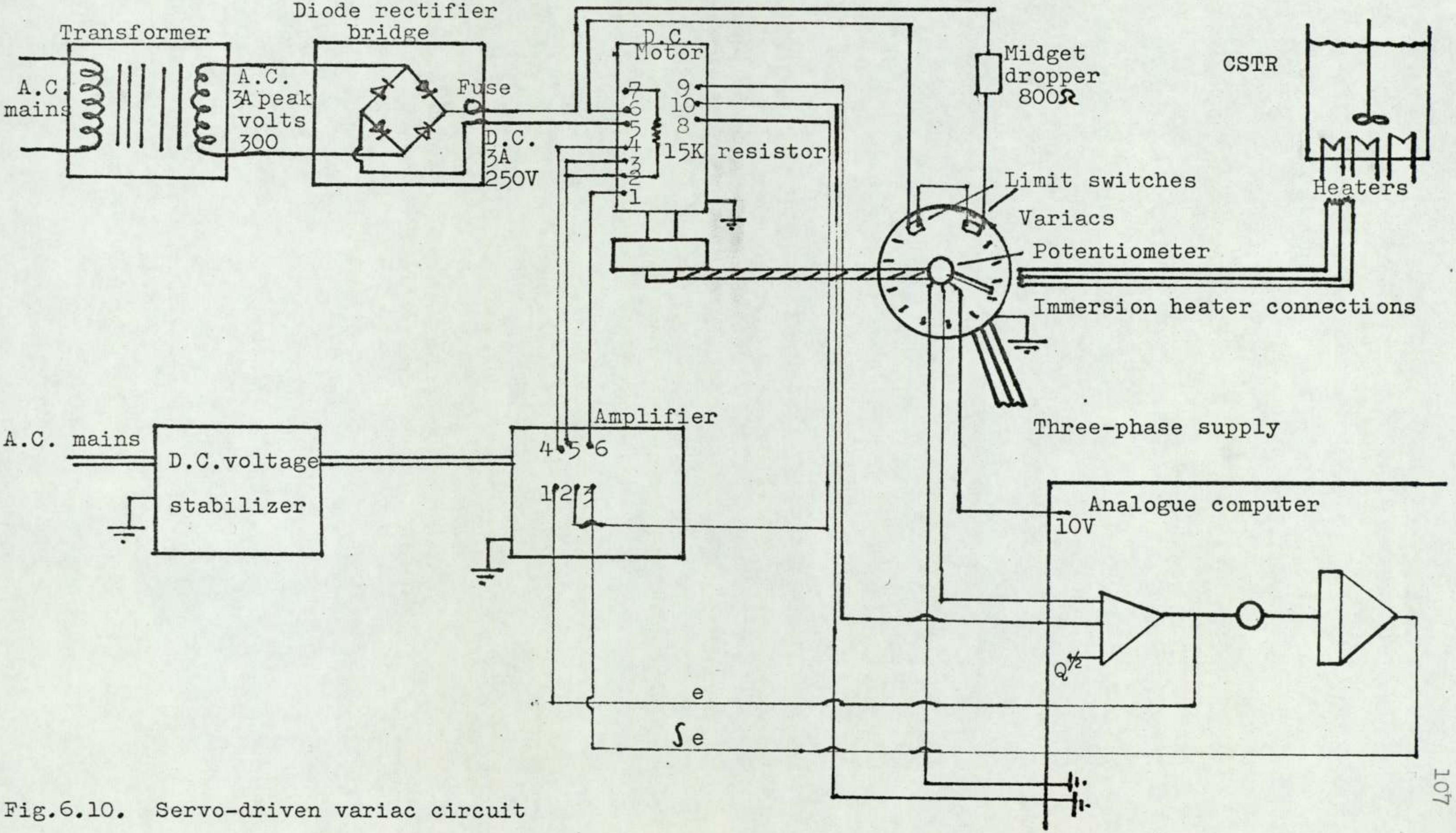

Fig.6.10. Servo-driven variac circuit

6.6.4. D.C. Reversible motor and variacs

The field produced force on the armature in the form of torque and hence the shaft on the motor drove the gears. The output from the gearbox drove a pinion which was linked by a chain to a pinion on the shaft of the variacs. Thus, when the motor received a field then it wound the shaft on the variacs up or down depending on the polarity of the field. The field polarity depended on whether the summed error was negative or positive. The position in which the shaft on the variacs settled determined the heat released by the immersion heaters. At the extremities of the scale on the variacs, limit switches were positioned to cut the motor out should the range be exceeded. This would prevent damage to the equipment but should it fail, a shear pin was also installed in the variac drive as a 'fail safe' method. A three-phase supply was connected to the set of three variacs on the common shaft, a single phase being linked to each variac which determined the power input to each of the three immersion heaters.

6.7. Controllability and stability of the servomechanism

The mechanism as it stands would be unstable without feedback control. Therefore position feedback was effected by means of a potentiometer driven by the variac shaft and a rate feedback generated by a tachogenerator in the D.C. reversible motor.

The reason for instability was evident with a simple mathematical investigation.

The servomechanism effectively carried out the following series of conversions:

field $\rightarrow$ force $\rightarrow$ acceleration $\rightarrow$ velocity $\rightarrow$ position

The latter three can be considered in terms of distance as:

$$\ddot{d} \rightarrow \dot{d} \rightarrow d$$

or in terms of Laplace transformation as:

$$G = \frac{K}{s^2} \qquad \text{(Eq.6.5.)}$$

where K is a constant.
This inverts to Kt in the time domain which indicates instability.

In reality the amplifier, motor, gearbox and load transfer functions have small time constants but these can be considered negligible in comparison with the time constants for the rest of the system, i.e. the electrical and mechanical time constants would be of the order of a fraction of a second or at the most a few seconds. The system time constant is greater than five minutes. Therefore an analysis based on negligible electrical time constants is valid.

6.7.1. Block diagram and Laplace transformation analysis

A block diagram was constructed for the servomechanism and this is illustrated in Fig.6.11. The simplified mathematics is as follows:

Block diagram for servomechanism control

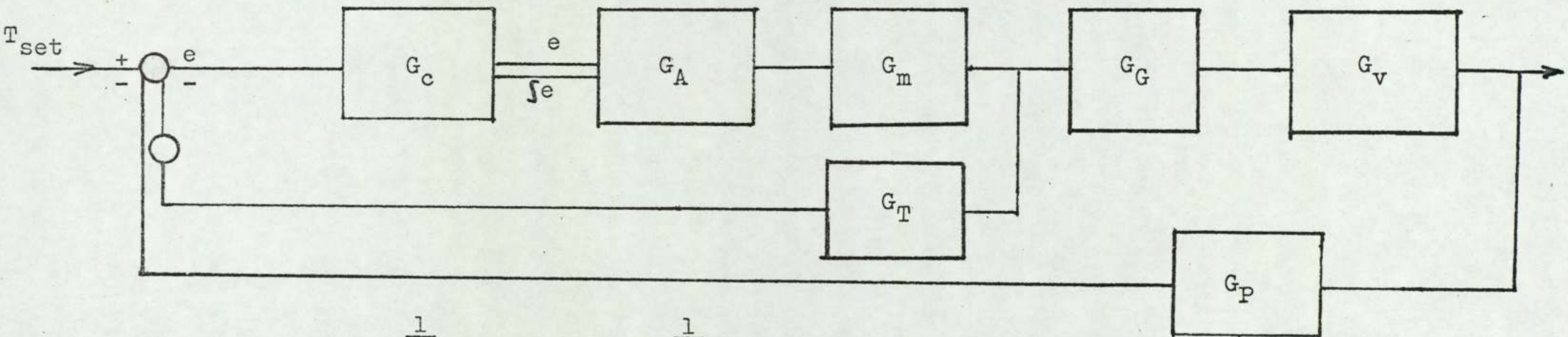

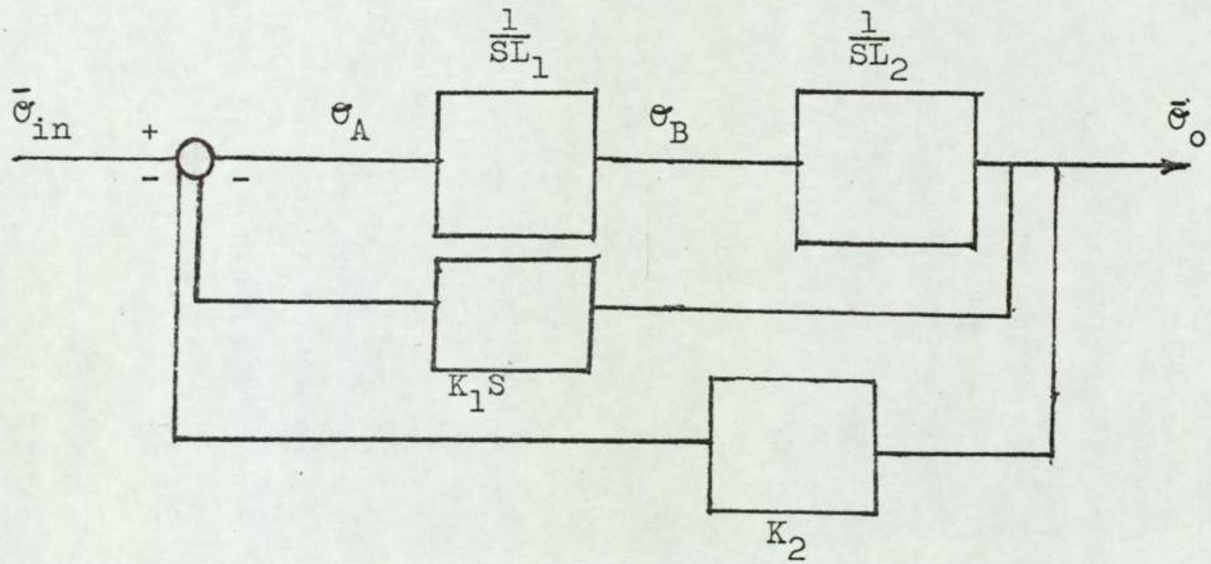

Simplified form of block diagram

Fig.6.11.

Table 6.3. Transfer functions re Fig.6.11.

G_c	Controller (TR 10)
G_A	Amplifier
G_m	Motor
G_G	Gears
G_V	Variac position
G_T	Tachogenerator
G_P	Potentiometer

$$\bar{\theta}_i - \bar{\theta}_o K_2 - K_1 s \bar{\theta}_o = \bar{\theta}_A \qquad \text{(Eq.6.6.)}$$

$$\frac{\bar{\theta}_B}{\bar{\theta}_A} = \frac{1}{s L_1} = G_1 \qquad \text{(Eq.6.7.)}$$

and
$$\frac{\bar{\theta}_o}{\bar{\theta}_B} = \frac{1}{s L_2} = G_2 \qquad \text{(Eq.6.8.)}$$

assuming no appreciable viscous loss in the motor.

$$\frac{\bar{\theta}_o}{\bar{\theta}_A} = G_1 G_2 = G = \frac{1}{s^2 L_1 L_2} \qquad \text{(Eq.6.9.)}$$

$$\bar{\theta}_i = \frac{\bar{\theta}_o}{G} + \bar{\theta}_o K_2 + K_1 s \bar{\theta}_o \qquad \text{(Eq.6.10.)}$$

$$= \left(\frac{1}{G} + K_2 + K_1 s \right) \bar{\theta}_o$$

$$\bar{\theta}_o = \frac{\bar{\theta}_i}{\frac{1}{G} + K_2 + K_1 s}$$

$$= \frac{\bar{\theta}_i}{s^2 L_1 L_2 + K_2 + K_1 s}$$

$$= \frac{\bar{\theta}_i}{a_1 s^2 + a_2 s + a_3} \qquad \text{(Eq.6.11.)}$$

This can be stable with the correct choice of feedback gain, i.e. if the real parts of the roots are negative (factors positive) then:

$$\bar{\theta}_o = \frac{\bar{\theta}_i}{(s + a)(s + b)}$$

If $\bar{\theta}_i$ is a unit step change, then after expanding into partial fractions:

$$\bar{\theta}_o = \frac{A_1}{s} + \frac{B_1}{s+a} + \frac{C_1}{s+b}$$

which inverts to:

$$\theta_o = A_1 - B_1 e^{-at} - C_1 e^{-bt} \qquad \text{(Eq.6.12.)}$$

which is stable if a and b are positive numbers. If the roots have imaginary parts then oscillation will be present also.

Position feedback only

If position feedback only is used (Fig.6.12.) this would change the mathematics as follows:

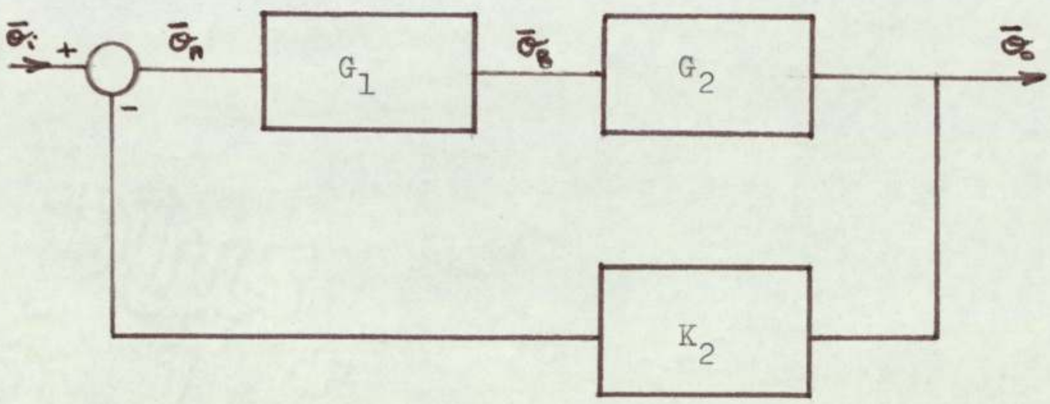

Fig.6.12.

$$\bar{\theta}_i - \bar{\theta}_o K_2 = \bar{\theta}_A \qquad \text{(Eq.6.13.)}$$

$$\frac{\bar{\theta}_B}{\bar{\theta}_A} = G_1 \qquad \frac{\bar{\theta}_o}{\bar{\theta}_B} = G_2$$

$$\therefore \; G_1 G_2 = G = \frac{\bar{\theta}_o}{\bar{\theta}_A}$$

$$\therefore \; \bar{\theta}_i - \bar{\theta}_o K_2 = \frac{\bar{\theta}_o}{G}$$

$$\bar{\theta}_i = \bar{\theta}_o \left(K_2 + \frac{1}{G}\right)$$

$$\bar{\theta}_o = \frac{\bar{\theta}_i}{K_2 + L_1 L_2 s^2} \qquad \text{(Eq.6.14.)}$$

Hence for a set-point step change:

$$\bar{\theta}_o = \frac{\theta_i}{(K_2 + L_1L_2s^2)\,s} \qquad \text{(Eq.6.15.)}$$

This cannot factorise into real roots as it stands.

viz.

$$\frac{(-b \pm \sqrt{b^2 - 4ac})}{2a}$$

$$= \frac{(-0 \pm \sqrt{0 - 4ac})}{2a}$$

$$= -0 \pm j\sqrt{\frac{4ac}{2a}}$$

Hence the roots have imaginary parts only and the response gives rise to sustained oscillations about an offset.

A practical test on the equipment was made by removing rate feedback. The mechanism was found to oscillate as predicted by the mathematics.

<u>Rate feedback only</u>

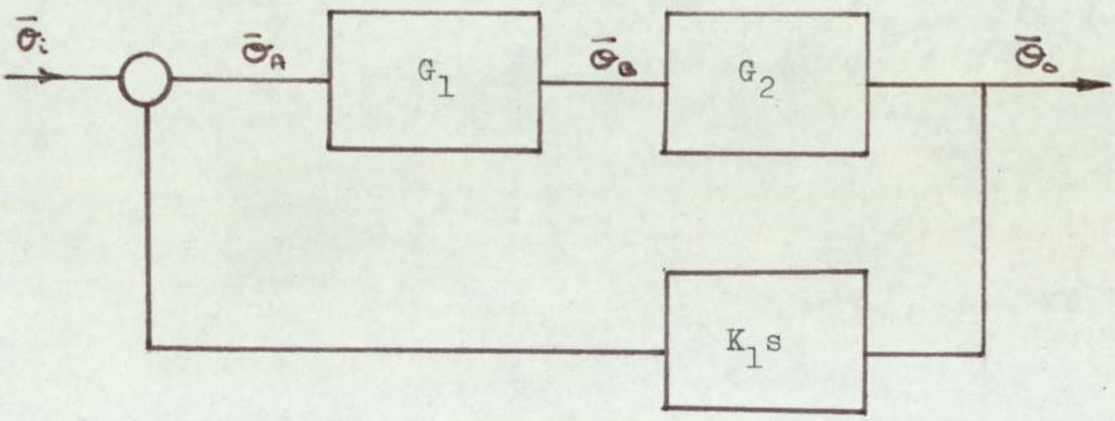

Fig.6.13.

$$\bar{\theta}_i - K_1s\,\bar{\theta}_o = \bar{\theta}_A \qquad \text{(Eq.6.16.)}$$

$$\frac{\bar{\theta}_o}{\bar{\theta}_A} = G = G_1G_2 = \frac{1}{L_1L_2s^2}$$

$$\therefore \quad \bar{\theta}_i - K_1s\,\bar{\theta}_o = \frac{\bar{\theta}_o}{G}$$

$$\bar{\theta}_i = \bar{\theta}_o (K_1 s + \frac{1}{G})$$

$$\bar{\theta}_o = \frac{\bar{\theta}_i}{(K_1 s + L_1 L_2 s^2)}$$

$$\bar{\theta}_o = \frac{\bar{\theta}_i}{s(K_1 + L_1 L_2 s)} \qquad \text{(Eq.6.17.)}$$

$\therefore$ for a step change: $\bar{\theta}_i = \frac{\theta_i}{s}$

$$\bar{\theta}_o = \frac{\theta_i}{s^2 (K + L_1 L_2 s)} = \frac{\theta_i}{L_1 L_2} \frac{1}{s^2} \frac{1}{(s + a)} \qquad \text{(Eq.6.18.)}$$

which inverts to:

$$\theta_o = A + Bt + C e^{-at} \qquad \text{(Eq.6.19.)}$$

which is unstable due to the Bt term being dominantly divergent.

Again, a practical test confirmed instability.

6.7.2. General consideration

If the small time constants were not ignored, the transfer functions would be more complex and of the form:

$$\frac{K_1}{L_1 s + 1} \quad \text{and} \quad \frac{K_2}{(L_1 s + 1)(L_2 s + 1)}$$

and powers of these. However, the dominant factors are retained in this analysis and a complete electrical control study would detract from the main theme of the research. In fact such a servomechanism has been the subject of much detailed study in its own right. Further details of servo-mechanism design and analysis can be found in ref.(28) which gives the complete transfer functions of a D.C. motor with viscous loss and an electronic amplifier.

Servomechanism nonlinearities

Nonlinearities enter into the circuit due to friction and viscosity, the nonlinear part in the friction being due to the difference between static and dynamic friction, as shown in Fig.6.14. below.

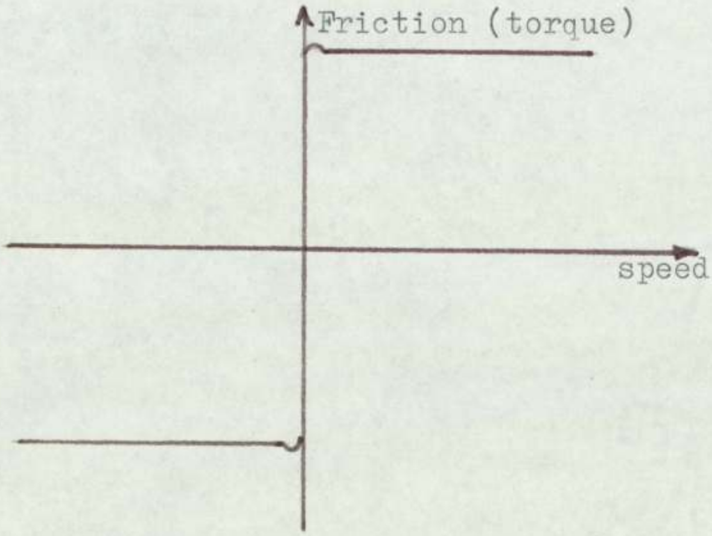

Fig.6.14.

These nonlinearities take action in opposite directions depending on motion and direction with the result that a small limit cycle may well develop. It is conceivable that if the feedback gain in the loop is increased enough, then the cycle can be eliminated completely.

A good elementary coverage of the transient analysis of servomechanisms is given in ref,(29).

6.8. Tests to prove acceptability of the servomechanism in the partial simulation

Earlier in the chapter, three conditions were stated which had to be satisfied by the servomechanism.

The first condition was clearly satisfied due to the small time constants of electrical equipment. As a practical test simple step changes were performed on the equipment. The response was found to be of the order of a second or two and therefore quite acceptably fast. From these tests also it was clear that the servomechanism was acceptably stable and furthermore little oscillation was present in the response. Any oscillations which were present were highly damped and soon died out. Practically, it is necessary to strike a happy medium between rapid response and some oscillation and this was not difficult to accommodate.

Nonlinearity provided the greatest problem. It was important to eliminate such errors as they would otherwise superimpose on the real system dynamics and distort the results. The hysteresis nonlinearity would tend to produce apparent limit cycles and two possible steady states. The position on the variac scale when hysteresis is present would describe the cycle illustrated in figure 6.15.

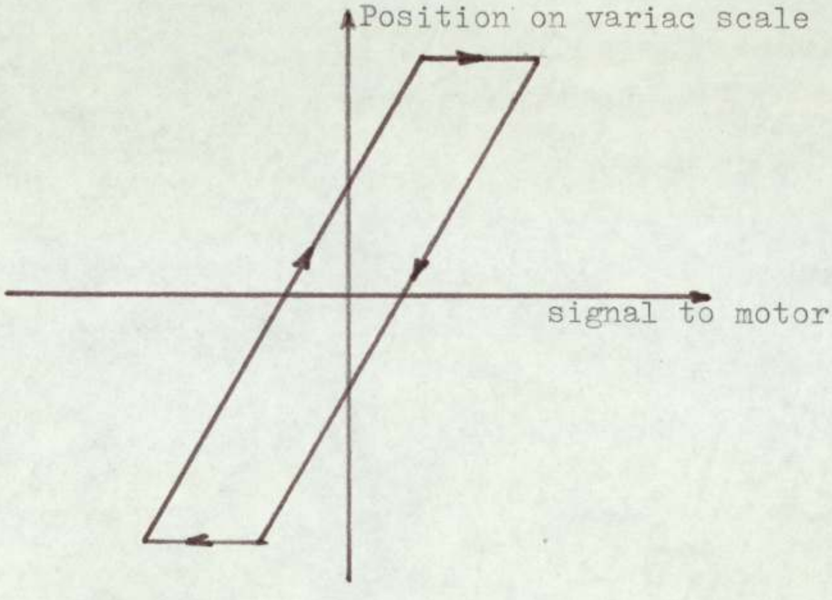

Fig.6.15.

The branch of the cycle being followed would depend on whether the signal to the motor and hence the direction of drive is up or down. Hence two possible final positions are obtainable depending on the final direction the shaft is moved in.

Initial tests on the equipment were marred by this fault being present to a far greater extent than anticipated. This was due to the hysteresis being reinforced by many factors. Causes of this in the mechanism were:

(1) loose linkage of pinions between the motor and the variac shaft

(2) chain slack

(3) loose variac shaft/brush connection

all of which contributed to produce excessive backlash.

Furthermore friction and viscosity hysteresis would also add to this effect.

The result of these combined factors on the partial simulation system was unreproducible steady states. The first step taken to remove this error was a general improvement of mechanical linkages throughout the mechanism. Although this produced a great improvement, a small deadband of about one division on the variac scale still persisted. This resulted in a very slow limit cycle with the one division magnitude. The small deadband was finally eliminated by the addition of integral control which also eliminated any proportional offset which would cause deviation from the desired value. This final arrangement proved quite satisfactory and all steady states were found to be reproducible.

Ref.(30) gives information on nonlinearity in servo-mechanisms due to backlash in linkages. For particularly bad cases nonlinear rate feedback or nonlinear phase-lead networks can be incorporated in the circuit. Fortunately in this instance the necessity did not arise.

6.9. Check for linearity between heat generation computed and power output from variacs to immersion heaters

The output of the amplifier on the TR 10 before the square root extraction was calibrated with power output from the variacs to the immersion heaters. To conduct this experiment a watt meter was connected to the output of each of the three variacs simultaneously and the output recorded for each input from the TR 10. The circuit connections necessary to measure the power output are given in Fig.6.16.

Details of the results obtained are shown in the Appendix (Table A.5. , Figs .A.8. to A.10.). The plots of voltage input vs. power output showed a good linearity, the lines passing through the origin which confirmed that there was no zero offset error. A graph was also constructed, as a further check, of voltage input vs. heat release, which was also linear (Fig.A.11.).

The checks conducted therefore ensured that the servo-mechanism functioned correctly, i.e. it converted computed heat generation into real heat release without distorting the computed value or rate of change of computed value to any harmful extent. It therefore approximated very well to the ideal case of instantaneous response. This allowed the dynamics of the system under consideration to be studied

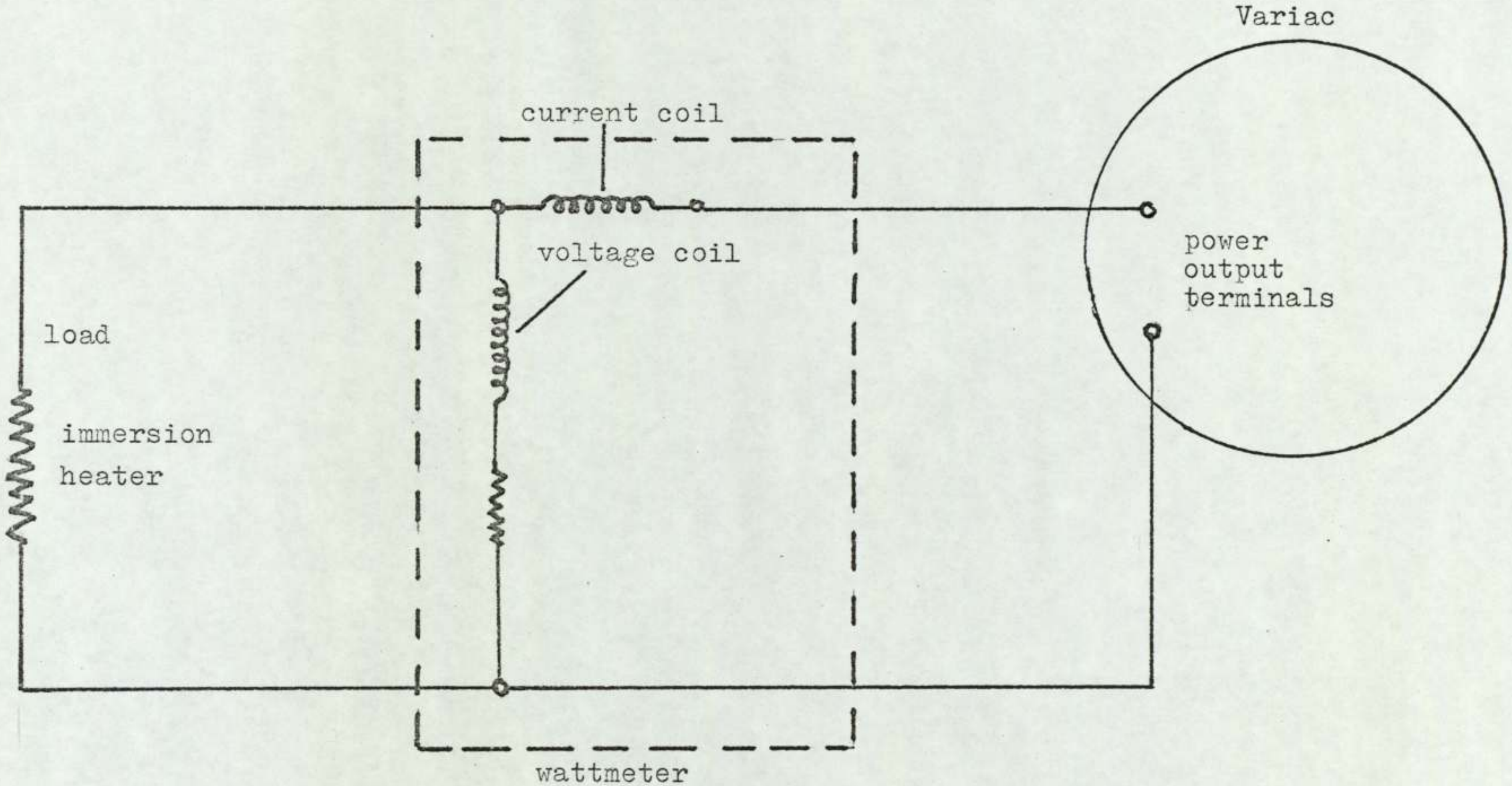

Fig.6.16. Measurement of power output of the variacs.
Three wattmeters were set up in this manner.

without taking into account any effects due to the servo-mechanism. If this could not have been achieved the partial simulation technique would have had to be abandoned, as the results obtained would not be representative of the real plant.

One further consideration which should be made is that unlike the real reaction, heat in the partial simulation will actually be released from three centres (i.e. the three immersion heaters) rather than at all points in the liquor. However, if well stirred conditions are maintained heat will be continually distributed evenly throughout and therefore the simulation should approximate reasonably well to the real case.

6.10. Monitoring of variables checks

6.10.1. Flowrate

Computer flowrate monitoring was compared against the flow through a rotameter which had itself been checked by a simple experiment using water collection and subsequent volume measurement and stopwatch timing. (Table A.4., Fig. A.7.).

The accuracy at the extemities of the scale was found to be within $\pm 2\%$ of full scale and close to linear. Considering the low flowrates and consequent small pressure drops available for measurement across the orifice plate this was considered acceptable. The response time for small changes was found to be negligible and of the order of five to eight seconds for changes of 1 litre/min. For changes of 3 - 4 litre/min. the response time was in the region of twenty seconds. When carrying out these tests some oscillation was observed in the response but this was well damped and died out rapidly after the first overshoot.

6.10.2. Temperature

The temperature device used first was that constructed utilising modules on the TR 10 and two external resistors to obtain the necessary amplification. Initially it appeared to function well especially after it had been equipped with a cold juction. It was tested by comparison with the temperature recorder controller's monitoring device. As a third check, mercury in glass thermometers were occasionally used. Often the system monitored well for times up to half an hour and occasionally longer. However, for longer periods of time it was found to be subject to drift and as this spoilt many runs it was finally decided to replace this temperature monitoring system by an amplifier designed particularly for the operation. It was hoped that this would be found more reliable as low drift characteristics were quoted.

The amplifier was delivered in mid-1969 and found to be non-operational. It was therefore returned to the factory and came back some three months later. After insulating the thermocouples from the static electricity in the tank reasonable results were obtained. Drift was found to be much less but noise was found to be a limiting factor in the accuracy of results obtainable. Efforts were made to reduce the noise level. The thermocouple leads were twisted and care was taken to ensure that they did not pass close to any mains leads where they might pick up static. The location of the thermocouple in the tank was moved into a zone away from the feed inlet pipe to prevent fluctuations caused by the feed flow . It was found possible with the above precautions to reduce the noise level to an acceptable value which was within the accuracy quotations of the amplifier manufacturers.

6.11. Analogue computer space

The computer space required to implement all of the operations exceeded that available on the TR 10. In order to gain more inverters a link was made to a servomultiplier unit which made available eight extra inverters to the TR 10. With this supplement the TR 10 was then capable of carrying out all the operations required of it.

6.12. Analogue computation accuracy confirmation

As the circuit for partial simulation must operate in real time it is necessary to deal with some potentiometer settings which are demanding on the accuracy limitations of the TR 10 computer.

Checks were made of the steady state results obtained from the computer operations with the calibration charts which were discussed in Section 3. The charts were constructed for a particular feed flowrate by utilising the steady state relationship:

$$c_1 = \frac{c_o}{1 + \frac{kV}{u}} \qquad \text{(Eq.6.20.)}$$

The graphs are given in the Appendix (Figs.A.4. and A.5.). The results obtained from the analogue computer were found to compare well with the graphs, the accuracy being usually better than five per cent.

Hybrid and TR 10 complete simulations at a later stage were implemented to a higher degree of accuracy due to the freedom to operate in computer time. These simulations gave a dynamic check of the partial simulation phase-plane portraits which were found satisfactory. The ten-fold accuracy of the Hybrid computer also increased confidence in the accuracy of the TR 10 results.

Tests were also carried out on the integrator in the material balance for the partial simulation to ensure that it was integrating correctly in seconds. This confirmed that the computer operated in real time and was in phase with the real equipment.

6.13. Valve positioner

Due to the presence of hysteresis in the control valve, a valve positioner was installed in the equipment to eliminate this imperfection and also to obtain the opportunity of comparing the system with and without the valve hysteresis. In this way the effect upon system stability and controllability could be studied.

The type of positioner installed was a Fisher V/P Type 3560 which was motion balance operated. An illustration of the valve layout is given in Fig.6.17. The position of the valve stem is compared with the bellows' position which receives the controller pressure via the

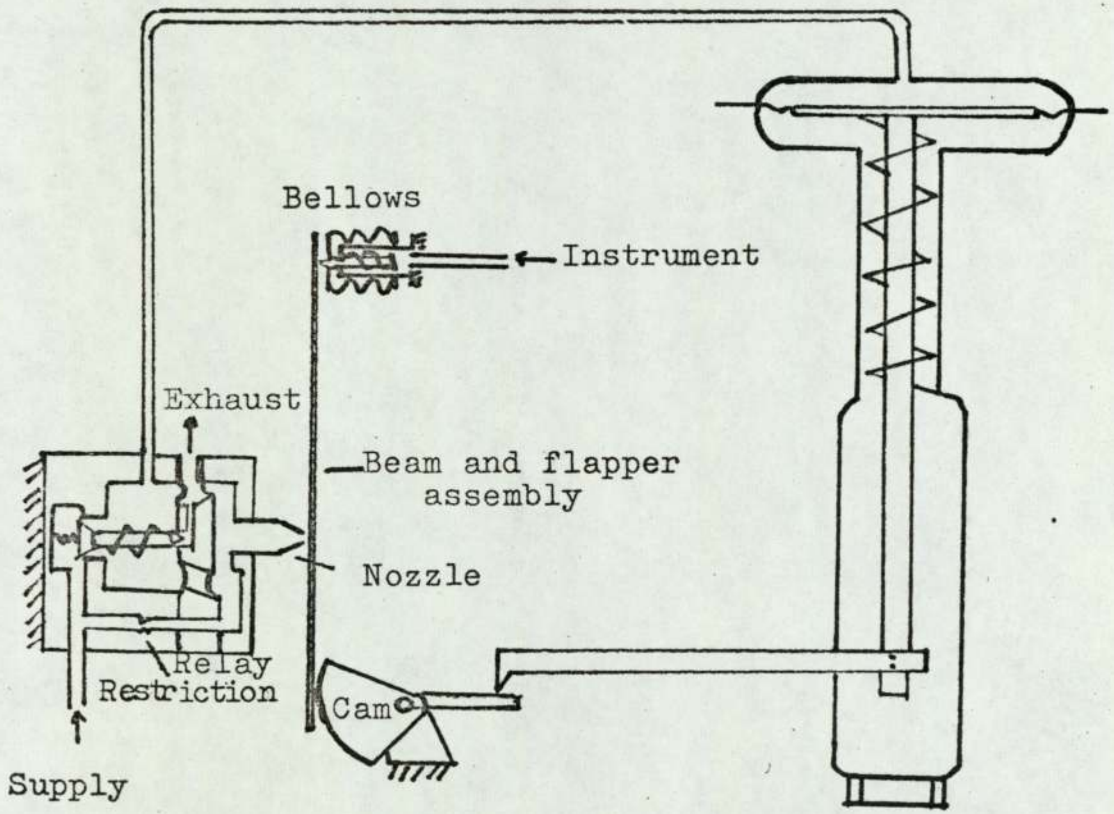

Fig.6.17. Valve positioner

motion of a beam and flapper device. Three cams are available which can be inserted into the feedback path to alter the characteristic of the valve. This is a useful addition where complex control systems require stabilising. When operational the controller output pressure acts on the bellows to make the beam and flapper assembly cover or uncover a relay nozzle. The cam position then balances the beam position by rotating due to valve stem movement. By this type of relay system a changing instrument pressure determines the corresponding stem position.

A more detailed coverage of the action can be found in literature supplied by the Fisher Governor Co. Ltd.

CHAPTER 7

7.1. Complete equipment consideration

At this stage each section of the equipment had been tested and found to operate satisfactorily. It was now necessary to test the whole equipment as one unit to determine if it operated correctly. To do this it is useful to conduct a steady state check and a dynamic check on the equipment.

Having verified that the partially simulated process functions correctly, a system is then available on which stability and controllability analyses can be made.

7.2. Verification of the steady state operation of the equipment

These tests were carried out by allowing the uncontrolled system to settle to its natural steady state for a particular coolant flowrate. (i.e. The Bristol temperature recorder controller was switched from automatic control to manual setting.) Having recorded the details necessary for mathematical check a new coolant flowrate was set and a new corresponding steady state obtained and recorded. This procedure was repeated until about ten steady states were recorded. Having done this enough information had been obtained to solve a steady state mathematical model of the system. The model was complex but contained only one variable and could therefore be solved by an iteration technique. Having calculated the heat of reaction for one of the steady states if the servomechanism operation was truly linear then all the other steady states should have been calculable using this value.

7.2.1. Parameter values chosen for experimental run

The following parameters were chosen for the experiment. This had to be done in order to evaluate the necessary potentiometer settings on the analogue computer. Some parameters were fixed or limited by the equipment design and other constraints whilst others had a fair degree of flexibility.

V = 16 litres

u = 3 litre/min.

c_p = 1 cal/g ^{o}C

c_o = 1 gmole/litre

T_o = Mains water temperature

T_{c1} = Mains water temperature or temperature of water in storage tank

ρ = 1 g/cm^3

Kinetics

Constant in the Arrhenius Equation (A) = 6.3×10^{15}

Activation energy (E) = 24000 cal/gmole

Gas constant (R) = 1.987 cal/gmole degC

Heat of reaction (ΔH) was calculated for each particular experiment.

The values chosen were used to give useful results in a range suitable for the equipment. Even with 9 kW of power available it was found advisable to restrict the temperature range because the consumption of the available heat by a cold feed obviously gets larger the greater the difference between the reactor and feed temperature. With 3 litre/min. of feed at say $10^{o}C$ and a reactor temperature of around $50^{o}C$, 9 kW of power was found to be consumed very readily, i.e. Heat required to heat up

$$\text{feed} = m_f\, c_p\, (T_1 - T_o)$$

$$= 3 \times 1000 \times 40 \left(\frac{g}{min}\right)\left(\frac{min}{60s}\right)\left(\frac{cal}{g\,deg\,C}\right) deg\,C$$

$$= 2000 \left(\frac{cal}{s}\right)$$

The maximum power available is 9 kW, or in heat units:

$$9\ kW \times \left(\frac{k\,cal\,/\,s}{kW\ 4.18}\right) = 2150 \left(\frac{cal}{s}\right)$$

This would leave only 150 cal/s which is very little with which to perturb the system. Therefore a range of 0 - 35 degC was chosen as the region for investigation. The other advantage which was mentioned earlier is that heat losses become negligible over this range (4% maximum) and therefore heat balance calculations were not complicated by this factor.

7.2.2. Arrhenius equation simulation

The setting up procedure for the VDFG can be found in the analogue computer manufacturers' manual. The data to be set up on the function generator was presented in the following manner. A table was constructed by splitting the temperature range under consideration (0 - 35 degC) into ten sections and spreading this range over 0 to 10 volts (Table 7.1.).

Table 7.1. VDFG Calibration (error curve)

Temperature	Input	Output
0	0	0 (ideally -0.038)
.	1	0.57
..	2	0.93
.	3	1.62
17.5	5	2.43
.	7	2.74
.	9	1.43
35.0	10	0

The output values for a given input can be measured directly from the graph of the exponential function and linear approximation (Fig.A.2.) when treated as shown in Fig.6.7.(c).

Conversion factor of $\frac{T}{T_m}$ $\rightarrow$ VDFG input was found to be 0.285 and the gradient of the straight line was calculated as 0.17.

Gains were distributed around the circuit to obtain maximum accuracy.

Thus $17.5^{o}C$ was represented as 5 volts for the input to the VDFG. By adjusting the break-points' gradients a calibration curve was constructed so that for a particular input value of temperature the appropriate value of error, obtained from the error curve, was generated. In this way the error curve was set up and after subtraction from the straight line approximation, the desired exponential curve was obtained.

7.2.3. Calculation of the heat of reaction

The heat of reaction was calculated from the total heat being released by the immersion heaters at a steady state. The heat release was calculated from the relationship:

Q_G = heat absorbed by feed and heat absorbed by coolant

which assumes that heat losses are negligible. From this value and the corresponding computed value of velocity constant then the heat of reaction could be evaluated. The heat of reaction is one of the constants which is absorbed in the gain relationship between rate of reaction and the servomechanism position and hence the actual heat release. The heat of reaction was obtained from:

$$
\begin{aligned}
Q_G &= rV(-\Delta H) \\
&= k c_1 V(-\Delta H) \\
&= \frac{k c_o}{1+\frac{kV}{u}} V(-\Delta H)
\end{aligned}
$$

Thus the only unknown was ΔH which could be calculated.

ΔH was assumed constant and once evaluated for one steady state, it was expected to be applicable to the remaining steady states if all other parameters were held constant.

7.2.4. Heat transfer coefficient

The heat transfer coefficient value was obtained for a particular coolant flowrate from the calibration graph (Fig.A.6.).

7.2.5. Analogue computer simulation

The scaling for the analogue circuit was as follows:

Considering the material balance:

$$\dot{c}_1 = \frac{u}{V}(c_o - c_1) - k c_1$$

The equation was scaled as shown in Section 6.5.2., Eq.6.3. The numerical values of u, V and c_o were given in Section 7.2.1. The following maxima were chosen:

$$c_{1m} = 1 \text{ gmole/litre}$$

$$\dot{c}_{1m} = 0.2 \text{ gmole/litre s}$$

$$k_m = 0.1 \text{ s}$$

$$T_{1m} = 100^\circ\text{C}$$

T_{1m} was chosen as 100°C in order to simplify reading. Similarly c_{1m} was chosen as 1 gmole/litre. Thus c_1 could be read directly and T_1 had a scale of 0.1 volts per deg.C. The Wheatstone bridge network potentiometer settings were fairly arbitrary being used as accuracy trimmers.

The $V\Delta H$ potentiometer was manipulated to give the desired heat release and the setting was dependent on various gains throughout analogue and servomechanism circuits. Its choice initially was dictated by the amount of heat release desired.

Experiments 1 to 4 were conducted to test the system operation at the steady state. Details of the results and digital checks are given in the Appendix. (pages 318 to 326).

7.2.6. Digital check of steady states using an iteration technique

The equation used to conduct the steady state check was constructed as follows.

Steady state material balance for the reactor

$$u c_o = u c_1 + k c_1 V$$

$$c_1 = \frac{u c_o}{u + kV}$$

Steady state energy balance

$$m_f c_p T_o = m_f c_p T_1 - k V c_1(-\Delta H) + UA(LMTD) + L$$

where: $m_f = \rho u$

L = heat losses

$\rho = 1$

$c_p = 1$

hence:

$$T_1 = T_o + \frac{kV(-\Delta H)u c_o}{m_f(u + kV)} - \frac{UA}{m_f} \frac{[(T_1 - T_{c1}) - (T_1 - T_{c2})]}{\ln[(T_1 - T_{c1})/(T_1 - T_{c2})]} - \frac{L}{m_f}$$

where: $k = A e^{-E/RT_1}$

T_{c2} varies with T_1 and was obtained from the relationship:

$$m_c c_p (T_{c2} - T_{c1}) = UA \frac{(T_{c2} - T_{c1})}{\ln[(T_1 - T_{c1})/(T_1 - T_{c2})]}$$

This expression was manipulated to give T_{c2} in terms of T_1 :

$$T_{c2} = T_1 - (T_1 - T_{c1})\, e^{-UA/m_c}$$

Allowing for units conversion the final forms used for the programme were:

$$T_1 = T_o + \frac{kV(-\Delta H)u\,c_o}{m_f(u + kV1000)} - \frac{UA\,(T_{c2} - T_{c1})}{3600\,m_f\,\ln[(T_{1o} - T_{c1})/(T_{1o} - T_{c2})]} - \frac{L}{m_f}$$

where: $k = A\,e^{-E/RT_{1o}}$

$$T_{c2} = T_{1o} - (T_{1o} - T_{c1})\, e^{-UA/m_c 60000}$$

T_{1o} was the first estimate of the value T_1

If $\pm(T_{1o} - T_1)$ was greater than 0.01 then the value of T_1 just calculated was fed back into the programme as the second estimate and so on. Having calculated T_1 then this value was substituted into the steady state material balance equation to compute c_1.

The programme is given in the Appendix (Programme 5, page 321). It was first written in Elliott Algol and later converted into both I.C.L. 1905 Algol and Fortran IV.

The equations were not linearised and therefore the results obtained were exact solutions.

7.2.7. Experimental results

Very early experiments are not recorded here as no useful results were obtained. This was primarily due to backlash in the servomechanism which made steady states somewhat arbitrary and irreproducible.

Experiment 1 was the first to be conducted which produced useful results. Still at this stage, however, minor errors were present which reduced the quality of the results. The most significant of these was a zero offset on the servomechanism. Another was due to the fact that proportional control only was being used on the servomechanism which in spite of improvements in linkages left a residual backlash effect. The inherent proportional offset would also produce errors from the desired value. Furthermore temperature monitoring drift was an important factor which undoubtedly had a serious effect on the results. Lastly due to imperfect Arrhenius equation implementation on the analogue computer, some error was present in the kinetics calculations. For the larger values of velocity constant this was very small but for the lower temperature values even a small deviation became significant.

The first of these faults, zero offset of the servomechanism, was eliminated simply by rotating the potentiometer driven by the variacs to the correct zero position. The hysteresis and proportional offset errors were eliminated by adding integral control. It was decided to watch the temperature monitoring drift and kinetics inaccuracy very closely and hence to try to eliminate or minimise their effects. At worst their effects could be assessed and taken into account. Errors in the value of k computed were expected to be within 5% normally except at very low temperatures when the accuracy could drop to 10%.

The results of Experiment 1 are tabulated in Table 7.2. Considering the errors discovered in the partial simulation the results were taken as promising. Whilst errors tended to be excessive at low temperatures this was felt to be not too surprising under the circumstances. For Experiment 2 all the errors mentioned had been eliminated or minimised. The results obtained were considered good enough to confirm that the system was performing correctly at the steady state within the accuracy expected. To reduce temperature drift errors the monitoring system was frequently checked against the temperature recorder during the experiment. One or two minor adjustments only were usually required to retain a high accuracy during a particular run. The final results of Experiment 2 are listed in Table 7.3.

By generally improving the accuracy, the results obtained were considered satisfactory. The parity between computed and experimental temperature waswell within experimental error with the exception of the starred result which showed a larger discrepancy but which was still within 10% of the range.

Improvements in accuracy could be expected when a better temperature monitoring system was employed and also when a more accurate computer was used. At this stage it was intended to carry out both of these modifications but due to lack of availability it was found impossible to link up a more accurate computer to the equipment.

Table 7.2.

Experiment 1 Comparison steady state results

T_1	c_1	T_1	c_1
Partial simulation values		Digital computed values	
34	0.05	34.2	0.056
31	0.07	30.7	0.085
28	0.10	26.7	0.136
25	0.14	23.5	0.197
22	0.18	19.2	0.308
20	0.19	15.5	0.433
26	0.12	24.0	0.187
29	0.08	28.0	0.118
33	0.05	32.3	0.070
24	0.15	21.2	0.251
33.5	0.05	33.0	0.068

Table 7.3.

Experiment 2 Comparison steady state results

T_1	c_1	T_1	c_1
Partial simulation values		Digital computed values	
34	0.060	34.25	0.055
30	0.090	30.17	0.091
25	0.180	25.27	0.161
23.2	0.200	22.90	0.209
‡18.2	0.36	19.20	0.307
16.5	0.38	16.20	0.407
24.2	0.170	25.00	0.164
28.1	0.102	28.80	0.106
32	0.068	32.7	0.066

Experiment 3 was a duplicate of Experiment 2. This was done as a check and as an attempt at accuracy improvement. Some results obtained were better while others were worse. The general trend was a verification of Experiment 2 and it was decided to go ahead with dynamic checks. If it was felt necessary, more static checks could be conducted when a better temperature monitoring device became available. This was done at a later date (Experiment 4) and still more accurate results were obtained.

One further comment on the results should be made. It was observed that in general errors tended to be due to a lag in the direction the system was moving. Therefore, it seemed possible that the variables recorded may have been slowly moving transients rather than actual steady state values. Therefore, if the equipment was allowed to settle for long periods of time it seemed likely that more accurate results could be obtained. However, temperature drift considerations made longer periods of time delay before result recording rather impractical. Therefore, at this stage, the results were accepted as satisfactory.

7.2.8. Computation of heat generation and removal curves

Another static check conducted was the evaluation of the heat generation and removal curves. The reasons for doing this were to determine if the steady state which is given by the intersection of the lines agrees with other computations and also to determine if there were any alternative steady states to which the system might settle, e.g. if two intersections are found then the system has two possible steady states and so on. Aris and Amundson investigated a three state system, two of which were stable, the other unstable. In this case the data for Experiment 5 was used and the curves plotted revealed the possibility of only one steady state for the parameters chosen (Fig.A.12.). The operating point found agreed very well with the other results obtained by alternative routes. Details of the calculation are given in the Appendix (page 327) and a comparison table of the results is shown later in this Chapter (Table 7.5.).

To calculate the heat generation and cooling curves, Algol programmes were written. An outline of the mathematics is given here. The complete programmes can be found in the Appendix (Programmes 3 and 4 , pages 330 and 331).

Calculation of heat generation curve

First, the computer calculated the velocity constant for the lowest temperature under consideration from:

$$k = A\,e^{-E/RT}$$

This value was then utilised in the heat generation expression:

$$Q_G = rV(-\Delta H) = k\,c_1\,V(-\Delta H)$$

$$= \frac{k\,c_o\,V(-\Delta H)}{1 + \frac{kV}{u}}$$

This equation was algebraically manipulated and the appropriate constants inserted in order to obtain consistent units before being programmed. Upon completing this calculation the computer jumped back to the start and repeated the procedure for $T + 5^{o}C$. This repetition was continued, stepping up temperature during each run through until the top of the range of temperature of interest was achieved.

The programme was actually made a little more complex than this so that a range of inlet concentrations and activation energies could be investigated. Clearly, as an alternative, a range of inlet concentrations could equally well be replaced by a range of heat of reaction values with inlet concentration held constant.

Calculation of heat removal line

The heat being removed from the system is that being absorbed by the feed and also that being carried away by coolant in the cooling coil, i.e.

$$Q_R = \frac{UA(T_{c2} - T_{c1})}{\ln\left[\frac{T_1 - T_{c1}}{T_1 - T_{c2}}\right]} + m_f c_p (T_1 - T_o)$$

where: Q_R = heat removal

T_{c2} was calculated as shown in Section 7.2.6.

Hence Q_R was computed and the whole operation repeated as in the heat generation computation in 5 deg.C intervals. The graph of the results obtained from Experiment 5 is given in the Appendix (Fig.A.12.).

7.3. Dynamic operation of the uncontrolled equipment

Experiments 5, 6, 7 and 10 produced dynamic information on the equipment used for the partial simulation.

It was decided to analyse the system using the phase plane analysis technique. This was particularly convenient as temperature and concentration are directly available for plotting from the computer. If temperature and concentration are the only state variables of the system (i.e. it is two-dimensional) then as state variables they can completely define the dynamic state of the system. A particular operating point was chosen for each experiment around which dynamic information was to be obtained. As in Section 7.2., values were recorded from the equipment at the steady state to enable a digital computer check to be carried out.

7.3.1. Phase-plane portrait

The phase-plane portrait was plotted on the variplotter for the partially simulated CSTR. This was done by disturbing the system in one of many ways, e.g.

(1) increasing feed concentration

(2) turning off immersion heaters

(3) turning off coolant pump.

When the system had reached a desired starting point, i.e. initial condition of concentration and temperature, the parameter or parameters which had been changed were reset to their original steady state values. If the system is stable the trajectory from the initial condition goes to the steady state and is displayed on the variplotter. If it is not stable the range of the servomechanism will be exceeded which is the equivalent of a runaway reaction or at the other extreme an effective shut down due to too low temperatures may be recorded. By choosing sufficient different initial conditions a phase-plane portrait of the system was constructed which described in full the stability of the system. All trajectories finally wound in to the same operating point.

Difficulties in plotting arose from the noise on the signal which produced a wavy line accentuated by the slow movement of the pen. As already explained, the system moves in real time and therefore the pen plot must be obtained in real time. In addition, the pen tended to dry up during the plot. It was therefore later decided to 'dot in' the curves and this proved the most satisfactory and neat method. The first few plots obtained were done in continuous lines therefore while the remaining ones are dotted. To start with, attempts were made to order a plotter more suited to real time plots but it soon became apparent that it would be difficult to obtain one. Information was promised by one firm on such an instrument but this never materialised. It was finally decided to retain the variplotter which seemed quite capable of producing satisfactory plots in the dotted form. Temperature monitoring drift reduced the quality of the plots and corrections for this drift were made when necessary in order to obtain the true portraits. The addition of an ice reference point to the circuit greatly reduced drift tendencies.

It should be noted that some low temperature trajectories could take about fifteen minutes to complete their uncontrolled approach to the steady state. Consequently a complete phase-plane portrait from the partial simulation equipment could easily take between one and two hours to be plotted. This is an important disadvantage of real time partial simulation in comparison with total simulation in which the solutions can be speeded up to a very great extent. An example of the portraits obtained for dynamic analysis of the equipment (Experiment 7) is given in Fig.7.1. Other portraits are included in the Appendix along with details of results obtained in these experiments.

From the literature it could be seen that the results being obtained were typical of two-dimensional system portraits. However, it was desirable to have a much closer check on the plot accuracy than this. It was decided to carry out this check by means of completely simulating the entire equipment. Without control this would not be too difficult and few approximations would be necessary to implement such a simulation.

7.3.2. Complete equipment simulation to effect dynamic verification of equipment

The analogue circuit used to implement the complete simulation of the uncontrolled equipment is shown in Fig.7.2. Definitions of potentiometer settings are given in Table 7.4.

It was now necessary to simulate both the material and energy balances. The analogue section of the Hybrid 48

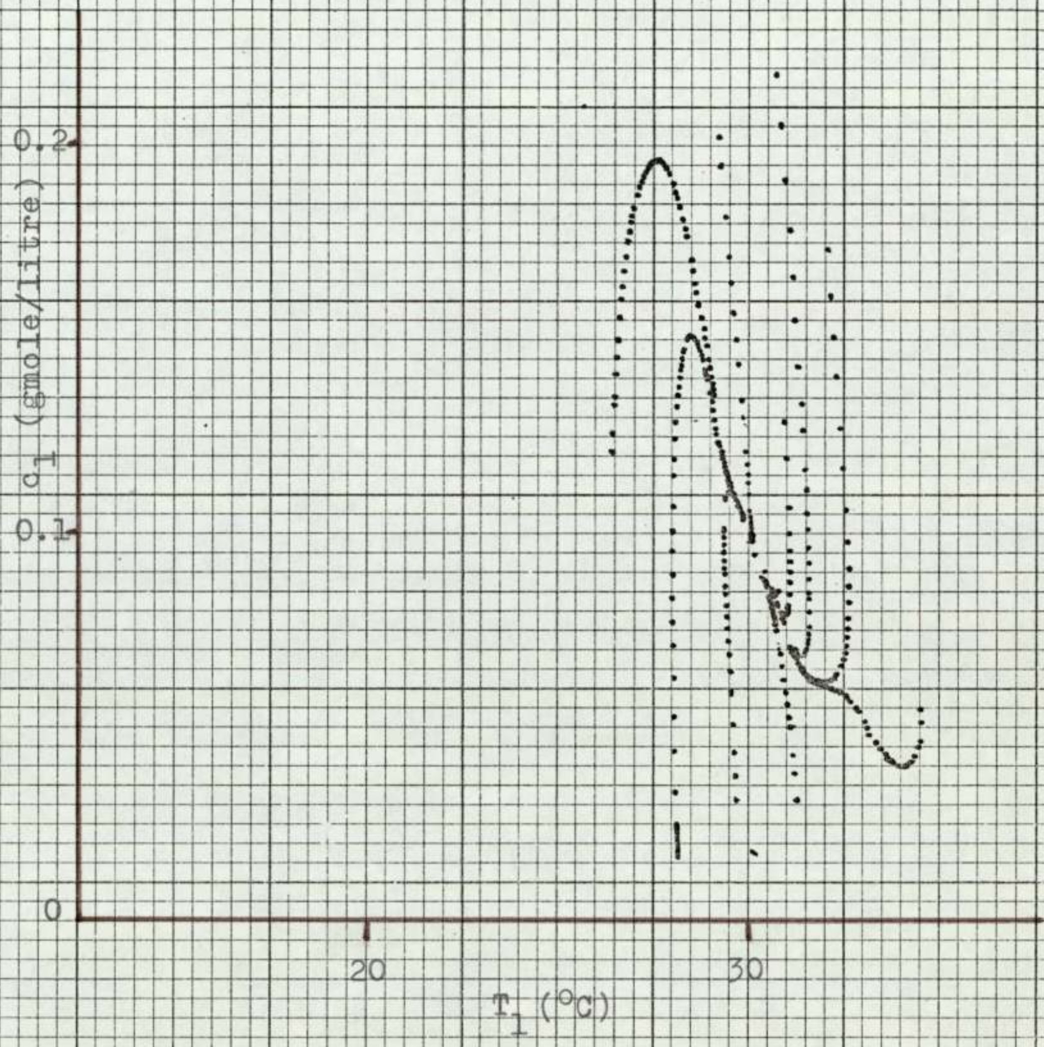

Fig.7.1.

Experiment 7. Partial simulation phase-plane portrait.

Concentration (c_1) vs. Temperature (T_1)

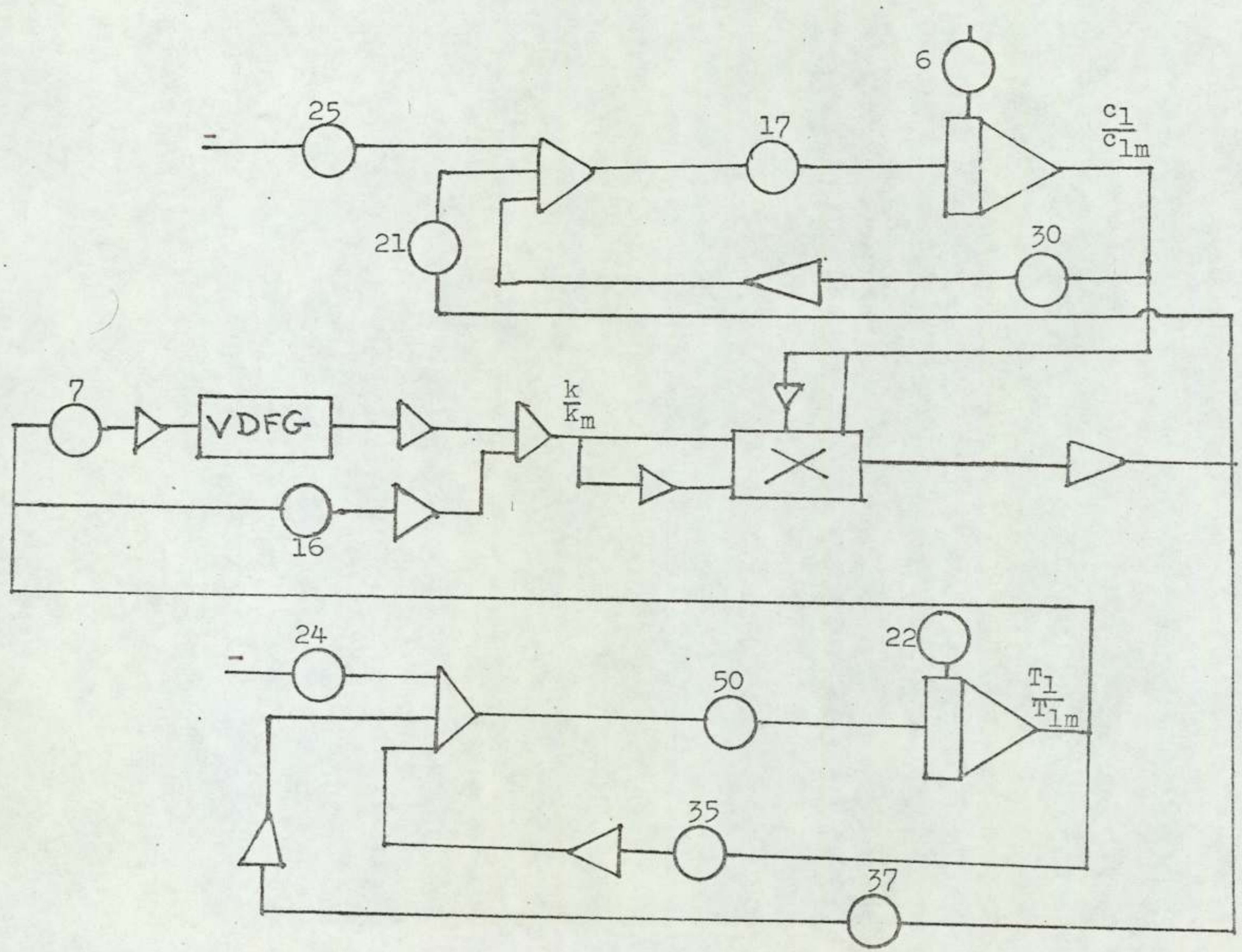

Fig.7.2. Complete simulation of uncontrolled equipment.

Table 7.5. Potentiometer settings definitions for circuit diagram shown in Fig.7.2.

Potentiometer number	Parameters involved
6	Initial condition of c_1
7	VDFG factor (0.4 x 0.2832)
16	Gradient of linear approximation to Arrhenius curve (0.4 x 0.1828)
17	$[\frac{\dot{c}_{1m}}{c_{1m}}]$
21	$[\frac{k_m c_{1m}}{\dot{c}_{1m}}]$
22	Initial condition of T_1
24	$[\frac{1}{\dot{T}_{1m}} (\frac{UA\, T_{cav}}{V} + \frac{u\, T_o}{V})]$
25	$[\frac{u\, c_o}{V\, \dot{c}_{1m}}]$
30	$[\frac{u\, c_{1m}}{V\, \dot{c}_{1m}}]$
35	$[\frac{T_{1m}}{\dot{T}_{1m}} (UA + \frac{u}{V})]$
37	$[\frac{\Delta H\, k_m\, c_{1m}}{\dot{T}_{1m}}]$
50	$[\frac{\dot{T}_{1m}}{T_{1m}}]$

computer was used because of its higher accuracy and greater space available.

For the particular steady state under consideration the coolant flowrate remained constant and therefore so did the heat transfer coefficient between coolant and liquor. To simplify the circuit an average fixed coolant temperature was assumed. A consequent limitation in the circuit was that if the feed temperature fell below the coolant average temperature assumed, then the heat transfer would change sign with heat being input into the reactor. Hence the approximation of an average coolant temperature did reduce the accuracy of results to some extent. The material balance circuit was set up as before except that it was speeded up by various gains.

As it was intended to utilize part of the same circuit for on-line analogue computation at a later date the scaling was done with this in mind (i.e. so that it could be switched over to real time operation without too much difficulty).

The energy balance model which was simulated was of the following form:

$$\frac{\dot{T}_1}{\dot{T}_{1m}} = \frac{uT_o}{V\dot{T}_{1m}} + \frac{(-\Delta H)}{(\dot{T}_{1m})}\frac{(k)}{(km)}\frac{(c_1)}{(c_{1m})} k_m c_{1m} - \frac{uT_{1m}}{V\dot{T}_{1m}}\left[\frac{T_1}{T_{1m}}\right]$$

$$- \frac{(UA)}{(\dot{T}_{1m})}\frac{(T_1)}{(T_{1m})} T_{1m} + \left[\frac{UA\,T_{cav}}{V}\right]\frac{1}{\dot{T}_{1m}}$$

[N.B. $\rho = 1$; $c_p = 1$]

The maxima chosen were:

$T_{1m} = 40$ $\qquad \dot{T}_{1m} = 16.67$ $\qquad k_m = 0.1$

The inconsistency for temperature maxima between material and energy balance was allowed for in the interactions between the balances. It was better to have a smaller maximum for the energy balance which was not to be used for on-line purposes. In this way, accuracy was improved in that part of the circuit.

The data recorded for the steady state check also furnished sufficient information to determine the numerical values of all the parameters required for the complete simulation potentiometer settings.

The variable diode function generators available on the Hybrid machine allowed greater accuracy in the Arrhenius equation implementation. Details for setting up the VDFG can be found in the service manual of the computer. The reason for greater accuracy was due to the fact that the positions of the breakpoints were movable so that where large changes in gradients were involved the breakpoints could be close together. Hence a closer approximation to the original curve was obtained.

Later the circuit was modified to allow flowrate in the material balance circuit to become a variable if desired, as in the TR 10 circuit. This was for on-line use in the future.

The phase-plane portraits obtained for the system when completely simulated are in general given in the Appendix with their corresponding partial simulation portraits. Fig.7.3. shows the complete simulation portrait which corresponds to Fig.7.1., the partial simulation portrait. Comparison between the two shows a good agreement.

Fig. 7.3. Experiment 7.

Complete simulation phase-plane portrait

Concentration (c_1) vs. Temperature (T_1)

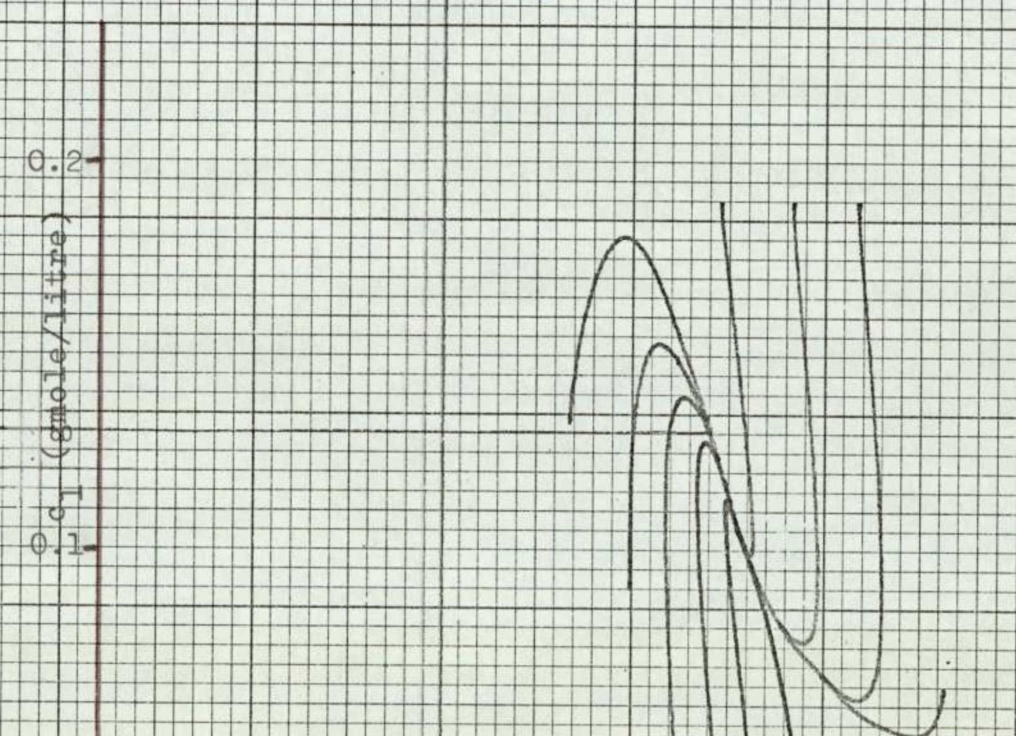

The general conclusion was that the equipment operated satisfactorily under transient as well as steady state conditions. Furthermore the final steady states obtained by the steady state checks, partial and total simulations, were in good agreement. Table 7.5. (obtained from Experiment 5) provides an example of the results.

Table 7.5.

	T	C
Heat generation/removal curve intersection	25.3	0.161
Static iteration	25.4	0.158
Dynamic partial simulation	25.0	0.155
Dynamic total simulation	25.3	0.161

CHAPTER 8. INVESTIGATION INTO THE STABILITY AND CONTROLLABILITY OF THE CONTINUOUS STIRRED TANK REACTOR EFFECTING THE CHOSEN EXOTHERMIC REACTION

8.1. Experimental Techniques employed for Partial Simulation of the Process under control

Experiments 11 to 86 were concerned with the investigation of stability and controllability. Useful phase-plane portraits were obtained from most experiments, the best of which are shown in the text, analysed and discussed. Supporting graphs and all useful experimental results appear in the appendix with example calculations where necessary.

8.1.1. Partial Simulation Tests

The equipment was set up with chosen system parameters set on the analogue computer and the chosen control parameters set on the three-term controller. After startup the system was allowed to settle to the steady state and all variables of interest were recorded. The state was then disturbed by one of the various means already mentioned until a chosen unsteady state initial condition was achieved. The parameters were then reset to the steady state values and the system allowed to return to the steady state under the influence of the controller. The trajectory of concentration versus temperature was plotted on the variplotter and hence the route the system took to reach its steady state recorded. In later tests when it was realised that much information was necessary for detailed analysis the steady state values of the system were recorded after each trajectory plot. Usually at least four trajectories were plotted, chosen to give an example of all possible combinations of initial conditions, i.e.

1. Low temperature, low concentration
2. Low temperature, high concentration
3. High temperature, high concentration
4. High temperature, low concentration

The range of the third initial condition was restricted due to equipment range limitations, i.e. if a too high value of heat generation was desired, the servo would be wound beyond its limits and thus the results become invalid.

As the results gave some unexpected features it was decided to extend the complete simulation a stage further to include some system tests under control.

8.2. Complete simulation on the Hybrid 48 computer, of the equipment under control

8.2.1. Consideration of the energy balance for proportional control

The addition of a feedback control loop to the complete simulation circuit increases its complexity to a surprising extent. This is best explained by consideration of the system's energy balance:

$$u\rho c_p T_o + rV(-\Delta H) = u\rho c_p T_1 + \rho V c_p \frac{dT_1}{dt} + UA(T_1 - T_{cav}) \qquad \text{(Eq.8.1.)}$$

where:

$$\rho u = m_f$$

$$\rho V = M$$

$$c_p = 1$$

An average constant cooling water temperature was again assumed.

The important difference from the uncontrolled situation is that now the heat transfer coefficient has become the control variable.

It is indirectly a function of temperature through the following relationship:

UA = f (coolant flowrate (m_c)) = f (controller output pressure (COP.)) = f (error from set-point (e_s)) = f (temperature in the stirred tank (T_1)).

(Eq.8.2.)

By substitution in equation 8.1. then:

$$m_f T_o + rV(-\Delta H) = m_f T_1 + M\frac{dT_1}{dt} + K_1(T_1 - T_{set})(T_1 - T_{cav})$$

(Eq.8.3.)

where: K_1 is a constant gain if the relationship between the heat transfer coefficient and the temperature in the tank is assumed linear.

This equation together with the material balance was then implemented on the Hybrid computer and typical two-dimensional portraits with trajectories approaching one steady state were obtained. A further check on the dimensionality of the system was made by considering the linearised equations using the Laplace transformation technique.

8.2.2. Laplace transformation consideration of the material and energy balances with proportional control

After linearisation of equation 8.3. and taking m_f, T_o and T_{set} as constants it can be represented in the form:

$$a_1 + a_2 T_1 + a_3 c_1 = a_4 T_1 + a_5\frac{dT_1}{dt} + a_6 T_1 - a_7 T_1 T_{set} - a_7 T_1 T_{cav} + a_7 T_{set} T_{cav}$$

(Eq.8.4.)

where: a_1 to a_7 are various constants for the system.

Similarly the material balance:

$$uc_o = uc_1 + V\frac{dc_1}{dt} + rV \qquad \text{(Eq.8.5.)}$$

can be linearised to the form:

$$b_1 = b_2c_1 + b_3\frac{dc_1}{dt} + b_4c_1 + b_5T_1 \qquad \text{(Eq.8.6.)}$$

taking c_o as a constant. Similarly b_1 to b_5 are constants for the system.

In perturbation variables equation 8.4. becomes:

$$a_2T_1 + a_3c_1 = a_4T_1 + a_5\frac{dT_1}{dt} + a_6T_1 - a_7T_{set}T_1 - a_7T_{cav}T_1 \qquad \text{(Eq.8.7.)}$$

and equation 8.6. becomes:

$$0 = b_2c_1 + b_3\frac{dc_1}{dt} + b_4c_1 + b_5T_1 \qquad \text{(Eq.8.8.)}$$

Collecting together and taking the Laplace transformation equation 8.7. gives:

$$0 = a_8\overline{T}_1 - a_3\overline{c}_1 + a_5\overline{T}_1s \qquad \text{(Eq.8.9.)}$$

where: $a_8 = (a_4 + a_6 - a_7T_{set} - a_7T_{cav} - a_2)$

and equation 8.8. gives:

$$0 = b_5T_1 + b_6c_1 + b_3\overline{c}_1s \qquad \text{(Eq.8.10.)}$$

where: $b_6 = b_2 + b_4$

then:

$$\overline{T}_1(a_5s + a_8) = a_3\overline{c}_1 \qquad \text{(Eq.8.11.)}$$

and:

$$\overline{c}_1(b_3s + b_6) = -b_5\overline{T}_1 \qquad \text{(Eq.8.12.)}$$

Then by elimination of concentration from equations 8.11 and 8.12:

$$\overline{T}_1(a_5s + a_8) = \frac{-a_3b_5\overline{T}_1}{(b_3s + b_6)}$$

$$\overline{T}_1(a_5s + a_8)(b_3s + b_6) = -a_3b_5\overline{T}_1$$

$$\therefore \quad \overline{T}_1(a_5 s + a_8)(b_3 s + b_6) + a_3 b_5 \overline{T}_1 = 0 \qquad \text{(Eq.8.13.)}$$

which is a quadratic equation. Therefore the system model has been shown by linear analysis to be a second order system and is therefore two-dimensional. This can be expected to hold unless high nonlinearities which cause the inclusion of a third variable are included in the model (e.g. backlash, dead band). This type of nonlinearity was not included in the complete simulation circuit.

The circuit for complete simulation on the Hybrid computer using parallel logic is given in Fig.8.1. The potentiometer settings are defined in Table 8.1. The scaled heat balance was of the form:

$$\frac{\dot{T}_1}{\dot{T}_{1m}} = \frac{u}{V}\frac{T_o}{\dot{T}_{1m}} + \frac{(-\Delta H)\,k_m}{\dot{T}_{1m}}\;\frac{k}{k_m}\;\frac{c_1}{c_{1m}}\;c_{1m} - \frac{u}{V}\frac{T_{1m}}{\dot{T}_{1m}}\;\frac{T_1}{T_{1m}}$$

$$- \frac{UAT_{1m}^{\;2}}{\dot{T}_{1m}V}\;\frac{T_1 - T_{set}}{T_{1m}}\;\frac{T_1}{T_{1m}} + \frac{UAT_{cav}T_m}{V\dot{T}_{1m}}\;\frac{T_1 - T_{set}}{T_{1m}}$$

(Eq.8.14.)

8.2.3. Constraints imposed on heat removal using parallel logic

As a linear relationship between heat transfer coefficient and deviation from set-point was to be assumed then the heat transfer effect can be determined as follows:

From the calibration of the heat transfer coefficient and coolant flow it was found that the maximum value of the coefficient was in the region of 300 Kcals/(h deg K). Thus there is available for feedback control purposes a range of heat transfer coefficient of 0 to 300 K cals/(h deg K). This can be spread across the chosen proportional band, i.e. for

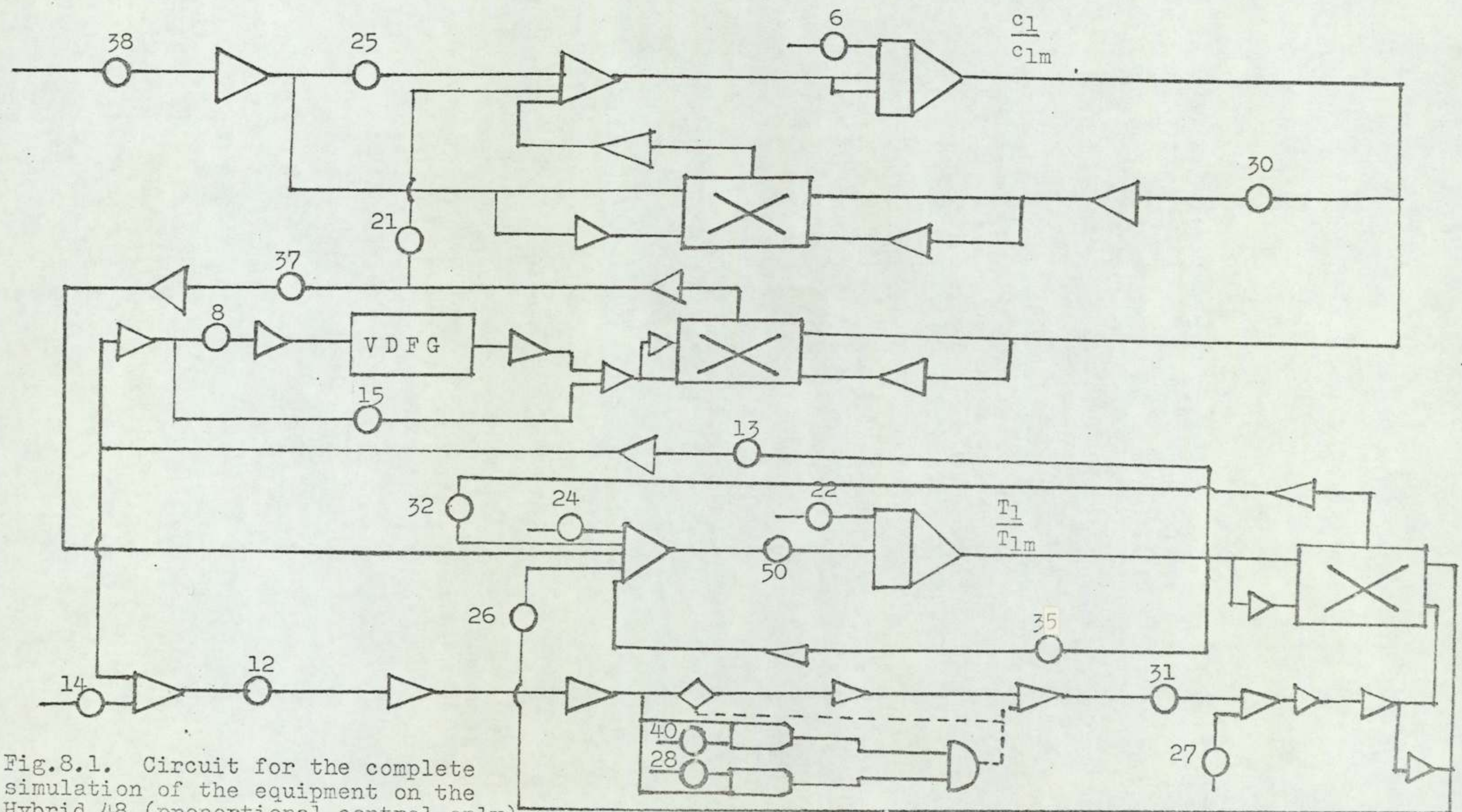

Fig.8.1. Circuit for the complete simulation of the equipment on the Hybrid 48 (proportional control only)
(The circuit also includes facility of simple alteration for on-line partial simulation use)

Table 8.1. Potentiometer settings definitions for circuit diagrams shown in Figs.8.1., 8.2. and 8.3.

Potentiometer number	Parameters involved
6	Initial condition of c_1
8	VDFG factor (0.2832)
12	PBW (setting 1.0 for 2 deg C)
13	T_{1m}
14	T_{set}
15	Gradient of linear approximation to Arrhenius curve (0.1828)
18	$\frac{1}{T_R}$ where T_R is the reset time constant
21	$[\frac{k_m c_{1m}}{\dot{c}_{1m}}]$
22	Initial condition of T_1
24	$[\frac{uT_o}{V\dot{T}_{1m}}]$
25	$[\frac{u_m c_o}{V \dot{c}_{1m}}]$
26	$[\frac{UA\ T_{cav}}{V \dot{T}_{1m}}]$
27	$[\frac{UA}{2V \dot{T}_{1m}}]$
28	Proportional band constraint (0.1)

Table 8.1. (continued)

Potentiometer number	Parameters involved
30	$[\frac{u_m c_{1m}}{V \dot{c}_{1m}}]$
31	$[\frac{UA}{2 V \dot{T}_{1m}}]$
32	T_{1m}
35	$[\frac{u T_{1m}}{V \dot{T}_{1m}}]$
37	$[\frac{\Delta H k_m c_{1m}}{\dot{T}_{1m}}]$
38	Feed flowrate $[\frac{u}{u_m}]$
40	Proportional band constraint (0.1)
41	Proportional band constraint (0.1)
43	Proportional band constraint (0.1)
50	$[\frac{\dot{T}_{1m}}{T_{1m}}]$

Maximum values used were: $T_{1m} = 40$ $c_{1m} = 1$

$\dot{T}_{1m} = 16.67$ $\dot{c}_{1m} = 0.2$

$k_m = 0.1$

a proportional band width of 2 deg.C. then there is 150 K cals/(h deg K) change in heat transfer coefficient per deg.C. of the band. Therefore if the process is controllable the final value of heat transfer coefficient will lie within the range available. Obviously if the error becomes negative the cooling system cannot be reversed to give an input of heat to the tank. The analogue computer would do this automatically unless programmed not to do so. Thus it must be programmed to have a minimum heat removal of zero corresponding to the coolant being turned off. The same applies if the maximum heat transfer coefficient available is exceeded by demand. In reality the cooling system cannot counter this and thus the computer programme has to have a constraint built in to limit the value to the maximum. The logic circuit deals with these factors. A further feature is that not only must the range limits not be exceeded but their values must be retained at their maximum or minimum whilst the demanded value is outside the range. Therefore the computer is required to store these values until the range limit is re-entered.

The logic section of the circuit alone is now considered to explain how these features were dealt with (see Fig.8.2.) Plus and minus error were included in order to allow the circuit to be easily adapted to the addition of integral control.

The error from the set-point was compared with two chosen limits on the logical comparators (e_1). The results were then transmitted to an AND GATE and depending on the result a digital/analogue (D/A) switch was opened or closed and a track/store (T/S) amplified was instructed to track or store.

Only if both limits on the comparators were not exceeded i.e. error lies within $\pm e_1$ will the D/A switch be left in the

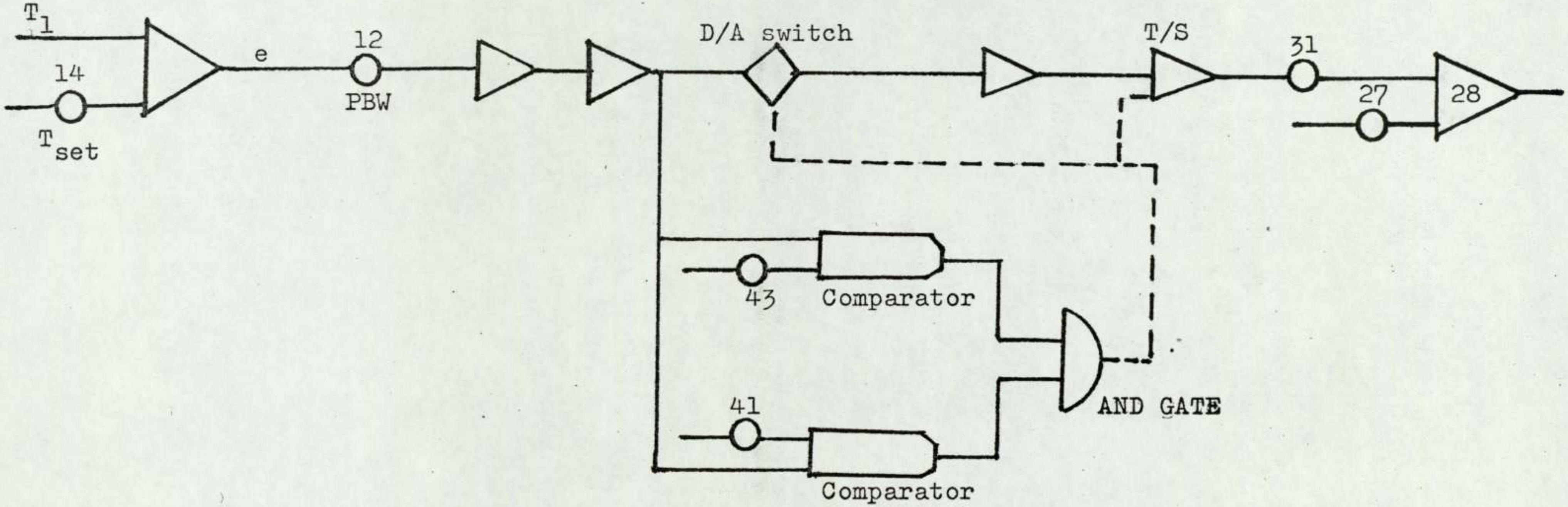

Fig.8.2. Logic circuit used to impose constraints on heat transfer coefficient..

'on' position and the T/S amplifier allowed to track. If either is exceeded then the D/A switch is closed and the last value in the T/S amplifier stored and transmitted constantly to amplifier 28. Amplifier 28 is constantly receiving a value through potentiometer 27 of half the maximum heat transfer coefficient available. This is then compared with the current value leaving potentiometer 31. The result will be the correct value of heat transfer actually available. e.g. If the maximum negative error from set-point has been stored by the T/S amplifier then the output from amplifier 28 will be zero, i.e.

$$\tfrac{1}{2}\,UA_{max} \;-\; \tfrac{1}{2}\,UA_{max} \;=\; 0$$

If the maximum positive error is stored then the maximum heat transfer coefficient available will be output from amplifier 28. i.e.

$$\tfrac{1}{2}\,UA_{max} \;+\; \tfrac{1}{2}\,UA_{max} \;=\; UA_{max}$$

Clearly anything in between the maximum and minimum value of error being tracked will produce the appropriate intermediate transfer coefficient.

8.2.4. Logic circuit required to add integral control to the circuit under discussion

The integral error circuit (Fig.8.3.) was set up to operate over the proportional band only. Thus over this range integration of the $\pm$ error would continue in the appropriate direction but would cease once either limit was exceeded. This was effected by means of the comparators and D/A switches in the circuit. It was necessary because if the integration was allowed to continue regardless of the size of

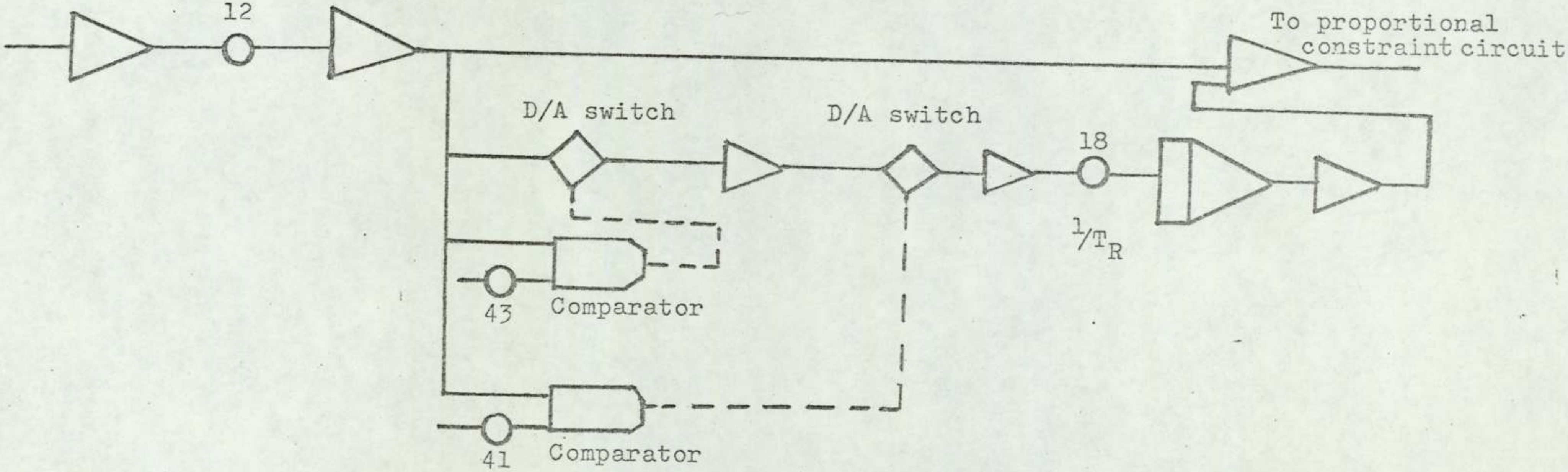

Fig.8.3. Integral control addition to complete simulation circuit. Logic circuit required.

error then for large proportional gains the integrator's range would become exceeded and hence overloaded. Therefore there would be an unrealistic representation of integral control which would distort the true values.

The integrated error was summed with the proportional value and this value then subjected to the constraints in the proportional section of the circuit as before. With the pneumatic controller which operates between 3 and 15 lbf/in^2 gauge it seems likely that the integral control would operate in excess of the range, i.e. it could drop the pressure to 0 lbf/in^2 gauge or increase it to 20 lbf/in^2 gauge which hence alters the operating time of the control. However when these limits are reached the controller is 'saturated' and further integral action is lost. It was therefore assumed that excessive errors would not be incurred by integrating only within the limits of the proportional band. These limits could no doubt be extended to include a large but still acceptable range of integration. However it was found impossible to exploit this circuit to its full advantages due to lack of computer availability.

From the results which were obtained a significant conclusion was that the portraits showed three-dimensionality when integral control was added to the complete simulation. Further proof of this was given by linear analysis in the s - domain.

8.2.5. Laplace transform analysis to show system three-dimensionality after the addition of integral control

In this case the energy balance shown in equation 8.3. has an additional term due to the integral action. The equation becomes:

$$m_f T_o + rV(- \ H) = m_f T_1 + M\frac{dT_1}{dt} + K_1(T_1 - T_{set})(T_1 - T_{cav})$$

$$+ K_2(T_1 - T_{cav})\int(T_1 - T_{set})\,dt$$

(Eq.8.15.)

As before this can be linearised and transformed into equation 8.9., plus the new term, i.e.

$$0 = a_8\overline{T}_1 - a_3\overline{c}_1 + a_5\overline{T}_1 s + \mathcal{L}\, K_2(T_1 - T_{cav})\int(T_1 - T_{set})\,dt$$

(Eq.8.16.)

The remaining nonlinear term can be linearised to a function of temperature (T_1) only. Hence the complete linear transformed expression is:

$$0 = a_8\overline{T}_1 - a_3\overline{c}_1 + a_5\overline{T}_1 s + a_9\frac{\overline{T}_1}{s} + a_{10}\overline{T}_1 \quad \text{(Eq.8.17.)}$$

which can be rearranged as:

$$\overline{T}_1(a_5 s + (a_8 + a_{10}) + \frac{a_9}{s}) = a_3\overline{c}_1$$

As before (equation 8.12.):

$$\overline{c}_1 = -\frac{b_5\overline{T}_1}{(b_3 s + b_6)}$$

Therefore eliminating $\overline{c}_1$ and multiplying through by $(b_3 s + b_6)s$ then:

$$\overline{T}_1[a_5 s^2 + (a_8 + a_{10})s + a_9](b_3 s + b_6) = -b_5\overline{T}_1 s \quad \text{(Eq.8.18.)}$$

or:

$$\overline{T}_1(A_1 s^3 + A_2 s^2 + A_3 s + A_4) = 0 \quad \text{(Eq.8.19.)}$$

where: a_1 to a_{10} and A_1 to A_4 are constants for the system.

Therefore even in the linear case the system is third order due to the addition of integral control and hence a three-dimensional representation is necessary for complete state space specification. Strictly a three-dimensional portrait is required, therefore, for complete system identification, i.e. portrait plots are required of the integrated error versus temperature and concentration (or alternatively $\ddot{T}$ vs. $\dot{T}$ vs. T plots). However integrated error is not available for plotting from the partially simulated system and the totally simulated system does not perfectly model the integral action of the controller. Therefore no portraits which included the integrated error were drawn - it was felt however that even in two dimensions (temperature and concentration) much useful information could be obtained by the plotting of these state variables.

8.2.6. General comments on results

A few results were obtained from these circuits while the computer was operational. However most of the results obtained were preliminary and whilst it is felt worthwhile to include the ones obtained it is unfortunate that further investigation was not possible.

The graphs obtained are presented in the Appendix and the discussion of the results is made in Section 8.14.

8.3. The requirement of the TR 10 computer for complete simulation

Since only a few results could be obtained from the Hybrid complete simulation, due to lack of computer availability, and as the partial simulation produced many interesting results which required a complete simulation comparison for a detailed analysis, it was decided to implement a complete simulation on the TR 10 computer. As this machine does not have parallel logic available and the analogue space is also much more restricted it was necessary to considerably simplify the original complete simulation. The new circuit implemented in shown in Fig.8.4. and the corresponding potentiometer definitions on Table 8.2.

The circuit was the same as the Hybrid one with the following limitations. Whilst negative heat removal could be prevented by an analogue comparator no maximum constraint could be imposed. Although a maximum value could be obtained by using another analogue comparator there are no facilities for storing the maximum value which would be replaced by zero leaving no feedback control. Clearly this is not acceptable and the alternative was to permit an unconstrained quantity of heat to be removed. The extent of inaccuracy depended upon the proportional band width under consideration. In the narrowest case it was necessary to produce a number of plots in order to build up a complete picture of the true situation. Also for reset control integration of the error was now a necessity over the entire range of temperature under consideration and care had to be taken not to overload the integrator. In all the circuits, gains and potentiometer settings were manipulated in order to obtain the highest accuracy possible.

8.4. Justification of the use of one- and two-term control on the system

During the dynamic verification of the equipment it was observed that the system had various natural single steady

Fig.8.4.

TR 10 Complete simulation circuit of equipment under integral and proportional control

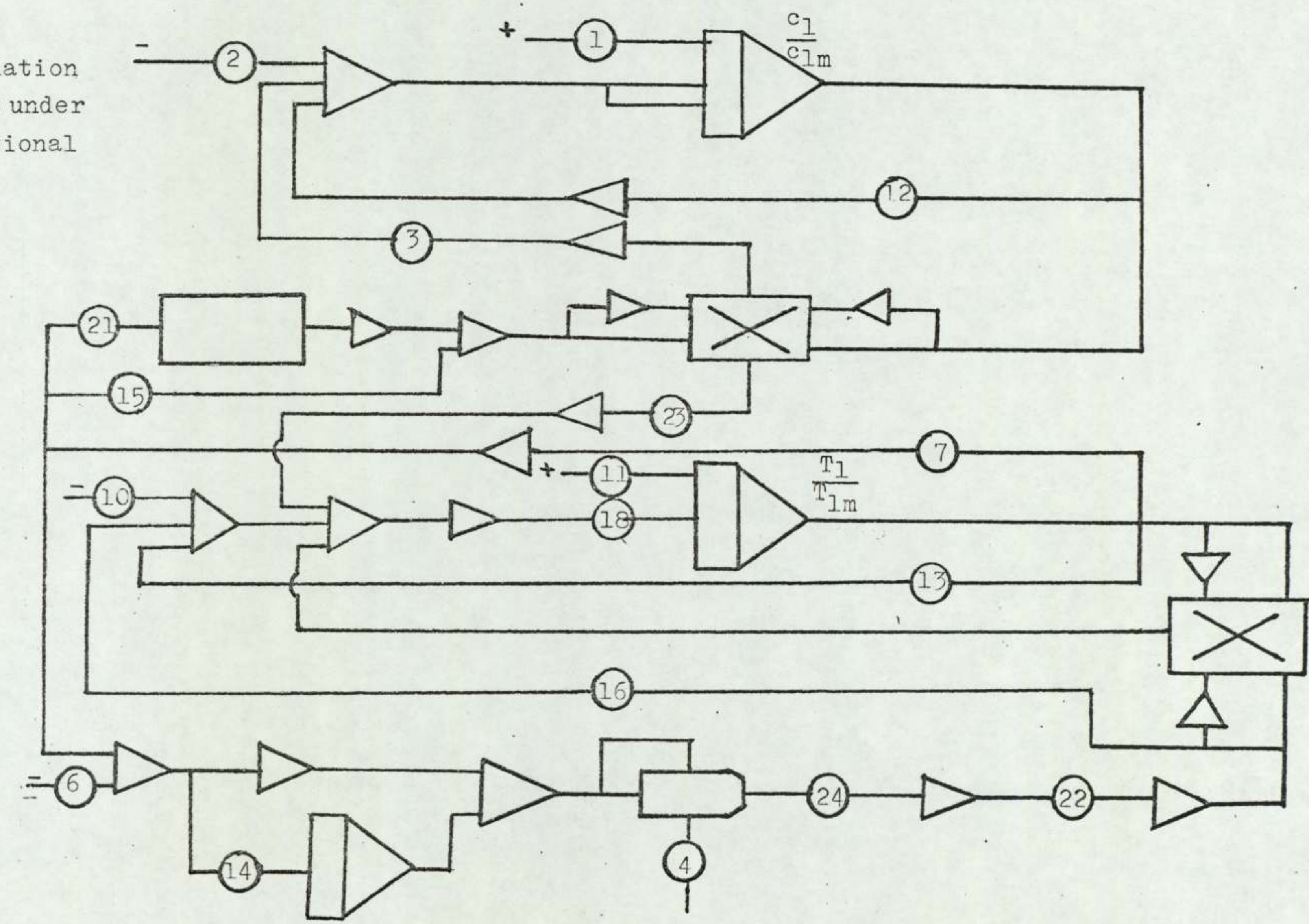

Table 8.2. Potentiometer settings definitions for circuit diagram shown in Fig.8.4.

Potentiometer number	Parameters involved
1	Initial condition of c_1
2	$[\frac{u\, c_o}{V\, \dot{c}_{1m}}]$
3	$[\frac{k_m c_{1m}}{\dot{c}_{1m}}]$
4	Zero
6	T_{set}
7	T_{1m}
10	$[\frac{u\, T_o}{V\, \dot{T}_{1m}}]$
11	Initial condition of T_1
12	$[\frac{c_{1m}\, u}{\dot{c}_{1m}\, V}]$
13	$[\frac{u\, T_{1m}}{V\, \dot{T}_{1m}}]$
14	$\frac{1}{T_R}$
15	Gradient of linear approximation to Arrhenius curve (0.17)

Table 8.2. (continued)

Potentiometer number	Parameters involved
16	$[\frac{T_{cav}}{T_{lm}}]$
18	$[\frac{\dot{T}_{lm}}{T_{lm}}]$
21	VDFG factor (0.287)
22	T_{lm}
23	$[\frac{\Delta H\, k_m\, c_{lm}}{\dot{T}_{lm}}]$
24	$[\frac{UA}{V\dot{T}_{lm}}]$

Maximum values used were: $T_{lm} = 40$ $c_{lm} = 1$

$\dot{T}_{lm} = 16.67$ $\dot{c}_{lm} = 0.2$

$k_m = 0.1$

states depending on the set coolant flowrate. However these operating points were poorly defined and trajectories from various initial conditions wound slowly in towards the steady state. Furthermore, the stability was not strong and under reasonably sized disturbances the heat removal capacity available could be expected to be exceeded causing a runaway reaction with consequent disastrous results in real plant.

The efficiency of the approach to the steady state is also poor since the coolant flowrate is maintained at a fixed value and therefore the system is being cooled even when it is far below the final operating temperature. Obviously it would be better to reduce the cooling effect or turn off completely the cooling water at such low temperatures. It could then be turned on again when the operating region was approached. In this way a much more optimal approach to the final steady state could be achieved. This could be done manually assuming the system is stable enough to be controlled in this manner when the steady state has been reached.

8.4.1. On/off control

The process could be controlled more satisfactorily by an on/off controller. Whilst a more optimal approach to the steady state is obtained, when the vicinity of control is reached there will be continuous cycling around the operating point - this will give a tendency towards instability and also large fluctuations in outlet concentration.

8.4.2. Proportional control

A proportional controller will give much less oscillation and a steady state value will be finally approached. For large proportional bands it will tend to be "sluggish" as it approaches the conditions which are faced without control and also there will be a large offset from the desired set-point. On the otherhand if a very narrow proportional band is chosen there will be a tendency towards instability and if too narrow the proportional controller will degenerate to the on/off type. The best solution is a compromise between the two. The narrowest proportional band usable is employed which does not cause the controller to act in the on/off mode. By using this form of control the coolant flow will be shut off for most of the time whilst the temperature is rising from its initial low value from startup to the control point. (see Fig.8.5.). Furthermore, at temperatues well above the proportional band the coolant will be left at the maximum rate until the control region is entered. Therefore the system approaches the proportional band in an optimal fashion. Upon reaching the band coolant flowrate will be modified according to the proportional action until the rate desired by the steady state is obtained. Thus the final value will lie within these limits, assuming there is a heat removal rate in the range which will satisfy the system's requirements.

If the system is overdamped there will be no overshoot. If critically damped there will be some overshoot and then the temperature will fall back and approach the steady state asymptotically. If underdamped there will be overshoot and subsequent oscillation around the controlled operating point.

8.4.3. Integral control

When integral control is added to a strong proportional action this should increase the rate at which the steady state

Fig.8.5. Temperature in reactor (T_1) vs. Time

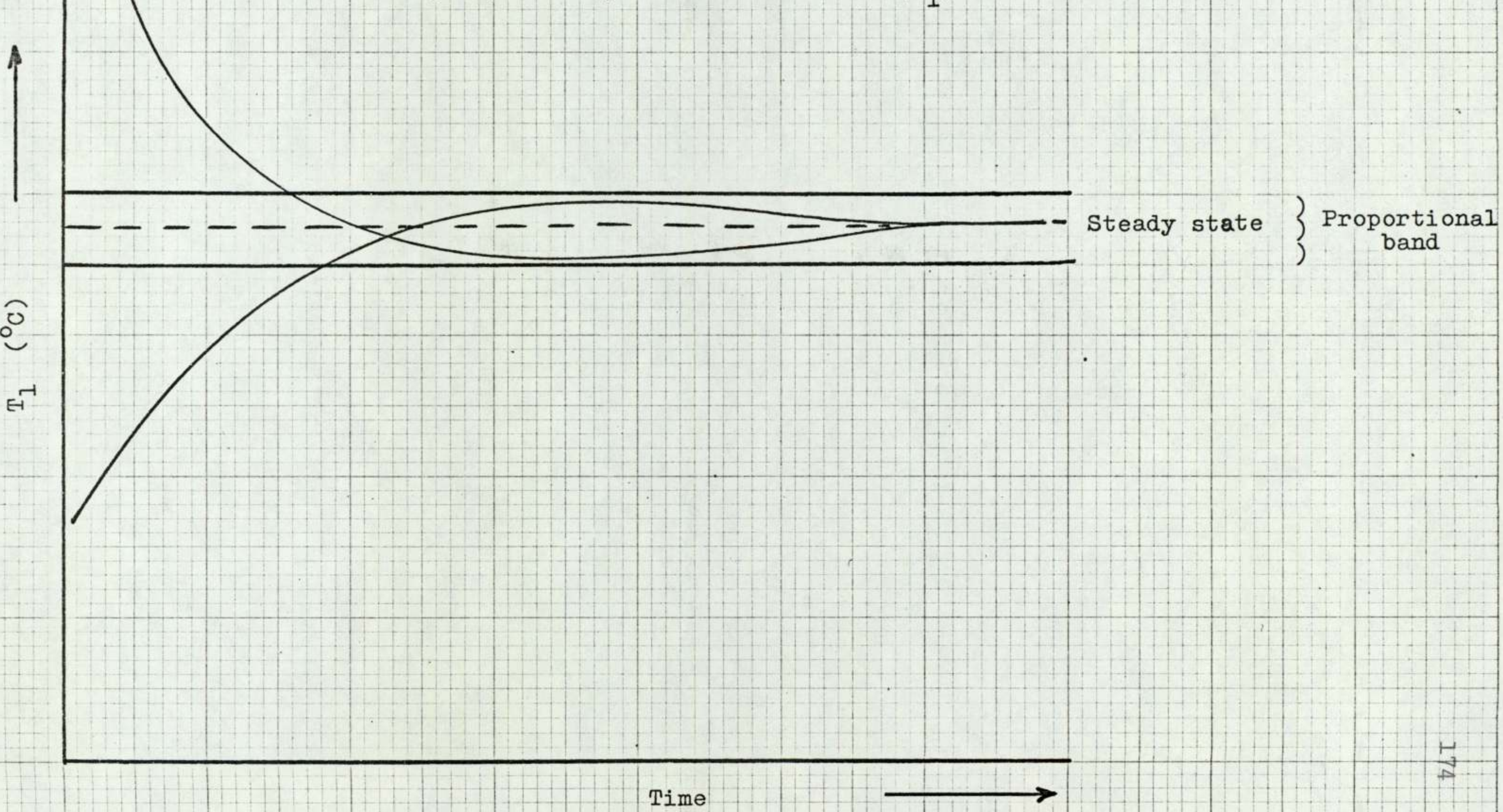

is achieved and also the offset inherent in the proportional action should be eliminated. With weak proportional action a tendency towards instability and limit cycles would be expected.

8.4.4. Derivative action

This mode should act as an anticipatory term and reduce overshoot. If the system does not change rapidly then advantages from this mode of control will be small.

8.5. Range of parameters chosen for investigation

Various combinations of the following three parameters were analysed:

Feed flowrate

Two feed flowrates were chosen for extensive analysis; one of 1.1 litre/min. and the other 3 litre/min. Greater feedrates increase excessively the demand for heat input and were therefore not chosen for investigation.

Proportional band widths

Ranges of 2 to 60 deg.C. band widths were chosen for investigation.

Integral action

Reset rates ranged between 0 and 70 repeats per minute.

8.6. Results and Analysis of the system under proportional control

Of the many results obtained the best examples are presented in this section. In order to carry out a complete analysis of the portraits early investigation of the results showed the need for further experiments. These are discussed and their implications considered when analysing the portraits.

8.6.1. Tests using 3 litres/min. of feed and 2 deg.C. proportional band width

Experiment 67 was chosen as a good example of this type of control. Other portraits with the same control band width were obtained in Experiments 38, 39(b), 61 and 85. Differences were imposed due to changes which could not be avoided (i.e. mains water temperature). More supporting plots were obtained but were substandard for various reasons (e.g. thermocouple noise, variplotter malfunctioning, temperature monitoring drift). They were therefore not chosen for inclusion in the thesis. Approximately forty partial simulation portraits are included in the thesis.

The results obtained in Experiment 67 are given in the Appendix (Table A24.2.). The portrait obtained is shown in Fig.8.6.

As anticipated, the narrow proportional band produces the most satisfactory form of control. The phase-plane portrait obtained established a much more rapid approach to the steady state by a more direct trajectory than with the weak or uncontrolled cases and the steady state region was much more clearly defined. Most noticeable however was the unanticipated existence of two operating points about 1 deg.C. apart. From a knowledge of the kinetics and steady state analysis it was known that multiple intersection of the heat generation and heat removal lines was impossible for the range of parameters available. Therefore an alternative explanation had to be

Fig.8.6. Experiment 67.

Partial simulation phase-plane portrait

Concentration (c_1) vs. Temperature (T_1)

sought and it was decided to implement a simulation of the complete equipment on the TR 10 computer. Numerical values obtained for the computer attenuator settings are given in the Appendix (Table A.37.). The portraits obtained are illustrated in Figs.8.7. and 8.8. More than one is required because of the limitations of the simple simulation. The final portraits obtained had to be considered in the light of these approximations. Although a circuit had been prepared the Hybrid computer was not utilised as it was unoperational at this stage. At a later date a portrait was obtained from the Hybrid circuit which compared well with the other portraits obtained (Fig.A.48.). The increase in complexity of the Hybrid simulation over the TR 10 circuit produced surprisingly little improvement in accuracy of simulation.

The complete simulation portraits were of the type normally expected for a two-dimensional system and in general compared well with the partial simulation portraits. However, only one steady state was defined and as anticipated trajectory intersection, which was recorded in some of the partial simulation plots, was not present in the corresponding complete simulations. It therefore followed that the idealised model with its approximations was omitting some important factor or factors which was affecting the character of the real system.

The logical place to investigate the differences was in the real system hardware. It seemed most likely that the assumed linear relationship between the error and heat transfer coefficient was so inaccurate as to have a pronounced effect on the final complete simulation results. It was therefore decided to conduct a series of tests on the control valve and recorder controller operation.

Fig.8.7. Experiment 67.

TR 10 Complete simulation phase-plane portrait

Concentration (c_1) vs. Temperature (T_1)

PBW 2 deg.C.

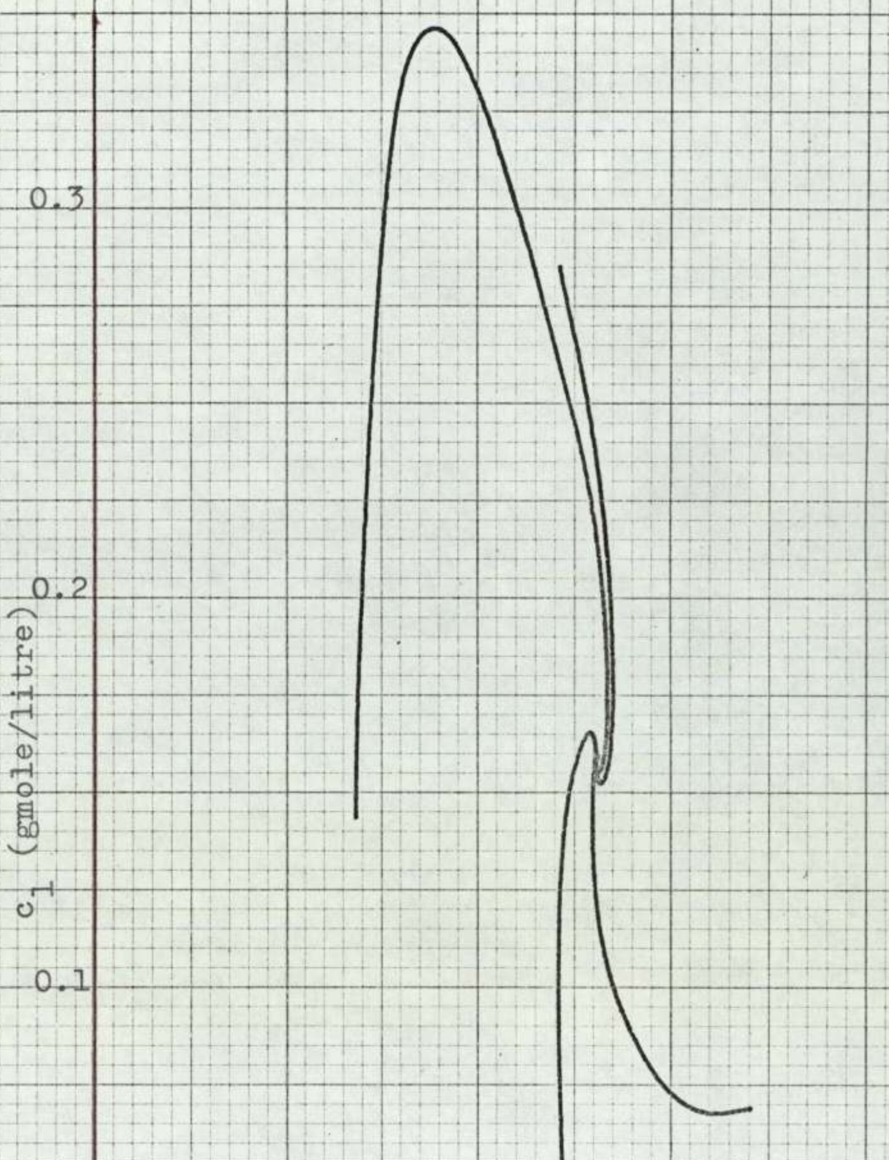

Fig.8.8. Experiment 67.

TR 10 Complete simulation phase-plane portrait

Concentration (c_1) vs. Temperature (T_1)

PBW 5 deg C.

8.7. Tests conducted on the automatic control valve and three-term recorder controllers

Initial tests established a hysteresis relationship existing between controller output pressure to the control valve and flowrate of water through the valve. This was eliminated by means of a valve positioner but hysteresis was still found to be present in the controller response, i.e. in the relationship between monitored temperature and output pressure.

8.7.1. Experimental procedure to calibrate the controller and control valve actions

The controller was used to control the temperature in the tank while the computer and servomechanism were rendered non-operational. The conditions for the tests were as follows:

Constant: Variac setting
Stirrer speed
Feedrate (except when employed to help force system)
Inlet coolant temperature
Inlet feed temperature

Coolant and feed temperatures were all monitored on the recorders and their steady values hence confirmed.

For Series 1 tests the proportional band width on the controller was set at 10 deg.C. The system was continually left under control but forced to a high or low temperature and then allowed to attempt to return to the original operating point with the original parameters under the control of the feedback loop. High starting temperatures were attained by switching off coolant and feed supply to the stirred tank which consequently heated up. Low temperatures were obtained by turning off the power supply to the variacs and by increasing the feedrate whilst disturbing the system. The system was tested both with and without the valve positioner in action. Readings of controller recorded temperature, controller output pressure and coolant flowrate were made during the approach to the final steady state and also at the final steady state. The first approach to the operating point was from a low temperature and the second from a high temperature. The system was also forced beyond the controlled operating point in order to obtain an extrapolation of the results. This was done by varying feed flowrate to obtain the controller's continuedresponse in that direction. This produced a better definition of the hysteresis because of the greater overlap of results from the two starting points.

Plots were then constructed between the following variables of the system for both cases of valve positioner acting and by-passed:

Controller output pressure vs. Coolant flowrate
Recorded temperature vs. Controller output pressure
Recorded temperature vs. Coolant flowrate

Series 2 and 3 tests were carried out for proportional band widths of 20 and 2 deg.C. respectively. Details of the results are given in the Appendix (Tables A.27. - A.30.). The graphs from Series 1 are presented in the text as examples for discussion. The remaining graphs are in the Appendix (Figs.A.49. - A.61.).

8.7.2. Consideration of the graphs obtained in Series 1 tests

(i) Controller output pressure vs. Coolant flowrate

Valve positioner not operating

Fig.8.9. shows the graph of the results obtained from Test 2 Series 1. The results clearly showed hysteresis and as a result two possible coolant flowrates are obtainable for a given controller output pressure depending only on whether the pressure is falling or rising. This was caused by factors such as packing box friction, valve plug and stem unbalance and diaphragm and spring hysteresis which cause the valve plug to assume a position which is not strictly proportional to the instrument signal.

Valve positioner operating

In this case a plot of the form shown in Fig.8.10. was obtained. The positioner had eliminated any hysteresis effect in the control valve.

The form of curve was as expected for the type of inner valve chosen (microflute) and also the cam employed in the valve positioner. This test therefore confirmed the effectiveness of the valve positioner.

It should also be mentioned that the valve positioner can adjust the stroke of the valve and hence the amount of coolant allowed to flow for a given controller pressure. For the setting chosen the superimposed plots were of the form shown in Fig.8.11. The dotted line could have been lowered or raised as desired by adjustment of a lever in the positioner.

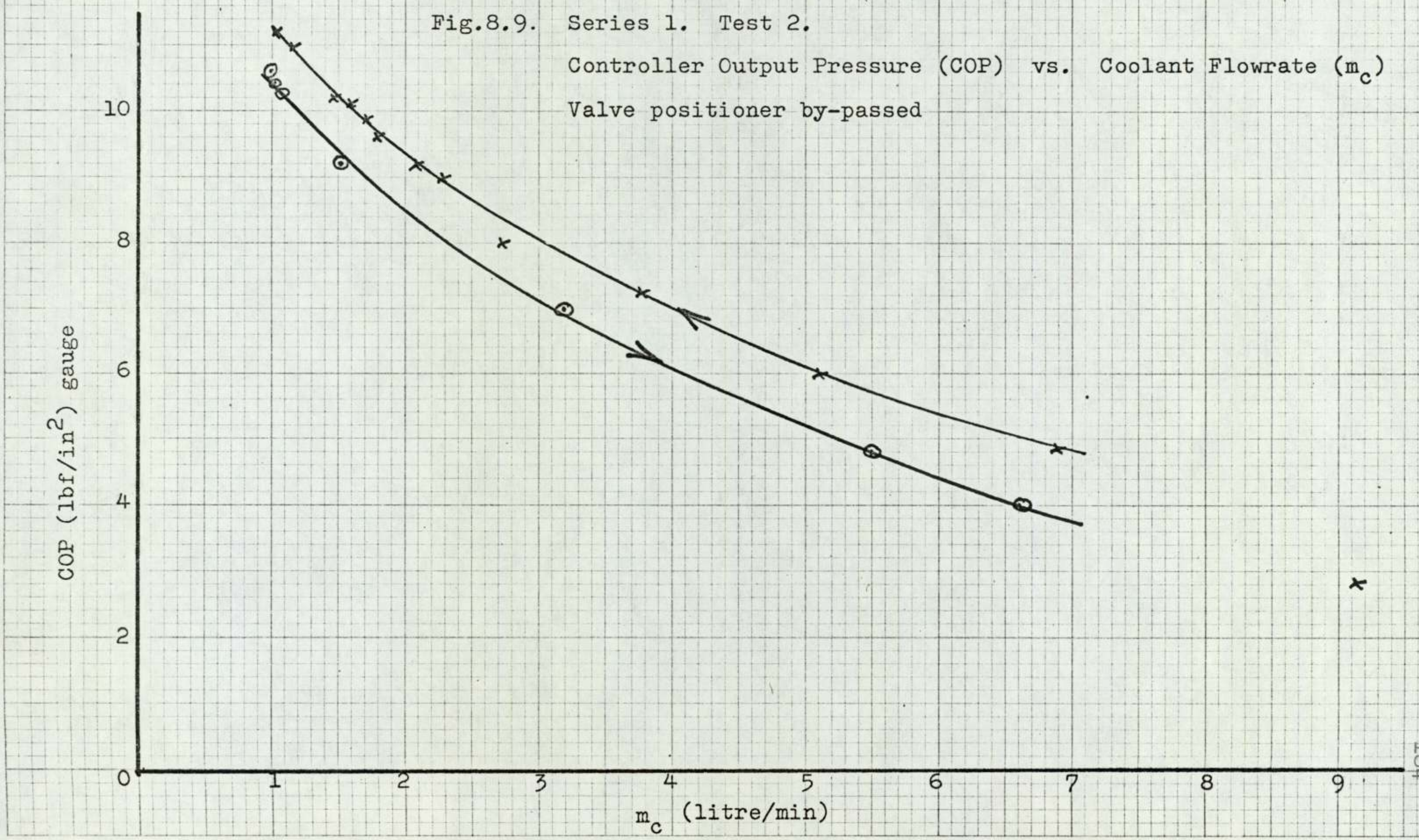
Fig.8.9. Series 1. Test 2.
Controller Output Pressure (COP) vs. Coolant Flowrate (m_c)
Valve positioner by-passed
COP (lbf/in^2) gauge
m_c (litre/min)
0
2
4
6
8
10
1
2
3
4
5
6
7
8
9

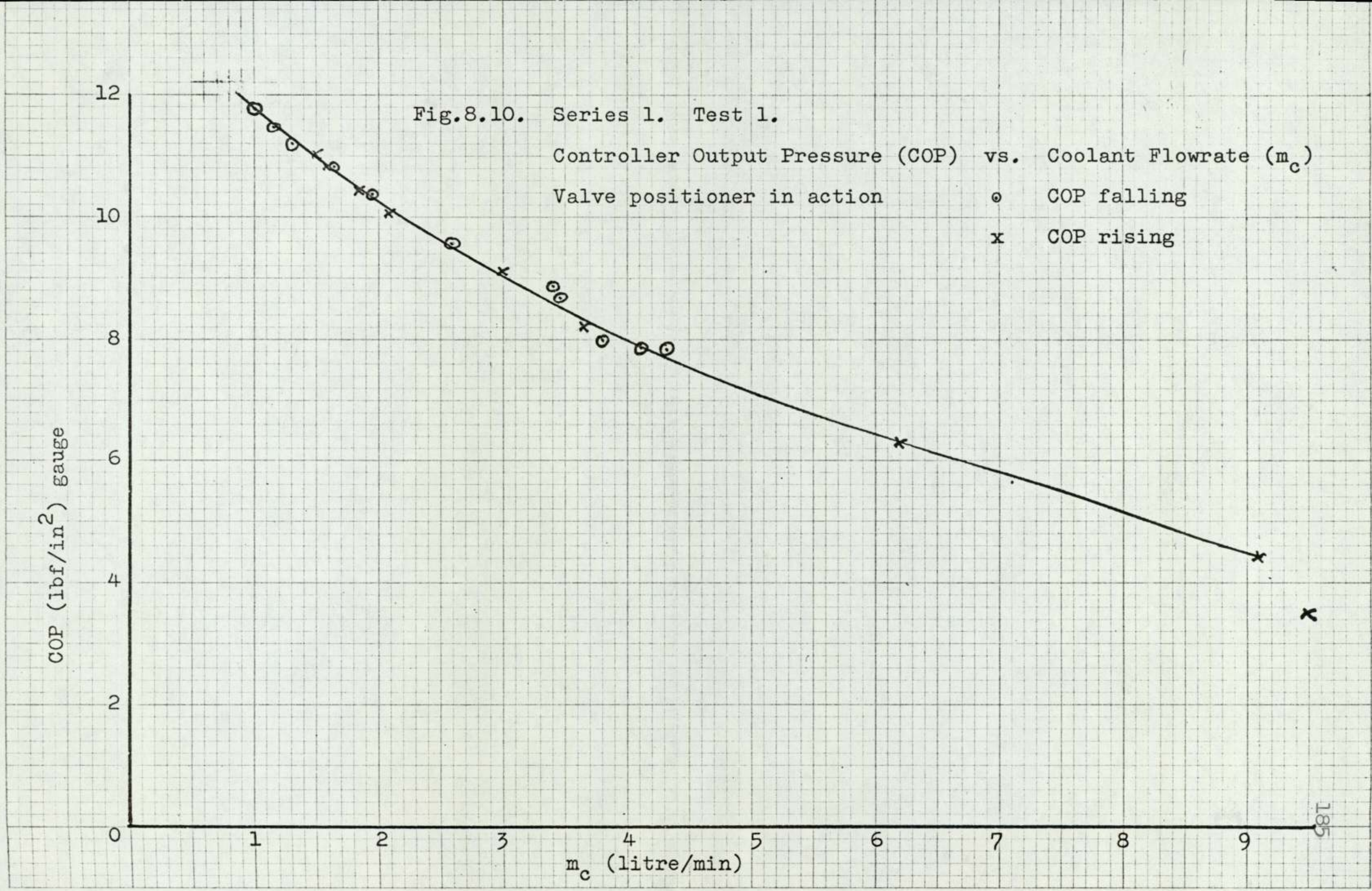

Fig.8.10. Series 1. Test 1.

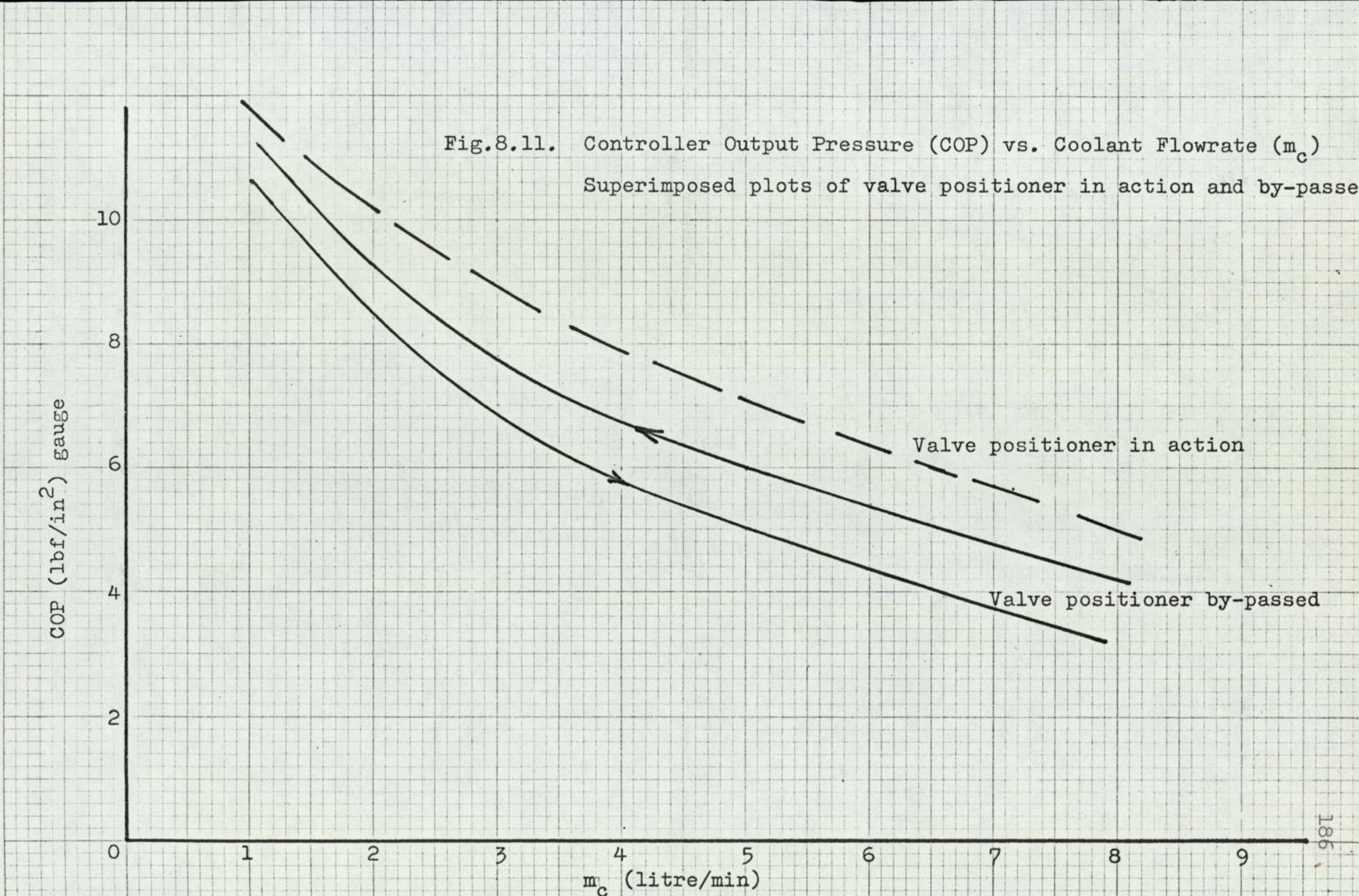

Fig.8.11. Controller Output Pressure (COP) vs. Coolant Flowrate (m_c)
Superimposed plots of valve positioner in action and by-passed

(ii) Recorded temperature vs. Controller output pressure

The only effect of the valve positioner is on the absolute value of output pressure from the controller. It was thought unlikely that there would be any other effects on these results due to the addition of the valve positioner. This was, however, checked in the plots produced and found to be the case. The graphs were of the form shown in Fig.8.12. The plots were linear to a good degree of accuracy. Again, however, hysteresis was present, i.e. two possible output pressures were obtainable depending on whether the temperature of the tank was rising from a low value or falling from a high value.

In Series 2 and 3 tests, proportional band widths of 20 and 2 deg.C. respectively were investigated. The hysteresis was found to be more pronounced for the narrow proportional bands and decreased as the band widened. This would be expected as the wider the proportional band the smaller the gain in terms of $lbf/in^2/deg.C.$ Thus for a narrow proportional band the effect of the dead band is larger on pressure output.

Despite the existence of the hysteresis in control action it should be stated that the effect was within the accuracy limit quotations for the apparatus. To improve the accuracy of the experiments a new controller was installed with a range of 0 to 100 deg.C. However, little if any improvement in hysteresis over the original controller was observed although again the accuracy was still within acceptable limits.

Results for the second controller are given in the Appendix (Tables A.34 and A.35, and (Series 10) Figs.A.66-69).

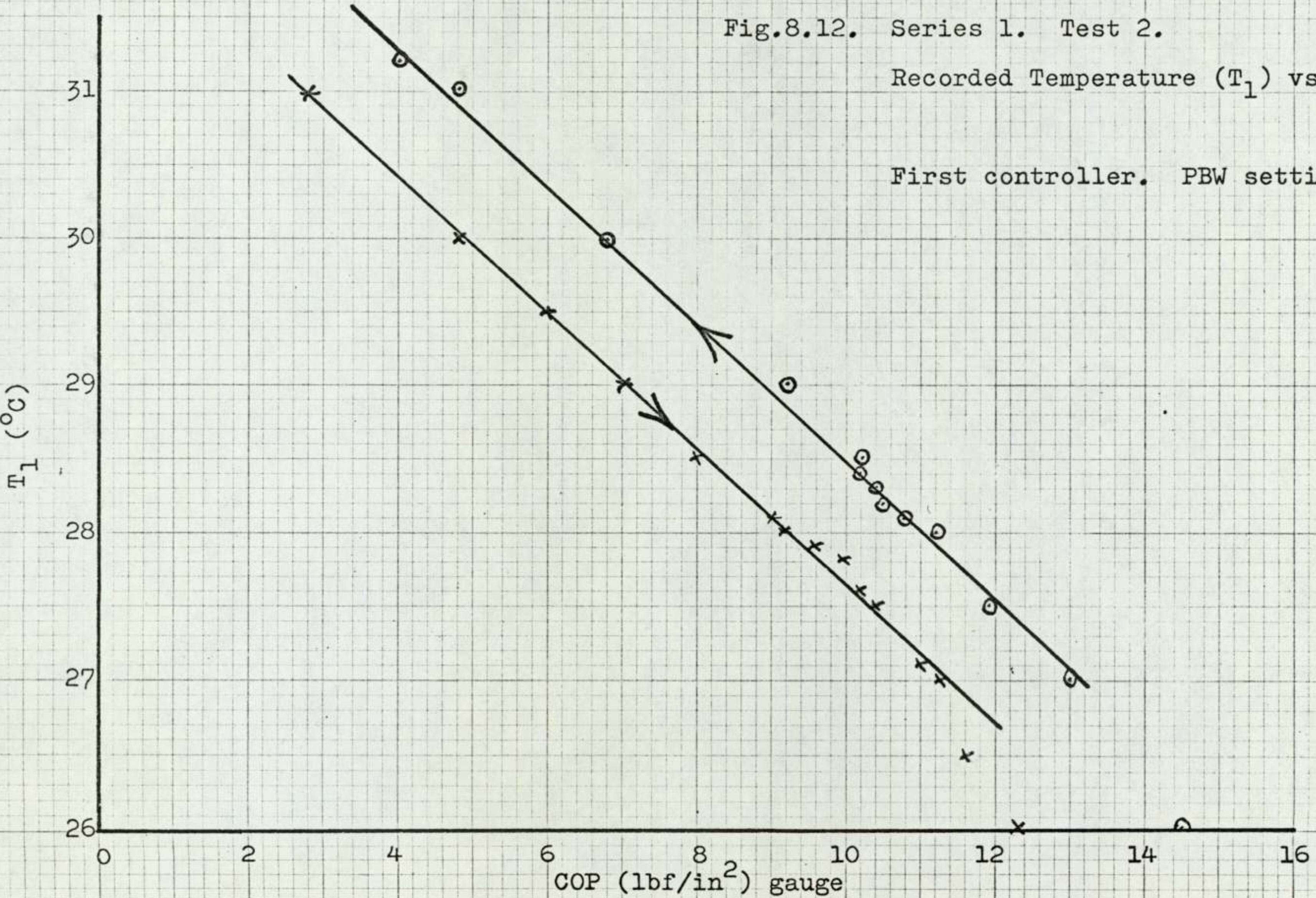

Fig.8.12. Series 1. Test 2.

Recorded Temperature (T_1) vs. Controller Output Pressure (COP)

First controller. PBW setting 10 deg. C

(iii) Recorded temperature vs. Coolant flowrate

Examples of the type of plots obtained are given in Figs.8.13. and 8.14. It was expected that hystereses would reinforce and this was indeed observed. With the valve positioner in action, the two lines were found to lie closer together than when it was by-passed. The combined effect of the two hystereses is readily observable.

Each test confirmed the general trend of results.

8.7.3. Further hysteresis consideration

The next problem was to explain why, although the high temperature trajectories homed on one state and the low temperature trajectories on another, finally the high temperature trajectories would slowly climb to the low temperature trajectories' steady state. This suggested that the latter was dominant and tests proved this to be so. e.g. If the trajectory approaching the lower temperature steady state overshot its target the reaction kinetics would start the servo-mechanism increasing the heat release again due to the high concentration and the dead band in the control system would be taken up before the coolant could be correspondingly increased. Thus the system could change branches of the hysteresis. This was found to be the case when going from high coolant rate to low coolant rate but not so in the reverse direction. This therefore explained the dominance of the high temperature steady state.

This was confirmed by an off-line test which was conducted simply by winding the variacs manually, instead of the servo in

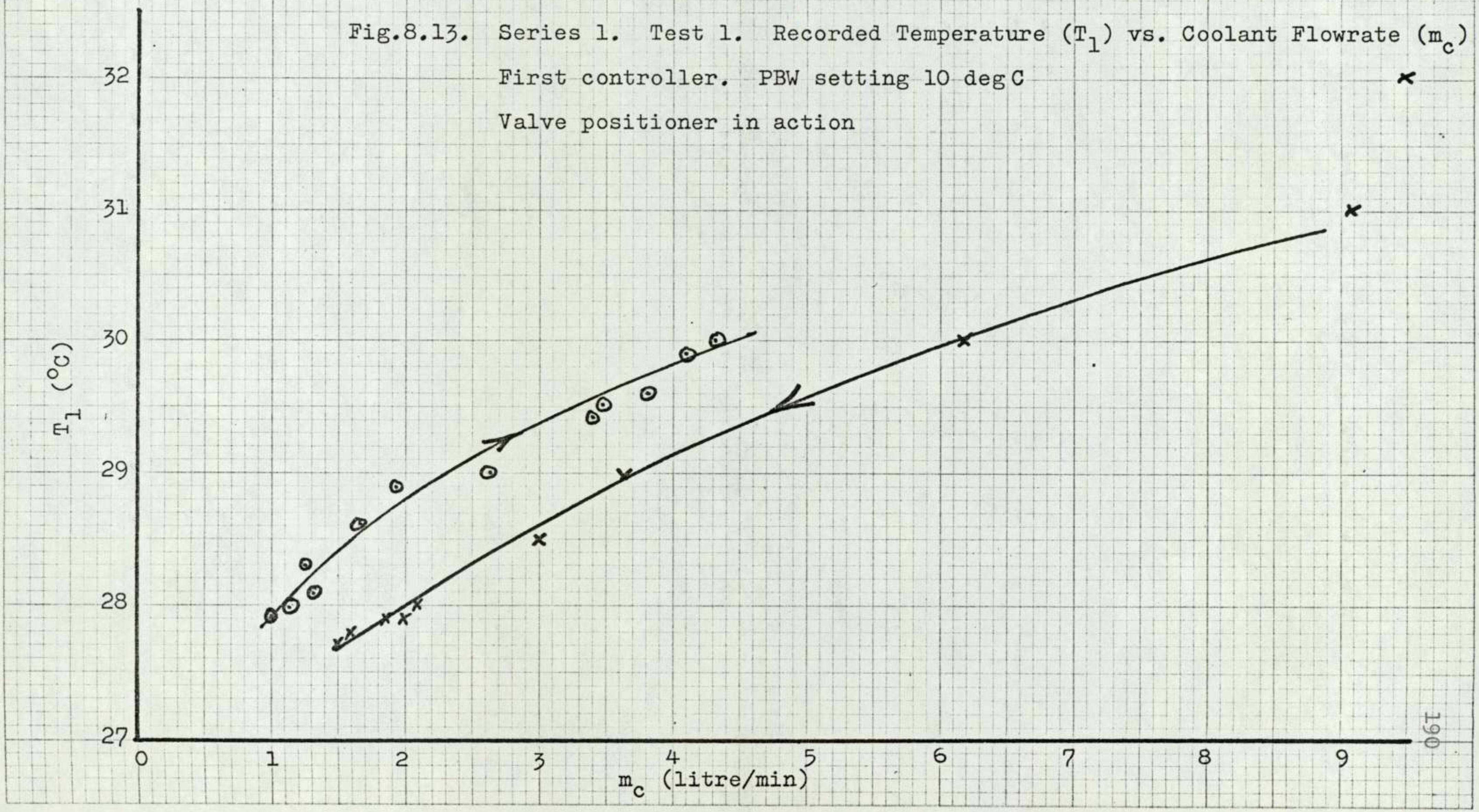

Fig.8.13. Series 1. Test 1. Recorded Temperature (T_1) vs. Coolant Flowrate (m_c)
First controller. PBW setting 10 deg C
Valve positioner in action

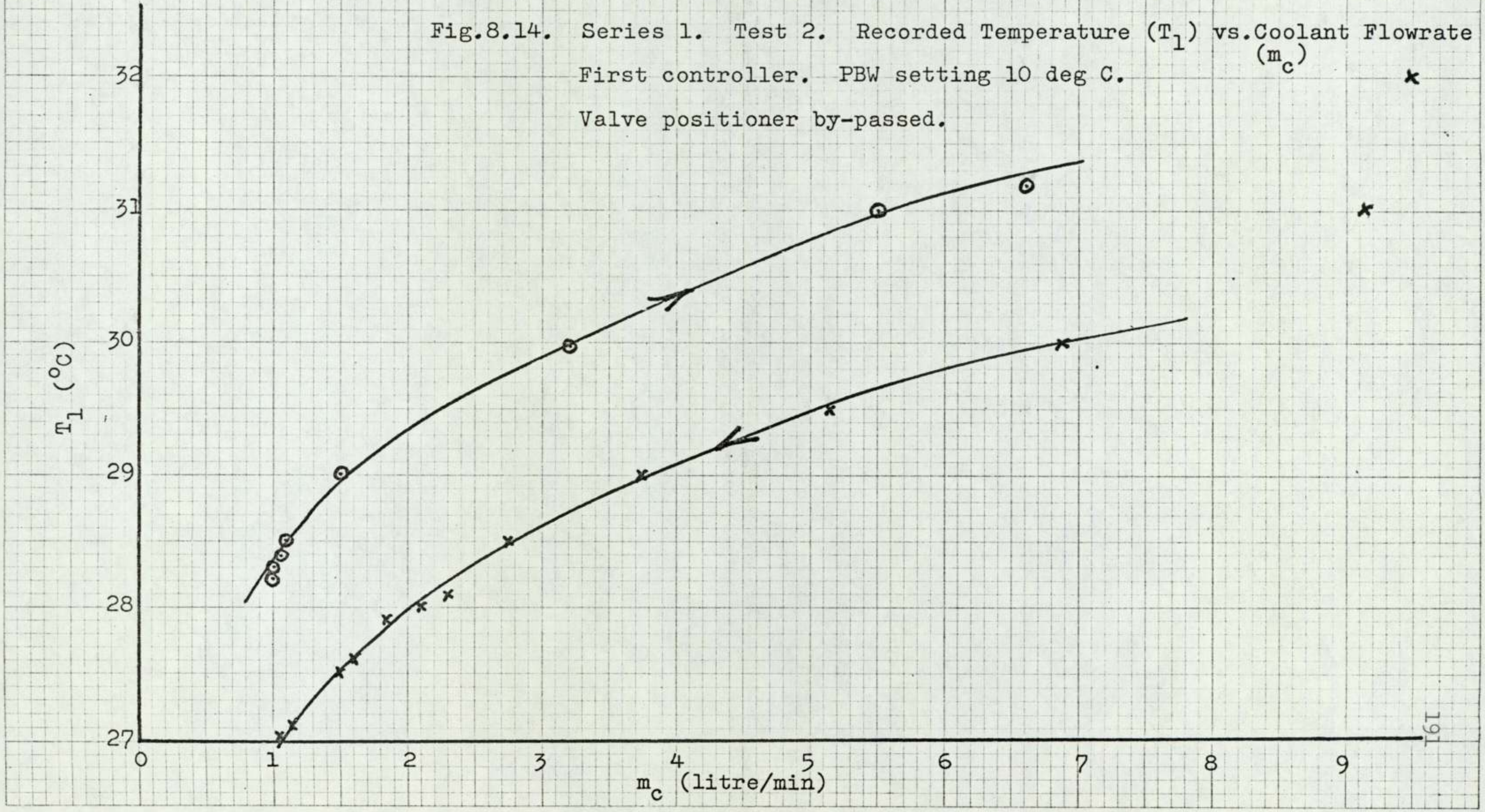

Fig.8.14. Series 1. Test 2. Recorded Temperature (T_1) vs. Coolant Flowrate (m_c)
First controller. PBW setting 10 deg C.
Valve positioner by-passed.

response to kinetics, to one side of a chosen variac value for a few seconds and then returning it to the original setting. Then the procedure was repeated in the opposite direction.

8.7.4. Controller drift

In some of the tests there was an indication of an overall very slow drift of controller set-point. This drift was in the opposite direction to the results recorded for hysteresis so there was no question of this being responsible for the hysteresis effect. In fact the drift would have tended to cause a diminishing effect on the hysteresis. One possible explanation of this drift was thought to be a warming up effect of the controller's electrical equipment. However very long runs of the order of many hours still showed a sustained drift even towards the end of the test. The controller was serviced by the manufacturers but some drift still persisted. The new controller which was installed later was also found to exhibit similar characteristics except for a drift in the opposite direction (Appendix page 436).

During the large majority of the partial simulation experiments zero or negligible drift took place. This was clear from the portraits obtained in that finally all trajectories approached a single steady state. As the portraits for the equipment under control usually only took between twenty minutes and half an hour to complete, this was not surprising when the low drift rate is considered. However, since the drift could not be eliminated, in later experiments the effects were monitored to confirm that the portraits had not been influenced. A portrait which was affected drastically by excessive drift is shown in the Appendix (Fig.A.34.) to illustrate that such effects can be readily detected.

The results obtained on controller set-point drift are given in the tests series 4 to 8. In Series 4 tests, a proportional band width of 10 deg.C. was set and the equipment was tested as in earlier runs but repeatedly in alternate directions. In this case the drift was found to be 0.25 deg.C./h or 0.4 lbf/in^2h. Test Series 5 was a repeat of Series 4 but with the valve positioner by-passed. The results showed that drift still occurred and a rate of 0.4 deg.C/h or 0.6 lbf/in^2h was recorded. Series 6 tested a 30 deg.C. proportional band and found a 1 deg.C./h or 0.8 lbf/in^2h drift rate. A longer test (Series 7) for the same conditions gave the rate at 0.8 deg.C/h. These rates would tend to diminish the measured hysteresis effect to some extent. The results also showed that drift was more rapid for wide proportional bands. Other test results are given in the Appendix (pages 416 to 436).

In conclusion, non-ideality of the controller performance must be considered as a combination of hysteresis and drift. However, these factors are usually distinguishable and hysteresis was generally found to produce the most significant effects.

8.8. Heat transfer coefficient vs. Coolant flowrate

In the complete simulation this was considered as part of the linear approximation of relationship between error and heat transfer coefficient. The calibration curve for the coolant flowrate, heat transfer relationship was as shown in Fig.8.15. A linear approximation will thus leave something to be desired and the partial simulation portraits must be interpreted with this in mind. Furthermore, the linear approximation will have a much more sensitive response of

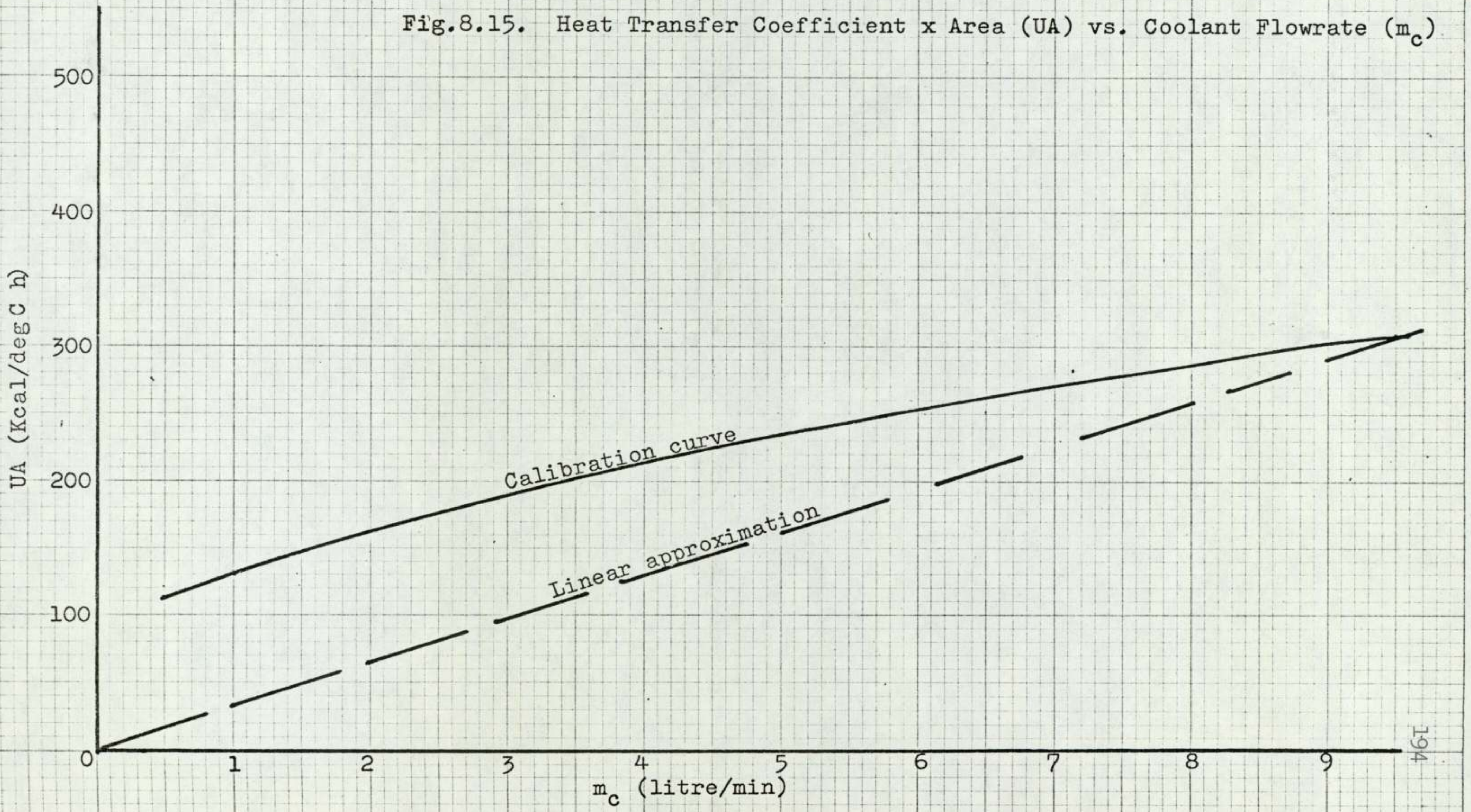

Fig.8.15. Heat Transfer Coefficient x Area (UA) vs. Coolant Flowrate (m_c)

heat transfer variation to coolant flowrate, and hence error from set-point, once the initial 0.5 litre/min. phase has been passed through. On the other hand as soon as the control valve is "cracked open" a significant heat removal can be assumed to be available. Therefore, initially, heat removal in reality will lead the linear approximation.

In general a less sensitive form of control is available in the real equipment.

8.9. Overall gain in the feedback loop

Assuming that the measurement gain is unity then the overall gain in the feedback loop is:

$$K = K_c K_v K_p \qquad \text{(Eq.8.20.)}$$

(see Fig.8.16.)

Omitting the hysteresis aspects initially, the gains may be established as follows and the hysteresis effects are incorporated at a later stage.

8.9.1. The controller gain (K_c)

This is the gain between the measured error and the output pressure from the controller.

$$K_c = \frac{\text{Output pressure (COP.)}}{\text{Error from set-point}} \qquad \text{(Eq.8.21.)}$$

For a 2 deg.C. proportional band width and an operating pressure range of about 7 lbf/in^2 then:

$$K_c = 3.5 \frac{\text{lbf/in}^2}{\text{(deg.C)}}$$

8.9.2. Valve gain (K_v)

This is the relationship between applied control pressure

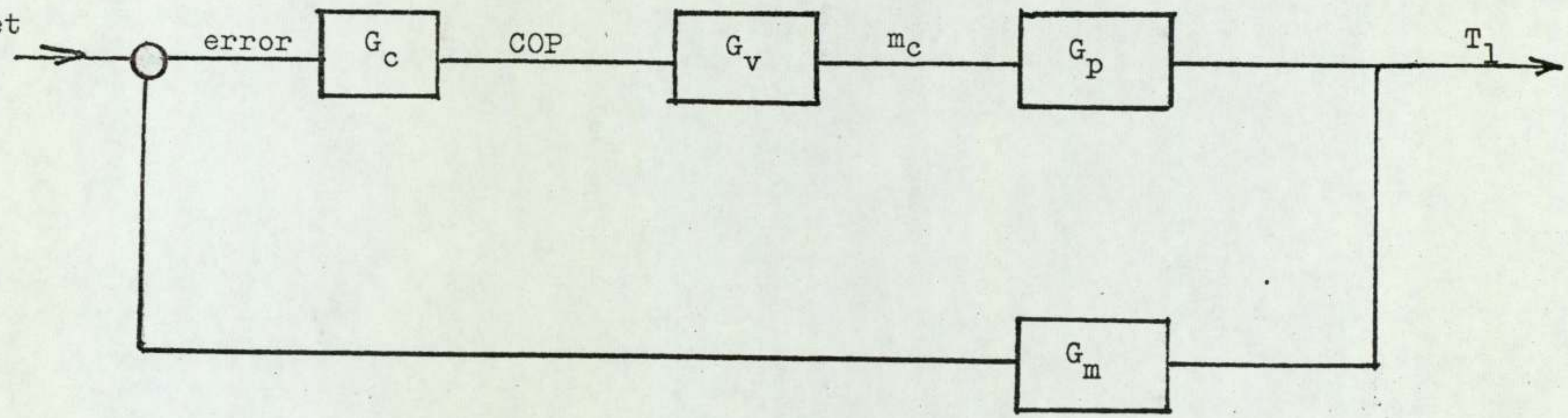

Fig.8.16.

and flow of coolant through the valve. The inner valve is of the microflute type having equal percentage characteristics. Using the 'A' cam in the valve positioner the characteristics of the valve plug are retained. The cam is shaped so as to produce a linear relationship between instrument pressure and valve travel. Other characterised cams which are available are intended to help solve stability problems caused by an oversized control valve or those problems resulting from the fact that the characteristic of the valve might not match the characteristic of the process controller. When one of the characterised cams is installed as the operating cam, the relationship between instrument pressure and valve travel is altered with the result that the characteristic will be changed in such a way that more or less instrument pressure increments will be necessary to create a given flow change.

As the inner valve is of the equal percentage type, it obeys the mathematical relationship:

$$u = u_o e^{nl} \qquad \text{(Eq.8.22.)}$$

where: u = flowrate

u_o = minimum controllable flow

l = valve travel

n = constant

The calibration curves of pressure vs. coolant flowrate have already been considered and as can be seen from Fig.8.17 a linear approximation to the curve does not involve excessive error.

Taking an operating range from 5 to 12 lbf/in^2 then the straight line law is:

$$u_c = K_v \times COP. + a_1 \qquad \text{(Eq.8.23.)}$$

where: K_v is the gradient

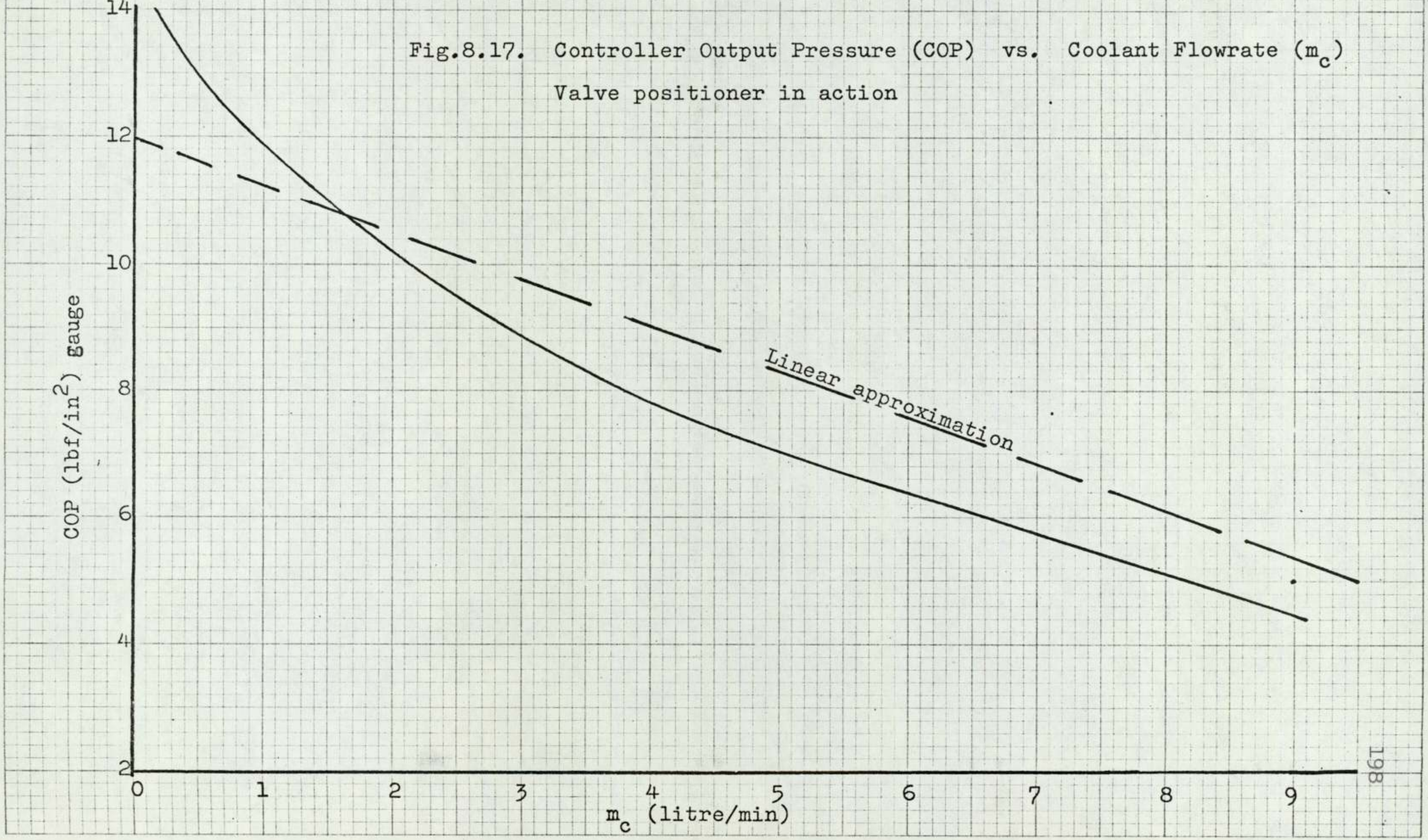

Fig.8.17. Controller Output Pressure (COP) vs. Coolant Flowrate (m_c)

Valve positioner in action

in which $a_1 = 0$ for the datum pressure 12 lbf/in^2 gauge (i.e. considered as a perturbation).

From the graph:

$$K_v = \frac{9}{7}$$

hence:

$$K_v = 1.29 \ \frac{\text{litre/min.}}{lbf/in^2}$$

8.9.3. Plant gain (K_p)

This is the gain between coolant flowrate and heat transfer coefficient x area.

$$K_p = \frac{\text{Heat removal/deg.C.}}{\text{Coolant flowrate litre/min.}} \qquad \text{(Eq.8.24.)}$$

Taking a linear relationship then the gradient can be obtained in perturbation variables from:

$$K_{p1} = \frac{UA_{max}}{m_{c\,max}} \qquad \text{(Eq.8.25.)}$$

In this case taking the calibration curve and extrapolating, a more representative line is:

$$UA = K_{p2}m_c + Z \quad \frac{Kcal}{h\,deg\,C} \qquad \text{(Eq.8.26.)}$$

where, from Fig. 8 . 15 .:

$$K_{p2} = \frac{200}{9} \quad \text{and the intercept } Z = 100$$

hence:

$$UA = \frac{200}{9} m_c + 100 \qquad \frac{Kcal}{h\,deg\,C}$$

In calories per second deg.C:

$$UA = \frac{200}{9 \times 3.6} m_c + \frac{100}{3.6}$$

$$UA = 6.18 \ m_c + 27.75$$

The direct linear approximation on the other hand gives: (from equation 8.25)

$$K_p = \frac{300}{9 \times 3.6}$$

$$\therefore \quad K_p = 9.27 \quad \frac{\text{cal/s deg C}}{\text{litre / min.}}$$

8.9.4. Calculation of the overall gain in the feedback loop

Using K_{pl} :

$$K_1 = K_c K_v K_{pl} \quad \frac{\text{lbf/in}^2}{\text{deg C}} \quad \frac{\text{litre/min}}{\text{lbf/in}^2} \quad \frac{\text{cals/s deg C}}{\text{litre/min}}$$

$$= 3.5 \times 1.29 \times 9.27$$

$$\therefore \quad K_1 = 41.8 \quad \frac{\text{cals/s deg C}}{\text{deg C error}}$$

or, from equation 8.26, then:

$$K_2 = 6.81 \times 1.29 \times 3.5 \text{ error} + 27.75$$

$$K_2 = 27.8 \times \text{error} + 27.75$$

These two overall gains were compared by feeding in values of error and checking the UA obtained. Graphs of UA vs. error are given in Fig.8.18. and illustrate the difference in the approximations between the intercept shifts.

A check for full proportional band should give identical values for the two approximations. Hence for 2 deg.C. proportional band width and 2 deg.C. set-point error then:

For linear approximation, non zero intercept

$$\begin{aligned} UA &= 27.8 \times \text{error} + 27.75 \\ &= 27.8 \times 2 + 27.75 \\ &= 83.35 \end{aligned}$$

Fig.8.18. Heat Transfer Coefficient x Area (UA) vs. Error from set-point

PBW 2 deg.C. (overall gain K)

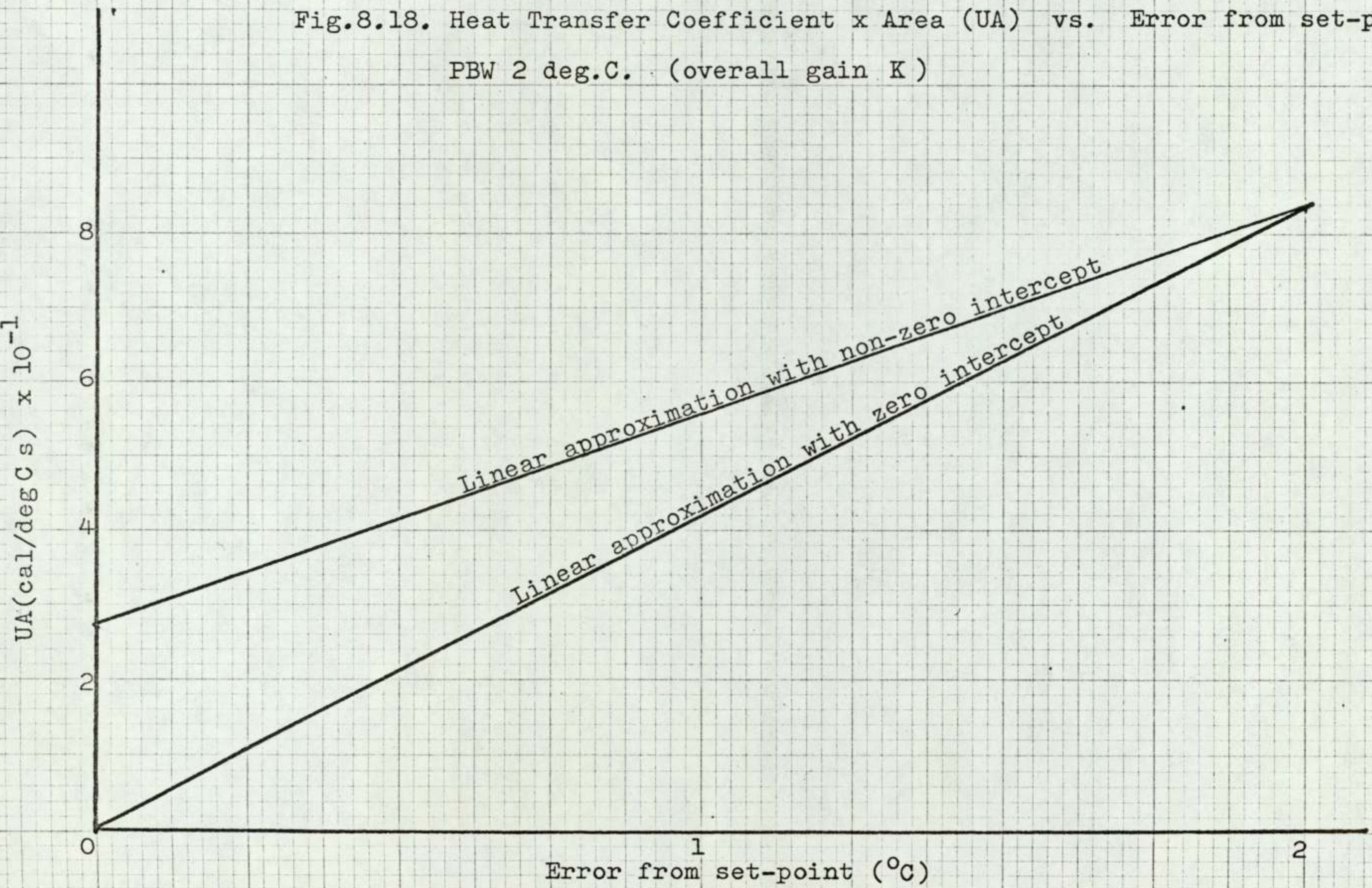

For linear approximation, zero intercept

$$UA = 41.8 \times \text{error}$$
$$= 41.8 \times 2$$
$$= 83.6$$

Thus the ratio of the operating gradients for complete and partial simulation is:

$$\frac{41.8}{27.8} \simeq 1.5$$

Therefore the sensitivity of control in the partial simulation will be one and a half times less than in the total simulation.

The addition of hysteresis effects leads to an even more significant difference between the two systems as can be seen in Fig.8.19.

8.10. Time delays in the feedback control loop

Time delays in controller, control valve and cooling coil dynamic response were considered in Sections 5.4. and 5.5. The total time lag can vary from 5 to 25 seconds depending mainly on the coolant flowrate and whether or not the valve positioner is in action or not. The general effect of the time delay in the feedback loop will be a decrease in its efficiency and a tendency to accentuate the hysteresis effects. Therefore there will be a reduction in system stability and controllability.

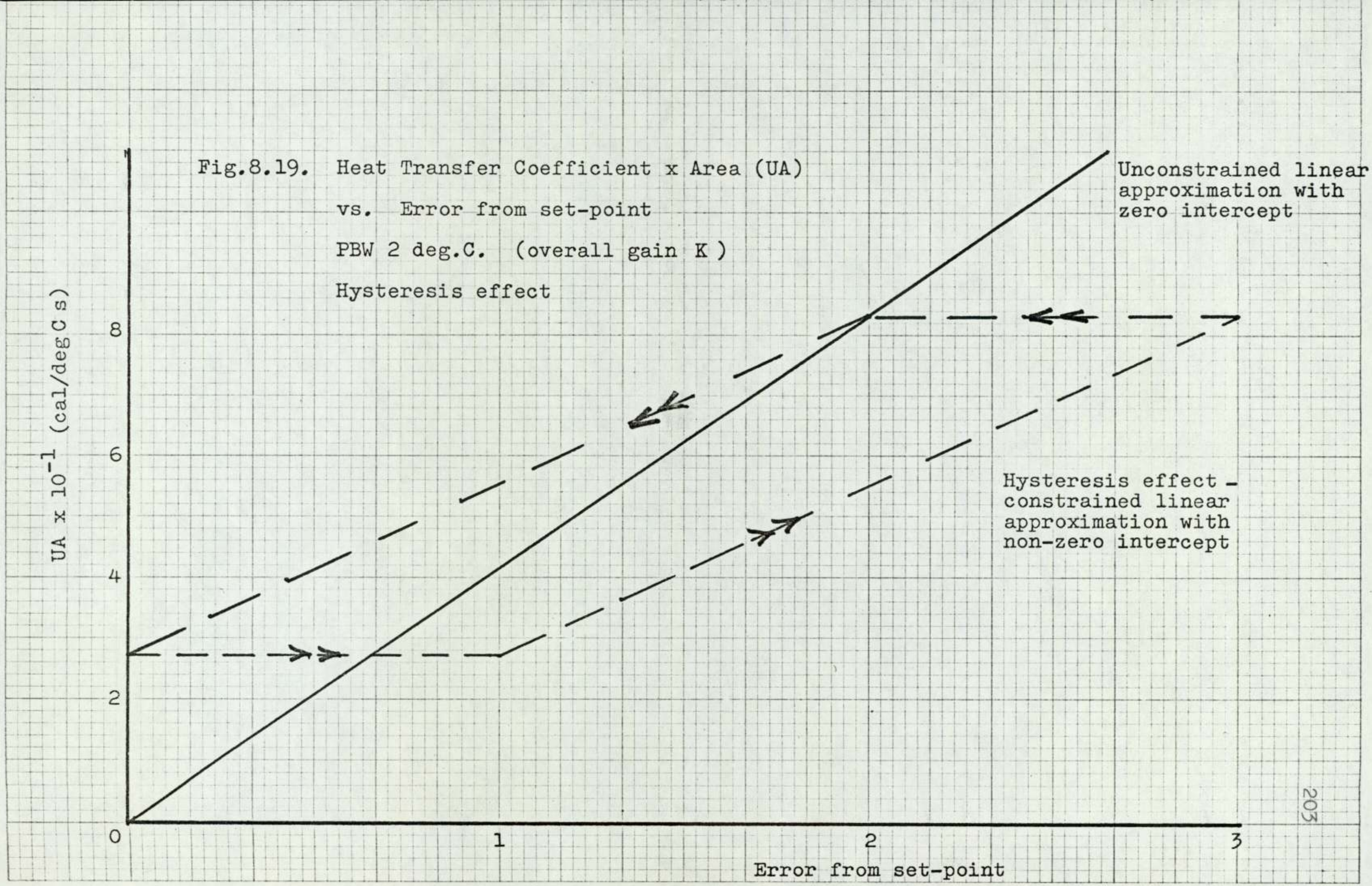

Fig.8.19. Heat Transfer Coefficient x Area (UA) vs. Error from set-point PBW 2 deg.C. (overall gain K) Hysteresis effect

8.11. Continuation of the analysis of the partial simulation results for the system under proportional control

8.11.1. Comparison between partial and complete simulation phase-plane portraits of Experiment 67

(Proportional band width 2 deg.C.)

Having considered the true variable relationships in the feedback controlloop of the real system the consideration of the results obtained can now be continued. Therefore the discussion on the portraits produced from Experiment 67 is resumed.

8.11.2. Consideration of particular trajectories in Experiment 67's phase-plane portraits

The four trajectories in the various simulations are identified by the letters A, B, C and D for explanation purposes. C and D will be considered in turn and the complete and partial simulations compared and their differences explained.

Partial simulation case (Fig.8.6.)

The initial condition for trajectory C was below the set-point and therefore at that stage the coolant would be turned off.

Initially the concentration rises rapidly and as a result of this the heat generation increases and consequently the temperature in the reactor starts to climb. This in turn increases the amount of heat released. Eventually the temperature in the tank passes the set-point value whilst the computed reactor concentration is still higher than that appropriate to the final steady state. Consequently the heat generation continues to rise and the trajectory overshoots its target temperature whilst the reactant concentration continues to fall rapidly. When the set-point was passed, the coolant flow was turned on at a rate determined by the hysteresis action appropriate. To assist the explanation of this action a diagram has been drawn to illustrate the effect (Fig.8.20.). As shown the coolant flow will remain at zero until the highest temperature curve of the hysteresis cycle is reached. It then flows at the low flowrate according to the curve and consequently the reactor temperature is allowed to overshoot the set-point until finally sufficient coolant is demanded to prevent further temperature rise in the reactor. As the concentration drops, the heat generation falls and the coolant flow starts to fall off and, after taking up the dead band, it now follows the high flowrate/low temperature branch of the hysteresis curve and the trajectory approaches the steady state appropriate to this control action. If the plot had been continued then again due to overshoot there would have been a final reversal to the high temperature steady state which is the dominant one of the two. Many other portraits illustrated the reversal but for clarity of presentation, this experiment was not pursued further than shown.

Trajectory D had an initial condition of temperature well above the final steady state value. Thus the coolant flowrate started on the maximum value, the reactor temperature fell rapidly and again overshoot of the final steady state occurred. Consequently the coolant was shut off, or very much reduced, and the temperature in the tank allowed to stop falling. Due to the increasing concentration the heat generation increases and the temperature in the reactor now climbs under the control of the low flowrate branch of the hysteresis curve, after taking

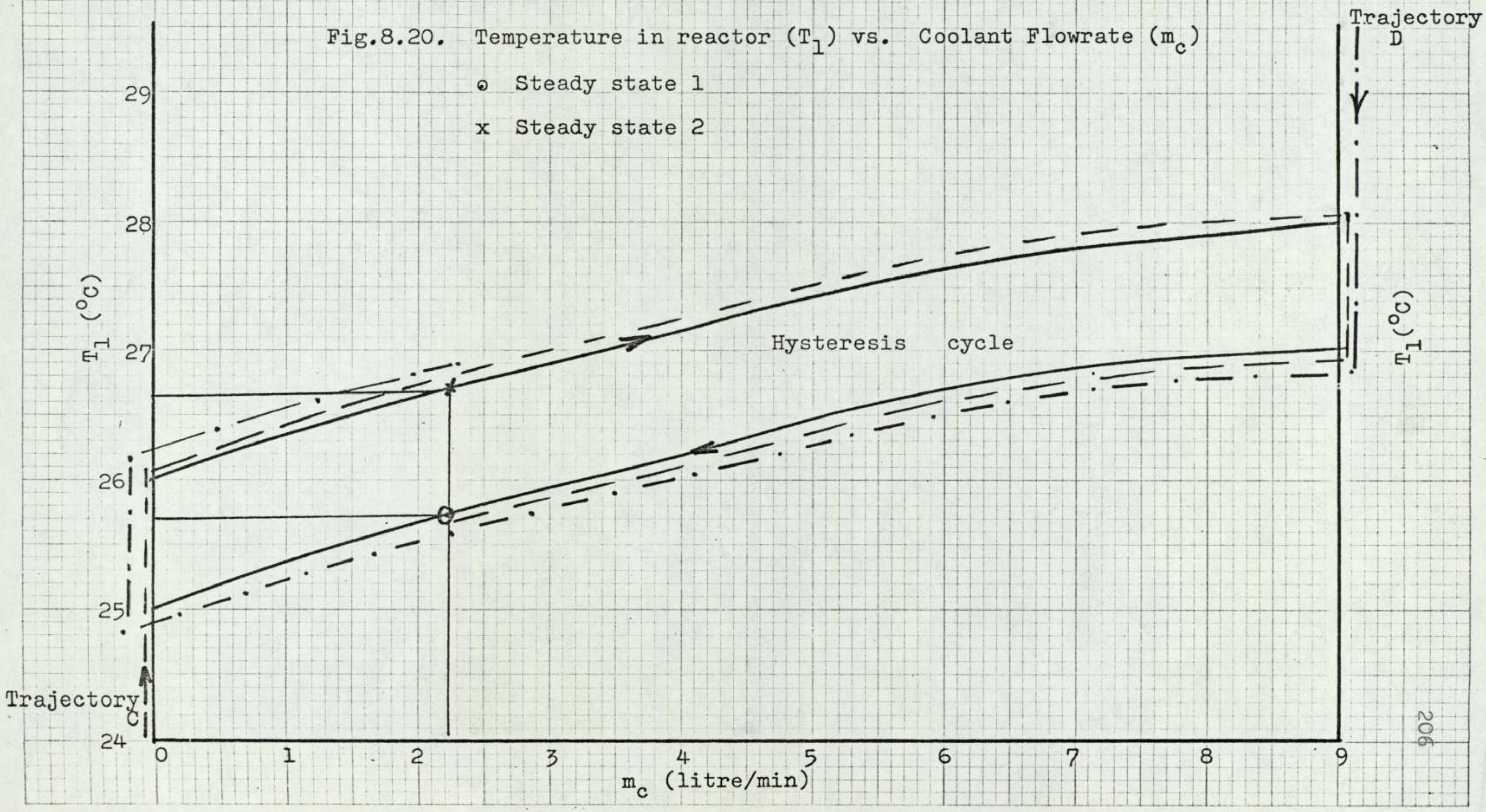

Fig.8.20. Temperature in reactor (T_1) vs. Coolant Flowrate (m_c)
⊙ Steady state 1
x Steady state 2
Trajectory D
Trajectory C
Hysteresis cycle
T_1 (^oC)
m_c (litre/min)
24
25
26
27
28
29
0
1
2
3
4
5
6
7
8
9

up the dead band and thus the steady state attained is due to the latter control action, i.e. the high temperature / low concentration steady state.

The same sort of consideration could be given to the trajectories A and B which start from different initial conditions.

Complete simulation on the TR 10

Proportional band width 2 deg.C. (see Fig.8.7.)

The plot indicated strong proportional control with negligible overshoot in the control band. Inaccuracies in this simulation apart from the linear approximation arise in temperatures in excess of the proportional band above the set-point. Thus the trajectory D at 34 deg.C. initial condition will have the equivalent of about four times the heat removal ability of the real system. This is shown in the more rapid fall of the trajectory towards the steady state temperature. The 1 deg.C. proportional band width illustrates this effect even more clearly (Fig.A.42.).

The Hybrid simulation obtained at a later date gives a closer simulation as would be expected due to the logic constraints on the coolant (Fig.A.48.).

The lack of overshoot and duality of the steady state confirmed that such features were caused by the feedback loop in the real system. Trajectories at temperatures below the set-point and hence outside the control band are almost identical in the two simulations which lends further support to the argument that discrepancies are arising from control loop operation and not reaction kinetics or other system features.

Proportional band width 5 deg.C. (see Fig.8.8.)

This portrait gave a closer simulation of the high temperature trajectory D than did the other TR 10 complete simulation as the simulated heat removal available was on the whole quite close to the real amount available. Trajectory D can be seen to have a similar heat transfer feedback to the partial case by mathematical consideration. On a 5 deg.C. proportional band width there was available a range of heat removal of 0 to U_{max}. The set-point was at 23.6^{o}C and thus a steady state value of 25.5^{o}C was in the range expected. Above 28.6^{o}C the proportional band was exceeded and thus above this temperature apparent excessive removal rates were available on the computer. At 34^{o}C just over double the maximum was assumed for total simulation. This was much better than the 2 deg.C. band width case and for most of the length of the trajectory a much closer approximation to the real value was given. However, as the effective set-point was now 23.6^{o}C, more inaccuracies were present in the lower temperature trajectories because the coolant was turned on at a lower temperature. Furthermore, control action was weaker leading to more oscillation around the steady state and because of this the portrait looks quite similar to the partial simulation portrait. However whereas the oscillations were due to the weaker control action in this case, they were caused by the hysteresis and time lags in the real feedback control loop for the partial simulation case. The dead band and the time lags reduced the rapidity of the change of direction of the control action and the hysteresis made even the delayed values high or low in comparison to the corresponding values before the direction change.

In general it was concluded that the nonidealities in the feedback loop caused more overshoot of the steady state, particularly trajectories C and D, and there could be convergence to a choice of two distinct states by a trajectory depending on the particular hysteresis branch in operation.

8.11.3. Consideration of the partial simulation portrait obtained from Experiment 39(b) - Proportional band width 2 deg.C. (Fig.8.21.)

The conclusions are similar to those drawn from Experiment 67 but this portrait was included in the text to show further features which were not covered by that experiment. The general picture differs in that it was run with different mains water temperatures and also a different value of heat of reaction was chosen. The portrait agrees well with the earlier conclusions on real plant nonidealities and the effects of hysteresis are well marked. The complete simulation (Fig.8.22.) on the TR 10 compared well with the partial simulation portrait. A proportional band width of 5 deg.C. for the complete simulation was chosen as it produced a more realistic picture than the 2 deg.C. band width because of the many high temperature trajectories. In this plot the trajectories were plotted to their final target and thus the final return of the high temperature trajectories to the high temperature steady state after initially going to the low temperature state was recorded. The reason for the reversal, as mentioned earlier, is that the high temperature state is dominant. Any disturbance on the lower temperature state in the direction of the higher temperature state will result in the system reverting to the high temperature

Fig.8.21. Experiment 39(b)

Partial simulation phase-plane portrait

Concentration (c_1) vs. Temperature (T_1)

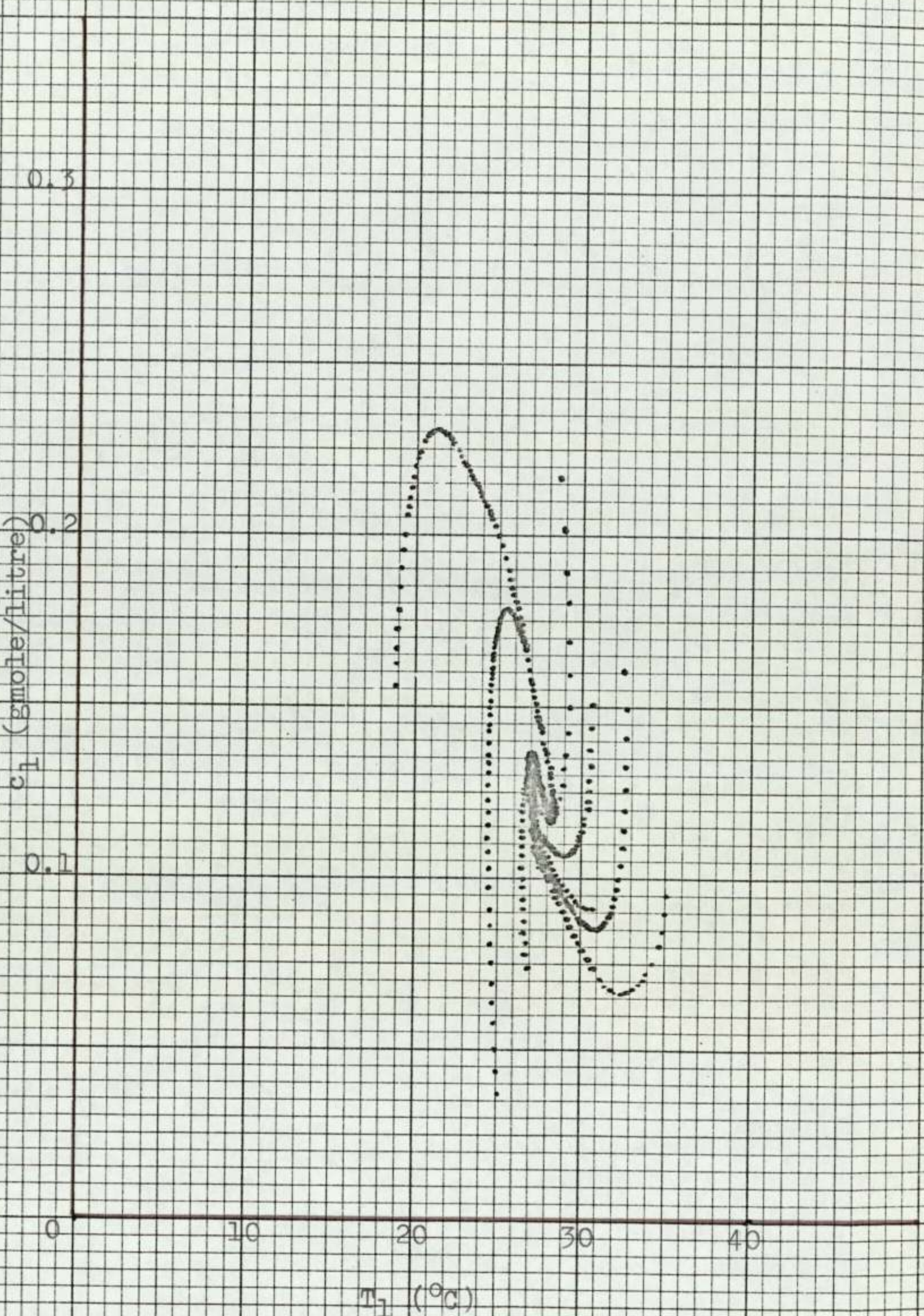

Fig.8.22. Experiment 39(b)

Complete simulation phase-plane portrait

Concentration (c_1) vs. Temperature (T_1)

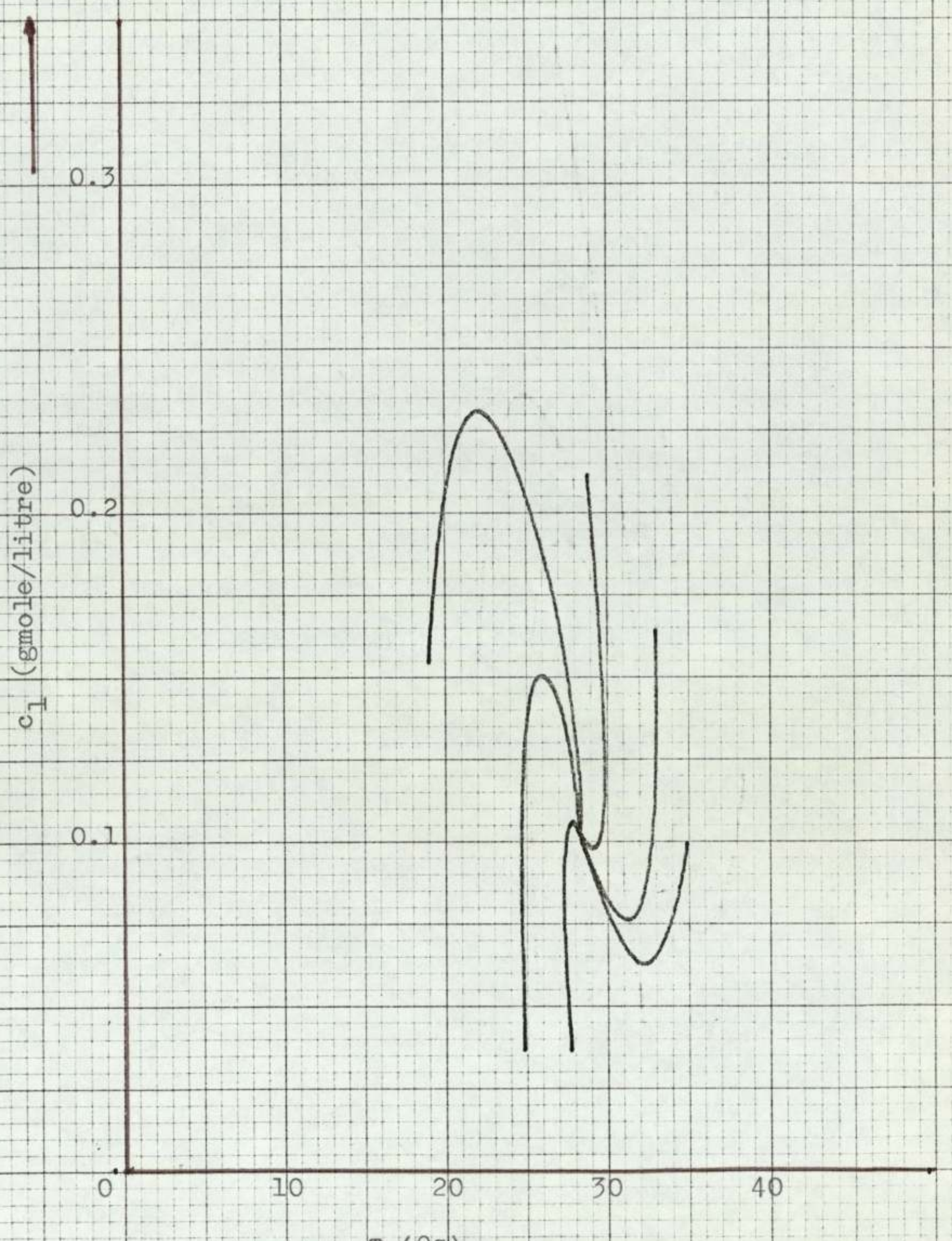

state. Nevertheless the lower temperature state is the original target for all the high temperature trajectories and has important influence until the vicinity of the two states is reached.

Another feature not shown, because of the choice of trajectories, in Experiment 67 was the intersection of trajectories due to the hysteresis effect. This can be seen on Experiment 39(b)'s portrait where both the trajectories starting from 28.6^{o}C and 27^{o}C intersect other trajectories on their way to the final steady state value.

8.11.4. Partial simulation portraits for a proportional band width of 5deg.C.

Experiment 58 gave a good example of this band width (Fig.8.23.). The complete simulation is given in Fig.8.24.

A similar portrait to Experiment 67 was obtained. The trajectories wind in a little more loosely due to the weaker proportional action. Hysteresis is well marked and the final return to the high temperature state shown.

The portraits considered to this point have had the valve positioner in action. An experiment was next conducted (Experiment 59) which had identical parameters set except that the positioner was by-passed (Fig.8.25.). Little if any increase in hysteresis effect was recorded. The only significant difference was a general steady state shift due to the change of valve stroke. It was therefore concluded that for proportional action only and this controller band setting the extra hysteresis effect and time delay caused by the control valve without the positioner was negligible. This conclusion was supported by the tests carried out on controller and control valve.

Fig. 8.23. Experiment 58

Partial simulation phase-plane portrait

Concentration (c_1) vs. Temperature (T_1)

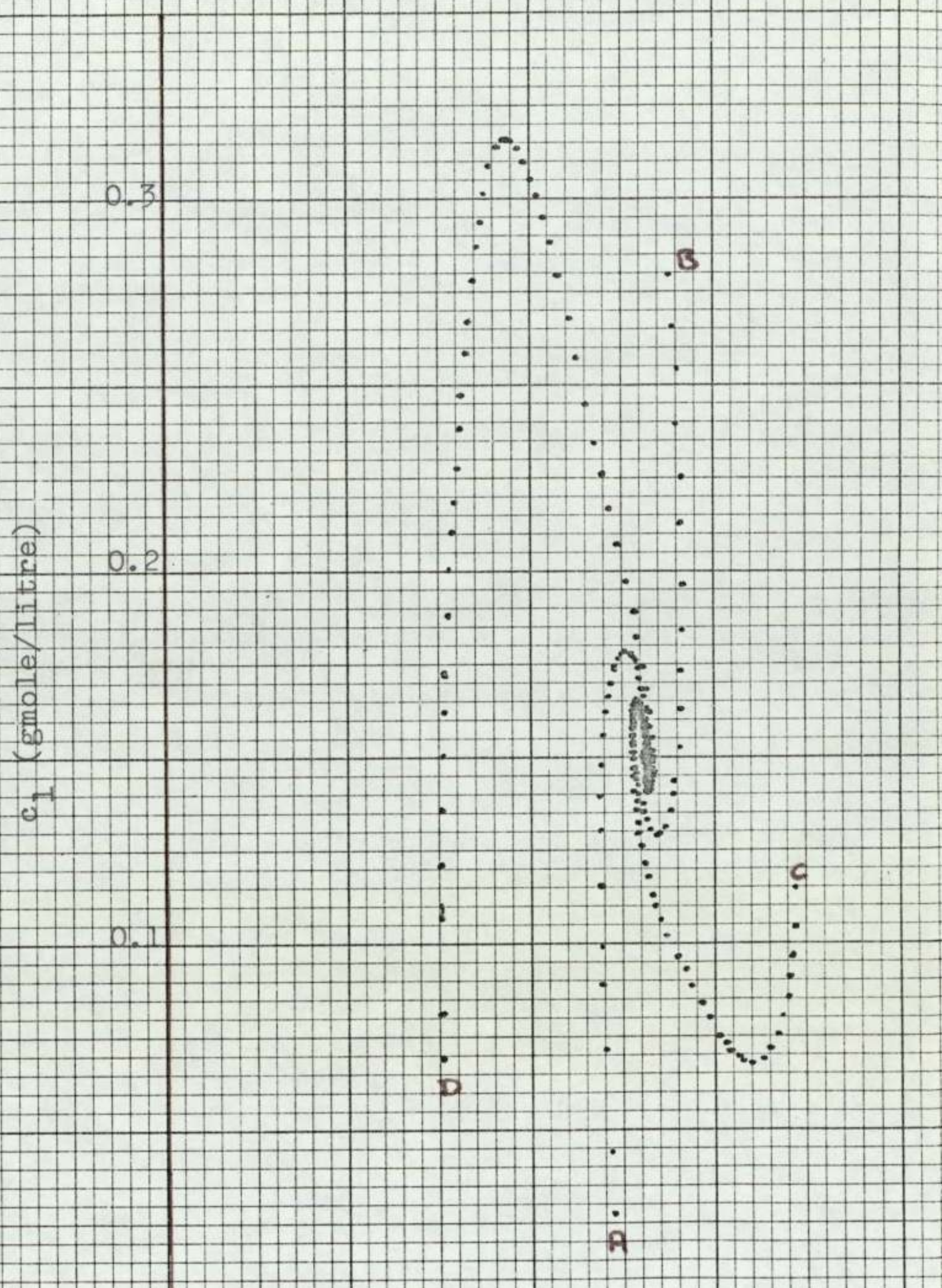

Fig.8.24. Experiment 58.

Complete simulation

Concentration (c_1) vs. Temperature (T_1)

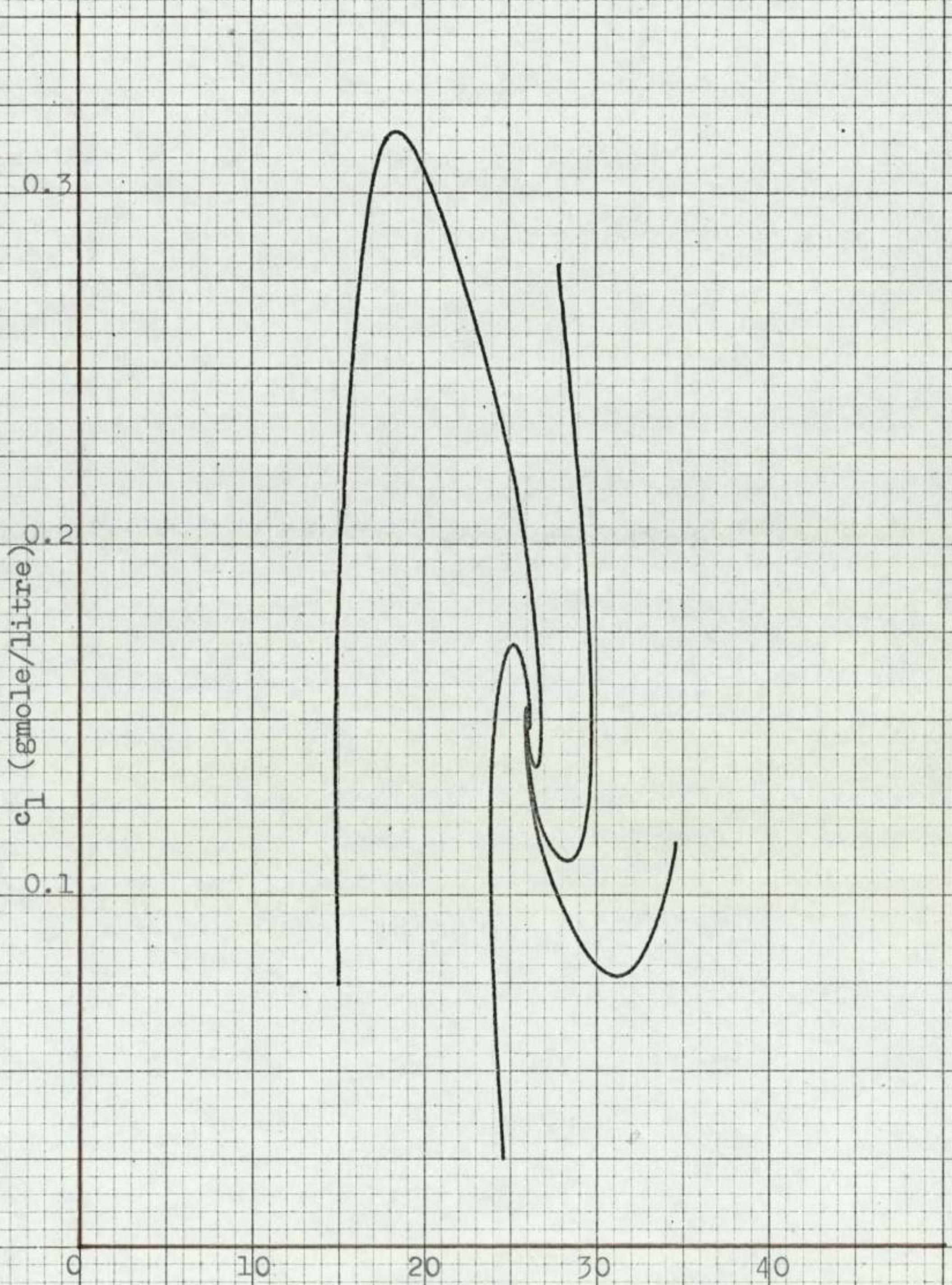

Fig.8.25. Experiment 59.
Partial simulation.
Concentration (c_1) vs. Temperature (T_1)

8.11.5. Partial simulation portraits for a proportional band width of 10 deg.C.

Experiment 40 (Fig.8.26.) gave a good example of this band width. The complete simulation is shown in Fig.8.27.

Due to the weaker control action the portrait shows a greater tendency for the higher temperature / concentration trajectories to overshoot. The trajectories approached the steady state at a much slower rate the whole dynamics being more retarded. The hysteresis effect was reduced but the two steady states were more marked due to the slow dynamics. Two separate steady state temperatures 0.7 deg.C. apart were recorded. The complete simulation compared well and clearly showed the differences of the ideal equivalent.

8.11.6. Partial simulation portraits for proportional band widths of 20 and 30 deg.C.

Experiments 65 and 82 gave portraits for a 20 deg.C. proportional band width and two different set-points (Figs. 8.28 and 8.29.). The complete simulations are given in Figs. 8.30 and 8.31. The simulations compare well and all show the weakness of the control action. When the partial simulations are compared with their corresponding complete simulations no hysteresis effect is detectable. This agrees with the results obtained from the controller when the hysteresis effect on a wide proportional band was measured (Fig.A.52.). Furthermore for such a wide proportional band little change in control action was demanded and the dynamic speed of the system was such that time lags in the feedback loop became small in comparison with the system response time. Therefore a good

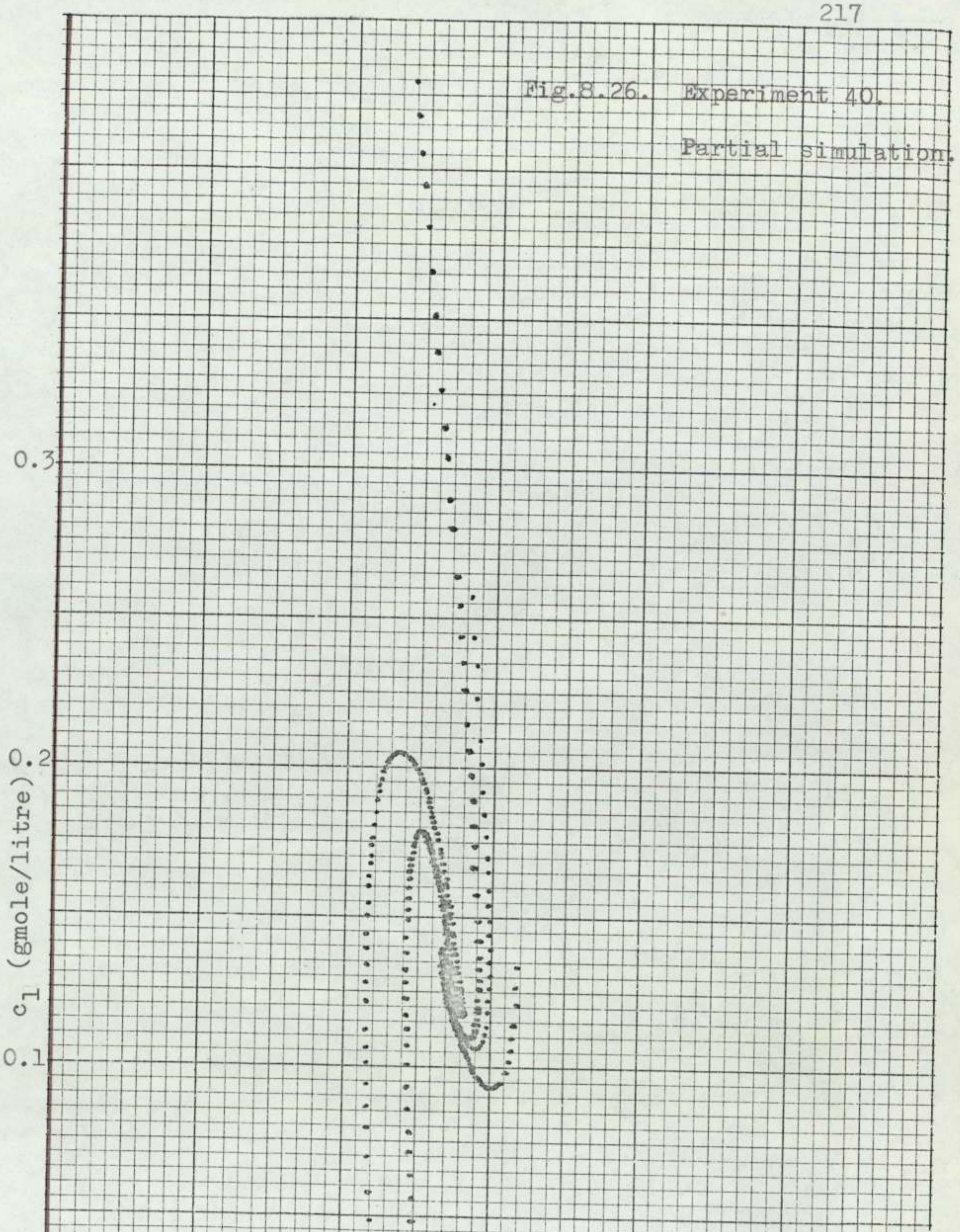
Fig.8.26. Experiment 40.
Partial simulation.
0.3
0.2
0.1
0
c_1 (gmole/litre)
10
20
30
40
T_1 (^oC)

Fig.8.27. Experiment 40.

Complete simulation

Concentration (c_1) vs. Temperature (T_1)

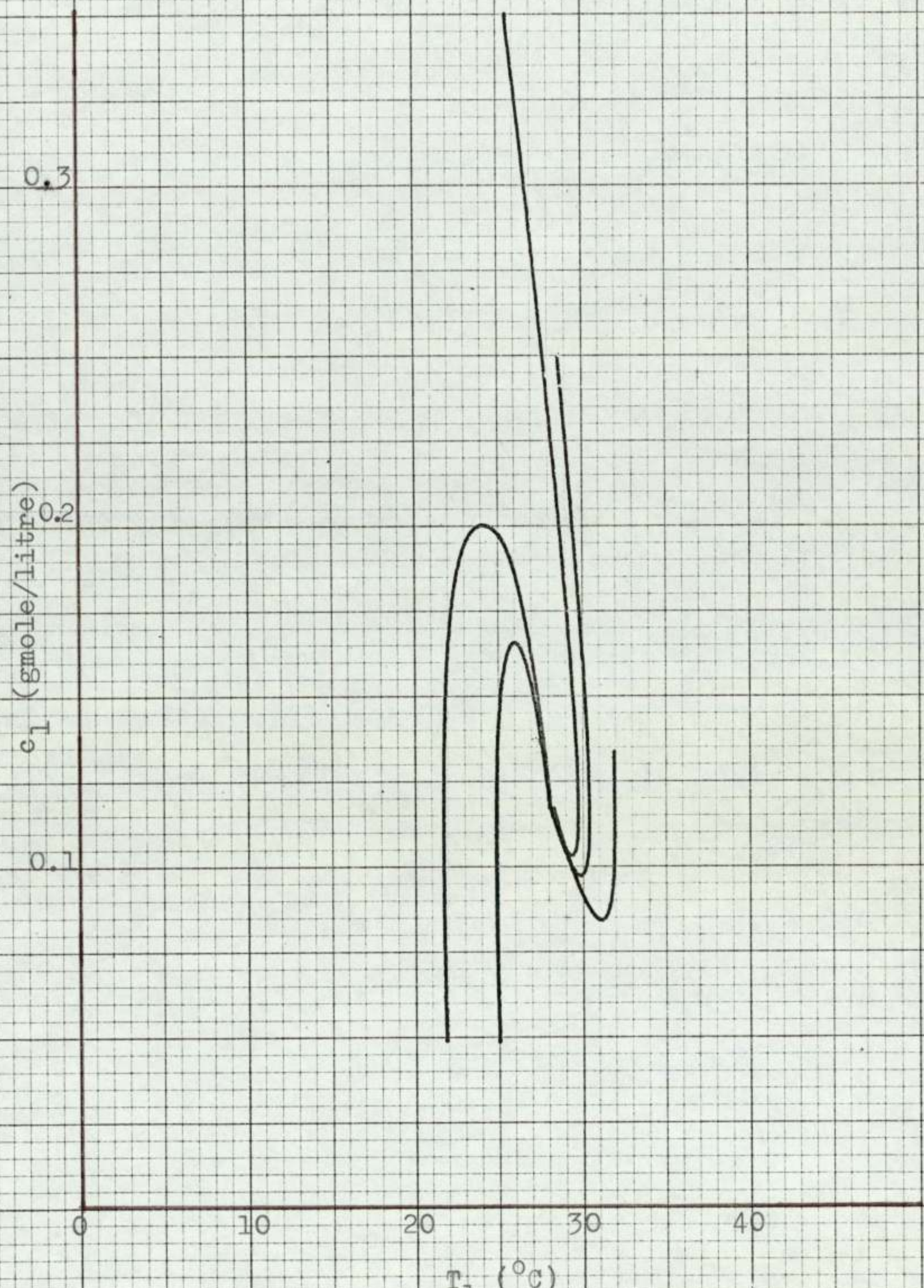

Fig.8.28. Experiment 65.

Partial simulation.

Concentration (c_1) vs. Temperature (T_1)

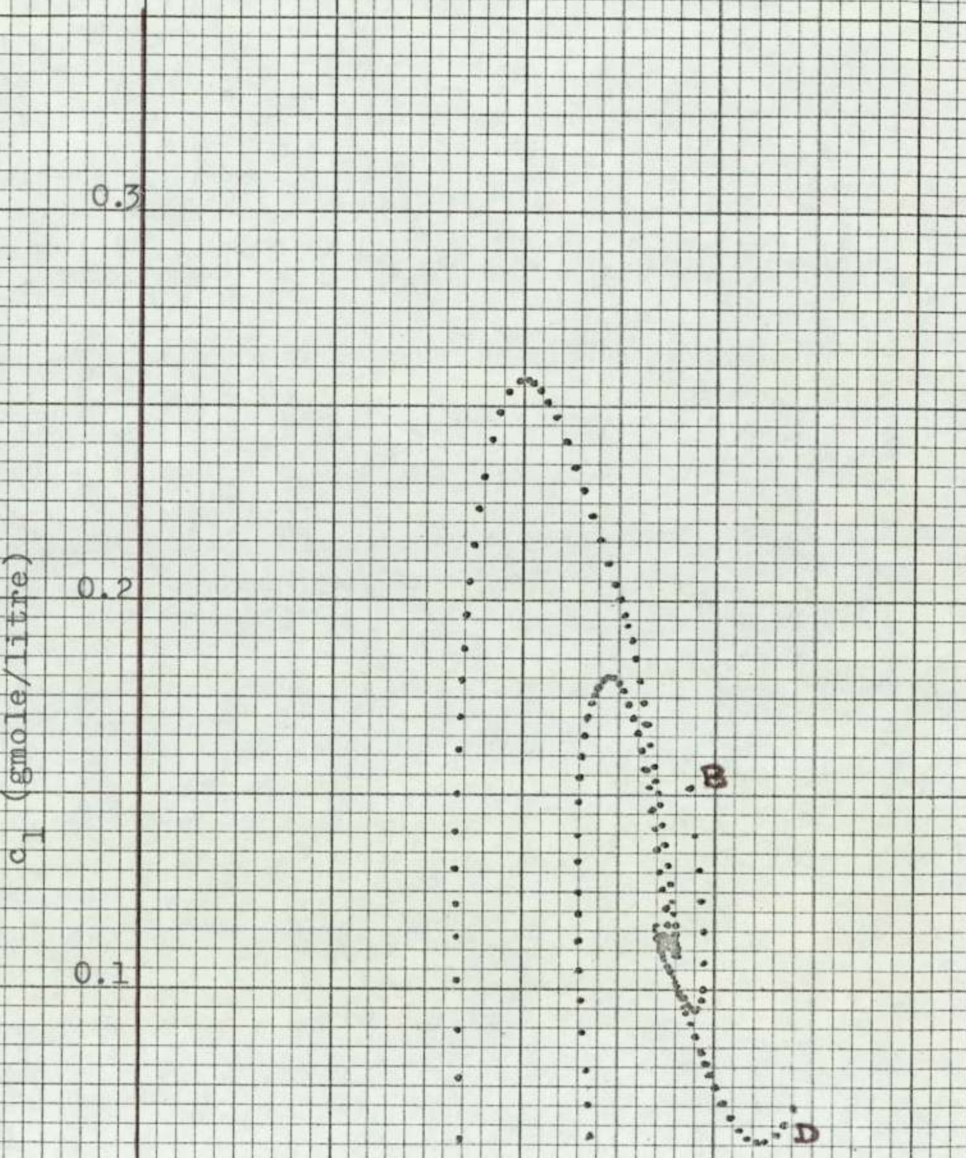

Fig.8.29. Experiment 82.

Partial simulation

Concentration (c_1) vs. Temperature (T_1)

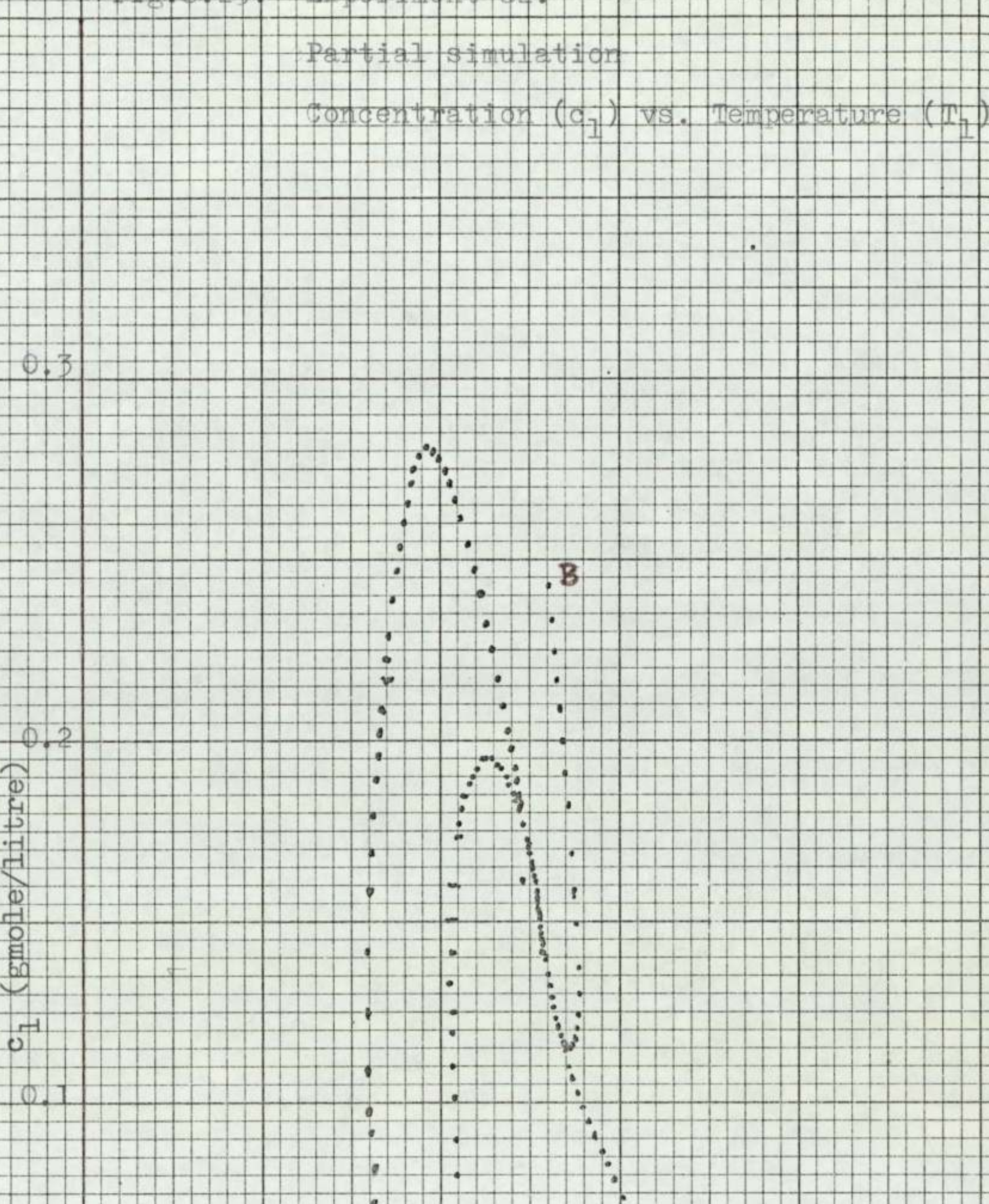

Fig. 8.30. Experiment 65.

Complete simulation.

Concentration (c_1) vs. Temperature (T_1)

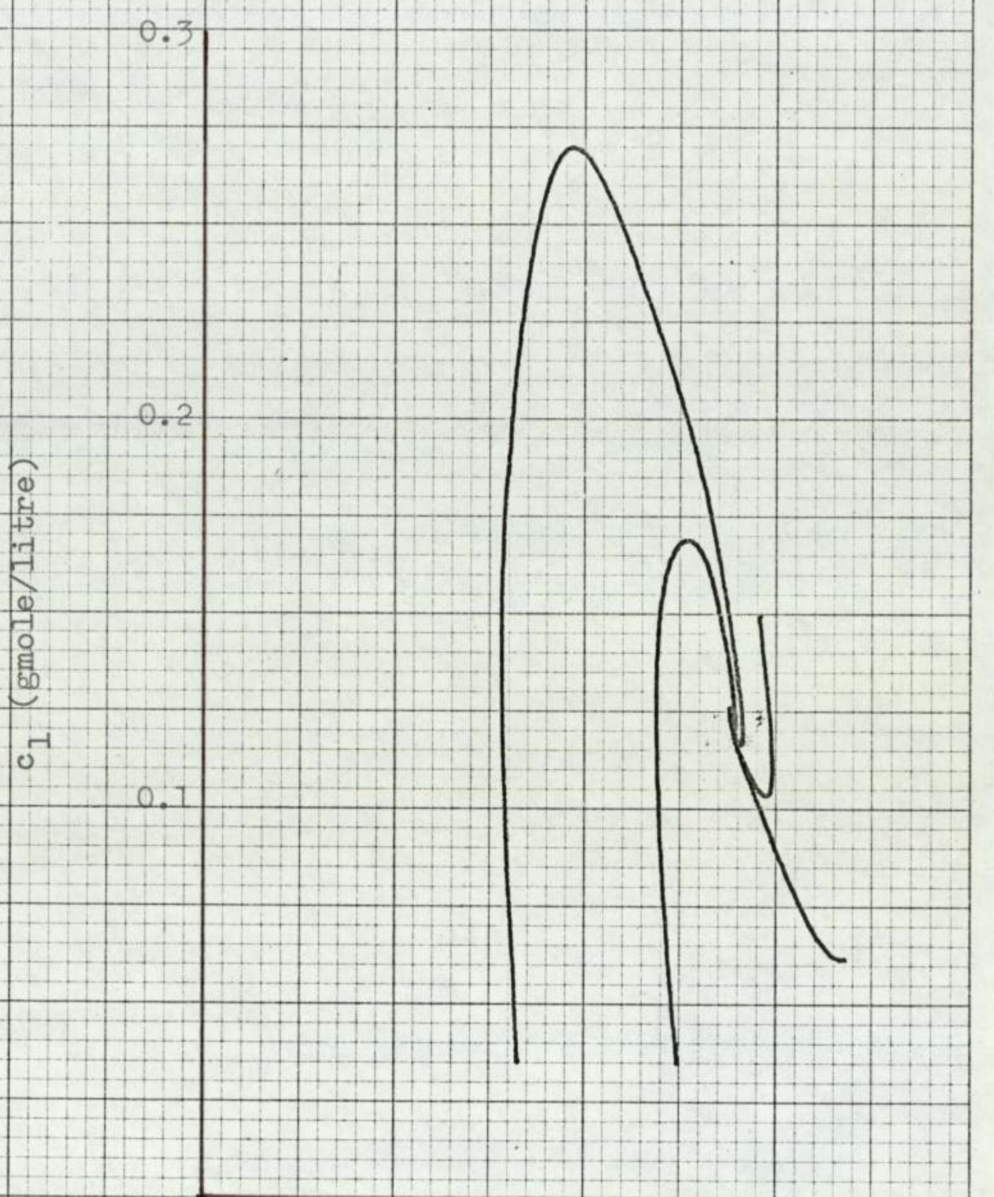

Fig.8.31. Experiment 82.

Complete simulation.

Concentration (c_1) vs. Temperature (T_1)

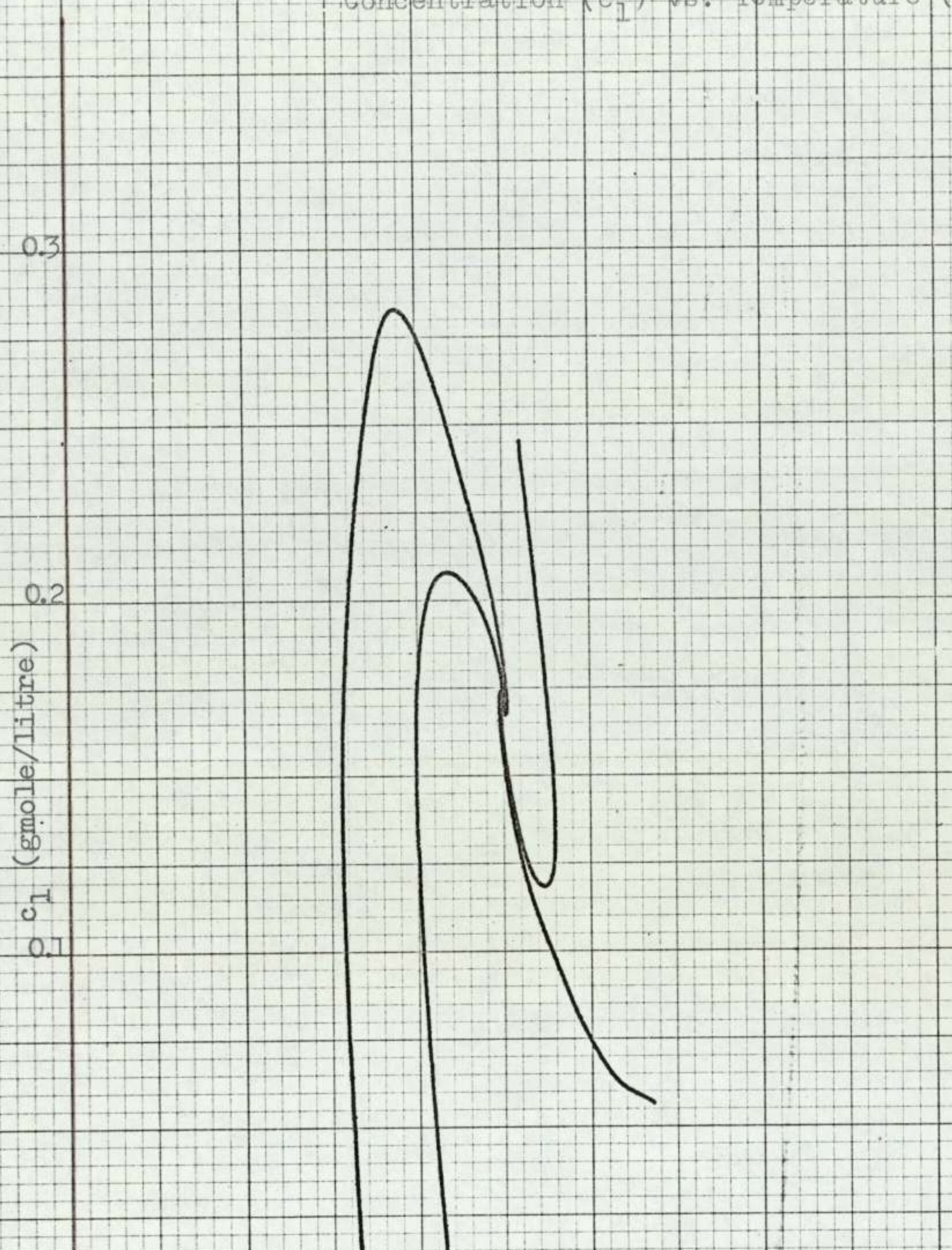

agreement between the portraits would be expected.

The proportional band width of 30 deg.C. was also tested and a comparison test done with the valve positioner by-passed (Experiments 56 and 57 - Figs.8.32 and 8.33.). Little if any hysteresis effect was recorded even with the positioner by-passed the only noticeable difference again being due to the general steady state shift. However, this is not surprising since, as can be seen from Fig.8.9. showing valve hysteresis, the effects are smallest at the lower flowrate / high pressure end of the graph. These were the conditions at the control point for this experiment. A complete simulation was also carried out which compared very well to the partial simulations (Fig.8.34.).

In general as the proportional band width was so wide the demand on the effectiveness of the feedback control loop was much reduced. Therefore the system approximated closely to the ideal case. On the other hand the efficiency of the approach to the steady state was low as it took a long time for the steady state to be achieved from the initial condition. The portraits now show much in common with the uncontrolled case and if the proportional band was much wider the control system would have effectively degraded to that case.

8.12. Results and analysis of the system under proportional plus integral control action

Varying amounts of integral control were added to various proportional bands. For strong proportional action the addition of integral control tended to strengthen the control. For weak proportional action the addition of integral action tended to cause oscillation and in the partial simulation oscillations

Fig.8.32. Experiment 56.

Partial simulation

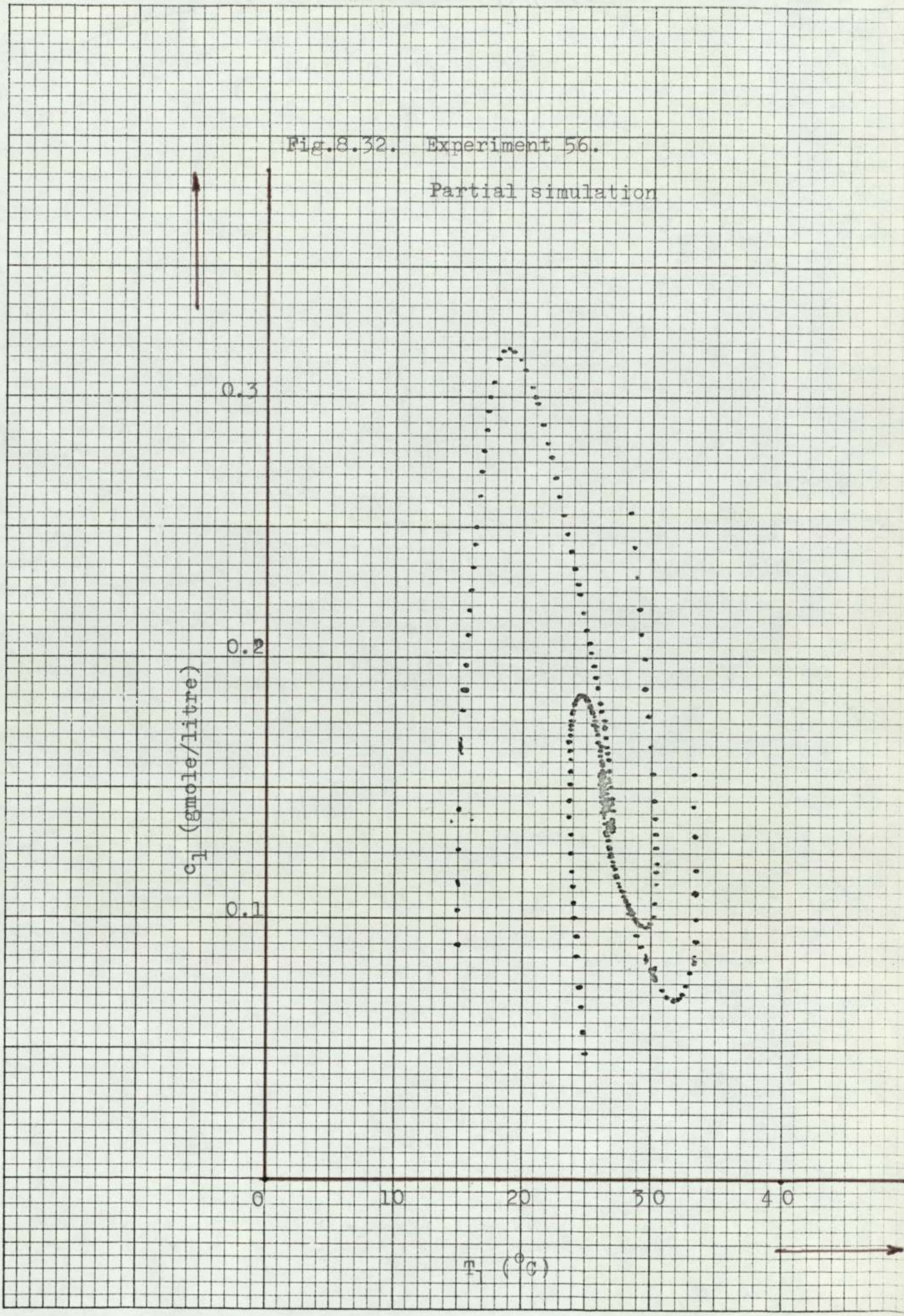

Fig.8.33. Experiment 57.

Partial simulation.

Concentration (c_1) vs. Temperature (T_1)

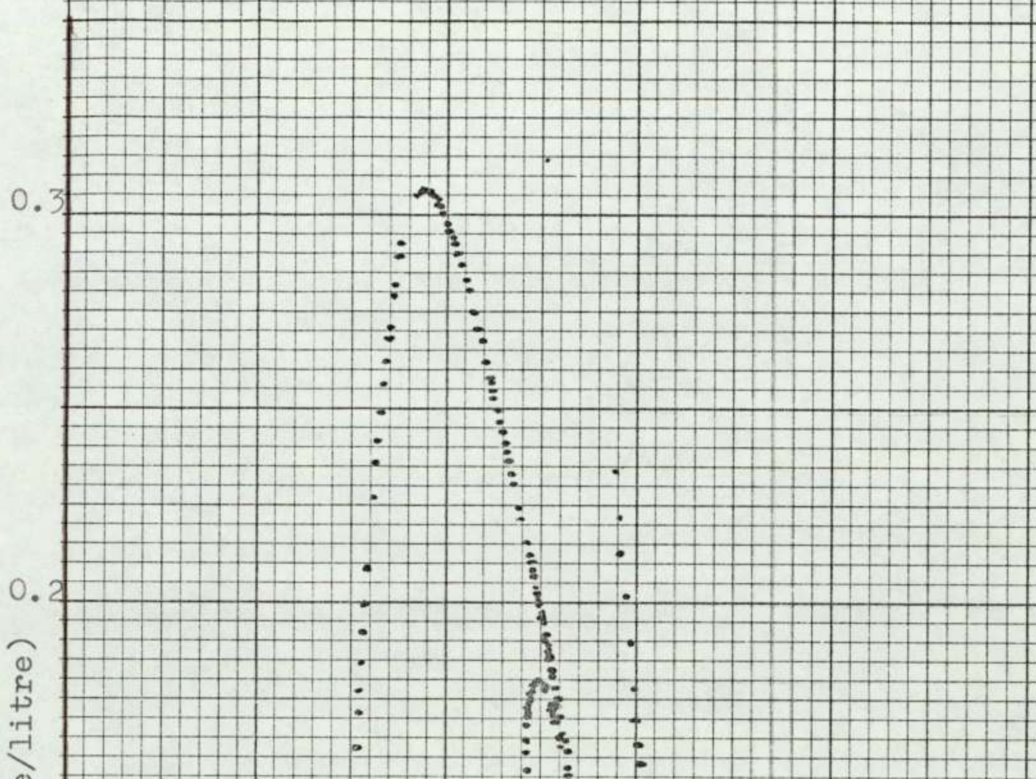

Fig.8.34. Experiment 56.

Complete simulation

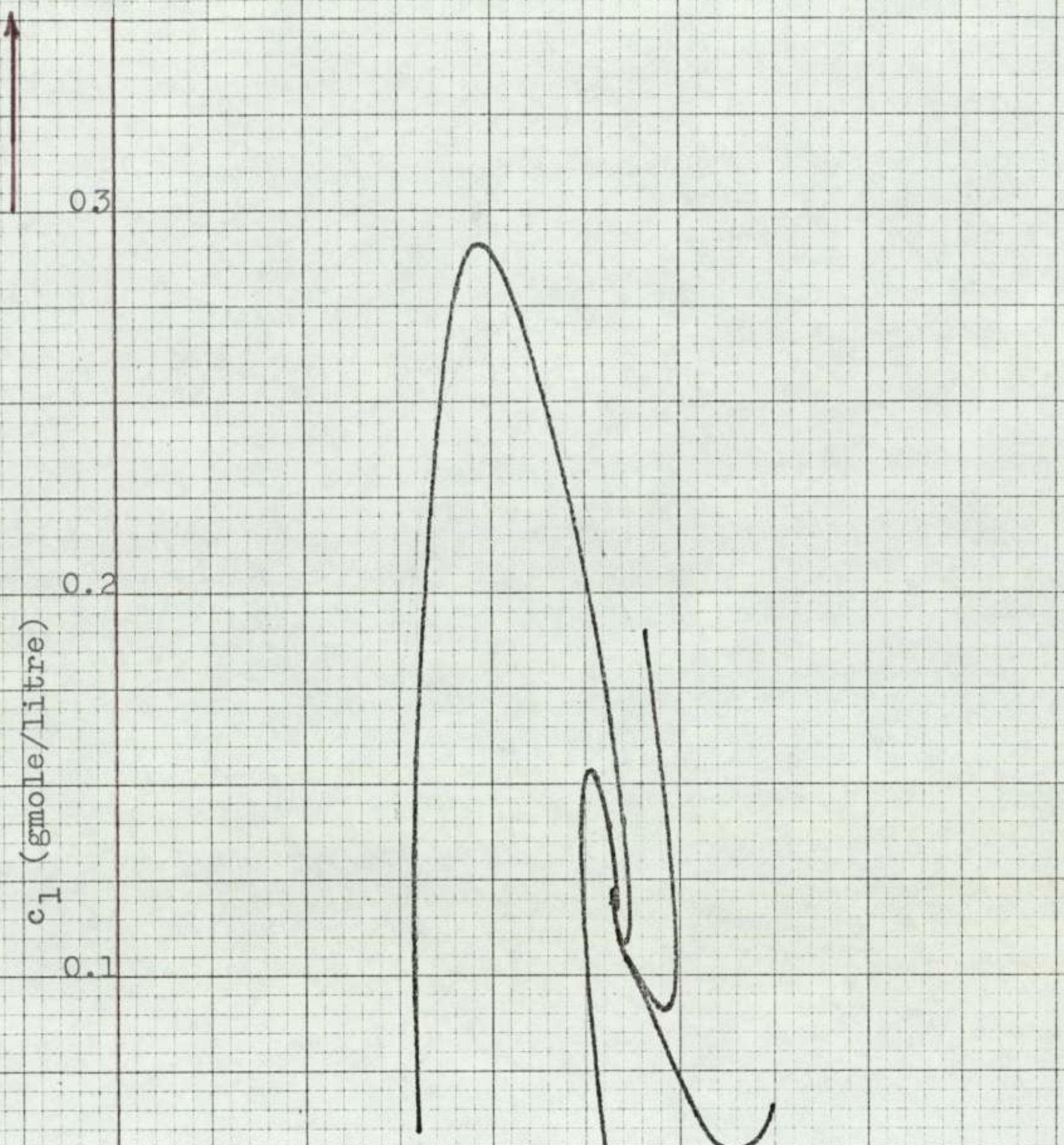

which were almost limit cycles were obtained. It rapidly became apparent that the addition of integral action tended to cause trajectory intersection. This was first attributed to a side effect of the hysteresis which itself is capable of causing trajectory intersection. To investigate this a complete simulation was implemented and it was quite apparent that the integral action was converting the two-dimensional system into a three-dimensional one. Clearly in the complete simulation hysteresis could not possibly enter into the results to cause this effect. Furthermore, trajectory intersection took place only in the control band for the Hybrid simulation reinforcing this view. The mathematical support to a conclusion of three-dimensionality was given in Section 8.2.5. Again specific cases will be considered for the 3 litre/min. feed flowrate case.

8.12.1. Partial simulation portraits for a proportional band width of 2 deg.C. - Reset action 70 repeats/min.

Experiment 71

The partial simulation portrait is given in Fig.8.35. and the complete simulation portrait in Fig.8.36.

The first portrait illustrates the multi-dimensionality well, in that the trajectories from both high and low starting temperatures intersected with ones starting from a temperature close to the final value. The offset could be seen to be eliminated with the corresponding value balanced by the pneumatic integrator.

The complete simulation agreed well with the partial one for the low temperature trajectories but this was not the case for the high temperature ones which initially showed no tendency

Fig.8.35. Experiment 71. Partial simulation

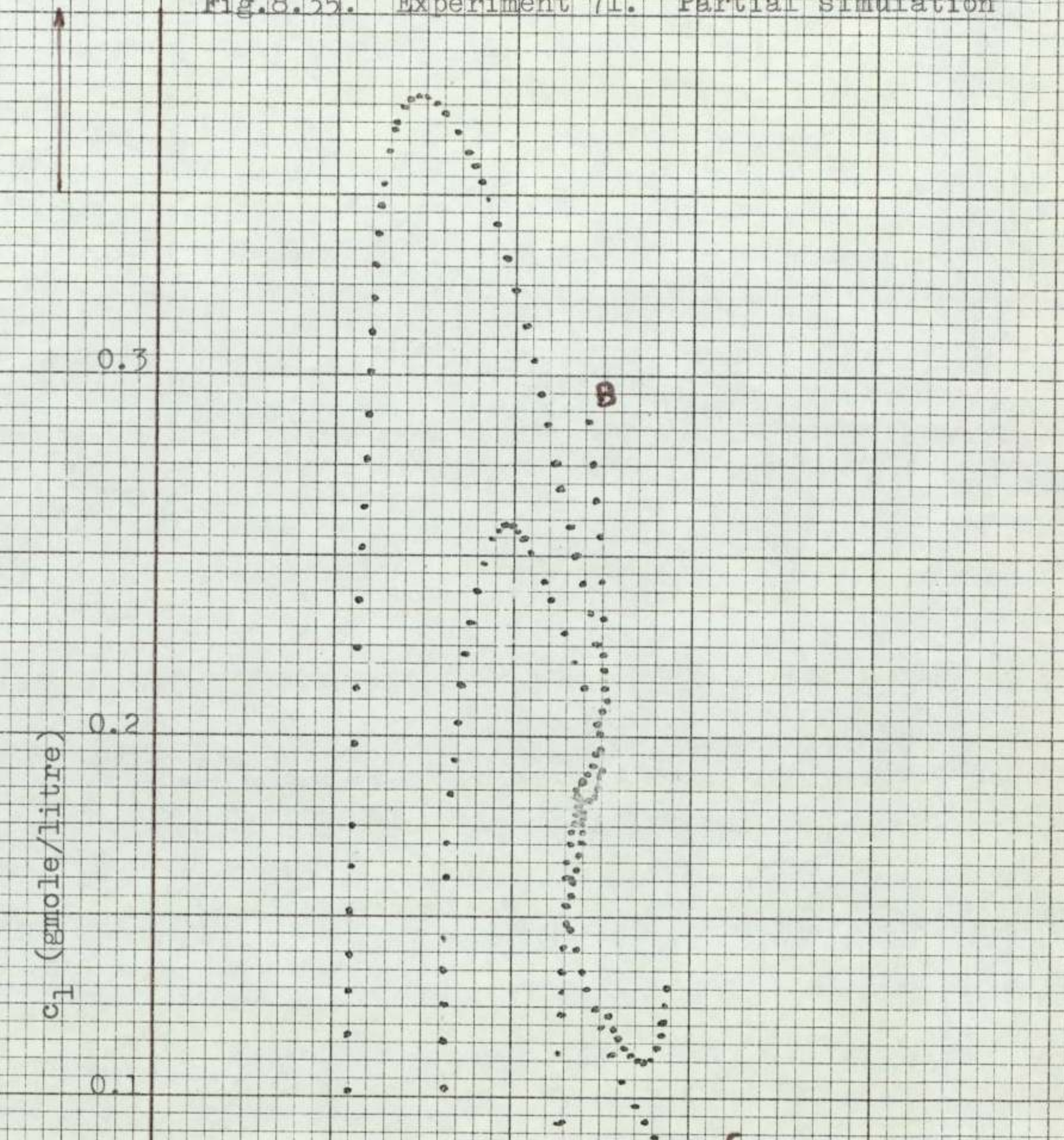

Fig. 8.36. Experiment 71.
Complete simulation.
Concentration (c_1) vs. Temperature (T_1)

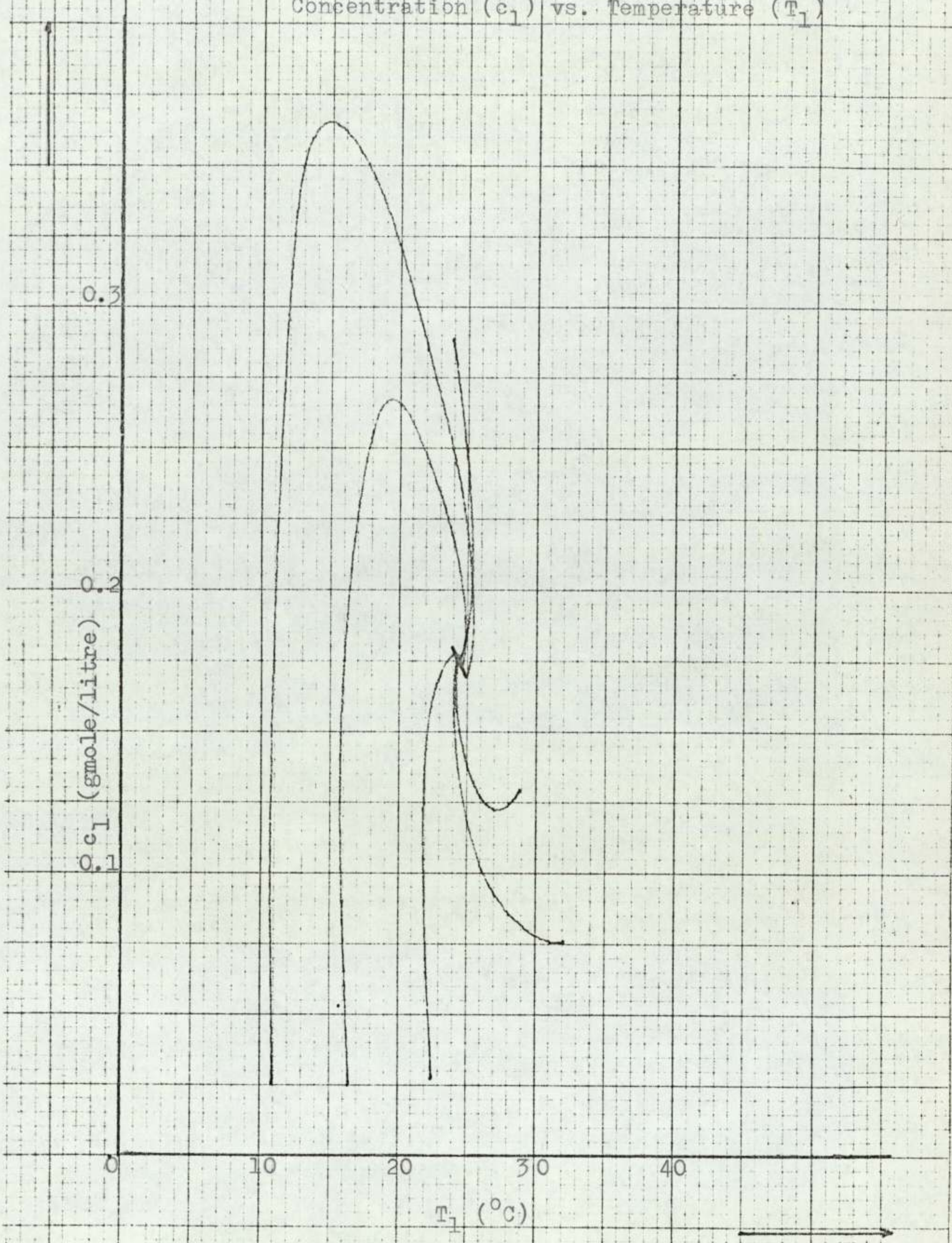

to intersect. The reason for the short comings of the simulations became apparent when the partial version's construction was considered. To obtain initial values from the practical equipment it will be remembered that the system had to be forced to reach them, i.e. the system could not be set to that value by simply resetting the integrators as in the case of the complete simulation. Whilst this forcing was taking place the pneumatic integrator would integrate the error from the set-point and before some of the initial conditions (viz. extreme temperature values) could be attained the pneumatic system would probably even have reached its saturation value. For the low temperature trajectories this value was successfully simulated as the integration from the initial condition would attain an equivalent value by the time the set-point temperature was reached. This was due to the fact that the low temperature trajectories are comparatively slow, giving time for the integral control action to function. In the case of the high temperature trajectories movement is comparatively rapid and the simulated integral control action has no time to reach a similar value to that attained by the real integral action. Consequently all the high temperature trajectories accumulate negligible integrated error and therefore the system dimensionality for them is two and therefore they do not intersect. To prove this statement a complete simulation portrait was plotted (Fig.8.37.) in which the high temperature trajectories were given an initial value of integrated error. Trajectories were then found to intersect as in the partial simulation case.

As in the servomechanism the hysteresis in the controller seems to be largely overridden by the integral control action.

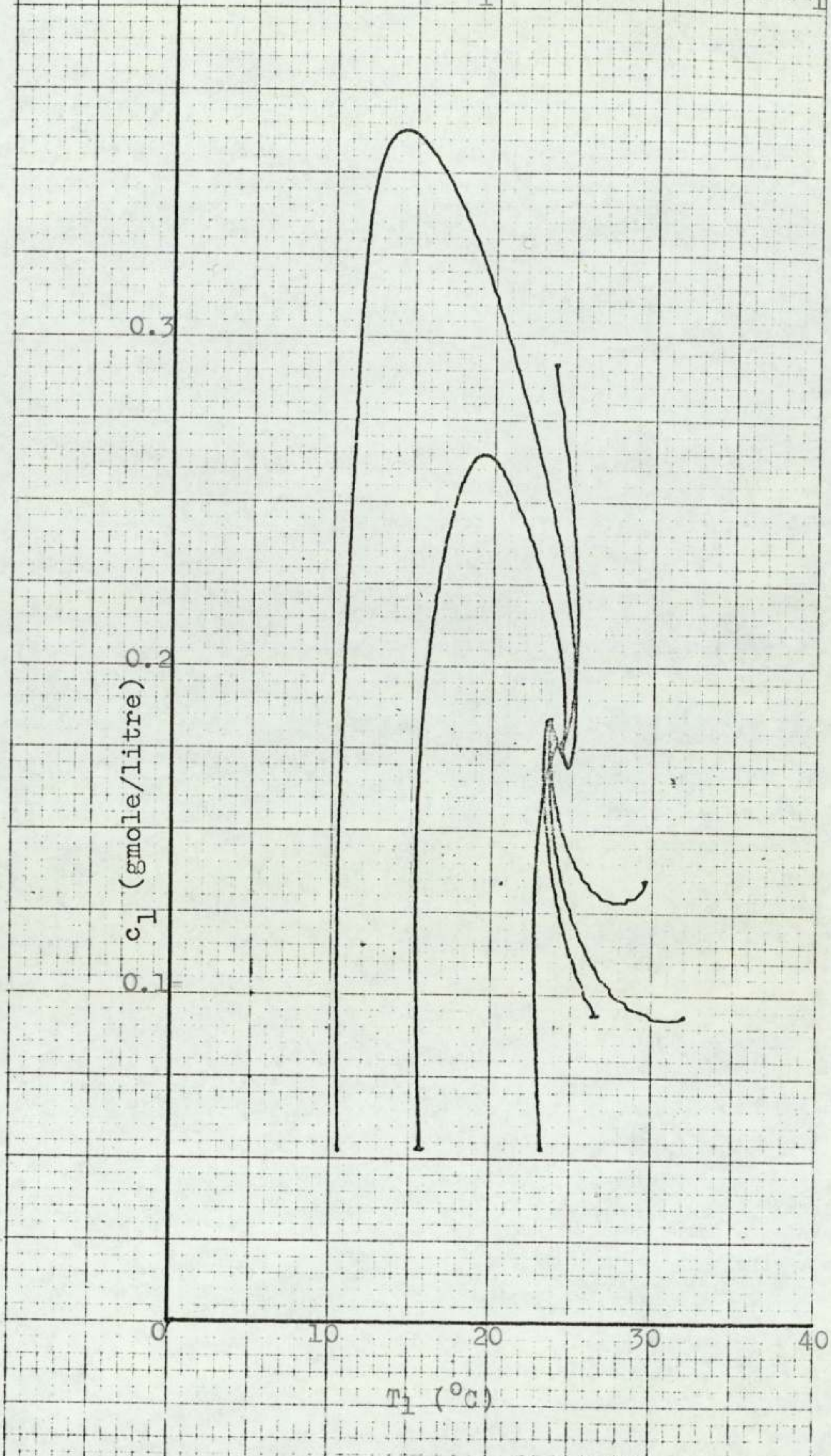

Fig. 8.37. Experiment 71.
Complete simulation.
Concentration (c_1) vs. Temperature (T_1)

From a general portrait comparison point of view, they compare well, the final steady states are in a similar position and the trajectories take routes to these states in a very similar fashion.

Experiment 70 was the same as 71 with the exception that the reset rate was 30 repeats per minute. The portrait (Fig.8.38.) was seen to resemble more closely that produced with proportional action only, i.e. a tendency to temperature overshoot due to hysteresis. It was therefore concluded that the lower reset rate was not able to fully override the hysteresis effect. The trajectory overshoot was not recorded in the comparison complete simulation as would be expected. (Fig.8.39.)

8.12.2. Partial simulation portraits for proportional band widths of 10 and 15 deg.C. - Reset action 70 repeats/min.

Difficulty was encountered when trying to obtain these portraits because of set-point drift. Example portraits which included set-point drift are included for completeness in the Appendix (Figs.A.34 - 36). Other portraits which were not marred by this effect are presented in the text and the Appendix.

With the wider proportional band widths the control action was weaker and the plots obtained were more oscillatory.

Experiments 74 and 78 provided examples of a 10 and 15 deg.C. proportional band width respectively (Figs.8.40 and 8.41.). Comparison complete simulation portraits are given in Figs.8.42. and 8.43. In general the portraits compared reasonably well. The differences which were present was again considered to be due to the difference of the two integral actions. It seemed likely that the partial simulation reset

Fig. 8.38. Experiment 70(c)

Partial simulation.

Concentration (c_1) vs. Temperature (T_1)

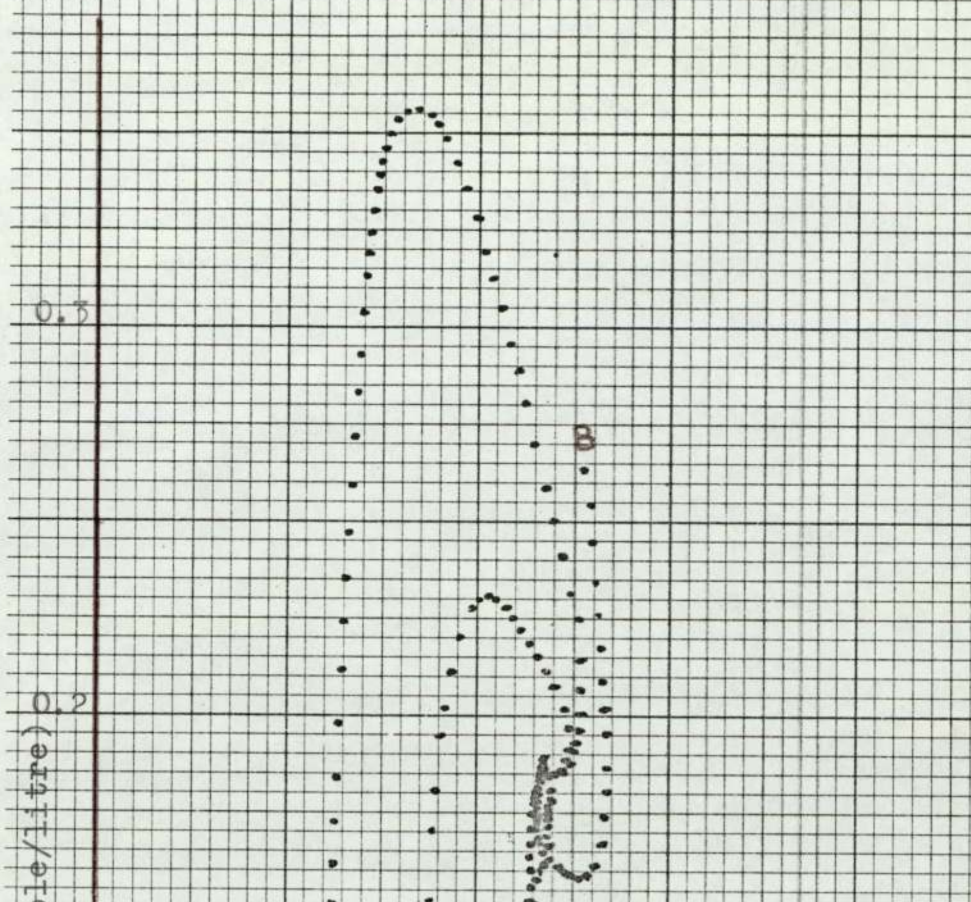

Fig.8.39. Experiment 70.
Complete simulation.
Concentration (c_1) vs. Temperature (T_1)

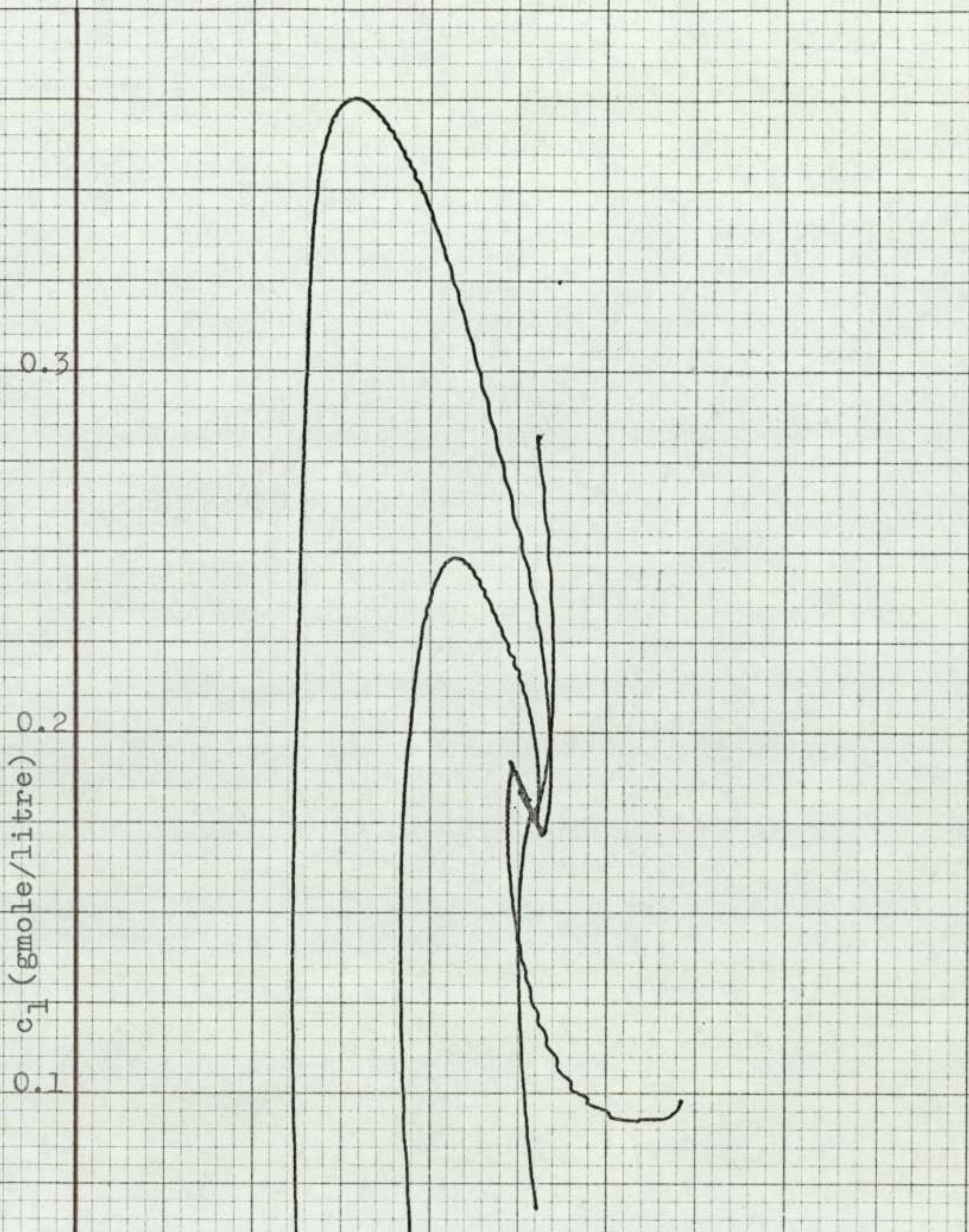

Fig.8.40. Experiment 74.
Partial simulation.
Concentration (c_1) vs. Temperature (T_1)

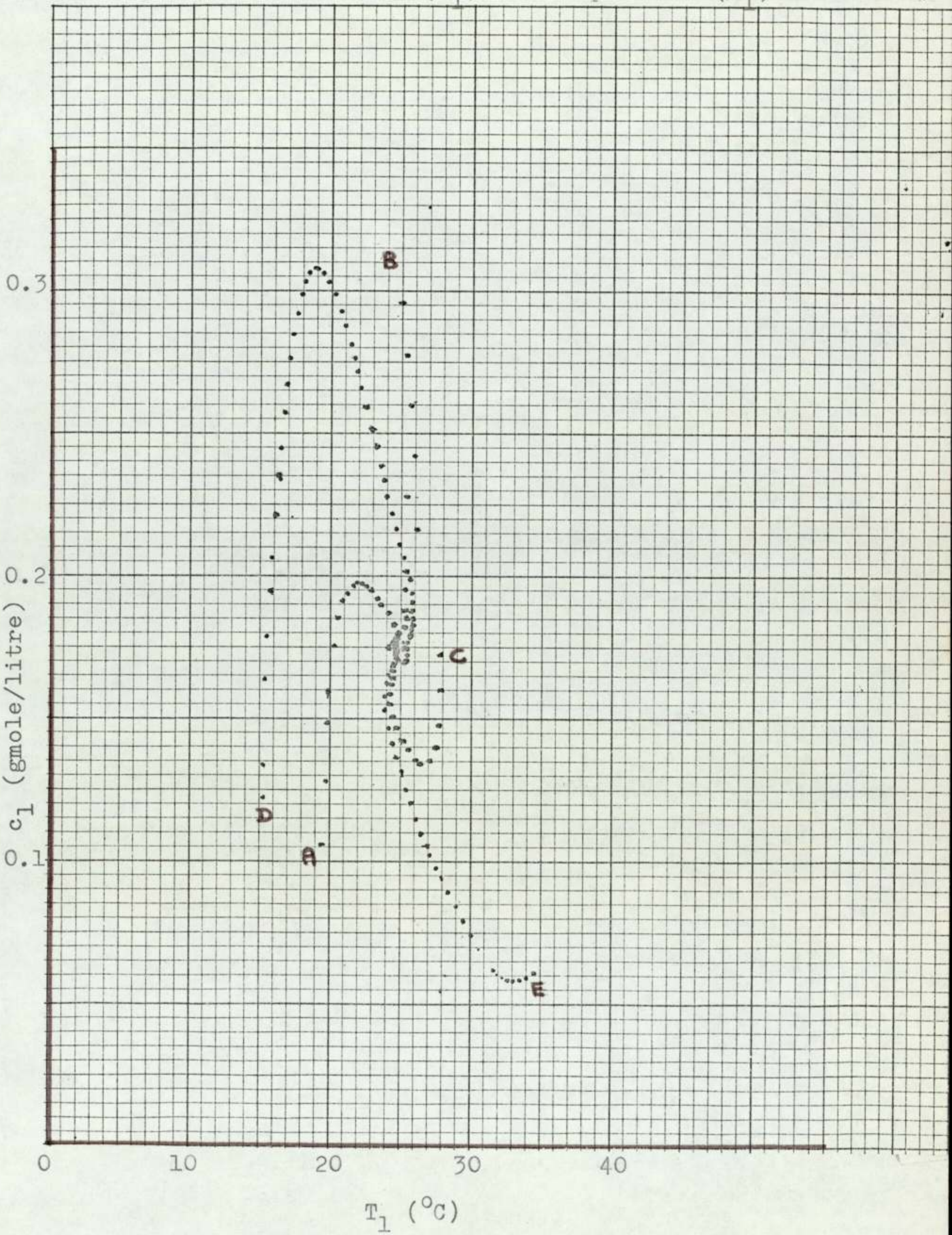

Fig.8.41. Experiment 78.

Partial simulation.

Concentration (c_1) vs. Temperature (T_1)

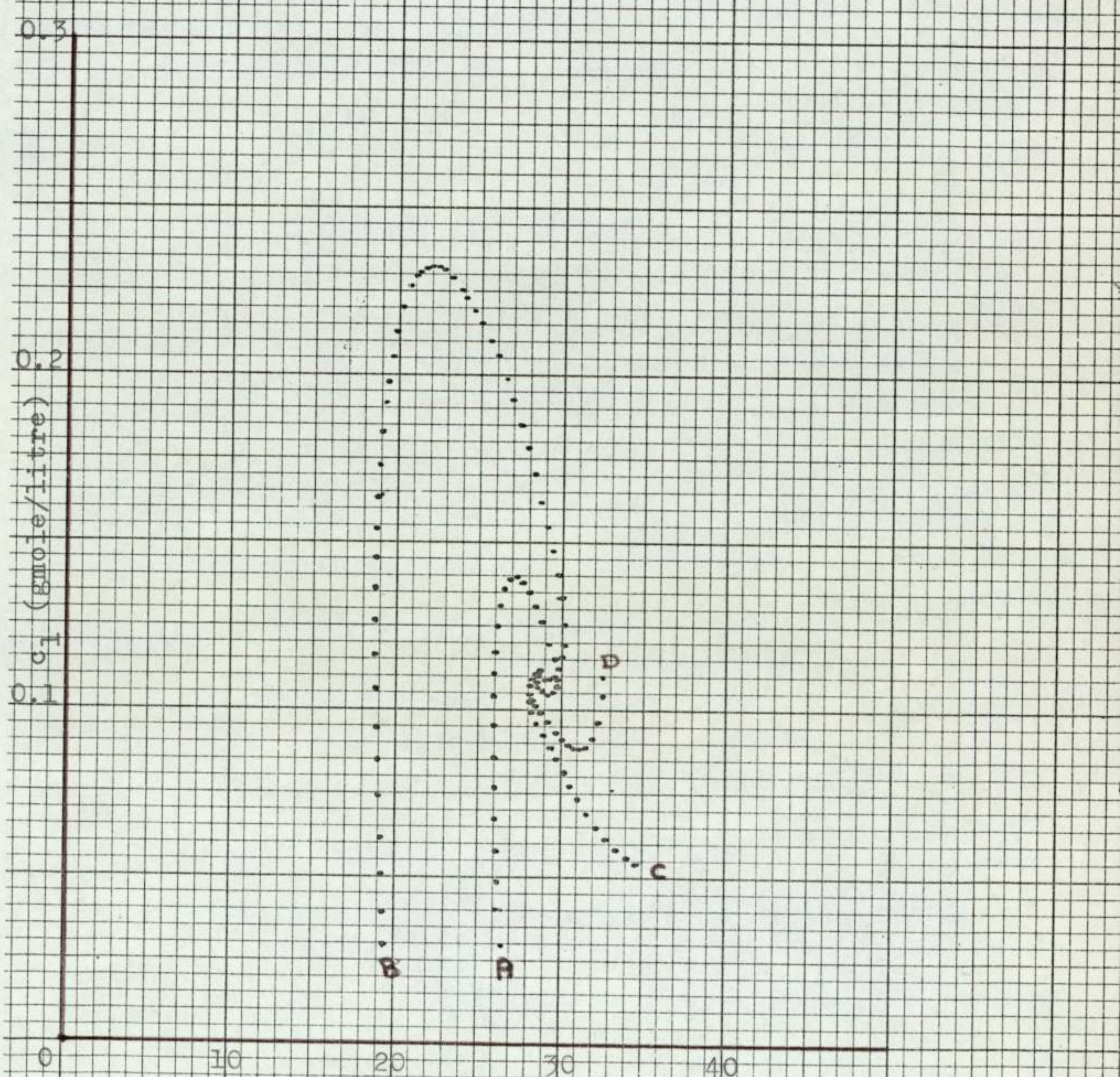

Fig. 8.42. Experiment 74.

Complete simulation.

Concentration (c_1) vs. Temperature (T_1)

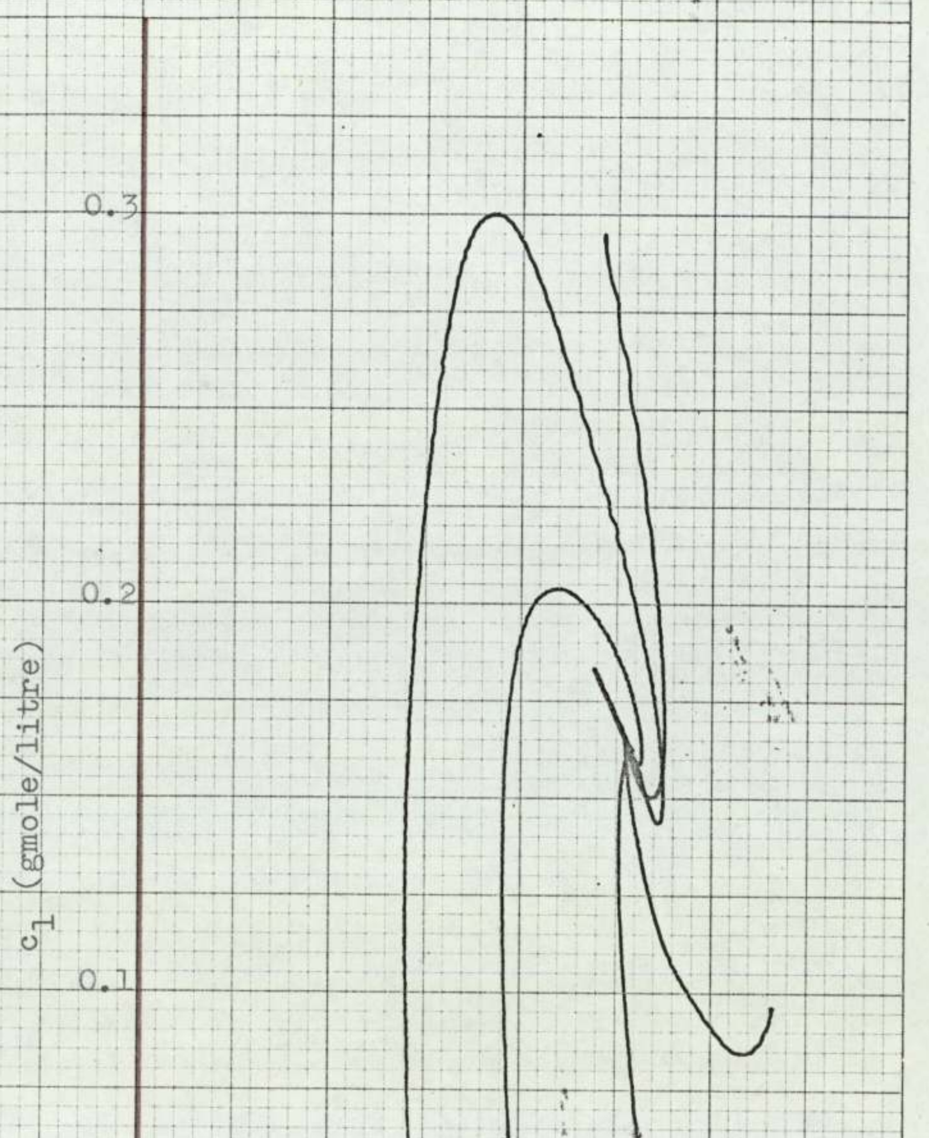

Fig.8.43. Experiment 78. Complete simulation

Concentration (c_1) vs. Temperature (T_1)

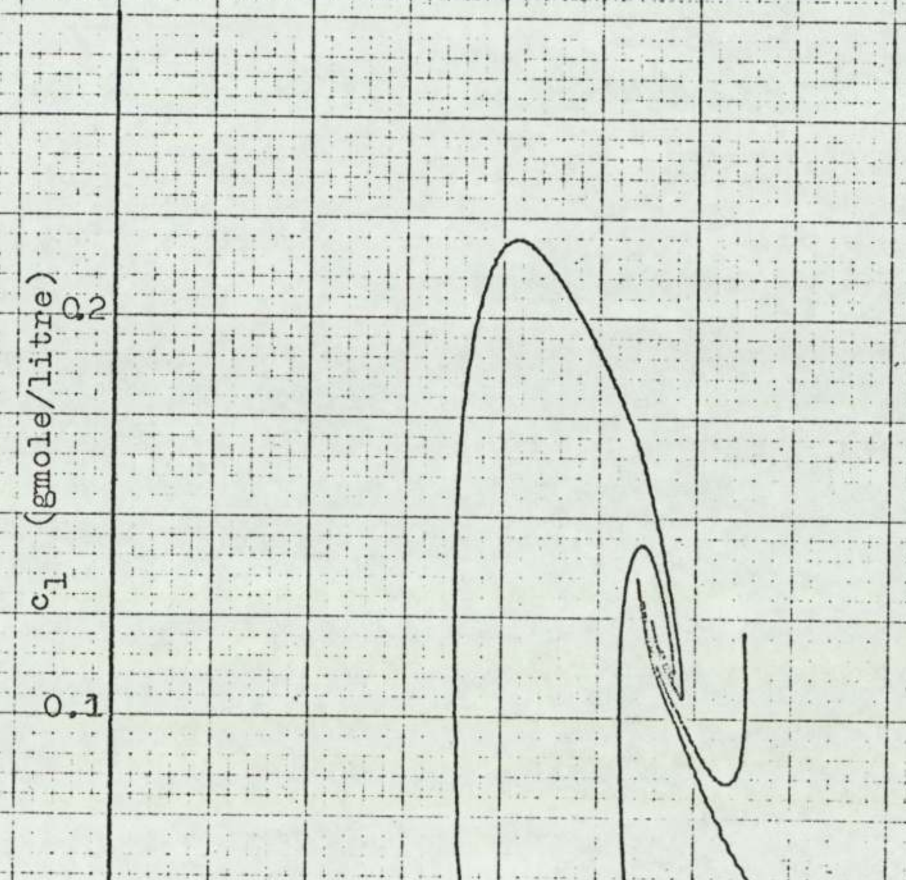

rates were faster but saturation prevented excessive trajectory overshoot. This could have caused the greater tendency for trajectory intersection, which was observed in the partial simulation portraits. In both partial and total simulation portraits the final fall towards the set-point due to the integral action was recorded. This part of the portrait takes a long time in real time and therefore only the start of this approach is shown in the partial simulation case. In the complete simulation a full but exaggerated picture of the situation is given.

With initial values on the control integrator a slower or faster approach to the final set-point value is given depending on the sign of the initial condition. For the high temperature / low concentration simulation (in Fig.8.43.) this caused a more rapid approach to the set-point. The overall effect is that the trajectories in general tend to converge on a line which finally reaches the set-point. Thus there is an operating line rather than a point.

8.12.3. Partial simulation portraits for proportional band widths of 30 to 60 deg.C. - Reset rate 0 to 70 repeats/min.

Useful portraits were obtained mainly from the first controller as this was the subject of most of this type of investigation.

For various reset rates the portraits showed an oscillatory response which wound in towards the steady state at a rate depending on the control parameters chosen and also on the presence or absence of the valve positioner. Complete simulations gave reasonable agreement even though the integral action set in the analogue circuit had to be estimated as the true integral characteristics were not known. This was because whilst the repeats per minute value was known from the setting on the controller no information of the saturation limits of the integral action was available. Clearly limits must be imposed due to the extreme ranges of pressure available to the instrument (0 to 20 lbf/in^2 gauge). If the saturation limits on the real system's integral action were reached then significant differences in control action between the two simulations could be expected. In all the portraits obtained it was noted that the low temperature / low concentration trajectory tended to overshoot the partial simulation trajectory around $31^{o}C$. This was attributed to the differences in the two integral actions as they were certainly capable of causing this effect. The fact that this trajectory has also got the most chance of integrating excessive error values due to its slow speed and large initial deviation from the set-point supports this argument. It was also noted that the trajectory overshot very slowly whilst waiting for coolant to be switched on. The stored integral error in the computer complete simulation could be seen to be falling slowly as its value of negative integrated error was diminished by the positive integrated error. The effect of saturation can be illustrated as in Fig.8.44. Other trajectories could escape this effect due to their smaller deviation from the set-point or the speed of the trajectory.

The other major feature of interest was the difference between the portraits in which the valve positioner was or was not functioning. Thus the control valve was given the opportunity of superimposing its hysteresis effect on the portrait. This effect was strongly apparent in all the comparison portraits

Fig.8.44.

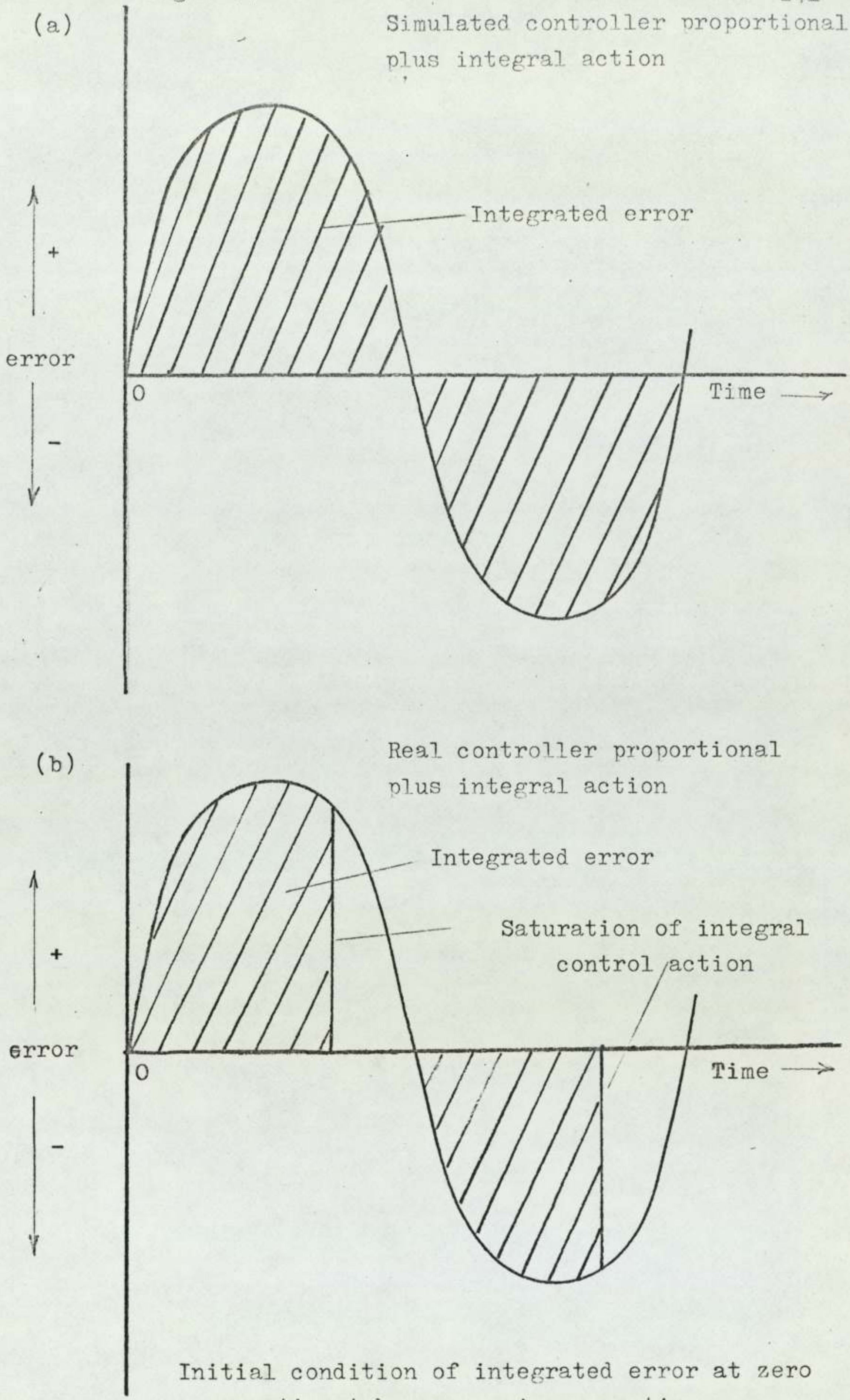

Initial condition of integrated error at zero time taken as maximum negative obtained and illustrated the beneficial action of retaining some of the real system rather than completely simulating it.

As the reset rate was high and the deviations from set-point large the integrated error was also large and proved a dominant factor. Therefore the coolant flowrate was either maximum or zero for most of the trajectories' lengths and nonidealities of feedback loop could only be expected to have an effect when change in direction of controller action took place. As illustrated in the investigations on proportional control action only, the hysteresis effect for wide proportional bands on the controller was small and therefore the complete simulations produced portraits which compared well with the partial ones when the valve positioner was in action. However the oscillations were more sustained in the partial simulation portrait case. This would be caused by the time delays in the real feedback loop. With valve hysteresis present, the limit cycle form was much larger and the oscillations far more sustained. If there was a gradual wind-in towards the operating point it was very slow indeed and undetectable on some of the portraits plotted.

For lower reset rates the oscillations diminished accordingly.

Example portraits:

Experiment 36(b)

Proportional band width 40 deg.C. - Reset rate setting 9

Valve positioner in action.

Comparison partial and complete simulation portraits were obtained (Figs.8.45. and 8.46.). Apart from the greater over-shoot of the trajectories starting from 21°C and 31°C in the

Fig.8.45. Experiment 36(b).

Partial simulation.

Concentration (c_1) vs. Temperature (T_1)

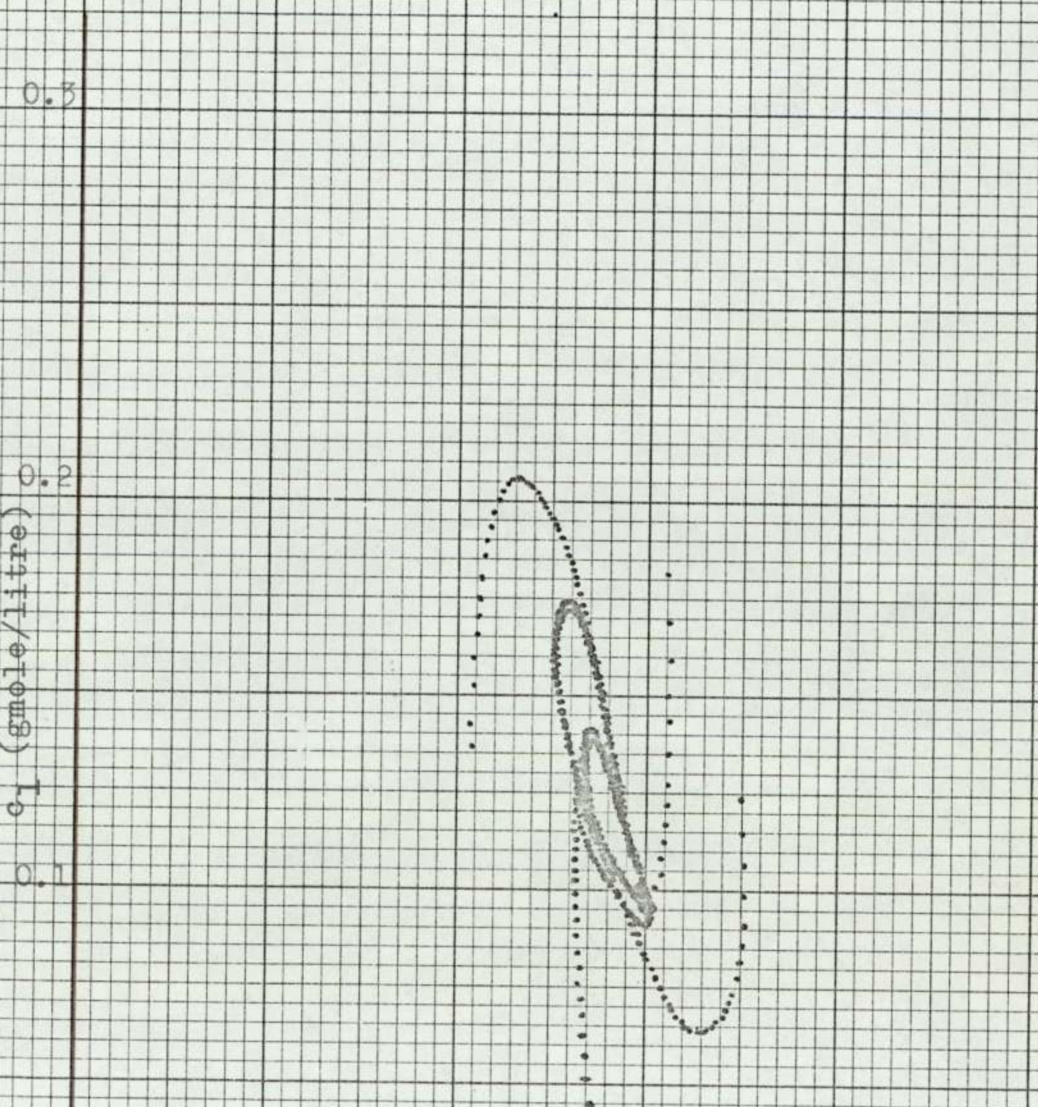

Fig. 8.46. Experiment 36(b).

Complete simulation.

Concentration (c_1) vs. Temperature (T_1)

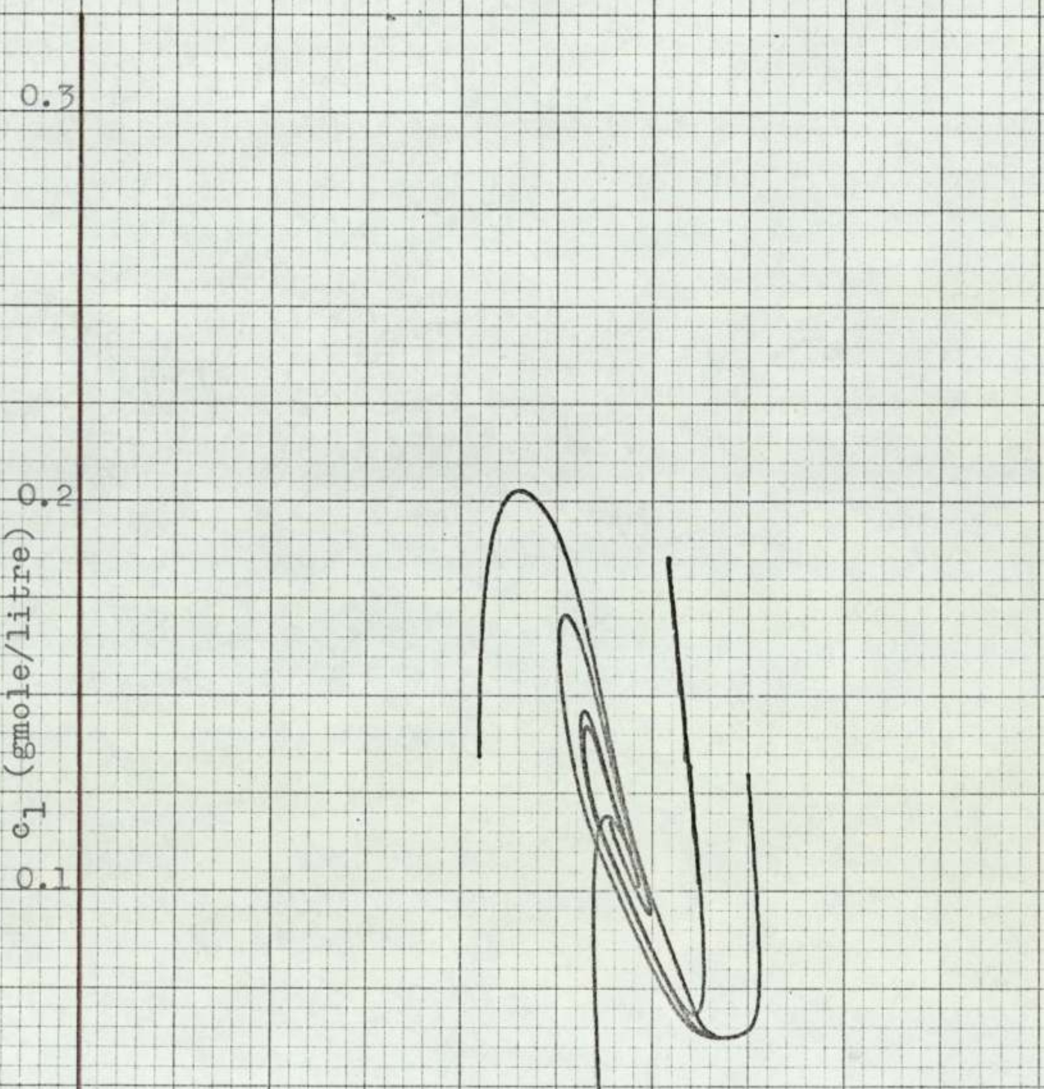

complete simulation, the reasons for which have already been dealt with, the portraits agree very well.

Experiment 35

Proportional band width 60 deg.C. - Reset rate setting 9
Valve positioner in action.

The partial and complete simulation portraits are shown in Figs. 8.47. and 8.48. Again with the same reservations the portraits are very closely related. The trajectory with initial conditions 29^{o}C and 0.055 gmole/litre in the complete simulation could have been made to approximate closer to the partial simulation case if an initial value of integrator error had been applied to the complete simulation controller integrated. The pneumatic integrator had obviously attained such a value.

Experiment 69

Proportional band width 30 deg.C. - Reset rate 30 repeats/min.
Valve positioner in action.

The partial and complete simulation portraits are shown in Figs.8.49. and 8.50. The portraits are again quite similar. Ambient / mains temperatures and heat of reaction were different for this experiment from the previous two experiments and also the second controller was used. Two complete simulation portraits were drawn to show the difference caused by the low temperature / high concentration trajectory overshoot due to the unconstrained integral action.

Single trajectory portraits

These plots are presented to show the effect of large

Fig.8.47. Experiment 35.
Partial simulation.
Concentration (c_1) vs. Temperature (T_1)

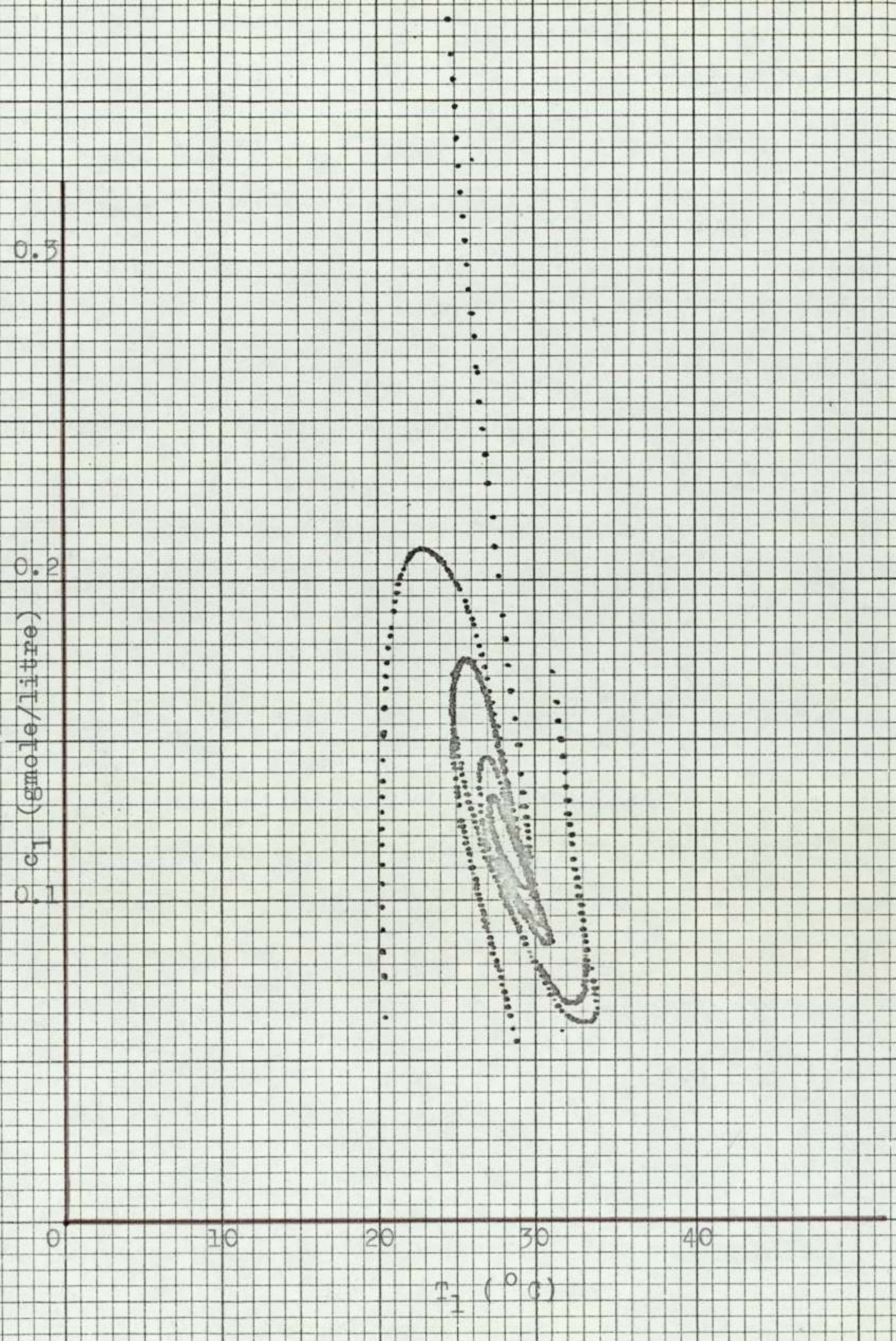

Fig.8.48. Experiment 35. Complete simulation.

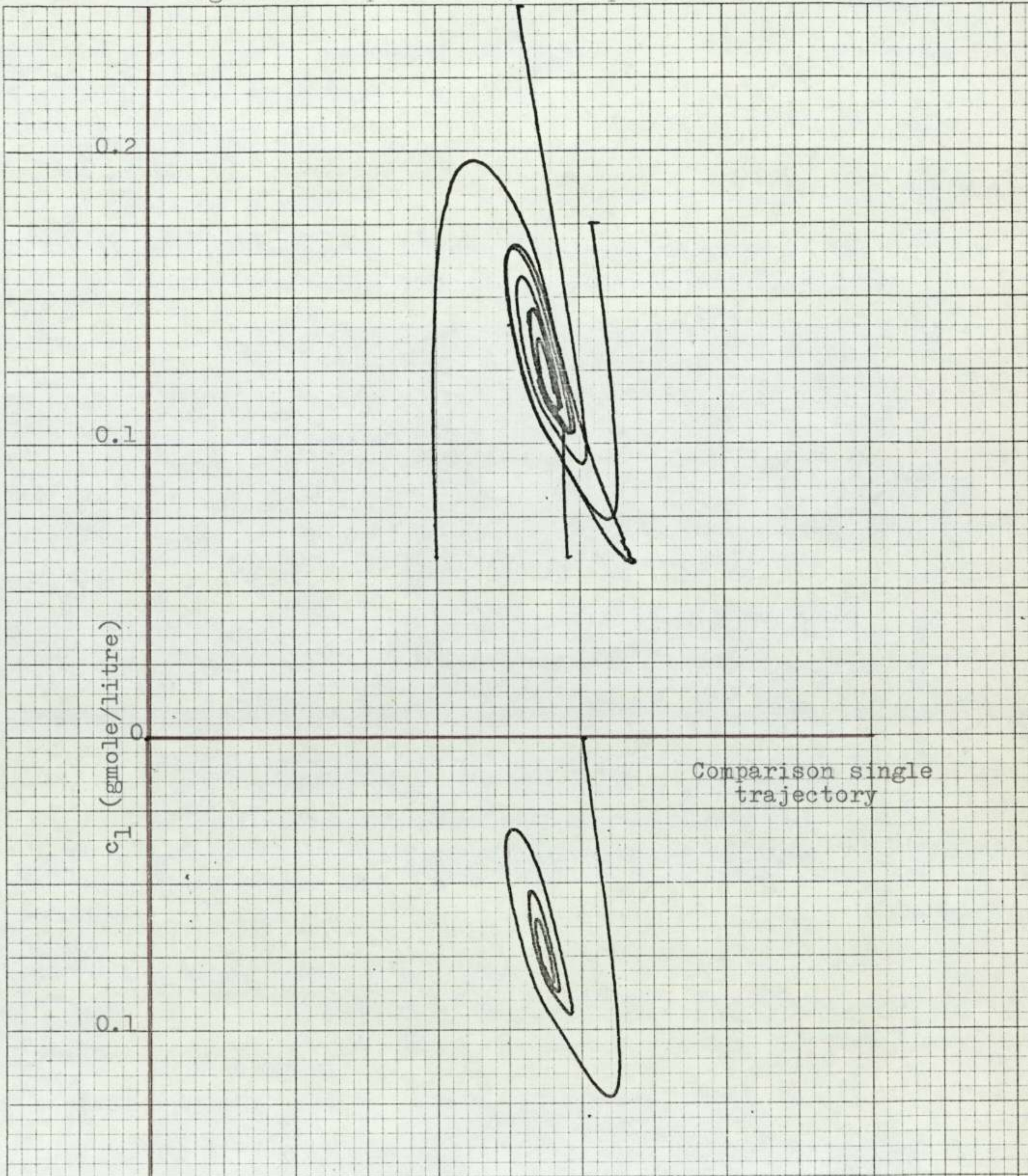

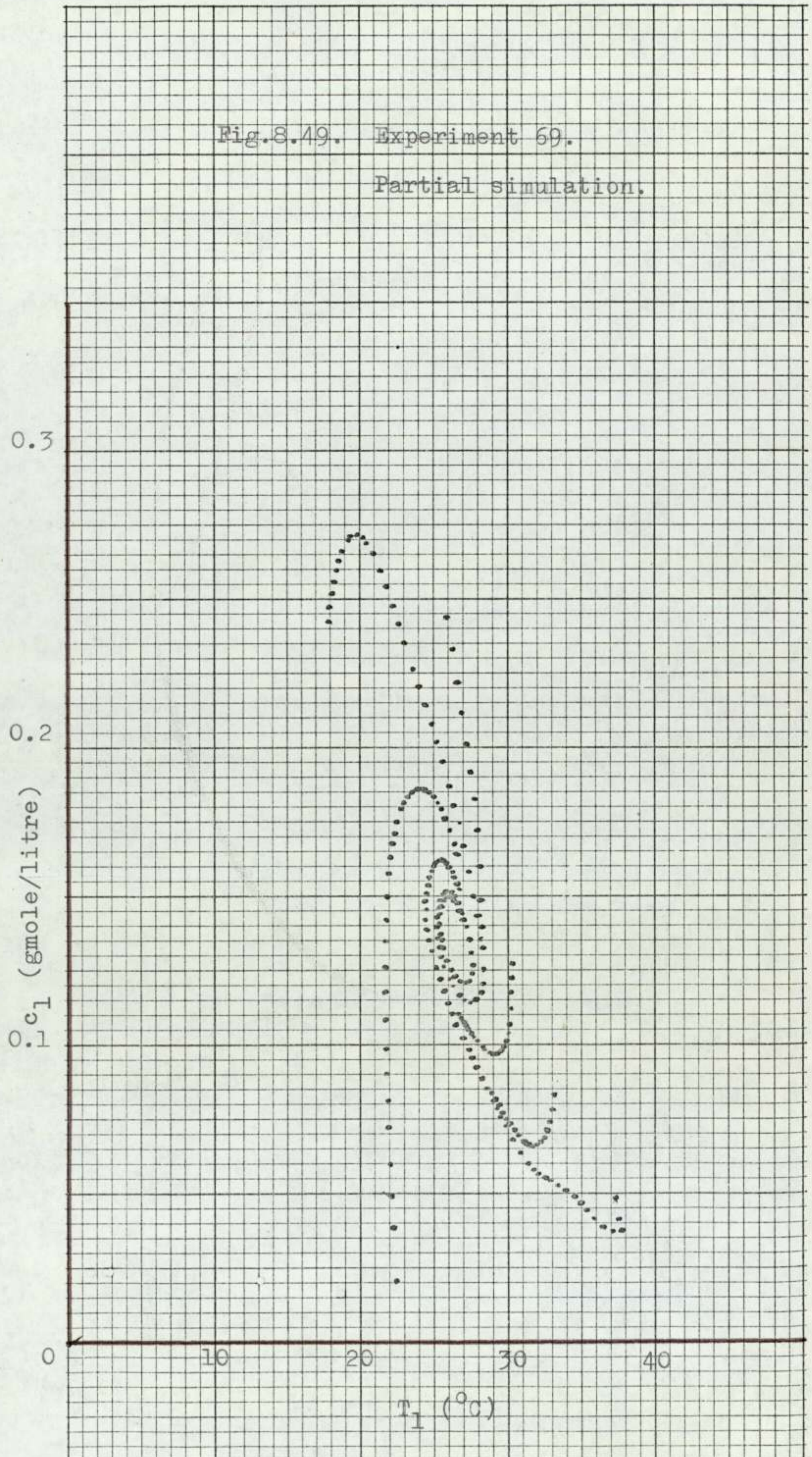
Fig.8.49. Experiment 69.
Partial simulation.
0.3
0.2
0.1
0
10
20
30
40
c_1 (gmole/litre)
T_1 (^{o}C)

Fig.8.50. Experiment 69.
Complete simulations.

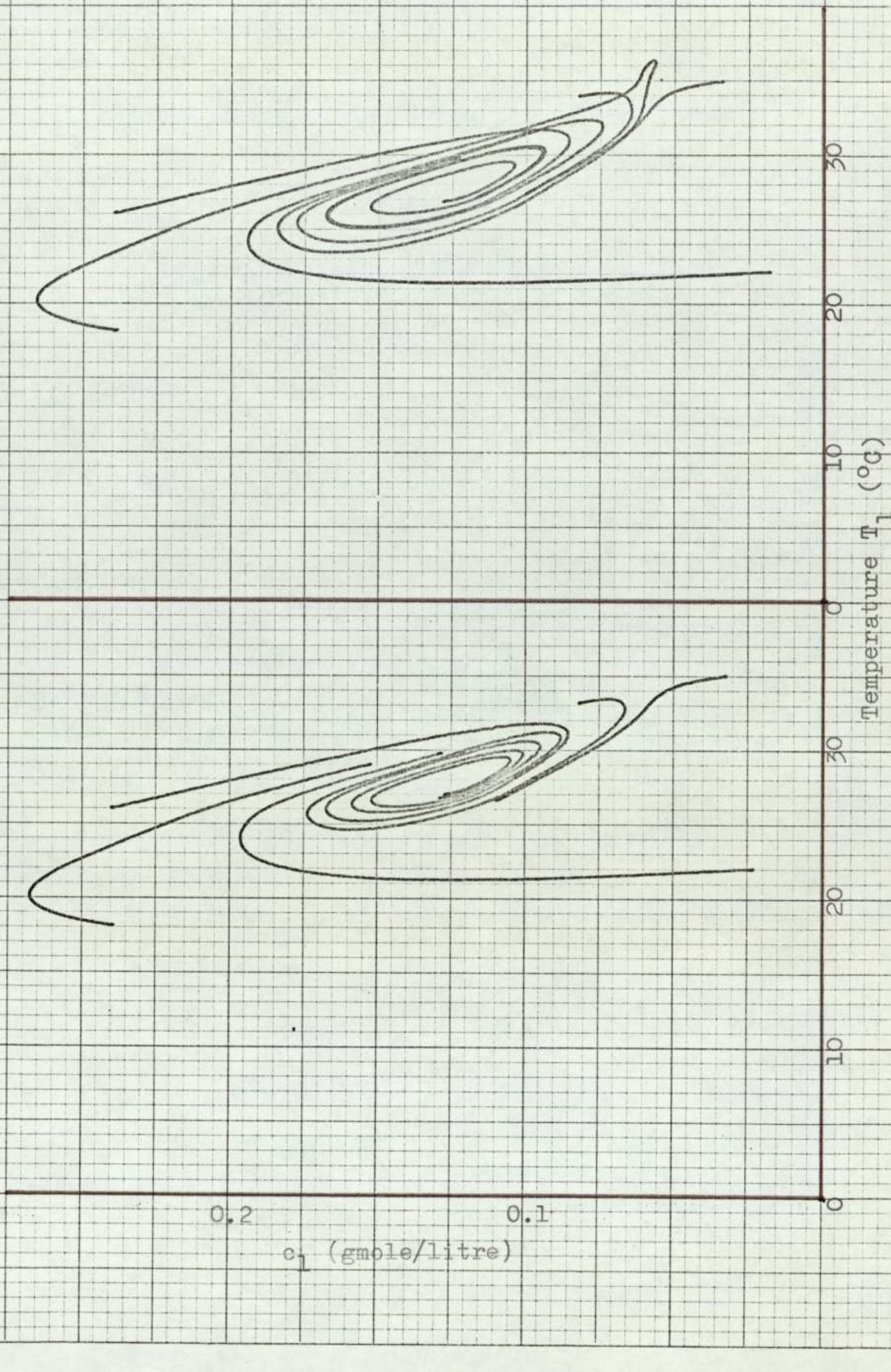

reset rate on weak proportional action more clearly and also to show how the hysteresis in the control valve causes oscillations of greater amplitude and slow decay towards the steady state.

Proportional band width 60 deg.C. - Reset rate setting 9

Several experiments were conducted in which the valve positioner was either in action or by-passed. These showed that the control valve without the positioner produced greater magnitude oscillations due to the hysteresis effect. With the high reset rate and weak proportional gain, oscillations caused by the integral action were numerous and thus provided the backlash effect with a good opportunity to superimpose on the results.

Experiments 44 and 45 (Figs.8.51.(a) and (b)) gave a good comparison. The oscillations were fairly sustained in both cases but the magnitudes showed an impressive difference. On the concentration axis the cycle at the beginning covered about eight squares or 0.04 gmole/litre for valve positioner in action whilst for the by-passed case the size was about twelve squares or 0.06 gmole/litre. The oscillations were less sustained when the positioner was in action and the trajectory could be seen to be slowly inward winding towards the steady state. A comparison complete simulation portrait was drawn (Fig.8.52.) and as expected it agreed more closely with the valve positioner in action case as the feedback loop was closer to the ideal case. Considering the approximations made in the complete simulation for this plot the comparison was thought to be good.

Fig.8.51. Experiments 44 and 45.

Partial simulations

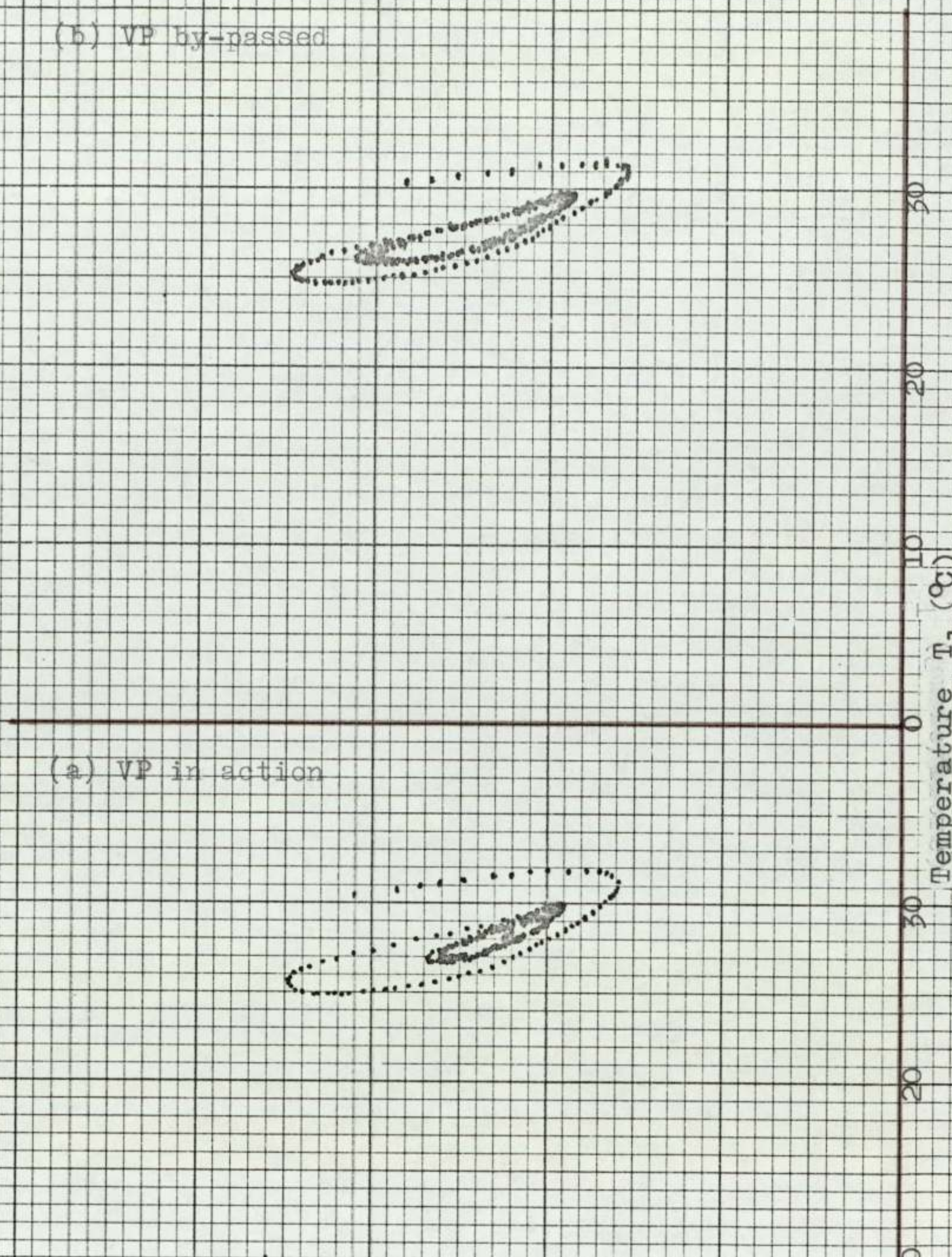

Fig. 8.52. Experiment 44.

Complete simulation.

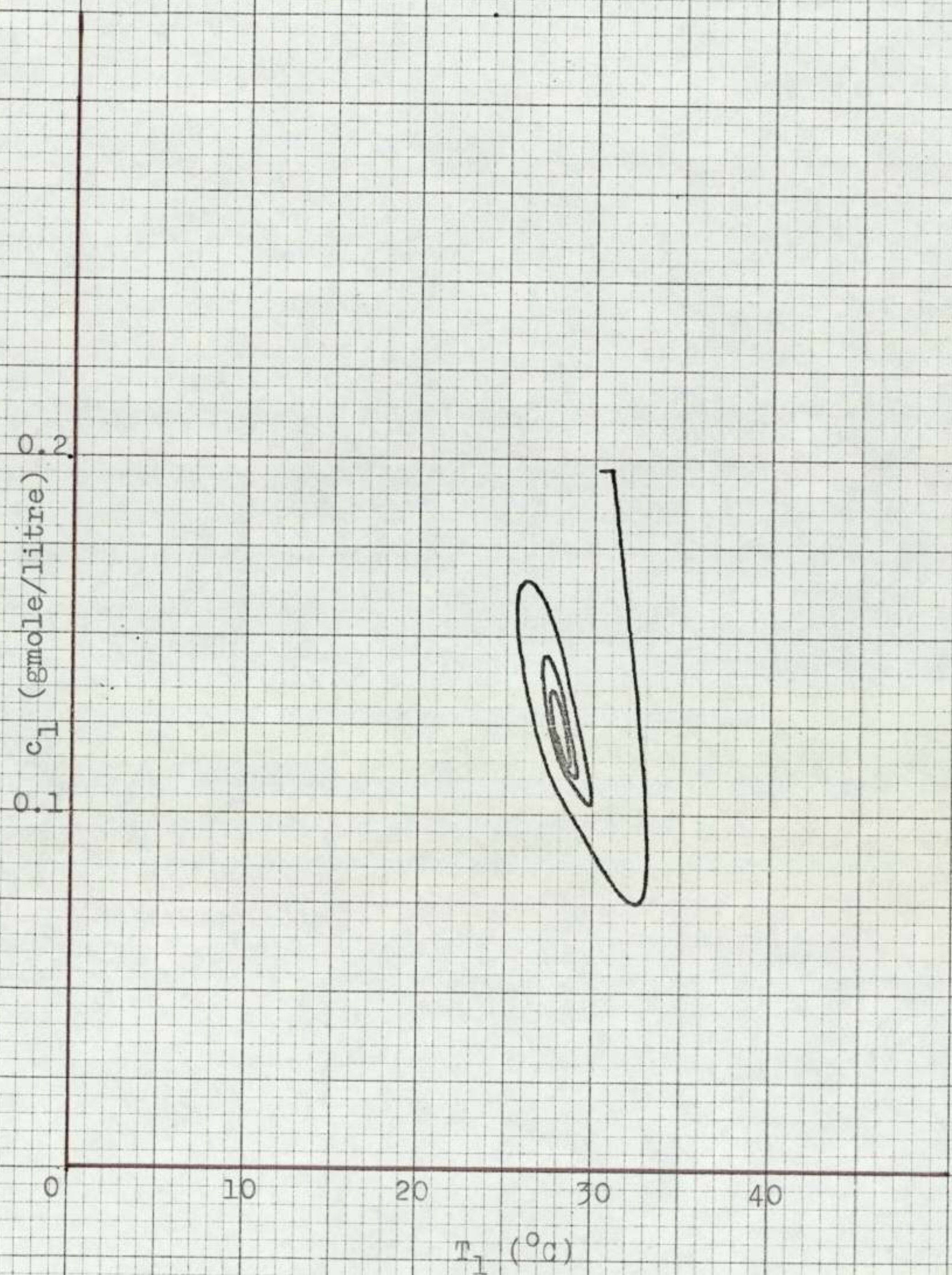

Experiments 46, 47, 48 and 49 for the same conditions but different trajectories supported these results with the differences in cycle magnitude being proportionately the same. The first two portraits are included in the text in Figs. 8.53.(a) and (b) and the other two in the Appendix (Fig.A.27.). Experiment 47 was completely simulated in order to try to duplicate the trajectory intersection with the cycle at $29\frac{1}{2}^{o}$C. The simulation was successful after an initial condition of integrated error was imposed on the simulation. Presumably a longer time elapsed before the initial condition of temperature / concentration was obtained in this partial simulation case than with the other cases and thus integrated error had a chance to accumulate. Unfortunately no record of this fact was available as a check. (Fig.A.41.).

The backlash effect produced by the control valve will be a combination of both its static and dynamic nonideal response. The time delay in the dynamic response could produce a significant contribution. However both the nonidealities combine to form effectively a time delay in control action. The time delay effect would be expected to be most pronounced when a rapid change in direction control action is required. The system cools at a much faster rate than it heats up when a high coolant flowrate is employed. This is the position for the trajectories cooling from about 30^{o}C in the cycle. The set-point is in the 28^{o}C region and thus after this point is passed, error will be integrated in the opposite direction. In the case of Experiment 44 the trajectory temperature falls rapidly and due to the more rapid reversals in action of the control valve with the positioner in action the coolant is switched off much sooner in this case and thus the temperature falls less and hence does not allow the concentration to rise

Fig.8.53. Experiments 46 and 47.

Partial simulations

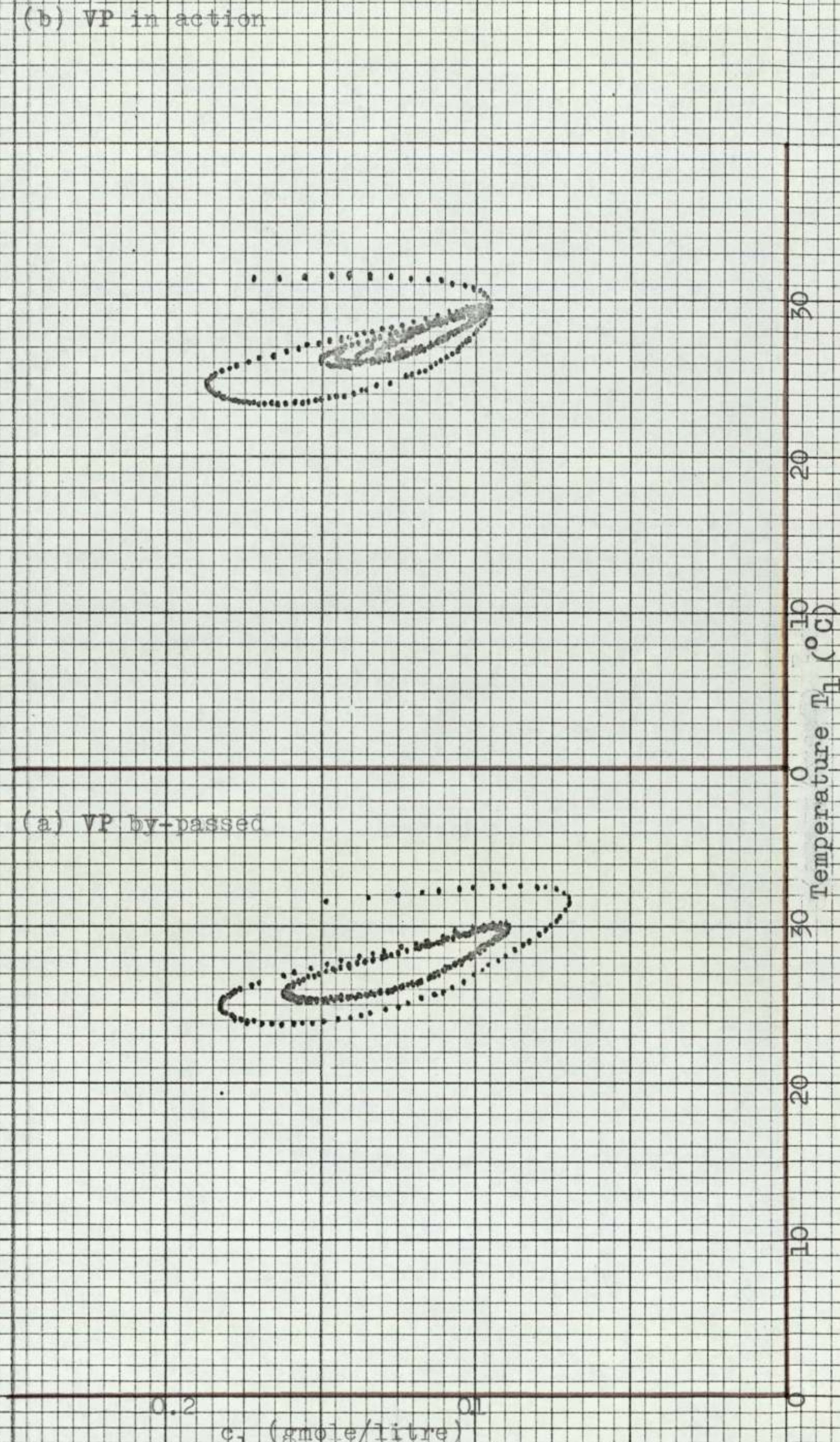

higher than 0.135 gmole/litre. For Experiment 45 the coolant is left on much longer and the temperature falls a degree further, allowing the concentration to reach 0.155 gmole/litre. In Experiment 44, as the trajectory winds in towards the set-point, due to reduction in integrated error because it overshoots the set-point less, the rapid response of the feedback loop allows further significant reductions in cycle size. For Experiment 45 the delay in control action allows the oscillations to be more sustained and only a slight inward winding effect is observable. The reduction in speed of the trajectory at the high temperature end of the cycle would be expected to produce a less marked effect on the nonideal control action and whilst an inward winding tendency is observable, it is smaller in magnitude and also the overshoot of the set-point is reduced.

Similar conclusions could be drawn from an examination of the other portraits obtained for these control parameters.

Proportional band width 30 deg.C. - Reset rate setting 6

Experiments 52 and 53 provided comparison portraits for these control parameters showing control valve hysteresis effect (Fig.8.54.). The stronger proportional action and reduced reset rate leads to fewer oscillations and a more rapid approach to the steady state. Therefore the backlash effect was less marked.

Fig.8.54. (a) and (b). Experiments 52 and 53.

Partial simulations.

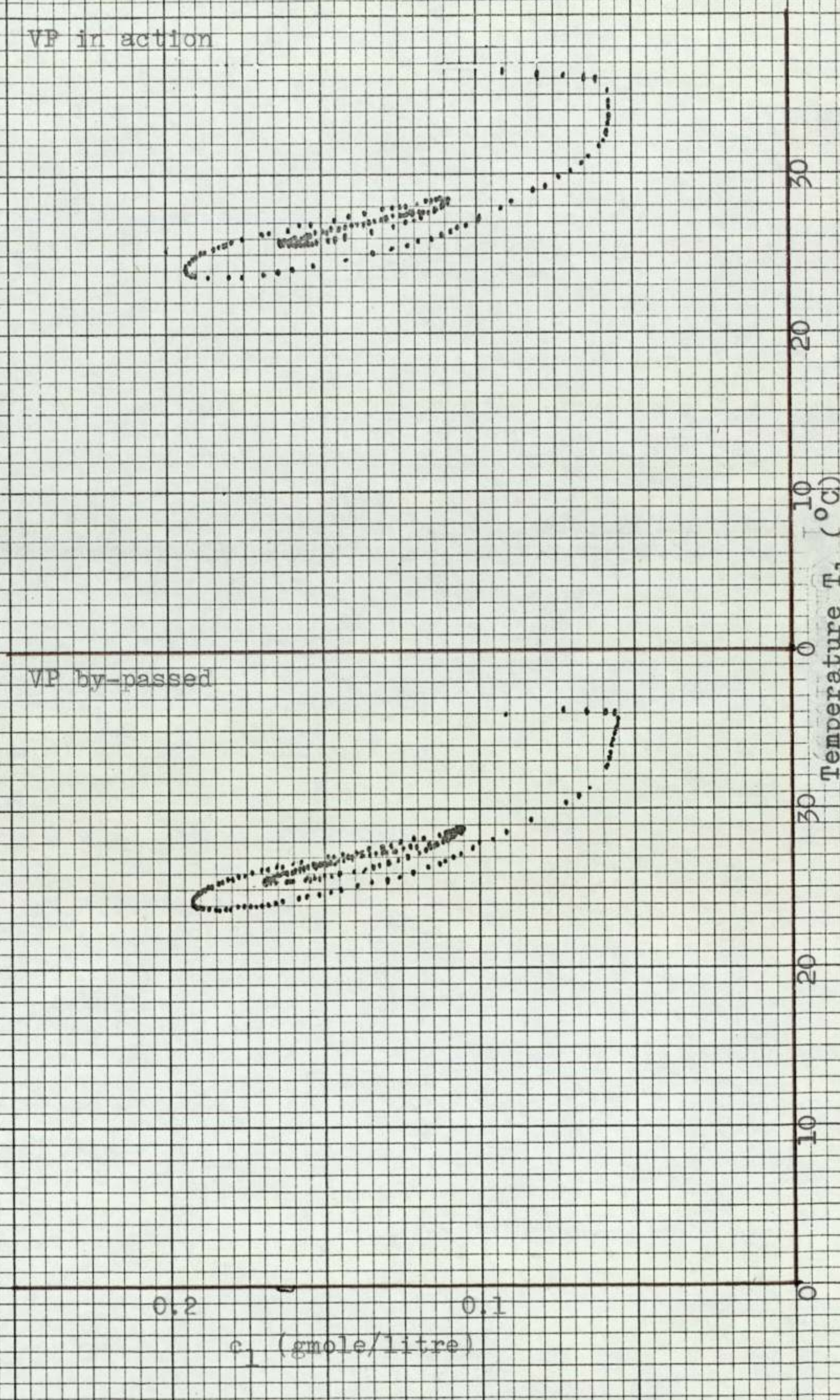

8.13. Analysis of the results obtained from the process with a 1.1 litre/min. feedrate

Portraits were obtained for various proportional band widths with or without the addition of reset action. Complete simulations were again conducted on the TR 10 for comparison purposes. The same sort of conclusions on hysteresis and multidimensionality as for the 3 litre/min. feedrate were drawn from these tests. As before, first proportional control with its various band widths and later proportional plus reset action tests were considered. Complete simulation potentiometer settings were based on Experiment 32 since its data was very similar to further experiments having the same feed flowrate. The only modifications for each experiment were the potentiometer settings determining proportional band width, set-point and reset rate.

8.13.1. Partial simulation portraits for the system under proportional control

The partial simulations for the narrower proportional band widths showed the hysteresis effect as expected from the 3 litre/min. feedrate results. The complete simulations confirmed again that these effects were not present in the two-dimensional system. In the portrait obtained in Experiment 28 (Fig.8.55.) with a proportional band width of 2 deg.C. the hysteresis was particularly noticeable and caused trajectory intersection. Fig.8.56. gives the comparison complete simulation portrait. Experiment 32 gave a particularly good example of the 10 deg.C. proportional band width. The complete and partial simulation portraits (Figs.8.57. and 8.58.) compared

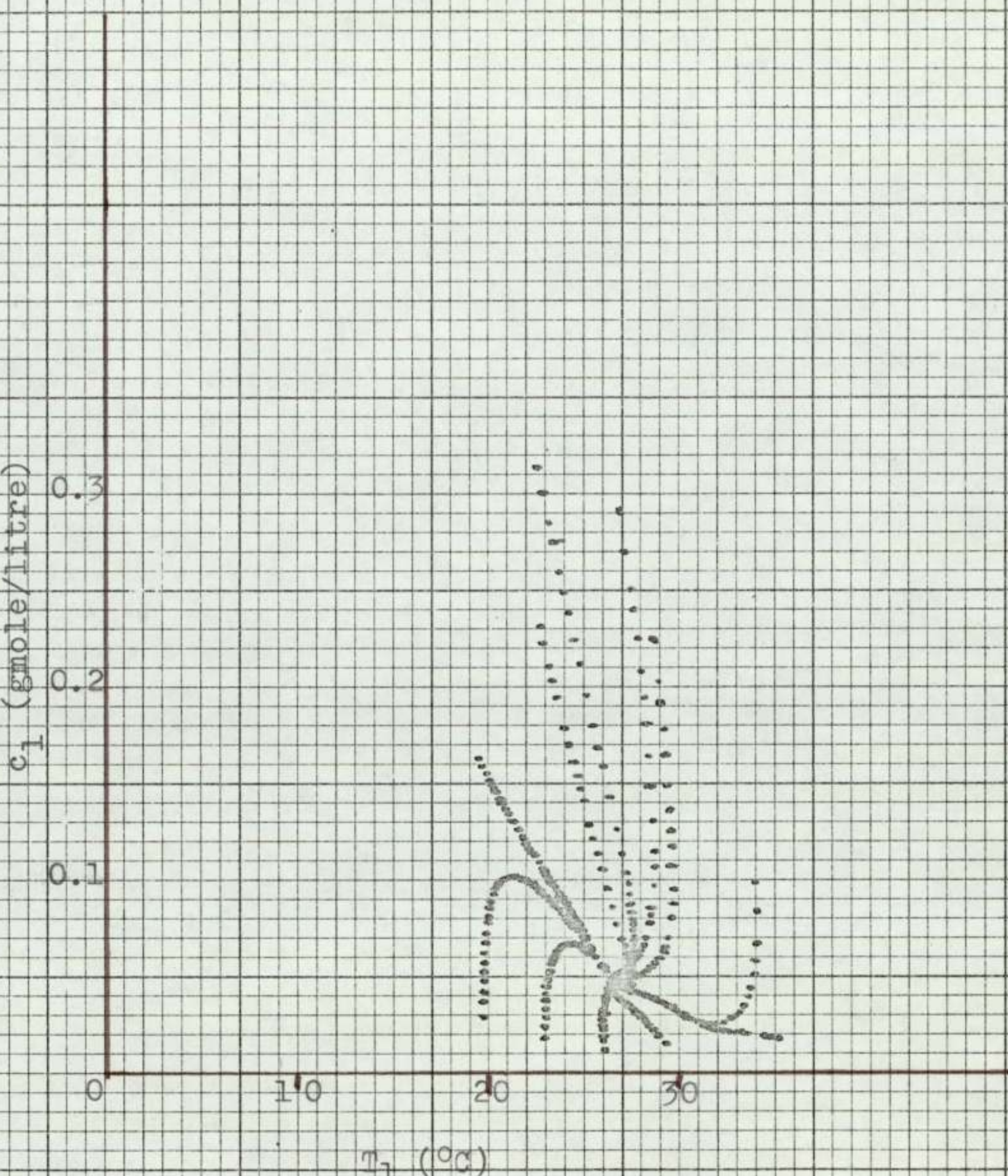

Fig.8.55. Experiment 28.

Partial simulation.

Fig. 8.56. Experiment 28.

Complete simulation.

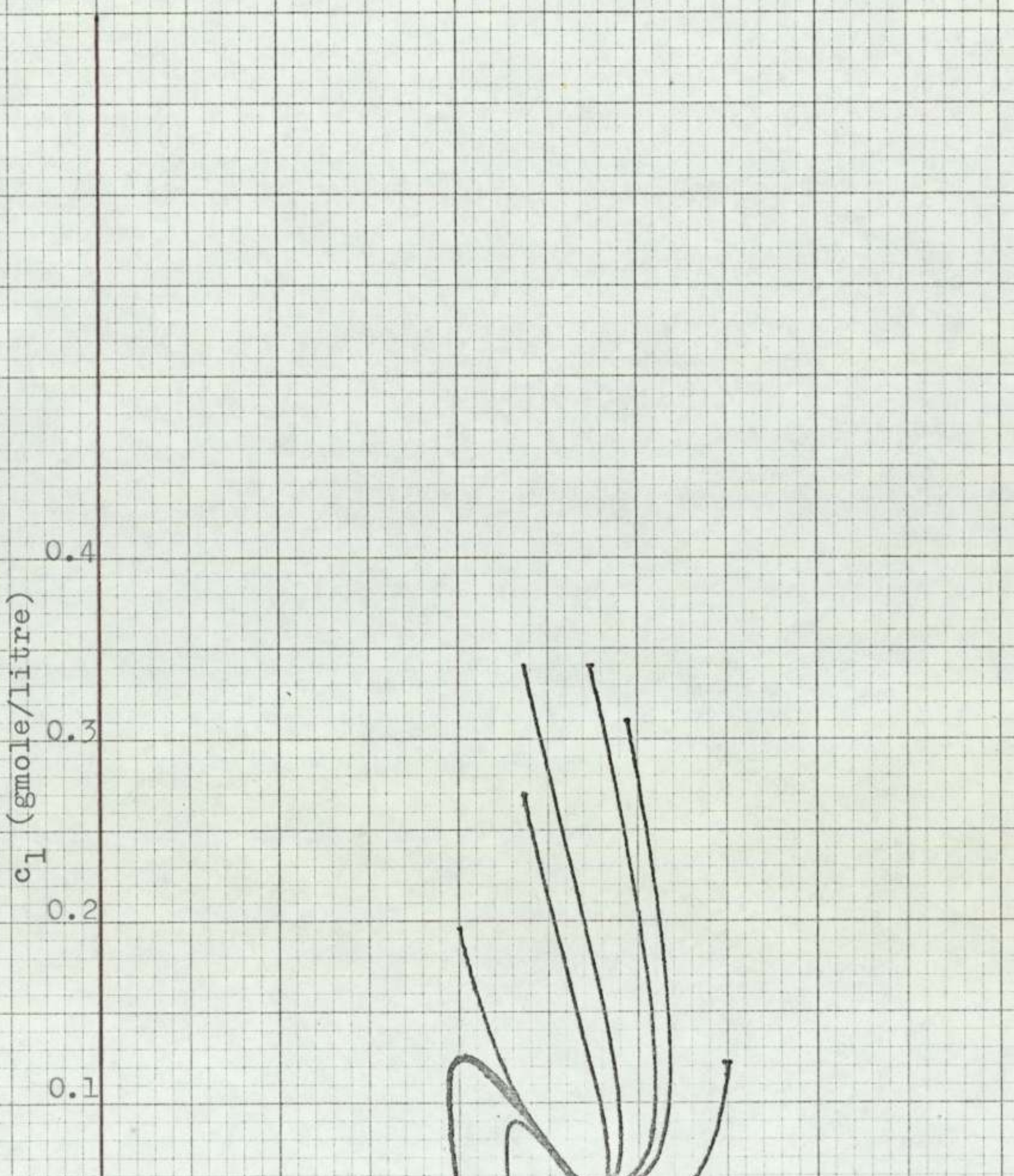

Fig. 8.57. Experiment 32.

Complete simulation.

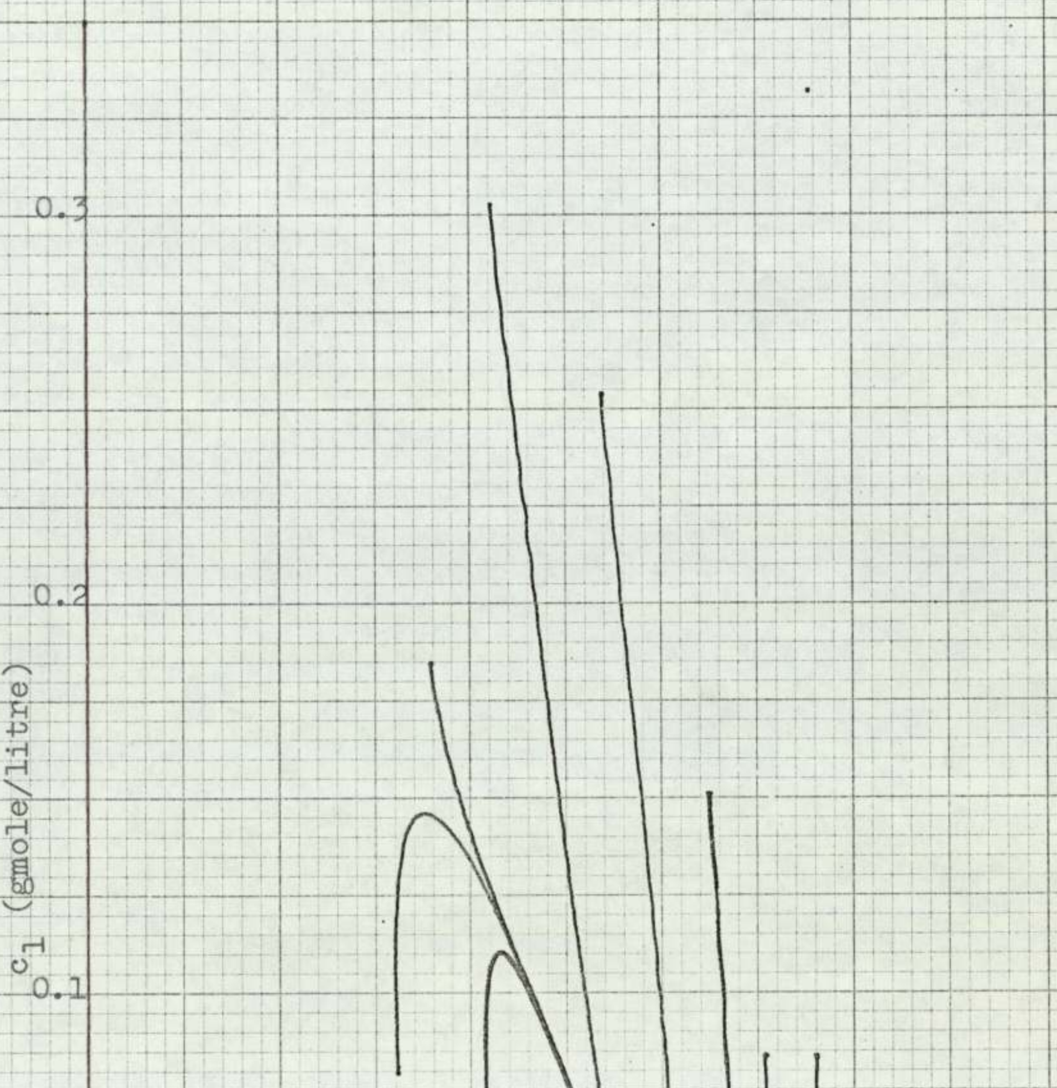

Fig.8.58. Experiment 32.

Partial simulation.

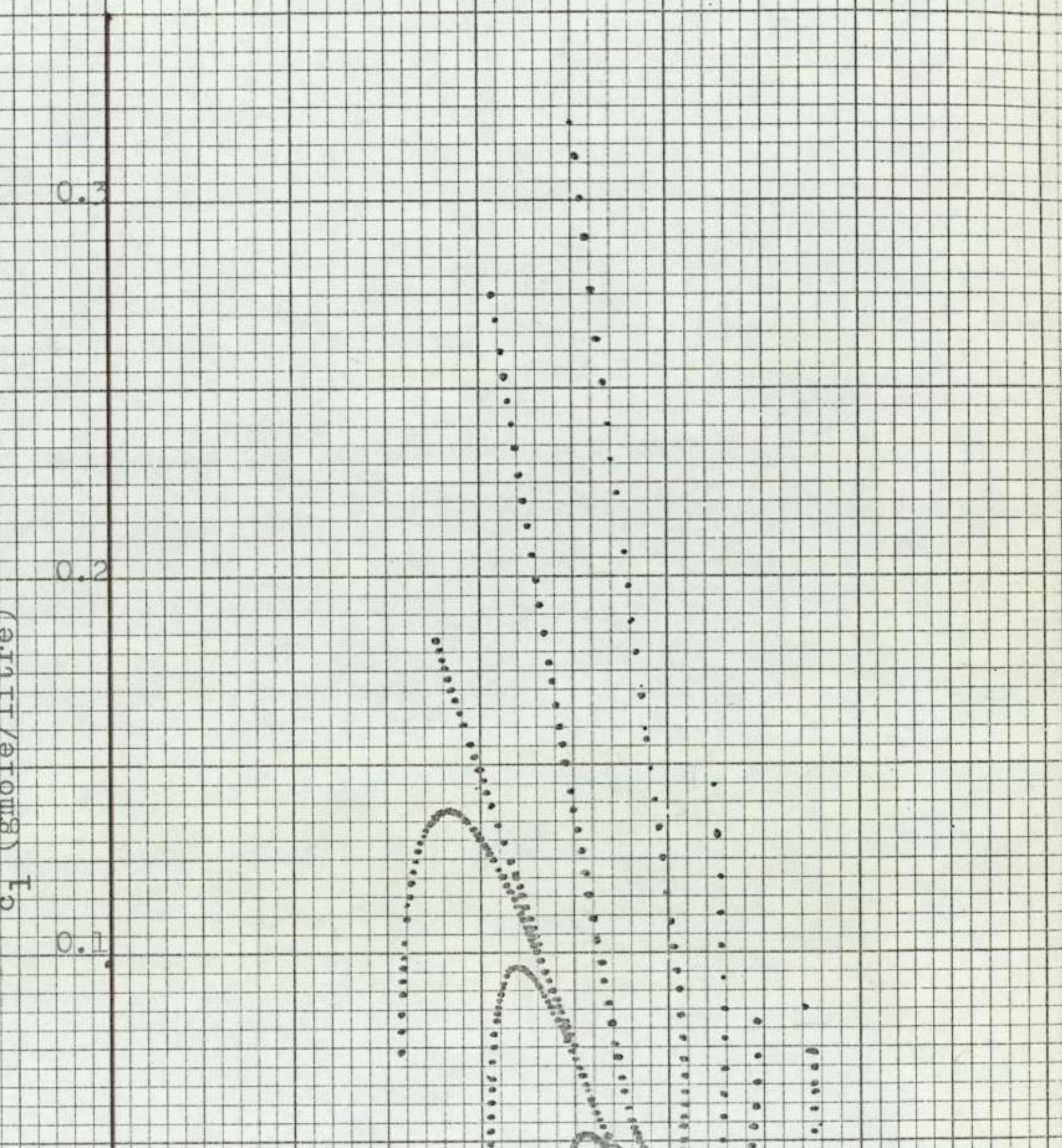

very closely indeed, the only noticeable difference being the hysteresis effect nearly causing the high temperature trajectories to overshoot on their approach to the steady state. Experiment 24 gave an example of the 30 deg.C. proportional band width. The complete and partial simulation portraits (Figs.8.59. and 8.60.) are virtually identical, the hysteresis effect being almost non-existent for such a wide band. This agrees with the 3 litre/min. tests and also the off-line tests on the controller. The little hysteresis that was present and caused the high temperature trajectory to overshoot in the partial simulation will have been largely due to the hysteresis control valve as the positioner was not in action during the run. The steady states recorded verified this conclusion by showing the two possible coolant flowrates. The values agreed with the calibration curve (Fig.A.60.). Experiment 25 confirmed this effect and the observed results also showed different coolant flowrates (portraits in Appendix - Figs.A.21 and 40.The reversal to the high temperature steady state did not occur in these tests due to the slow build up of reactor concentration. If the tests had been carried on long enough it is likely that the reversal would have eventually taken place. An intermediate proportional band width of 20 deg.C. is given in Experiment 33 (Fig.A.23.). The valve positioner was in action and little if any hysteresis was recorded.

8.13.2. Partial simulation portraits for the system under proportional plus reset control action

Experiment 31 provides an example of a proportional band width of 2 deg.C. with high reset rate (Fig.8.61.) As expected

Fig.8.59. Experiment 24.

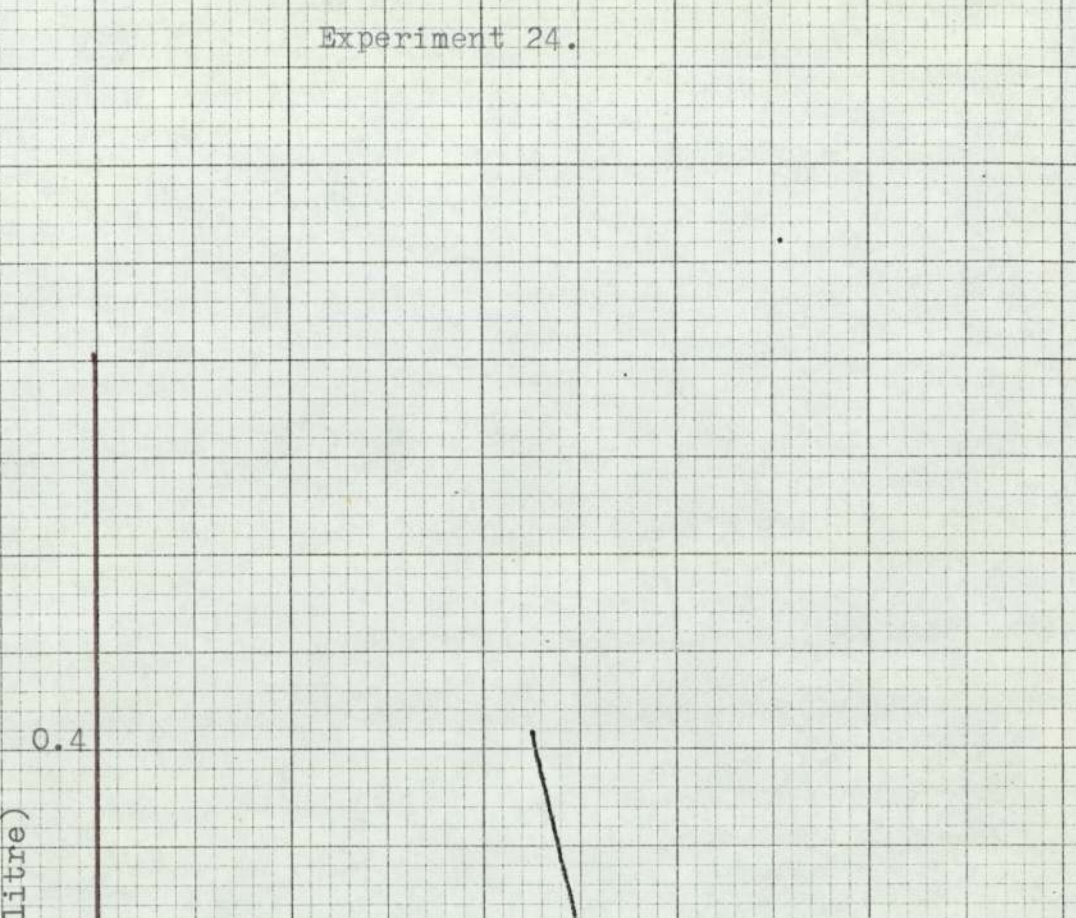

Fig.8.60. Experiment 24.

Partial simulation

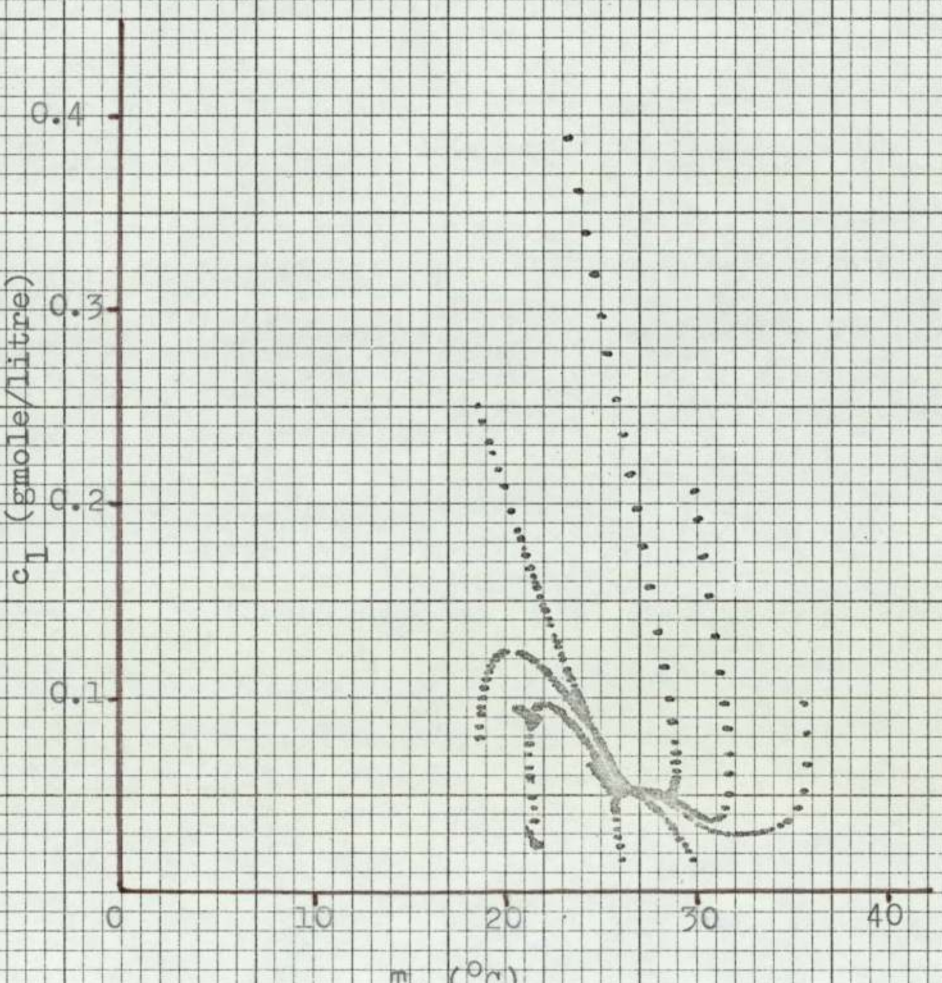

Fig. 8.61. Experiment 31.

Partial simulation.

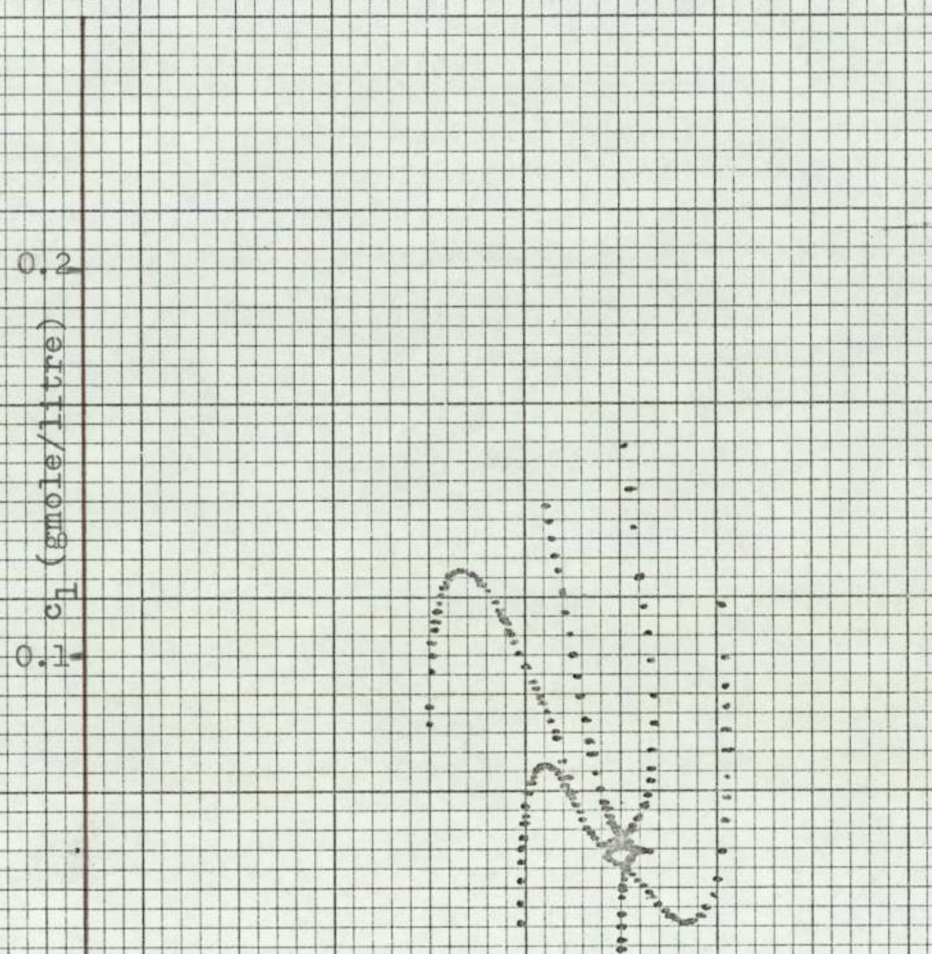

multiple trajectory intersection was recorded due to the three-dimensionality and a line oscillation observed. The complete simulation (Fig.8.62.) agreed reasonably well but as previously the accuracy of complete simulation was reduced due to controller integral action saturation limits not being simulated ; nevertheless a useful comparison was obtained. Experiment 19 gives an example of a lower reset rate. Intersection of trajectories occur in both partial and complete simulation portraits (Figs.8.63. and 8.64.).

Finally, Experiment 30 was included as an example of a 15 deg.C. proportional band width with high reset rate. The simulations were similar (Figs.8.65. and 8.66.) but the hysteresis effect of the controller seems to have caused more distinct oscillations around the set-point. Nevertheless, a live oscillation was recorded in both cases and the simulations in general were very close indeed.

8.14. Complete simulation results obtained from the Hybrid computer

These were mainly conducted in advance of the partial simulation experiments in order to gain insight into the portraits to be expected from the rig. Thus the potentiometer settings at that stage did not pertain to any particular partial simulations. However, they succeeded in aiding the analysis at that stage and gave the first indications of the presence of hysteresis in the partial simulations and the three-dimensionality of the system when reset action had been added. At a very late stage in the research the Hybrid computer became operational for a short length of time and

Fig.8.62. Experiment 31.

Complete simulation

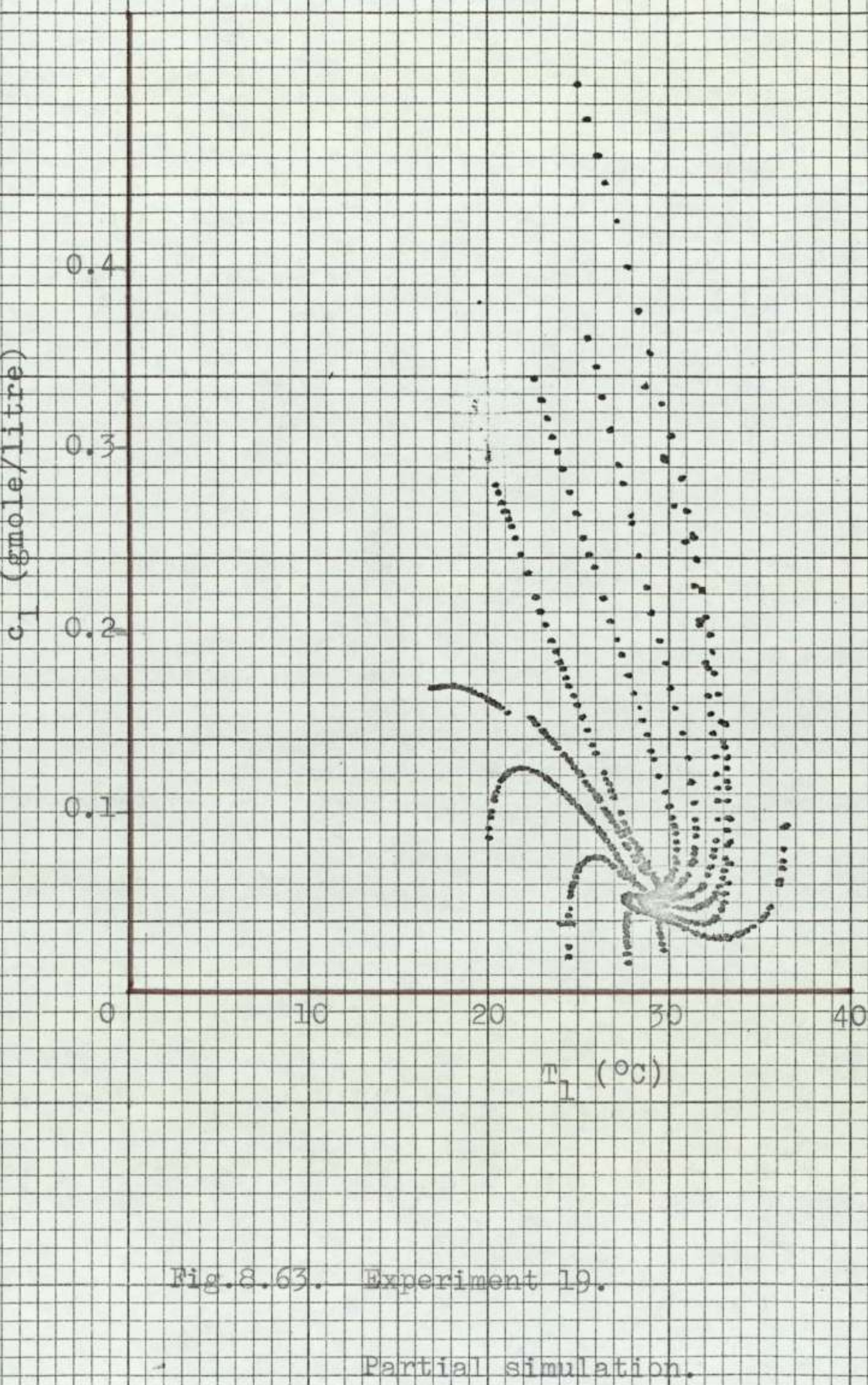

Fig.8.63. Experiment 19.

Partial simulation.

Fig. 8.64. Experiment 19.

Complete simulation.

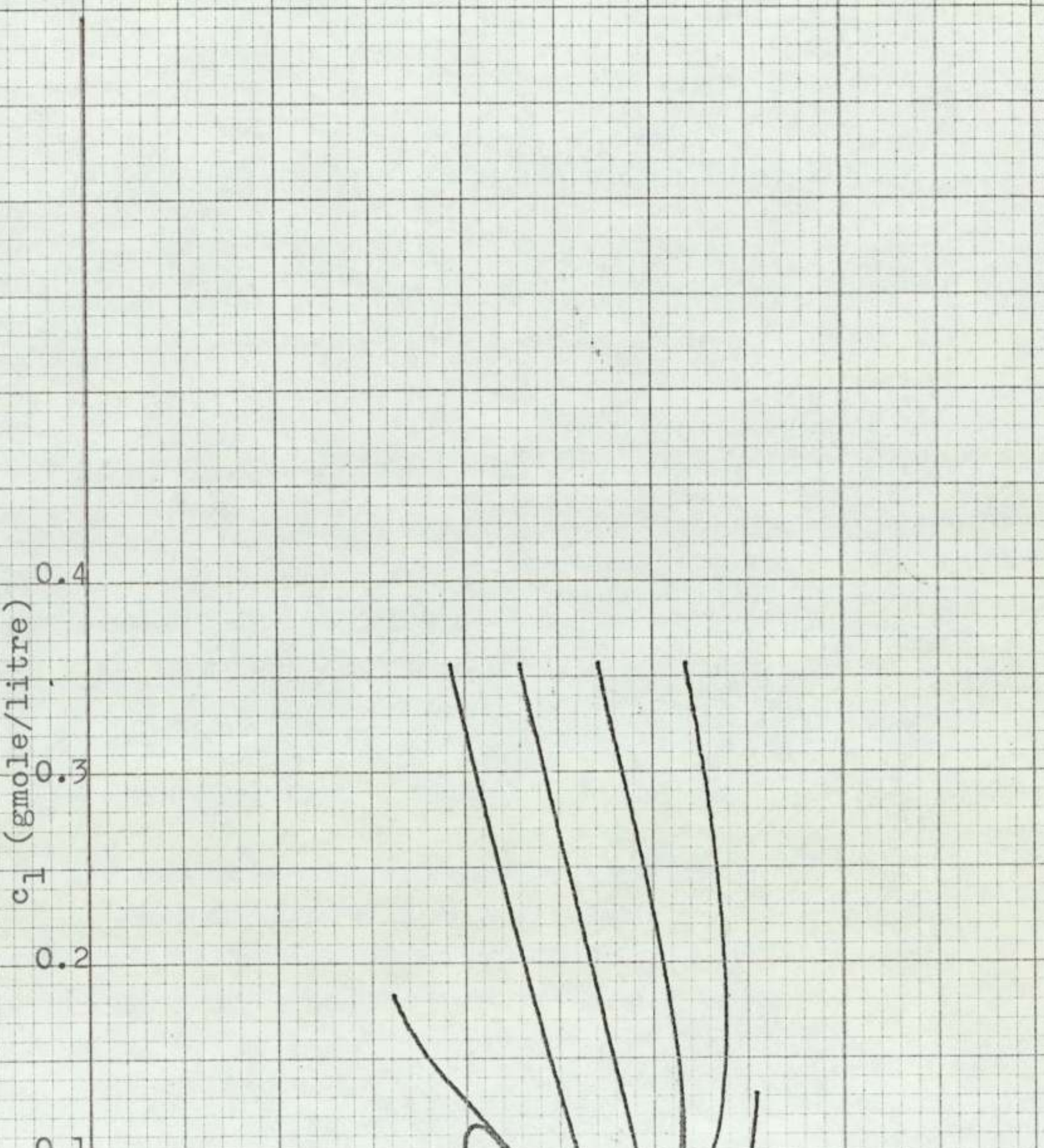

Fig.8.65. Experiment 30.

Partial simulation.

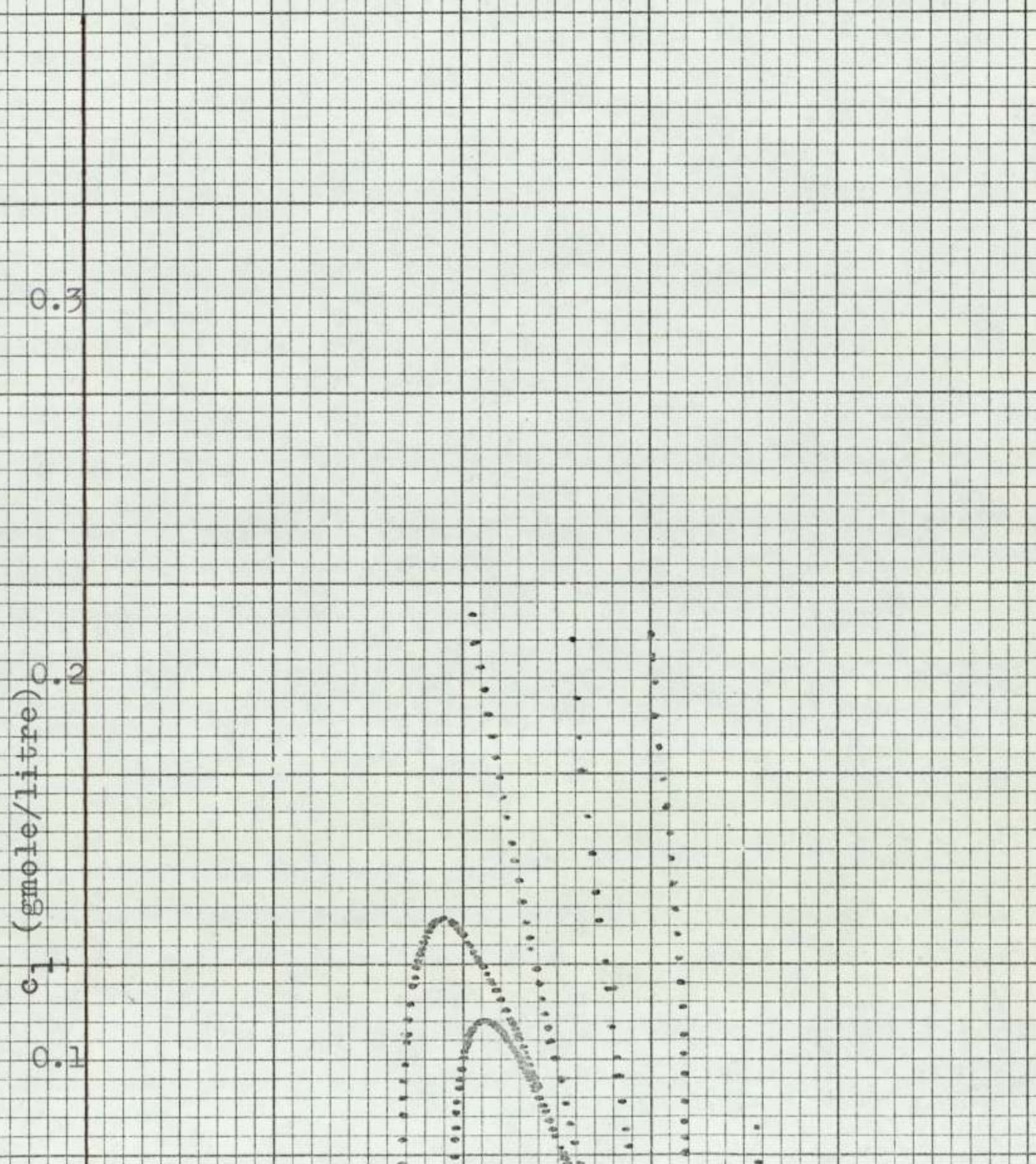

Fig.8.66. Experiment 30.

Complete simulation.

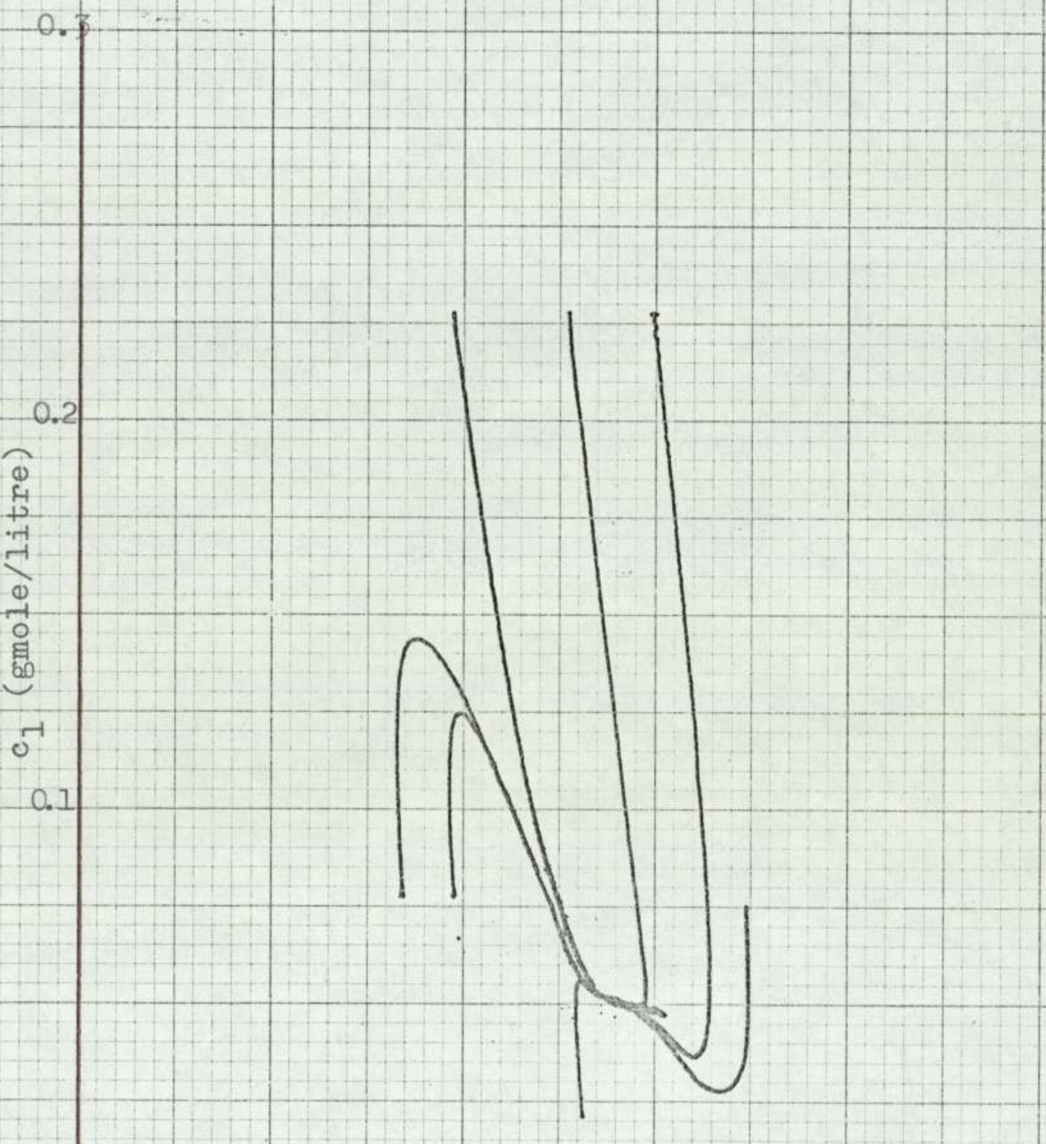

complete simulations of Experiments 67 and 28 were obtained (Figs.A.46 and 48). They produced more accurate simulations than did the TR 10 and verified previous conclusions. However, considering the increased complexity of the Hybrid circuit it was considered very doubtful whether the increased accuracy obtained for proportional control only was worth the much greater complexity of energy balance simulation. Certainly it is remarkable how close the TR 10 simulations compare with the ones from the Hybrid 48 considering the simplicity of the TR 10 circuit.

An example of the early results obtained for strong proportional action and high reset rate is also included in the Appendix (Fig.A.47.). It clearly shows three-dimensionality, in that the trajectories intersect, and the value of imposing limits on the integration of the error. These limits simulate saturation in the pneumatic controller and intersection similar to this in the partial simulation portraits was recorded (Fig.8.61.) which were not present in the TR 10's complete simulation because it was conducted without reset constraints (Fig.8.62.)

8.15. Simulation of hysteresis on the Hybrid computer

Hysteresis was simulated on the Hybrid computer by constructing the circuit shown in Fig.8.67(a). Helpful information which assisted in doing this was given in the E.A.I. "Handbook of Analogue Computation"

The potentiometer settings used are given in the Appendix (Table A.36.). A sinewave was chosen to represent the variable which undergoes a hysteresis cycle. Hence having generated

Fig.8.67.(a) Hybrid circuit diagram for hysteresis simulation

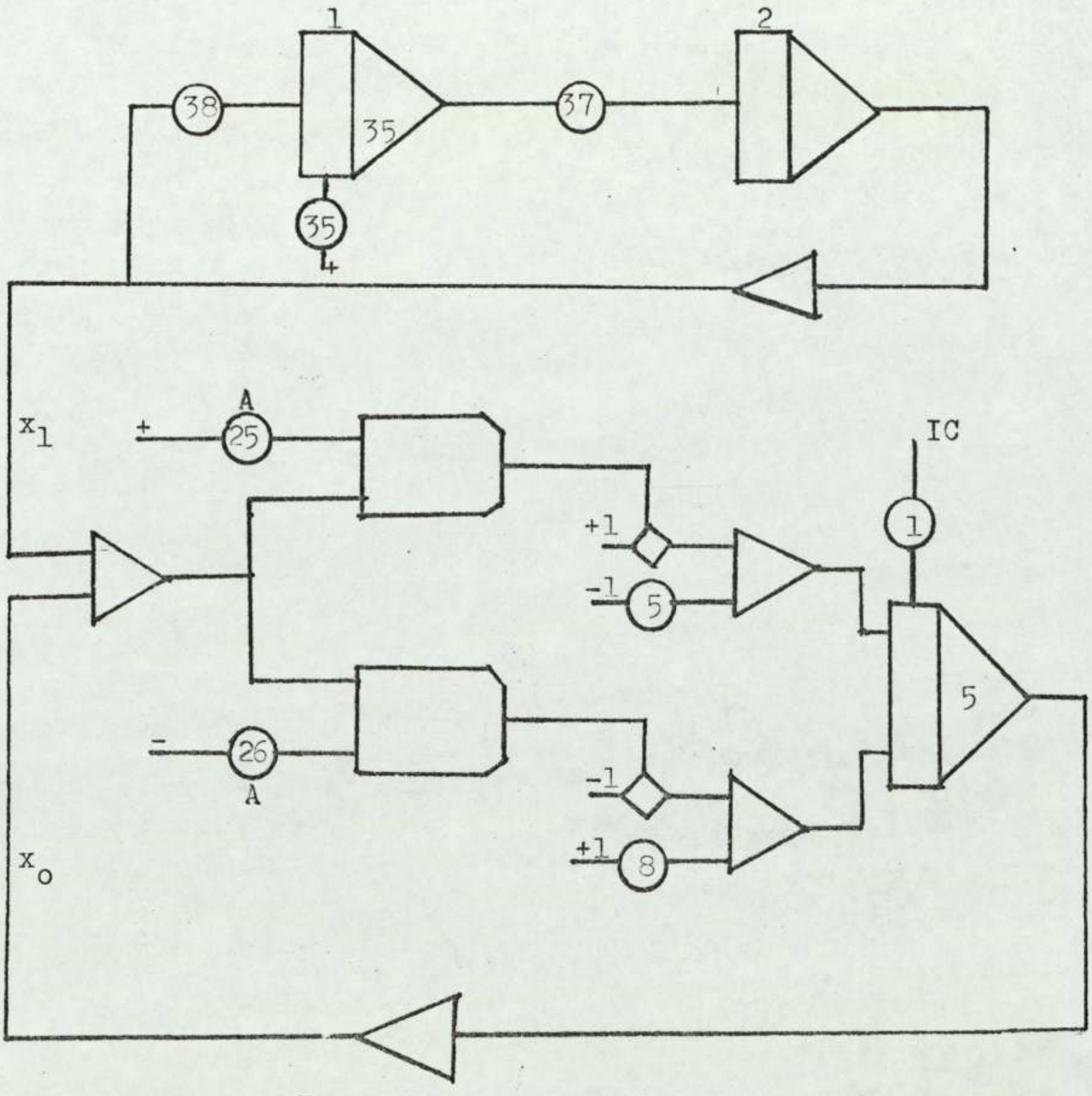

Fig.8.67.(b)

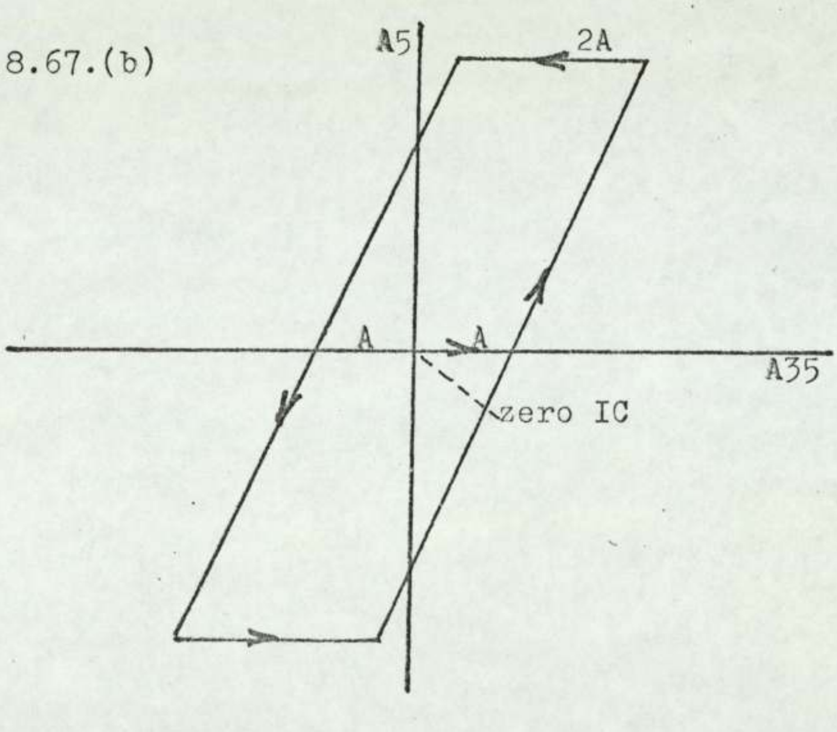

this variable it was fed into the circuit and a hysteresis loop of the form expected was displayed on the oscilloscope. Whilst it was interesting to see that the computer was capable of simulating such nonlinearities it was decided to leave this line of investigation at that stage as the circuit used up valuable computer space and it would have been difficult, if not impossible, to simulate the equipment and even one hysteresis loop on the computer due to lack of space. Also, at this stage, the computer became non-operational. Had a larger Hybrid computer been available this direction of research could most likely have been pursued profitably aiming at a very close simulation of the complete equipment.

A sketch of the hysteresis cycle produced is given in Fig.8.67(b).

Circuit operation

When x_1 increases from zero, the dead zone does not allow any input to the integrator until $x_1 - x_0$ input exceeds the limit A. Then the integrator operates at a very high rate and tracks $x_1 - x_0$ input with virtually no time lag. When x_1 drops, the integrator output does not alter until $x_0 - x_1$ becomes less than -A. There is no fixed upper limit but the width is a constant determined by the dead band which is set on the potentiometers.

8.16. Derivative controller action

A few experiments were conducted using this mode of control. Comparison portraits were obtained for the control system with a 2 deg.C. proportional band width and with or without maximum derivative action. No significant difference between the portraits could be detected.

The controller was then tested with fixed heating or cooling rates in the tank and the chart record was observed to try to detect any effect of the derivative action. Even for weak proportional control and high reset rate (i.e. oscillatory response) no effect of any consequence was observed. It was therefore decided not to carry out any further analysis of this control action. It was not considered surprising that the derivative action had no appreciable effect as it was known that the system's rate of change of temperature was never very rapid and the derivative action which depended on this as a feedback factor would have been expected to have little effect. For rapid rates of change the action should reduce overshoot but no decrease was observed.

8.17. Block diagram consideration of the entire equipment

In the analysis the complete process has been broken down into various sections and analysed in order to simulate and understand its dynamic behaviour. It was therefore felt that it would be useful finally to gather together all the analysed sections and present the entire process in block diagram form of notation. Where a linear section is being considered these blocks can be taken to represent transfer functions. Where the relationship is nonlinear they should then be considered only as a nonlinear mathematical expression which links the input and output variables.

The complete block diagram is presented in Fig.8.68. and definitions of each block are listed in Table 8.3.

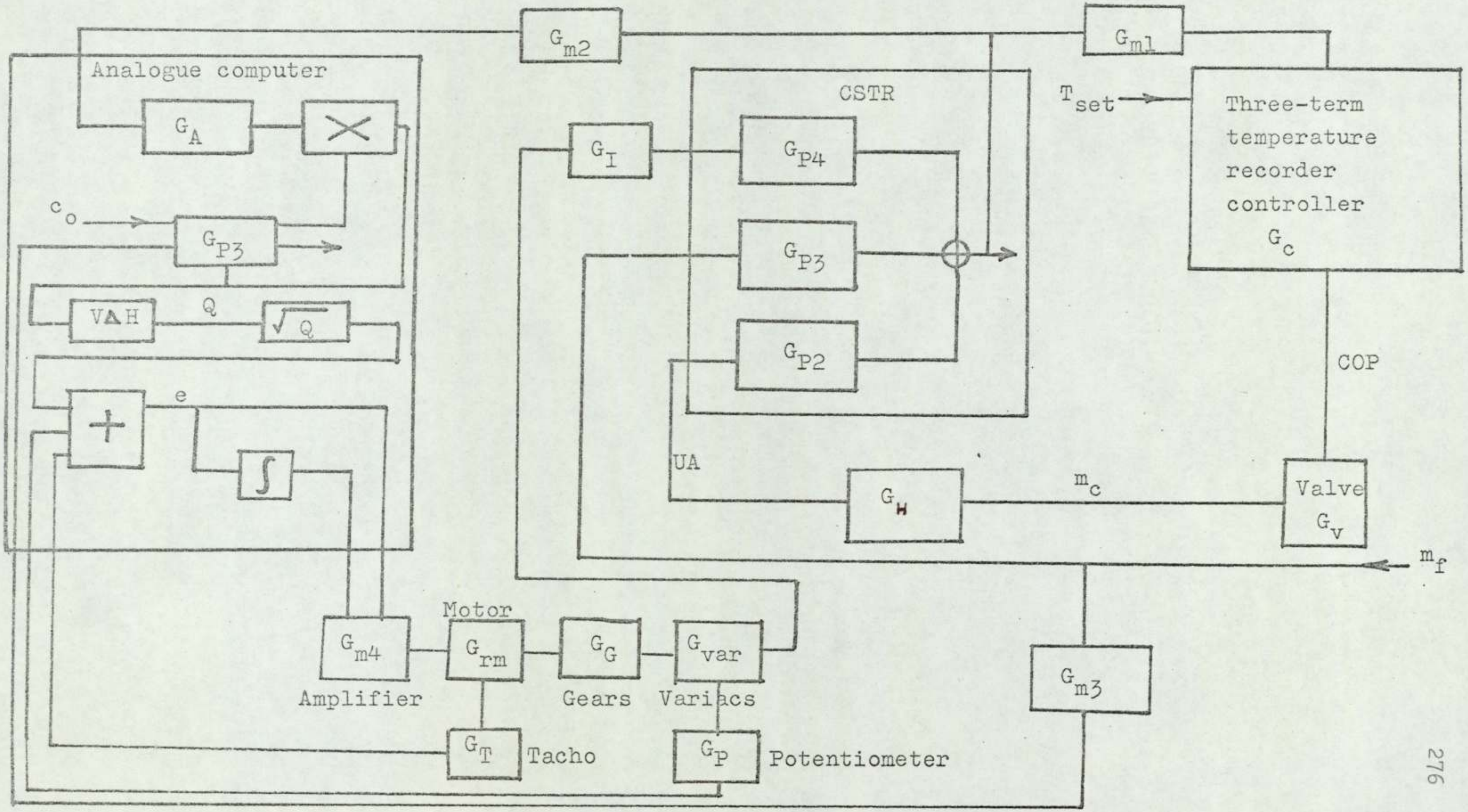

Fig.8.68. Block diagram for complete equipment

Table 8.3.

re Fig.8.68.

Transfer functions/Mathematical relationships between variables

G_{m1}, G_{m2}, G_{m4}	are transfer functions for amplifiers, time constants assumed negligible.
G_{m3}	is a resistance flowmeter, whose time constant is also small, and represents a linear relationship between pressure drop across an orifice plate and an output voltage supplying a measurement of feed flowrate to the TR 10.
G_{P1}	Nonlinear mathematics connecting feed flow-rate variable to temperature (T_1) in tank.
G_{P2}	Nonlinear mathematics connecting heat transfer coefficient to temperature (T_1) assuming a constant average coolant temperature.
G_{P3}	A nonlinear material balance connecting velocity constant [$f(T_1)$], inlet concentration and feed flowrate with concentration of A in liquor.
G_{P4}	Nonlinear mathematics connecting heat generation [$f(T_1, c_1)$] with temperature (T_1) in tank.
G_A	Nonlinear Arrhenius equation relating the specific rate (k) to temperature (T_1)

G_c Relationship between temperature (T_1) error from the set-point and output pressure from the controller (COP). Ideally this should be linear with three-term controller, the mathematics for proportional and proportional plus integral action being:

$$COP = K_c e$$

and $$COP = K_c \left(e + \frac{1}{T_R} \int e\,dt\right)$$

Investigation showed nonlinearity due to hysteresis and also slow drift of output signal.

G_v Relationship between controller output pressure to the control valve and coolant flowrate through the valve. Calibration curves were constructed with and without valve position action. The latter was found highly nonlinear due to hysteresis.

G_H Relationship between coolant flowrate and heat transfer coefficient multiplied by area of cooling coil. Calibration curve determined and found to be nonlinear.

G_{rm} Transfer function for D.C. reversible motor. The time constants were assumed negligible due to no appreciable viscous loss within the motor.

G_G Gearing ratios.

G_{var} Relationship between position on variacs to power output to the immersion heaters (square law).

G_I	Power/heat relationship. Joules equivalent.
G_P	Variac position feedback potentiometer.
G_T	Derivative feedback from tachogenerator due to motor velocity.

CHAPTER 9.

9.1. Conclusions

9.1.1. The effectiveness of the research

Various advantages of partial simulation have come to light during the analysis of the results on the controllability and stability of the system. It is first beneficial to compare this approach with the alternative routes available.

9.1.2. Comparison of partial simulation with complete simulation

Advantages over complete simulation on an analogue or Hybrid computer have been clearly shown. It was found necessary to make many approximations when simulating the whole equipment in order to fit it onto the Hybrid 48. No space was available for adding complex kinetics, hysteresis effects and other nonlinear features. It was illustrated in the results that omission of such features could have a real effect on the character of the system being simulated and thus the results obtained are much less representative. Simulations conducted on the TR 10 involved even grosser approximations since parallel logic was not then available for the representation of various system constraints. A larger computer than either the TR 10 or the Hybrid 48 would have given the facility for a much closer approximation to the system under investigation. However, all the features of the system's components to be simulated require the programmer to have a good foreknowledge of their complete characteristics. By simulating only part of the system this demand was very much reduced and the nonidealities of some components which might have been overlooked were retained in the analysis. Also in the partial simulation computer space on the Hybrid would still be available for the representation of reasonably complex kinetics.

9.1.3. Comparison of partial simulation technique with the operation and analysis of a real plant or pilot plant with a real reaction taking place

Reduced expense is one of the major advantages of the partial technique. Assuming that access to an analogue computer is possible, then the technique is cheaper in that no real chemicals need be purchased and chemical plant need only be purchased to stand up to the chosen heat transfer fluid and not to corrosive chemicals. Also no effluent or chemical recovery problems are faced. Furthermore, there are no safey hazards in the form of explosion due to runaway reactions or dangers to health due to toxic chemicals.

The real plant has no versatility in that it will have to be designed for a chosen process, whilst with only minor modifications the partial simulation equipment could be employed to investigate a range of reactions by programming the computer for the various kinetics and perhaps altering the heat transfer fluid and its flowrates in order to correspond more closely to the actual system under consideration.

For the ranges in which the real plant is marginally stable, little investigation on the real plant is possible as, if a runaway reaction is obtained, disastrous results follow.

With the partial simulation the servomechanism range is simply exceeded with no dangerous consequences.

9.1.4. Partial simulation advantages

Apart from the advantages over the other techniques already mentioned, the research highlighted the effects of nonideality in the feedback loop of the chemical plant. It thus illustrated a way of breaking down the problem yielding the possibility of analysing the effects of particular sections.

It seems likely that such a partial simulation technique could be employed to analyse other systems in which it is more convenient to simulate a particular operation. Mass transfer, absorption with chemical reactions and other types of chemical processes should lend themselves particularly well to such an approach.

Summarising, the advantages suggested by the previous two sub-sections are:

(1) Versatility - any exothermic reaction may be analysed from a range of starting points
(2) Computer space used economically
(3) Low cost
(4) No risk of explosion or health hazard
(5) Retention of chemical plant character
(6) Less demand on foreknowledge
(7) Rapid stability analysis and controllability analysis
(8) Increased investigation range to the stability limit.

9.1.5. Value of the approach used

The gap in knowledge between the analysis of completely idealised models of the chemical process and real plant problems has been narrowed by this research approach. The effects of nonlinearity in plant functioning have been illuminated. A comparison between electrical, mechanical and chemical engineering control theory showed the close analogy between the three studies and that a knowledge of all fields is really necessary in order to obtain complete assessment of a chemical plant and the operations it carries out. The problems faced are usually related and thus their solutions can be obtained by utilising know-how from all fields. In this case a knowledge of electrical time constants, servomechanism design and nonlinearities associated with the design enabled the research to be conducted and assisted in the solution of some of the problems which arose from the results. Much of the classical control analysis which originated in electrical and mechanical engineering has already been utilised in the chemical engineering industry. It seems likely that as chemical engineering systems become better defined, modern control theory will also be utilised in a similar manner.

9.1.6. Disadvantages of the research approach

An analogue computer must be available for long periods of time in order to allow its on-line use. This could be inconvenient where a large demand on computer time exists.

For systems with very long time constants a computer with higher accuracy than the one utilised would be required.

However, with the computers now available on the market this restriction would probably not be too severe.

Solutions must be carried out in real time and thus one of the analogue / Hybrid advantages of rapid problem evaluation is lost.

At least three-phase power supply is required if the size of plant under consideration is to be of reasonable proportions.

Heat transfer problems are no more overcome in this work than in the ordinary design approach. Thus a separate initial study of what the system heat transfer coefficients are likely to be for the physical properties of the liquor in the reactor must be conducted for each case under consideration. Scaling-up of the tubes and other factors, including nonideality of mixing, must be considered. To deal with the heat transfer differences, liquids other than water would have to be used or alternatively loading of the equipment's heat transfer capabilities introduced. Nonideality of mixing would have to be dealt with in the modelling of the material balance and also in the temperature monitoring for this computation.

A further point to be considered is that the partial simulation must be scaled up to real plant proportions. However, there has been much work conducted in this field and no difficulty is anticipated here (e.g. Ref.31).

For chemical systems with small time constants, electrical and immersion heater time lags could become important and render the partial simulation impracticable.

Ranges of temperature investigation are limited by the power supply available but to some extent this could be offset by utilising low specific heat liquids as simulated reactants.

Ranges of kinetics available for investigation were limited in the research by analogue computer accuracy. However, with more modern machines with higher accuracy, this difficulty could be overcome.

Large system disturbances are limited by the extent of range on the servomechanism scale which is itself dependent upon power supply per unit shaft rotation on the variacs.

9.2. Suggested direction of future research

There are several fields which could be entered utilising the partial simulation equipment. The most obvious is an extension to more complex kinetics. Several possible forms of reactions could readily be investigated by this method. It would be useful to choose a particular reaction at this stage and conduct the initial heat transfer, kinetics, heat generation and mixing studies and then from this data go forward to the partial simulation loading and modifying the equipment where necessary. By utilising the Hybrid computer instead of the TR 10, sufficient computer space would be available for this work. Should the kinetics' demand for computer space become excessive the servomultipliers could again be used as an extension unit.

The equipment could also be linked to a digital computer and data logging unit from which digital control considerations of the plant could be made. Modelling techniques could be utilised which could lead to optimal control considerations. Possibly an optimally switched control technique could be developed as suggested by the utilisation of a narrow proportional band in the three-term control. Once the temperature under control enters the control band after a prescribed number of switchings or other constraint, the control action could then be switched to the optimal setting. Work conducted in this field utilising idealised mathematical models was conducted by Aris et al (ref.(32)). The control action would have three possible settings:

Maximum coolant rate

Minimum coolant rate

Optimum coolant rate (steady state value required for chosen operating point)

Consideration could be given to the utilisation of partial simulation as an analysis technique for other chemical processes.

Work could also be considered utilising digital simulation techniques which could incorporate all the nonlinear features identified in the current research. The results could be compared with the results obtained here and also with any future system analyses.

The equipment was designed to facilitate a switch to control of the system by using feedrate as the control variable. However, work was not conducted on this due partially to time restrictions and also to the long term failure of the variplotter which did not function well enough for partial simulation. With only minor modifications to the existing plant this field of controllability and stability could be investigated.

Load changes to the system could also be imposed by utilising plant which was constructed but not commissioned. The plant allowed the variation of feed or coolant temperature as an artificial disturbance. This type of variation would produce less heat absorption by the liquids and thus produce more unstable situations.

Investigations could be conducted by testing the system with alternative cams in the valve positioner. More or less beneficial forms of control could be determined.

Feed-forward control could be considered but this should be supplemented by feedback control unless all the forms of the disturbances can be anticipated.

More complex systems such as stirred tanks in series, interacting systems and cascade control could also be tested utilising this technique.

Clearly a very wide range of applications is available and there is scope for more versatility than has so far been exploited.

A P P E N D I X

INDEX TO APPENDIX

INDEX TO FIGURES IN THE APPENDIX

INDEX TO TABLES IN THE APPENDIX

INDEX TO PROGRAMMES

Fig.A1.

Temperature vs. Chromel/Alumel thermocouple output

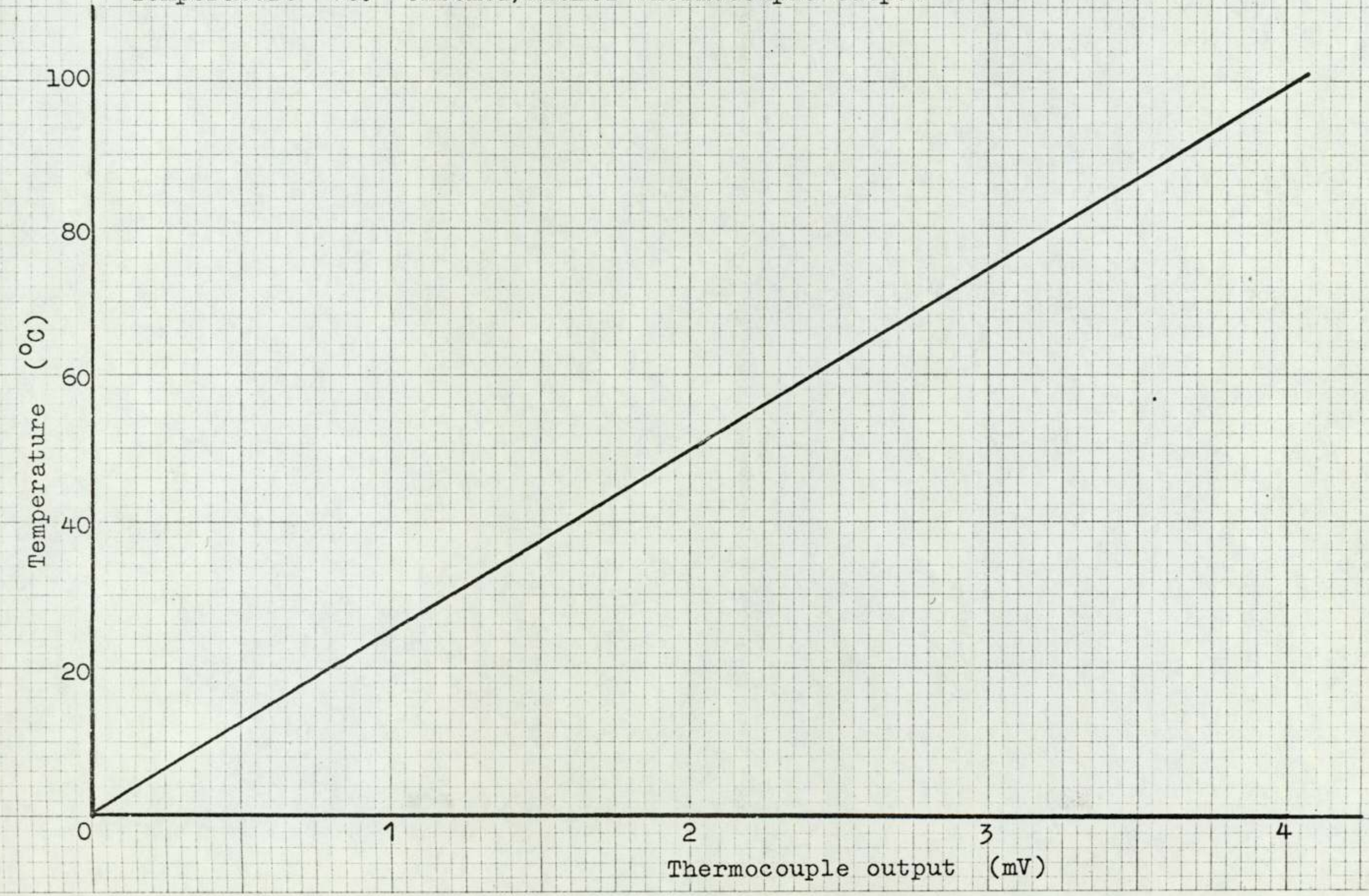

Programme 1. Elliott 803 in Algol.

Calculation of velocity constant from the Arrhenius equation:

$$k = Ae^{-E/RT}$$

where: $A = 6.3 \times 10^{15}$

$E = 24000$ cal/gmole

$R = 1.987$ cal/gmole degK

$T = 313^{\circ}K$

```
CALCULATION OF VELOCITY CONSTANT'

BEGIN REAL K'
INTEGER E,T,N'
PRINT ££LS?T£S11?K?'
READ E,T'
FOR N:=273 STEP 5 UNTIL T DO
BEGIN K:=(6.3*10**(15))*EXP(-(E/(1.987*N)))'
PRINT DIGITS(3),T,SAMELINE,££S9??,SCALED(6),K'
END'
END'
```

A graph of the results obtained with temperature vs. velocity constant is shown in Fig.A.2.

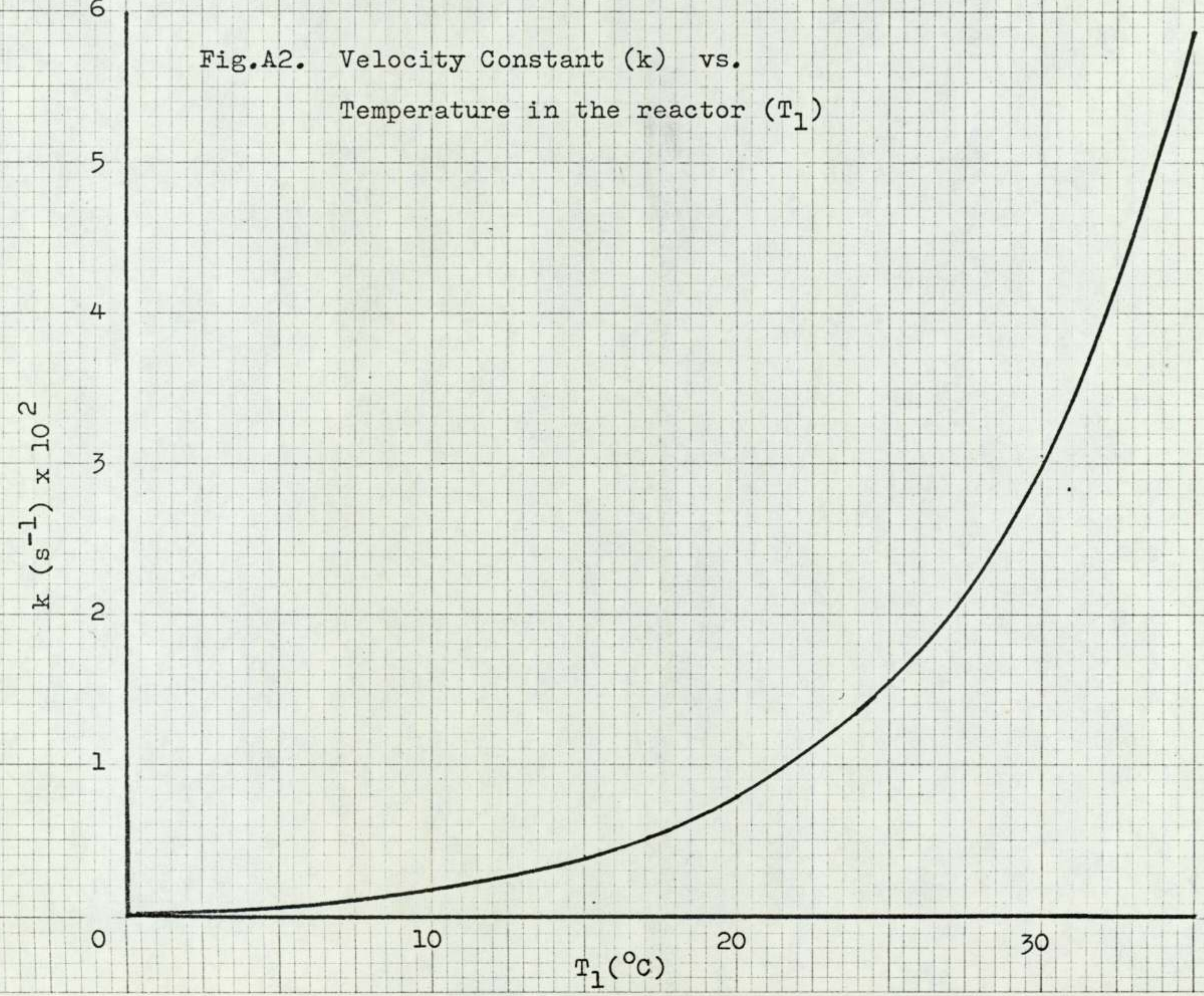

Fig.A2. Velocity Constant (k) vs. Temperature in the reactor (T_1)

Table A.1.

Calibration of variacs on maximum electrical setting

T_o = 18.8°C

m_c = 0

m_f = 3 litre/min. for variac settings 10 to 50 and
5 litre/min. for variac settings 60 to 85

Variac setting scale	Reactor temperature °C	Heat produced Kcals / hour
10	19.1	54
20	21.0	396
30	23.0	755
40	27.0	1470
50	30.5	2480
60	38.5	3540
70	35.7	4920
80	40.0	6350
85	42.5	7100

A graph of the results is given in Fig. A.3.

Fig.A3.
Heat output from immersion heaters (Q) vs. Variac Setting
(Maximum power output from the variacs)

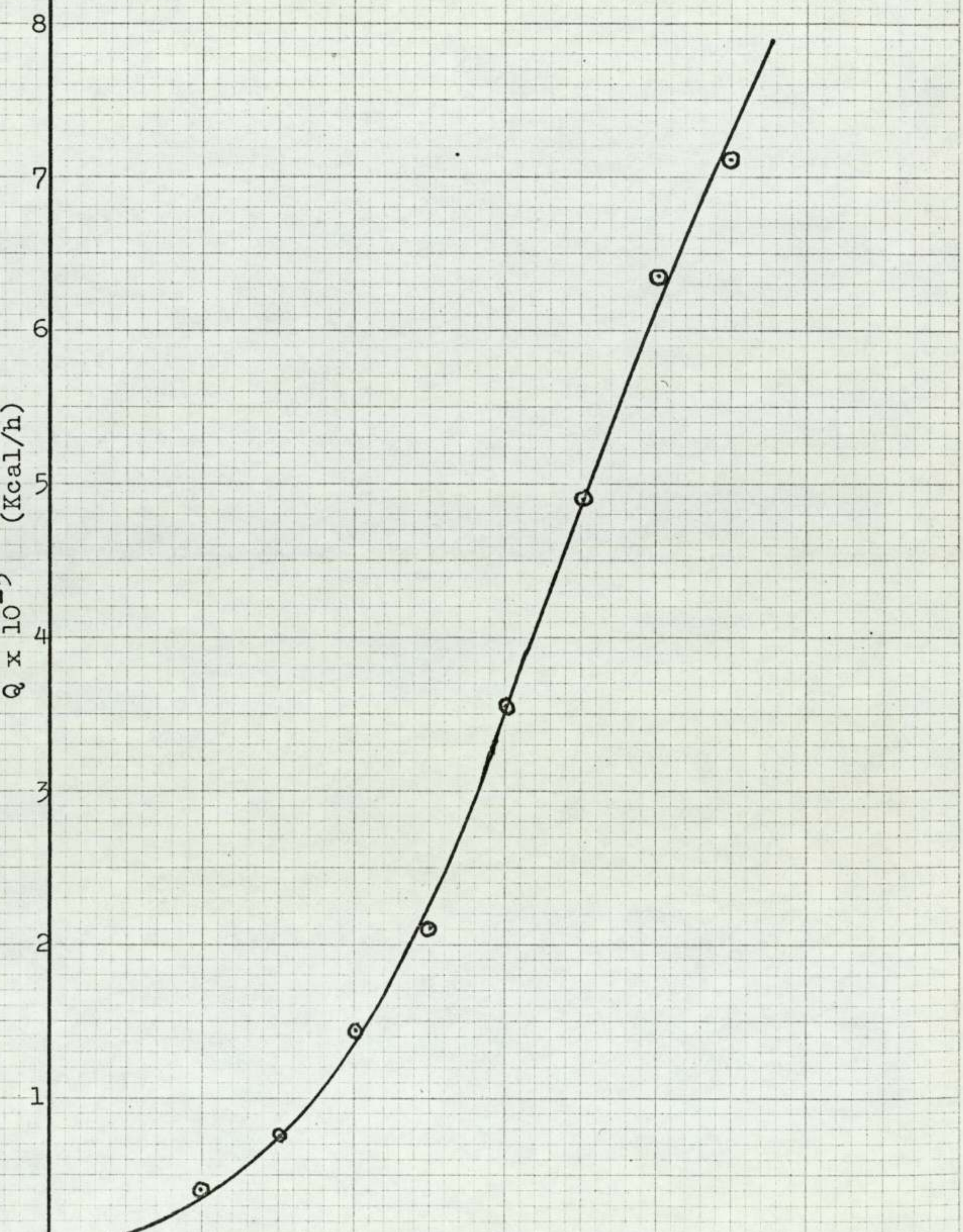

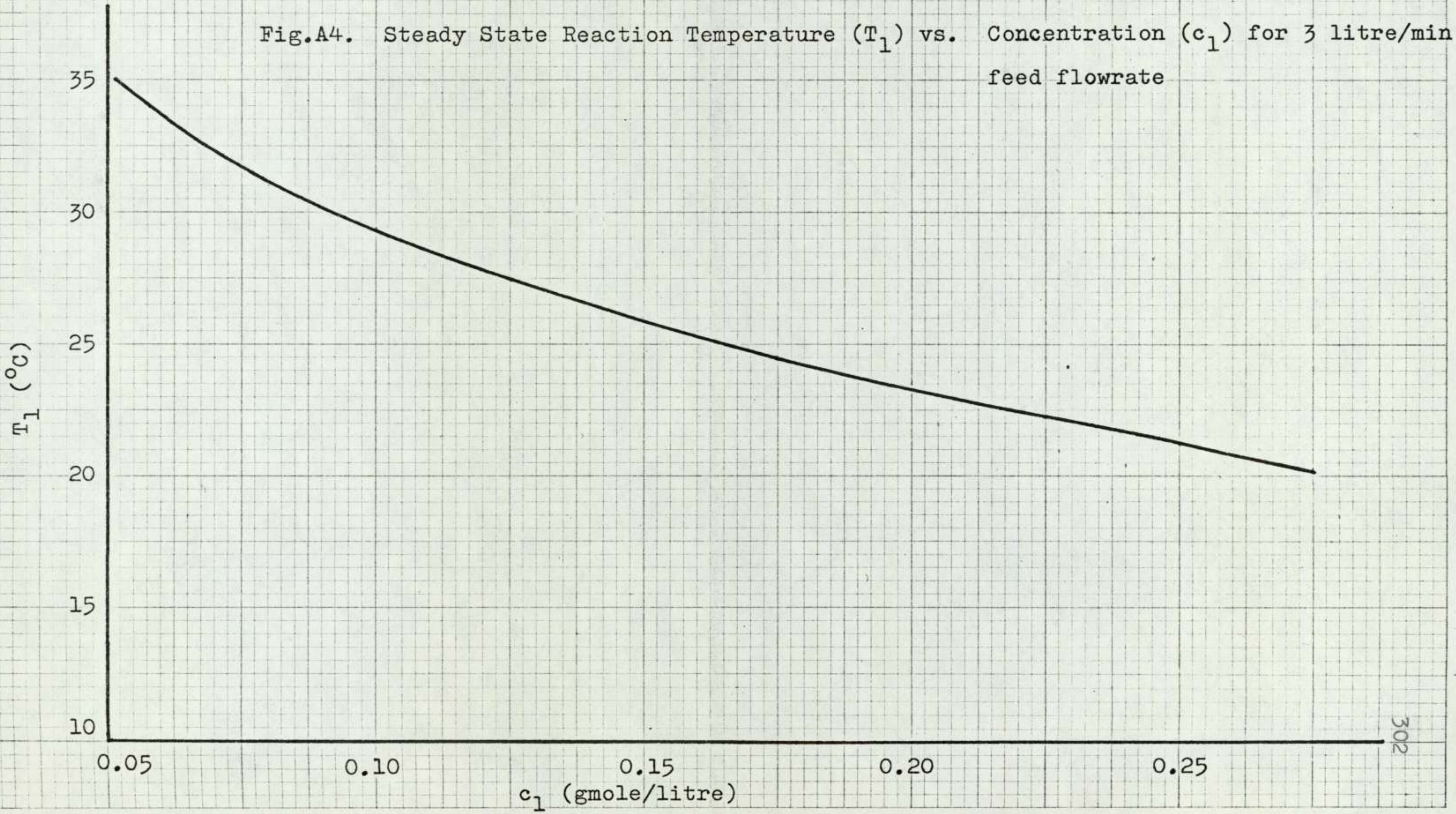

Fig.A4. Steady State Reaction Temperature (T_1) vs. Concentration (c_1) for 3 litre/min feed flowrate

Fig.A5.

Steady state reaction temperature (T_1) vs. Concentration (c_1) for 1.1 litre/min. feed flowrate

Table A.2. Experimental results

Calibration of heat transfer coefficient vs. coolant flowrate

Range of coolant flowrate 0.5 - 5 litre/min. Rotameter 14s

Stirrer set at 40 Variacs set at 60

m_c litre/min.	T_{c1} ^oC	T_{c2} ^oC	T_1 ^oC
0.70	17.0	69.8	73.0
0.80	16.4	64.0	68.0
0.95	16.0	57.6	62.8
1.13	15.9	51.5	57.8
1.26	15.9	48.1	54.2
1.39	15.5	47.2	53.8
1.57	15.2	45.2	52.1
1.70	15.1	42.8	50.0
1.90	15.7	38.0	45.0
2.10	15.5	37.8	45.6
2.15	15.4	36.6	44.5
2.38	15.2	34.7	43.0
2.55	15.2	33.2	41.6
2.70	15.2	32.0	40.5
2.88	15.2	31.0	39.1
3.25	15.0	29.1	37.4
3.40	16.0	29.1	37.5
3.63	15.1	28.1	36.3
3.80	14.7	27.0	35.5

continued

Table A.2. (continued)

m_c litre/min.	T_{c1} ^oC	T_{c2} ^oC	T_1 ^oC
4.03	14.8	26.6	34.9
4.28	14.5	25.6	34.0
4.50	14.7	24.9	33.0
5.10	14.8	23.8	31.5
5.40	14.7	23.1	31.0

Table A.2.1.

Range of coolant flowrate 1 - 11 litre/min. Rotameter 18s

Variacs set at 40

m_c litre/min.	T_{c1} ^oC	T_{c2} ^oC	T_1 ^oC
3.80	19.1	25.0	29.8
4.92	19.0	24.6	29. 2
5.96	19.0	23.7	28.1
6.96	19.0	23.0	27.5
7.47	19.0	22.6	27.0
8.52	19.0	22.2	26.5
9.42	18.9	21.9	26.0
10.08	19.0	21.7	25.7
10.98	19.0	21.5	25.4

The heat transfer coefficient was evaluated from the equation:

$$Q = m_c c_p (T_{c2} - T_{c1}) = UA \times LMTD$$

UA was calculated using programme 2 given on page 308.

The results obtained are presented in Table A3 and the calibration curve obtained in Fig.A.6.

Table A.3. Computed Results

Calibration of heat transfer coefficient vs. coolant flowrate

Range of coolant flowrate 0.5 - 5 litre/min.

Q K cal/h	LMTD degC	UA K cal/h deg C	m_c litre/min.
2217.6	18.4	120.2	0.70
2284.8	18.6	122.7	0.80
2371.2	18.9	125.2	0.95
2403.0	18.7	127.8	1.12
2424.6	17.5	138.3	1.25
2634.2	18.0	146.1	1.38
2826.0	17.8	157.9	1.57
2825.4	17.5	160.9	1.70
2542.2	15.5	163.2	1.90
2809.8	16.5	170.1	2.10
2734.8	16.2	168.2	2.15
2778.7	16.1	172.2	2.37
2754.0	15.7	175.2	2.55
2721.6	15.4	176.7	2.70
2728.3	14.6	186.8	2.87

continued

Table A.3. (continued)

Q K cal/h	LMTD degC	UA K cal/h deg C	m_c litre/min.
2749.5	14.2	193.5	3.25
2703.8	13.9	193.9	3.44
2816.6	13.7	205.2	3.62
2804.4	13.7	204.0	3.80
2853.2	13.3	213.8	4.03
2850.4	13.1	216.2	4.28
2754.0	12.5	220.0	4.50
2754.0	11.6	236.9	5.10
2721.6	11.5	234.6	5.40

Table A.3.1.

Calibration of heat transfer coefficient vs. coolant flowrate

Range of coolant flowrate 1 - 11 litre/min.

Q K cal/h	LMTD degC	UA K cal/h deg C	m_c litre/min.
1345.2	7.36	182.7	3.80
1653.1	7.03	235.0	4.92
1680.7	6.46	259.8	5.96
1680.0	6.28	267.1	7.00
1613.5	6.02	267.9	7.47
1635.8	5.75	284.3	8.52
1695.6	5.46	310.3	9.42
1632.9	5.23	311.9	10.08
1647.0	5.04	326.3	10.98

Programme 2. Elliott 803 in Algol.

```
CALCULATION OF HEAT TRANSFER COEFFICIENT VARIATION
WITH COOLING RATE AND REACTOR TEMPERATURE'

BEGIN REAL T1,TC1,TC2,LMTD,UA,MC,Q' COMMENT Q IS
THE HEAT INPUT FROM IMMERSION HEATERS MINUS LOSSES'
INTEGER N,NMAX'
SWITCH L:=AGAIN
PRINT ££S2?Q£S14?LMTD£S14?UA£S12?MC?'
READ NMAX'
N:=0'
AGAIN:READ TC1,TC2,MC,T1'
LMTD:=(TC2-TC1)/(LN((T1-TC1)/(T1-TC2)))'
Q:=MC*60*(TC2-TC1)'
UA:=Q/LMTD'
PRINT ££L??,FREEPOINT(5),Q,SAMELINE,
££S7??,FREEPOINT(3),LMTD,££S12??,
FREEPOINT(4),UA,££S7??,FREEPOINT(3),MC'
N:=N+1'
IF N LESS NMAX THEN GOTO AGAIN'
END'
```

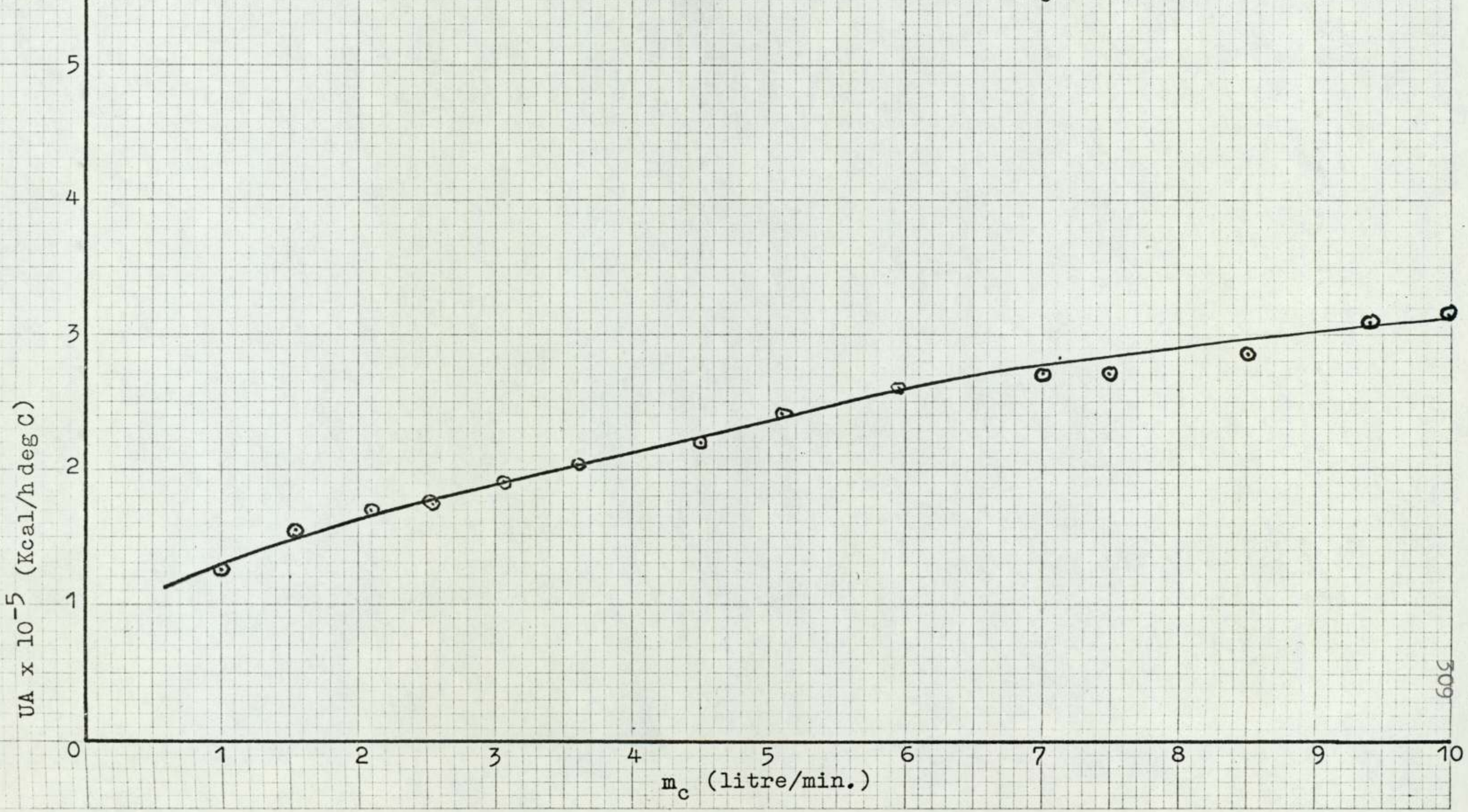

Fig.A6.

Heat Transfer Coefficient x Area (UA) vs. Coolant Flowrate (m_c)

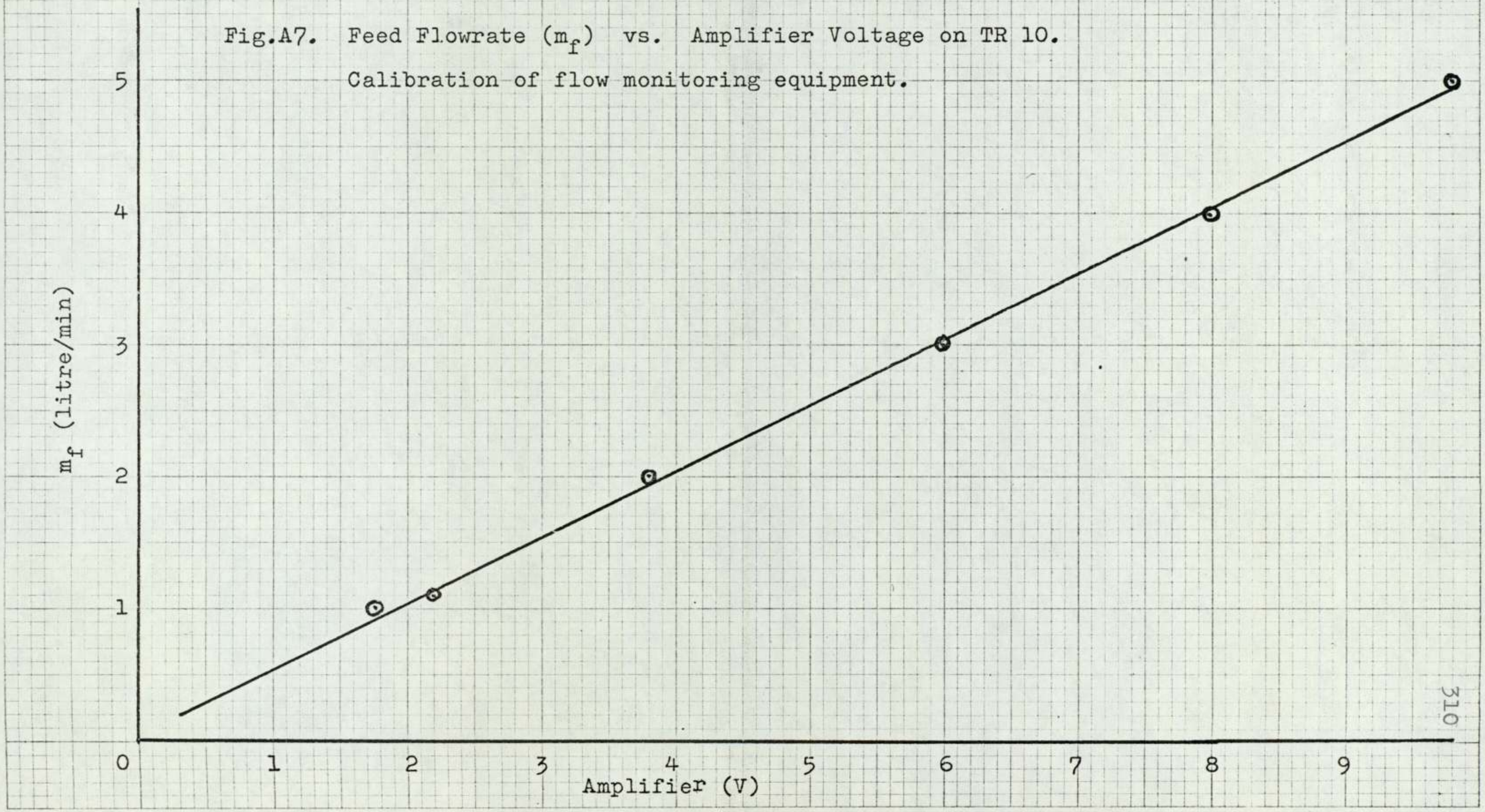

Fig.A7. Feed Flowrate (m_f) vs. Amplifier Voltage on TR 10.
Calibration of flow monitoring equipment.
m_f (litre/min)
Amplifier (V)
0
1
2
3
4
5
6
7
8
9

Table A.4.

Calibration of flow monitoring equipment on computer vs. flowrate monitored on rotameter

Rotameter reading	m_f litre/min.	A13 Amplifier on computer volts
3.5	1.0	1.78
4.6	1.1	2.20
10.0	2.0	3.8
15.8	3.0	6.0
21.0	4.0	8.0
26.0	5.0	9.8

The graph of feed flowrate vs. amplifier voltage is given in Fig.A.7.

Table A.5.

Results on check for linearity between TR 10 voltage input to servomechanism (before square root extraction) and the power output from the variacs

Variac setting	TR 10 Amplifier 2 (equivalent of heat generation) volts	Meter 1 watts	Meter 2 watts	Meter 3 watts
86.5	7.8	3045	3100	Meter range exceeded
82.1	7.0	2740	2800	
76.3	6.0	2380	2430	
75.5	5.8	2272	2337	2337

continued

Table A.5. (continued)

Variac setting	TR 10 Amplifier 2 (equivalent of heat generation) volts	Meter 1 watts	Meter 2 watts	Meter 3 watts
74.2	5.6	2200	2210	2260
70.2	5.0	2000	2015	2040
66.8	4.5	1800	1855	1840
63.5	4.0	1600	1630	1615
60.0	3.5	1440	1472	1458
55.5	3.0	1225	1250	1227
51.0	2.5	1032	1023	1040
46.2	2.0	840	831	835
40.0	1.5	584	592	600
33.5	1.0	420	400	408
24.8	0.5	224	208	208

The graphs of these results are shown in Figs.A.8., A.9. and A.10. They show a linear relationship and the lines passed through the origin showing no zero offset.

From the first two columns in Table A.5. and Fig.A.3., a graph of the voltage on Amplifier 2 vs. total heat released from the immersion heaters was plotted (Fig.A.11.). This was also found to be linear with no zero offset. A check between calculated total power output and heat release at a given variac position gave good agreement.

Fig.A8.

Power output vs. TR 10 Computed heat generation value. Watt meter 1.

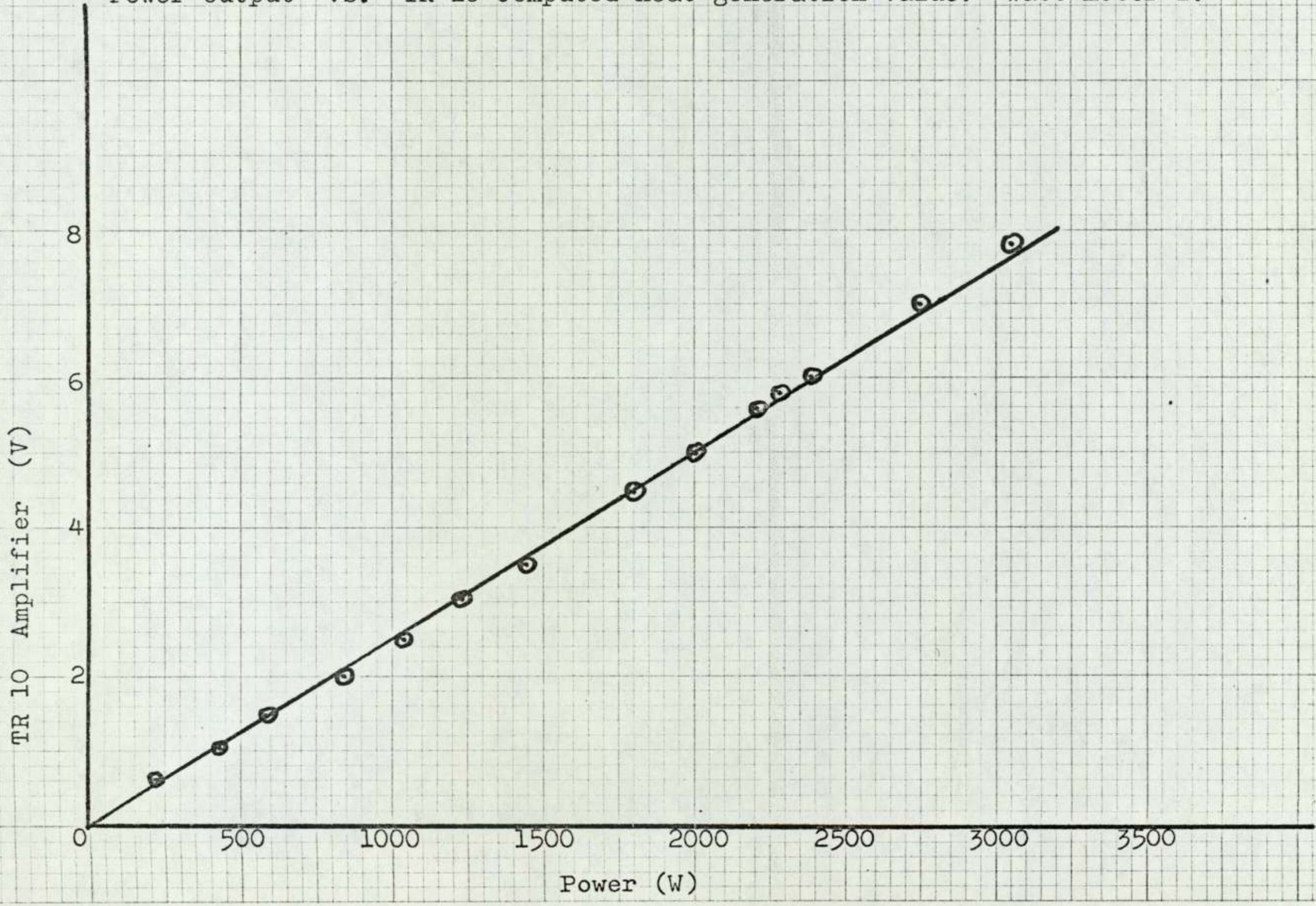

Fig.A9.

Power output vs. TR 10 Computed heat generation value. Watt meter 2

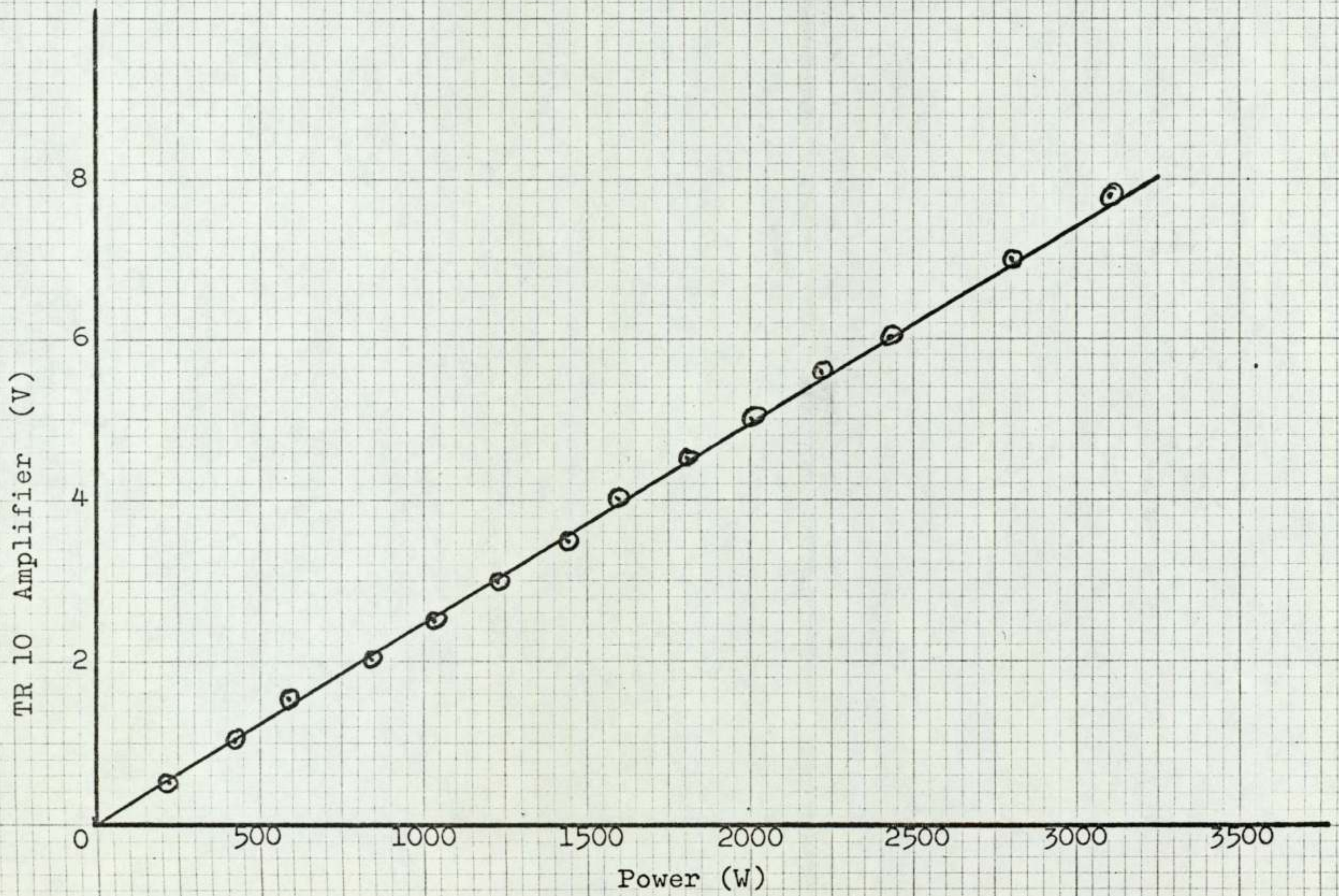

Fig.A10.

Power output vs. TR 10 Computed heat generation value. Watt meter 3

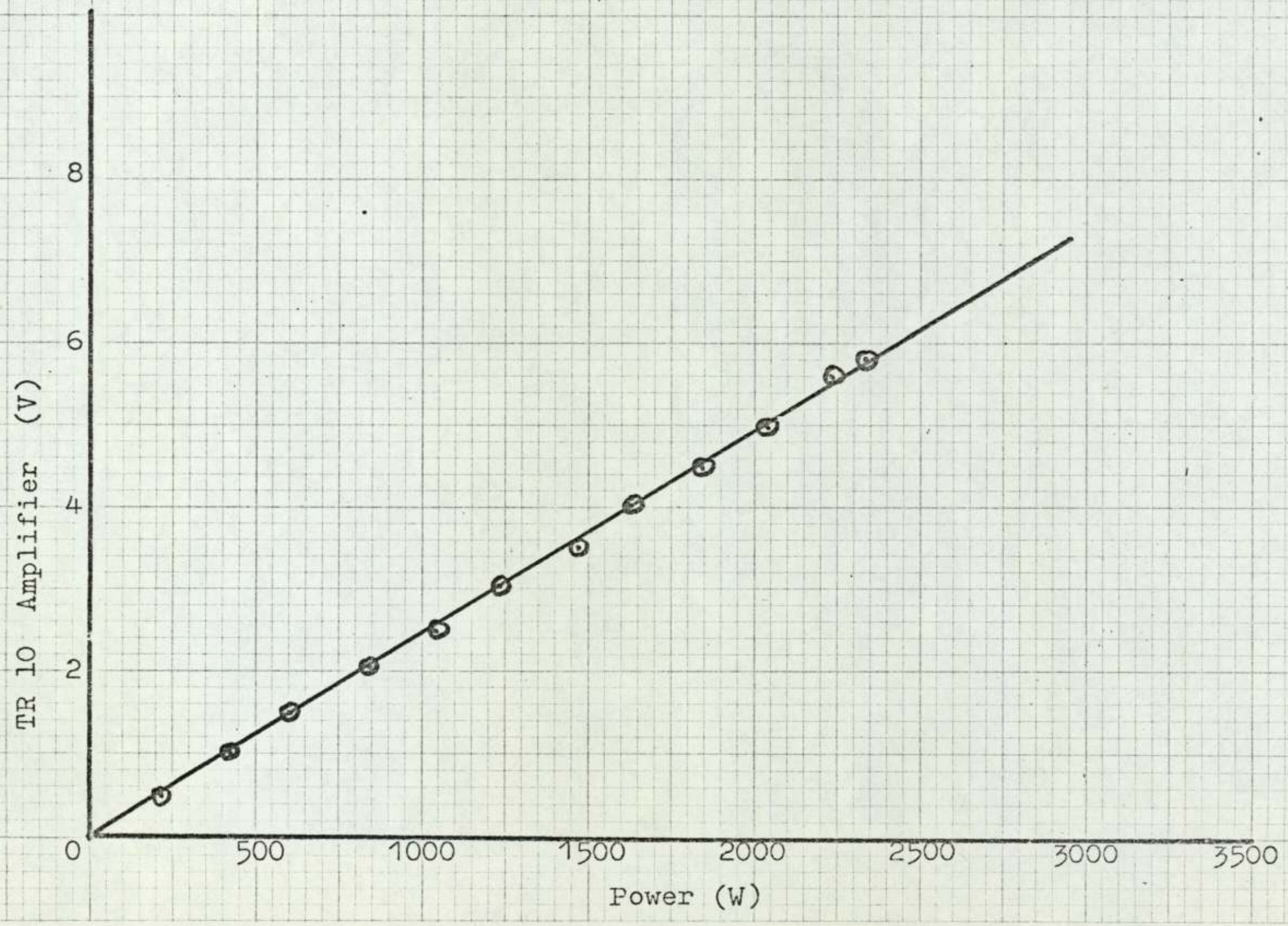

Fig.A.11.

Total heat output from immersion heaters vs. TR 10 computed heat generation value.

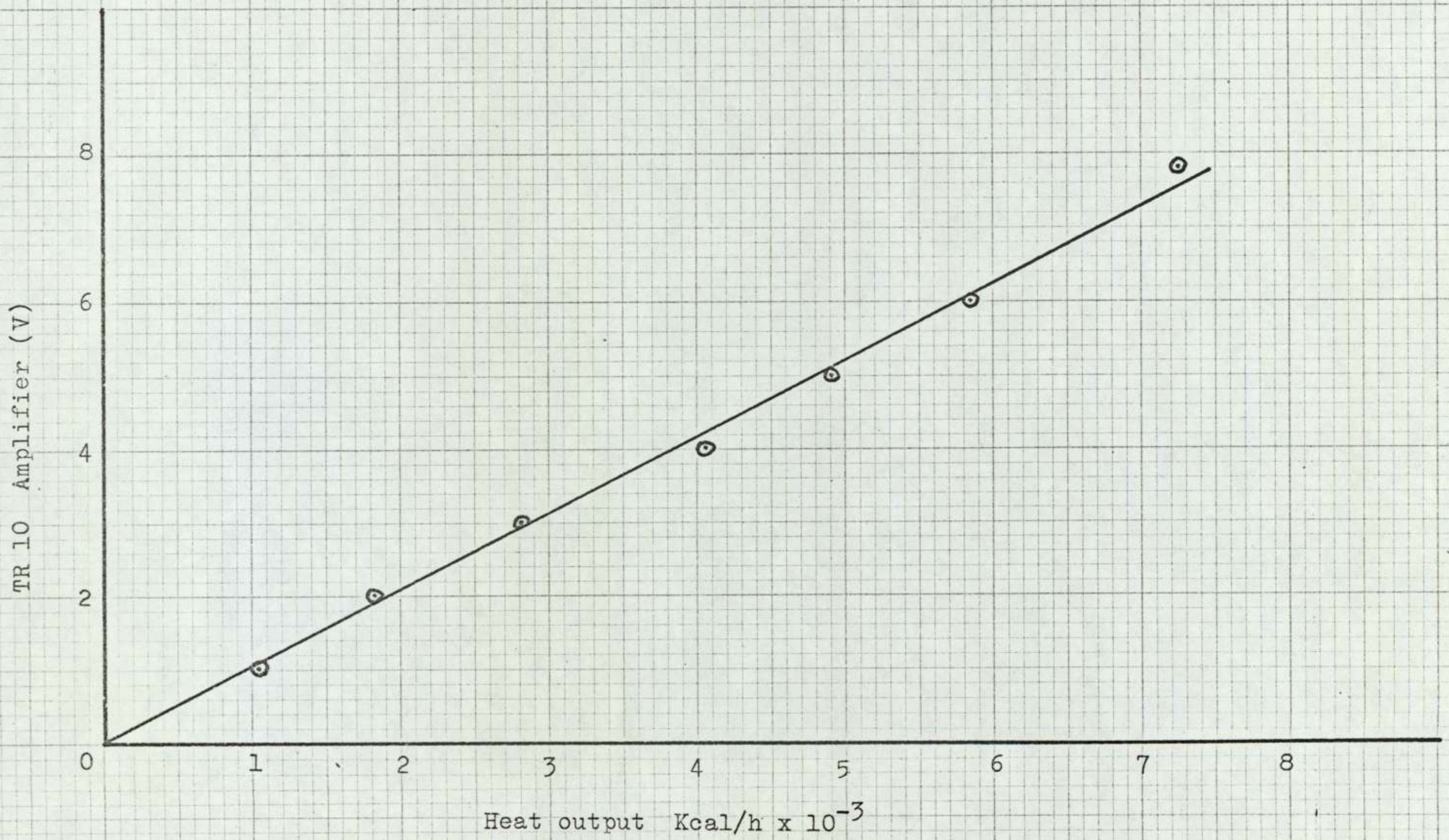

Table A.6.

First controller parameter settings

Derivative/Time minutes delay	Scale setting	Reset rate minutes
0	0	0
0.10	1	0.12
0.15	2	0.18
0.20	3	0.25
0.40	4	0.35
0.75	5	0.50
1.20	6	0.75
2.00	7	1.20
3.00	8	1.90
5.00	9	3.00

These were the correct values as far as could be ascertained from the manufacturers.

Experiments 1 to 4

Steady state verification of equipment

Experiment 1

This was the first experiment which produced useful results. Previous experiments had been spoilt by backlash effects. These effects were eliminated before this run.

The experimental results are presented in Table A.7. UA values were obtained from the calibration curve (Fig.A.6.)

Experiments 1, 2, 3 and 5 were conducted with the variacs connected for a low power output. The heat generation was calculated from:

$$Q_G = m_c c_p\,(T_{c2} - T_{c1}) + m_f c_p (T_1 - T_o)$$

For Experiment 1 this yielded a value of:

$$Q_G = 10\,(32.6 - 5.8) + 50\,(34 - 5.8)$$

$$= 1678 \text{ cal/s}$$

The heat of reaction was calculated from the data obtained at 34°C. If the heat of reaction is assumed constant over the temperature range then this value should be the same for all the steady states obtained.

Calculation of heat of reaction

$$Q_G = r\,V(-\Delta H)$$

For a first order reaction:

$$(-\Delta H) = \frac{Q_G}{rV} = \frac{Q_G}{Vkc_o/1+\frac{kV}{u}} = \frac{1678}{0.053 \times 16000 \times 1/1 + \frac{0.053 \times 16000}{50}}$$

$$= 35400 \text{ cal / gmole}$$

Table A.7.

Experiment 1 Results

Feedrate 3 litre/min. * Stirrer speed Torovolt setting 40

c_o = 1 gmole/litre

T_1 °C	T_{c1} °C	T_{c2} °C	T_o °C	k x 10 s^{-1}	c_1 gmole/litre	m_c litre/min.	A2 V	V variac scale	UA x 10^{-5} K cal/h
34	5.8	32.6	5.8	0.53	0.05	0.59	7.5	85.0	1.15
31	5.8	27.1	5.8	0.37	0.07	1.00	7.3	83.0	1.30
28	5.7	21.1	5.7	0.26	0.10	1.75	7.1	82.2	1.60
25	5.3	17.7	5.3	0.18	0.14	2.38	6.8	80.0	1.78
$\frac{22}{23}$ ‡	5.0	14.8	5.0	0.12	0.18	3.50	6.5	78.8	2.04
$\frac{20}{22}$	5.0	12.0	5.0	0.10	0.19	5.30	6.4	77.8	2.35
$\frac{26}{27}$	5.2	19.0	5.2	0.22	0.12	2.10	7.0	81.0	1.70
29	5.0	23.8	5.0	0.30	0.08	1.28	7.4	83.0	1.42
33	5.0	30.5	5.0	0.46	0.05	0.65	7.7	84.5	1.17
$\frac{24}{25}$	4.9	16.1	4.9	0.16	0.15	2.73	6.7	79.8	1.90
33.5	6.0	32.8	5.5	0.50	0.05	0.60	7.7	84.5	1.10

‡ Temperature above line monitored by controller
Temperature below line monitored by TR 10
When in agreement, only one value shown.

* This setting wasused for all experiments.

Check of experimental steady states using idealised mathematical models and a digital computer

The Algol program employed is shown on page 321. Data was presented in the form shown in Table A.8. A summary of the comparison results obtained is included in the text (Table 7.2.)

Table A.8.

u	cm^3/s	
T_o	^oK	
A	6.3×10^{15}	
V	litre	
UA	cal/deg C h	
c_o	gmole/litre	
m_f	g/s	
T_{c1}	^oK	
m_c	kg./min.	
T_{1o}	^oK	Initial estimation of temperature in reactor
E	cal/gmole	
ΔH	cal/gmole	
L	cal	Losses considered negligible over temperature range

Programme 5. I.C.L.1905 in Algol.

Calculation of steady state temperature (T_1) and concentration (c_1) for non-linearised equations

```
'BEGIN''REAL'U,T1,TO,A,V,UA,CO,MF,C1,TC1,TC2,T10,K,MC;
'INTEGER'E,H,L,J,I;
J:=READ;
'FOR' I:=1 'STEP' 1 'UNTIL' J 'DO'
'BEGIN'
WRITETEXT('('T1')');SPACE(14);WRITETEXT('('C1')');NEWLINE(1);
U:=READ;TO:=READ;A:=READ;V:=READ;UA:=READ;CO:=READ;MF:=READ;
TC1:=READ;MC:=READ;T10:=READ;E:=READ;H:=READ;L:=READ;
AGAIN:K:=A*EXP(-(E/(1.987*T10)));
TC2 :=T10-EXP(-(UA/(MC*60000)))*(T10-TC1);
T1 :=TO+K*V*H*U*CO/(MF*(U+K*V*1000))-UA*((T10-TC1)-
(T10-TC2))/(3600*MF*LN((T10-TC1)/(T10-TC2)))-L/M;
PRINT (T1,3,6);NEWLINE(1);
'IF' ABS(T10-T1) 'GE' 0.01 'THEN' 'BEGIN' T10:=T1;
'GOTO' AGAIN;
'END';
C1:=U*CO/(U+K*V*1000);
PRINT(T1,3,6);SPACE(2);PRINT(C1,3,6);NEWLINE(1);
'END';
'END';
```

Experiment 2

This experiment was conducted after improvements had been made to the servomechanism. These were discussed in Chapter 7.

The experimental results are given in Table A.9. and the final comparison table of experimental and computed tank temperatures and concentration were presented in the text (Table 7.3.).

Table A.9.

Feedrate 3 litre/min. Stirrer speed Torovolt setting 40

c_o = 1 gmole/litre

T_1	T_{c1}	T_{c2}	T_o	k x 10	c_1	m_c	A2	V	UA x 10^{-5}
°C	°C	°C	°C	s^{-1}	gmole/litre	litre/min.	V	variac scale	K cal/h
34.0	6.8	33.0	6.5	0.48	0.06	0.50	7.1	82.6	1.20
30.0	6.1	26.0	6.0	0.32	0.09	1.00	6.7	80.0	1.30
25.0	5.9	19.5	5.9	0.13	0.18	1.88	6.0	76.5	1.63
23.2	5.8	17.0	5.9	0.11	0.20	2.50	5.8	76.0	1.80
18.2	5.2	12.5	5.5	0.06	0.36	3.40	4.6	68.5	2.00
16.7	5.2	11.0	5.5	0.04	0.38	4.70	4.4	67.5	2.30
24.2‡	5.5	19.6	5.5	0.13	0.17	1.75	6.1	77.0	1.60
28.1	5.8	24.0	5.8	0.25	0.10	1.13	6.6	80.0	1.35
32.0	6.1	30.9	5.6	0.40	0.07	0.55	6.9	82.0	1.10

‡ Temperature monitoring drift correction

($-\Delta H$) calculated to be 34250 cal/gmole.

Experiment 3

This experiment was a further check on the equipment's steady state operation. The experimental results are given in Table A.10. and the comparison values of experimental and computed tank temperature and concentration in Table A.11.

These results confirmed those from Experiment 2 although it was noticed that accuracy was reduced at the lower temperatures. This would be due to the reduction in accuracy of the computed velocity constant due to the VDFG's limitations and also to the fact that the system would be moving slowly dynamically. It is very likely that eventually if the system had been left long enough it would have attained a steady state condition much closer to the one computed.

Table A.10.

Feedrate 3 litre/min. Stirrer speed Torovolt setting 40

c_o = 1 gmole/litre

T_1	T_{c1}	T_{c2}	T_o	k x 10	c_1	m_c	A2	V	UA x 10^{-5}
^oC	^oC	^oC	^oC	s^{-1}	$\frac{\text{gmole}}{\text{litre}}$	$\frac{\text{litre}}{\text{min.}}$	V	variac scale	K cal/h
34.7	6.8	34.0	6.1	0.52	0.054	0.53	7.5	84.6	1.10
30.0	6.0	25.5	6.0	0.30	0.075	1.15	7.1	83.0	1.35
25.5	6.0	20.0	6.0	0.16	0.165	2.13	6.6	79.9	1.70
‡ 23.6	6.0	16.5	6.0	0.12	0.190	3.20	6.5	79.0	1.97
20.0	5.8	13.3	6.0	0.08	0.295	4.70	5.8	75.3	2.30
29.1	6.1	24.5	6.1	0.28	0.099	1.38	7.2	83.2	1.45
25.0	6.0	19.0	6.0	0.14	0.155	2.13	6.3	78.5	1.70

‡ Temperature drift correction

$(-\Delta H)$calculated to be 35150 cal/gmole.

Table A.11.

Comparison steady state results

T_1	c_1	T_1	c_1
Partial simulation values		Digital computed values	
34.7	0.054	34.7	0.053
30.0	0.094	30.0	0.093
25.5	0.165	25.5	0.158
23.6	0.190	22.1	0.229
20.0	0.300	18.5	0.330
29.1	0.099	28.8	0.106
25.0	0.155	25.4	0.158

Experiment 4

This was conducted much later than the other experiments after the new temperature monitoring device had been installed. The variacs were set at maximum output (Fig.A.3.).

The experimental results are given in Table A.12. and the comparison steady state values in Table A.13. Good agreement was recorded.

Table A.12.

Feedrate 3 litre/min. Stirrer speed Torovolt setting 40

c_o = 1 gmole/litre

T_1 °C	T_{c1} °C	T_{c2} °C	T_o °C	kx10 s^{-1}	c_1 gmole/litre	m_c litre/min.	A2 V	V variac scale	UAx10^{-5} Kcal/h
33.0/32.0 ‡	16.9	24.0	16.9	0.40	0.068	0	3.0	54.8	0
29.2	17.0	27.6	17.0	0.27	0.103	1.00	2.8	53.2	1.30
26.6	17.0	22.9	16.9	0.18	0.145	2.85	2.6	51.6	1.85
24.8	16.8	20.6	16.8	0.14	0.180	5.15	2.5	50.7	2.35
23.8	16.9	19.8	16.9	0.13	0.190	7.30	2.5	50.3	2.70
23.4	17.0	19.2	17.0	0.12	0.195	9.45	2.4	50.1	3.05
25.0	17.0	21.1	17.0	0.14	0.181	4.50	2.5	50.8	2.25
28.7/28.3	17.0	26.0	17.0	0.24	0.110	1.30	2.7	52.4	1.35
33.0/32.0	16.9	24.2	16.9	0.38	0.073	0	2.9	54.3	0

‡ Temperature above line monitored by controller
Temperature below line monitored by TR 10

$(-\Delta H)$ was calculated at 17550 cal/g mole.

Table A.13.

Comparison steady state results

T_1	c_1	T_1	c_1
Partial simulation values		Digital computed values	
$\frac{33.0}{32.0}$	0.068	33.5	0.061
29.2	0.103	29.2	0.102
26.6	0.145	26.2	0.144
24.8	0.180	24.6	0.174
23.8	0.190	23.7	0.192
23.4	0.195	23.0	0.206
25.0	0.181	24.9	0.168
$\frac{28.7}{28.3}$	0.110	28.5	0.110
$\frac{33.0}{32.0}$	0.073	33.5	0.061

Experiments 5, 6, 7 and 10

Steady state and dynamic operation of equipment verification

Experiment 5

The steady state reactor conditions chosen for investigation were:

$$T_1 = 25^\circ C$$

$$c_1 = 0.155 \text{ gmole/litre}$$

The steady state values recorded from the experimental run were:

Table A.14.

Feedrate 3 litre/min. c_o = 1 gmole

T_1	T_{c1}	T_{c2}	T_o	k x 10	c_1	m_c	A2	V	UA x 10^{-5}
25.0	6.0	19.0	6.0	0.14	0.155	2.125	6.3	78.5	1.70

The heat of reaction was calculated at 35150 cal/gmole.

The comparison steady state results were:

Table A.15.

T_1	c_1	T_1	c_1
Partial simulation values		Digital computed values	
25.0	0.155	25.4	0.157

As a further check and also to investigate the possibility of more than one operating point the heat removal and heat generation curves were computed. The equations used were given in the text (Section 7.2.7.) The programmes (3 and 4) are included in the Appendix (pages 330 and 331). The form in which the data was fed to the computer is given in Tables A.16. and A.17. The lines obtained for Experiment 5 are shown in Fig.A.12. They intersected at the steady state value of temperature (T_1) computed by programme 2. It was clear from the lines obtained that multiple intersection was impossible and therefore only one steady state could be obtained.

The computer programme for the determination of the heat generation curve which was written in a form to enable a series of heat generation curves to be computed for different activation energies, inlet concentrations and heats of reaction. Thus results were obtained which provided extensive information for the various combinations of parameters. The programme for computing heat removal could also deal with several sets of data, i.e. for various coolant flowrates and heat transfer coefficients.

Further investigation showed that for the range of parameters chosen for research, multiple intersection of the lines was impossible.

Complete simulation of the equipment

The circuit constructed to completely simulate the partial simulation equipment was discussed in Section 7.3. The potentiometer settings were defined in the text. The partial and complete simulation portraits produced were similar. They are not, however, presented in the thesis as they were considered below standard due to noise, variplotter malfunctioning and temperature monitoring drift. Other portraits obtained from Experiments 6, 7 and 10 gave much better examples and these are therefore included in the thesis. It is however worth mentioning that the steady state values recorded from the complete simulation agreed well with those of the partial simulation.

Programme 3. Elliott 803 in Algol.

```
CALCULATION OF HEAT REMOVAL LINE'

BEGIN REAL TC2,TC1,MC,TO,MF,UA,Q'
INTEGER T,TMAX,X,XMAX'
SWITCH S:=AGAIN'
PRINT ££LS?T£S12?Q£S17?TC2£S17?MC?'
READ TC1,TO,MF,TMAX,XMAX'
X:=0'
AGAIN:READ MC,UA'
FOR T:=283 STEP 5 UNTIL TMAX DO
BEGIN TC2:=T-EXP(-(UA/(MC*60000)))*(T-TC1)'
Q:=UA*(TC2-TC1)/(LN((T-TC1)/(T-TC2)))+MF*(T-TO)*3600'
PRINT DIGITS(3),T,SAMELINE,££S4??,SCALED(6),Q,££S8??,
FREEPOINT(4),TC2,££S12??,FREEPOINT(3),MC'
END'
X:=X+1'
IF X LESS XMAX THEN GOTO AGAIN'
END'
```

$Q \equiv Q_R$

Programme 4. Elliott 803 in Algol

```
DETERMINATION OF HEAT GENERATION CURVE FOR
VARIOUS CO AND E AND T'

BEGIN REAL K,V,H,A,Q,U'
INTEGER T,TMAX,E,EMAX,CO,COMAX'
SWITCH S:=AGAIN,REPEAT,RETURN'
PRINT ££LS?T£S11?Q£S17?E£S18?CO£S21?K?'
READ TMAX,COMAX,EMAX,V,H,A,U'
E:=4000'
AGAIN:E:=E+5000'
CO:=0'
REPEAT:CO:=CO+1'
FOR T:=273 STEP 5 UNTIL TMAX DO
BEGIN K:=A*EXP(-(E/(1.987*T)))'
Q:=K*CO*V*H*0.1*3600*U/(U+60*K*V)'
PRINT DIGITS(3),T,SAMELINE,££S4??,SCALED(6),Q,££S8??,
DIGITS(5),E,££S12??,FREEPOINT(3),CO,££S17??,SCALED(3),K'
END'
IF CO LESS COMAX THEN GOTO REPEAT'
IF E LESS EMAX THEN GOTO AGAIN'
END'
```

$Q \equiv Q_G$

Fig.A12. Experiment 5. Heat Generated (Q_G) and Heat Removal (Q_R) vs. Temperature in the reactor (T_1)

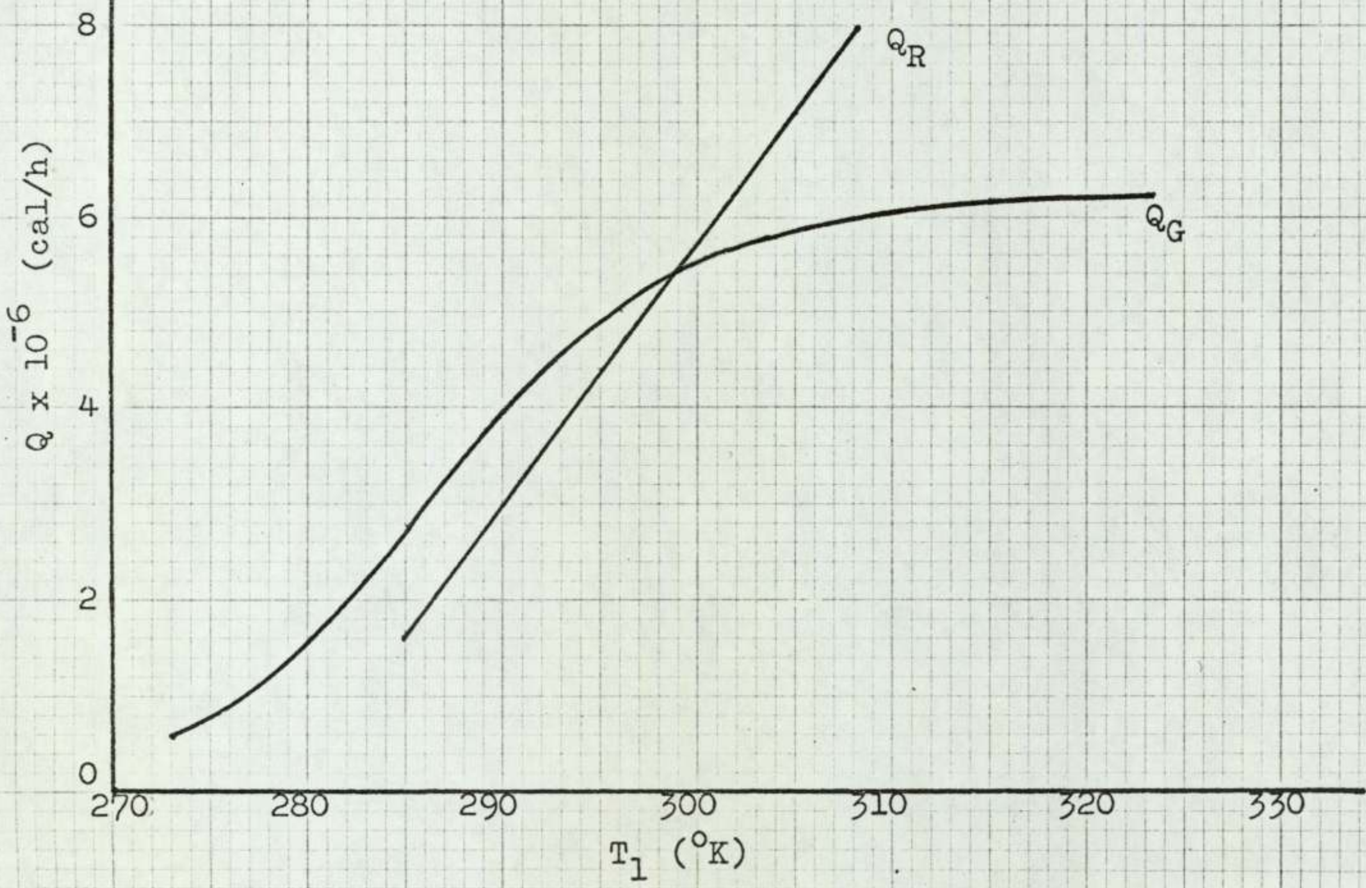

Table A.16.

Data format for programme to compute heat removal line

T_{cl}	^oK
T_o	^oK
m_f	g/s
T_{lm}	^oK
X_m	number of sets of data
m_c	kg./min.
UA	cal/deg C h

Table A.17.

Data format for programme to compute heat generation curve

T_{lm}	^oK
c_{om}	gmole/litre
E_m	cal/gmole
V	litre
ΔH	cal/gmole
A	6.3×10^{15}
u	litre/min.

Experiments 6 and 7

Experiment 6 was the first experiment conducted using an ice point reference for the temperature monitoring device. This reduced the drift from which the previous experiments had suffered.

The power output from the variacs was also increased at this stage to a maximum by different electrical connections. The new rate of power release was calibrated (Fig.A.3.). The two portraits plotted were obtained around the same operating point and hence the grouping together. The steady state obtained experimentally was:

Table A.18.

Feedrate 3 litre/min. c_o = 1 gmole/litre

T_1	T_{c1}	T_{c2}	T_o	$k \times 10$	c_1	m_c	A2	V	$UA \times 10^{-5}$
30	19	27	19	0.32	0.097	2.15	2.7	53.2	1.70

Heat from immersion heaters 842 cal/s

$(-\Delta H)$ = 18600 cal/gmole

The better portrait of the two was presented in the text along with the comparison complete simulation portrait (Figs.7.1. and 7.3.). The other is included in the Appendix (Fig.A.13.). The complete simulation is given in Fig.A.14. A good agreement between total and partial simulation was obtained as would be expected after making only minor approximations in the complete simulation at this stage.

The digital steady state check gave:

T_1 = 30.0°C c_1 = 0.092 gmole/litre

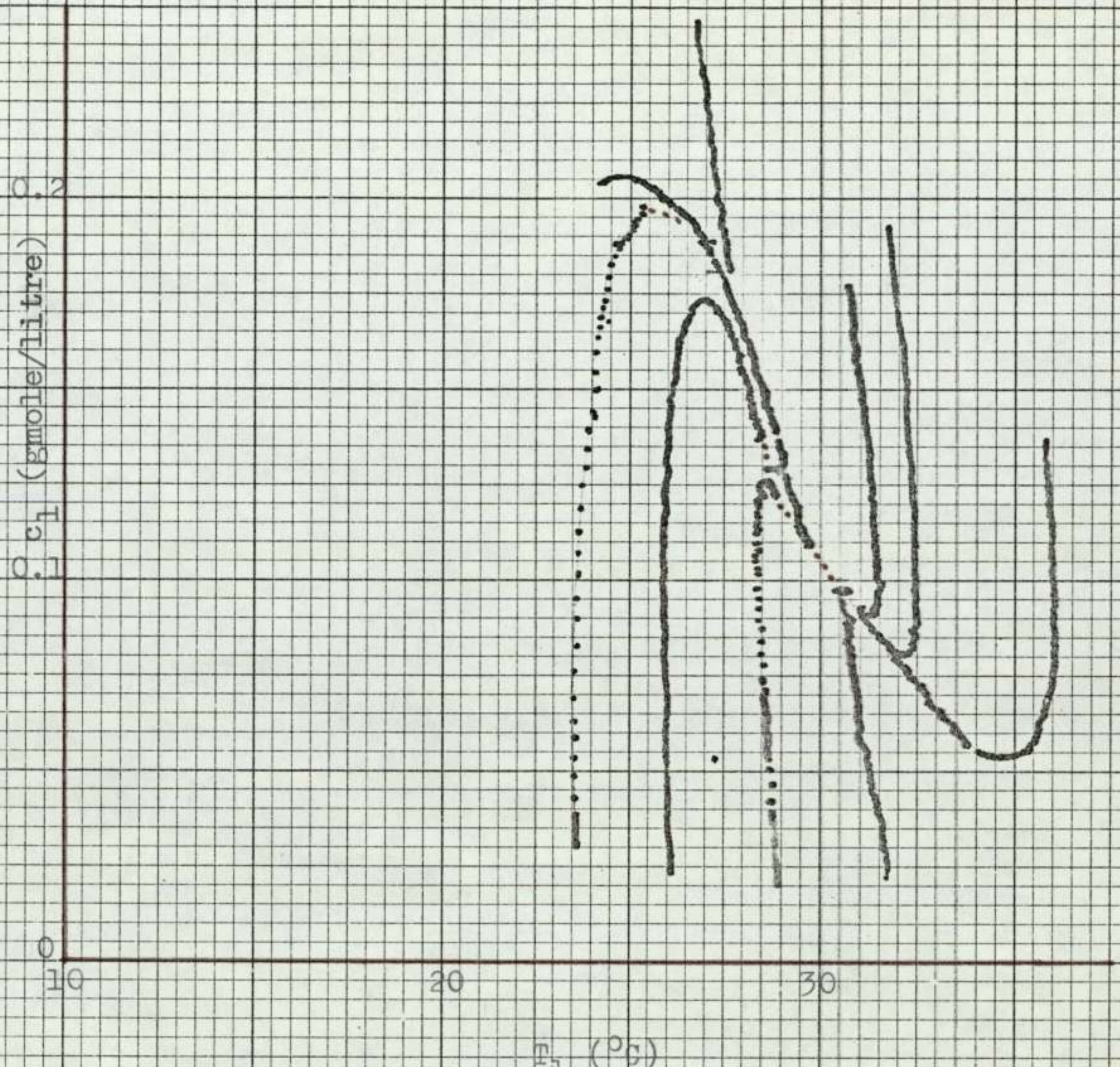

Fig.A.13. Experiment 6.

Partial simulation.

Fig. A.14. Experiment 6.

Complete simulation.

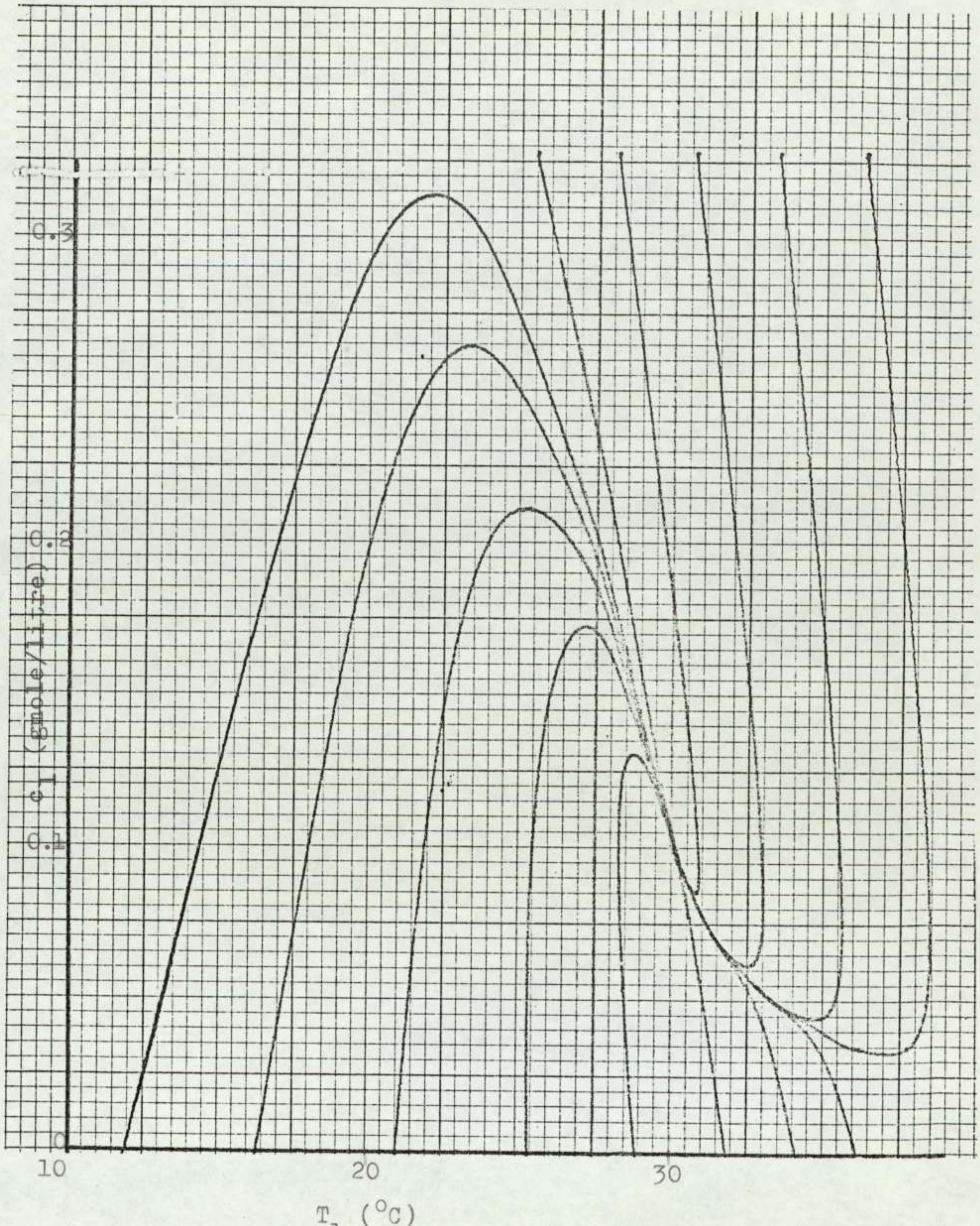

while the complete simulation produced steady state values:

$$T_1 = 29.4^\circ C \qquad c_1 = 0.100 \text{ gmole/litre.}$$

Experiment 8

At this stage the flow monitoring equipment was installed and tested. The experiments dealt with forcing the system by means of changing the feed flowrate and concentration.

Table A.19.

Feedrate 1 litre/min. c_o = 1 gmole/litre

T_1	T_{c1}	T_{c2}	T_o	k x 10	c_1	m_c	A2	V	A13
29.9	20	25.6	20	0.32	0.04	3.61	1.7	41.3	1.8

The steady state recorded in Table A.19. was used as a centre for the investigation of forcing the system by load changes of feed flowrates only. The portrait shown in Fig.A.15. was obtained. It could be seen that the extra heat generation available for higher feed rates tended to be absorbed by the greater demand for heating up of the feed and vice versa for a drop in feedrate.

Experiment 9.

Table A.20. shows the steady state values recorded for two feed flowrates.

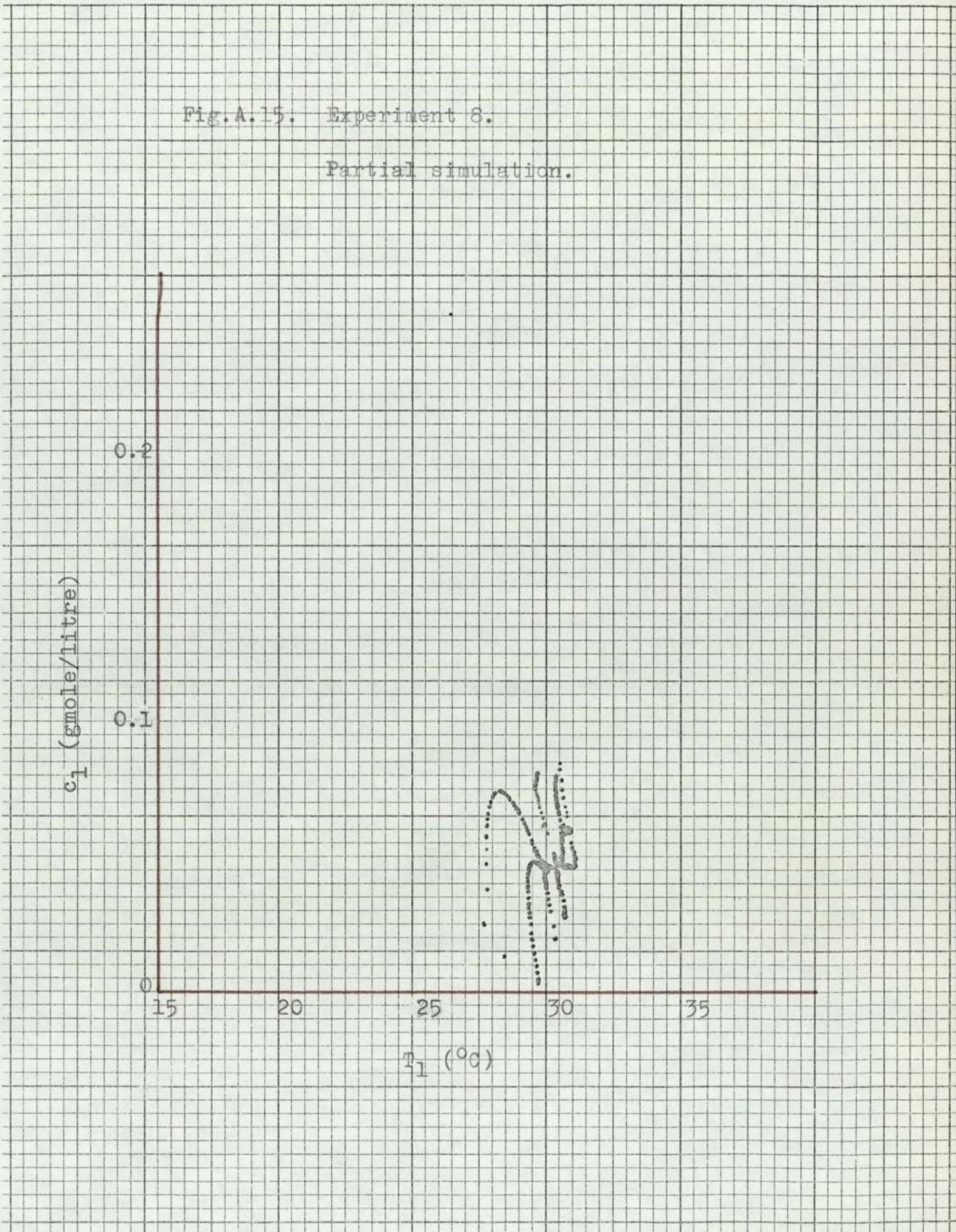
Fig.A.15. Experiment 8.
Partial simulation.
0.2
0.1
0
c_1 (gmole/litre)
15
20
25
30
35
T_1 (°C)

Table A.20.

T_1	T_{c1}	T_{c2}	T_o	k x 10	c_1	m_c	A2	V	A13
Feedrate 3 litre/min.					c_o = 1 gmole/litre				
34	19.8	28	20	0.49	0.062	3.61	4.5	67.2	5.8
Feedrate 1.4 litre/min.					c_o = 1 gmole/litre				
31	19.5	27	19.7	0.38	0.038	2.91	1.8	43.5	2.6

No detailed analysis was conducted during these tests. A general 'feel' for the equipment was obtained by forcing it with step changes in feed flowrate and inlet concentration. In this way its range of operation, limitations etc. were ascertained.

Experiment 10

This was the final verification of the dynamic operation of the equipment.

The steady state of the equipment is given in Table A.21:

Table A.21.

Feedrate 1.4 litre/min. c_o = 1 gmole/litre

T_1	T_{c1}	T_{c2}	T_o	k x 10	c_1	m_c	A2	V	A13
28.5	22	26.5	22	0.255	0.067	3.1	1.4	38.5	2.5

Heat from immersion heaters 375 cal/s

$(-\Delta H)$ = 16400 cal/gmole

Due to the availability of feed flowrate as a forcing function it was found possible to obtain a portrait over a greater range of temperature and concentration (Fig.A.16.) The comparison complete simulation portrait is shown in Fig.A.17. The steady state values recorded from the complete simulation were:

T_1 = 29.0^{o}C c_1 = 0.058 gmole/litre

Good agreement was obtained between the portraits.

Fig.A.16. Experiment 10.

Partial simulation.

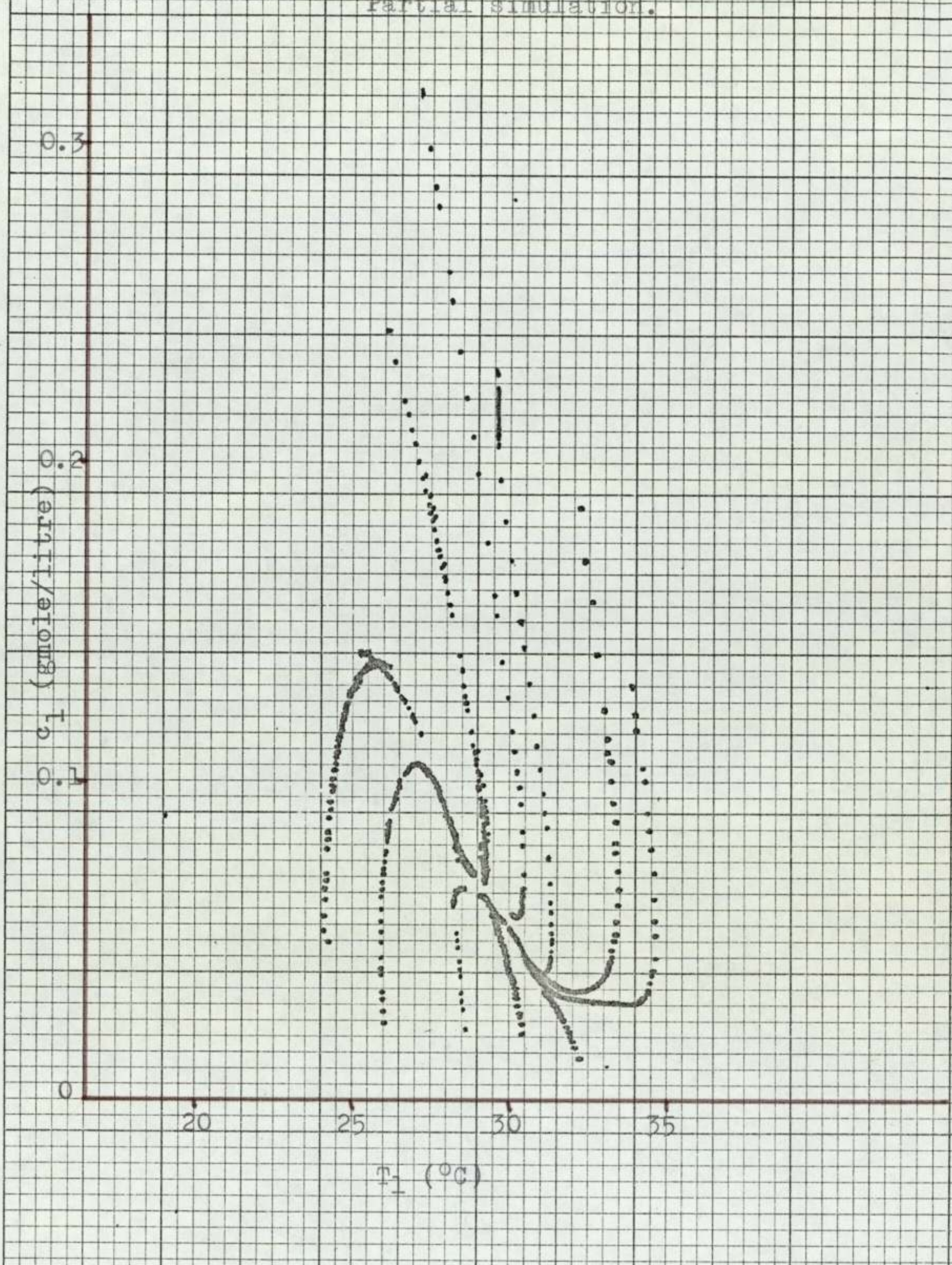

Fig. A.17. Experiment 10.

Complete simulation.

Experiments 11 to 15

The experiments dealt with general testing of the system by forcing the steady state with or without feedback control.

Experiment 11 dealt with the forcing of the steady state obtained in Experiment 10. The other steady states recorded in Experiments 12 to 15 are given in Table A.22.

During these experiments, experience was obtained in operating the equipment and the effectiveness of strong control was demonstrated. However, the tests were preliminary and therefore no phase-plane portraits were obtained.

Experiments 16 to 86

These experiments dealt with the investigation of the system stability for various system parameters and control parameters.

The steady state values recorded are given in Tables A.23 and A.24.

Definition of column headings

E	Experiment number	
T_1	Temperature in reactor	^oC (if disagreement, upper value controller recorded, lower value TR10 monitored)
c_1	Concentration in reactor	gmole/litre
k	Velocity constant	per second
A2	TR 10 Amplifier no.2. Computed heat generation	volts
A13	TR 10 Amplifier no.13. Monitored feed flowrate	volts
V	Variac position on the scale	
m_c	Coolant flowrate	litre/min.
m_f	Feed flowrate	litre/min.
T_{c1}	Coolant inlet temperature	^oC
T_{c2}	Coolant outlet temperature	^oC
T_o	Feed temperature	^oC
SPI	Set-point indicator on controller	^oC
VP	Valve positioner action i.e. in action = in, or by-passed = out	
T	Trajectories	
COP	Controller output pressure	lbf/in^2 gauge
	Control action:	
PBW	Proportional band width setting	deg C
I	Reset action - setting number (see Table A.7.)	
D	Derivative action - setting number (see Table A.7.)	

Table A.22.

E	T_1	c_1	k x 10	A2	A13	V	m_c	m_f	T_{c1}	T_{c2}	T_o	c_o	Control PBW	Control I	Control D
12	35.0	0.130	0.53	5.5	7.8	73.0	2.00	4.0	20.5	31.5	20.5	1.6	-	-	-
13	29.0	0.067	0.28	1.5	2.5	39.0	2.30	1.4	21.1	27.0	21.1	1.0	-	-	-
	33.0	0.120	0.44	4.5	7.7	66.0	2.35	4.0	20.5	29.0	20.5	1.4	2	-	-
	29.7	0.160	0.32	4.2	7.5	65.0	5.50	3.9	20.0	24.0	20.0	1.4	"	3	-
	29.0	0.140	0.28	3.3	5.7	58.0	5.15	3.0	20.0	24.9	20.0	1.4	"	"	-
	33.0	0.100	0.42	3.5	5.7	59.0	2.40	5.9	20.1	29.2	20.1	1.4	-	-	-
	29.0	0.140	0.29	3.4	5.8	58.0	5.50	3.0	19.9	24.1	19.9	1.4	10	9	-
14	30.0	0.130	0.33	3.5	5.8	59.5	5.50	3.0	19.9	24.8	19.9	1.4	4	9	9
15	27.8	0.054	0.23	1.2	2.1	35.2	2.40	1.1	19.9	25.1	19.5	1.0	2	-	-
	30.0	0.168	0.32	4.4	6.1	65.7	9.30	3.0	19.5	23.8	19.2	1.7	"	-	-

Table A23 Experiments 16 to 26

Recorded steady states of the System under control.
First controller 200 deg.C. proportional band width
$c_o = 1$

E	T_1	c_1	k x 10	A2	A13	V	m_c	m_f	T_{c1}	T_{c2}	T_o	SPI	VP	Control PBW	Control I	Comments
16/17	28.8	0.056	0.28	1.3	2.1	36.5	1.75	1.1	21.1	26.8	19.6	29.0	out	2	3	
18	27.1	0.130	0.22	1.3	5.8	56.0	2.75	3.0	25.1	26.1	23.0	"	"	20	3 & 9	
19	28.8	0.045	0.27	1.3	1.8	37.2	0.90	1.1	17.6	27.8	15.5	"	"	2	3	
20	27.3	0.048	0.25	1.3	2.0	38.0	1.50	1.1	17.0	24.8	16.1	28.0	"	2	0	
21	27.6	0.083	0.25	2.2	3.9	48.5	3.00	2.0	18.2	24.1	16.0	"	"	2	0	
21a	26.1/25.9*	0.110	0.18	2.2	3.8	48.5	2.60	2.0	16.5	23.1	16.0	"	"	2	0	
22	27.8	0.047	0.26	1.3	2.0	37.5	1.85	1.1	19.5	25.1	16.5	"	"	2	9	
22a	27.0	0.050	0.23	1.3	2.1	38.5	0.80	1.1	19.0	27.5	16.5	"	"	14	9	
23	26.8	0.050	0.22	1.3	2.0	38.5	2.70	1.1	18.5	24.0	16.5	"	"	20	0	
24	26.4	0.049	0.21	1.3	2.0	38.0	2.10/2.75	1.1	17.0	23.2	16.2	"	"	30	0	Control valve hysteresis recorded
25	26.0	0.050	0.20	1.3	2.0	38.0	2.00	1.1	16.3	23.5	16.2	"	"	30	0	
	24.5	0.069	0.15	1.3	2.1	37.5	3.00	1.1	16.4	21.4	15.9	"	"	30	0	
26	27.8	0.130	0.24	3.0	6.0	60.0	3.40	3.0	15.2	22.5	14.9	28.5	in	2	0	

* Controller recorded temperature
TR 10 monitored temperature

Table 23.1 Experiments 27 to 37

E	T_1	c_1	k x 10	A2	A13	V	m_c	m_f	T_{c1}	T_{c2}	T_o	SPI	VP	Control PBW	I	D	Comments
27	27.5/28.0*	0.046	0.27	0.8	2.0	39.0	1.60	1.1	16.0	24.5	15.1	28.5	in	2	0	0	
28/29	27.5	0.046	0.24	1.5	1.9	38.5	1.25	1.1	15.1	25.1	14.9	"	"	2/10	0/6	0/0	
30/31	28.5	0.045	0.29	1.4	2.0	39.0	1 to 1.80	1.1	15.5	27.2	15.0	"	"	15/2	9/9	0/0	
32	29.2	0.042	0.32	1.4	2.0	38.2	0.90	1.1	17.2	28.2	14.0	"	"	10	0	0	
33	31.0	0.026	0.38	1.4	2.0	38.2	0.70	1.1	18.0	31.0	14.0	"	"	20	0	0	
34				3.3	6.2	58.8		3.0				"	"	30	9	0	Oscillatory results ∴ not all values recorded
35				3.3	6.2	58.8		3.0				"	"	60	9	0	
35a				3.3	6.2	58.8		3.0				"	"	30	6	0	
35b	27.9	0.125	0.23	3.3	6.2	58.8	1.80	3.0	14.5	24.2	13.5	"	"	30	6	0	
35c				3.3	6.2	58.8		3.0				"	"	30	1	0	
35d	27.5	0.155	0.20	3.4	6.2	58.5	1.85	3.0	14.5	23.5	13.3	"	"	30	0	0	
36/36b	28.0					60.0		3.0	14.0		13.0	"	"	30/40	9	0	
37	28.6	0.115	0.29	3.3	5.8	58.9	2.20	3.0	14.5	26.0	12.5	"	"	2	0	9	

Table 23.2 Experiments 38 to 44

E	T_1	c_1	k x 10	A2	A13	V	m_c	m_f	T_{c1}	T_{c2}	T_o	SPI	VP	Control PBW	I	D	Comments
38	28.8	0.105	0.28	3.5	6.1	58.9	1.40	3.0	14.1	25.5	12.9	28.5	in	2	0	0	) Controller) hysteresis
	28.0	0.115	0.25	3.4	6.1	59.5	1.80	"	13.9	23.8	12.9	"	"	2	0	0	) recorded
39a	28.5	0.111	0.26	3.4	6.1	59.5	1.30	"	14.1	25.1	12.8	"	"	2	0	0	
39b	28.1	0.115	0.26	3.4	6.0	59.5	1.20	"	15.0	25.9	12.5	"	"	2	0	0	Trajectories from:
40	27.4	0.130	0.23	3.4	6.1	59.5	1.40	"	14.2	24.7	12.5	"	"	10	0	0	high T_1^o
	27.9	0.122	0.24	3.4	6.1	60.0	1.40	"	14.0	24.8	12.5	"	"	10	0	0	low T_1^o
41	27.0 / 26.8 *	0.140	0.21	3.4	6.1	60.0	1.60	"	14.0	23.9	12.5	"	"	20	0	0	high T_1^o
	27.9	0.120	0.24	3.4	6.1	59.0	1.10	"	14.5	25.5	12.5	"	"	20	0	0	low T_1^o
42	28.1	0.110	0.27	3.4	6.1	59.8	1.30	"	14.0	24.6	12.3	"	"	2	0	0	
43	28.0	0.115	0.25	3.4	6.1	59.8	1.40	"	13.8	24.5	12.3	"	"	20	0	0	
44	29.0 to 27.0	0.100 to 0.110	0.29	3.3	5.9	59.0	1.25	"	13.5	25.0	11.1	"	"	60	9	0	E.44 to 50 oscillatory results hence data incomplete
	28.0	0.110	0.26				1.00	"	13.5	26.0	11.1	"	"	60	9	0	

Table 23.3 Experiments 45 to 56

E	T_1	c_1	k x 10	A2	A13	V	m_c	m_f	T_{c1}	T_{c2}	T_o	SPI	VP	Control PBW	Control I	Comments
45				3.3	5.9	59.0		3.0	13.5		11.1	28.5	out	60	9	sustained oscillation
46		as 45 but different trajectory						"	13.5		11.1	"	out	60	9	
47		as 44	"	"		"		"			11.1	"	in	60	9	inward-winding oscillation
48		as 47	"	"		"		"			11.1	"	in	60	9	
49		as 48 except for valve positioner						"			11.1	"	out	60	9	
50	29.0	0.100	0.32	3.4	5.9	60.0	0.90	"	15.5	27.0	10.9	28.0	out	60	9	
51	28.5	0.110	0.28	3.5	6.0	60.0	0.90	"	14.5	27.5	10.9	"	out	30	6	
52	28.0							"	14.1	27.1	10.9	"	out	30	6	
53		as 52 except for valve positioner						"			10.9	"	in	30	6	
54	27.3	0.122	0.23	3.4	6.1	59.5	0.95	"			10.9	"	in	30	3	
55	27.9	0.110	0.26	3.4	6.0	59.5	1.00	"	13.0	25.9	10.9	"	out	30	3	
																Trajectories from:
56	26.0	0.152	0.19	3.3	6.2	59.5	1.45	"	12.1	23.0	10.9	"	in	30	0	high T_1^o
	26.5	0.140	0.21	3.3	6.2	59.5	1.25	"	12.1	23.9	10.9	"	in	30	0	low T_1^o

Table 23.4 Experiments 57 to 59

E	T_1	c_1	k x 10	A2	A13	V	m_c	m_f	T_{c1}	T_{c2}	T_o	SPI	VP	COP	Control PBW	T	Comments
57	26.6	0.135	0.22	3.3	6.2	59.0	1.25	3.0	12.5	24.1	10.9	28	out	-	30	-	Trajectories from: high T_1^o
	27.1	0.120	0.23	3.3	6.2	59.2	0.95	"	12.9	25.2	10.9	"	out	-	30	-	low T_1^o
58	26.0	0.150	0.19	3.4	6.1	59.5	1.65	"	12.5	23.0	11.2	"	in	11.0	5	A	
	26.1	"	0.20	"	"	"	1.60	"	12.3	22.9	"	"	"	"	"	B	
	26.1	"	"	"	"	"	"	"	"	"	"	"	"	"	"	C	
	"	0.145	"	"	6.0	"	"	"	"	"	"	"	"	"	"	D	
59a	27.0	0.130	0.23	3.6	6.1	61.0	1.50	"	12.2	23.8	"	"	out	9.8	5	A	
	26.5	0.140	0.20	3.5	6.1	60.0	1.25	"	12.5	24.0	"	"	"	10.3	"	B	
59b	27.1	0.125	0.23	3.6	6.1	60.5	1.40	"	12.5	24.1	"	"	"	10.1	"	A	
	27.0	"	"	3.7	6.2	61.5	"	"	12.2	23.9	"	"	"	"	"	B	
	27.5 to 27.1	0.122	0.24	3.8	"	61.0	1.65	"	"	23.8	"	"	"	9.7	"	C	
	27.5 to 27.0	0.130	0.24	3.7	"	61.5	1.40	"	12.1	"	10.9	"	"	9.8 to 10.1	"	D	

Table 23.5 Experiments 60 to 61

E	T_1	c_1	k x 10	A2	A13	V	m_c	m_f	T_{c1}	T_{c2}	T_o	SPI	VP	COP	Control PBW	T	Comments
60	26.2	0.142	0.21	3.40	6.0	59.5	0.90	3.0	12.8	24.5	9.5	28	in	12.3	2		
	"	"	"	"	"	59.0	"	"	12.5	25.0	"	"	"	12.6	"	A	
	"	"	"	"	"	"	"	"	"	"	"	"	"	"	"	B	
	26.5							"	12.4	25.0	9.7	"	"	"		C	
	26.4	0.140	"	"	6.2	"	"	"	11.9	25.0	9.5	"	"	12.3	"	D	
61	27.1	0.130	0.22	3.5	"	60.0	0.80	"	12.4	26.6	9.5	"	out	12.0	"	A	
	"	0.122	0.23	3.4	"	"	0.90	"	12.0	25.4	"	"	"	11.6	"	B, C & D	

Table A24 Experiments 62 to 63

Recorded steady states of the System under control.
Second controller 100 deg.C. proportional band width
c_o = 1 Set-point checked for drift before and after each experiment

E	T_1	c_1	k x 10	A2	A13	V	m_c	m_f	T_{c1}	T_{c2}	T_o	SPI	VP	COP	Control PBW	T
62	32.3	0.062	0.43	5.3	5.8	74.0	1.25	3.0	9.1	28.0	7.9	30	in	11.0	10	
	32.5	0.062	0.45	5.7	6.1	75.0	1.40	"	9.0	28.1	"	"	"	"	"	
63	29.5	0.094	0.32	4.9	5.8	72.5	2.25	"	10.1	23.0	8.6	28	"		"	
	$\frac{28.8}{29.0}$	*0.098	0.31	5.3	6.0	72.0	2.50	"	10.0	22.0	8.6	"	"	9.2	"	A
	$\frac{29.0}{29.2}$	*0.094	0.32	5.2	5.75	72.0	2.25	"	10.0	22.5	8.5	"	"	9.9	"	B
	$\frac{29.0}{29.5}$	*0.088	0.33	5.3	5.8	72.5	2.25	"	10.0	22.5	8.5	"	"	9.5	"	C
	29.3	0.093	0.32	5.3	5.8	72.0	2.10	"	10.0	23.6	8.2	"	"	10.0	"	D
	$\frac{29.1}{29.8}$	*0.087	0.33	5.1	5.8	72.6	2.20	"	9.8	22.9	8.1	"	"	10.0	"	E
	28.9	0.096	0.29	5.0	5.8	72.0	2.30	"	9.4	22.0	8.0	"	"	9.7	"	F

Table 24.1 Experiments 64 to 65

E	T_1	c_1	k x 10	A2	A13	V	m_c	m_f	T_{c1}	T_{c2}	T_o	SPI	VP	COP	Control / PBW	T
64	Not recorded															A
	27.4/27.7 *	0.110	0.25	5.2	6.0	72.8	2.90	3.0	8.8	20.0	8.0	28	in	9.0	5	B
	28.3/28.6 *	0.096	0.29	5.0	5.8	71.5	2.00	"	9.0	22.8	7.9	"	"	10.0	"	C
	27.8/28.1 *	0.102	0.27	5.0	5.7	71.0	2.00	"	"	22.3	8.0	"	"	10.0	"	D
	28.2/28.6 *	0.094	0.29	4.9	5.7	70.5	1.90	"	8.9	23.0	7.9	"	"	10.2	"	E
	28.2/29.1 *	0.095	0.32	5.1	5.8	71.8	2.25	"	"	21.8	"	"	"	9.9	"	F
65	27.5	0.110	0.25	5.1	6.0	72.0	2.70	"	8.3	21.1	7.6	26	"	9.3	2	A
	27.0	0.110	0.23	5.0	5.9	71.0	"	"	"	20.0	"	"	"	"	"	B
	28.0 to 27.6	"	0.26	5.1	6.0	72.0	2.80	"	"	20.1	7.5	"	"	9.1	"	C
	27.2/27.0 *	0.115	0.23	"	"	71.8	"	"	8.1	20.0	7.4	"	"	"	"	D

Table 24.2 Experiments 66 to 69

E	T_1	c_1	k x 10	A2	A13	V	m_c	m_f	T_{c1}	T_{c2}	T_o	SPI	VP	COP	Control PBW	Control I	T
66	$\frac{28.1}{28.0}$*	0.106	0.26	5.0	5.8	71.0	1.75	3.0	8.5	23.1	6.9	26	in	10.2	2	0	A
	27.6	0.112	0.25	5.2	5.8	72.2	2.25	"	7.9	21.0	"	"	"	9.9	"	"	B
67	26.0	0.145	0.19	4.8	5.9	70.2	2.40	"	7.8	19.5	"	25	"	9.6	"	"	A
	25.5 to 25.6	0.152	0.18	"	5.8	69.5	2.25	"	7.7	20.0	6.8	"	"	10.0	"	"	B
68	26.5 to 26.6	0.141	0.20	5.0	6.0	71.5	2.25	"	7.9	20.2	6.5	"	"	"	30	"	A
	26.3 to 26.2	0.140	0.20	5.1	6.0	71.3	2.40	"	7.8	19.8	"	"	"	9.5	"	"	B
69	25.8	0.141	0.17	4.6	5.9	69.0	1.05	"	6.9	22.7	6.3	"	"	11.8	30	30	
	26.6	0.135	0.21	4.9	5.8	69.5	4.60	"	6.5	16.5	"	"	"	9.7	"	"	
	26.1						2.40	"	7.5	19.7	6.4	"	"	"	"	"	

Table 24.3 Experiments 70 to 71

E	T_1	c_1	k x 10	A2	A13	V	m_c	m_f	T_{c1}	T_{c2}	T_o	SPI	VP	COP	Control		T
															PBW	I	
70a	25.7	0.158	0.17	4.8	5.8	70.3	3.10	3.0	9.0	18.9	6.5	25	in	9.0	2	30	A & B
70b	25.1	0.166	0.16	"	"	70.0	2.65	"	7.8	18.8	6.8	"	"	9.1	"	"	A
	24.9 / 24.7	* 0.175	0.15	4.7	5.7	69.5	2.80	"	7.5	18.1	"	"	"	"	"	"	B
	24.1	0.190	0.13	"	"	"	3.45	"	7.3	16.8	6.7	"	"	8.9	"	"	C
70c	23.7	0.175	0.14	4.6	"	68.6	2.95	"	"	17.0	6.5	"	"	9.0	"	"	A
	23.5	0.188	0.13	4.8	5.8	69.5	4.10	"	7.0	15.5	6.7	"	"	8.0	"	"	B & C
	23.2	0.184	"	4.7	"	69.0	4.40	"	"	15.1	6.5	"	"	7.7	"	"	D
	23.5	0.181	0.13	"	"	"	3.55	"	7.1	16.1	"	"	"	8.1	"	"	E
71	23.5	0.182	0.13	"	5.9	69.5	3.30	"	"	16.3	"	"	"	8.5	"	70	A & B
	23.7	0.180	0.14	4.8	5.8	69.6	3.80	"	7.0	16.0	"	"	"	8.1	"	"	C
	23.9	0.178	"	4.7	"	69.5	"	"	"	"	"	"	"	"	"	"	D
	23.8	0.176	0.14	"	"	69.0	3.05	"	7.1	17.0	"	"	"	9.0	"	"	E

Table 24.4 Experiments 72 to 73

E	T_1	c_1	k x 10	A2	A13	V	m_c	m_f	T_{c1}	T_{c2}	T_o	SPI	VP	COP	Control PBW	Control I	T
72	25.3	0.167	0.15	4.8	5.7	69.0	2.90	3.0	9.9	19.4	7.5	26	in	9.0	10	70	A
	25.0				Not recorded												B
	26.0	0.148	0.18	"	5.8	69.8	2.30	"	9.1	20.0	"	"	"	9.8	"	"	C
	25.9	0.160	0.18	"	"	69.2	2.10	"	8.7	"	7.1	"	"	10.0	"	"	D
	25.0	0.175	0.16	"	5.9	69.5	2.90	"	8.1	18.2	"	"	"	9.0	"	"	E
	25.0	0.173	0.15	"	5.8	"	2.80	"	8.0	18.3	"	"	"	"	"	"	F
	25.0	0.175	"	"	5.9	69.9	3.00	"	"	18.2	7.0	"	"	"	"	"	G
	25.0	"	"	4.9	"	70.0	2.80	"	"	"	"	"	"	"	"	"	H
73	25.8	0.150	0.18	"	5.8	"	1.85	"	7.9	20.9	6.5	"	"	10.1	"	"	A
	26.1	0.140	0.19	"	5.9	70.2	2.10	"	7.8	20.0	6.6	"	"	10.0	"	"	B
	25.8	0.151	0.18	"	5.8	69.9	1.85	"	7.9	21.0	"	"	"	10.2	"	"	C
	25.9	0.145	"	4.8	5.7	69.5	1.50	"	8.0	21.9	6.5	"	"	10.9	"	"	D
	$\frac{24.8}{24.6}$*	0.165	0.15	4.7	"	"	2.00	"	7.9	20.0	"	"	"	10.1	"	"	E

Table 24.5 Experiments 74 to 77

E	T_1	c_1	k x 10	A2	A13	V	m_c	m_f	T_{c1}	T_{c2}	T_o	SPI	VP	COP	Control PBW	Control I	T
74	24.8	0.175	0.15	4.8	5.8	69.2	2.00	3.0	7.9	20.0	6.5	26	in	10.0	10	70	A B C & D
	24.5	0.175	0.14	"	""	"	3.00	"	7.1	17.6	"	"	"	9.0	"	"	E
75	26.0	Repeat of Experiment 73															
76	27.1		0.23		6.0		2.70	3.0				"	"	9.2	"	1	A
	26.4				"		"	"				"	"	9.0	"	"	B
	27.1				"		"	"				"	"	"	"	"	C
	26.7		0.22		"		2.60	"				"	"	9.1	"	"	D
	26.9/27.0*	0.118	0.22	5.1	"	71.5	2.70	"	7.8	19.9	6.8	"	"	9.2	"	"	
77	29.7	0.084	0.33	4.9	5.9	70.8	1.95	"	10.9	24.2	9.2	28	"	10.1	"	"	A & B
	29.5/29.4*	0.092	0.32	5.1	6.0	71.5	2.20	"	10.1	23.1	9.0	"	"	10.5	"	"	C
	28.9	0.097	0.30	5.0	6.1	71.5	2.40	"	10.0	22.1	"	"	"	9.8	"	"	D
	28.5 to 28.2	0.105	0.27	4.9	6.0	70.0	2.25	"	9.9	"	8.9	"	"	"	"	"	E

Table 24.6 Experiments 78 to 80

E	T_1	c_1	k x 10	A2	A13	V	m_c	m_f	T_{c1}	T_{c2}	T_o	SPI	VP	COP	Control PBW	I	T
78	28.5	0.110	0.25	4.9	6.0	70.3	2.25	3.0	9.9	22.9	8.5	28	in	9.9	15	70	A
	28.7	0.108	0.26	5.1	"	71.9	2.15	"	"	"	8.4	"	"	10.0	"	"	B
	28.5	0.110	0.24	4.8	6.1	69.9	2.20	"	9.8	22.4	"	"	"	"	"	"	C
	"	0.108	0.25	5.1	6.0	71.2	2.50	"	9.5	21.9	8.8	"	"	9.7	"	"	D
79	29.9	0.096	0.30	5.1	6.1	71.7	1.70	"	9.9	25.0	8.5	"	"	10.8	"	0	A
	30.0 to 29.9	0.092	0.31	5.0	"	71.0	1.65	"	"	24.8	"	"	"	10.6	"	"	B
	29.2 to 29.5	0.098	0.28	"	6.0	71.3	1.70	"	"	24.3	8.3	"	"	"	"	"	C
	29.5	0.095	0.29	5.0	5.9	71.0	"	"	"	24.2	8.4	"	"	10.1	"	"	D
80	26.9 to 26.7	0.125	0.21	4.7	5.8	68.0	2.75	"	10.0	20.2	8.9	32	"	9.1	10	"	B

Table 24.7 Experiments 81 to 83

E	T_1	c_1	k x 10	A2	A13	V	m_c	m_f	T_{c1}	T_{c2}	T_o	SPI	VP	COP	Control / PBW	T
81	25.8	0.152	0.16	4.5	5.9	68.7	3.10	3.0	9.1	18.9	8.9	32	in	9.1	10	A
	25.8 / 26.0 *	"	"	"	"	"	"	"	"	"	"	"	"	"	"	B
	24.5 / 25.0 *	"	0.15	"	"	"	"	"	"	"	"	"	"	"	"	C
	25.0 / 25.2 *	0.148	0.16	4.2	"	67.0	3.15	"	9.0	18.3	8.7	"	"	8.8	"	D
82	25.3	0.155	0.16	4.6	6.1	69.0	3.10	"	8.9	18.5	8.5	"	"	9.0	20	A
	25.2	"	"	4.5	6.0	68.0	3.20	"	"	18.3	"	"	"	8.8	"	B & C
	25.2 to 26.0	0.152	"	"	"	68.8	2.95	"	9.0	19.0	"	"	"	9.0	"	D
83	30.5 to 30.0	0.076	0.34	4.8	5.8	70.8	1.60	"	10.0	25.9	8.6	"	"	10.8	1	A
	29.7	0.083	0.32	"	5.7	70.0	1.25	"	"	26.0	8.5	"	"	11.1	"	B

Table 24.8. Experiments 83 (continued) to 85

E	T_1	c_1	k x 10	A2	A13	V	m_c	m_f	T_{c1}	T_{c2}	T_o	SPI	VP	COP	$\frac{\text{Control}}{\text{PBW}}$	T
83	29.6	0.087	0.32	5.0	5.8	71.8	1.80	3.0	9.5	24.0	8.3	32	in	10.2	1	C
	30.0	0.082	0.33	"	"	72.5	2.00	"	"	23.5	"	"	"	10.1	"	D
	"	0.083	"	"	6.0	73.0	1.90	"	9.2	24.0	8.1	"	"	"	"	E
84	27.5	0.105	0.24	4.9	"	69.6	2.40	"	9.5	21.0	8.5	28	"	9.9	2	A
	27.2	"	0.23	5.0	"	70.0	2.70	"	9.1	20.1	"	"	"	9.2	"	B
	26.5	0.115	0.22	4.8	6.1	69.9	2.75	"	"	19.9	8.3	"	"	9.1	"	C
85	27.5 to 27.2	0.105	0.24	5.0	"	70.3	2.70	"	9.2	20.2	8.1	"	"	9.2	"	A
	$\frac{26.7}{26.9}$*	0.115	0.22	4.8	"	69.8	2.85	"	9.0	19.8	8.0	"	"	9.0	"	B
	$\frac{27.0}{27.2}$*	0.108	0.23	"	6.0	"	2.75	"	9.1	20.0	"	"	"	9.1	"	C
	27.5 to 27.2	0.102	0.24	"	"	69.6	2.80	"	9.0	20.2	8.1	"	"	"	"	D

Table 24.9 Experiments 85 (continued) to 86

E	T_1	c_1	k x 10	A2	A13	V	m_c	m_f	T_{c1}	T_{c2}	T_o	SPI	VP	COP	Control / PBW	T
85	26.8	0.110	0.22	4.9	6.0	70.0	2.85	3.0	9.0	19.9	8.1	28	in	9.0	2	H
	$\frac{26.6}{26.8}$*	"	"	4.7	"	"	2.65	"	"	20.0	8.0	"	"	9.2	"	J
86	$\frac{26.8}{26.5}$*	"	"	4.8	"	"	2.70	"	"	"	"	"	"	9.1	"	A
	$\frac{27.4}{27.0}$*	0.105	"	"	"	69.5	2.90	"	"	19.8	"	"	"	9.0	"	B
	$\frac{27.1}{27.0}$*	0.102	0.24	4.9	"	70.2	3.10	"	"	20.0	8.1	"	"	9.1	"	C

Figs. A.18. to A.39. are partial simulation portraits obtained for some of the experiments shown in Tables A.23. and A.24.

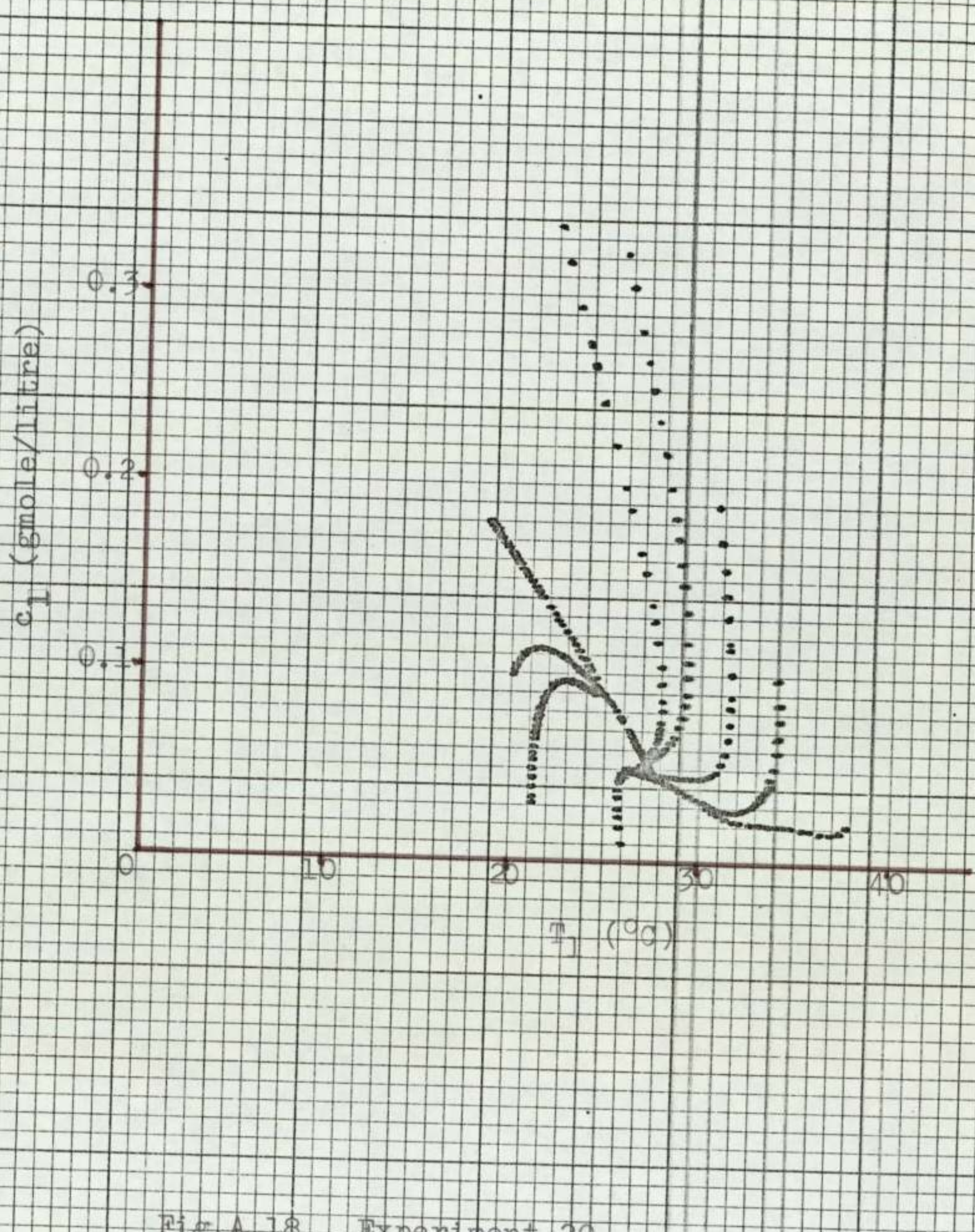

Fig.A.18. Experiment 20.

Partial simulation.

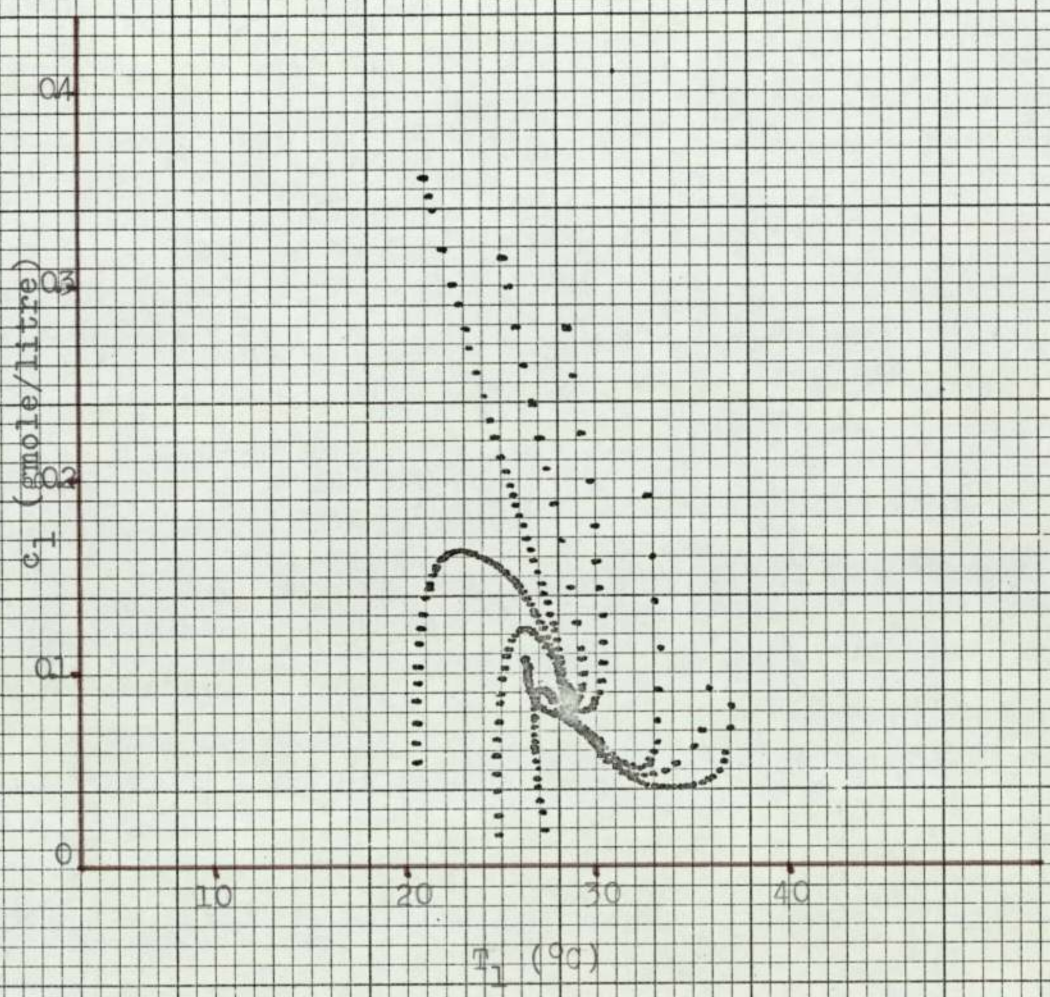

Fig. A.19. Experiment 21.

Partial simulation.

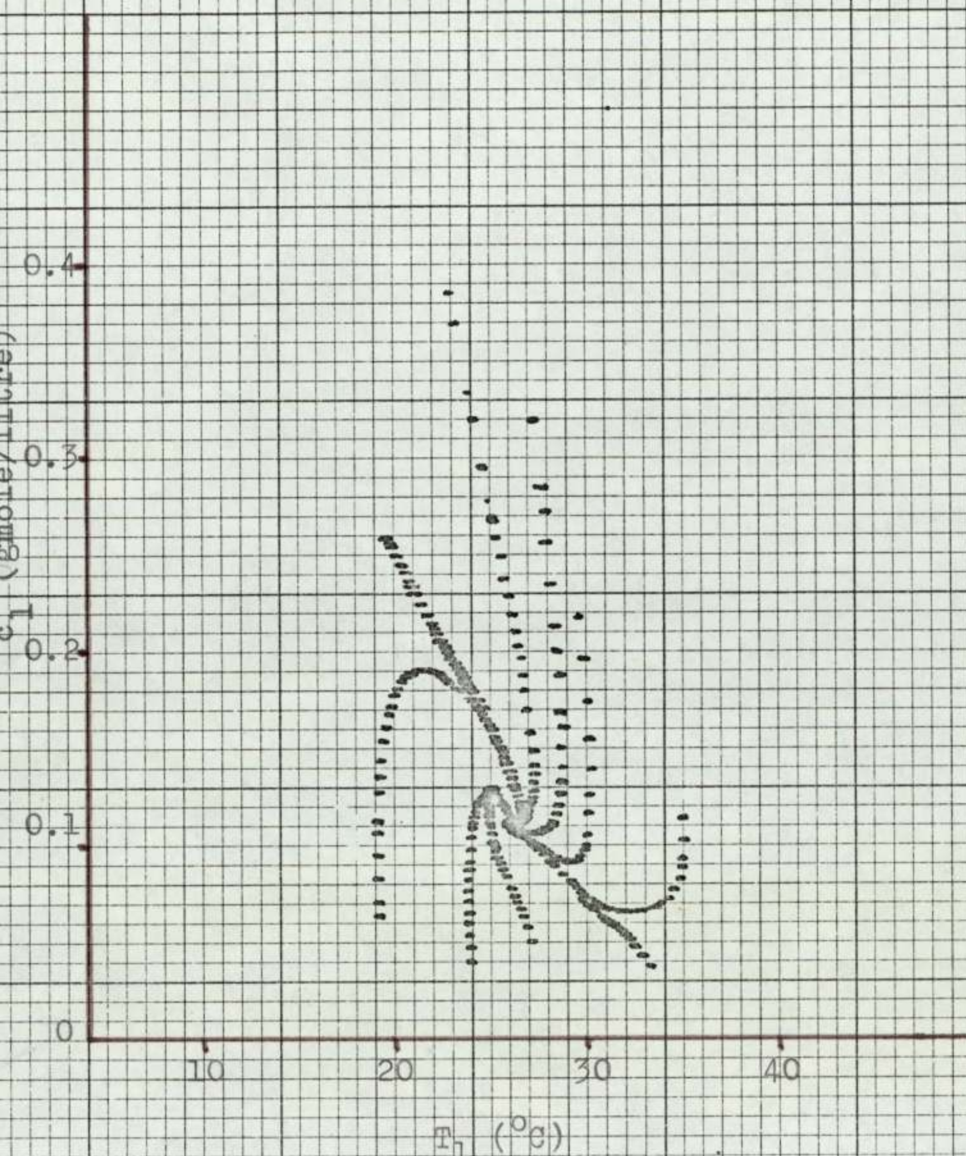

Fig. A.20. Experiment 21(a).

Partial simulation.

Fig. A.21. Experiment 25.

Partial simulation.

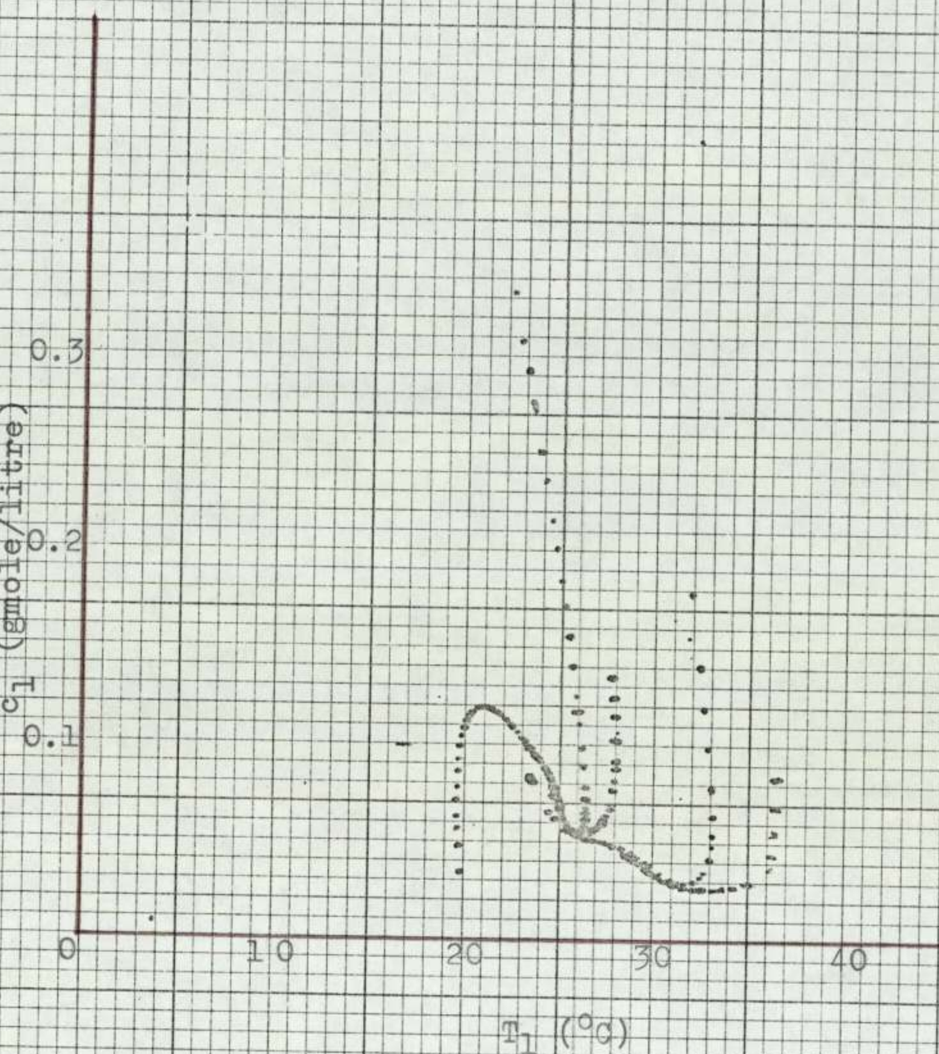

Fig.A.22. Experiment 29.

Partial simulation.

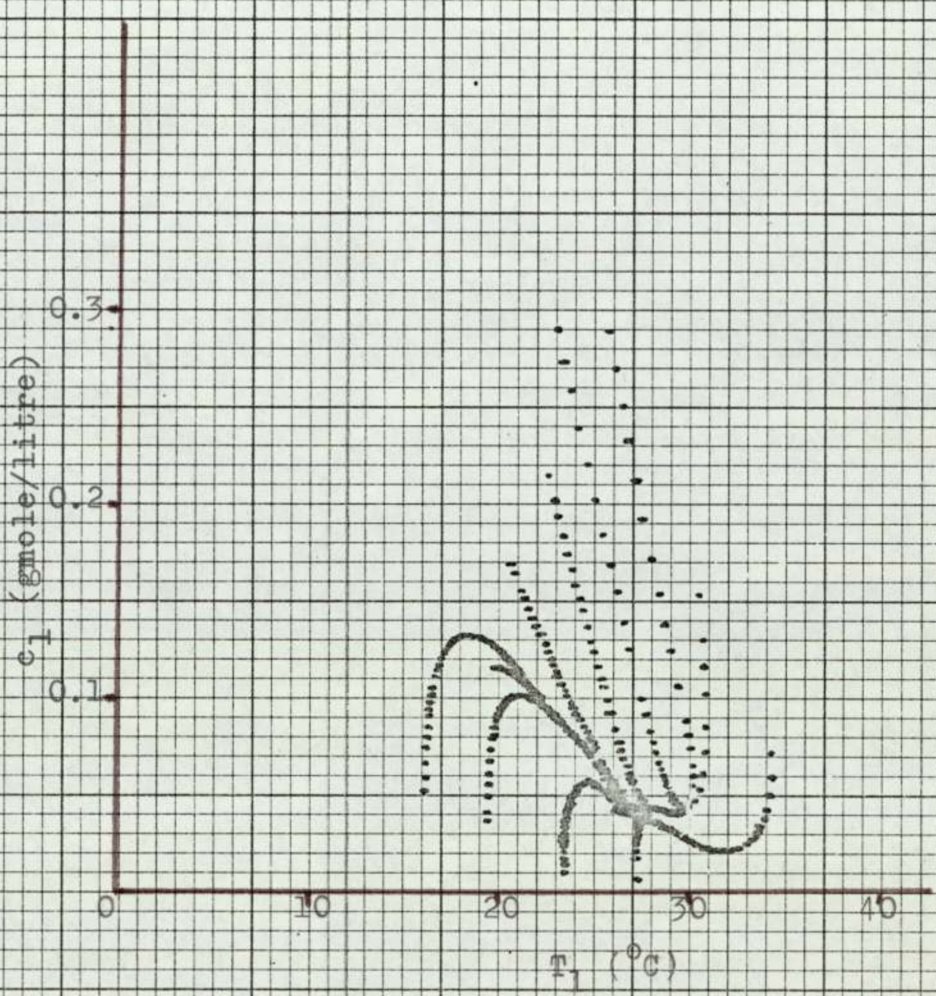

Fig. A.23. Experiment 33.

Partial simulation.

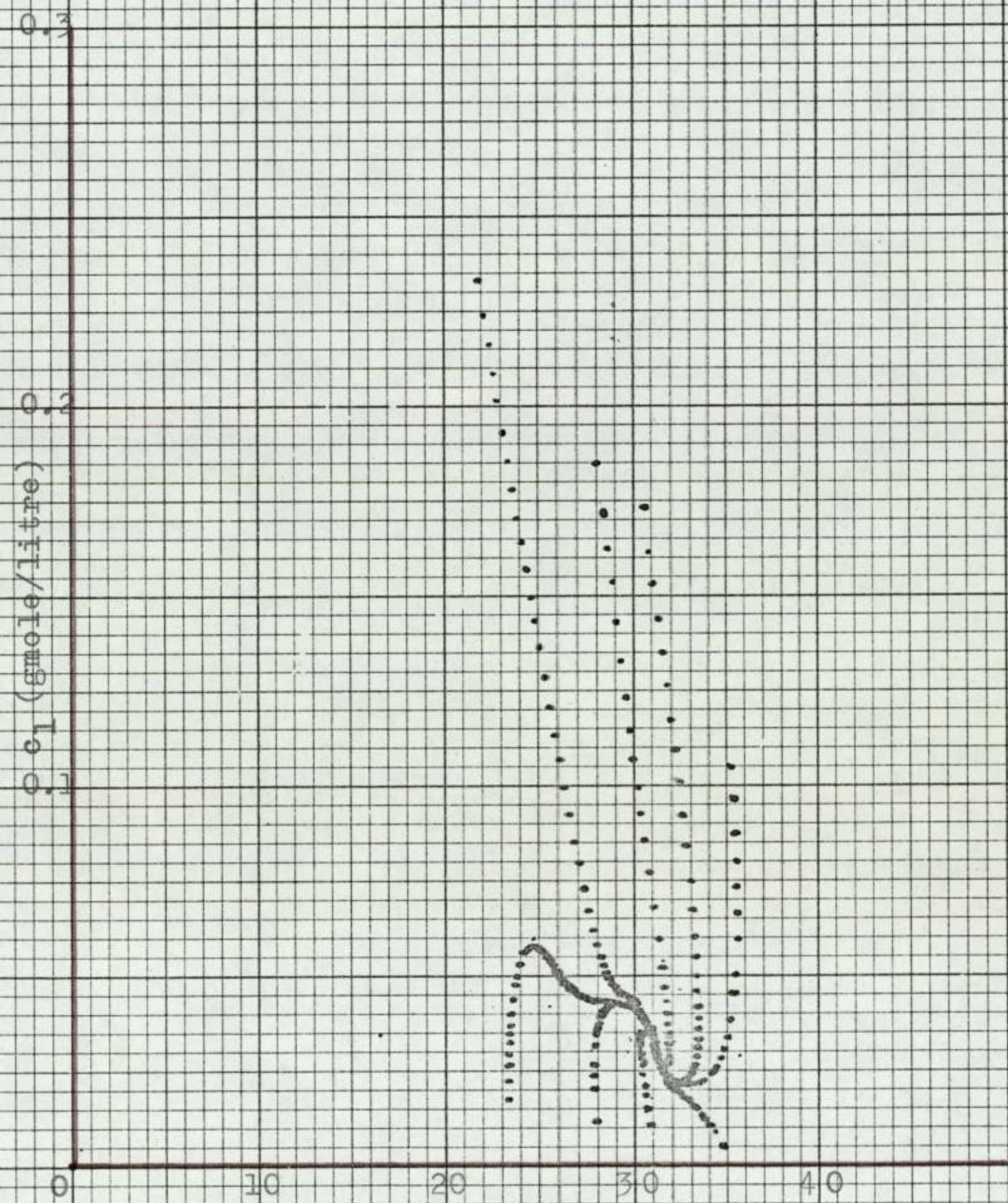

Fig.A.24. Experiment 34.

Partial simulation.

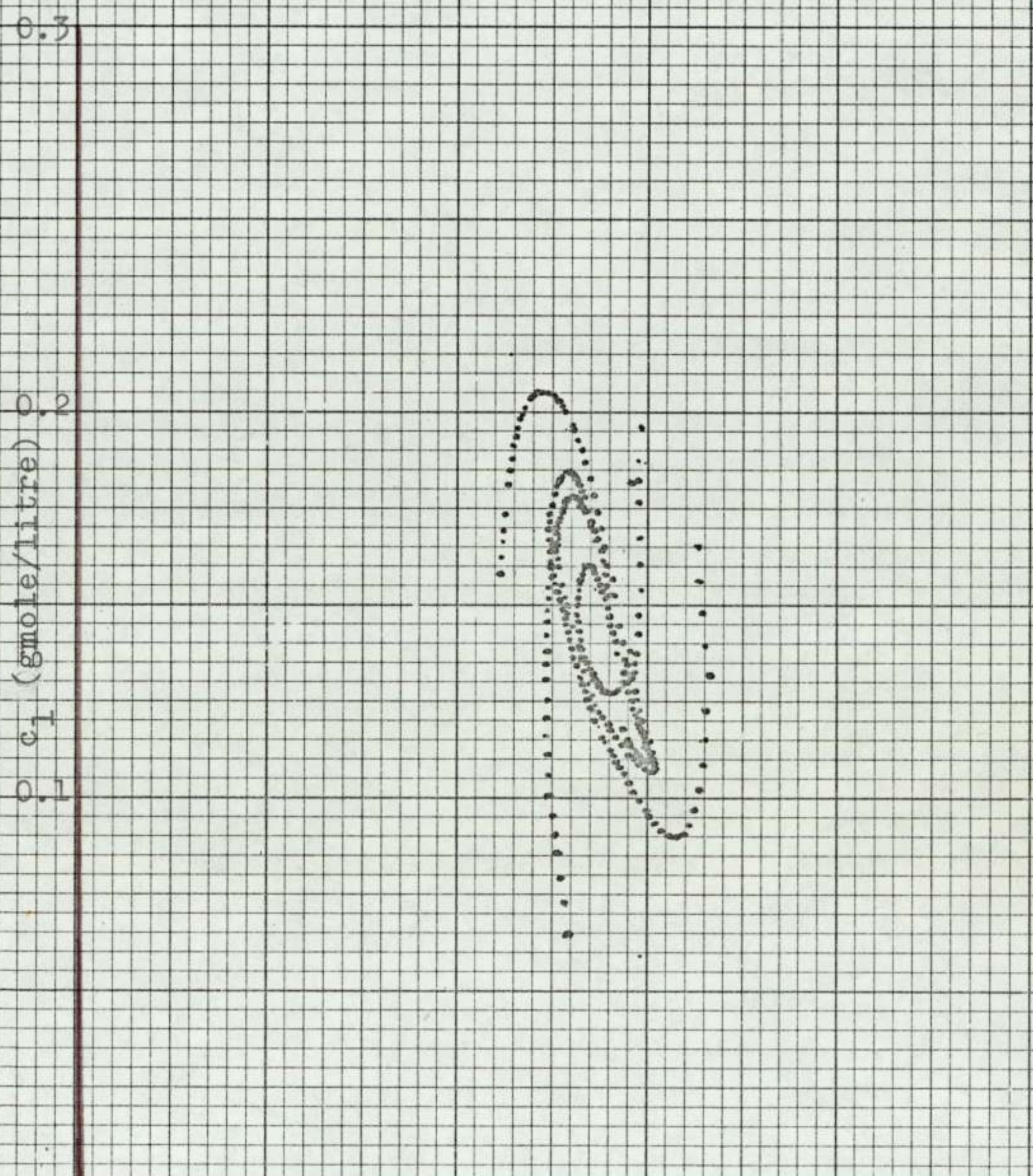

Fig. A.25. Experiment 37.

Partial simulation.

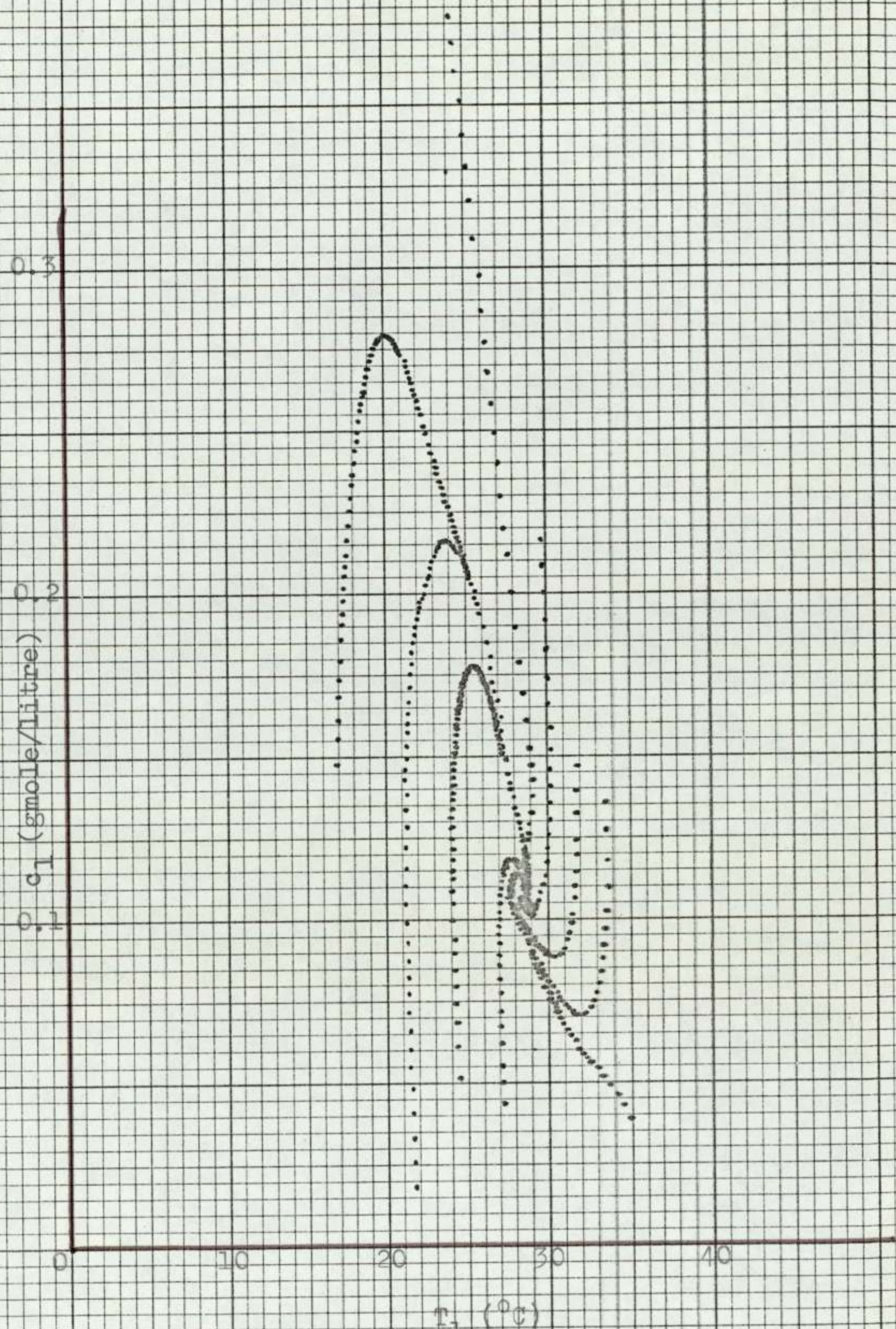

Fig. A.26. Experiment 38.

Partial simulation.

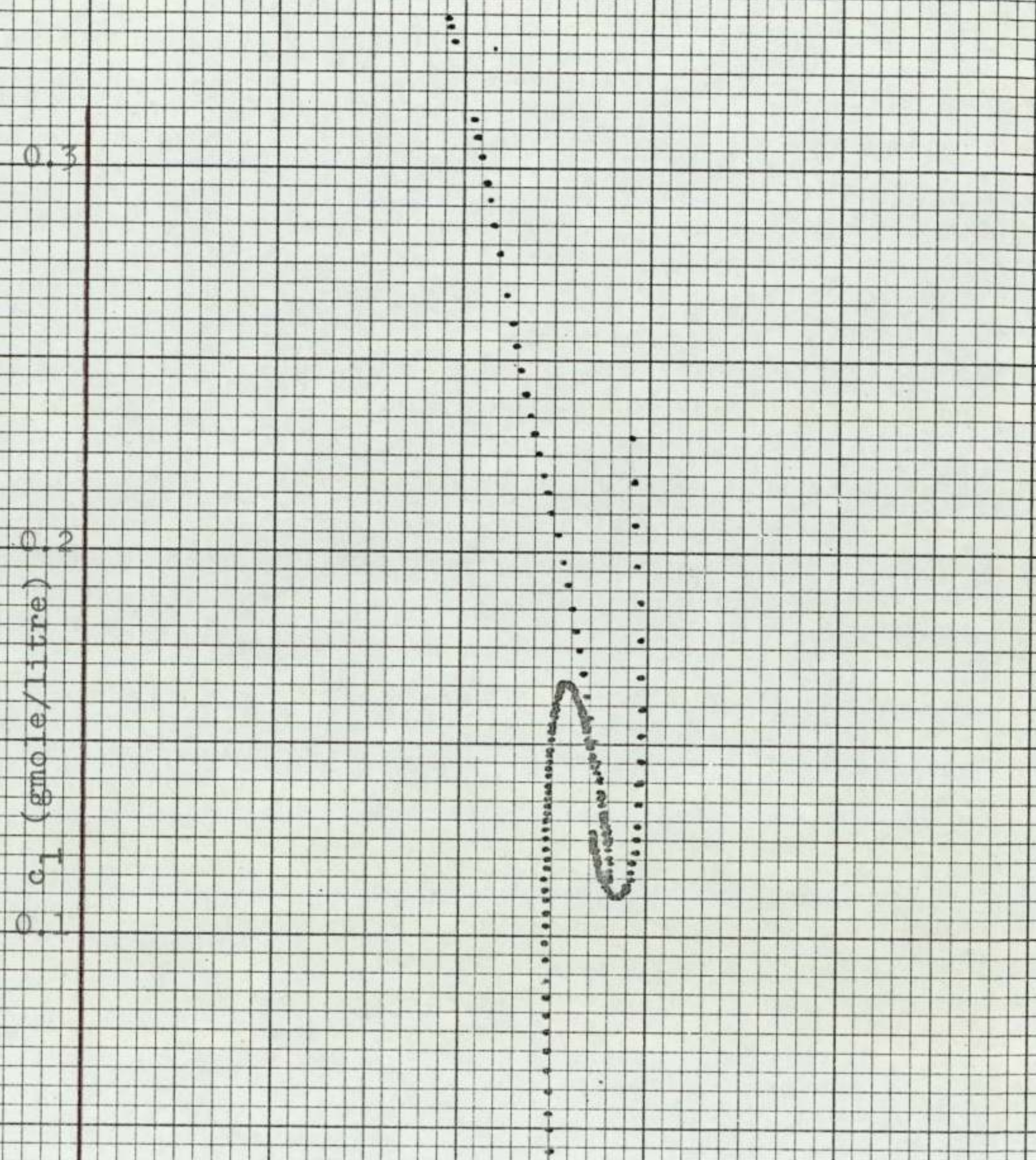

Fig.A.27. Experiments 48 and 49.

Partial simulations.

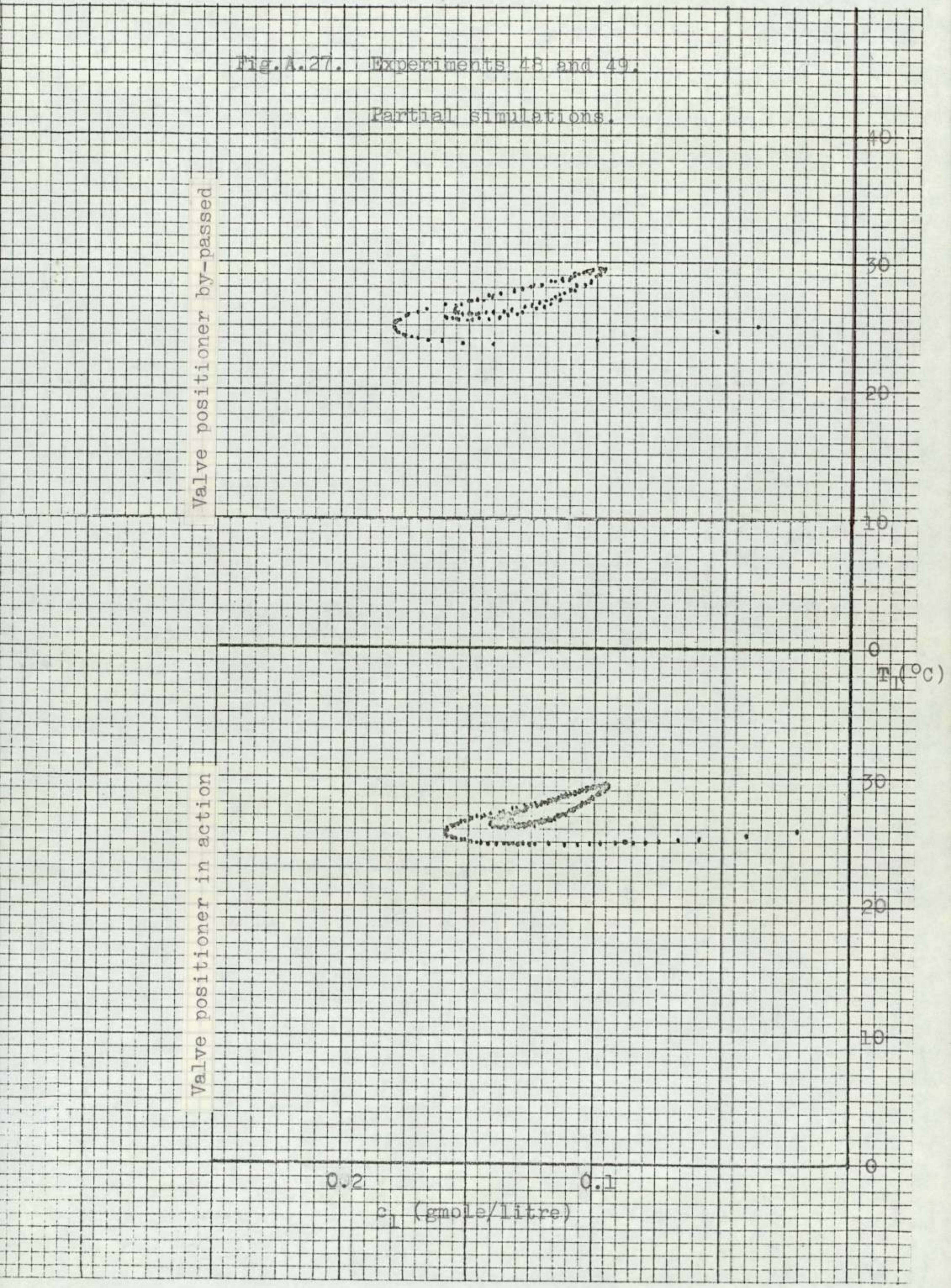

Fig.A.28. Experiments 54 and 55. Partial simulation
Concentration (c_1) vs. Temperature (T_1)

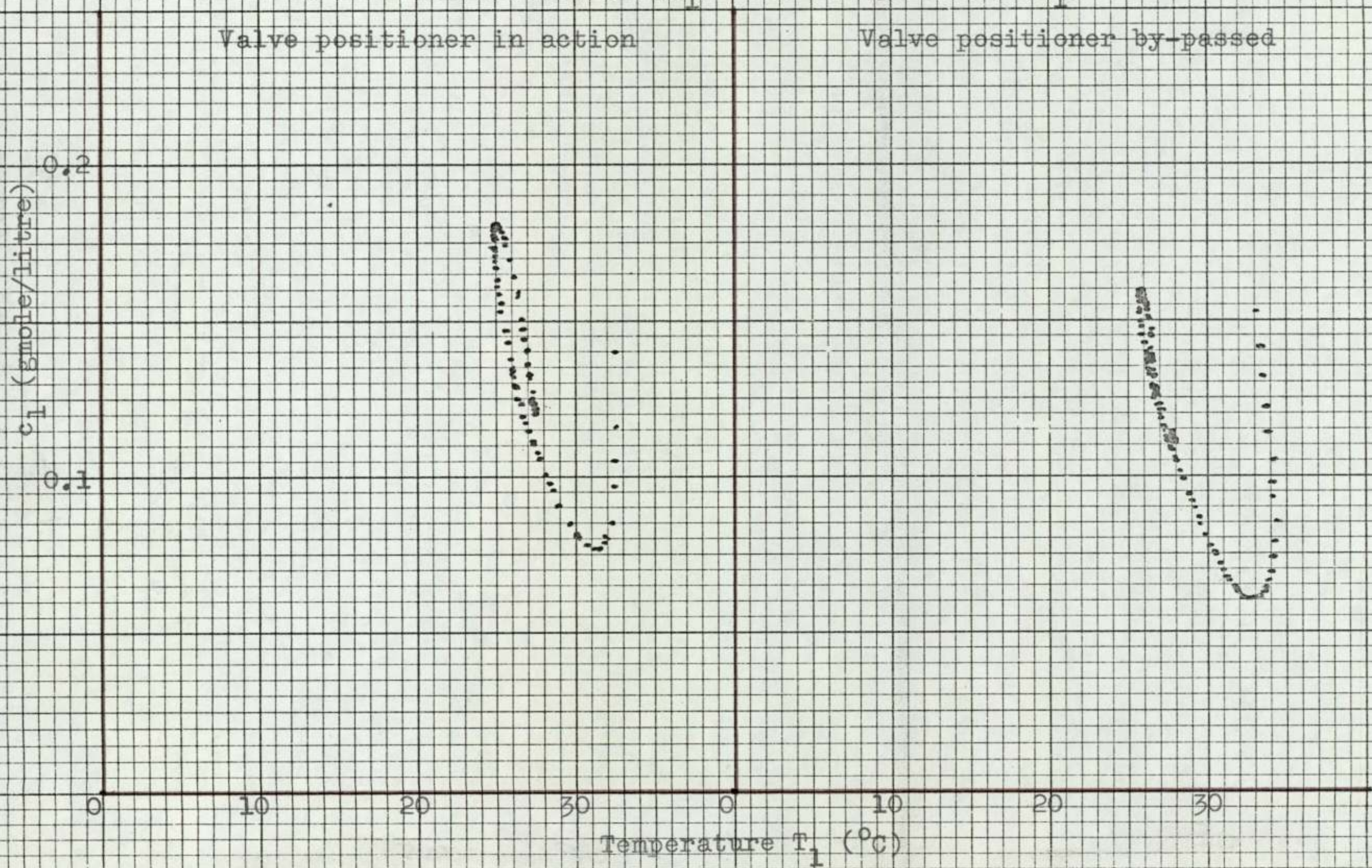

Fig. A.29. Experiment 60.

Partial simulation.

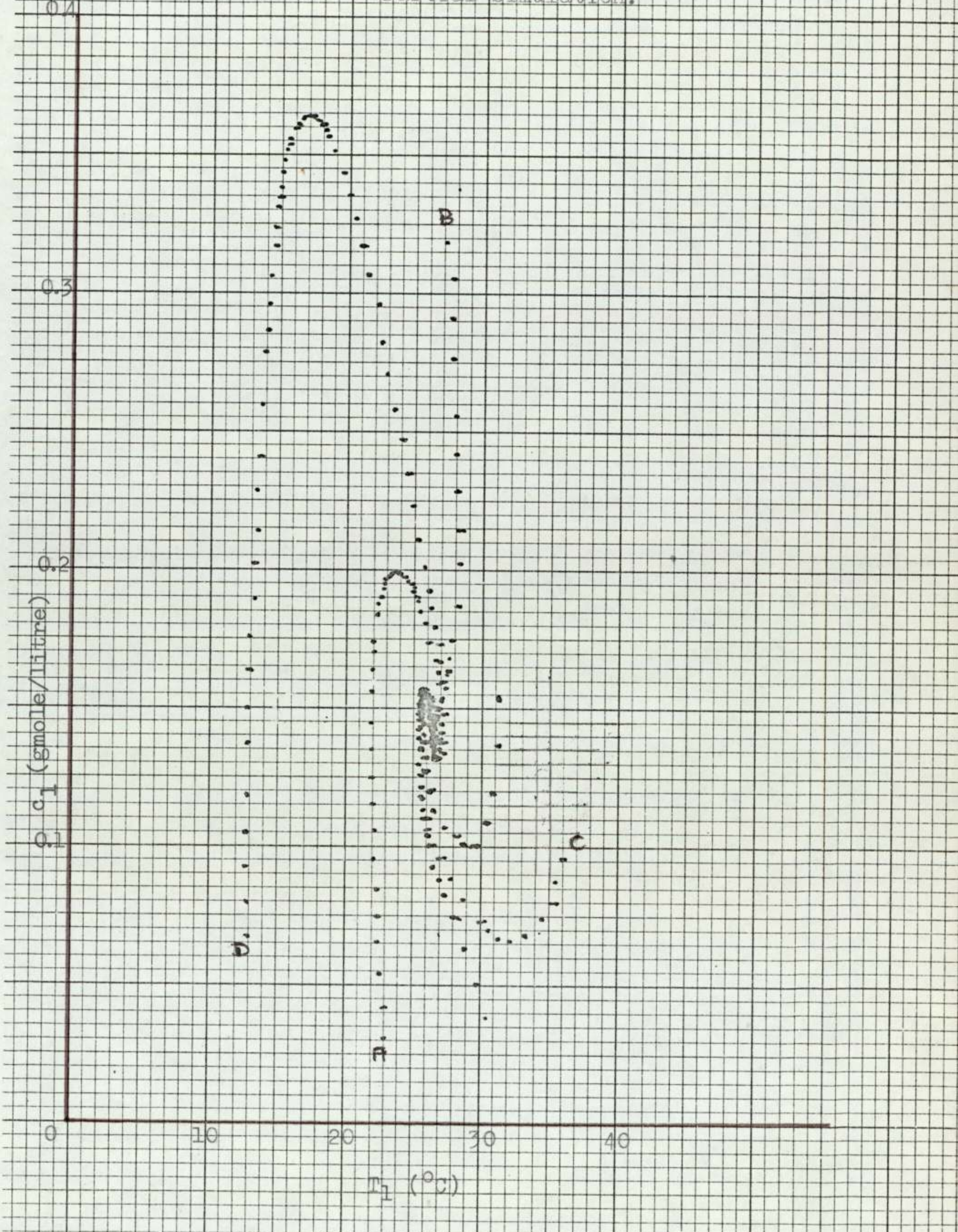

Fig. A.30. Experiment 61.

Partial simulation.

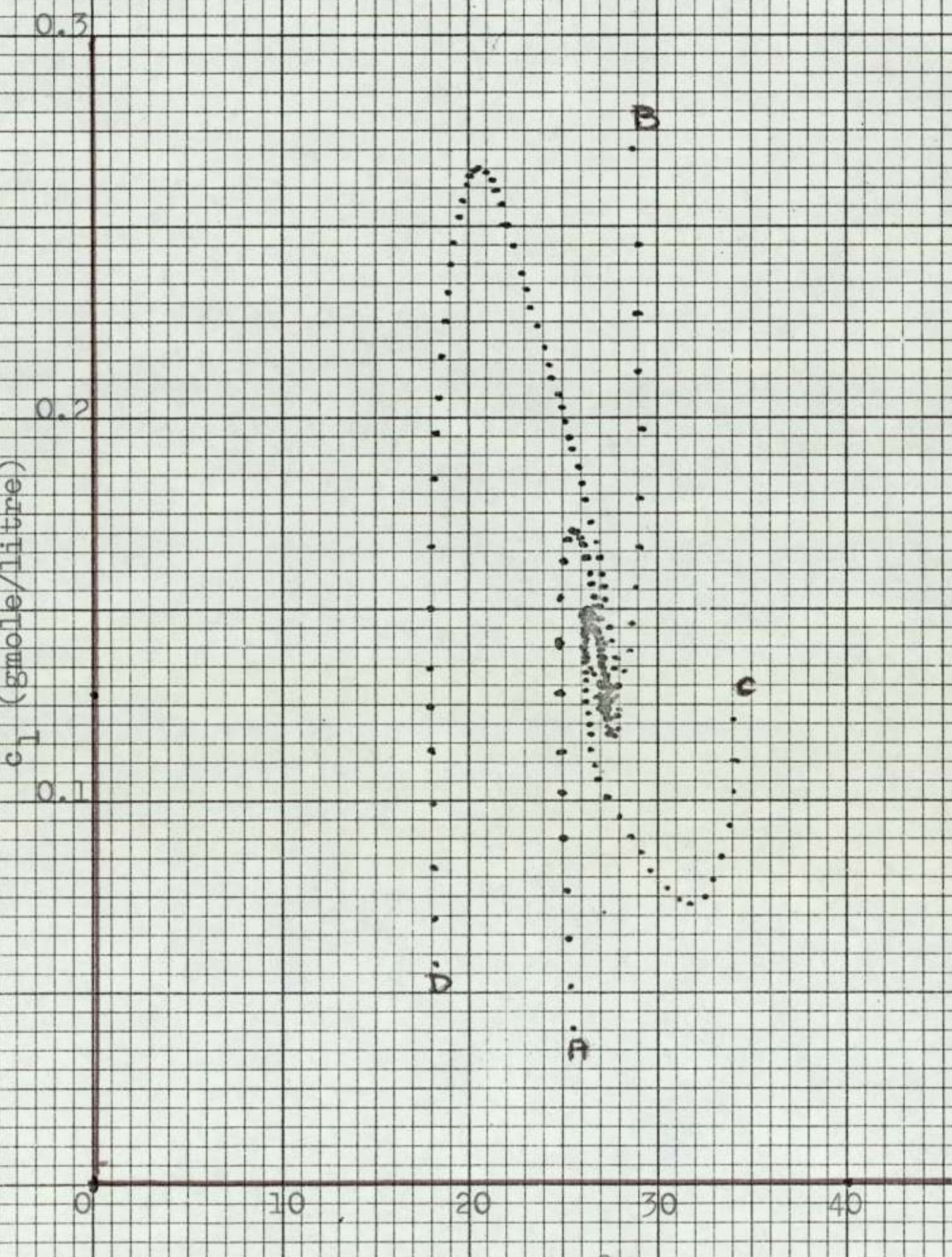

Fig. A.31. Experiment 63.

Partial simulation.

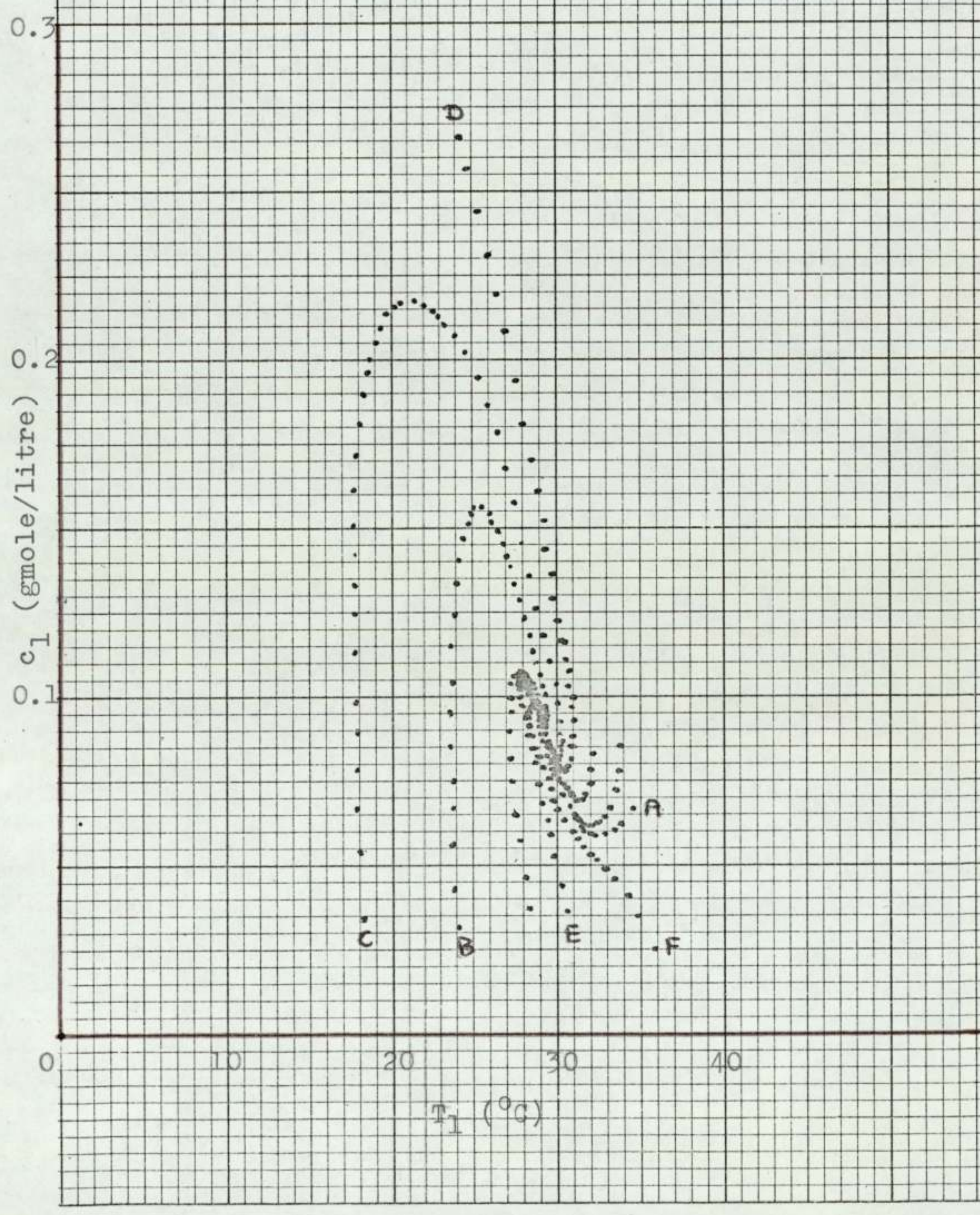

Fig. A.32. Experiment 64.

Partial simulation

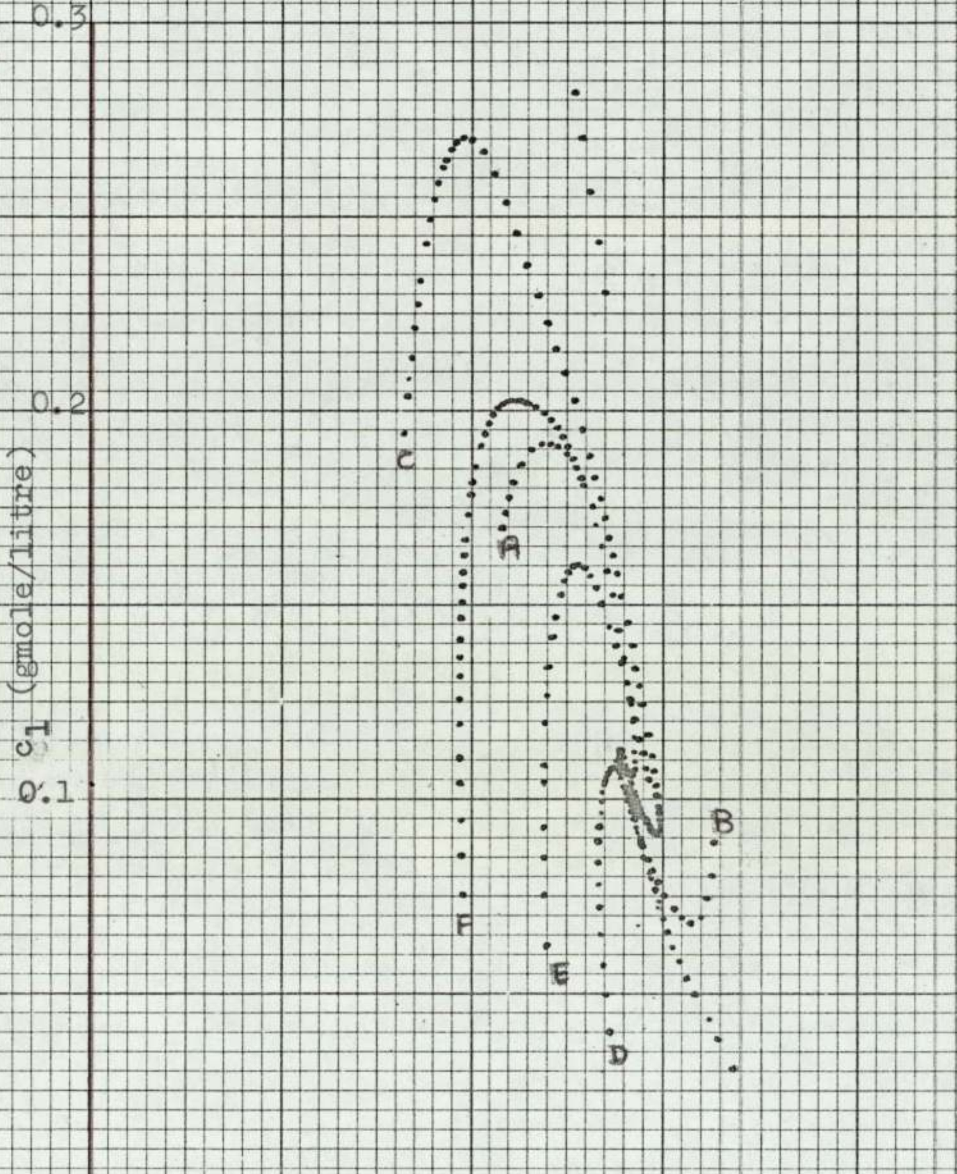

Fig. A.33. Experiment 68.

Partial simulation

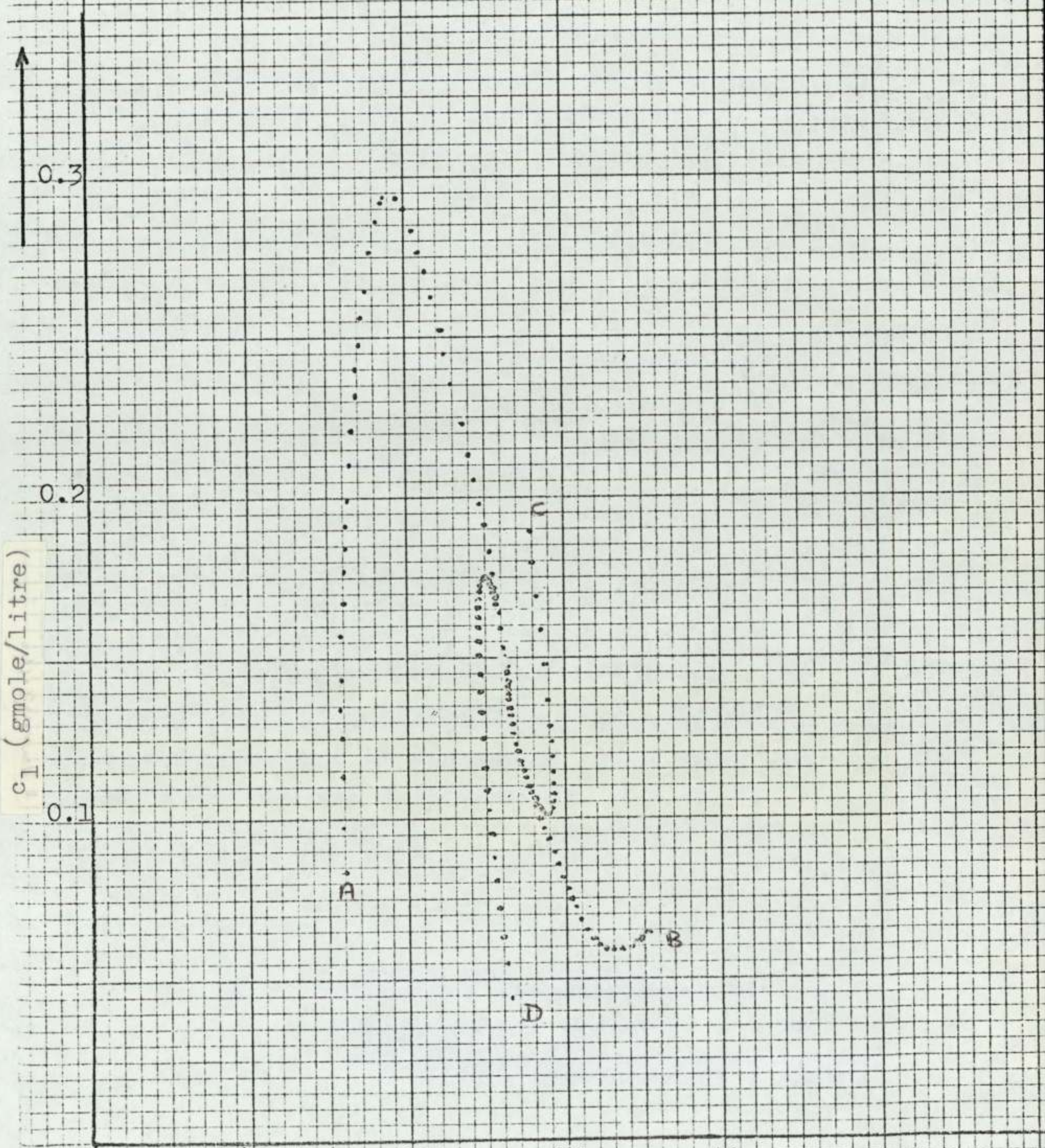

Fig.A.34. Experiment 70(b).

Partial simulation.

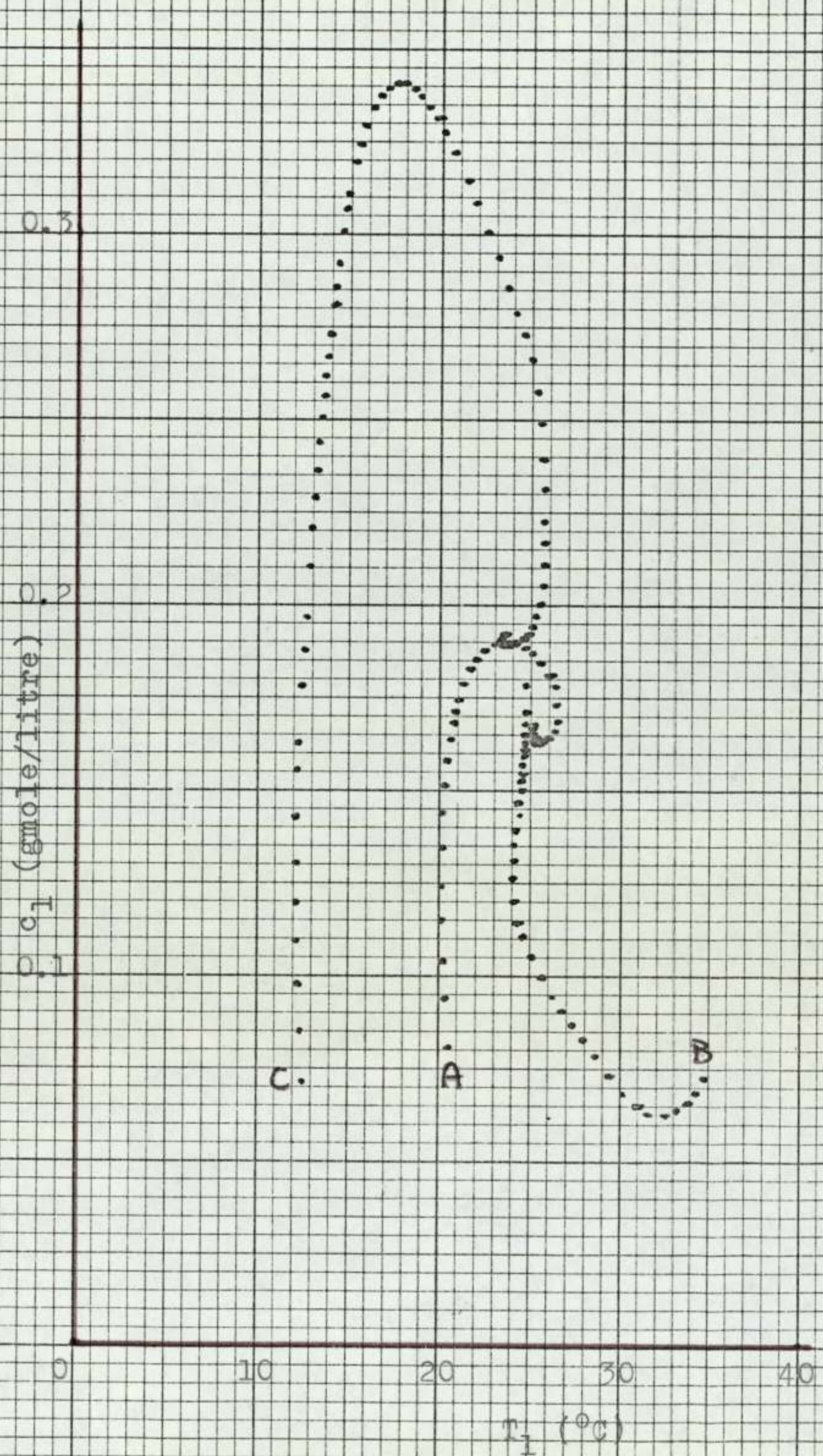

Fig.A.35. Experiment 72.

Partial simulation.

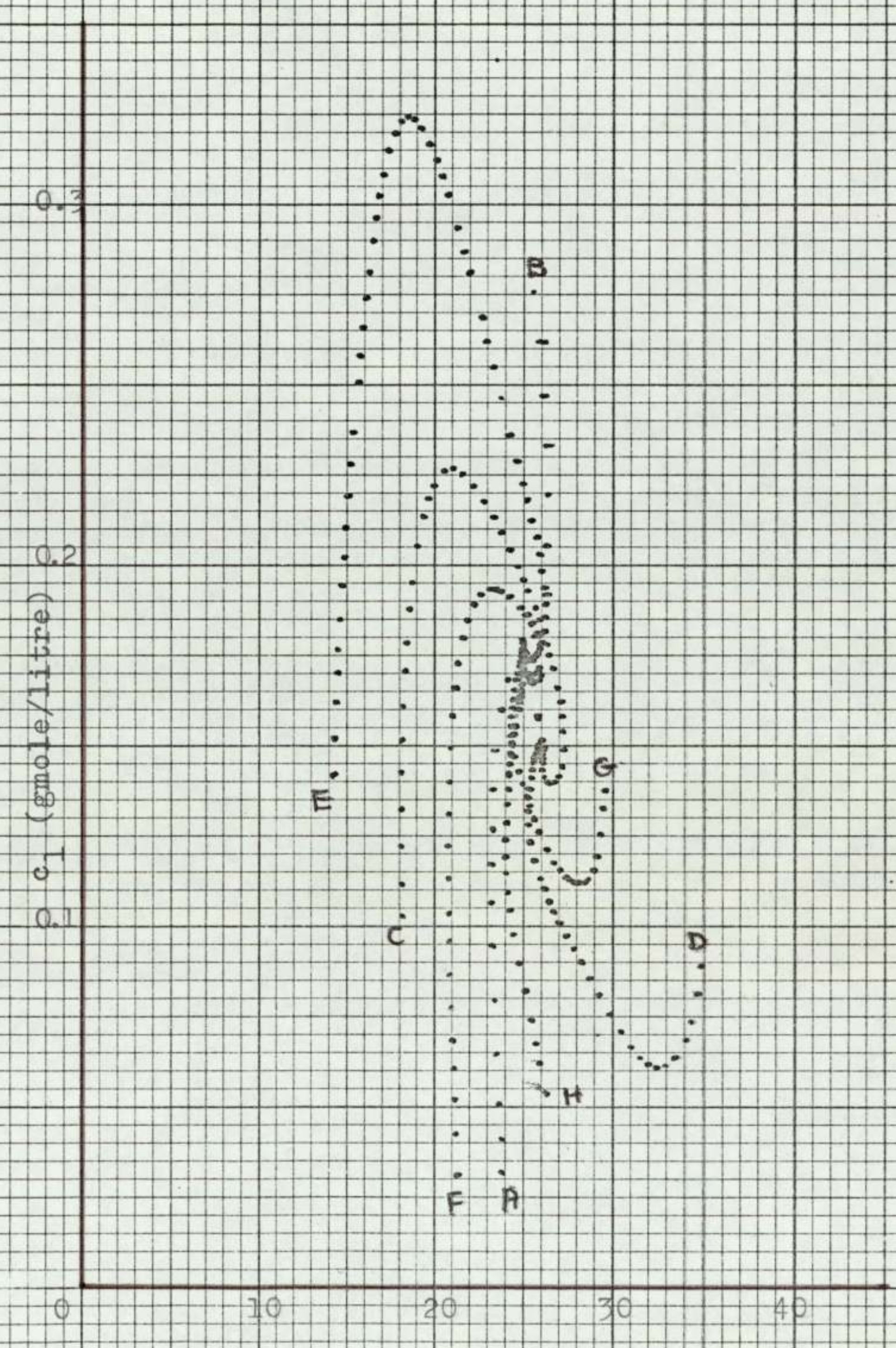

Fig. A.36. Experiment 73.

Partial simulation.

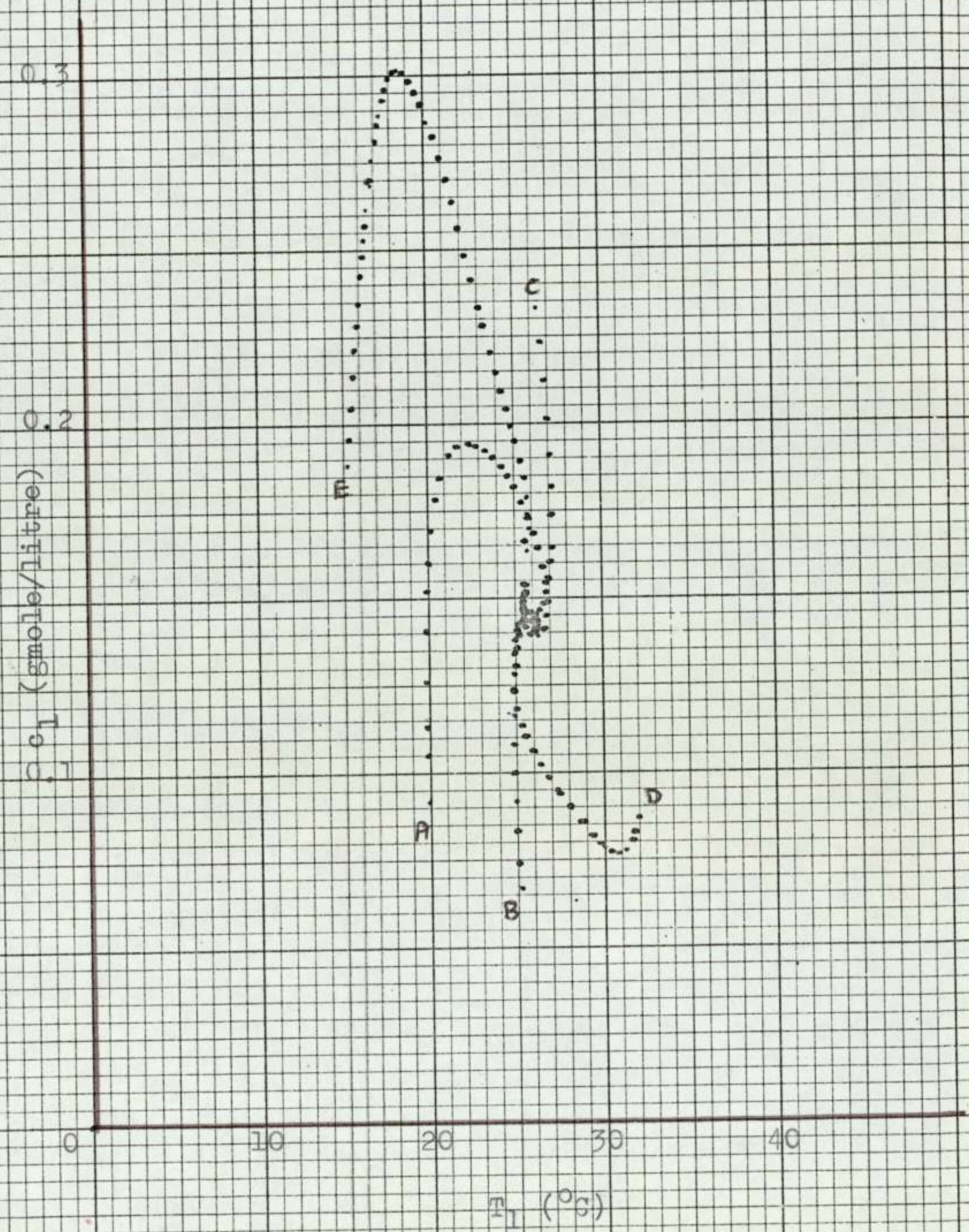

Fig. A.37. Experiment 75.

Partial simulation.

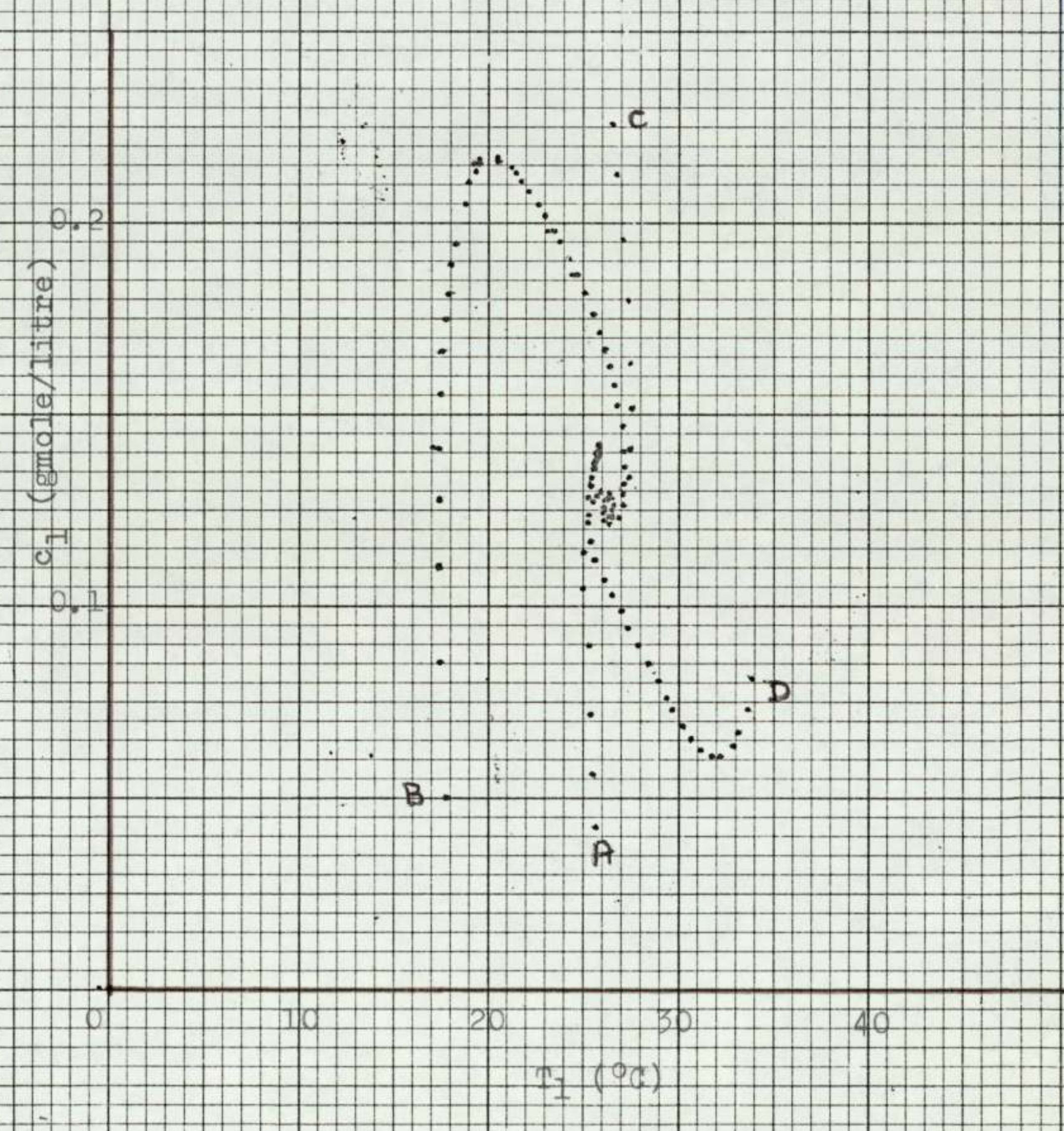

Fig.A.38. Experiment 79.

Partial simulation

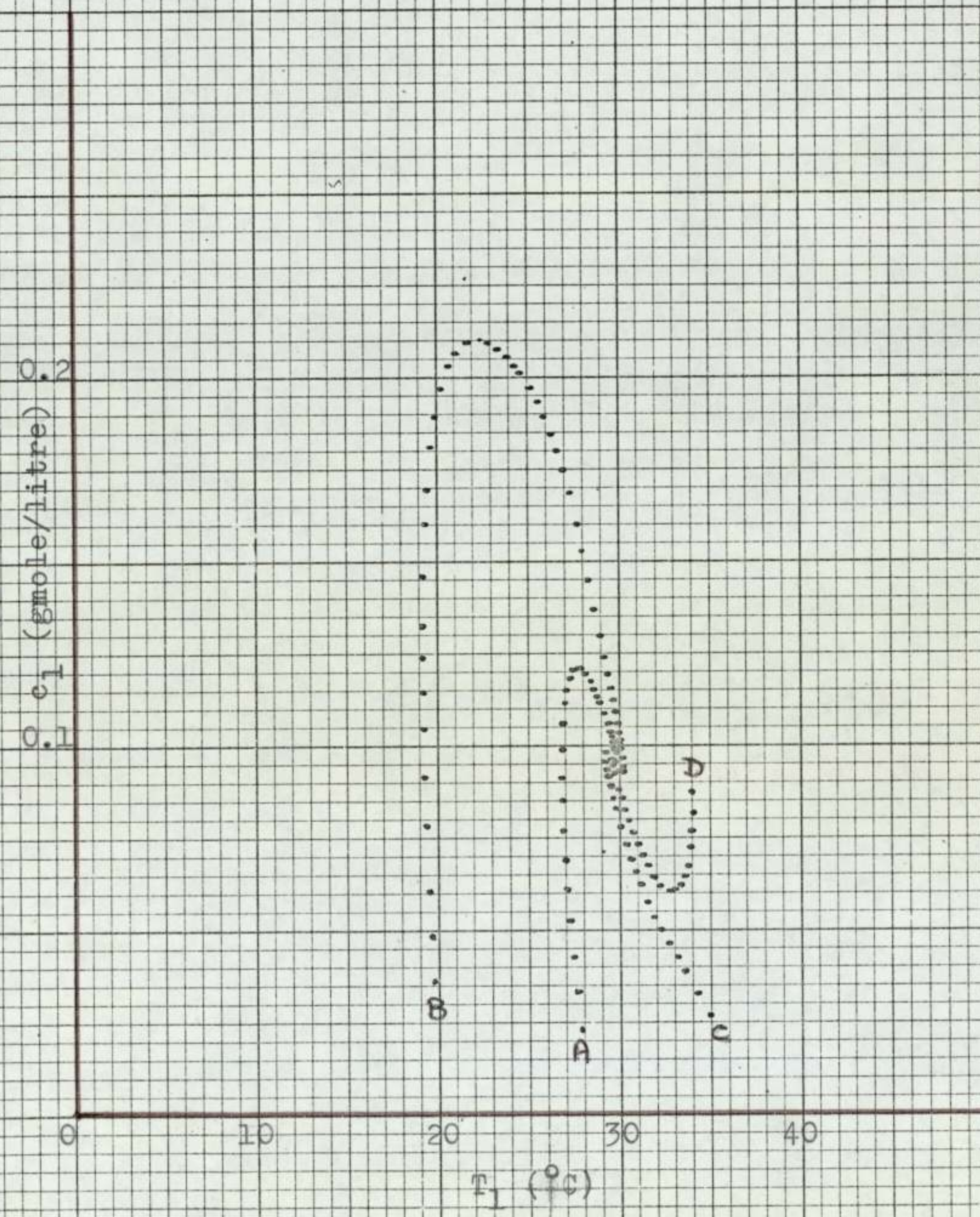

Fig. A.39. Experiment 85.

Partial simulation.

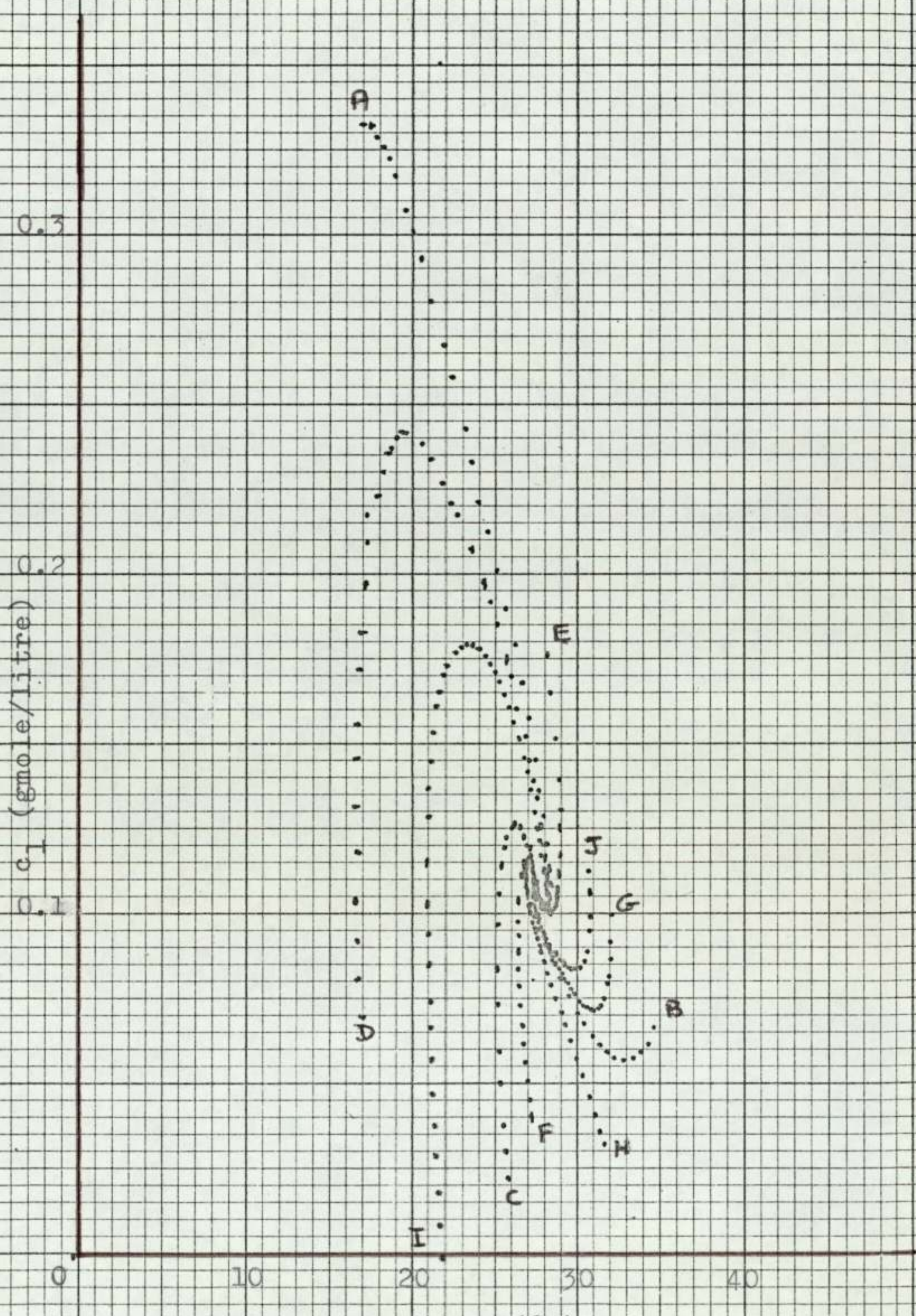

Figs. A.40. to A.45. are some TR 10 complete simulation portraits shown for comparison with their corresponding partial simulation portraits.

Fig. A.40. Experiment 25.

Complete simulation.

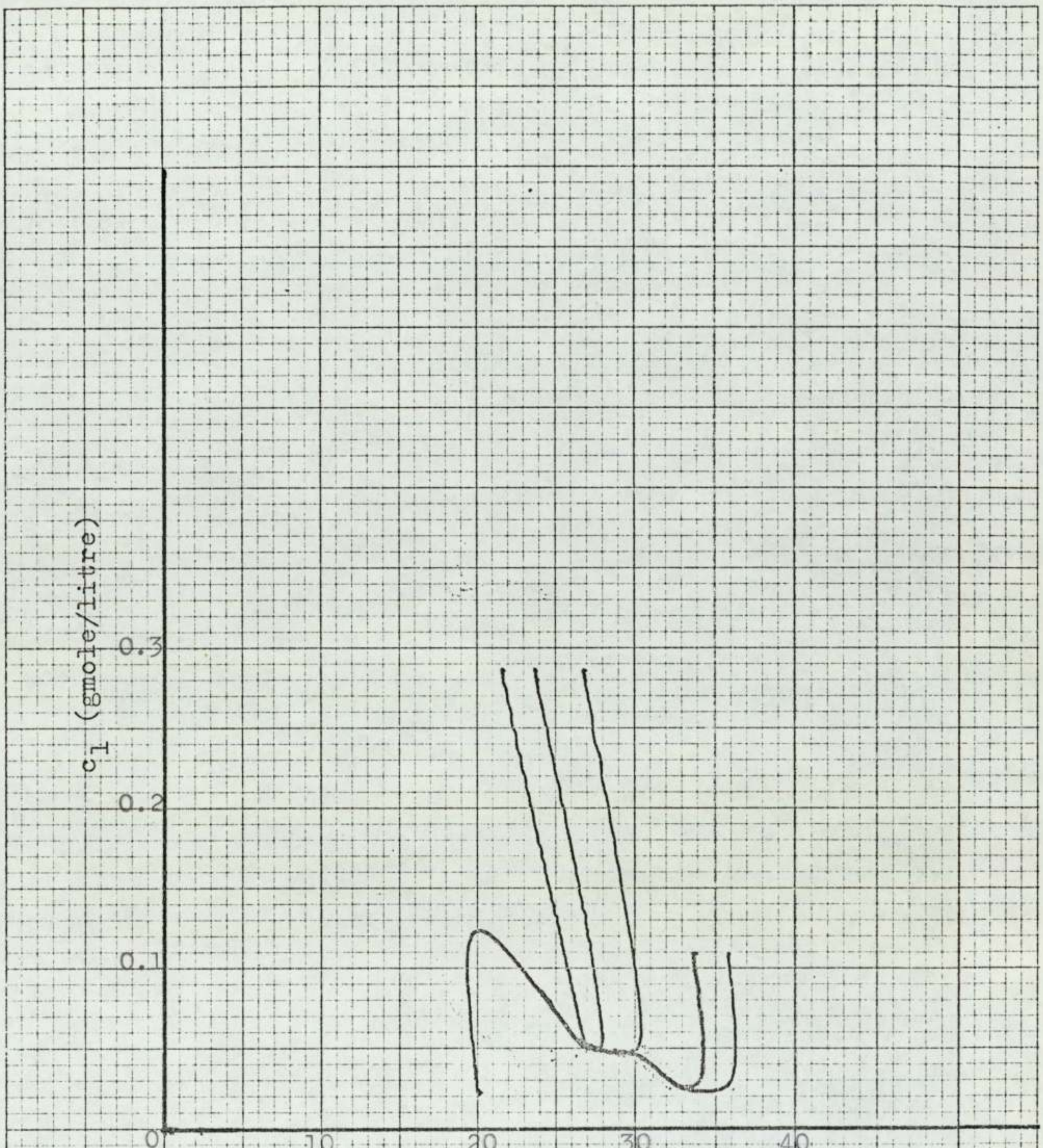

Fig. A.41. Experiment 47.

Complete simulation.

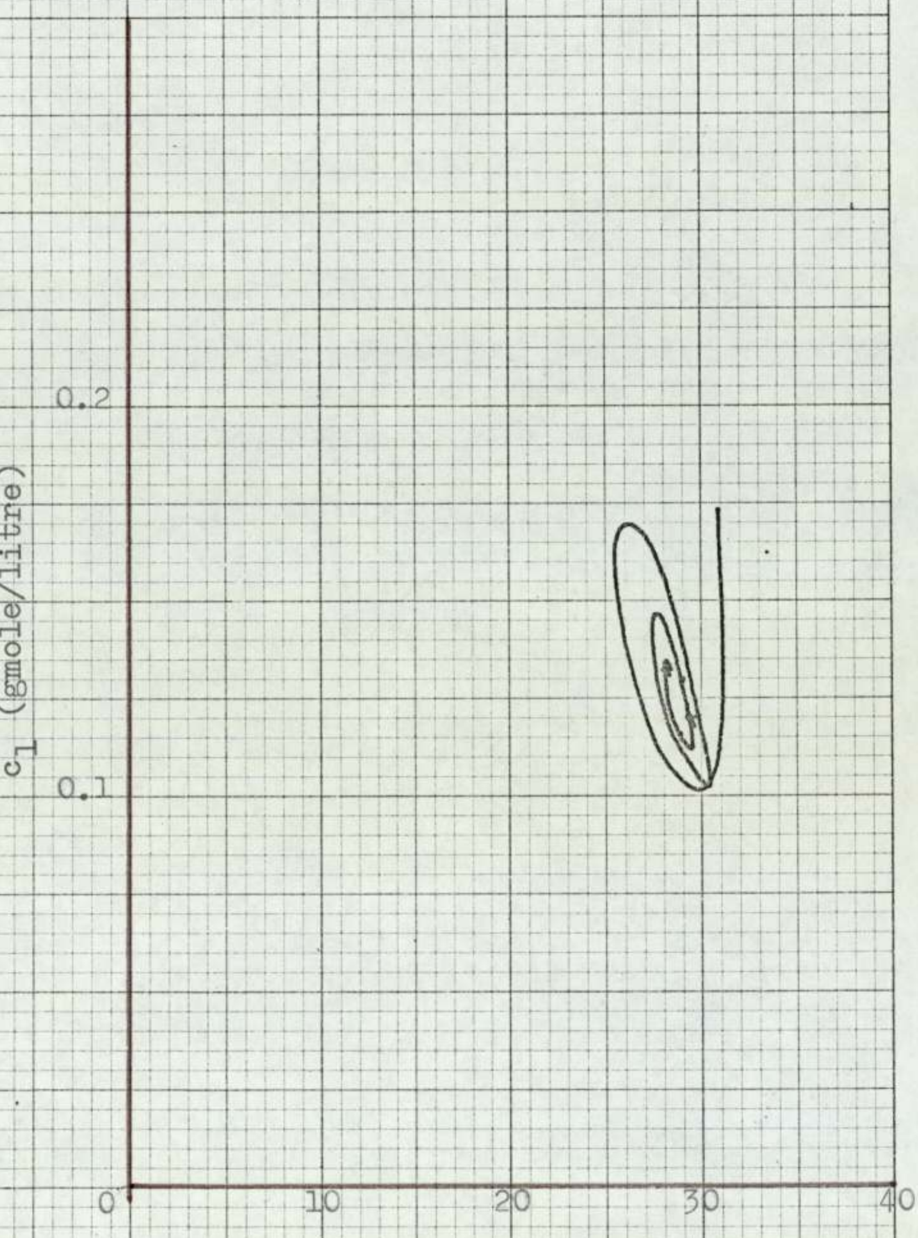

Fig. A.42. Experiment 67.

Complete simulation.

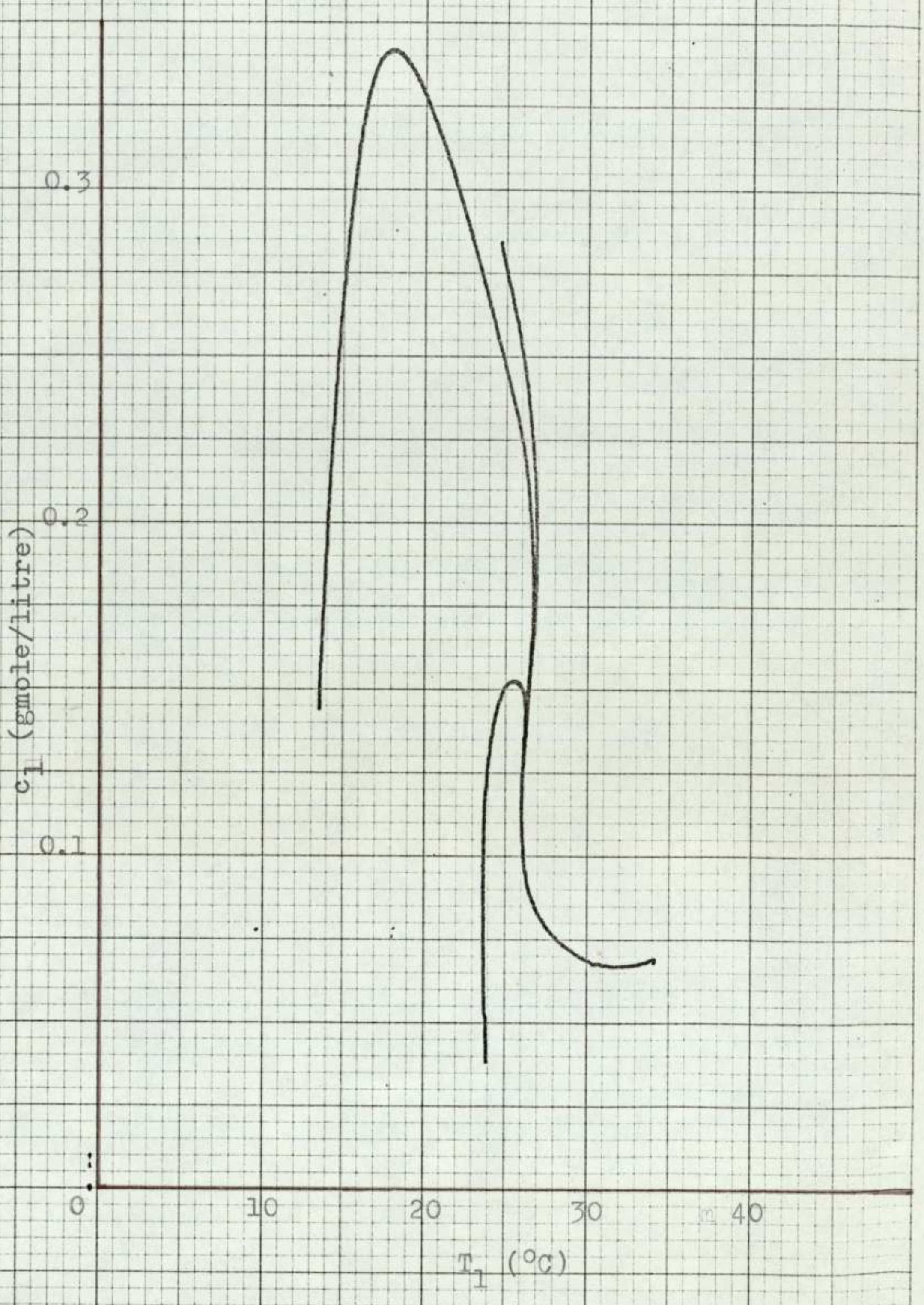

Fig. A.43. Experiment 72.

Complete simulation.

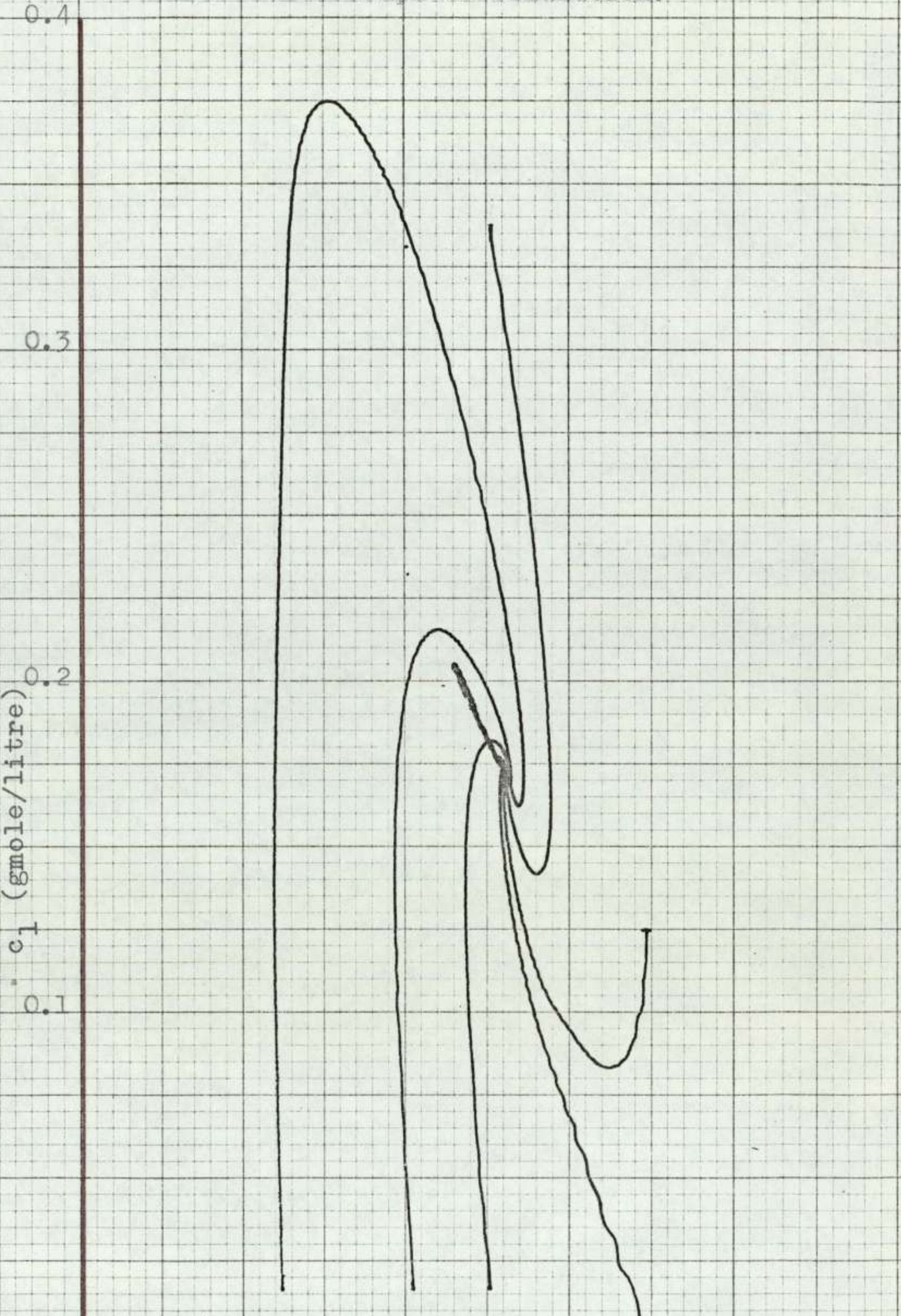

Fig. A.44. Experiment 75.

Complete simulation.

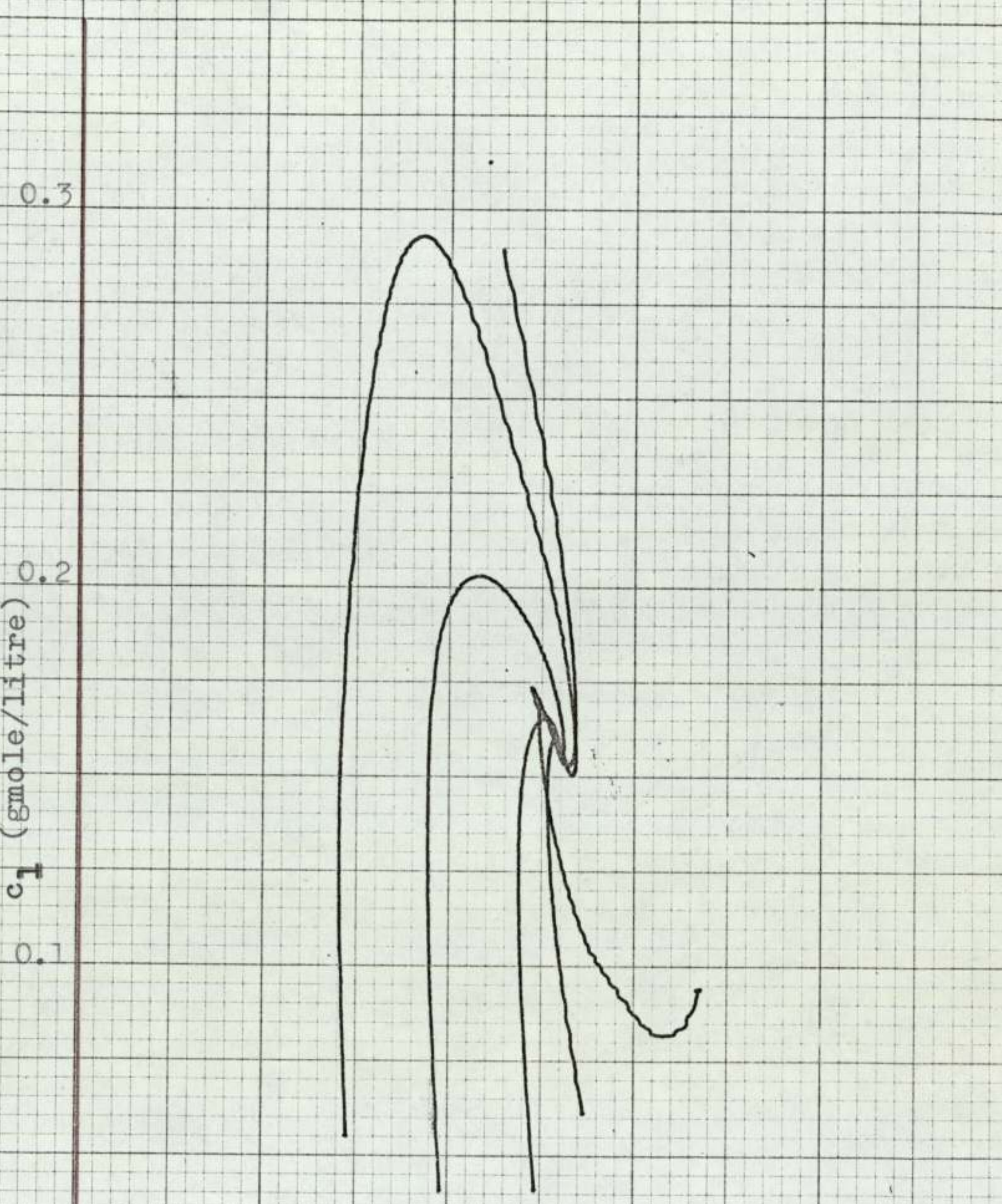

Fig. A.45. Experiment 85.

Complete simulation.

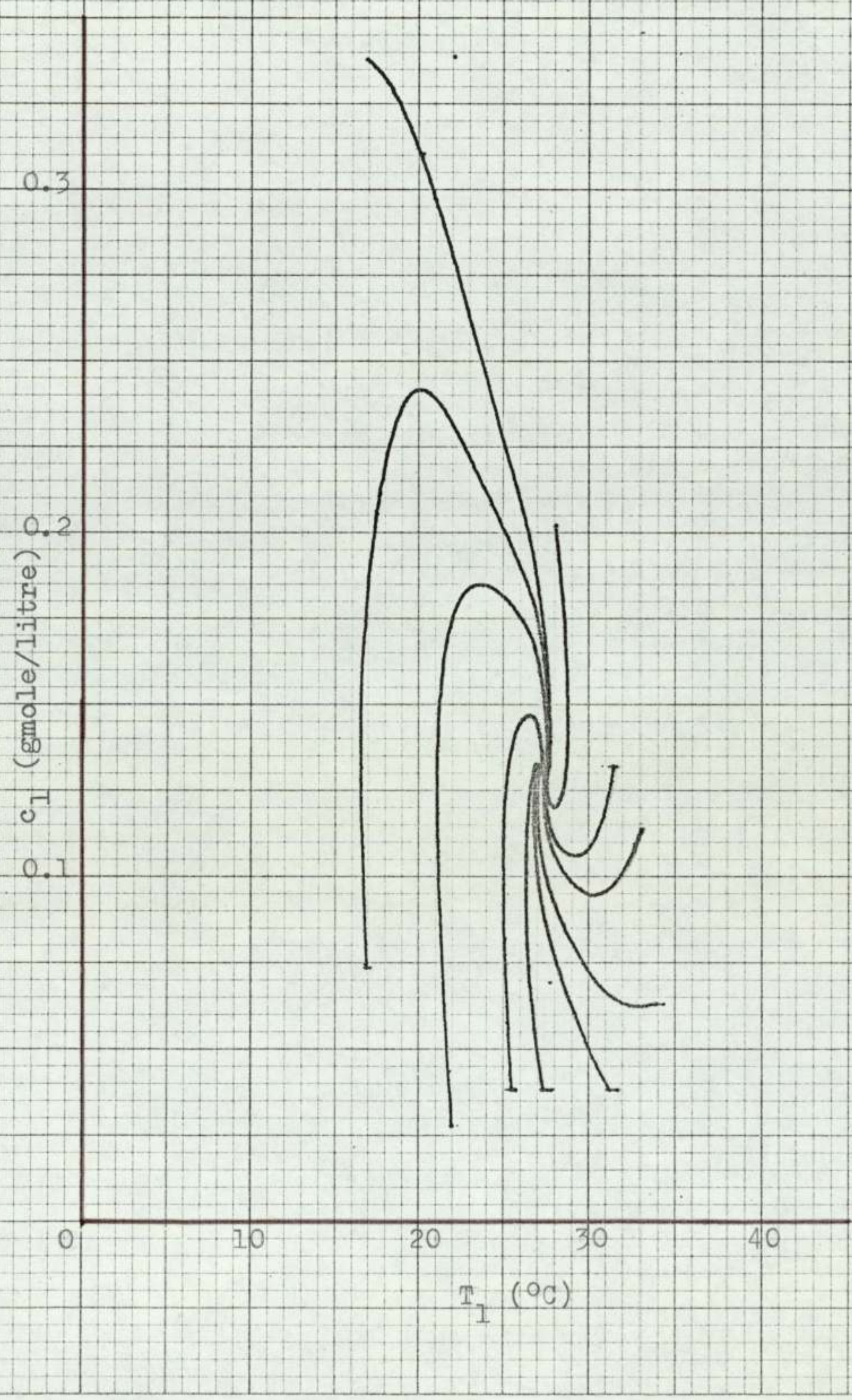

Figs. A.46. to A.48. are Hybrid complete simulation portraits shown for comparison with partial simulation and TR 10 complete simulation portraits.

Fig. A.46. Experiment 28.

Complete simulation.

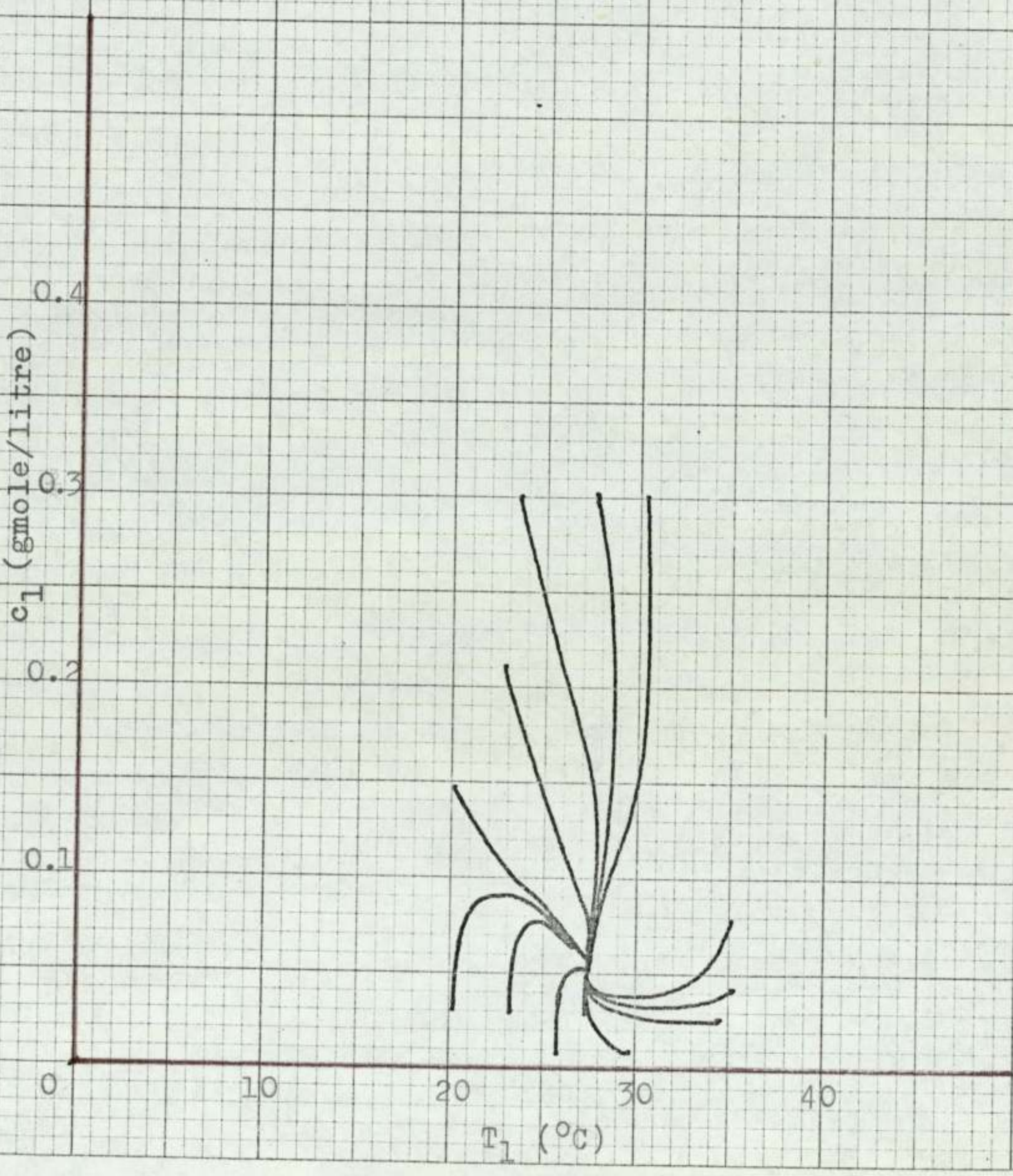

Fig. A.47. Experiment 31.

Complete simulation.

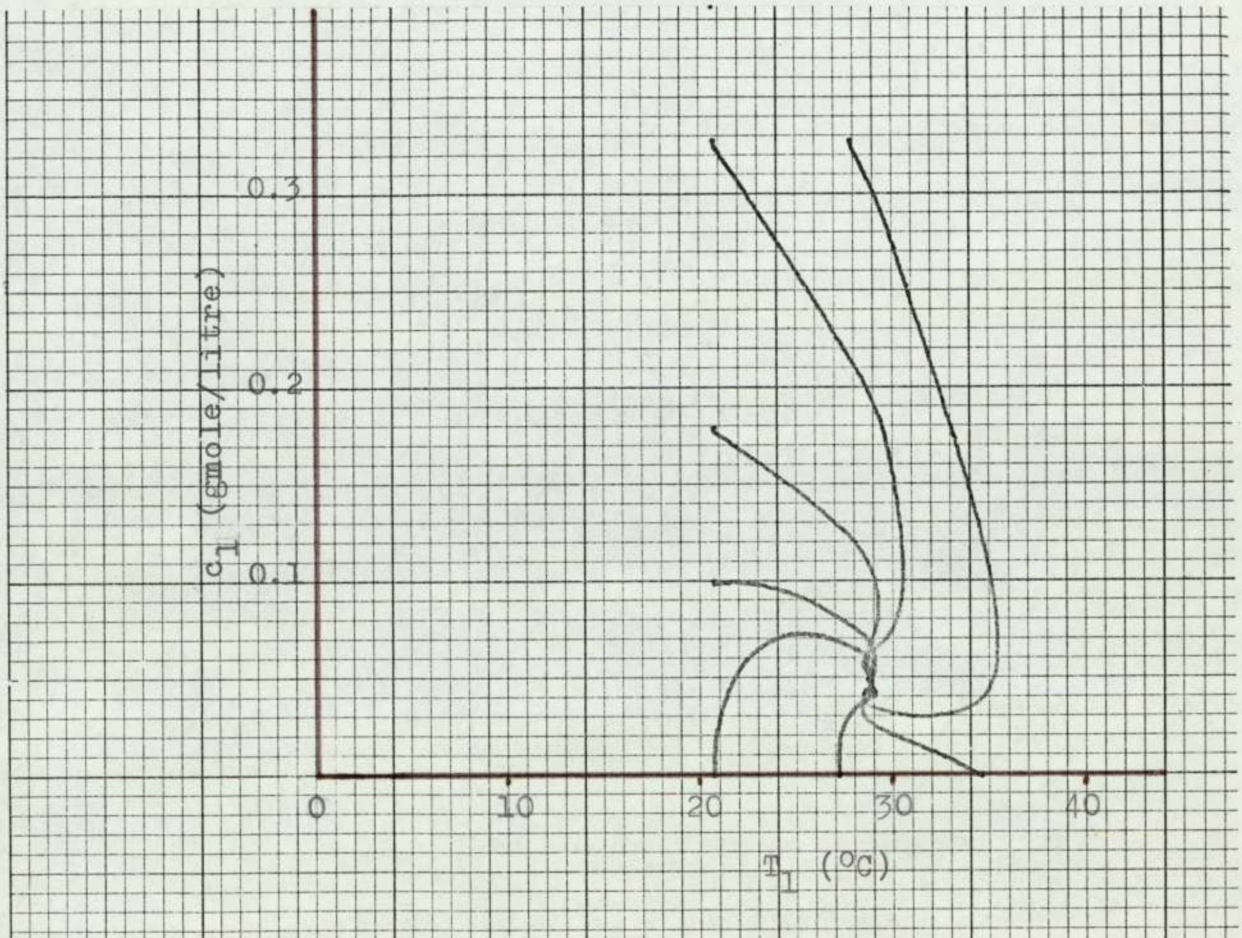

Fig. A.48. Experiment 67.

Complete simulation.

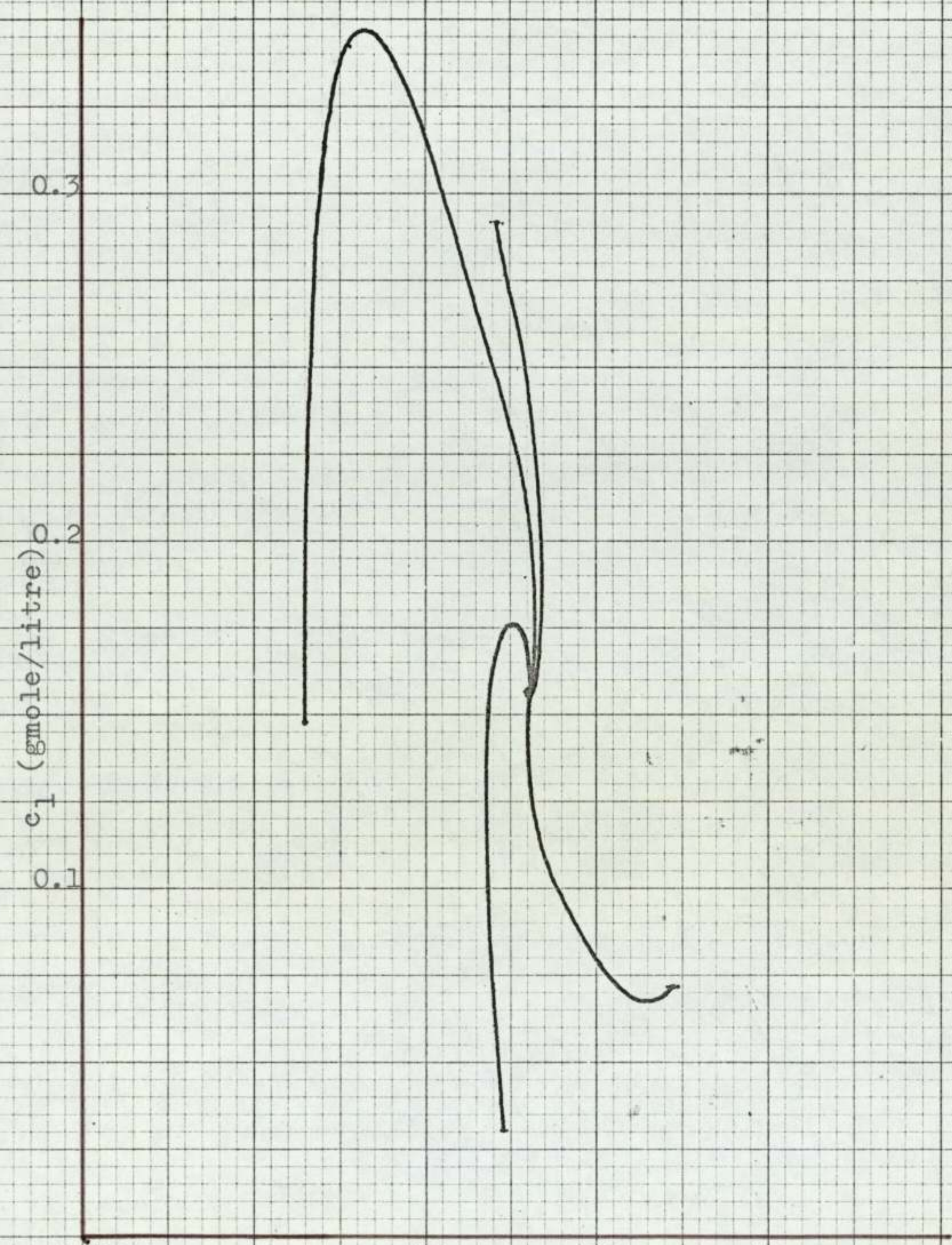

Tests on controllers and control valve

The experimental procedure was considered in Chapter 8. Only the results obtained are therefore considered here. The results are shown in the order that they were recorded. It was noted from these results that for wider proportional bands on the first controller, the actual proportional band widths were wider than those indicated by the controller setting. Consideration of this discrepancy was made when analysing the results and effecting complete simulations. The effect on the portraits was found to be very small or negligible.

The first controller (200°C range) was used in Series 1 to 7. The stirrer speed - Torovolt setting 40 - was used for all tests on controllers and control valve.

Table A.25.

Series 1 Test 1

PBW setting 10 deg C — Other control actions set to zero

Valve positioner in action — Variac setting 59

T_{c1} = 12.0°C — m_f for steady state = 3 litre/min.

T_1 rising			T_1 falling		
T_1 °C	COP lbf/in^{2}gauge	m_c litre/min.	T_1 °C	COP lbf/in^{2}gauge	m_c litre/min.
26.5	12.8	0.50	34.0	0	9.50
27.5	12.5	0.80	32.0	2.5	"
27.8	12.0	0.98	31.0	4.2	9.10
27.9	11.8	1.00	30.0	6.3	6.20
28.0	11.5	1.15	29.0	8.2	3.65
28.1	11.2	1.30	28.5	9.1	3.00
28.4	"	1.25	28.0	10.1	2.10
steady state reached			27.9	10.2	1.85
forced readings			27.8	10.8	1.60
28.6	10.8	1.65	27.7	11.0	1.50
28.9	10.2	1.95	27.6	"	"
29.0	9.6	2.60	27.9	10.9	1.60
29.4	8.9	3.40	steady state reached		
29.5	8.7	3.45	forced readings		
29.6	8.0	3.80	27.0	12.5	0.80
29.9	7.9	4.10	26.0	13.8	0
30.0	7.8	4.30			

T_1 steady state hysteresis = 0.5°C

(see Figs.8.10., 8.13. and A.49. for graphs of results)

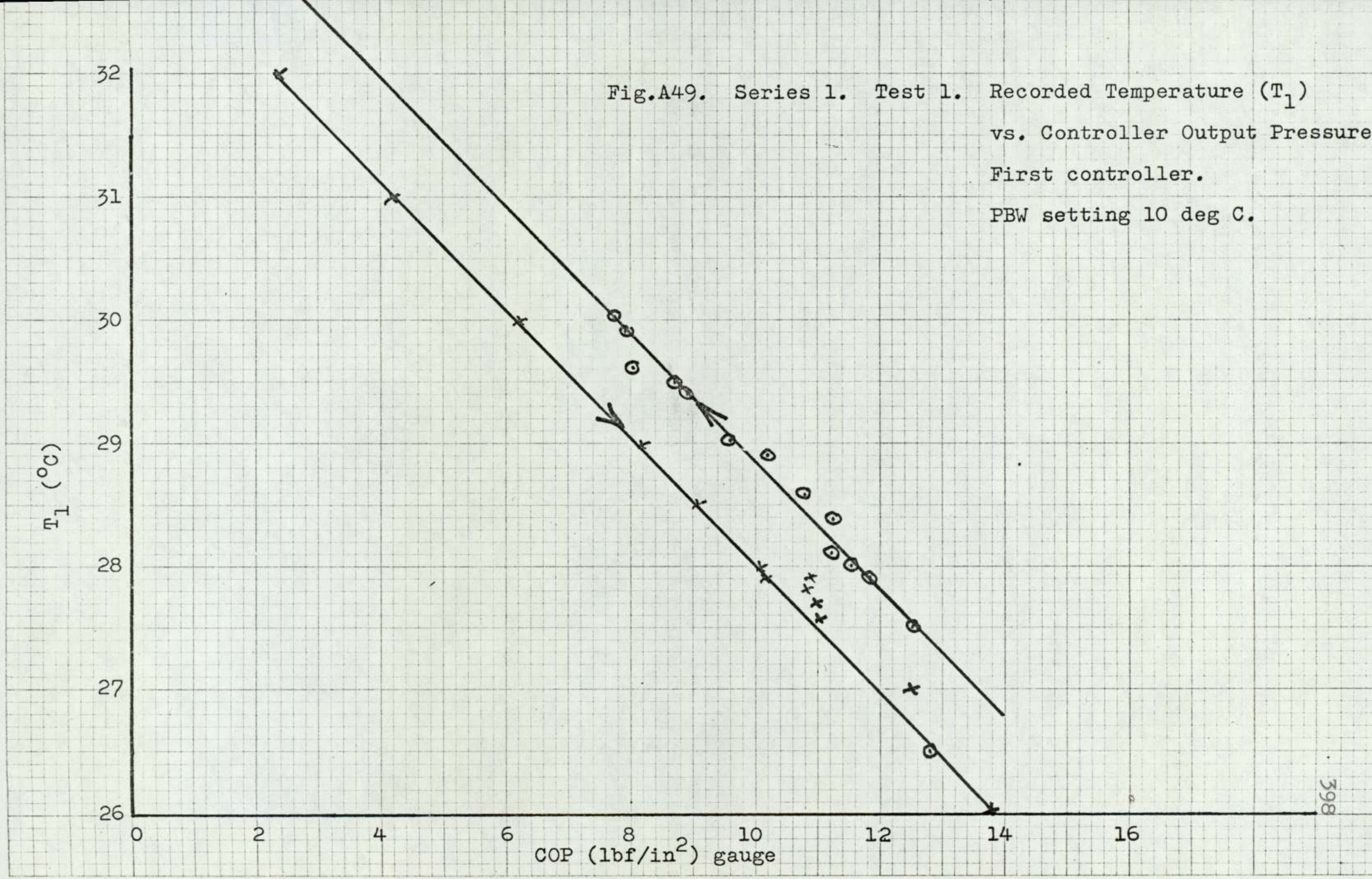

Fig.A49. Series 1. Test 1. Recorded Temperature (T_1) vs. Controller Output Pressure(CO
First controller.
PBW setting 10 deg C.

Table A.26.

Series 1 Test 2

PBW setting 10 deg C Valve positioner by-passed

Other parameters as Test 1

T_1 rising			T_1 falling		
T_1 ^oC	COP lbf/in^2 gauge	m_c litre/min.	T_1 ^oC	COP lbf/in gauge	m_c litre/min.
25.0	15.5	0	32.0	0	9.50
26.0	14.5	0	31.0	2.8	9.15
27.0	13.0	0.20	30.0	4.8	6.90
27.5	11.9	0.60	29.5	6.0	5.15
28.0	11.2	0.90	29.0	7.2	3.75
28.1	10.8	0.98	28.5	8.0	2.75
28.2	10.5	1.00	28.1	9.0	2.30
28.3	10.4	"	28.0	9.2	2.10
28.4	10.2	1.05	27.9	9.6	1.85
28.5	"	"	27.8	9.9	1.75
steady state reached			27.6	10.1	1.60
forced readings			27.5	10.2	1.50
29.0	9.2	1.50	steady state reached		
30.0	6.8	3.20	forced readings		
31.0	4.8	5.50	27.1	11.0	1.15
31.2	4.0	6.60	27.0	11.2	1.05
			26.5	11.6	1.00
			26.0	12.3	0.80

T_1 steady state hysteresis = 1.0^oC

(see Figs.8.9., 8.12. and 8.14. for graphs of results)

Table A.27.

Series 2 Test 1

PBW setting 20 deg C

Variac setting 50

Other parameters as Series 1

Valve positioner in action

m_f = 0 litre/min.

T_1 rising			T_1 falling		
T_1 °C	COP lbf/in^{2}gauge	m_c litre/min.	T_1 °C	COP lbf/in^{2}gauge	m_c litre/min.
17.0	12.7	0.90	30.0	0	9.25
18.0	11.8	1.15	29.0	0	"
19.0	10.9	1.75	28.0	2.9	"
20.0	10.1	2.35	27.0	3.9	"
21.0	9.3	2.70	26.0	4.7	9.00
22.0	8.3	3.75	25.0	5.3	8.25
23.0	7.6	4.65	24.5	6.0	7.40
24.0	6.9	5.85	24.3	6.1	7.00
24.1	6.6	6.20	24.2	"	6.90
24.2	"	6.30	24.1	6.2	6.85
24.4	6.5	6.40	steady state reached		
"	"	6.50	coolant temperatures:		
24.5	6.4	6.45	T_{c1} = 9.2		
steady state reached			T_{c2} = 15.9		
coolant temperatures:					
T_{c1} = 9.2					
T_{c2} = 16.0					

T_1 steady state hysteresis = 0.4°C

(see Figs.A.50., A.51. and A.52. for graphs of results)

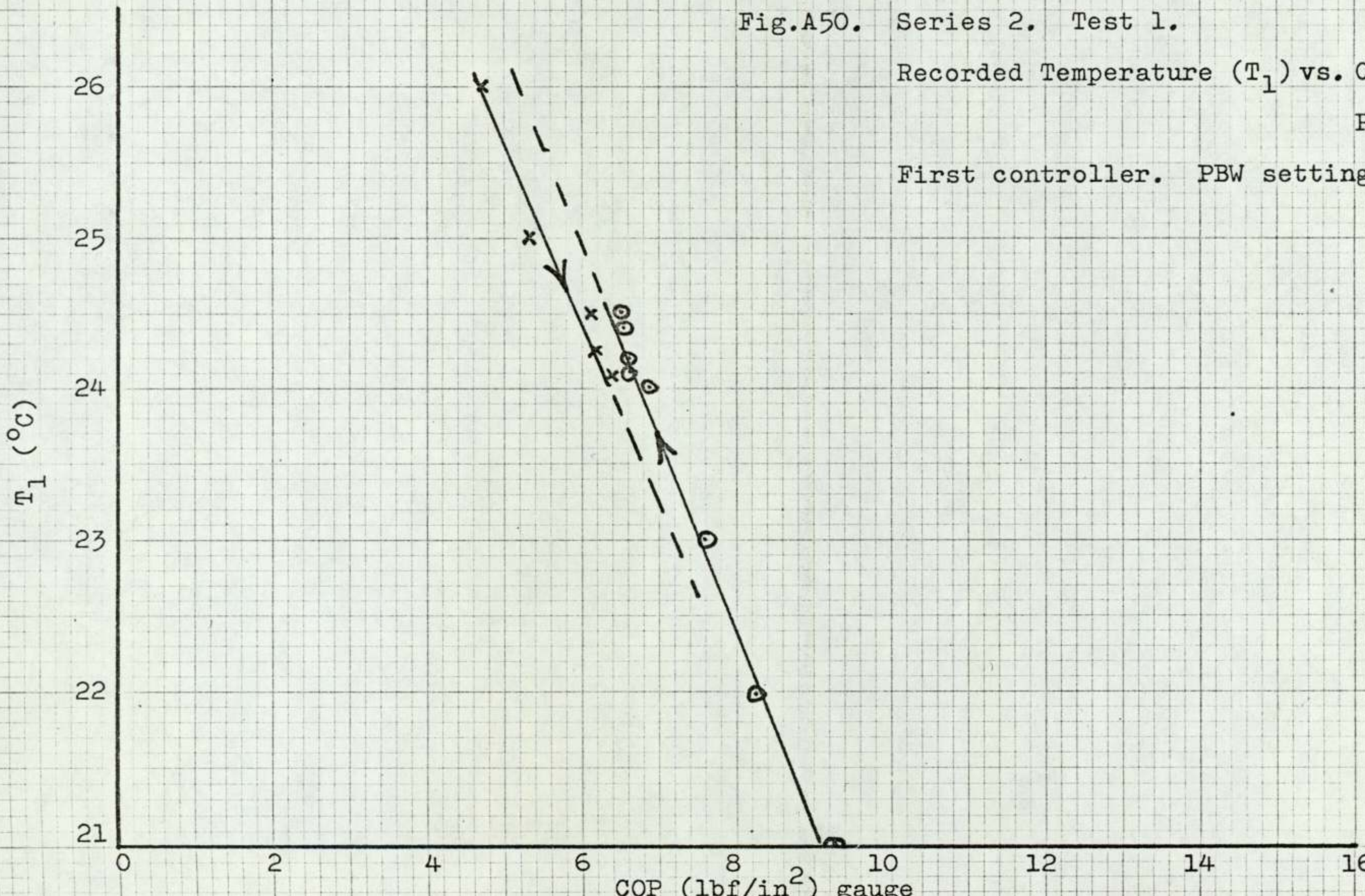

Fig.A50. Series 2. Test 1.
Recorded Temperature (T_1) vs. Controller Output Pressure (COP)
First controller. PBW setting 20 deg.C.

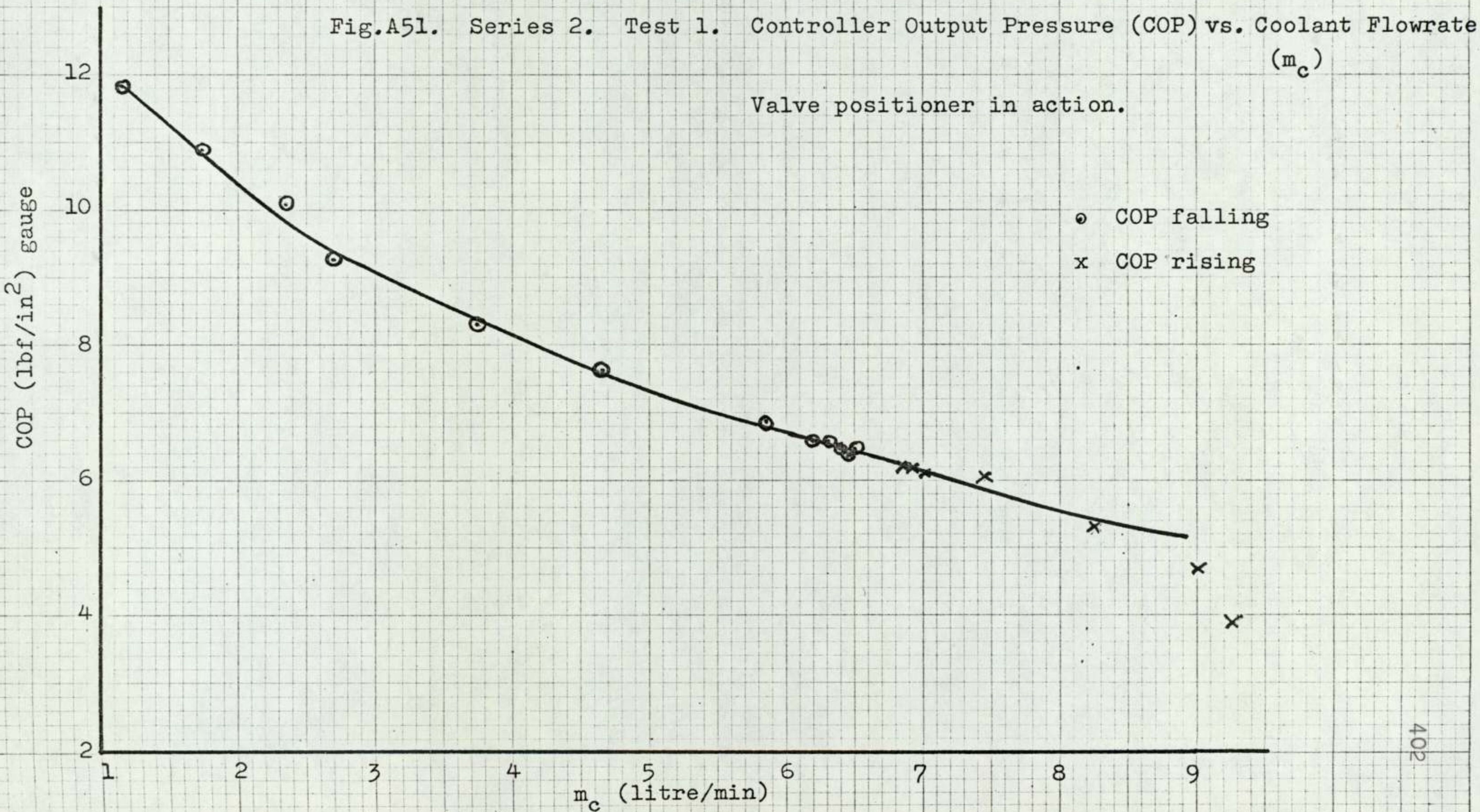

Fig.A51. Series 2. Test 1. Controller Output Pressure (COP) vs. Coolant Flowrate (m_c)

Valve positioner in action.

Fig.A52. Series 2. Test 1. Recorded Temperature (T_1) vs. Coolant Flowrate (m_c)
First controller. PBW setting 20 deg C.
Valve positioner in action.

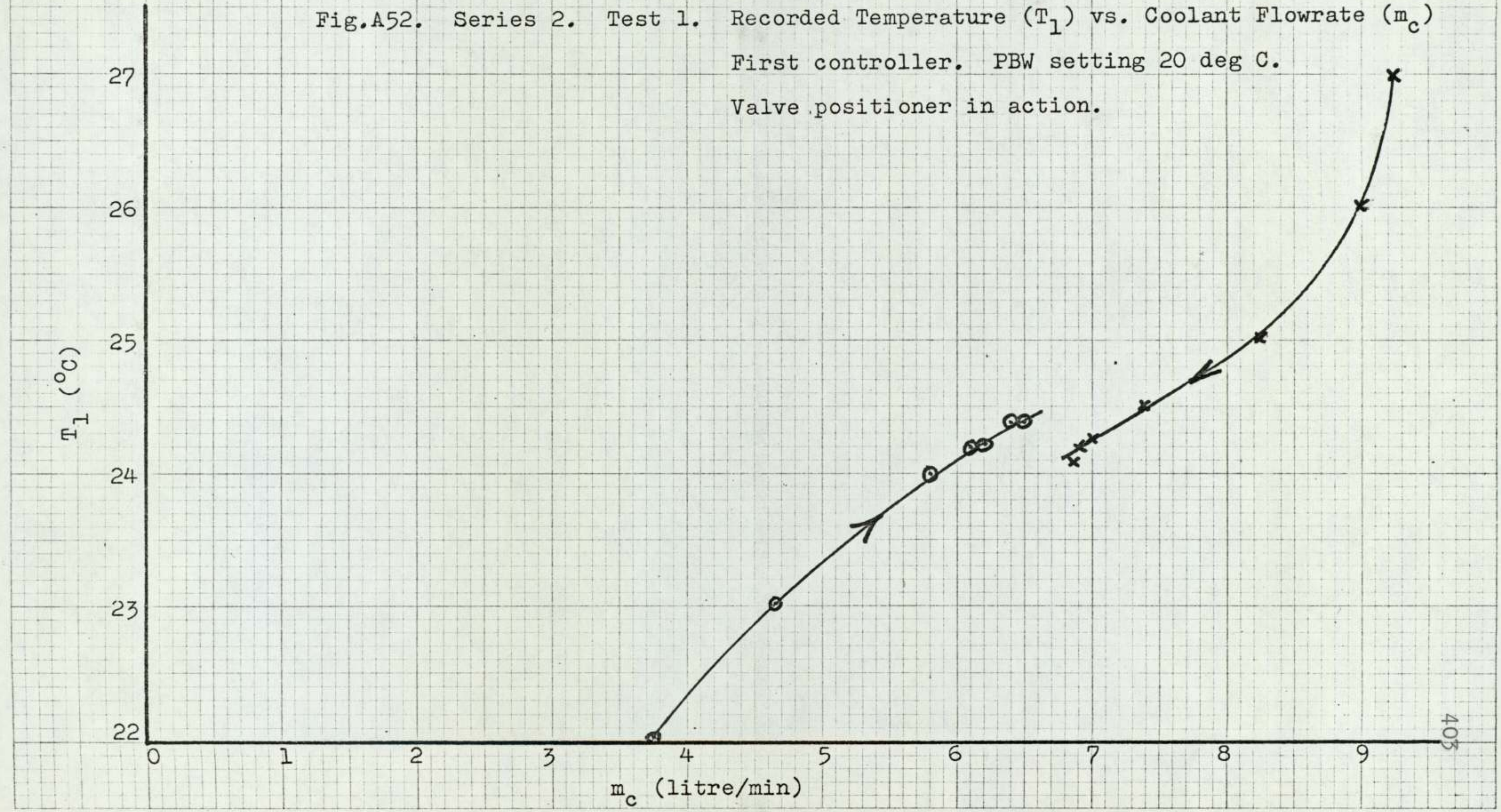

Table A.28.

Series 2 Test 2

PBW setting 20 deg C   Valve positioner by-passed

Other parameters as Test 1

T_1 rising			T_1 falling		
T_1 °C	COP lbf/in^{2}gauge	m_c litre/min.	T_1 °C	COP lbf/in^{2}gauge	m_c litre/min.
16.0	13.0	0.30	35.0	0	9.40
17.0	12.0	0.50	32.0	0	"
18.0	11.2	0.90	29.0	0	"
19.0	10.2	1.08	28.0	0	"
20.0	9.6	1.35	27.0	3.0	8.85
21.0	9.1	1.80	26.0	4.0	7.95
22.0	8.0	2.30	25.0	4.8	6.75
23.0	7.2	2.85	24.9	4.9	6.30
24.0	6.4	3.60	"	5.0	6.28
25.0	5.5	4.60	steady state reached		
25.5	4.9	5.45	coolant temperatures:		
25.8	"	5.55	T_{c1} = 9.2		
26.0	"	"	T_{c2} = 16.2		
25.8	"	5.60			
steady state reached					
coolant temperatures:					
T_{c1} = 9.1					
T_{c2} = 17.2					

T_1 steady state hysteresis = 0.9°C

(see Figs.A.53., A.54. and A.55. for graphs of results)

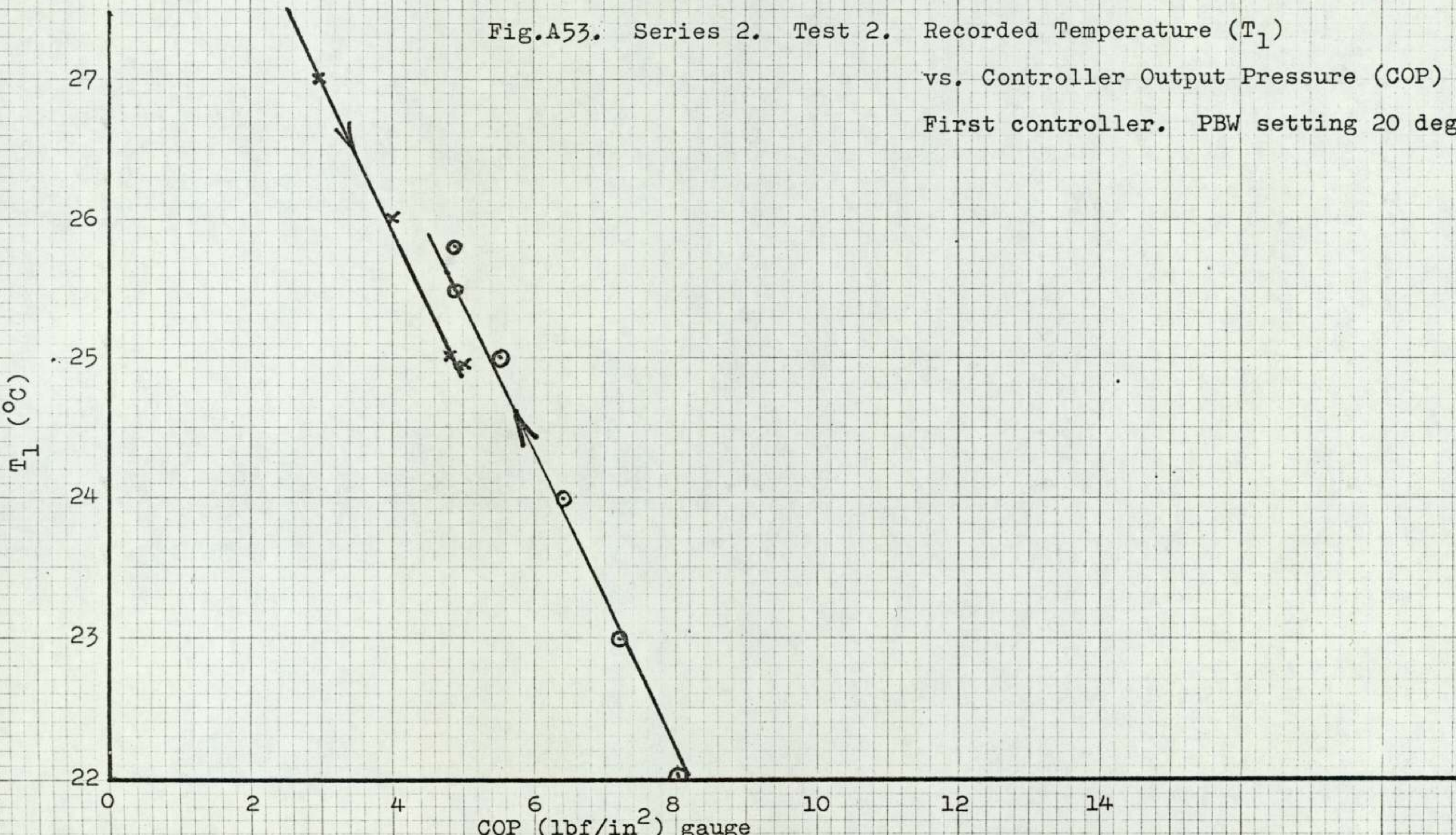

Fig.A53. Series 2. Test 2. Recorded Temperature (T_1) vs. Controller Output Pressure (COP) First controller. PBW setting 20 deg C.

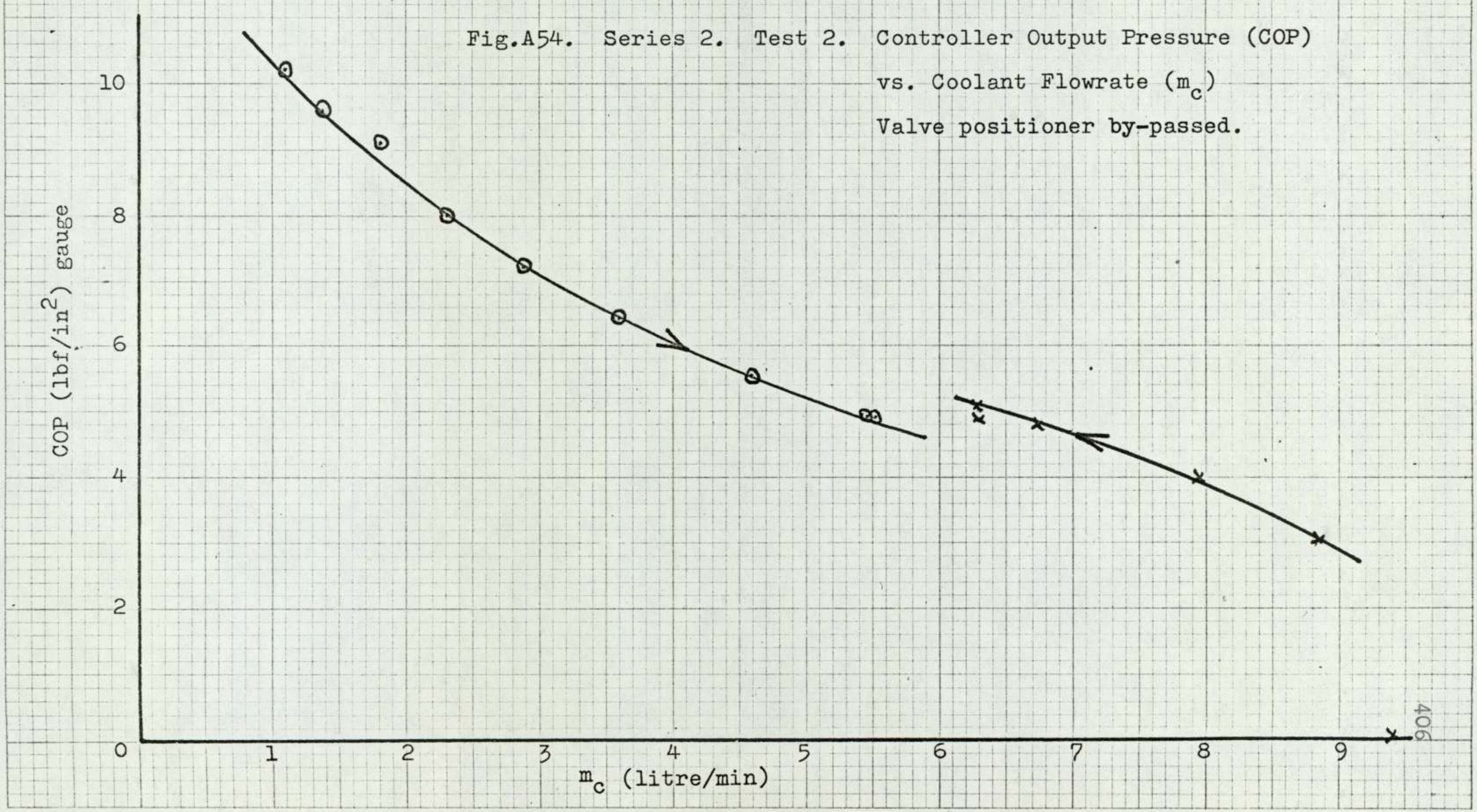
Fig.A54. Series 2. Test 2. Controller Output Pressure (COP)
vs. Coolant Flowrate (m_c)
Valve positioner by-passed.
COP (lbf/in^2) gauge
10
8
6
4
2
0
1
2
3
4
5
6
7
8
9
m_c (litre/min)

Fig.A55. Series 2. Test 2. Recorded Temperature (T_1) vs. Coolant Flowrate (m_c)

First controller. PBW setting 20 deg.C.

Valve positioner by-passed.

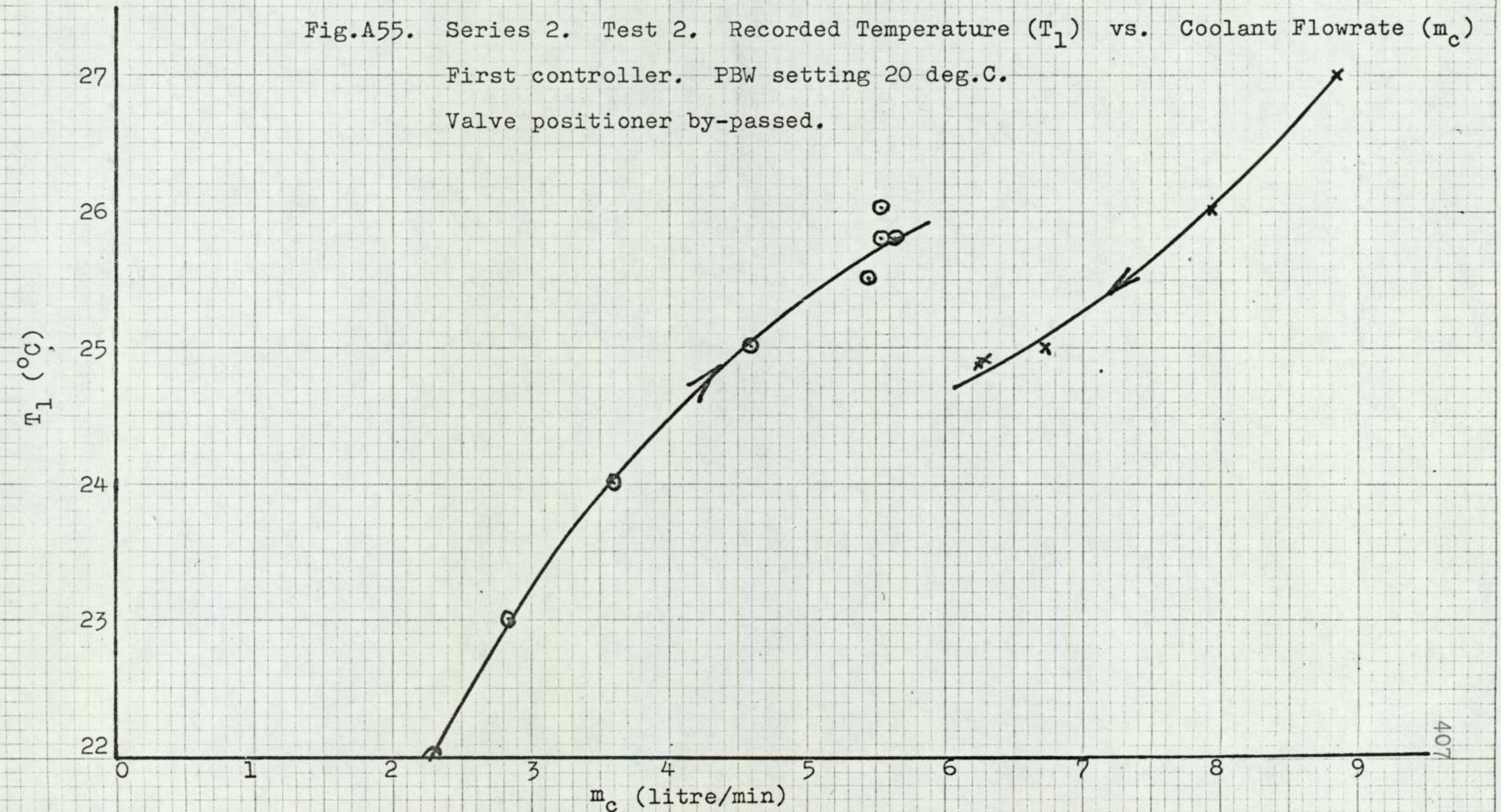

Table A.29.

Series 3 Test 1

PBW setting 2 deg C Valve positioner in action

Variac setting 46 Other parameters as Series 2

T_1 rising			T_1 falling		
T_1 ^{o}C	COP lbf/in^2 gauge	m_c $\frac{litre}{min.}$	T_1 ^{o}C	COP lbf/in^2 gauge	m_c $\frac{litre}{min.}$
19.0	22.0	0	33.0	0	9.55
21.0	"	0	30.0	0	"
24.0	20.5	0	27.0	0	"
25.0	17.7	0	26.5	4.8	8.90
26.0	12.8	0.80	26.1	6.1	7.00
26.1	11.0	1.55	26.0	7.6	4.55
26.2	9.8	2.60	25.9	8.1	4.30
26.5	9.0	3.40	"	8.2	4.00
26.8	8.2	4.00	steady state reached		
26.9	7.9	4.40	coolant temperatures:		
"	7.8	4.50	T_{c1} = 8.0		
26.8	8.0	4.20	T_{c2} = 17.2		
"	"	4.00	forced readings		
steady state reached			25.5	9.8	2.40
coolant temperatures:			25.2	10.5	1.85
T_{c1} = 8.1					
T_{c2} = 18.0			25.1	10.9	1.55
27.0	7.0	5.50	"	11.3	1.25
27.1	6.3	6.50	25.0	11.8	1.05
27.2	6.0	7.30			
27.3	5.8	7.90			
27.6	4.0	9.40			

T_1 steady state hysteresis = $0.9^{o}C$

(see Figs.A.56., A.57. and A.58. for graphs of results)

Fig.A56. Series 3. Test 1. Recorded Temperature (T_1) vs. Controller Output Pressure (COP)

First controller. PBW setting 2 deg C.

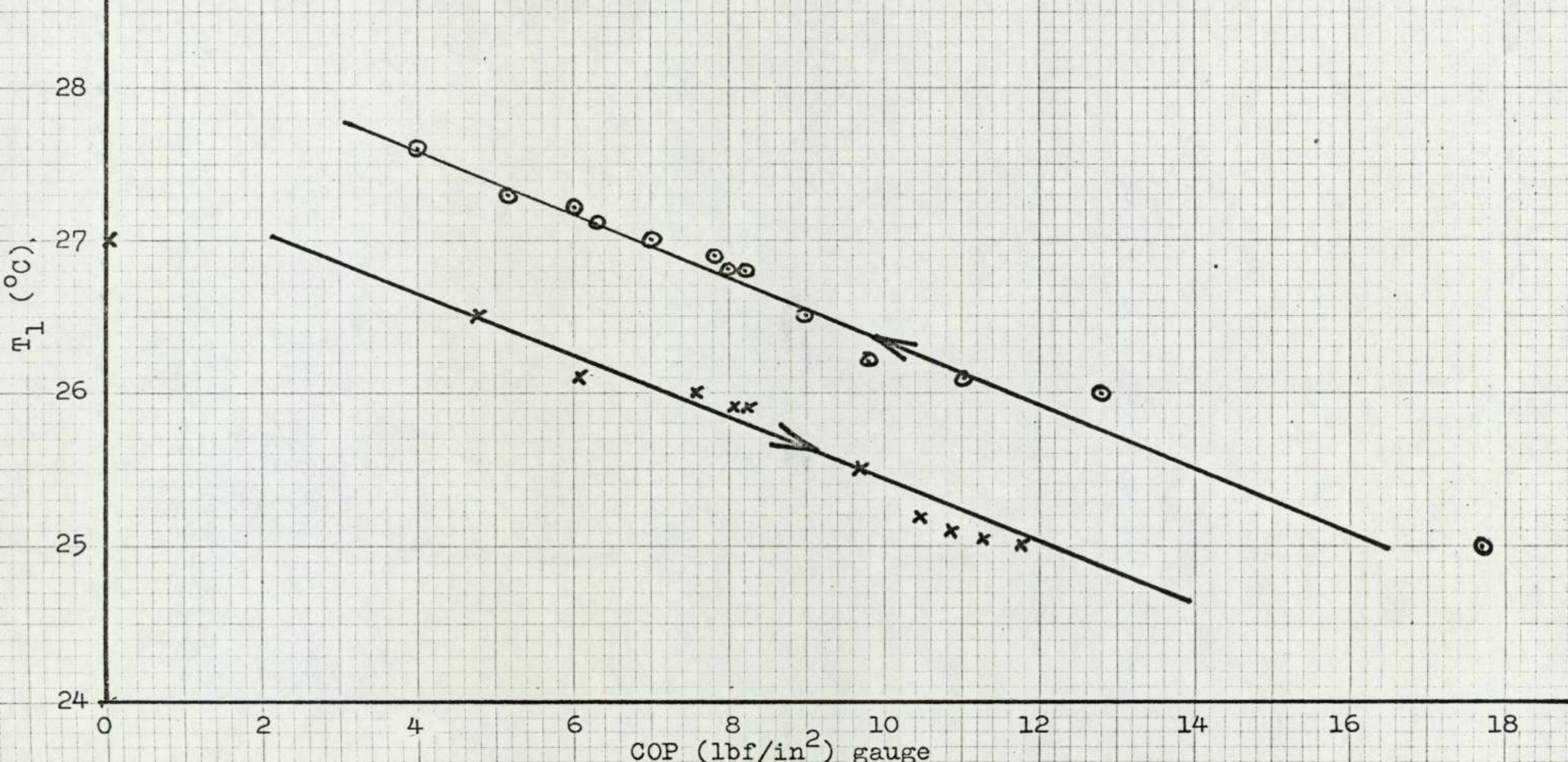

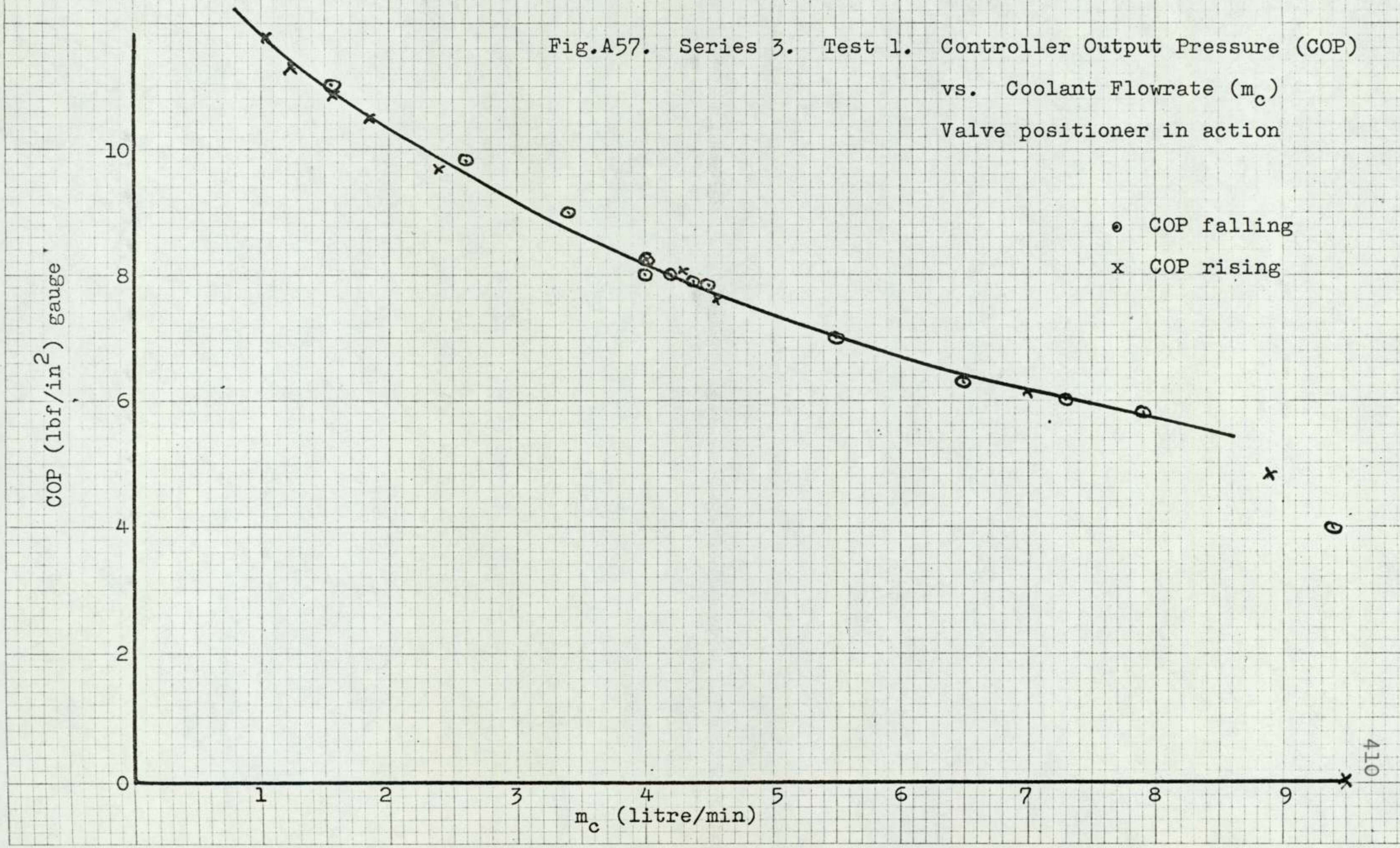

Fig.A57. Series 3. Test 1. Controller Output Pressure (COP) vs. Coolant Flowrate (m_c)
Valve positioner in action

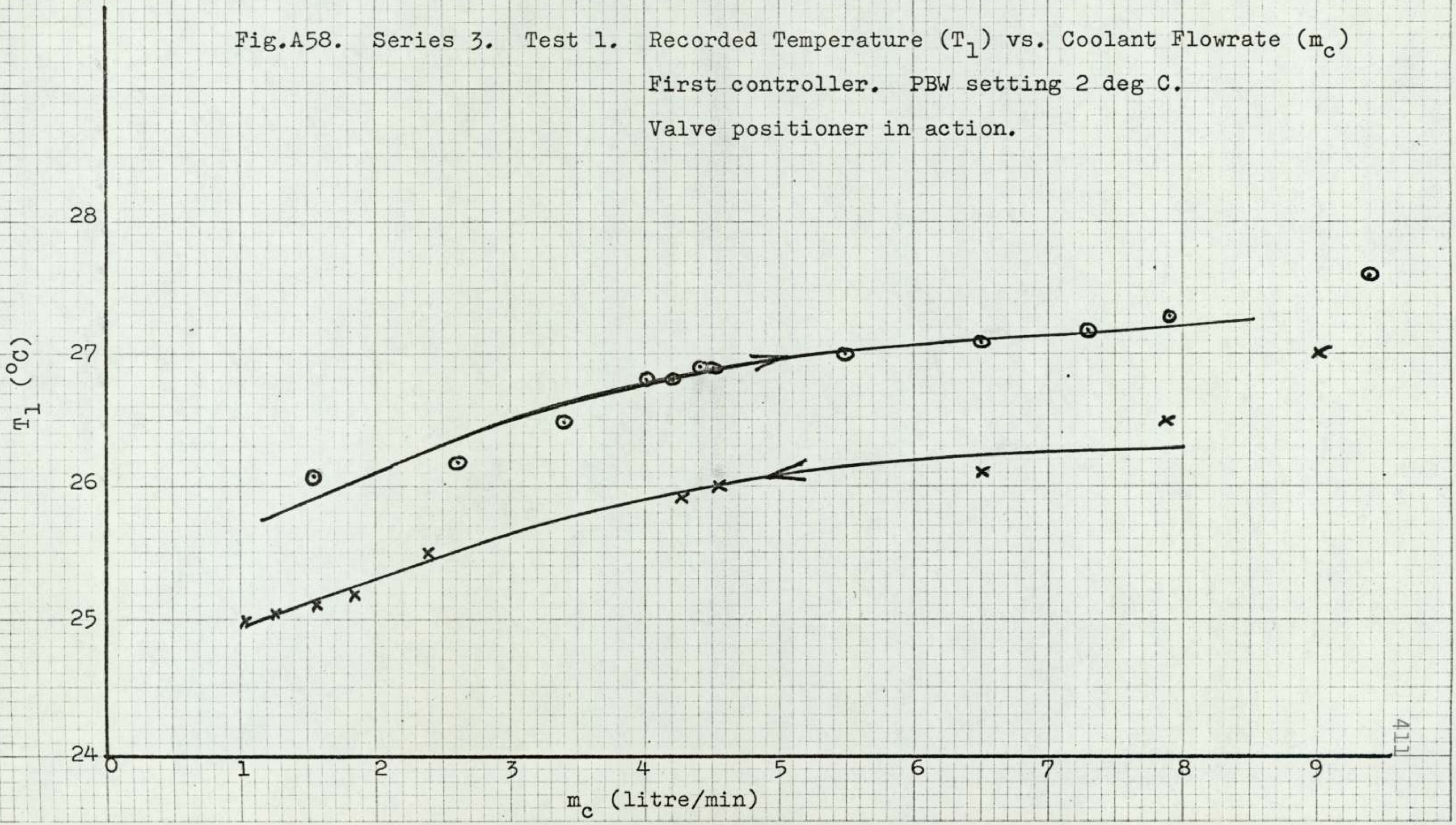

Fig.A58. Series 3. Test 1. Recorded Temperature (T_1) vs. Coolant Flowrate (m_c)
First controller. PBW setting 2 deg C.
Valve positioner in action.

Table A.30.

Series 3 Test 2

PBW setting 2 deg C Valve positioner by-passed

Other parameters as Test 1

T_1 rising			T_1 falling		
T_1 °C	COP lbf/in^{2}gauge	m_c litre/min.	T_1 °C	COP lbf/in^{2}gauge	m_c litre/min.
25.0	15.2	0	30.0	0	9.50
26.2	10.5	1.05	27.0	0	"
26.5	9.4	1.50	26.9	4.5	7.75
26.8	8.6	1.90	26.5	5.2	6.20
26.9	8.1	2.30	26.3	5.8	5.30
27.1	7.2	2.85	26.2	6.1	4.95
27.2	6.9	3.15	26.1	6.3	4.40
"	6.7	3.30	"	6.8	4.15
"	6.4	3.55	"	7.1	3.80
27.1	6.6	3.60	steady state reached		
steady state reached			coolant temperatures:		
coolant temperatures:			T_{c1} = 8.05		
T_{c1} = 8.1			T_{c2} = 17.90		
T_{c2} = 18.7			forced readings		
forced readings			26.0	8.0	3.00
27.4	6.0	4.00	25.9	8.2	2.70
27.5	5.5	4.55	25.5	9.6	1.85
27.6	5.1	5.00	25.2	10.6	1.50
27.7	4.5	5.75	25.1	11.2	1.15
27.8	4.2	6.20			
27.9	3.5	7.15			
28.0	3.0	8.25			
"	2.0	9.60			

T_1 steady state hysteresis = 1.0°C

(see Figs.A.59., A.60. and A.61. for graphs of results)

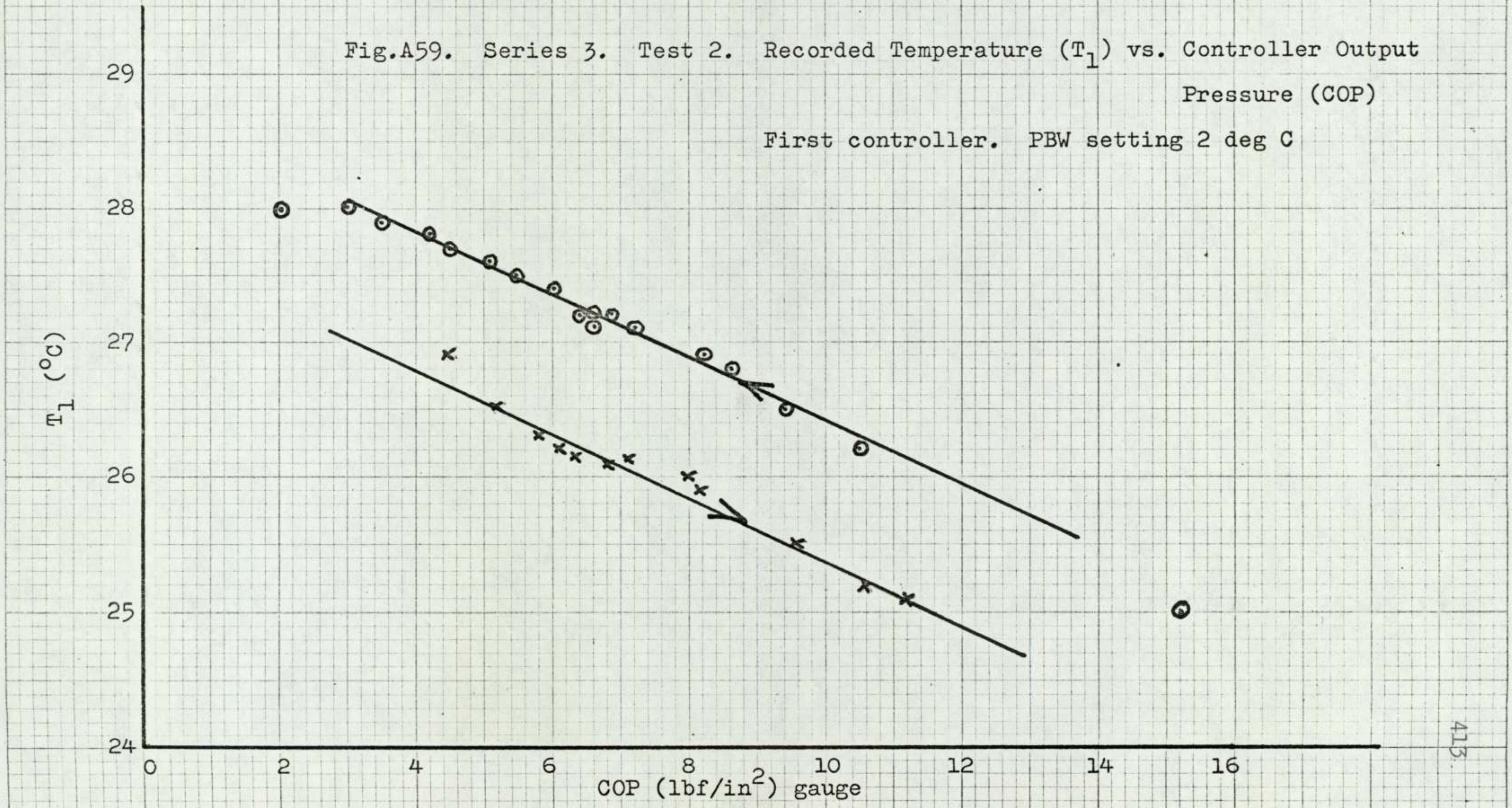
Fig.A59. Series 3. Test 2. Recorded Temperature (T_1) vs. Controller Output Pressure (COP)
First controller. PBW setting 2 deg C
T_1 (°C)
29
28
27
26
25
24
0
2
4
6
8
10
12
14
16
COP (lbf/in^2) gauge

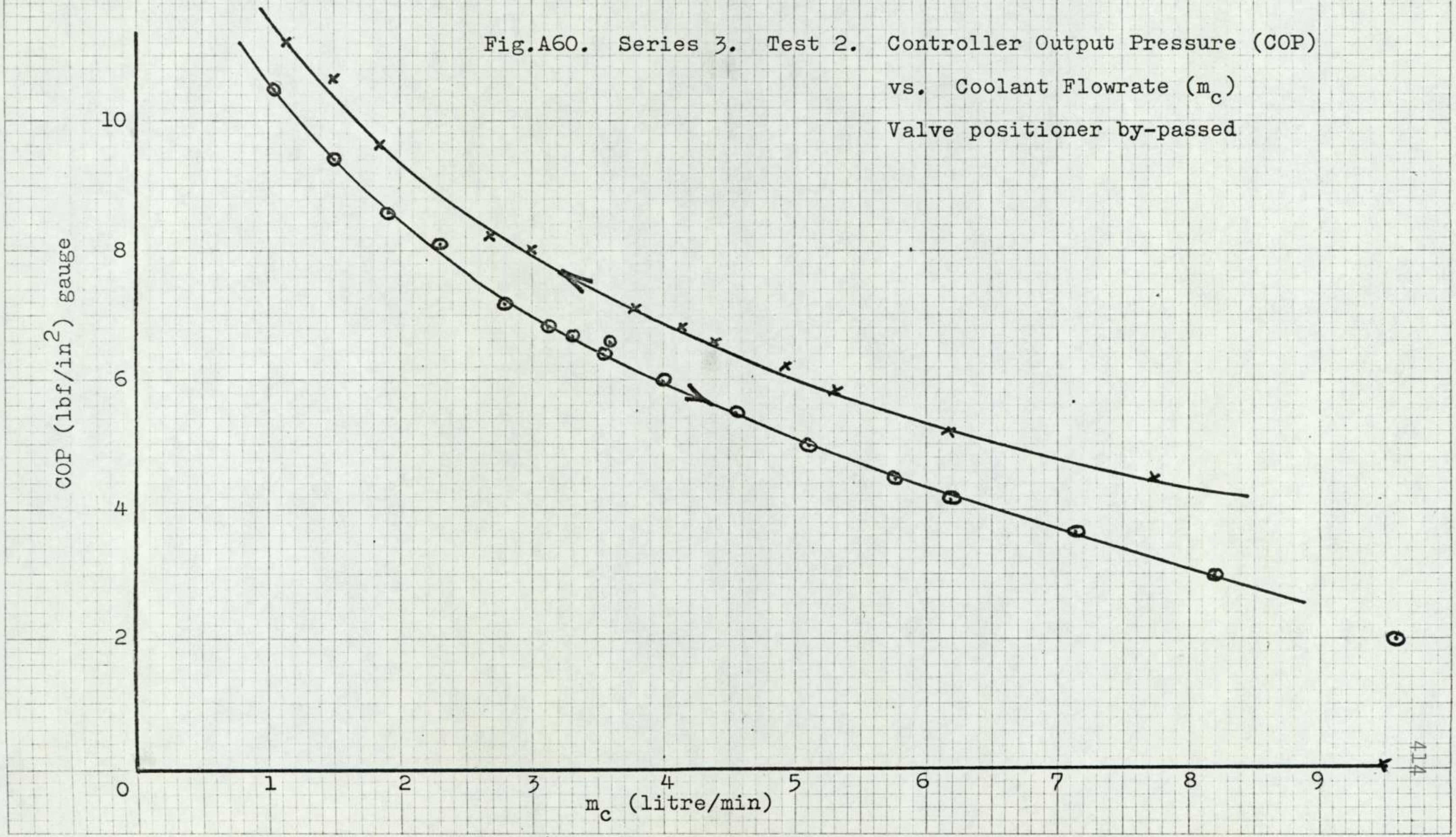

Fig.A60. Series 3. Test 2. Controller Output Pressure (COP) vs. Coolant Flowrate (m_c) Valve positioner by-passed

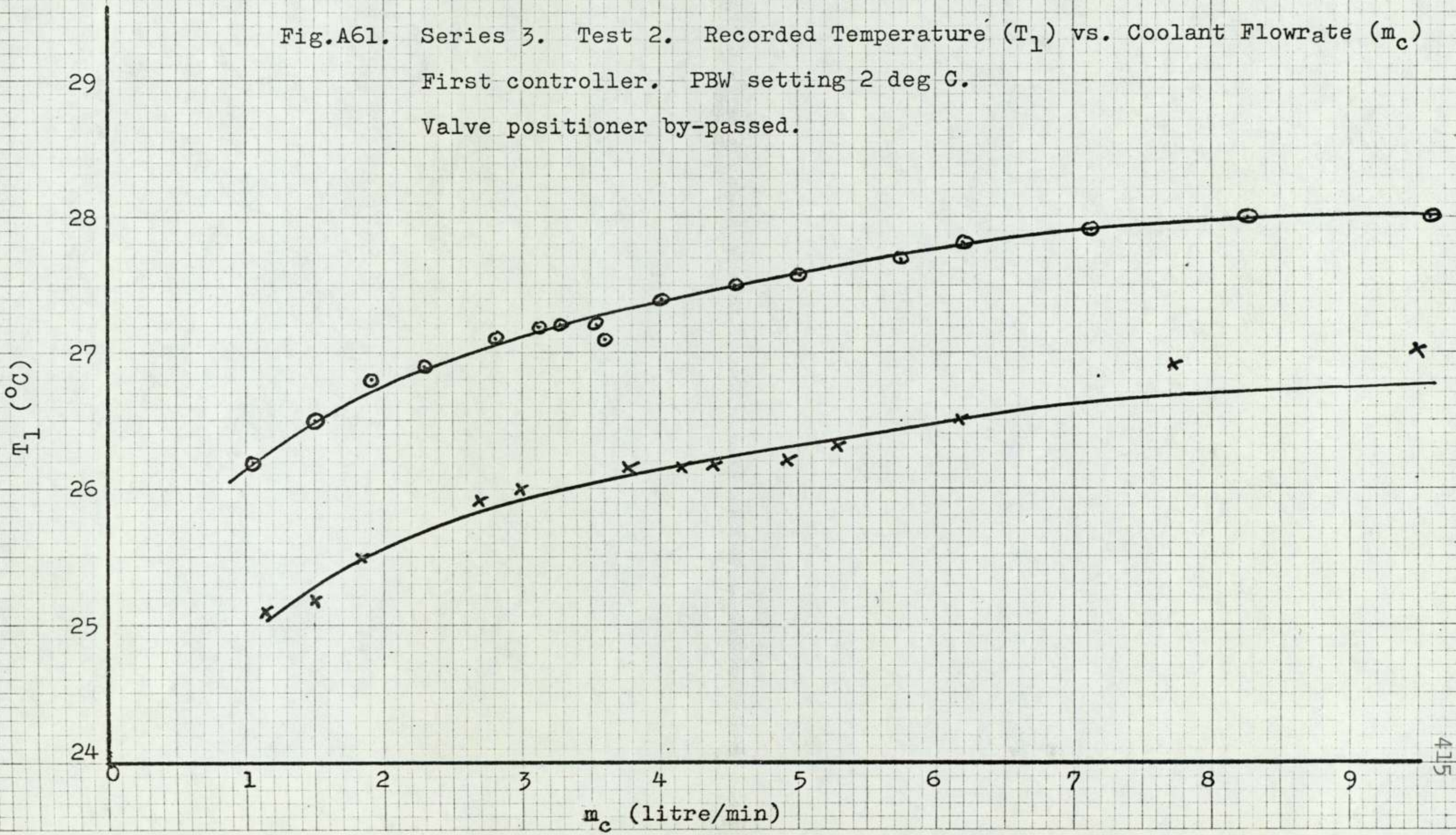

Fig.A61. Series 3. Test 2. Recorded Temperature (T_1) vs. Coolant Flowrate (m_c)

First controller. PBW setting 2 deg C.

Valve positioner by-passed.

Reproducibility tests on the first controller

Series 4

Tests were run alternately from low and high temperatures T_1 except for two consecutive runs from a low starting temperature T_1 before the final run from a high T_1 value. Drift was found to continue at the same rate regardless of the direction of approach to the steady state.

Table A.31.

PBW setting 10 deg C Valve positioner in action

Other parameters as Series 3

T_1 rising			T_1 falling		
T_1 ^oC	COP lbf/in^{2}gauge	m_c $\frac{\text{litre}}{\text{min.}}$	T_1 ^oC	COP lbf/in^{2}gauge	m_c $\frac{\text{litre}}{\text{min.}}$
Run 1			Run 1		
20.0	17.0	0	32.0	0	9.60
21.0	14.6	0	28.0	0	9.60
22.0	13.0	0.50	27.0	3.0	9.60
23.0	11.1	1.50	26.5	4.0	9.60
24.0	9.6	2.70	26.0	5.2	8.75
24.5	8.4	3.60	25.5	5.9	7.75
24.9	8.1	3.90	25.0	6.7	5.90
24.9	8.0	4.40	24.9	7.1	5.10
25.0	7.9	4.40	24.8	7.3	4.80
steady state reached			steady state reached		
coolant temperatures:			coolant temperatures:		
T_{c1} = 8.9			T_{c1} = 8.5		
T_{c2} = 16.9			T_{c2} = 16.1		

Table A.31. (continued)

T_1 rising			T_1 falling		
T_1 °C	COP lbf/in^{2}gauge	m_c $\frac{\text{litre}}{\text{min.}}$	T_1 °C	COP lbf/in^{2}gauge	m_c $\frac{\text{litre}}{\text{min.}}$
Run 2			Run 2		
23.0	12.0	0	28.0	0	9.60
24.0	10.8	1.80	27.0	4.5	9.25
24.5	9.5	2.75	26.5	5.3	8.30
24.9	9.0	3.20	26.0	6.0	7.10
25.0	8.3	3.75	25.5	6.7	6.20
25.1	8.2	3.85	25.2	7.0	5.40
25.2	8.1	4.00	25.1	7.2	5.00
25.3	8.0	4.10	25.0	7.4	4.70
steady state reached			steady state reached		
coolant temperatures:			coolant temperatures:		
T_{c1} = 8.5			T_{c1} = 8.5		
T_{c2} = 17.2			T_{c2} = 16.6		
Run 3			Run 3		
21.0	15.3	0	28.0	0	9.60
22.0	13.8	0	27.0	4.2	"
23.0	12.2	0.98	26.5	5.1	8.50
24.0	10.8	1.80	26.1	5.7	7.75
24.5	10.0	2.40	26.0	6.2	6.90
24.8	9.5	2.75	25.9	6.3	6.60
24.9	9.2	3.00	25.5	6.7	6.20
25.0	9.1	3.25	25.3	7.0	5.60
25.0	8.8	3.40	25.2	7.1	5.25

Table A.31. (continued)

T_1 rising			T_1 falling		
T_1 ^oC	COP lbf/in^2 gauge	m_c litre/min.	T_1 ^oC	COP lbf/in^2 gauge	m_c litre/min.
Run 3 (continued)			Run 3 (continued)		
25.1	8.6	3.55	25.1	7.3	5.25
25.2	8.2	3.80	"	7.4	4.80
25.3	8.0	4.00	25.0	7.6	4.60
25.4	"	"	steady state reached		
steady state reached			coolant temperatures:		
coolant temperatures:					
T_{c1} = 8.5			T_{c1} = 8.4		
T_{c2} = 17.2			T_{c2} = 16.8		
Run 4			Run 4		
24.2	10.8	1.80	27.0	4.8	9.00
24.5	10.2	2.20	26.5	5.8	7.80
24.8	10.0	2.40	26.1	6.1	7.10
24.9	9.8	2.60	26.0	6.6	6.25
25.0	9.6	2.80	"	7.0	5.75
25.1	9.0	3.10	25.9	7.1	5.40
25.2	"	3.25	25.8	"	5.10
25.3	8.8	3.40	25.6	7.3	4.80
25.4	8.6	3.60	25.5	7.4	4.75
25.5	8.3	3.70	25.3	7.6	4.60
25.6	8.2	3.75	"	7.7	4.40
25.7	"	3.80	25.2	7.9	4.30
			steady state reached		
			coolant temperatures:		
			T_{c1} = 8.45		
			T_{c2} = 17.00		

Table A.31. (continued)

T_1 rising		
T_1 ^oC	COP lbf/in^2 gauge	m_c $\frac{litre}{min.}$
Run 4 (continued)		
25.8	8.1	3.90
25.9	8.0	4.00
"	"	4.10
steady state reached		
coolant temperatures:		
T_{c1} = 8.4		
T_{c2} = 17.5		
Run 5		
23.0	13.5	0
23.9	12.0	1.10
24.0	11.0	1.35
24.5	10.5	1.90
25.0	9.5	2.80
25.1	9.0	3.10
25.2	8.9	3.25
25.3	8.7	3.40
25.4	8.6	3.50
25.5	8.5	3.60
25.6	8.4	3.70
25.7	8.3	3.80
25.8	8.2	"
25.9	8.1	4.00

steady state reached   coolant temperatures: T_{c1} = 8.4
T_{c2} = 17.7

The greatest rate of drift of the temperature (T_1) was:

$$0.25\,^{o}C\,/\,h$$

or COP $0.4\ lbf/in^2\ h$

the total duration of the test being 3.5 hours.

Hysteresis effect on steady state temperatures varied from a difference of 0.2 to 0.7 ^{o}C due to the drift effects.

A graph of the results is given in Fig.A.62.

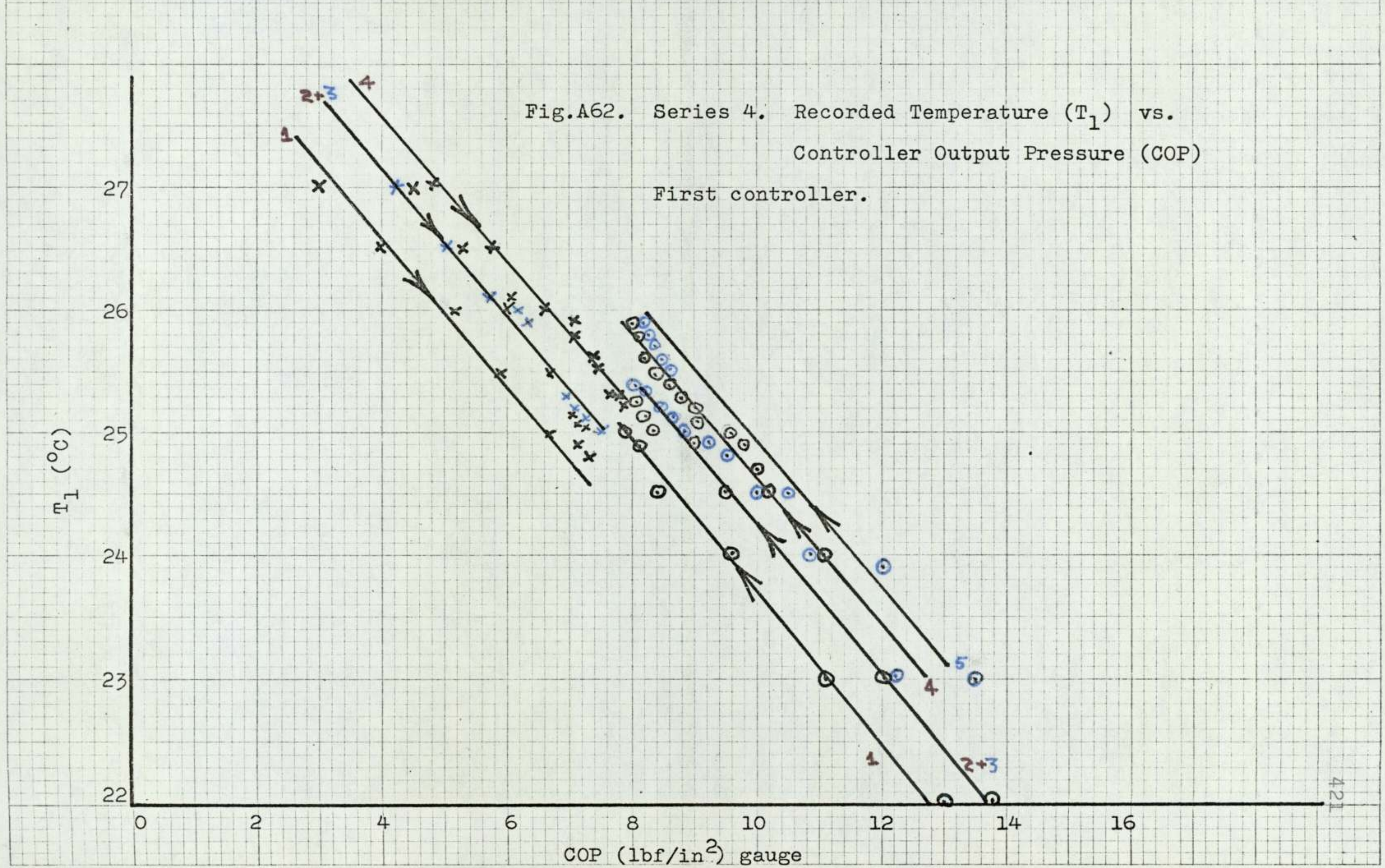

Fig.A62. Series 4. Recorded Temperature (T_1) vs.
Controller Output Pressure (COP)
First controller.
T_1 (^oC)
COP (lbf/in^2) gauge
22
23
24
25
26
27
0
2
4
6
8
10
12
14
16
1
2+3
4
5

Series 5

Table A.32.

PBW setting 10 deg C Valve positioner by-passed

Other parameters as Series 4

T_1 rising			T_1 falling		
T_1 ^oC	COP lbf/in^2 gauge	m_c $\frac{litre}{min.}$	T_1 ^oC	COP lbf/in^2 gauge	m_c $\frac{litre}{min.}$
Run 1			Run 1		
18.0	22.0	0	28.0	0	9.50
19.0	21.0	0	27.5	1.0	"
20.0	19.0	0	27.2	3.0	9.00
21.0	15.5	0	27.0	3.8	8.50
23.0	12.2	0.50	26.7	4.0	7.80
24.0	10.5	1.00	26.5	4.5	7.30
24.5	9.7	1.25	26.2	4.9	6.75
25.0	8.7	1.85	26.1	5.1	6.25
25.5	7.9	2.40	26.0	5.3	5.80
26.0	7.0	3.00	25.9	5.7	5.50
26.1	6.7	3.40	25.8	6.0	5.00
"	6.5	3.50	25.7	6.1	4.70
26.2	6.3	3.60	25.6	"	4.60
26.3	6.2	3.75	25.5	6.2	4.50
26.4	6.1	3.80	"	"	"
"	"	4.00	25.4	6.3	4.40

steady state reached

coolant temperatures:

T_{c1} = 9.6

T_{c2} = 18.4

steady state reached

coolant temperatures:

T_{c1} = 9.0

T_{c2} = 16.9

Table A.32. (continued)

T_1 rising			T_1 falling		
T_1 °C	COP lbf/in^{2}gauge	m_c litre/min.	T_1 °C	COP lbf/in^{2}gauge	m_c litre/min.
Run 2			Run 2		
19.0	21.5	0	28.0	0	9.50
22.0	14.6	0	27.5	3.0	9.20
23.1	12.5	0.20	27.0	4.0	7.80
24.5	10.2	1.05	26.6	5.1	6.25
25.0	9.3	1.50	26.1	5.8	5.30
25.5	8.2	2.20	26.0	6.0	4.90
26.0	7.5	2.55	25.9	6.1	4.75
26.1	7.1	2.90	25.8	6.2	4.55
26.2	6.9	3.10	"	6.4	4.20
26.3	6.8	3.25	25.7	6.5	4.30
26.4	"	3.40	steady state reached		
26.5	6.6	"	coolant temperatures:		
26.6	6.3	3.60	T_{c1} = 8.4		
26.7	6.2	3.70	T_{c2} = 17.1		
steady state reached					
			Run 3		
coolant temperatures:			27.1	3.9	8.30
T_{c1} = 8.8			27.0	4.5	7.40
T_{c2} = 18.4			26.9	4.8	7.00
Run 3			26.5	5.2	6.10
18.0	22.0	0	26.1	5.6	5.60
22.0	15.0	0	"	5.9	5.20
23.0	13.2	0.20	26.0	6.0	4.90

Table A.32. (continued)

T_1 rising			T_1 falling		
T_1 ^oC	COP lbf/in^{2}gauge	m_c $\frac{\text{litre}}{\text{min.}}$	T_1 ^oC	COP lbf/in^{2}gauge	m_c $\frac{\text{litre}}{\text{min.}}$
Run 3 (continued)			Run 3 (continued)		
24.0	11.5	0.80	25.9	6.1	4.70
24.5	10.7	1.00	25.8	6.2	4.50
25.0	9.6	1.30	"	6.5	4.40
25.1	9.1	1.60	"	6.6	4.25
25.5	8.5	1.90	steady state reached		
26.0	8.0	2.30	coolant temperatures:		
26.1	7.7	2.50	T_{c1} = 8.4 T_{c2} = 17.1		
26.2	7.3	2.75	Run 4		
26.4	7.0	2.90			
26.5	"	3.00	27.5	3.2	9.25
26.6	6.9	3.20	27.1	4.2	7.75
26.8	6.7	3.70	27.0	4.8	7.00
26.9	6.4	3.50	26.9	5.0	6.30
"	"	3.70	26.8	5.2	6.00
27.0	6.3	"	26.5	5.5	5.65
steady state reached			26.2	5.8	5.40
coolant temperatures:			26.1	6.0	5.10
T_{c1} = 8.9			"	"	4.80
T_{c2} = 19.0			"	6.1	4.75
			26.0	6.2	4.50
			"	6.5	4.40
			"	"	4.30

Table A.32. (continued)

	T_1 falling	
T_1 ^oC	COP lbf/in^2 gauge	m_c $\frac{litre}{min.}$
Run 4 (continued)		
26.0	6.6	4.25
"	"	"
"	"	4.20
"	6.7	"
steady state reached		
coolant temperatures:		
T_{c1} = 8.5		
T_{c2} = 17.3		

It was concluded from the results that the valve positioner was not causing the drift effect. In fact the rate of drift was a little higher in Series 5 than it was in Series 4.

The greatest rate of drift of temperatures (T_1) was:

$0.4^oC / h$

or COP $0.6 \; lbf/in^2 \; h$

T_1 steady state hysteresis = 1.0^oC

A graph of the results is given in Fig.A.63.

Fig.A63. Series 5. Recorded Temperature (T_1) vs. Controller Output Pressure (COP)

First controller.

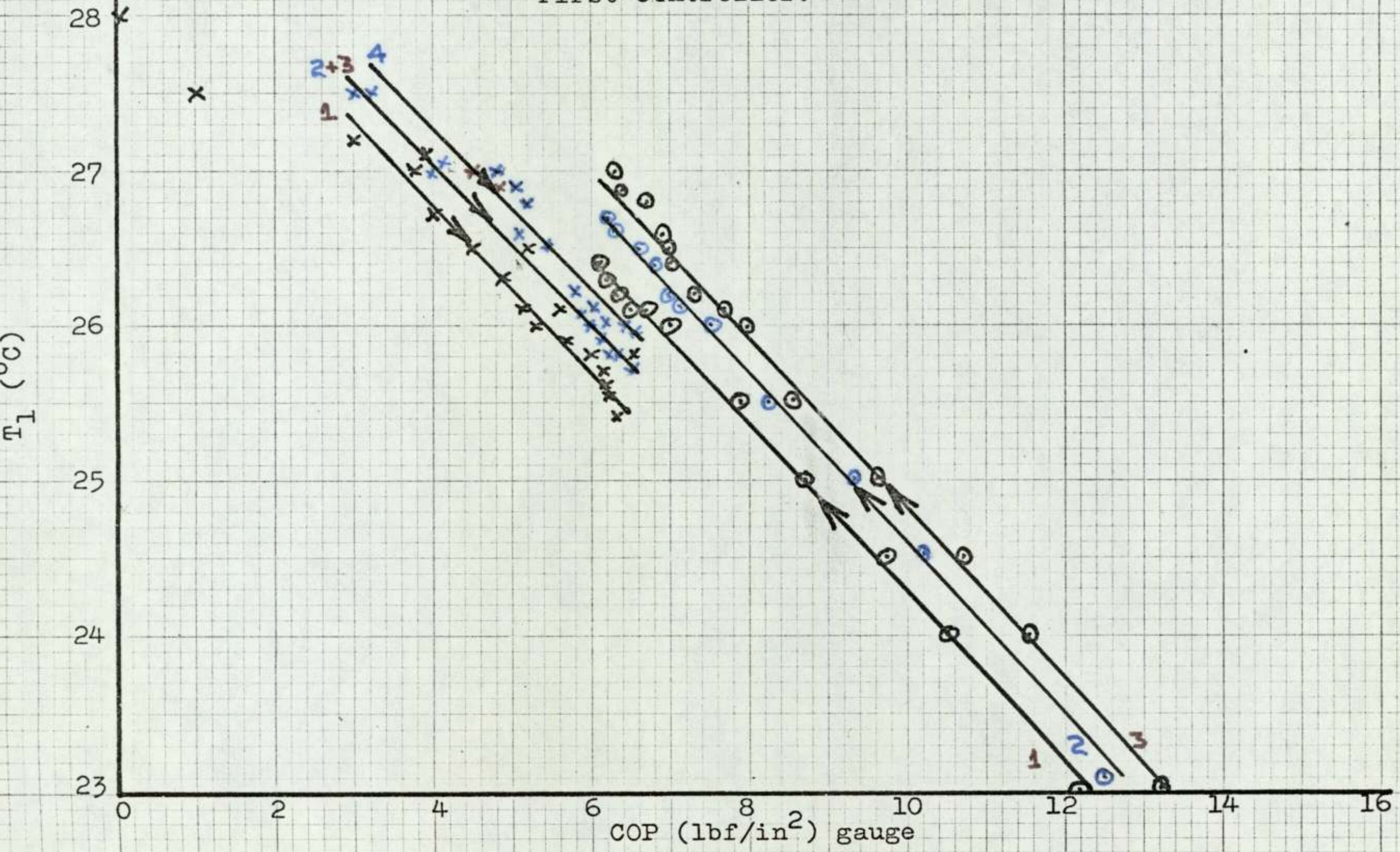

Series 6

Table A.33.

PBW setting 30 deg C Valve positioner in action

Other parameters as Series 5

T_1 rising			T_1 falling		
T_1 ^oC	COP lbf/in^2 gauge	m_c $\frac{litre}{min.}$	T_1 ^oC	COP lbf/in^2 gauge	m_c $\frac{litre}{min.}$
Run 1			Run 1		
13.2	11.8	1.10	32.0	0	9.50
14.1	11.7	1.20	30.1	2.5	"
14.5	11.2	1.30	29.0	3.5	"
15.0	11.1	1.40	28.0	4.1	"
16.0	10.9	1.75	27.5	4.7	9.20
17.0	10.2	2.15	27.1	4.9	9.00
18.0	9.9	2.50	27.0	5.0	8.85
19.0	9.1	3.00	26.5	5.1	8.60
20.0	8.7	3.40	26.1	5.4	8.25
21.0	8.1	3.80	26.0	5.5	8.10
21.2	8.0	4.20	25.9	5.7	7.80
21.6	7.9	4.40	25.5	5.9	7.50
22.0	7.7	4.55	25.1	6.0	7.35
22.2	7.5	4.70	25.0	6.1	7.10
22.5	7.3	4.80	24.9	6.2	6.80
22.8	7.2	"	24.8	"	6.75
22.9	7.1	4.90	24.7	6.3	6.50
23.0	"	4.95	24.5	6.4	"
23.1	"	5.05	24.4	6.5	6.40

Table A.33. (continued)

T_1 rising			T_1 falling		
T_1 °C	COP lbf/in^2 gauge	m_c $\frac{litre}{min.}$	T_1 °C	COP lbf/in^2 gauge	m_c $\frac{litre}{min.}$
23.2	7.0	5.2	24.3	6.6	6.40
steady state reached			24.2	"	6.35
coolant temperatures:			24.1	6.7	6.20
T_{c1} =	9.0		24.0	6.8	6.00
T_{c2} =	15.5		23.9	6.9	5.80
			23.8	"	5.75
Run 2			23.7	7.0	5.60
13.2	13.0	0.70	23.5	7.1	"
14.0	12.8	0.80	23.6	7.0	"
15.0	12.0	1.00	steady state reached		
16.0	11.6	1.25	coolant temperatures:		
17.0	11.0	1.50	T_{c1} =	8.5	
18.0	10.6	1.90	T_{c2} =	15.2	
19.0	10.1	2.25			
20.0	9.6	2.60	Run 2		
21.0	9.0	3.10	32.0	2.5	9.50
22.0	8.5	3.60	30.0	3.9	"
22.5	8.2	3.90	29.0	4.5	9.30
22.9	8.1	4.00	28.0	5.1	8.70
23.0	8.0	4.10	27.0	5.8	7.75
23.1	7.9	4.25	26.0	6.2	6.70
23.5	7.8	4.50	25.5	6.6	6.45
23.8	7.6	4.60	25.1	6.8	6.10

Table A.33. (continued)

T_1 rising			T_1 falling		
T_1 °C	COP lbf/in^{2}gauge	m_c litre/min.	T_1 °C	COP lbf/in^{2}gauge	m_c litre/min.
Run 2 (continued)			Run 2 (continued)		
24.0	7.5	4.75	25.0	6.9	5.80
24.1	7.2	4.90	24.9	7.0	5.60
24.2	7.1	"	24.8	"	5.50
24.3	"	5.00	24.7	7.1	5.40
steady state reached			24.5	"	5.25
coolant temperatures:			steady state reached		
T_{c1} = 8.4			coolant temperatures:		
T_{c2} = 15.9			T_{c1} = 8.4		
			T_{c2} = 16.0		
Run 3			Run 3		
13.0	13.8	0.20	32.0	3.8	9.50
14.0	13.5	"	30.0	4.6	9.10
15.0	13.0	0.65	29.0	5.3	8.40
16.0	12.5	0.90	28.0	6.0	7.12
17.0	12.0	1.00	26.9	6.8	6.00
18.0	11.3	1.25	26.1	7.0	5.50
19.0	11.0	1.60	26.0	"	5.30
20.0	10.3	2.05	25.9	7.1	5.15
21.0	10.0	2.40	25.8	"	5.00
22.0	9.5	2.80	25.5	7.3	4.80
23.0	9.0	3.25	25.4	7.4	4.75
23.5	8.7	3.45	25.1	7.6	4.70

Table A.33. (continued)

T_1 rising

T_1 ^oC	COP lbf/in^{2}gauge	m_c $\frac{litre}{min.}$
Run 3 (continued)		
24.0	8.5	3.60
24.1	8.2	3.80
24.5	8.1	4.00
24.8	8.0	4.20
24.9	"	4.25
25.0	7.9	4.30
25.1	7.8	4.50
steady state reached		
coolant temperatures:		
T_{c1} = 8.3		
T_{c2} = 16.7		
Run 4		
13.0	14.5	0
14.0	14.0	0
15.0	13.8	0.20
16.0	13.1	0.50
17.0	12.7	0.80
18.0	12.1	1.00
19.0	11.6	1.20
20.0	11.0	1.45
21.0	10.8	1.80
22.0	10.1	2.25

T_1 falling

T_1 ^oC	COP lbf/in^{2}gauge	m_c $\frac{litre}{min.}$
Run 3 (continued)		
25.1	7.6	4.60
steady state reached		
coolant temperatures:		
T_{c1} = 8.4		
T_{c2} = 16.5		
Run 4		
32.0	4.8	9.10
31.0	5.0	8.75
30.0	5.1	8.40
29.0	6.1	7.05
28.0	6.8	6.10
27.5	7.0	5.60
27.1	"	5.25
27.0	"	5.10
26.9	7.1	5.00
26.5	7.4	4.85
26.1	7.6	4.60
26.0	7.8	4.45
25.9	7.9	4.40
steady state reached		
coolant temperatures:		
T_{c1} = 8.4		
T_{c2} = 17.0		

Table A.33. (continued)

	T_1 rising	
T_1	COP	m_c
^oC	lbf/in^2gauge	$\frac{litre}{min.}$
Run 4 (continued)		
23.0	9.8	2.55
24.0	9.1	3.00
24.5	9.0	3.25
25.0	8.7	3.50
25.1	8.5	3.60
25.2	8.4	3.70
25.3	8.3	3.75
25.5	8.2	"
25.7	8.1	3.80
25.9	"	3.90
26.0	"	4.00
"	8.0	4.10
steady state reached		
coolant temperatures:		
T_{c1} =	8.5	
T_{c2} =	17.4	

The greatest rate of drift of the temperature (T_1) was:

$1.0^oC / h$

or COP $1.0\ lbf/in^2\ h$

the total duration of the test being 2.75 hours.

Hysteresis effect on steady state temperatures varied from a difference of 0 to $0.3^{\circ}C$ due to the drift effects.

A graph of the results is given in Fig.A.64.

From the Test Series 4 to 6 it was clear that the drift in Temperature (T_1) was directly due to the drift in controller output pressure for a particular recorded temperature.

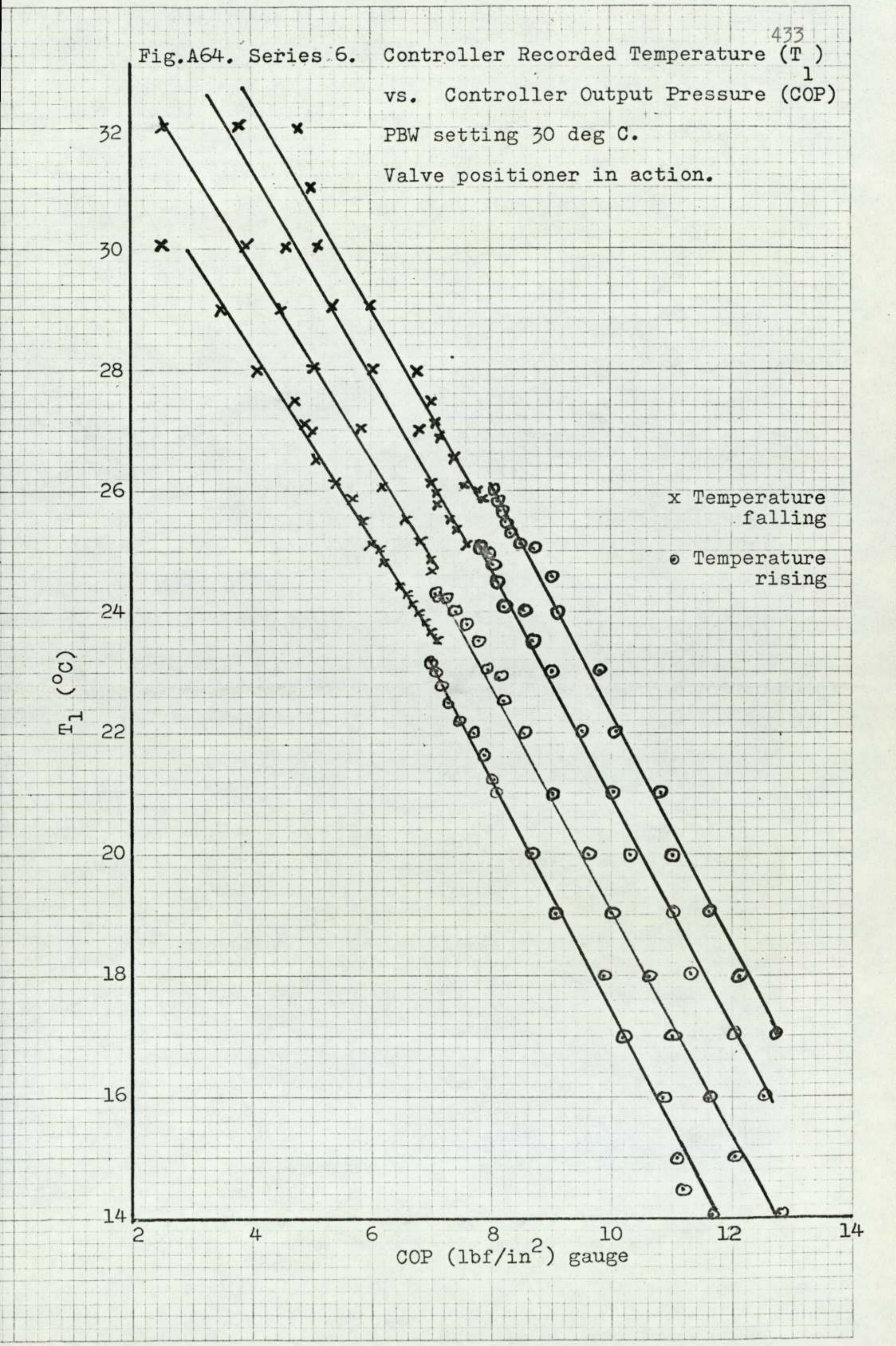
Fig.A64. Series 6. Controller Recorded Temperature (T_1) vs. Controller Output Pressure (COP)
PBW setting 30 deg C.
Valve positioner in action.
x Temperature falling
⊙ Temperature rising
T_1 (°C)
32
30
28
26
24
22
20
18
16
14
2
4
6
8
10
12
14
COP (lbf/in^2) gauge

Series 7 Test 1

This experiment was the same as Series 6 except that it was conducted over five consecutive hours to try to observe any tailing off of the drifting effect. The system was disturbed as before but only the value of T_1 and the corresponding time was recorded at intervals during the test. A plot of the results obtained is given in Fig.A.65. No tailing off was observed and a rate of drift of $0.8^{\circ}C/h$ was recorded.

Series 7 Test 2

The system was also tested without imposing any changes upon it. The steady state was found to drift at the rate of $0.6^{\circ}C/h$. This was slower than the other rates of drift but still substantial.

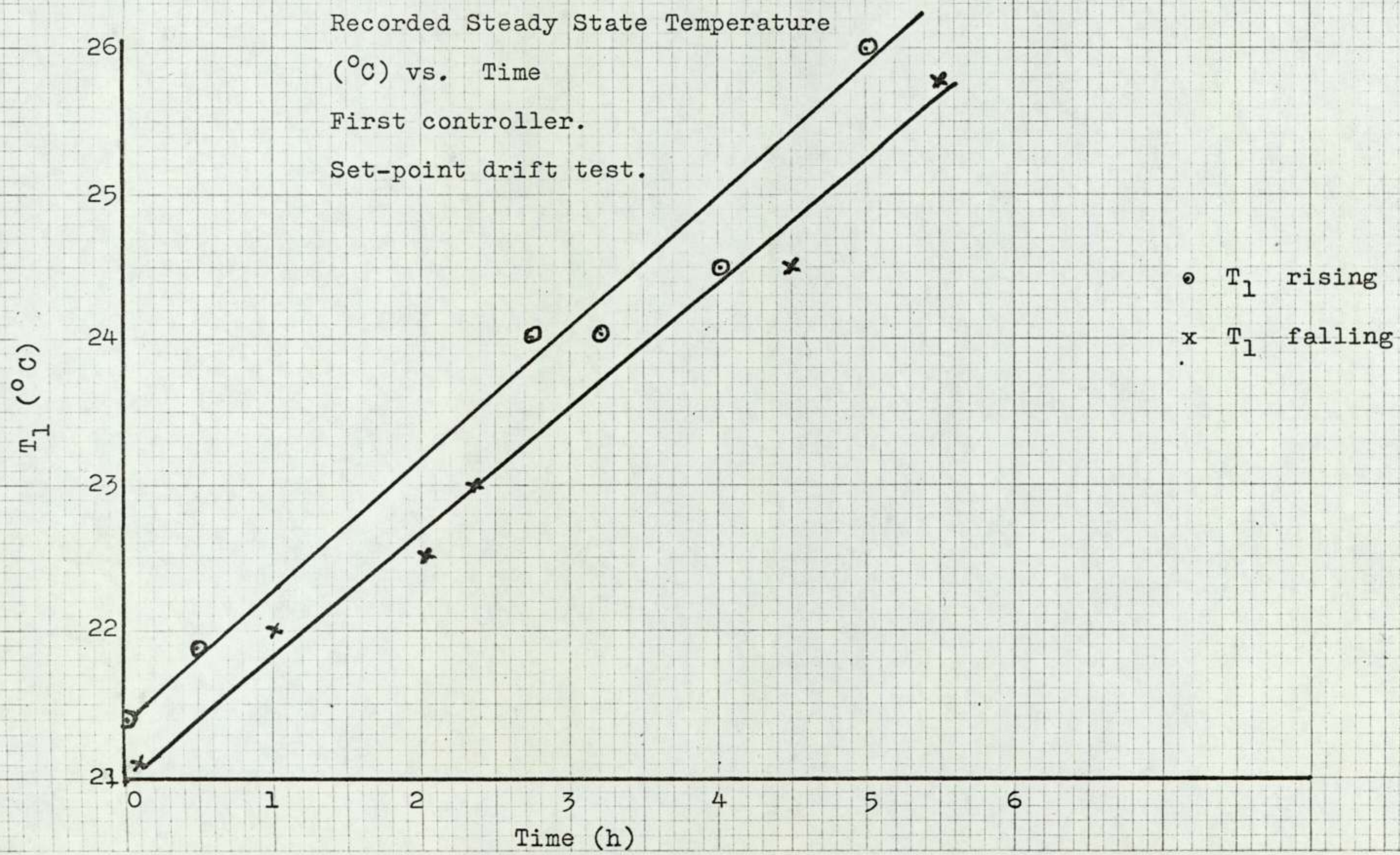

Fig.A65. Series 7. Test 1.
Recorded Steady State Temperature
(°C) vs. Time
First controller.
Set-point drift test.

Tests on second controller

The first controller was removed from the system because of the drift and hysteresis effects recorded. It was hoped that by incorporating a new controller such errors would be overcome or at least reduced. Furthermore, the range of the new controller was 100°C and because of this it was expected to offer greater accuracy in its action than its predecessor.

Series 8

Table A.34.

PBW setting 6 deg C — Valve positioner in action

Variac setting 59 — Other parameters as Series 6

Steady states recorded over 3 hours from both high and low starting temperatures (T_1).

T_1 °C	COP lbf/in^{2}gauge	m_c $\frac{\text{litre}}{\text{min.}}$	T_{c1} °C	T_{c2} °C	Direction of Approach of temperature (T_1)
29.8	6.8	5.85	7.9	18.0	rising
28.7	6.1	6.55	"	17.0	falling
29.5	6.7	6.20	"	"	rising
29.3	6.5	6.25	7.8	17.5	"
29.2	"	"	"	"	"
28.2	6.0	7.15	"	16.6	falling

The rate of drift of temperature (T_1) was 0.2°C / h

T_1 steady state hysteresis = 1.0°C

From this and similar tests, it was concluded that this controller suffered from the same drift tendencies as the first controller, the only difference being that the drifting was in the opposite direction.

Series 9

Table A.35.

PBW setting 15 deg C Valve positioner in action

Other parameters as Series8

T_1 °C	COP lbf/in^{2}gauge	m_c litre/min.	T_{c1} °C	T_{c2} °C	Direction of approach of temperature (T_1)
33.1	7.0	5.50	10.0	21.2	rising
32.5	6.6	5.75	10.2	20.9	falling

T_1 steady state hysteresis = 0.6°C

Series 10

Other tests were also carried out on this controller to determine the static hysteresis. In Series 10 tests, steady state hysteresis was recorded by leaving the measured value pointer (T_1) at a fixed position (23°C) and moving the set-point in a cycle around this pointer. As the readings were recorded at steady state there was sufficient time available to record the values obtained directly in graphical form. Proportional band widths of 1, 5, 20 and 30 deg C were tested and the graphs obtained are shown in Figs. A.66. to A.69. The hysteresis was clearly marked and it diminished as the proportional band width increased. The graphs agreed well with results obtained from the tests on the first controller for proportional band widths of similar magnitudes. The drift in the earlier tests appeared to have diminished the measured hysteresis effect on wide proportional band widths as expected.

This was indicated by the fact that Series 10 tests showed diminished yet significant hysteresis even at proportional band widths of 20 and 30 deg C.

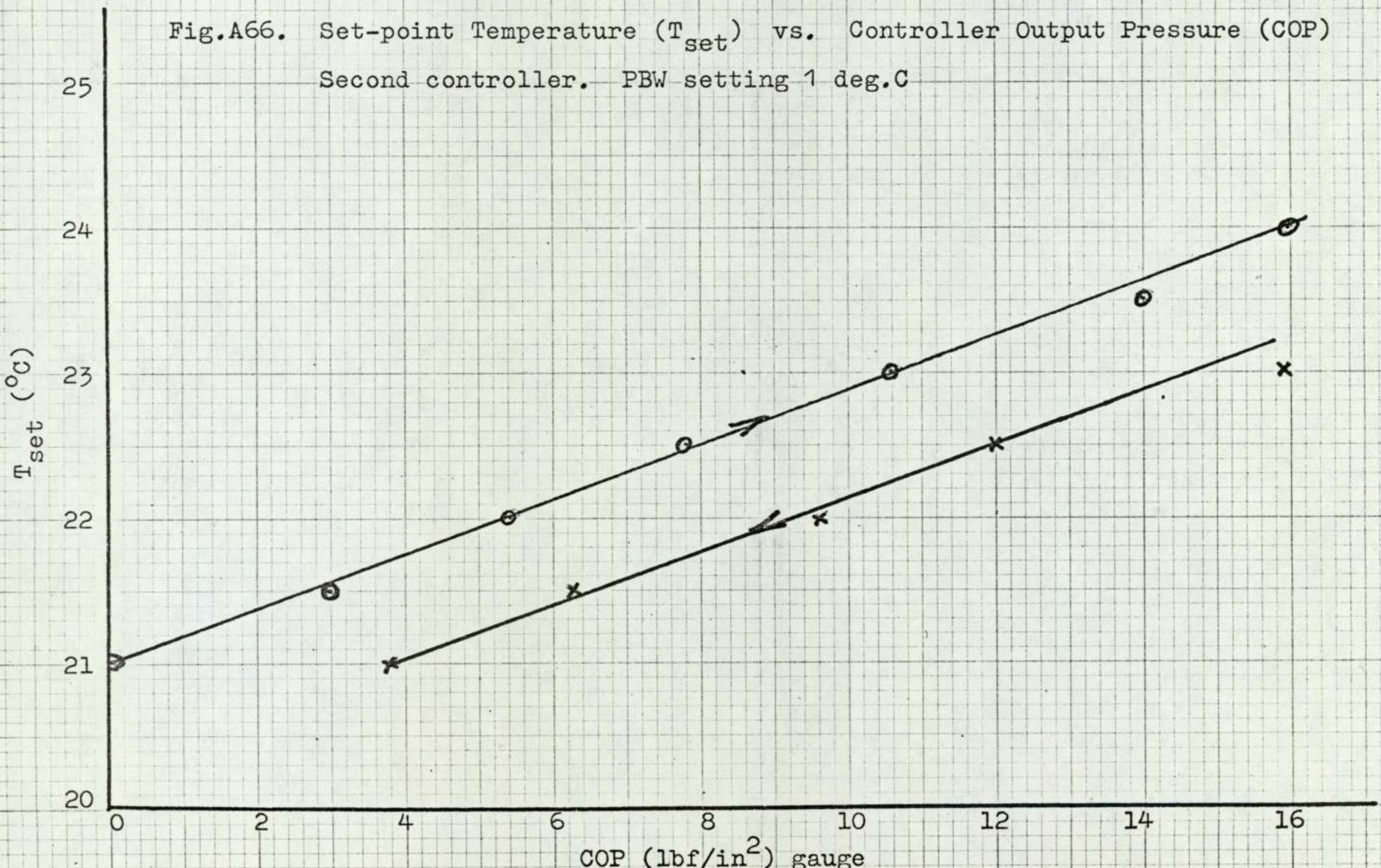

Fig.A66. Set-point Temperature (T_{set}) vs. Controller Output Pressure (COP)

Second controller. PBW setting 1 deg.C

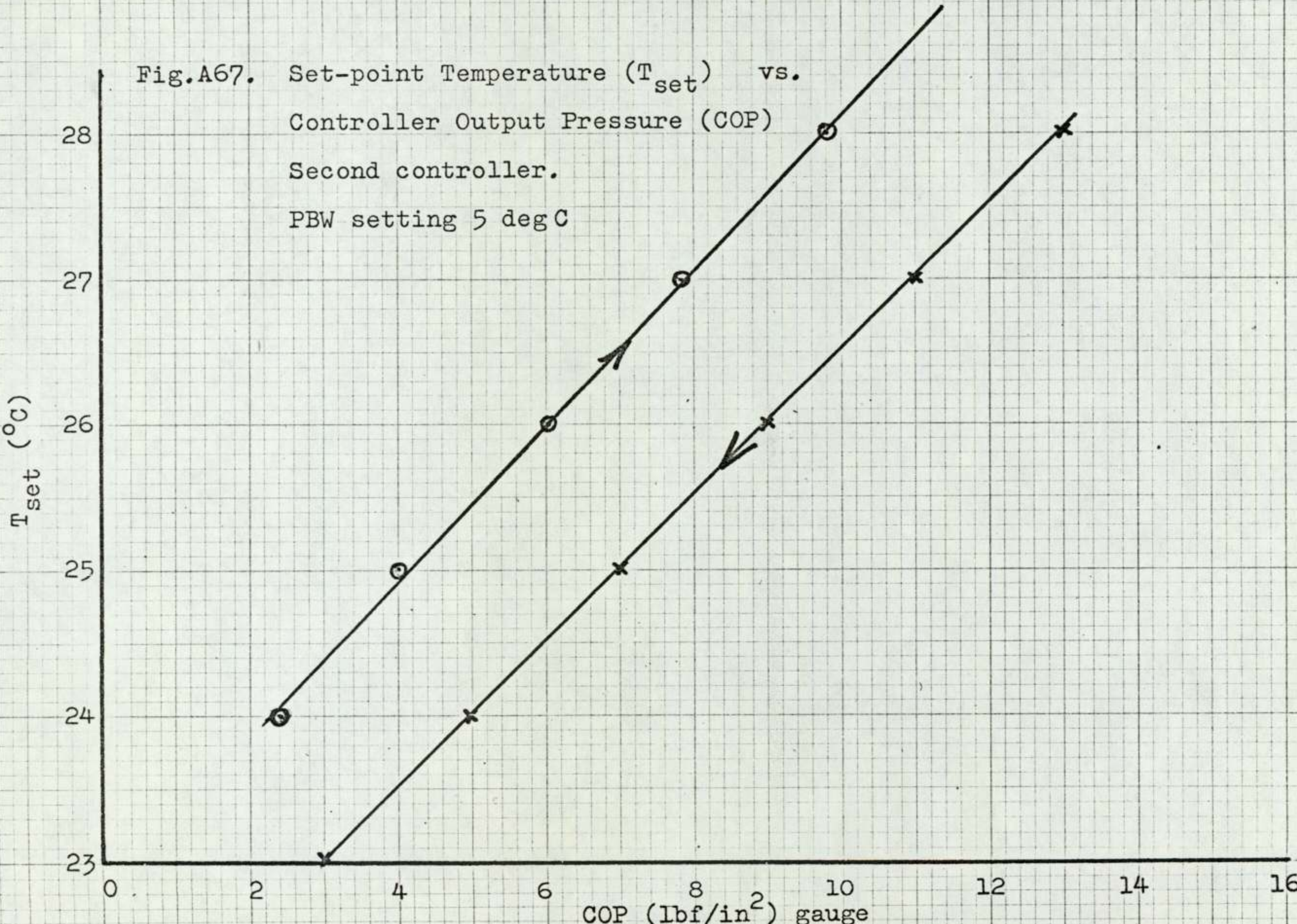

Fig.A67. Set-point Temperature (T_{set}) vs. Controller Output Pressure (COP)

Second controller.

PBW setting 5 deg C

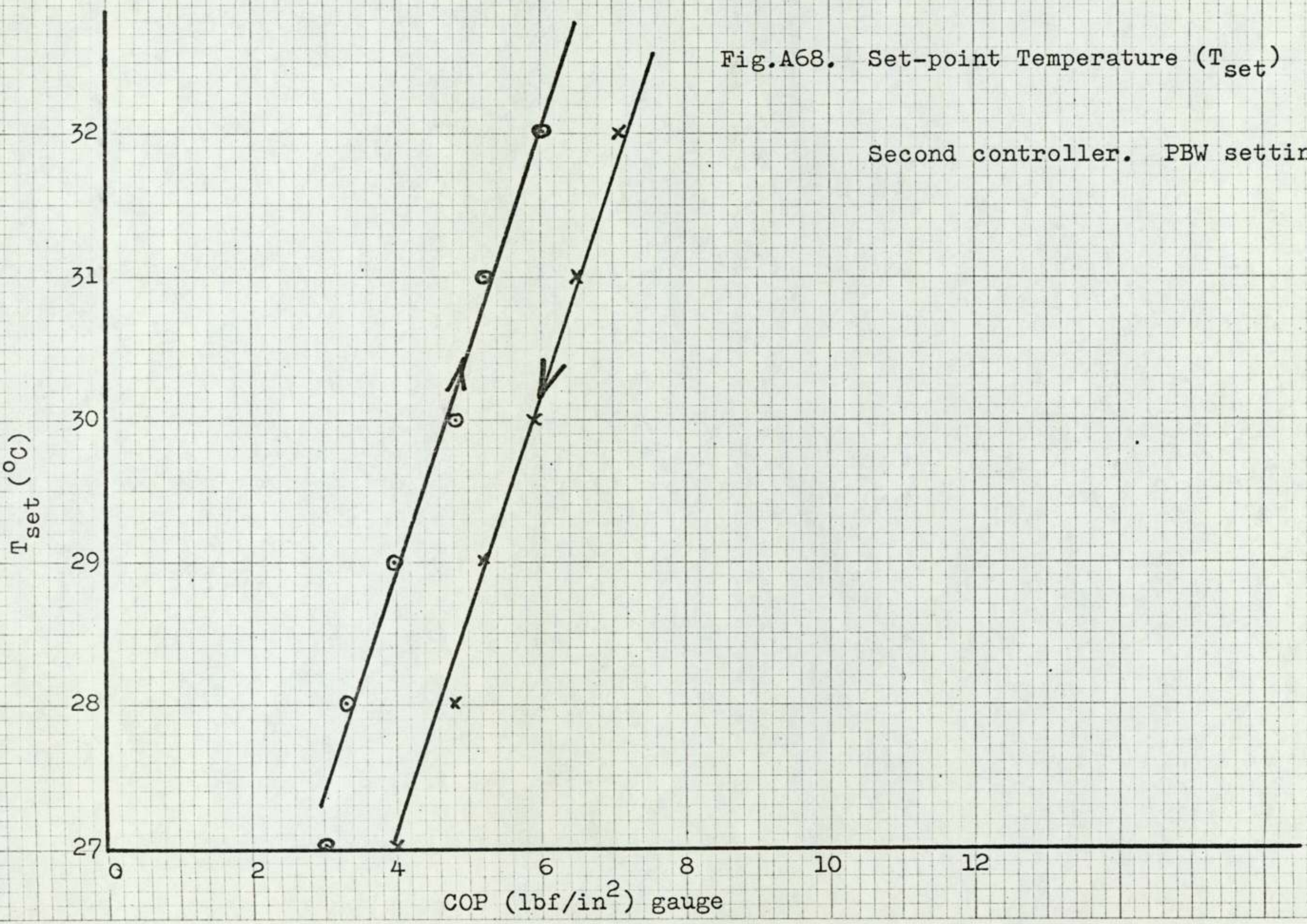

Fig.A68. Set-point Temperature (T_{set}) vs. Controller Output Pressure(COP)

Second controller. PBW setting 20 deg C

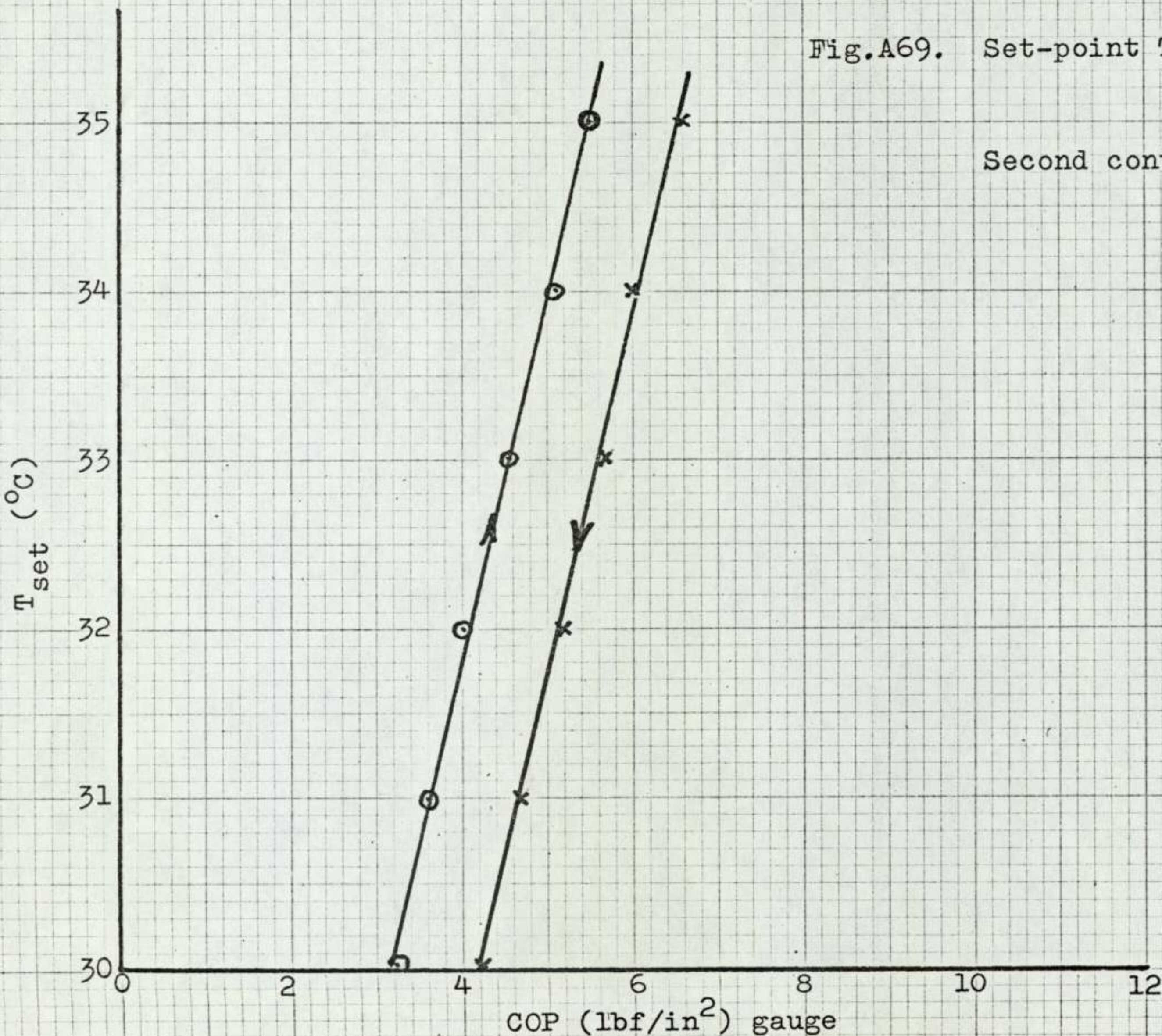

Fig.A69. Set-point Temperature (T_{set}) vs. Controller Output Pressure (COP)

Second controller. PBW setting 30 deg C

Table A.36. re Fig.8.67.(a) and (b)

These potentiometer settings were those actually used when simulating on the Hybrid computer. Gains of 10 were put on integrators 1 and 2.

Potentiometer number	Potentiometer setting
1	Initial condition
5	0.5
8	0.5
25	A
26	cycle width/2
35	0.5
37	0.2 frequency
38	0.2 frequency

Example of calculation of numerical values for potentiometer settings in complete simulations

Experiment 67 was used to supply numerical values for TR 10 complete simulation potentiometer settings.

Table A.37.
Parameter values

From values recorded at steady state:

$$m_f = \rho u = 3 \text{ litre/min.} \times \rho = 50 \text{ g/s.}$$

$$M = \rho V = 16 \text{ litres} \times \rho = 16000 \text{ g}$$

$$c_o = 1 \text{ gmole/litre}$$

$$T_o = 6.8^{\circ}\text{C}$$

$$T_{cav} = \frac{T_{c1} + T_{c2}}{2} = \frac{7.7 + 20.0}{2}$$

$$= \frac{27.7}{2} = 13.9^{\circ}\text{C}$$

T_1 steady state $= 26^{\circ}$C

$m_c = 2.3$ litre/min.

$k = 0.019 \text{ sec}^{-1}$

$T_{set} = 25.2$ (chosen for analogue circuit)

PBW 2 deg C Maximum heat removal (UA) = 300 Kcal/h

$\therefore$ 150 Kcal/h deg C = 41.7 cal/s deg C

Calculation of heat released from immersion heaters

$$Q = m_c(T_{c2} - T_{c1}) + m_f(T_1 - T_o) = 1422 \text{ cal/s.}$$

$$\therefore (-\Delta H) = \frac{Q}{rV} \quad \left(\text{where } r = kc_1 = \frac{kc_o}{1 + k\frac{V}{u}}\right) = 33200 \text{ cal/gmole}$$

Maximum values of variables

$$c_{1m} = 1 \text{ gmole/litre}$$

$$T_{1m} = 40^{\circ}C$$

$$k_m = 0.1 \, s^{-1}$$

$$\dot{c}_{1m} = 0.2 \text{ gmole/litre s.}$$

$$\dot{T}_{1m} = 16.7^{\circ}C/s.$$

From this information all the potentiometer settings defined in Table 8.2. were calculable. Gains of 10 or 0.1 were distributed throughout the circuit as necessary.

Using the information obtained from the system at steady state all complete simulations were implemented in a similar fashion.

BIBLIOGRAPHY

(1) Raven F.H.
Automatic Control Engineering 2nd. Edition
pp.355 - 376 McGraw-Hill

(2) Giordano P., A. Mathis and G. Schandellari
Automatica 3, no.2. pp.73 - 89

(3) Paradis W.D. and D. D. Perlmutter
A.I.Ch.E.J., 12, 1, p.131

(4) Luus R. and L. Lapidus
Chem.Eng.Sci. 1966, 21, pp.159 - 181

(5) Aris, R. and R. N. Amundson
An Analysis of Chemical Reactor Stability and Control
I Chem.Eng.Sci. 1958, 7, pp.121 - 130
II " " " " 7, pp.132 - 147
III " " " " 7, pp.148 - 155

(6) Amundson R. N. and O. Bilous
A.I.Ch.E.J., 1, no.4, pp.513 - 521

(7) Raven F. H. [see (1)] p.114

(8) Gille J. C. et al
Feedback Control Systems, McGraw-Hill, New York 1959
p.239

(9) Ellingson W. R. and N. H. Ceaglske
A.I.Ch.E.J., March 1959, pp.30 - 36

(10) Kermode R. I. and W. F. Stevens
Can.J.C.E., April 1961, pp.81 - 85

(11) Bilous O., H. D. Block and E. L. Piret
A.I.Ch.E.J., June 1957, pp.248 - 260

(12) Ogata K.
State Space Analysis of Control Systems
Prentice-Hall, p.115

(13) Bollinger R. E. and D. E. Lamb
I.E.C. F., 1, no.4, Nov.1962, pp.245 - 252

(14) Ogata K. [see (8)] p.372

(15) " " " " pp.385 and 403

(16) " " " " p.461

(17) Porter W. A.
Modern Foundations of Systems Engineering, Macmillan Co.

(18) Leondes C. T. (editor)
Modern Control Systems Theory, McGraw-Hill

(19) Mickley, Sherwood, and Reed
Applied Mathematics in Chemical Engineering, p.193

(20) Sabo D. S. and J. S. Dranoff
A.I.Ch.E.J., 1966, 12, no.6, p.1223

(21) Warden R. B., R. Aris and N. R. Amundson
An Analysis of Chemical Reactor Stability and Control
VIII Chem.Eng.Sci. 1964, 19, pp.149 - 172
IX " " " " 19, pp.173 - 190

(22) A.I.Ch.E.J., 10, no.2, pp.233 - 245
Berger J. S. and D. D. Perlmutter

(23) Berger J. S. and D. D. Perlmutter
Chem. Eng. Sci. 1965, 20, pp.147 - 156

(24) Lueke R. H. and M. L. McGuire
I.E.C. F., 6, no.3, August 1967, p.432

(25) Lueke R. H. and M. L. McGuire
A.I.Ch.E.J., 11, no.4, 1965, p.749

(26) Ogata K. [see (8)] Chapter 8

(27) Gurel O. and L. Lapidus
I.E.C., 60, no.6, June 1968, pp.13 - 26

(28) Murphy G. J.
Basic Automatic Control Theory
Van Nostrand Series.

(29) Thaler G. J. and R. G. Brown
Servomechanism Analysis, Chapter 4, McGraw-Hill

(30) Mahalanabis A. K.
A.I.E.E., Nov.1961, 80, no.2, pp.277 - 285

(31) Kafarov V.V. and V.V. Eremenko
Zhurnal Prikladnoi Khimii, 35, no.10,
October 1962, pp.2251 - 2262

(32) Siebenthal C.D. and Aris R.
Chem. Eng. Sci. 1964, 19, pp.729 - 761